ISSN 0289-842X

RIKEN Accelerator Progress Report

1992

vol. 26

理化学研究所
The Institute of Physical and Chemical Research (RIKEN)

RIKEN Accelerator Progress Report
January-December 1992

理化学研究所
The Institute of Physical and Chemical Research (RIKEN)
Wako-shi, Saitama, 351-01 JAPAN

CONTENTS

I. INTRODUCTION

M. Ishihara

This Report covers activities at the RIKEN Accelerator Research Facility for the year of 1992. The major facility involved is an intermediate energy heavy ion accelerator complex consisting of an energy booster, RIKEN Ring Cyclotron (RRC) with k=540 and two injectors, an energy tunable linear accelerator (RILAC) and a k=70 AVF cyclotron. The RILAC has also been used in stand alone mode, while such a utility with the AVF is under preparation. In addition a 1-MeV Tandetron is in operation. Thus a variety of heavy ions with energies ranging from 1 to 100 MeV/u have served for experimental studies.

The heavy-ion beams have been used for multiple disciplines including nuclear physics, atomic physics, condensed matter physics, nuclear chemistry, radiation biology and space science. Users have ranged over 12 among 49 laboratories in RIKEN. Besides a large number of outside users, about 250 researchers and 70 graduate students, have participated in the activities. International collaborations with groups from more than 15 laboratories have also contributed to the activities on the basis of institutional agreements or individual initiatives. This year new collaboration programs with INFN (Italy), Jyvaskyla University (Finland), Kansas State University (USA) and University of Frankfurt (Germany) have become operational.

The Report includes construction status reports of two developing projects: One is a joint project between RIKEN and JEARI to build an 8-GeV synchrotron radiation source (SPring-8) at the site of Harima Science Garden City. The other is an international joint project between RIKEN and RAL (UK) to facilitate a pulsed muon beam at the RAL synchrotron.

The accelerators have well worked through the year. The RRC beam hour on the target has exceeded the level of 5000 hours. Ions as heavy as Ta have been used. With improving performance of the ECR ion sources at the RILAC and AVF beam intensities have been considerably strengthened. Meanwhile a polarized ion source for hydrogen beams has been completed at the AVF.

There has been steady development also on the experimental apparatus at the RRC beam channels. A projectile fragment separator RIPS has been supplemented with a large-acceptance magnetic spectrometer to analyze secondary reactions using radioactive beams. Another magnetic spectrometer SMART, a high-precision particle analyzer, has become available for experiments. A new setup to produce high-spin isomer beams has been newly installed in the E1 room.

Studies on nuclear physics have been made primarily at the RRC by consuming about 70 % of its beam hours. A strong emphasis has been placed on the studies on unstable nuclei. Three different types of radioactive beams available, i.e., intermediate-energy beams of projectile fragments, spin-polarized projectile-fragment beams and high-spin-isomer beams of fusion residues have been used. By virtue of the appreciable beam intensities secondary reactions can be comfortably studied.

Extensive works on near-drip-line isotopes have continued to study unique properties of neutron-halo nuclei such as soft modes of excitation and particle correlation in the halo. Attempts to determine masses of off-drip-line nuclei have been also made in several ways. Studies on reaction rates of astrophysical interests have been made by observing secondary reactions of unstable nuclei. In particular electro-magnetic dissociation processes were used to study inverse radiative capture reaction rates such as on ^{7}Be (p,γ)^{8}B, which is related with solar neutrinos. Spin polarized unstable nuclei have been used to determine g-factors of neutron-rich isotopes.

Development of isomer beams is in progress to facilitate secondary reactions with nuclei at high-spin states. Application to synthesis of cold and very rapidly rotating nuclei is intended. A challenging program to synthesize super heavy elements has made a steady progress. A pilot experiment using a (HI,αxn) reaction yielded a positive indication.

The SMART spectrometer was primarily used to study charge-exchange reactions with deutron and heavy-ion beams. A promissing prospect of high-energy heavy-ion direct ractions as sprectroscopic probes was indicated.

Experiments on atomic physics have been made using the RRC, the RILAC and the ECR ion source to cover a wide range of beam energy. A study on radiative processes such as

radiative electron rearrangement and radiative Auger effect has been started in the high-energy domain to investigate effects of the interaction between two electrons. A study on ionization and electron transfer processes in ion-atom close impact collisions has been also initiated by observing the impact parameter dependence. Beam-foil spectroscopy has been applied to Ne-like Fe ions. A study on micro cluster formation was continued by means of heavy-ion irradiation on various frozen gas targets.

In the field of nuclear chemistry studies have been continued using tracer techniques, hyperfine techniques, and analyzing methods in terms of positron annihilation, Rutherford scattering, PIXE and channelling effects. A major development was achieved on the multi-tracer technique in which a variety of radioactive nuclides produced in high-energy heavy-ion irradiation are utilized simultaneously to trace circulation of different elements in various systems. New methods for preparing multi-tracer solutions from different targets were established. The technique has been broadly applied to analytical chemistry, environmental chemistry and biochemistry. Mossbauer, TDPAC and positron annihilation studies were continually performed using accelerator-produced radioactive sources on the properties of high-Tc super conductors, magnetic materials and semi-conductors.

Biological studies have extended over both basic and applied researches on heavy-ion irradiation effects. A variety of samples such as DNA molecules, bacterial cells and spores, cultured mammalian cells and shrimp eggs were irradiated to systematically study the difference in induced damages between heavy-ion and other coventional ionizing radiations. Studies on radiotherapy, space biology and genetic improvement in plant were also pursued. In the domain of radiotherapy R$D, a beam with a homogeneous dose distribution has been prepared by means of spreading out the Bragg peak. The curing probability was then studied for tumer-bearing mice.

Beside experimental studies theoretical studies were also pursued. There were also a large number of activities for seminars , workshops and symposia. For example six international meetings were organized this year. In particular a winter school was initiated primarily for graduate students. It was held at Yuzawa and will be continued every year on a different subject. A joint symposium between INFN and RIKEN on heavy ion collisions was also held for the first time at Catania.

As a whole the Facility has reached a stage of steady operation with increasing productivity. In anticipation for further development in a larger scale a working group to formulate a future project has been set up.

II. OPERATION OF ACCELERATORS

II-1. RRC Operation

A. Goto, M. Kase, T. Kageyama, T. Nakagawa, O. Kamigaito, H. Isshiki,*
H. Akagi,* R. Ichikawa,* N. Tsukiori,* R. Abe,* K. Takahashi,* S. Otsuka,*
T. Maie,* T. Kawama,* T. Honma,* and Y. Yano

Table 1 lists the characteristics of ion beams that were delivered from November 1991 to October 1992. We operated the ring cyclotron for 161 days for beam services to users (excluding tuning time) during this period. We started to accelerate polarized deuterons of 135 MeV/nucleon. The ^{40}Ar ions of 7.5 MeV/nucleon were accelerated without charge stripping between RILAC and the ring cyclotron. There was one cancellation of scheduled machine-time (2 days) because of a vacuum trouble in one of the resonators, which was compensated later.

We took a long summer-time shutdown (for 45 days) for the following improvements:

1) 464 pieces of joints of cooling-water pipes for all the trim coils, located just outside the acceleration chamber, were removed, and the pipes were directly rejointed by welding, because the joints had been damaged due to electrical corrosion.
2) 128 pieces of O-rings of cooling-water joints used in the movable-boxes of the resonators were replaced from P9 to P10A having a slightly larger cross section, because the vacuum of the acceleration chamber had been sometimes broken down due to leaking troubles at these joints.
3) The EDC (deflector) was replaced by a new type whose high-voltage feed-throughs are accommodated in a chamber filled with high-pressure SF_6 gas.
4) The MDC1 (magnetic channel) was replaced by a spare.
5) The nylon hoses used for cooling-water inside trim-coil power supplies were replaced by Synflex hoses, because the nylon hoses had been deteriorated.
6) A twenty-first phase probe was newly installed.

In an attempt to increase the beam intensity from RILAC, we decided to add a new beam buncher of the second harmonic on the injection beam line. The design of it was finished and the whole system will be completed at the end of next March. Besides, a new ECR ion source and a frequency-variable RFQ, which is planned to be installed as another injector of RILAC in the same attempt, is being designed.

Table 1. RRC beams accelerated in November 1991 - October 1992.

Particle	Charge	RF F (MHz)	h	Energy (MeV/nucleon)	Beam time (days)
d†	1	29.0	5	100	1
	1	32.6	5	135	9
pol. d†	1	32.6	5	135	3.5
H_2†	1	32.6	5	135	3.5
^{12}C†	6	28.0	5	92	8
†	6	29.0	5	100	10.5
	6	32.6	5	135	17.5
^{14}N	7	32.6	5	135	7
^{16}O†	8	26.2	5	80	3.5
^{18}O	8	29.0	5	100	21.5
^{20}Ne†	10	32.6	5	135	4
^{22}Ne†	10	24.6	5	70	4
^{40}Ar†	5	18.8	11	7.5	25.5
†	14	30.0	9	30	2
†	14	33.0	9	38	8
	17	29.1	5	95	24
^{136}Xe†	23	19.5	10	10	6.5
	31	28.0	9	26	2
				Total	161

† New beams

* Sumijyu Accelerator Service, Ltd.

II-2. RILAC Operation

E. Ikezawa, M. Hemmi, M. Yanokura, M. Kase, T. Aihara,* T. Ohki,*
H. Hasebe,* T. Chiba, Y. Chiba, and Y. Miyazawa

This year, RILAC has been operated for 164 days, and has supplied various kinds of ion beams for experiments. Table 1 gives the statistics of operation from Jan. through Dec. 1992. Table 2 summarizes the time sharing for individual research groups. The percentage of the beam time for RIKEN Ring Cyclotron (RRC) was about 32 %. Ions of ^{40}Ar, ^{136}Xe, and ^{181}Ta accelerated by RILAC were injected to RRC. Table 3 gives the statistics of ions used this year. Beams of 27 ion species have been used for experiments. About 57 % of the total beam time was devoted to ^{40}Ar ions. Metallic ions were also requested frequently and the beam time for those ions amounted to about 20 %.

Table 1. Statistics of the operation from Jan. 1 through Dec. 31, 1992.

	Day	%
Beam time	164	44.8
Frequency change	15	4.1
Overhaul and improvement	27	7.4
Periodic inspection and repair	34	9.3
Machine trouble	2	0.5
Scheduled shut down	124	33.9
Total	366	100

Table 2. Beam time for individual research groups.

	Day	%
Atomic physics	44	26.8
Solid-state physics	21	12.8
Nuclear chemistry	19	11.6
Radiation chemistry	16	9.8
Accelerator research	11	6.7
Beam transportation to RRC	53	32.3
Total	164	100

Table 3. List of ions used in this year.

Ion	Mass	Charge state	Day
He	4	1	6
C	12	2	2
N	14	2, 3	5
N	15	2	1
O	16	3	1
Ne	20	4	4
Si	28	5	1
Ar	40	5, 6, 8, 9	94
Ti	48	5	3
Cr	52	7	4
Fe	56	6, 9	12
Kr	84	9, 11	4
Xe	129	13	2
Xe	136	9, 15, 16	13
Ta	181	16	5
Bi	209	14, 16, 21, 22	7

We have made the following improvements: 1) An electrostatic quadrupole lens (ESQ) was replaced with a new one, because in ion production of ferromagnetic materials such as Fe, magnetized sputtered particles frequently formed a bridge shorting between the electrodes and the wall ; the new lens was improved for rapid exchange of the whole and easy maintenance. 2) An einzel lens was installed between the ECR ion source and ESQ in order to focus the spread beams from the source. As a result, the beam transmission efficiency of the injection beam line increased by 20 % compared with that without the lens. 3) The power supplies for the drift tube magnets used in the cavities No. 4 and 5 were remodeled by replacing the obsolete power transistors with

*Sumijyu Accelerator Service, Ltd.

the modern ones.

We have made the following developments: 1) Ions of ^{11}B, ^{19}F, and ^{32}S were newly produced by the ECR ion source. At present we can supply ions of 10 gaseous and 35 solid elements. 2) A high speed beam chopper was installed in the injection beam line. The details are reported in this issue.[1] 3) We succeeded on accelerating 115 MeV $^{40}Ar^{9+}$ and 324 MeV $^{209}Bi^{22+}$ ion beams. These are new records of the maximum energies accelerated at RILAC.

Two days of the scheduled beam time were canceled owing to faults in NO. 1 rf amplifier and in the screen grid power supply of NO. 5 rf amplifier. The former was induced by water splashed due to an accident in a piping. The other machine troubles in this year hardly affected the beam time schedule and were as follows: 1) In a 40 MHz test operation, thin copper sheets (10 cm wide, 7 cm long, and 0.3 mm thick), which formed an rf path between the upper and the lower structure of NO. 3 and 6 resonators, melted over one meter with an anomalous rf current. 2) A screen grid power supply of NO. 2 rf amplifier, a wide band amplifier for the buncher, and the DC blocking capacitor of the final stage of NO. 1 rf amplifier had troubles.

References

1) M. Hemmi et al.: This report, p. 141.

II-3. AVF Cyclotron Operation

A. Goto, M. Kase, T. Nakagawa, T. Kageyama, O. Kamigaito, H. Isshiki,*
H. Akagi,* R. Ichikawa,* N. Tsukiori,* R. Abe,* K. Takahashi,* S. Otsuka,*
T. Maie,* T. Kawama,* T. Honma,* and Y. Yano

Table 1 lists the characteristics of ion beams that were delivered from November 1991 to October 1992. The beam intensities of these ions are around several eμA. We operated the AVF cyclotron for 124 days for beam services to users (excluding tuning time) during this period with no serious troubles.

We accelerated polarized deuterons from a newly completed ion source. The acceleration was done several times in order to measure the polarization with a polarimeter located just downstream from the AVF cyclotron, and to deliver the beam for further acceleration with RIKEN Ring Cyclotron. The beam intensity was typically 300 nA and the vector polarization about 60 % of the ideal value.

In the summer-time overhaul, we checked the positions of elements such as the deflector, the magnetic channel and the RF dees. We found that the position of one of the two RF dees in the central region was shifted (rotated) in azimuthally direction by about 3 mm, which we put back to the original position. We also checked the electrical damage of RF contact fingers used in various places with a result that there was no damage. We replaced the electrode meshes of the injection beam buncher with new ones, because the color of their surfaces had changed due to beam during three-year's use.

Recently some user groups have made strong demands to use AVF cyclotron beams for their experiments. Until now, we have completed a chamber for use in isotope production in the AVF cyclotron vault. We also plan to prepare other experimental ports in E7 experimental room, which is located below the AVF cyclotron vault.

Table 1. AVF beams accelerated in November 1991 - October 1992.

Ion	RF Frequency (MHz)	Energy + (MeV/nucleon)	Operation++ time (days)
H_2^+	16.3	7.0 (135)	3.5
d	14.5	5.5 (100)	1
d	16.3	7.0 (135)	9
pol. d	16.3	7.0 (---)†	7
pol. d	16.3	7.0 (135)	3.5
$^{12}C^{4+}$	14.0	5.1 (92)	8
$^{12}C^{4+}$	14.5	5.5 (100)	10.5
$^{12}C^{4+}$	16.3	7.0 (135)	17.5
$^{14}N^{5+}$	16.3	7.0 (135)	7
$^{16}O^{5+}$	13.1	4.5 (80)	3.5
$^{18}O^{6+}$	14.5	5.5 (100)	21.5
$^{20}Ne^{7+}$	16.3	7.0 (135)	4
$^{22}Ne^{6+}$	12.3	4.0 (70)	4
$^{40}Ar^{11+}$	14.05	5.2 (95)	24
		Total	124

+ The values in the parentheses show the energies obtained by the coupled operation with RRC.

++ The time served to experiments.

† These ions were accelerated only with the AVF cyclotron.

* Sumijyu Accelerator Service, Ltd.

II-4. Tandetron Operation

E. Yagi, T. Urai, T. Kobayashi, and M. Iwaki

The Tandetron was operated for 90 days for the experiments in the period from Nov. 1, 1991 to Oct. 31, 1992. In the maintainance much time was taken for the improvement of the stability of the acceleration voltage and that of the duoplasmatron ion source. The experimental studies on the following subjects were made.

(1) Rutherford Backscattering Spectroscopy (RBS)
  (a) Behavior of Kr atoms implanted into aluminum by a channeling method (Metal Physics Lab.).
  (b) Analysis of radiation damage in a Tb- and Eu-implanted CaF_2 (Semiconductor Lab. and Surface Characterization Center).
  (c) Silicide formation in Ni-deposited Silicon (Metal Phys. Lab.).

(2) Radiation Effects
  (a) Radiation damage of diamond (Earth Sciences Lab.)

(3) Nuclear Reaction Analysis
  (a) Lattice location of hydrogen in niobium alloys by a channeling method (Metal Physics Lab.)

(4) Particle-Induced X-ray Emission
  (a) Application of PIXE to biomedical, environmental and material sciences; Trace element analysis using energy-dispersive X-ray spectrometry, and Chemical state analysis using wave-dispersive X-ray spectrometry (Inorganic Chemical Physics Lab.).

III. RESEARCH ACTIVITIES

1. Nuclear Physics

III-1-1. Study of α Decays Following ^{40}Ar Bombardment on ^{238}U

T. Nomura, M. Wada, N. Ikeda, S. Kubono, I. Katayama, K. Morita, A. Yoshida, T. Inamura, M. Kurokawa, T. Motobayashi, H. Murakami, S. Furuya, Y. Nagai, H. Kudo, K. Sueki, M. Tanikawa, I. Nishinaka, H. Nakahara, T. Shinozuka, H. Sunaoshi, M. Fujioka, H. Miyatake, Y. Fujita, T. Shimoda, and K. Tsukada*

[NUCLEAR REACTION, $^{238}U(^{40}Ar,\alpha 2n)$, $^{238}U(^{40}Ar,4n)$, E=5.1 MeV/u; measured α decays, spontaneous fission; gas-filled separator.]

Because the α emission from a highly excited nucleus can efficiently cool it down both in energy and angular momentum, the (HI,αxn) type reaction is expected to be a promising way of producing heavy fissile nuclei, in which the fission width is far larger than the neutron emission width. Therefore, we have recently carried out a measurent on the $^{238}U(^{40}Ar,\alpha 2n)$ reaction by using the RIKEN gas-filled separator (GARIS). Since the detailed analysis is now in progress, we will briefly describe here its experimental set-up shown in Fig. 1.

A 7.5 MeV/u ^{40}Ar beam of about 100 pnA in intensity was supplied from the Ring Cyclotron. The beam energy was degraded down to 5.14 MeV/u through a 5.55 μm Havar foil placed between the GARIS and vacuum regions as well as through a target backing (15 μm Al foil), onto which a $^{238}U_3O_8$ target of about 1 mg/cm^2 thickness was mounted. In this set-up the reaction products collected by the GARIS first pass the TOF system consisting of two micro-channel plate assemblies placed 50 cm apart from each other, and then enter a two dimensional position-sensitive Si detector (PSD) set at the focal plane of the GARIS. Each micro-channel plate assembly is composed of a 1 μm mylar

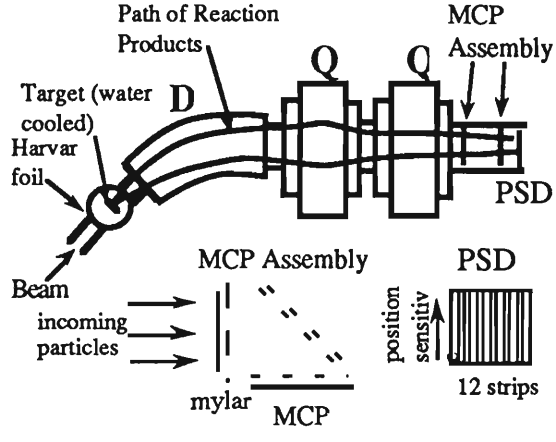

Fig. 1. The present experimental set-up.

foil of 80 mm in diameter and a micro-channel plate of 70 mm in diameter, while the PSD is 60 mm high and 60 mm wide.

The measured space resolution of the PSD turned out to be 0.3 mm for fission fragments, whereas it was around 3 mm for 5.5 MeV α particles. The PSD signals were used to trigger the data taking. Each event array consists of signals of the MCPs, TOF if both the MCPs are on, the energy signal detected in the PSD, and the absolute clock signal. The mass analysis of the residual nuclei reaching the PSD will be done from the measured TOF and energy signals.

* Jpn. At. Energy Res. Inst.

III-1-2. Electromagnetic Transition Probabilities in the Natural-Parity Rotational Bands of ^{155,157}Gd†

H. Kusakari, M. Oshima, A. Uchikura,*1 M. Sugawara, A. Tomotani,*1
S. Ichikawa,*2 H. Iimura,*2 T. Morikawa, T. Inamura, and M. Matsuzaki*3

[NUCLEAR REACTIONS ^{155,157}Gd(^{58}Ni,^{58}Niγ), E=240 MeV; ^{155,157}Gd(^{81}Br, ^{81}Brγ), E=305 MeV; measured Eγ, γ-ray angular distributions, γ branchings and $E2/M1$ mixing ratios, nuclear lifetimes.]

The ground-state rotational bands of ^{155}Gd and ^{157}Gd have been investigated through the multiple Coulomb excitation with beams of 240-MeV ^{58}Ni and 305-MeV ^{81}Br from the tandem accelerator at Japan Atomic Energy Research Institute at Tokai.

We have previously reported the "inverted" signature dependence of $M1$ strength $B(M1)$ in the natural-parity rotational band of ^{163}Dy.[1,2] This has drawn considerable attention since the signature dependence is unexpectedly large and the phase of the zigzag pattern as a function of spin contradicts the well-known selection rule for unique-parity rotational bands based on high-j orbits.[3] In terms of the cranking model we have shown that the inverted signature dependence is likely to originate from the characteristic coherence between the orbital spin configurations in the spin-down ($\Omega=\Lambda-1/2$) dominant one-quasiparticle states.[2] On the other hand, the counterpart, i.e., the spin-up ($\Omega=\Lambda+1/2$) dominant configurations show almost no signature dependence of $B(M1)$, being consistent with the cranking model.[4] In order to further study the general feature in this mass region, we carried out multiple Coulomb excitations of ^{155,157}Gd whose ground states possess comparable magnitudes of the spin-down and spin-up configurations.

The ground-state rotational bands of ^{155,157}Gd are commonly based on the natural-parity Nilsson state ν[521,3/2]. We have assigned levels up to $J^{\pi}=25/2^-$ in ^{155,157}Gd. Measured were γ-rays and their branchings, $E2/M1$ mixing ratios; nuclear lifetimes were also measured by the recoil distance method and the absolute intraband transition probabilties up to the $21/2^-$ state in ^{155}Gd and the $23/2^-$ state in ^{157}Gd were determined.

By comparing the present results especially for ^{155}Gd with those for ^{163}Dy and ^{173}Yb which were previously reported,[2,4] it has been found that, in terms of the cranking model, the signature-averaged magnitude of $B(M1)$ becomes smaller than the experimental one and the inverted signature dependence does more conspicuous as the spin-down components increase. For the case of ^{157}Gd, the calculation somewhat deviates from the observed $B(M1)$ at high spins. As for $B(E2)$ values, however, the experimental trend as a function of spin is well reproduced by the calculation.

References

1) E. Minehara, M. Oshima, S. Kikuchi, T. Inamura, A. Hashizume, and H. Kumahora: Phys. Rev., **C35**, 858 (1987).
2) M. Oshima, E. Minehara, S. Kikuchi, T. Inamura, A. Hashizume, H. Kusakari, and M. Matsuzaki: Phys. Rev., **C39**, 645 (1989).
3) I. Hamamoto: Phys. Lett., **106B**, 281 (1981).
4) M. Oshima, M. Matsuzaki, S. Ichikawa, H. Iimura, H. Kusakari, T. Inamura, A. Hashizume, and M. Sugawara: Phys. Rev., **C40**, 2084 (1989).

† Condensed from the article in Phys. Rev., C46, 1257 (1992).

*1 Chiba Univ.
*2 Jpn. At. Energy Res. Inst.
*3 Fukuoka Univ. of Education.

III-1-3. Lifetime Measurement of a New Isomeric State in ^{145}Sm

A. Ferragut, Y. Gono, T. Murakami, T. Morikawa, Y.H. Zhang, K. Morita, A. Yoshida, M. Oshima, H. Kusakari, M. Sugawara, M. Ogawa, M. Nakajima, J.C. Kim, S.J. Chae, B.J. Min, S. Mitarai, E. Ideguchi, T. Shizuma, and A. Odahara

[Nuclear reaction, isomeric state, secondary beam, recoil-ion separator, ^{145}Sm.]

Secondary beams give the possibility to explore high-spin physics by means of Coulomb excitation or nuclear reactions of the high-spin nuclei in a second target. To estimate the counting rate of high-spin nuclei at the latter position, the knowledge of their half-life is required.

An isomeric state of 13 ns half-life and 1105 keV energy in ^{145}Sm has already been found by using light ions as projectiles,[1] and fusion-neutron evaporation as a production reaction. By means of a heavy ion reaction, ^{16}O(^{136}Xe,7n)^{145}Sm at a bombarding energy of 7.5 MeV/A, we were able to populate higher excited levels and we found an excited state with a half-life of 956.8 ns (+192.5 ns, -148.9 ns).

The reaction products were collected by using a gas filled recoil ion separator[2] and stopped on a catcher which consisted of a plastic scintillator placed at the focusing position and kept in vacuum. Seven BGOACS Germanium (Ge) detectors were placed around the catcher where the high-spin states decayed. Coincidence events obtained with Ge-Ge and Ge-plastic coincidences (triggers) were recorded, and the corresponding gamma energy spectra were measured by the Germanium detectors (Fig. 1 for the Ge-plastic events). Time difference distributions between the germaniums and the plastic were measured for the Ge-plastic coincidence events.

Figure 1 shows clearly all the transitions previously observed in Ref. 1 and therefore, proves that ^{145}Sm is produced with a high efficiency. Since the time of flight of ^{145}Sm from the production target to the catcher is at least 150ns, and since all the reported states above the known isomeric state (1105 keV) have half-lives below the nanosecond range,[1] another isomeric state must be produced at the production target. Moreover, by using the Ge-Ge coincidence data, we determined that most of the important transitions shown in Fig. 1 are coming from the decay of the new isomeric state.

Therefore, the structure observed in the distribution of the time difference between the plastic scintillator and the germaniums is attributed to the decay of the new isomeric state. After a proper background substraction, the distribution shown in Fig. 2 is obtained and the half-life mentionned above is extracted.

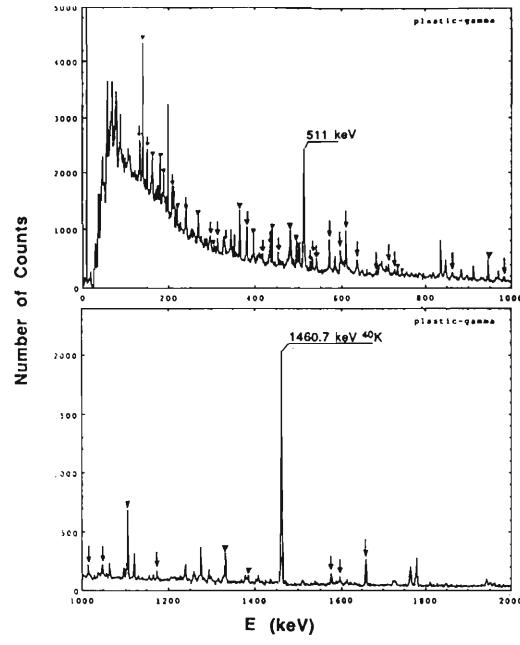

Fig. 1. Gamma energy spectrum for Ge-plastic events. Triangles show the known transitions in ^{145}Sm and arrows the new ones.

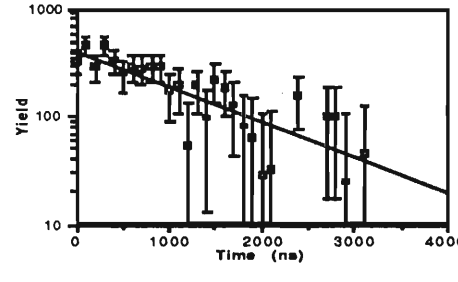

Fig. 2. Distribution of the time difference between the plastic and the germaniums for the Ge-plastic coincidences. Background substracted.

References

1) M. Piiparinen et al.: Z. Phys., A338, 417 (1991).
2) K. Morita et al.: RIKEN Accel. Prog. Rep., 21, 155 (1987).

III-1-4. High-Spin Isomer Beams

Y. Gono, T. Murakami, T. Morikawa, A. Ferragut, Y.H. Zhang, K. Morita,
A. Yoshida, M. Oshima, H. Kusakari, M. Sugawara, M. Ogawa
M. Nakajima, S. Mitarai, A. Odahara, E. Ideguchi,
T. Shizuma, M. Kidera, J.C. Kim,
S.J. Chae, and B.J. Min

[Nuclear Reactions $^{14}N(^{136}Xe,6n)^{144}Pm$, $^{16}O(^{136}Xe,7n)^{145}Sm$, $^{20}Ne(^{136}Xe,9n)^{147}Gd$, 8.5-10MeV/u; Gas Filled Recoil Separator; found new High-Spin Isomers of ^{144}Pm, ^{145}Sm, High-Spin Isomer Beams.]

Experiments to search for high-spin isomers were performed using ^{136}Xe beams of 8.5 and 10 MeV/u. The beams were provided by the RIKEN Ring Cyclotron. The reactions used were the $^{14}N(^{136}Xe,6n)^{144}Pm$, $^{16}O(^{136}Xe,7n)^{145}Sm$ and $^{20}Ne(^{136}Xe,9n)^{147}Gd$. The reaction products were transported to a catcher which was made of a 0.2mm plastic scintillator and placed at 6m down stream from the target position. The beam lines were filled with He, N_2,Ne or Ar gases to equilibrate the charge states both of the reaction products and the primary beams so that the width of the charge state distribution could be reduced. The N_2 and Ne gases worked as targets to produce ^{144}Pm and ^{147}Gd as well. A SiO_2 target of 2mg/cm^2 was used to produce ^{145}Sm. Two new isomers were found in ^{144}Pm and ^{145}Sm at the excitation energies of 7.5 and 8.7 MeV, respectively, which were determined tentatively by the analysis of $\gamma\gamma$-coincidence data. Their probable spin values are assigned to be 27^+ and $49/2^+$ based on the systematics of isomers and the argument of tilted Fermi surface of N=83 isotones.

It is worth noting that these isomers including that of ^{147}Gd have the recoil energies which are high enough to be used as secondary beams when they are produced by the inverse kinematics just as of the present cases. The interesting utilizations of these isomer beams are the Coulomb excitation of the isomers and the fusion reactions of isomer beams to produce the cold high spin states.

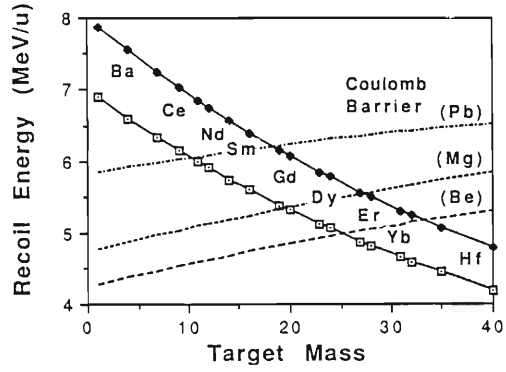

Fig. 1. The recoil energies of Xe induced reactions with inverse kinematics and Coulomb barriers between the reaction products and secondary targets, Be, Mg and Pb.

Though the isomer beam intensities under the present conditions, a little more than 10^4 s^{-1}, are weak, the Coulomb excitation experiment will be possible within ten days if there are E2 collective states based on these isomers with enhancement of more than 20 single particle units.

There are many possibilities to produce unstable nuclear beams by the fusion reactions of inverse kinematics as shown in Fig.1. In this figure, the recoil energies of reaction products of various targets bombarded by the ^{136}Xe beams of 7 and 8 MeV/u are shown as well as the Coulomb barrier heights between these products and the Be, Mg and Pb targets.

III-1-5. Neutron Emission for the Fusion of ^{40}Ar + Ni, ^{92}Mo, ^{122}Sn Reactions at E/A=26 MeV†

K. Yoshida, J. Kasagi, H. Hama,*1 M. Sakurai,*2 M. Kodama,*2
K. Furutaka, K. Ieki, W. Galster,*3 T. Kubo, M. Ishihara, and
A. Galonsky

[NUCLEAR REACTIONS : ^{40}Ar + Ni, ^{92}Mo, ^{122}Sn at E / A = 26 MeV; measured neutron energy spectra and angular distributions; statistical model analysis; deduced level density parameters.]

Coincidence measurements between residues and neutrons were performed and the level density parameters were deduced for the nuclei with excitation energies 3 - 6 MeV/nucleon where the strong reduction of the level density parameters was reported by Wada et al.[1)]

Foils of Ni, ^{92}Mo, and ^{122}Sn were irradiated with ^{40}Ar beams of E/A = 26 MeV extracted from the RIKEN Ring Cyclotron. Neutrons were detected with seven NE213 detectors and residues were observed with an annular PPAC. The neutron spectra were analyzed with the moving source model for different residue velocities represented by the ratios $<R>$ between the average residue velocities and those for the complete-fusion residues. Two sources, the fusion source and the pre-equilibrium source, were assumed in the model and the multiplicities and the temperature parameters for both sources were deduced from the fitting.

The relation between the initial temperature and the temperature parameter for the neutron emission from hot nuclei was deduced numerically through CASCADE calculations. It is found that the relation $T = (12/11)\tau$ is valid only for $\tau < 3$ MeV, and the relation $T = 1.15\tau$ is a good approximation at higher temperatures. The initial excitation energy of the fused system was kinematically evaluated from the amount of linear momentum transferred to the fusion residue taking into account the pre-equilibrium emission. The extracted neutron multiplicity and the initial temperature increase from $<R>$ = 0.6 to 1.0. Thus, the neutron emission can be regarded as the decay of the thermally equilibrated fused system. As shown in Fig. 1, the initial-temperature vs. excitation-energy relation is well explained with the level density parameter $a = A/(9 \pm 1)$ for excitation energies of 2.5 - 5.0 MeV/nucleon. No strong variation of a has been deduced.

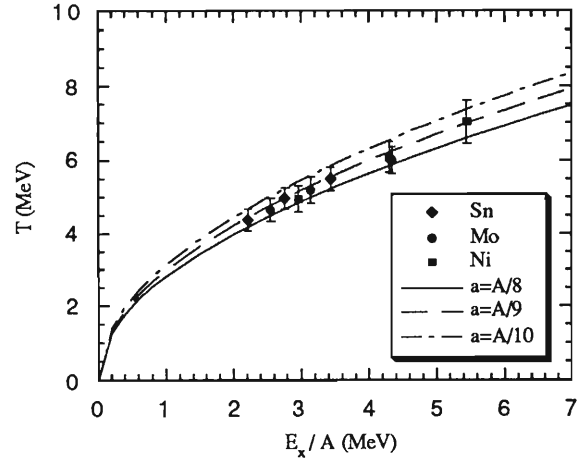

Fig. 1. Initial temperature versus excitation energy per nucleon obtained in the ^{40}Ar + Ni (squares), ^{92}Mo (circles) and ^{122}Sn (diamonds) reactions. The solid, dashed, and dotted curves correspond to the level density parameter $a = A/8$, $A/9$, and $A/10$, respectively.

References

1) R. Wada et al.: Phys. Rev., C39, 497 (1989).

† Condensed from the article in Phys. Rev., C46, 961(1992).

*1 Ultraviolet Synchrotron Orbital Rad. Lab., Inst. Mol. Sci.
*2 Dept. Phys., Tokyo Inst. Technol.
*3 Universite Catholique de Louvain.

III-1-6. Complex Fragment Distributions in ^{84}Kr + ^{27}Al at E_{lab}=10.6 MeV/u†

T. Nakagawa, K. Yuasa-Nakagawa, S. C. Jeong,* T. Mizota, Y. H. Pu, Y. Futami, B. Heusch, K. Ieki, T. Matsuse, and S. M. Lee

[NUCLEAR REACTION $^{84}Kr+^{27}Al$, E(^{84}Kr)=10.6MeV/nucleon: measuredcomplex fragment emitted from hot compound nucleus.]

In order to study the decay mechanism of complex fragments from a hot compound nucleus, we measured the complex fragment emitted in the reaction of $^{84}Kr+^{27}Al$ at the incident energy of 10.6 MeV/u. According to the empirical formula for complete and incomplete fusion reactions, the complete fusion is still dominant and sequential decay is expected at the incident energy of 10.6MeV/u.

An experiment was performed using a large cylindrical scattering chamber ASCHRA[1] of RIKEN Ring cyclotron Facility. Experimental details were previously reported. [2,3]

Figure 1 shows the angle integrated Z distribution of complex fragments. One notices some even-odd effect for Z<10 and for heavier elements the cross section becomes smooth. At Z~40, there is a spurious peak which originates from the evaporation residues. The cross sections for evaporation residues and complex fragment emissions are 550±100 and 500±50 mb, respectively. The total fusion cross section obtained by summing up the cross section of evaporation residues and complex fragment emission is 1050 mb.

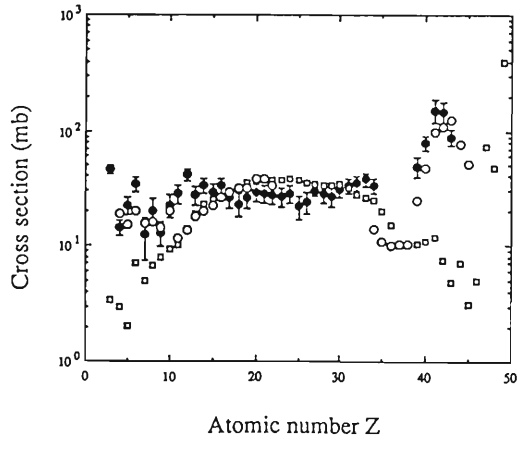

Fig.1. The calculated results of Z-distribution for $^{84}Kr+^{27}Al$ at 10.6 MeV/u: Closed circles are the experimental data. Open squares and circles show the results of the first-step and multi-step calculations, respectively.

In order to investigate the decay mechanism more in detail, we compared the experimental results with the theoretical calculation of Extended Hauser-Feshbach method(EHFM).[4] In Fig. 1, open squares show the first step calculation and circles show the calculation with the sequential decay. From the detailed comparison between the experimental Z distribution and the results of EHFM, it turns out that the intermediate mass fragment (IMF) (3≤Z≤10) emission competes with the light-particle evaporation in the first step decay and as a consequence there is a sizable contribution of the IMF sequential decay after the light particle evaporation in the final IMF yields. On the contrary, the fission decay is dominant in the first step calculation. To verify this conclusion more directly we are planning to perform a correlation experiment between complex fragments and light particles using a 3π phoswich detector system.[5]

References

1) T. Nakagawa et al.: RIKEN Accel. Prog. Rep., **22**, 147 (1988).
2) K. Yuasa-Nakagawa et al.: Phys. Lett., **B283**, 185 (1992).
3) K. Yuasa-Nakagawa et al.: Proc. Int. Symp. Nikko '91(Nikko, June 1991) AIP Conf. Proc., 250, p.100.
4) T. Matsuse et al.: ibid., p.112.
5) Y. Futami et al.: Nucl. Instrum. Method, A, in press.

† Condensed from the article in Phys. Lett., B283, 185 (1992).

* Inst. Phys., Univ. Tsukuba.

III-1-7. Search for a Bound State of a Negative Pion and Neutrons in ^{18}O + Be Collisions

T. Suzuki, M. Fujimaki, S. Hirenzaki, N. Inabe, T. Kobayashi, T. Kubo, T. Nakagawa, S. Shimoura, Y. Watanabe, and I. Tanihata

[NUCLEAR REACTIONS, $^{18}O + Be, E = 100$ MeV / nucleon; particle-identification, deduced upper limits of $\sigma(\pi^- n^N)$, coalesence model.]

A bound system of a π^- and neutrons (pineuts), denoted by $(\pi^-)n^N$, was searched in the fragmentation region of ^{18}O + Be collisions at 100 A MeV.

So far, no experiment has been carried out for the pineut production using a neutron-rich projectile in the projectile fragmentation region, although the Berkeley group recently searched pineuts in the central region using heavy-ion beams.[1] In this note we report on a search for singly charged pineuts (N = 2-3) using a 100 A MeV ^{18}O beam from the RIKEN Ring Cyclotron. Experimental details can be found in Ref. 2. Eighteen among the initially recorded 3×10^6 events survived through the analysis.

Figure 1 shows the two-dimensional distributions of the time spectrum versus the radius of curvature (ρ) in the magnetic field, where the time spectrum is defined between the scintillator (H1) and the radio frequency of the cyclotron (TRF). Eighteen events are in the figure. The hatched regions estimated from calibration runs indicate the location where $\pi^- n^2$ or $\pi^- n^3$ with zero binding energy is expected. The widths of the bands reflect the mass resolution of respective ^2H and ^3H events. Two (six) of the 18 events are within the region of the pion neutron cluster scenario as candidates for the $\pi^- n^2$ ($\pi^- n^3$). However all the surviving 8 events locate on the fringes of the reference distribution.

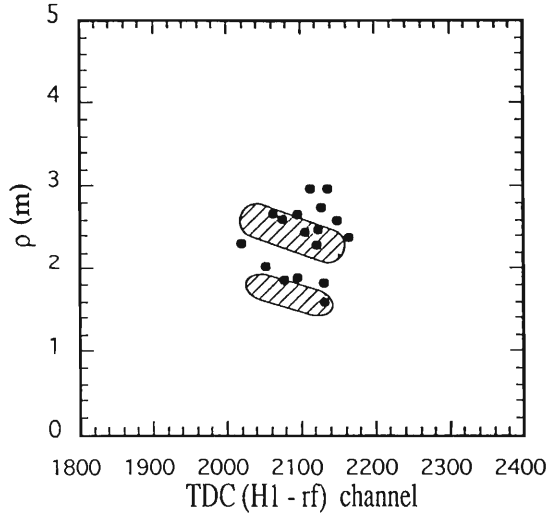

Fig. 1. Plot of time spectrum versus radius of curvature ρ, corresponding to the rigidity, where the time spectrum is defined between the scintillator and TRF. Pineuts might be expected in hatched region with zero binding energy.

Several background sources were examined since the background and reference distribution could not be well separated. Among them protons converted at the most front scintillator by numerous forward neutrons (10^8) might be likely the background. About 30 protons were estimated to remain through the process using a cross section, $\sigma(n\rightarrow p)$, of 0.07 b for 100 A MeV neutrons, which is a comparable number to that of the candidates. The possibility that the survived 2(6) events were due to background sources could thus not be excluded.

If we assume that pineuts distribute uniformly in the phase space of Δy =0.36-0.45 and $\Delta(p_\perp/m) <$ 0.025 the upper limits of double differential cross section at 90% confidence level, $d^2\sigma/d\Omega dp$, are 0.46 (1.07) nb/sr (MeV/c) for $\pi^- n^2$ ($\pi^- n^3$). Here we took into account the minimum lifetime of 26 ns for the survival probability of pineuts. The data were compared with a theoretical calculation based on the coalesence model. [3]

References

1) F. W. N. de Boer *et al.*: Phys. Rev., D 43, 3063 (1991).
2) T. Suzuki *et al.*: submitted to Phys. Rev. C.
3) S. Hirenzaki *et al.*: submitted to Phys. Rev. C.

III-1-8. Pion Absorption in the GeV Region

I. Nomura, I. Arai,[*1] T. Fukuda, H. Kitayama,[*1] P. Kitching,[*2] T. Kobayashi, K. Maeda, H. Matsuyama,[*3] T. Nagae,[*4] Y. Nagasaka,[*1] M. A. Prokhvatilov,[*5] V. I. Rasin,[*5] D. Rowntree,[*6] M. Sekimoto,[*4] T. Suda, K. Tomizawa,[*1] S. Ueno,[*1] and K. Waki[*1]

[Nuclear reaction, ^{4}He(π^+, pp), (π^+, pn), $P\pi$= 1GeV/c, Pion absorption.]

Recently the intensive study of the pion absorption on ^{3,4}He was carried out in the energy region below $T\pi$ = 0.5 GeV at LAMPF, PSI and TRIUMF.[1-3] This energy region is characterized by the dominance of the Δ resonance, and, therefore, the absorption on the nucleon pair with isospin T= 0 is enhanced.

In the GeV region there are resonances which are much weaker than the Δ resonance. As in the Δ region, the effect of the resonances on pion absorption can be expected to result from a mechanism of this region. The energy dependence of the absorption cross sections on Deuteron,[4] however, shows no clear structure. This can be considered to be due to that the reaction is not affected by the resonances or the effect of resonances are smeared out. The measurements on a Deuteron target show directly the absorption cross section on the nucleon pair with T=0, and there is no data of that for the T=1 pair in this region. One of our aims is to obtain the elementary absorption cross sections on the nucleon pair with T=1 and T=0, in order to investigate the absorption mechanism in this region.

As the first experiment, we have measured the (π^+, pp) and (π^+, pn) cross sections on ^{4}He at $P\pi$ = 1 GeV/c using 12GeV Proton Synchrotron at National Laboratory for High Energy Physics(KEK). The preliminary analysis shows that the angle-integrated cross section ratio $R = \sigma(\pi^+, pp) / \sigma(\pi^+, pn)$ is the order of one, while in the Δ region it is about 20. This measured ratio R is connected to the elementary absorption cross sections by inserting the numbers of nucleon pairs and the Clebsch-Gordan Coefficients as below,

$$R = \sigma(\pi^+, pp) / \sigma(\pi^+, pn)$$

$$= \sigma(\pi^+ + pn[T=0,1] \rightarrow pp[T=1]) / \sigma(\pi^+ + nn[T=1] \rightarrow pn[T=0,1])$$

$$= [\,\langle 11\ 10 \mid 11\rangle^2 N_{1,0}\,\sigma_{11} + \langle 11\ 00 \mid 11\rangle^2 N_{0,0}\,\sigma_{01}\,] / [\,\langle 11\ 1{-1} \mid 10\rangle^2 N_{1,-1}\,\sigma_{11} + \langle 11\ 1{-1} \mid 00\rangle^2 N_{1,-1}\,\sigma_{10}\,]$$

$$= (1/2\,\sigma_{11} + 3\,\sigma_{01}) / (1/2\,\sigma_{11} + 1/3\,\sigma_{10})$$

here, $\sigma_{i,f}$ shows the elementary cross section for absorbing a pion on a nucleon pair with initial isospin T = i and final isospin T = f. $N_{i,j}$ shows the number of nucleon pairs in ^{4}He with isospin T = i and Tz = j. Same as above, we can get the ratio $R_D = \sigma[^4\mathrm{He}(\pi^+, pp)] / \sigma[D(\pi^+, pp)]$. Assuming that the σ_{01} is given by the cross section on Deuteron, the elementary cross section ratio $r_{10} = \sigma(T=1) / \sigma(T=0) = (\sigma_{11} + \sigma_{10}) / \sigma_{01}$ is obtained from R.

Consequently, our preliminary ratio R indicates that the contribution of T = 1 pair absorption is by a few times to one order stronger than that of T = 0. In order to confirm the resonance effect and to obtain the difference between the elementary cross section σ_{01} and that of Deuteron, the measurements of the pion energy dependence of the absorption cross sections, on- and off-resonance, and the measurements of π^+ and π^- absorption cross section should follow.

References

1) S.Mukhopadhyay et al.: Phys. Rev., **C43**, 957 (1991).
2) L.C.Smith et al.: Few Body XIII, Adelaide, Australia, Jan.6-11, 1992.
3) H.J.Weyer: Phys. Rep., **195**, 295(1990), and references therein.
4) M.Akemoto et al.: Phys. Lett., **149B**, 321(1984).

*1 Institute of Physics, University of Tsukuba.
*2 Nuclear Research Center, University of Alberta, TRIUMF and Institute for Nuclear Study, University of Tokyo(INS).
*3 Laboratory of Nuclear Science, Tohoku University.
*4 INS.
*5 Institute for Nuclear Research, Academy of Science (INR) and INS.
*6 Department of Physics and laboratory of Nuclear Science, Massachusetts Institute of Technology(MIT).

III-1-9. $^{12}C(^{12}C,^{12}N)^{12}B$ Charge-Exchange Reaction at E/A=135 MeV

T. Ichihara, Y. Fuchi, K. Hatanaka, M. Hosaka, S. Ishida , S. Kato, H. Kawashima, S. Kubono, S. Miyamoto, T. Niizeki, H. Ohnuma, H. Okamura, H. Orihara, N. Sakamoto, Y. Tajima, S. Takaku, M.H. Tanaka, H. Toyokawa, T. Yamamoto, M. Yosoi, and M. Ishihara

[NUCLEAR REACTION $^{12}C(^{12}C,^{12}N)^{12}B$, E/A=135 MeV.]

Heavy-ion charge-exchange reaction has been expected to be used as a new probe for studying spin-isosipn excitations of nuclei. However, in the E/A < 50 MeV region, the reaction mechanism is complex and the successive nucleon transfer process is dominant. One-step and two-step DWBA calculations show that in the E/A >100 MeV region, the two step process becomes negligible and the direct charge-exchange is safely dominant.[1,2)]

Charge-exchange reaction of $^{12}C(^{12}C,^{12}N)^{12}B$ has beam measured at E/A=135 MeV using the high resolution spectrograph SMART in RIKEN.[3)] Figure 1 shows the typical spectra. The overall energy resolution was 700 keV FWHM. Figure 2 shows the measured differential cross sections of the $^{12}C(^{12}C,^{12}N)^{12}B$ for the ^{12}B (1^+) ground state in closed circles.

Microscopic one-step DWBA calculations were performed using the code of Lenske et al. [1)] First, single particle wave functions of ^{12}C were calculated to reproduce the binding energy of orbits using a Wood-Saxon potential. Then transition densities for both target and projectile were constructed with the one-body transition amplitude of Winfield et al. Form factors were then calculated by folding the nucleon-nucleon effective interactions of Franey and Love. Single nucleon knock-out exchange contributions in the local momentum approximation and direct tensor term are included. The optical potentials were taken from ^{12}C + ^{12}C elastic scattering at 84 MeV/A.

The solid curve in Fig. 2 shows the result of the DWBA predictions. The normalization factor for the calculated cross sections is 0.9 and this is very close to unity. An excellent fit has been obtained for all the angle region. The dotted and dashed curves in Fig.2 show the L=0 component and L=2 component, respectively. The dot-dashed curve in Fig.2 shows the DWBA calculation using only the central part of the nucleon-nucleon effective interaction (without tensor interaction). As noticed by these calculations, L=0 component is mainly excited by the central part of the effective interaction, while L=2 component is mainly excited by the tensor part of the effective interaction.

The experiment and analysis of the $^{12}C(^{12}C,^{12}N)^{12}B$ charge-exchange reaction at E/A=135 MeV show that the cross sections for the $\Delta J^{\pi}=1^+$ transition can be quantitatively reproduced by the one-step DWBA calculation using the realistic nucleon-nucleon effective interaction. This suggests that the heavy-ion charge-exchange reactions in this energy region is a good spectroscopic tool for nuclear spin-isospin excitations.

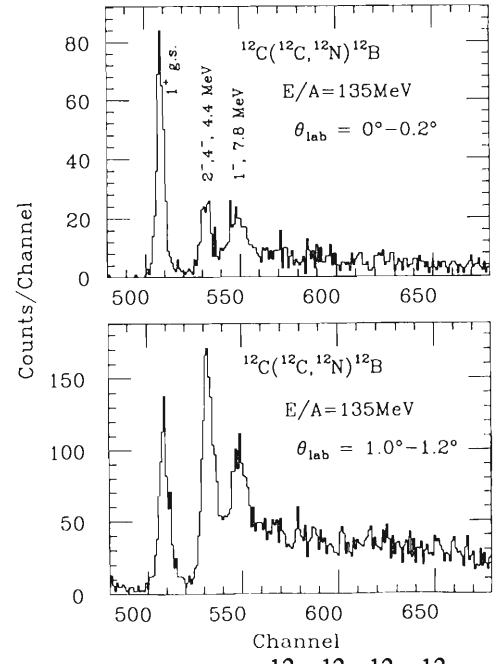

Fig.1. Observed Spectra for $^{12}C(^{12}C,^{12}N)^{12}B$ reaction.

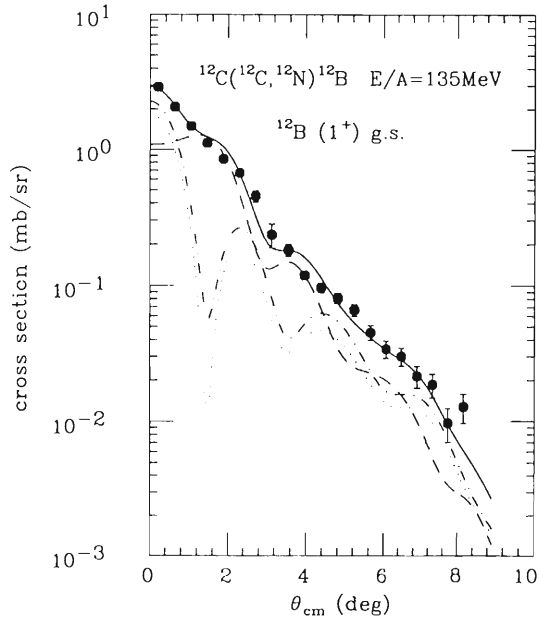

Fig.2. Observed angular distributions.

References

1) H. Lenske et. al.: Phys. Rev. Lett.,62,1457 (1989).
2) N. Anantaraman et al.: Phys. Rev.,C44, 398 (1991).
3) T. Ichihara et. al.: submitted to Phys. Lett. B.

III-1-10. Deuteron Breakup Reaction at Intermediate Energies

H. Okamura, K. Hatanaka, T. Ichihara, S. Ishida, T. Niizeki, H. Ohnuma, H. Otsu, H. Sakai, N. Sakamoto, Y. Tajima, H. Toyokawa, T. Uesaka, T. Wakasa, and M. Yosoi

[NUCLEAR REACTION ^{12}C, ^{28}Si, ^{40}Ca, ^{90}Zr, ^{118}Sn, ^{165}Ho, ^{208}Pb(d,pn) E_d = 140, 270 MeV.]

The breakup of the deuteron is a simple but fundamental process and has been the subject of extensive investigations. Kinematically complete measurements have provided valuable information on this problem, although there exists no data above 100 MeV. The RIKEN Ring Cyclotron can accelerate the deuteron beam up to 270 MeV and gives us opportunities to shed light on the possible new aspect of the breakup reaction.

Our special interest is the mechanism of the Coulomb breakup at intermediate energies. In our previous study at 56 MeV,[1] a conspicuous double-peaked structure was observed in the triple differential cross section $d^3\sigma/d\Omega_p d\Omega_n dE_p$ for the (d,pn) elastic breakup at $\theta_p = \theta_n = 0°$. It turned out to be clear evidence for the Coulomb breakup of the deuteron. The strong effect of the Coulomb distortion was also observed as the characteristic target-dependence of the cross section and as the asymmetric shape of the double-peaked structure. This effect is expected to be small at intermediate energies.

We have studied the (d,pn) elastic breakup reaction on ^{12}C, ^{28}Si, ^{40}Ca, ^{90}Zr, ^{118}Sn, ^{165}Ho and ^{208}Pb at E_d = 140 and 270 MeV. Protons were detected by the SMART spectrograph system[2] and neutrons were detected by 6 sets of NE213 liquid scintillation counters. The flight path length of neutron was 22 (12) m for E_d = 270 (140) MeV. The resolution of $E_p + E_n$ was 2.2 MeV FWHM or better depending on the target. The detection efficiency of neutron was calibrated by using the ^{7}Li$(p,n)^7$Be reaction at E_p = 135 and 70 MeV.[3] The proton beam was obtained by accelerating H_2^+ with the same magnetic field of cyclotron as that for the deuteron beam just before the breakup experiment. The optics property of the SMART spectrograph was also studied by using protons elastically scattered from a gold target.

The $(d,^2$He) and $(d,d_{S=0})$ reactions as well as the (d,nX) and (d,pX) inclusive breakup reactions were also measured simultaneously.

Figure 1 shows the triple differential cross section for the ^{12}C, ^{40}Ca, ^{90}Zr and ^{208}Pb targets at E_d = 270 MeV. The energy-integrated double differential cross section $d^2\sigma/d\Omega_p d\Omega_n$ has the target dependence of $Z^{1.78}$ and clearly indicates the dominance of the Coulomb breakup process. The inclusive (d,nX) reaction, on the other hand, exhibits the target dependence of $A^{0.61}$.

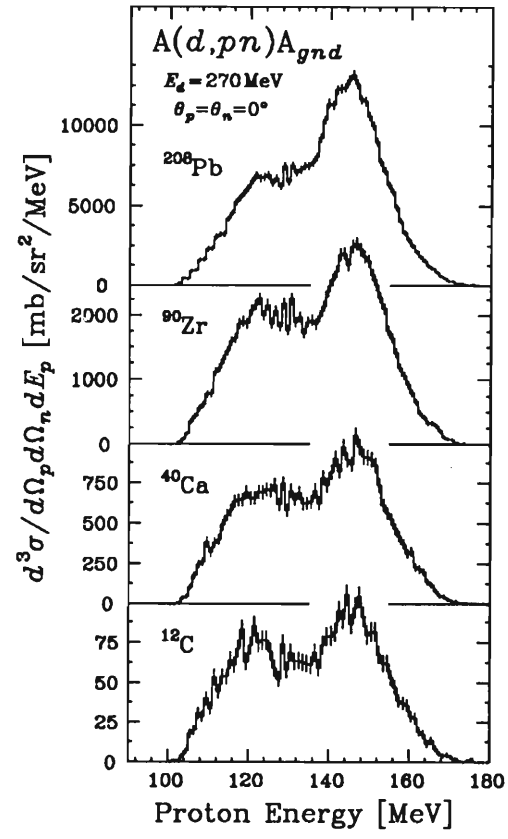

Fig. 1. Triple differential cross sections for ^{12}C, ^{40}Ca, ^{90}Zr and ^{208}Pb at E_d = 270 MeV.

References

1) H. Okamura *et al.*: Contribution to 7th Int. Conf. on Polarization Phenomena in Nuclear Physics, Paris (1990).
2) H. Okamura *et al.*: *RIKEN Accel. Prog. Rep.*, **25**, 128 (1991) and references therein.
3) T.N. Taddeucci *et al.*: *Phys. Rev.*, **C41**, 2548 (1990).

III-1-11. Coulomb Breakup of ^{8}B

T. Motobayashi, M. Gai, N. Iwasa, Y. Ando, Th. Delbar, R.H. France III, K. Furutaka, Y. Futami, K.I. Hahn, N. Inabe, M. Ishihara, T. Kubo, M. Kurokawa, H. Murakami, T. Nakamura, J. Ruan(Gen), S. Shimoura, S. Shirato, T. Teranishi, Y. Watanabe, and Z. Zhao

[NUCLEAR REACTION ^{208}Pb(^{8}B,^{7}Be p)^{208}Pb, E/A = 47MeV; measured coincidence $\sigma(\theta)$.]

The ^{7}Be(p,γ)^{8}B reaction was studied through the ^{8}B breakup process in the Coulomb field of ^{208}Pb. The Coulomb breakup process ^{8}B$\rightarrow$^{7}Be+p can simulate the photo-absorption reaction ^{8}B(γ,p)^{7}Be, the inverse reaction of ^{7}Be(p,γ)^{8}B. The (p,γ) reaction on ^{8}B is the major process producing solar neutrinos observed in the experiments of Davis et al.[1] and Kamiokande,[2] where the observed flux was 1/3 to 1/2 of the that expected in the standard solar model. A possible explanation is due to the neutrino oscillation, but it failed to reproduce the recent results of SAGE and Gallex experiments with lower energy threshold.[3]

The calculation of the high-energy neutrino flux is based on the ^{7}Be(p,γ)^{8}B cross section, which has been studied in many experiments. The astrophysical S-factor used in the calculation is S(0)=0.0238±0.0023 keV-b, which is a weighted mean of the experimental data.

Recently, Barker and Spear[4] pointed out possible uncertainties in above determination of S(0). New measurements with independent methods are highly desirable. We performed the present Coulomb breakup experiment as such a measurement.

A ^{8}B beam of about 47 A MeV was provided by the RIPS facility of RIKEN Ring Cyclotron. The breakup products, ^{7}Be and proton, were detected in coincidence by ΔE-E telescopes of plastic scintillators set 5 m from the target. The particle identification was achieved by the E and time-of-flight (TOF) information as well as the ΔE-E method. The energies of the proton and ^{7}Be were determined by the TOF obtained by the signals from the telescopes and the cyclotron RF signal. A helium-bag was set between the target and hodoscopes to reduce the probability of parasitic reactions.

Since the product ^{7}Be has its excited state at E_{ex}=429 keV ($1/2^{-}$), the breakup process feeding this state is possible. To evaluate the cross section of this process, a BaF2 scintillator array with 60 crystals detected the γ-rays emitted from the excited ^{7}Be. Analysis is now in progress.

References

1) R. Davis: Workshop on Neutrino Telescopes, ed. M. Baldo-Ceolin, Palazzo Lorendan, Venice, p. 1 (1990).
2) M. Mori: *ibid.*, p. 61.
3) J.F. Wilkerson: 1992 Annual Fall Meet. of APS, Santa Fe, p. 1297(1992); W. Hampel, *ibid.*, p. 1297.
4) F.C. Barker and R.H. Spear: Astrophys. J., **307**, 847 (1986).

III-1-12. Sub-barrier Fusion with Unstable Neutron-rich Nuclear Beams

A.Yoshida, T.Fukuda, T.Sekine, Y.Watanabe, K.Kimura, H.Okuno, H.Ueno, Y.Mizoi, H.Izumi, M.Tanikawa, K.Asahi, M.Ishihara, I.Nomura, S.Shimoura, T.Nakamura, T.Kubo, and H.J.Kim

[Sub-barrier fusion, neutron-rich beam reaction.]

Recently, it has been argued that the use of a neutron-rich beam is of great advantage to reach the super heavy element region. However the feasibility depends upon the cross section that we can actually expect for fusion reaction, especially regarding the sub-barrier fusion cross section.

A large number of data concerning sub-barrier fusion using beams of stable nuclei show an enhancement as compared with the estimations using an one-dimensional barrier penetration model .[1] On the other hand, it is argued that an extremely neutron-rich nucleus may be dynamically polarized in the collision(soft E1-dipole mode) and excess neutrons may be transferred easily to the target nucleus, thus facilitating fusion. But this type of experiment has not yet been done, so we tried, for the first time, to measure the fusion cross section of the unstable neutron-rich isotope ^{29}Al plus Au system.

The experiment was done by using the RIPS, where ^{29}Al was produced by bombarding 95MeV/u Ar beams on a Be production target and separated, and after secondary focus position(F2), the energy of ^{29}Al was reduced to 5MeV/u by using an Al-energy degrader plate. Then the low energy ^{29}Al beam was again focused at the third focus position(F3) where the secondary reaction Au targets were located. To gain a reaction yield, we used a multi-target system comprised of a stack of 22 thin Au foils(170ug/cm^2 each). In the ^{29}Al+Au reaction, almost 100% of compound nucleus will decay by fission. Fission fragments were measured by two sets of MWPC positioned both left and right relative to the Au target

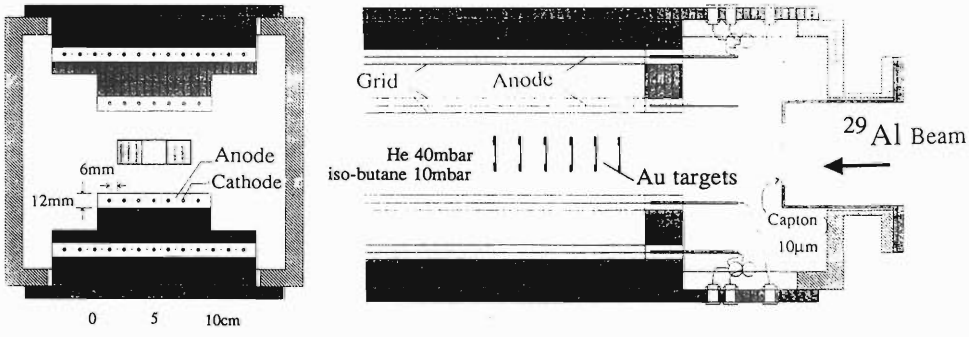

Fig. 1. The schematic view of secondary reaction target position. A stack of 22 thin Au foil targets is sorounded by two sets of MWPC.

stack(Fig.1).

We picked up the fusion-fission event by selecting 4-plane wire coincidence events, and knew the reaction target position by tracing the fission fragment track. Each ^{29}Al beam energy was measured by the TOF method between F2 and F3(6.2m), and the energy loss in each Au foil and filled gas was corrected for.

By using information on the deposit energy and hit pattern of MWPC, we could clearly distinguish the fusion-fission events from ^{29}Al elastic scattering and transfer-like light particle emission events. The analysis is now in progress. Experiments with more neutron rich Al isotopes will follow.

References

1) P.H. Stelson: Phys.Lett., **B205**,190(1988).

III-1-13. Measurements of ^{11}Li + p and ^{9}Li + p Elastic Scatterings at 60 MeV

C.-B. Moon, M. Fujimaki, S. Hirenzaki, N. Inabe, K. Katori, J.C. Kim,* Y.K. Kim,*
T. Kobayashi, T. Kubo, H. Kumagai, S. Shimoura, T. Suzuki, and I. Tanihata

[Inverse reactions, elastic scatterings, phenomenological optical model.]

Proton elastic scattering from neutron rich nuclei ^{9}Li and ^{11}Li have been measured for the first time at E_{lab}/A = 60 and 62 MeV, respectively, under the inverse kinematical conditions.[1)]

While the angular distribution of ^{9}Li scattering follows the systematic trend from those of ^{6}Li and ^{7}Li scatterings, the ^{11}Li cross section is smaller by factor of about two.

To understand the measured elastic cross sections, we applied a phenomenological optical model with the standard potential U_N represented as follows,

$$U_N = -V_R f_R - iW_V f_I + 4ia_I W_S (d/dr) f_I + 2(\hbar/m_\pi c)^2 1/r (r/dr) V_{SO} f_{SO} (\mathbf{L}\cdot\mathbf{S}) + V_{coul}$$

with $R_i = r_i A^{1/3}$, $f_i = [1+\exp\{(r-R_i)/a_i\}]^{-1}$, i = R,I and SO, where subscripts R, I, and SO denote real, imaginary, and spin-orbit, respectively.

This phenomenological optical potential model fit to the ^{11}Li suggests that both the real and the imaginary potentials should be considerably modified from the global fit parameters that reproduce the proton elastic scatterings from the other Li isotopes, ^{6}Li, ^{7}Li, and also ^{9}Li. The best fit as shown by the solid curve in Fig.1 was obtained with a combination of a shallow real potential and an imaginary potential with a long tail. The dotted curve in Fig.1, on the other hand, is the fit result as obtained by fixing the depth of the real potential as the global parameters of ^{7}Li. It should be emphasized that the reaction cross section predicted by this potential, 456 mb, is somewhat larger than the estimated empirical value of 359 - 414 mb.

To understand the present ^{11}Li data, we need more detailed microscopic studies that include the reaction mechanisms, such as a break up process, due to loosely bound neutrons in ^{11}Li.

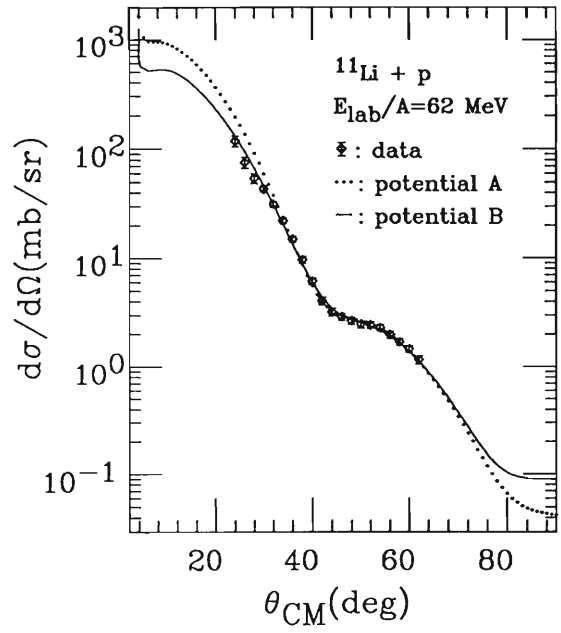

Fig. 1. Elastic scattering angular distribution for the ^{11}Li + p system at E_{lab}/A = 62 MeV. The dotted and the solid curves are the fits by the optical model calculations with the potential A and B described below, respectively. Parameters corresponding to the potential A (B) are, in the usual notation where depths are in MeV and lengths are in fm, as follows ; V_R = 35.96 (18.06), r_R =1.13 (1.385), a_R = 0.69 (0.546), W_V = 6.64 (4.26), W_S = 4.58 (4.60), r_I = 1.11 (0.56), a_I = 0.81 (1.16), V_{SO} = 5.9 (5.9), r_{SO} = 0.8 (0.8), a_{SO} = 0.63 (0.63). The calculated reaction cross sections are 456 and 388 mb, respectively.

References

1) C.-B. Moon *et al.* : *Phys. Lett.*, **B 297**, 39 (1992).

* Seoul National University, Korea.

III-1-14. Coulomb Dissociation of ^{11}Li on a Lead Target at 43 A MeV

S. Shimoura, N. Inabe, M. Ishihara, T. Kobayashi, T. Kubo,
T. Nakamura, R.H. Siemssen,* I. Tanihata, and Y. Watanabe

[NUCLEAR REACTIONS heavy-ion collision, radioactive beam, Coulomb dissociation, Pb(^{11}Li,^{9}Li + 2n)X, soft $E1$ mode.]

The Coulomb dissociation reaction of ^{11}Li nucleus, Pb(^{11}Li,^{9}Li+2n)X, was measured at an incident energy of 43 A MeV. Secondary beams of ^{11}Li were produced at the RIPS using the fragmentation of 100 A MeV ^{18}O beams on a Be target. The experimental setup and method are presented elsewhere.[1)]

Figure 1 shows an excitation energy spectrum of ^{11}Li* obtained by making an invariant mass of the observed three-body system (^{9}Li+2n) event-by-event. The peak position and the average of the spectrum are 1 MeV and 1.9 MeV, respectively. Because of the dominace of $E1$ excitation in the Coulomb dissociation reaction, the peak indicate a notable $E1$ strength in the excitation of the ^{11}Li nucleus, which is suggested in Refs. 2 and 3.

A relative energy spectrum between two neutrons coincident with ^{9}Li is shown in Fig. 2, whose average is 0.3 MeV. This indicates that the excitation is dominated by the relative motion of ^{9}Li and the center-of-mass of 2n system rather than that of two neutrons, which is consistent with the picture of an oscillation between the core and the neutron halo. This spectrum is much sharper than the prediction based on the Migdal-Watson model describing a final state interaction (FSI) between two neutrons. This may indicate the distance between the two neutrons is too large to make FSI.

The present work is supported by the Grant-in-Aid for Scientific Research (No. 0242005) by the Ministry of Education, Culture and Science of Japan.

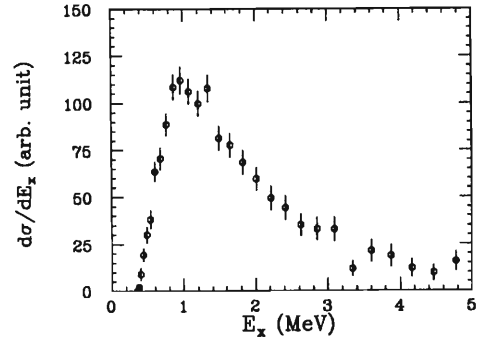

Fig. 1. Excitation energy spectrum of ^{11}Li nucleus deduced from invariant mass of ^{9}Li+2n system.

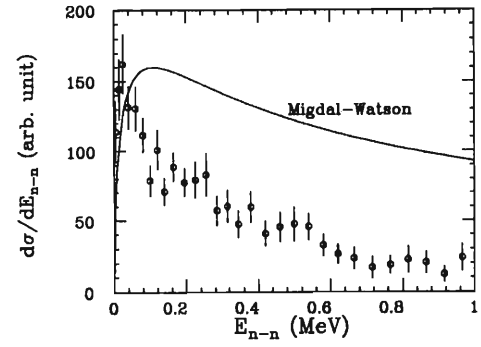

Fig. 2. Relative energy spectrum between two neutrons. Solid line represents the shape of the density of state in terms of the Migdal-Watson model.

References

1) S. Shimoura *et al.*: *6th Int. Conf. on Nuclei far from Stability*, Bernkastel-Kues, July, 1992.
2) T. Kobayashi *et al.*: *Phys. Lett.*, **232B**, 51 (1989).
3) R. Anne *et al.*: *ibid.*, **250B**, 1219 (1990).

* KVI, Groningen, the Netherland.

III-1-15. Mass Measurements of Neutron-Rich Unbound Nuclei by Break-Up Reactions

T. Teranishi, K. Abe, N. Aoi, Y. Doki, M. Fujimaki, N. Inabe, N. Iwasa, K. Katori, T. Kobayashi, T. Kubo, T. Nakamura, H. Okuno, S. Shimoura, T. Suzuki, I. Tanihata, Y. Watanabe, A. Yoshida, and M.Ishihara

[NUCLEAR REACTIONS, heavy-ion collision, radioactive nuclear beam, C(^{8}He,^{7}He)X.]

Recent development of radioactive beams has opened a wide domain of unstable nuclei to be studied. One of the interesting subjects is determination of masses of these nuclei. This paper reports on an attempt to develop a new method of mass determination by means of nuclear reactions. The method is, in particular, useful for particle-unbound nuclei, therefore, nuclei beyond the drip lines.

A classical method using nuclear reactions is a missing mass method, where the Q value is measured in a binary reaction between stable nuclei. The method usually provides a good mass resolution, but is limited in the range of unstable nuclei to be reached.

In the present method for particle-unbound nuclei, we use the "invariant-mass" technique, where particles in the final state are detected and their momentum vectors are used to construct the invariant mass of the intermediate state. The mass resolution is insensitive to the resolution of the incident energy. Any types of reactions may be used to populate the state. In addition the range of accessible nuclei may be enlarged using radioactive beams. In the present case, neutron-unbound ^{5}He, ^{7}He, and ^{10}Li nuclei were studied in the break-up processes of ^{6}He, ^{8}He, and ^{11}Li projectiles. Known masses of ^{5}He and ^{7}He were studied to examine the method with radioactive beams.

The secondary beams of energy 72A MeV were provided from the radioactive beam line (RIPS) using a 100A MeV ^{18}O primary beam onto a Be target. The secondary projectile was projected on C and Pb targets and was broken into one charged particle and two neutrons. The detector system consisted of neutron counters and a magnetic spectrometer, which covered nearly 4π solid angle in the projectile frame.

Figure 1 shows preliminary results on the ^{6}He+n system. Figure 1(a) shows a scatter plot of the relative momentum (p) between ^{6}He and neutron in the x-y plane perpendicular to the beam direction z. Events with p_z=0 are plotted.

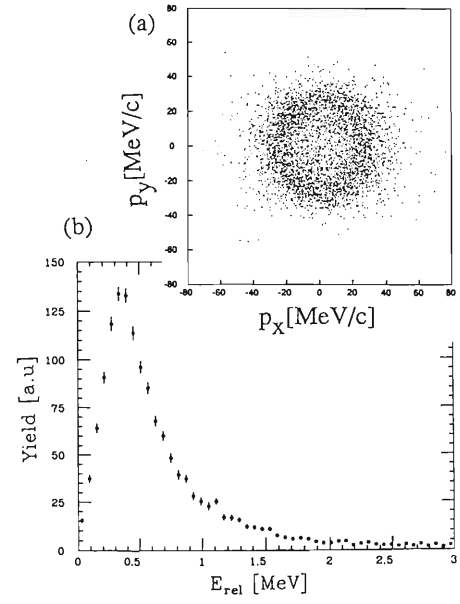

Fig.1. (a) Cross-sectional view of the 6He-n relative momentum distribution at p_z=0 in C+^{8}He -> ^{6}He+n+X reaction. (b) ^{6}He-n relative energy spectrum.

The circular distribution of the events is consistent with the decay of a resonance state. Figure 1(b) shows a relative energy spectrum for the ^{6}He-n system. Events over the whole measured phase space are included. A dominant peak appears at 350 keV, which is roughly consistent with but smaller than a previous result[1] of 440±30 keV. The source of the slight difference is not understood yet. Examinations are still under progress to understood it. The apparent width (480 keV (FWHM)) observed is widened as compared to the known value of Γ=170 keV, indicating the mass resolution of 450 keV (FWHM) of the present experiment.

The analysis on ^{4}He+n and ^{9}Li+n systems is in progress.

References

1) Richard H. Stokes and P. G. Young: Phys. Rev., **178**, 2024 (1969).

III-1-16. Momentum Distribution of Projectile-Rapidity Neutrons from ^{6,8}He, ^{9,11}Li Projectiles at 800 and 72 MeV/nucleon

T. Kobayashi, K. Yoshida, I. Tanihata, K. Matsuta, T. Minamisono, K. Sugimoto, S. Shimoura, D. Olson ,* H. Wieman ,* W. Christie ,* Y. Watanabe, T. Nakamura, M. Ishihara, T. Teranishi, and N. Iwasa

[NUCLEAR REACTIONS C,Pb(^{6,8}He,^{4,6}He+n+x), C,Pb(^{9,11}Li,^{7,8,9}Li+n+x) E/A=800 and 72MeV; measured momentum distribution dσ/dp.]

Projectile fragmentation is one of the experimental methods to study the properties of nuclei far from stability. Although the reaction mechanism is believed to be simple due to its peripheral nature, the effect of the fragmentation mechanism for extracting the nuclear structure information from the experimental data is not clear. We have systematically studied the momentum distribution (MD) of projectile fragments and neutrons in coincidence for few-neutron-removal processes from ^{6,8}He and ^{9,11}Li projectiles on C and Pb targets.[1] Measurements were performed at two incident energies: 800 MeV/nucleon (LBL Bevalac) and 72 MeV/nucleon (Riken Ring Cyclotron).

The MD of neutrons in coincidence with ^{4,6}He and ^{9}Li from ^{6,8}He and ^{11}Li at 800 MeV/nucleon showed two-Gaussian structure. The width of the narrow component is shown in Fig.1 as a function of the separation energy of valence neutrons. The dashed line in Fig.1 is from a simple model assuming the sudden approximation and no correlation between valence neutrons. Apparently, this model does not explain the general tendency, especially for neutrons from ^{8}He and ^{9}Li. If one neutron is removed from the projectile, the intermediate state, such as ^{5,7}He or ^{10}Li, is unstable against neutron emission. Therefore, the sequential decay mechanism via such an intermediate state can be important. The solid line in Fig.1 is an estimate assuming the sequential decay mechanism, and reproduces the general tendency. This is a first experimental indication that the sequential decay mechanism is important even for the two-neutron-removal process from neutron-rich nuclei.

The width of the neutron MD in coincidence with ^{9}Li from ^{11}Li is shown in Fig.2 together with the GANIL data[2] for studying the dependence on incident-energy and target. The systematics showed two features: (1) target-independence, and (2) slight incident-energy dependence. The latter might result from probing the density distribution of ^{11}Li at a different radius due to a different nucleon-nucleon cross section: we need more quantitative estimate.

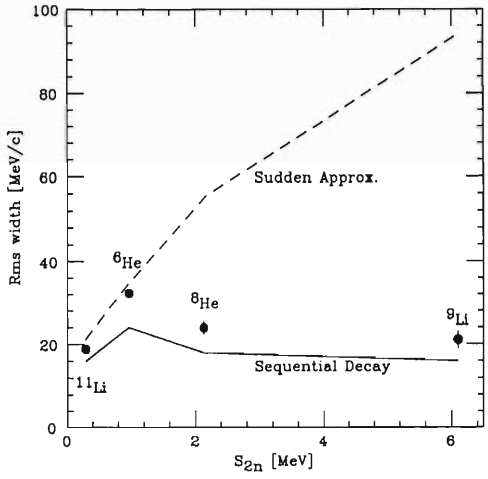

Fig. 1. The momentum width of neutrons for the two-neutron-removal process from ^{6,8}He and ^{9,11}Li projectiles on a C target as a function of the separation energy of valence neutrons.

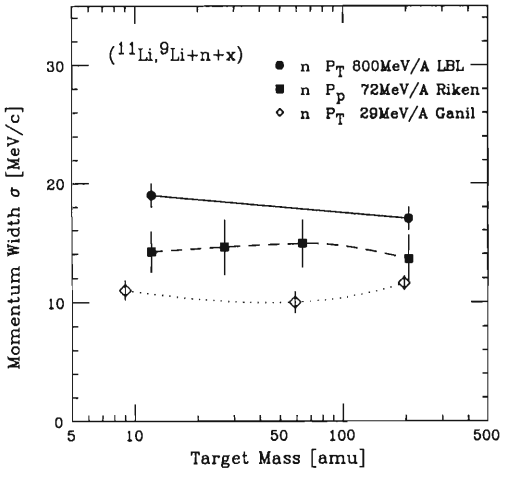

Fig. 2. The width of the neutron momentum distribution for the (^{11}Li,^{9}Li) reaction on various targets at 29, 72, and 800 MeV/A.

References

1) T. Kobayashi: *Nucl. Phys.*, **A** (1992) in press.
2) R. Anne et al.: *Phys. Lett.*, **B250**, 19 (1990).

* LBL, Berkeley, USA.

III-1-17. Revelation of Thick Neutron Skins in Nuclei†

I. Tanihata, D. Hirata, T. Kobayashi, S. Shimoura, K. Sugimoto,* and H. Toki

[Exotic nuclei, neutron skin, nuclear reaction, radioactive nuclear beam.]

In spite of detailed studies of stable nuclei of a large neutron excess (N - Z), no evidence of a thick neutron skin had been observed. For example, the root-mean-square (rms) radius of the neutron distribution is larger than that of the protons only by ~0.2 fm in ^{48}Ca (N-Z = 8) and by ~0.15 fm for ^{208}Pb (N-Z = 44).

Recently a development of high-energy radioactive nuclear beams enabled us to determine nuclear radii of β-unstable neutron-rich nuclei in which one may expect thick neutron skins due not only to the neutron excess but also to the large difference between the neutron and the proton Fermi energies. Nuclear matter radii of light nuclei were determined by measurements of the interaction cross sections (σ_I) .[1] Although these measurements provided the determinations of the matter radii, the neutron and the proton radii were not determined separately before.

Using the relations between the interaction cross sections and the neutron removal cross sections, thick neutron skins have been found out in ^{6}He and ^{8}He nuclei. Observed relations,

$\sigma_I(^6\text{He})-\sigma_I(^4\text{He}) = \sigma_{-2n}(^6\text{He})$ and

$\sigma_I(^8\text{He})-\sigma_I(^4\text{He}) = \sigma_{-2n}(^8\text{He})-\sigma_{-4n}(^8\text{He})$,

between interaction cross sections (σ_I) and fragmentation cross sections (σ_{-2n}, σ_{-4n}) [2] indicate that the ^{4}He core in ^{6}He (or ^{8}He) has same density distribution as ^{4}He nucleus.[3] Then we used the harmonic oscillator density distributions to fit the σ_I's using Glauber calculation under the constraint that core ^{4}He is fixed. We found following differences:

$\langle r^2_n\rangle^{1/2} - \langle r^2_p\rangle^{1/2} = 0.87$ fm for ^{6}He and

$\langle r^2_n\rangle^{1/2} - \langle r^2_p\rangle^{1/2} = 0.93$ fm for ^{8}He.

To study other possibilities of neutron skin formations, we applied the relativistic mean field (RMF) theory to many isotopes.[4] We have analyzed the behavior of

$\Delta r = \langle r^2_n\rangle^{1/2} - \langle r^2_p\rangle^{1/2}$

against the $\Delta E_F = E_{Fn} - E_{Fp}$ (Difference of Fermi energies of proton and neutron). We found a linear relation between those differences as shown in Fig. 1. The differences ;

$\langle r^2_n\rangle^{1/2} - \langle r^2_p\rangle^{1/2} = 0.98$ fm for ^{6}He

and $\langle r^2_n\rangle^{1/2} - \langle r^2_p\rangle^{1/2} = 1.1$ fm for ^{8}He

are in good agreement with the experimental results shown above. The calculated proton radii are in good agreement with experimental data and the neutron skin of 0.75 fm is predicted for ^{31}Na.

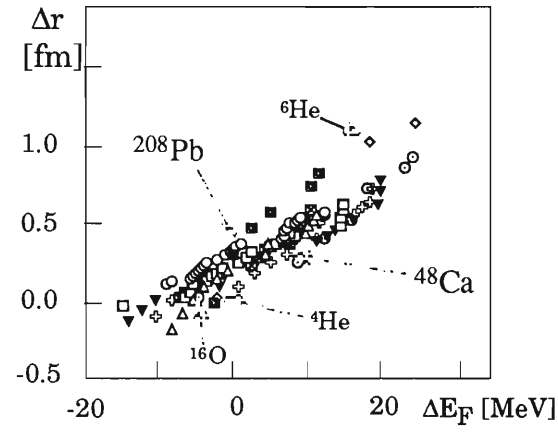

Fig. 1. The difference between the rms radius from neutrons and protons as a function of the difference between the Fermi energies of neutrons and protons for several isotopes.

References

1) I. Tanihata, et al.: Phys. Lett., **160B**, 380 (1985); I. Tanihata, et al.: Phys. Rev. Lett., **55**, 2676 (1985); I. Tanihata, et al.: Phys. Lett., **B206**, 592 (1988).
2) T. Kobayashi, et al.: Phys. Rev. Lett., **60**, 2599 (1988).
3) Y. Ogawa, K. Yabana, and Y. Suzuki: Nucl. Phys., in press.
4) D. Hirata, et al.: Phys. Rev., **C44**, 1467 (1991).

† Condensed from the article in Phys. Lett., B289, 261 (1992).

* Fac. Sci., Osaka Univ.

III-1-18. g-Factor Measurement of ^{21}F Ground State

H. Okuno, H. Ueno, K. Asahi, M. Ishihara, T. Nakamura, M. Adachi, H. Sato, H. Izumi, T. Sekine, N. Inabe, T. Kubo, A. Yoshida, T. Shimoda, H. Miyatake, and N. Takahashi

[NUCLEAR REACTION ^{93}Nb + ^{22}Ne, E/A = 70 MeV/nucleon ; measured β-ray asymmetry of ^{20}F and ^{21}F, nuclear magnetic resonance ; deduced g-factor of ^{21}F ground state.]

Recent experiments[1] have revealed that ejectile nuclei in the fragmentation of intermediate-energy heavy-ions are largely spin-polarized. Previously,[2] we reported the application of this phenomenon, resulting in the first measurements of the ground-state g-factors of neutron-rich nuclei ^{14}B and ^{15}B. We present, in this report, the extension of the measurement to the g-factor of ^{21}F ($T_{1/2}$ = 4.32 s). The ^{21}F is a nucleus rather close to the stability but its g-factor had not been measured before.

The experiment was carried out by using a radioactive beam line RIPS.[3] Short lived nuclei ^{20}F and ^{21}F were produced by fragmentation of ^{22}Ne projectiles at 70 MeV/nucleon on a ^{93}Nb target (300 μm in thickness). Those nuclei which were emitted at angles around 2.5 degrees were isotope-separated and momentum-selected by the RIPS and implanted into a CaF crystal placed at the final focus of the RIPS as shown in Fig. 1. The g-factor was deduced from the frequency of NMR detected by the change of β-ray asymmetry. The NMR spectrum finally obtained is shown in Fig. 2. The g-factor of ^{20}F, which was already known with good accuracy, was used for the calibration. From the peak position extracted from the least-squares fitting, we obtained the g-value as g(^{21}F) = 1.57 ± 0.02.

The experimental value agrees well with the g-factor for the $\pi d_{5/2}$ configuration, 1.58, by assuming a spin-quenching factor of 0.7. The experimental value is in fair agreement with the g-factor, 1.52, obtained from a shell model calculation[4] using OXBASH code.[5]

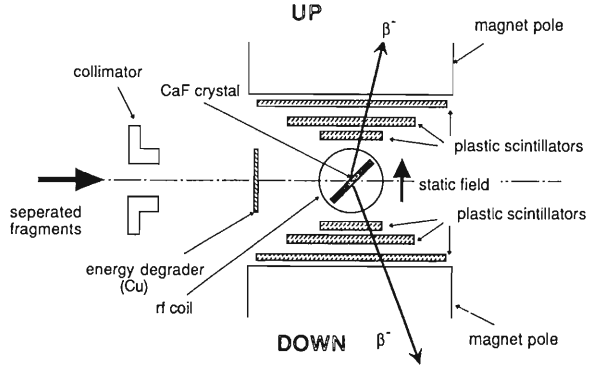

Fig. 1. Schematic diagram of the NMR apparatus at the final focus of the RIPS.

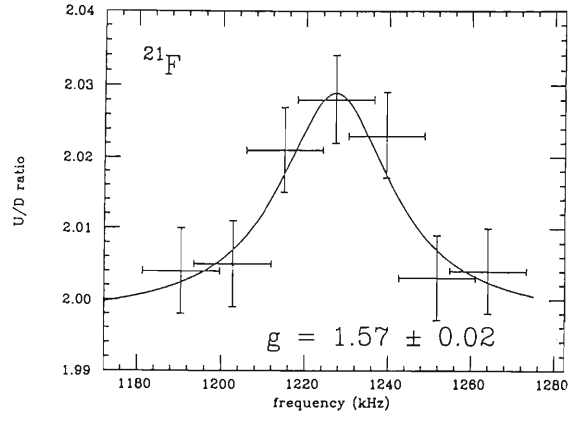

Fig. 2. Nuclear magnetic resonance spectrum of ^{21}F. Up/down ratios of β-rays emitted from ^{21}F are plotted as a function of the rf-frequency.

References

1) K. Asahi *et al.*: Phys. Lett., **B251**, 488 (1990).
2) H. Okuno *et al.*: RIKEN Accel. Prog. Rep., **24**, 14 (1990).
3) T. Kubo *et al.*: Proc. 1st Int. Conf. on Radioactive Nuclear Beams 1989 Berkeley, p.563 (1990).
4) B. A. Brown : OXBASH user's manual. 1985. unpublished.
5) T. Otsuka *et al.*: private communication.

III-1-19. Spin Polarization of ^{43}Ti Fragment from 116 A MeV ^{46}Ti Beam

K. Matsuta,* A. Ozawa, T. Minamisono, Y. Nojiri,* M. Fukuda, A. Kitagawa,* T. Ohtsubo,* S. Momota,* S. Fukuda,* K. Sugimoto,* I. Tanihata, K. Yoshida, K. Omata, J. R. Alonso,** G. F. Krebs,** and T. J. M. Symons**

[NUCLEAR REACTION ^{197}Au, ^{12}C+ ^{46}Ti, E=116 A MeV; measured β-ray asymmetry of ^{43}Ti nucleus; deduced spin polarization of ^{43}Ti.]

A 116 A MeV ^{46}Ti beam was used to bombard Au and C targets. Spin polarization as well as angular distribution of ^{43}Ti fragments were measured at forward angles (θ~2°). These measurements were performed at the LBL's Bevalac. The experimental setup was essentially the same as the one used in a previous work.[1)]

Observed angular distributions were broader than those predicted on the basis of the Goldhaber model[2)] although the model explained the widths of the momentum distributions quite well. This is a characteristic feature of the projectile fragmentation process in the present energy region, as shown by Van Bibber et al.[3)] For comprehension of the broadening, nuclear spin polarization of the fragments is the best observable. It reflects the sign of the scattering angle by changing its sign depending upon whether positive or negative angle scattering dominates in the reaction.[4)]

The momentum dependence of the polarization observed for the case of a C target is shown in Fig.1. Although the dependence observed for the case of an Au target was essentially the same as the one reported for ^{39}Ca and ^{37}K fragments in the ^{40}Ca on Au collision,[1)] the dependence was reversed in the case of a C target. It was concluded from the measurements that positive angle scattering dominates in the case of an Au target and negative angle scattering dominates in the case of a C target. This result strongly suggests that orbital deflection of the projectile is caused by the Coulomb potential in the case of an Au target and by the nuclear potential in the case of a C target prior to the breakup. Even in the present energy region, these potentials play an important role and cause the broadening of the angular distributions of the fragments.

This work was partly supported by the Grant-in-Aid for Scientific Research Program from The Ministry of Education, Culture and Science, Japan. Support was also given by the USA-Japan Collaborative Research, given by both the Japan Scientific Foundation and the National Science Foundation, USA. This work was also supported in part by the US Department of Energy under the contract No. DE-AC03-76SF0098.

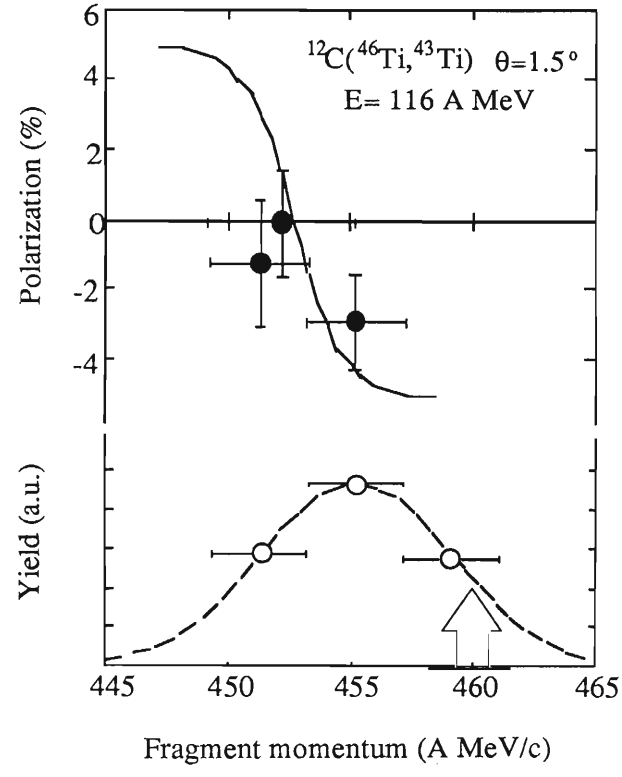

Fig. 1. Momentum dependence of the fragment polarization of ^{43}Ti. Closed circles are observed polarizations. Open circles are relative yields of ^{43}Ti. The momentum corresponding to the beam velocity is shown by the arrow. The solid line represents the polarization calculated using a simple projectile fragmentation model[4)] and multiplied by 1/20. Negative angle scattering and an additional energy-loss (2.5 A MeV/c) were assumed in the calculation.

References

1) K. Matsuta et al: Phys. Lett., B 281, 214 (1992).
2) A.S. Goldhaber: Phys. Lett., B 53, 306 (1974).
3) K. Van Bibber et al: Phys. Rev. Lett., 43, 840 (1979).
4) K. Asahi et al: Phys. Lett., B 251, 488 (1990).

* Osaka Univ.
** LBL, Berkeley, U.S.A.

III-1-20. Proton Elastic Scattering with ^{9}Li and ^{11}Li and Its Halo Structure

S. Hirenzaki, H. Toki, and I. Tanihata

[Proton elastic scattering, neutron halo.]

In the study of unstable nuclei, one of the most exciting findings was the neutron halo around the ^{9}Li core in ^{11}Li. The structure and reactions of ^{11}Li have been studied extensively both theoretically and experimentally. In this report, we study the proton elastic scattering on ^{9}Li and ^{11}Li using the Born approximation and the optical potential model.[1] The experiment was recently performed at 60 MeV for ^{9}Li and at 62 MeV for ^{11}Li at the RING Cyclotron facility in RIKEN by C.-B. Moon *et al.* The data for p+^{6}Li and p+^{7}Li also exist at 65 MeV.[2] In the angular range of 25 to 50 degrees in c.m. system, the data show that the cross section of ^{11}Li is about 70 % of the cross section of other Li isotopes and the slopes of the cross sections are almost the same for all four isotopes.

First, we study the data of ^{9}Li and ^{11}Li using the Born approximation and try to explain qualitatively the essential features of the data. The important conclusion from this qualitative study is that fragile halo neutrons are responsible to the smaller cross section through the imaginary part of the p+^{11}Li optical potential. We can evaluate the imaginary potential from halo neutrons using the experimental proton-neutron total cross section σ_{pn} as follows;

$$V_{2n}(\mathbf{r}) = -i\frac{\hbar v}{2}\sigma_{pn}\,\rho_{2n}(\mathbf{r}) \quad , \qquad (1)$$

where v is the velocity of the incident proton. We find that $V_{2n}(0) = -1.7\,i$ MeV.

We then look for the optical potential parameters using the experimental data. We assume that ^{11}Li has the configuration of ^{9}Li as the core plus two weakly bound neutrons. We take the optical potential of ^{9}Li as the basic potential for ^{11}Li and add a long range component, which is supposed to arise from the halo neutrons. The additional optical potential due to halo neutrons is assumed to have only an imaginary part which is justified by the qualitative study within the Born approximation. We added the halo potential eq. (1) to the potential that is obtained by fitting the ^{9}Li data. The result is shown in Fig. 1 by the broken line. We find that the data of p+^{11}Li elastic scattering can be reproduced qualitatively well, except for the discrepancy near the dip (45 degree).

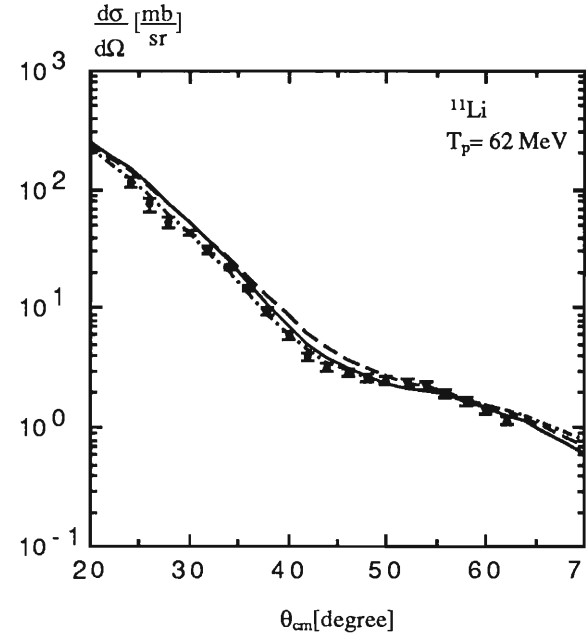

Fig. 1. The proton elastic scattering cross sections for ^{11}Li as a function of c.m. angle. The broken line is the result calculated with the core potential fitted to ^{9}Li data plus the halo potential shown in eq. (1). The solid line shows the result of the optical model fit obtained by modifying only the halo potential. The dot-dashed line is the result of the fit obtained by modifying only the core potential.

We could explain the essential features of the data of p+^{11}Li scattering by assuming that ^{11}Li has the halo structure. We found that the features of the data can be understood as the break up effect of halo neutrons of ^{11}Li which should be taken into account as an imaginary part of the optical potential. The imaginary potential of halo is weak because of a low halo neutron density and a mean free path in this potential is around 25 fm for 60 MeV proton. Thus we can think the halo as the "cloudy crystal ball".

References

1) S. Hirenzaki, H. Toki, and I. Tanihata: *Nucl. Phys.*, A, in press.
2) M. Tosaki: Ph.D. thesis, Osaka Univ. (1989).

III-1-21. Langevin Approach to Pre-scission Neutron Multiplicities and Fragment Kinetic Energies

T. Wada, N. Carjan,* and Y. Abe

[Langevin equation, pre-scission neutron multiplicity, fragment kinetic energy distribution, one-body dissipation.]

Experimental evidence of fission as a slow process has come from pre-scission multiplicities of neutrons, charged particles, and γ rays. Hinde *et al.*[1] observed a pre-scission neutron multiplicity much larger than the value obtained with a simple statistical model. To analyze the pre-scission neutron data, they had to introduce a long delay time. The delay time has been interpreted as a transient time during which the fissioning degree of freedom attains the quasi-stationary distribution in the phase space. The kinetic energy distribution of fission fragments is another important observable related to fission dynamics; it is related to the descent from saddle to scission. Recently, realistic calculations were made for these two physical quantities using the two-dimensional Langevin equation.[2] However, the transient time is not a measured quantity but extracted from the pre-scission neutron multiplicity with some assumptions. The aim of this report is to study fission dynamics consistently from the ground state to scission under continuous cooling due to evaporation of particles and to calculate the neutron multiplicity and the kinetic energy distribution at the same time. Insight into the dissipation mechanism of nuclear collective motion at high excitation energy will be thus obtained.

Table 1. Calculated results for the cases of the one-body friction and of the two-body viscosity with μ = 0.20 TP. The columns contain: the excitation energy (E^*(MeV)), the fusion cross section (σ_{fus} (mb)), the fusion-fission cross section (σ_{fiss} (mb)), the fusion-evaporation cross section (σ_{ev} (mb)), the pre-scission multiplicity of neutron (ν_{pre}), proton (π_{pre}), α particle (α_{pre}), the average total kinetic energy of the fission fragments (*TKE* (MeV)), and the variance (σ_{TKE} (MeV)).

E^*		σ_{fus}	σ_{fiss}	σ_{ev}	ν_{pre}	π_{pre}	α_{pre}	*TKE*	σ_{TKE}
80.7	1-body	1150	790	360	2.93	0.0092	0.0037	135.1	8.46
	2-body	1150	817	333	2.84	0.0108	0.0037	108.6	9.92
	exp.	1150	767	383	3.2±0.3	–	–	–	–
195.8	1-body	1400	1244	156	7.33	0.363	0.140	137.0	10.2
	2-body	1400	1261	139	7.03	0.350	0.137	107.4	11.5
	exp.	1400	–	–	7.7±0.3	–	–	139	16.5

We solved a two-dimensional Langevin equation and calculated the pre-scission multiplicities of neutrons, protons, and α particles as well as the kinetic energy distribution of fission fragments. Particle emission was included in the continuous limit.[3] Temperature dependence of the nuclear surface energy was included as, $E_s(q,T) = E_s(q,T=0)\ (1 - \xi T^2)$.[4] Calculations have been made for the symmetric fission of ^{200}Pb nucleus since the following reactions have been studied experimentally: ^{19}F+^{181}Ta (E^* = 80.7 MeV)[5] and ^{16}O+^{184}W (E^* = 195.8 MeV).[6] The spin distribution of the compound nucleus is determined to reproduce the experimental fusion cross section. We assign an event as fusion-evaporation if the corresponding trajectory does not escape before the fission width becomes comparable to the γ decay width. Calculated results for the wall-and-window one-body dissipation case are given in Table 1. The value of ξ adopted here is 0.014 MeV^{-2}. It is remarkable that the calculated pre-scission neutron multiplicity (ν_{pre}) coincides with the experimental one within the error bar. The fusion-fission cross section is also quite well reproduced. As for the kinetic energy distribution, the calculated mean value (*TKE*) is in good agreement with Viola systematics.[7] The calculated variance (σ_{TKE}), however, is too small to reproduce the experiment at E^* = 195.8 MeV. Results with the hydrodynamical two-body viscosity are also given in Table 1. Unusually strong (μ = 0.2 TP) two-body viscosity is necessary to reproduce the observed neutron multiplicity, but *TKE* is far smaller than Viola systematics with this strong viscosity. A consistent explanation of neutron multiplicities and fragment kinetic energies supports the one-body friction and not the hydrodynamical two-body viscosity. It is, therefore, extremely interesting to derive or explain the one-body friction by microscopic theories.

References
1) D.J. Hinde *et al.*: *Nucl. Phys.*, **A502**, 497c (1989).
2) T. Wada *et al.*: *Nucl. Phys.*, **A538**, 283c (1992).
3) H. Delagrange *et al.*: *Z. Phys.*, **A323**, 437 (1986).
4) X. Campi *et al.*: *Z. Phys.*, **A309**, 239 (1983).
5) D.J. Hinde *et al.*: *Nucl. Phys.*, **A452**, 550 (1986).
6) D.J. Hinde *et al.*: *Phys. Rev.*, **C45**, 1229 (1992).
7) V.E. Viola *et al.*: *Phys. Rev.*, **C31**, 1550 (1985).

* Centre d'Etudes Nucléaires de Bordeaux, France.

RIKEN Accel. Prog. Rep. 26 (1992)

III-1-22. Systematics of Isotope Production Rates

Fission Products and Their Barrier Penetration

H. Sato and A. Mizobuchi*

[NUCLEAR FISSION fission-product yields.]

In a previous work,[1] we showed that systematics of isotope production rates of the nuclear collision is well expressed by two different thermalization processes: first fast high energy thermalization and second evaporation. At low incident energy, especially, the isotope production rate is found to be expressed by

$$\sigma(Y) \propto \exp(-\frac{M_Y}{T}) ,$$

where T is the temperature parameter, and M_Y is the mass excess of the nucleus Y produced. Here, we study the relationship between the experimental mass distribution of fission products and its mass excesses by employing the above equation. As for the mass excess, we employ the minimum mass excess M_{ex} for a given mass number. Then we find, in many fissioning nuclei, that the gross shape of the mass distribution coincides nicely with the distribution of its mass excess with a constant T except in the gap region A = 100 ~ 130. The case of ^{235}U(n,f) fissions with the thermal, 3 MeV, and 14 MeV neutrons[2] is shown in Fig.1. The temperature T of 2.6 MeV obtained is very close to ones observed in isotope productions in 24 GeV p-U and 33.6 GeV ^{16}O-Pb collisions.[1]

Note: A naive liquid drop model predicts the symmetric fission, where the fissioning to equal mass nuclei (half of the parent nucleus) is most probable. In the ^{235}U(n,f) fissions, this most probable mass number is 118 which coincides, "accidentally", with the one that gives the smallest minimum mass excess. However, if the incident energy dependence of the mass distribution of the single fission fragment is taken into account, the mass excess dependence of the distribution seems to be plausible.

We also study the gap shape in the region A = 100 ~ 130 in terms of the barrier penetrability generated by the mass formula and the density distribution generated by the Hartree-Fock type variational calculation with shell model correction, and find that the shapes are semiquantitatively understood as the competition of many heavy particle decay modes.

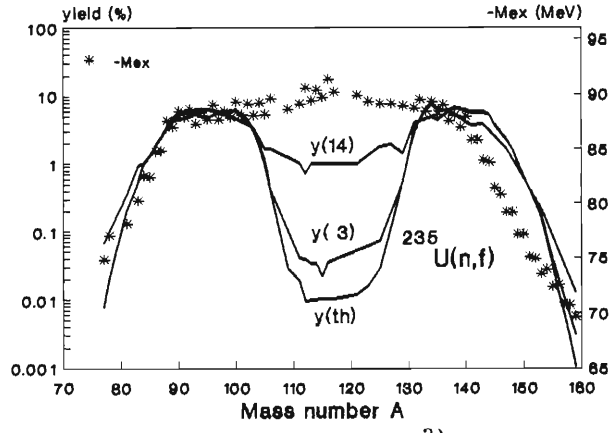

Fig.1. The fission yields[2] and minimum mass excesses M_{ex} in the ^{235}U(n,f) fissions.

References

1)H.Sato: *Phys.Rev.*,**C37**, 2902 (1988).
2)E.A.C.Crouch: *Atomic Data and Nuclear Data Tables*,**19**, 419 (1977).

* Inst. for Nucl. Study, Univ. Tokyo.

RIKEN Accel. Prog. Rep. 26 (1992)

III-1-23. Nucleus as a Canonical Ensemble: Deformed Nucleus

H. Sato

[NUCLEAR STRUCTURE w, E and thermal properties of deformed nuclei.]

In previous works, we have studied the nuclear system both at low and high excitation energies in terms of the canonical ensemble with the employment of the temperature dependent anti-symmetrized many particle density matrix in a harmonic oscillator (HO) potential.[1] We found that this ensemble is equivalent to the ground state of the HO shell model at a low temperature limit, and that various phenomena observed in medium and high energy nuclear collisions are nicely explainable as the property of this ensemble at high temperatures. In this work, we extend the study to the spheroidal symmetric HO potential,

$$h=\frac{p^2}{2m}+\frac{m}{2}(\omega_3^2 z^2+\omega_\perp^2(x^2+y^2)),$$

$$\omega_\perp=\omega_0\eta^{1/3},\ \omega_3=\omega_0\eta^{-2/3} \text{ and } \eta=\frac{3+\delta}{3-2\delta},$$

where ω_0 is an HO constant for the spherical one. Theoretical treatments are identical with those of the spherical case except the unnormalized one particle density matrix. We study the deformation δ and particle number N dependence of the internal energy and the entropy.[2] As an example, the entropy S_N calculated with temperature T = 0.25 MeV is summarized in Fig. 1. The peaks in the entropy at the deformation δ = -0.75, 0.0, and 0.6 correspond to simple integer ratios of the HO constants $\omega_\perp$ and ω_3. Since the entropy relates to the level density of the system, Fig.1 corresponds to the level density distribution discussed by Strutinsky in the study of fission phenomena.[3] This point is expected to be seen more clearly, if a Nilsson type potential is employed. Such kind of study is now in progress.

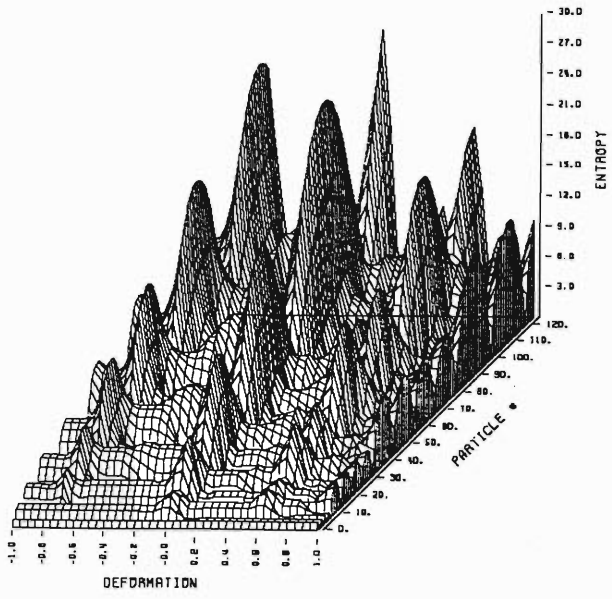

Fig.1 The deformation dependence of the entropy S_N at T= 0.25 MeV.

References

1)H.Sato: *Phys.Rev.*,**C36**, 785 and 794 (1987).

2)H.Sato: in *Proc. of the Symp. on Group Theory and Special Symmetries in Nucl. Phys.*, p.359 (*World Scientific*, 1992).

3)V.M.Strutinsky: *Nucl.Phys.*,**A122**, 1 (1968).

RIKEN Accel. Prog. Rep. 26 (1992)

III-1-24. An Application of Multi-precision Arithmetic in Physics

Nucleus as a Canonical Ensemble

H. Sato

[NUCLEAR STRUCTURE w, E and thermal properties.]

The study of multi-precision arithmetic has progressed very far due to an effective usage of a high speed computer and a practical study of the capability of computers. However, except the calculation of π, its actual applications are scarcely found, in physics especially. In this work, we show that multi-precision arithmetic plays an important role in the study of nuclear physics.

In a previous work,[1] we studied nuclear thermodynamical quantities in terms of the temperature dependent antisymmetrized density matrices of many fermions in a harmonic oscillator (HO) well. For a temperature T(=1/β) and particle number N system with an HO constant ω, the trace Z_N of the density matrix is found to satisfy the recurrence relation

$$Z_N=\frac{1}{N}\sum_{n=1}^{N}(-1)^{n+1}H_{n\beta}Z_{N-n},$$

where $H_{n\beta} = N_g/(2\sinh\frac{1}{2}n\beta\hbar\omega)^3$ with $N_g = 2(4)$ for spin(isospin) formalism, and $Z_0 = 1$. With these traces, we showed that this ensemble is equivalent to a ground state of an HO shell model at a low T limit. We also showed the relationship between thermodynamical quantities and the nuclear level density.

Since the trace Z_N behaves like an $\exp(-\beta E_N)$ at a low T with the sum of single particle energies E_N, the accuracy of an $\exp(-\beta E_N)$ must be reserved in the calculation of Z_1 to satisfy the recurrence relation. To study this point, we perform three different multi-precision arithmetics[2]: Case(1) a mixture mode of integer and real numbers with a 10^8 arithmetic, Case(2) a real number mode with a 10^8 arithmetic, and Case(3) a real number mode with a 10^6 arithmetic with Fast Fourier Transformation (FFT).[3] Figure 1 shows a comparison of calculational times of three cases for each N. The calculation is performed with FACOM-M380 at RIKEN.

While this nuclear model is applicable to a wide range of nuclear study, a much faster fully equiped subroutine package of the arithmetic is eagerly needed.

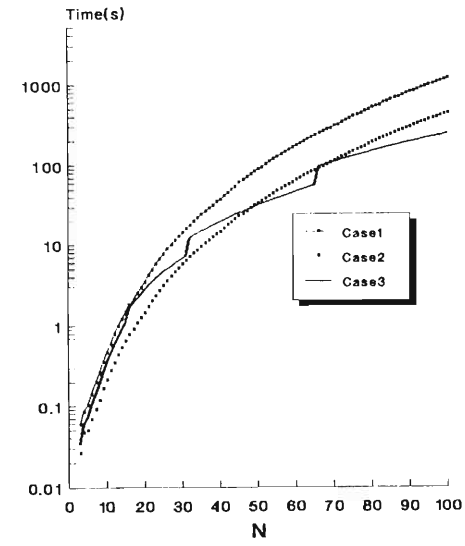

Fig.1. The N dependence of the calculational time in second.

References

1)H.Sato: *Phys.Rev.*,**C36**, 785 and 794 (1987).

2)D.E.Knuth: *SEMINUMERICAL ALGORITHMS Arithmetic in The Art of Computer programming*, II, Addison-Wesley (1981).

3)H.Hirayama: private communications.

III-1-25. Strength Distribution of Isoscalar Vibrations around Thermal Equilibrium

S. Yamaji, H. Hofmann,* and A. S. Jensen**

[Large scale collective motion, giant resonance, linear response theory.]

Thermal properties of finite nuclei have become of great interest. Usually theoretical studies concentrate on thermodynamical features in the proper sense, such as the free energy, entropy or nuclear density. These quantities characterize static states. We wish to focus on dynamical proreties, such as positions and widths of specific excitations and their relative strengths, and study their temperature dependence.

The aim of the present study[1] is threefold. Firstly, computation of the strength has its own merits. We believe that the case chosen is typical of isoscalar modes in general. Secondly, we hope to contribute to the understanding of the transition from microscopic to macroscopic dynamics. Indeed, for the static energy one knows how the disappearance of shell effects turns the energy functional into one given by the liquid drop model. The variation of strength distribution with frequency provides information about quantities representing dynamical features, like e.g. the vibrational inertia. Thirdly, such a study may help to understand recent fission experiments, which indicate that motion is storongly overdamped at finite excitations.

We study collective response as functions of excitation for a typical isoscalar mode. We apply a quasi-static picture in which the effective coupling constant changes with temperature T.

The dissipative part of collective response function for the quadrupole mode has been evaluated for ^{208}Pb. The important features of our results are summarized as:

a) For a comparatively small value of T = 0.5 MeV we observe the usual structure with pronounced resonances at low and higher frequencies.

b) With increasing T this structure is wiped out. This is expected since the widths of the intrinsic single particle states effectively become broader.

c) More exciting is the clear evidence of a shift of strength from high frequencies to lower ones. This effect is mainly due to the T-dependence of the effective coupling constant.

d) At larger T there is a clear concentration of strength in one prominent mode at very low frequency. The associated inertia is the one of irrotational flow.

e) The transition from low to high T-behaviour seems to occur at temperatures of 1.5 - 2 MeV.

f) The degree of damping increases steadily up to temperatures of 3 - 4 MeV. The motion is strongly overdamped at high T.

References

1) H. Hofmann, S. Yamaji, and A.S. Jensen: Phys. Lett., **B286**, 1(1992).

* Physikdepartment der Technischen Universität Müchen.
** Inst. Phys. Astronomy, Univ. Aarhus.

III-1-26. Quantal vs. Semi-Classical Treatment of Nucleon–Nucleon Collisions

M. Tohyama

[Heavy-ion reaction theories, numerical simulation.]

The numerical solution of the Vlasov-Uehling-Uhlenbeck (VUU) equation is compared with that of the time-dependent density-matrix theory (TDDM).[1] It is known that VUU is a semi-classical limit of TDDM. We consider a collision of two identical 2-dimensional slabs which are finite in one direction (the z direction) and infinite in the other direction (the x direction). The thickness of the slab is about 2fm and the incident energy is Ecm/A=10MeV/nucleon. We show in Fig.1 the time evolution of Q_{zx} defined by $Q_{zx} = < p_z^2 > - < p_x^2 >$ where $< A >$ denotes a mean value of a variable A. The quantity Q_{zx} is a measure of the deviation from equilibrium in momentum space. The curves denoted as Vlasov and TDHF are the results of classical and quantal calculations without nucleon-nucleon (NN) collisions. Each peak of Q_{zx} in Fig.1 corresponds to the maximum compression of the colliding slabs and the decrease in Q_{zx} towards the final stage corresponds to the expansion of the system. The Vlasov result shows a temporal behavior which is similar to the TDHF one. The maxima of Q_{zx} calculated in VUU and TDDM are reduced as compared with the mean-field values. This is an expected effect of NN collisions: the momentum transfer from the z direction to the x direction caused by NN collisions reduces the anisotropy in momentum space, resulting in small values of Q_{zx}. To compare the relaxation speed between VUU and TDDM, we show in Fig.2 the ratio of Q_{zx} with to that without NN collisions for the initial stage of the time evolution. There is a significant difference between TDDM and VUU: the initial relaxation of the anisotropy in momentum space is slower in TDDM than in VUU. This may be attributed to a difference in the collision term: the VUU collision term treats NN collisions as Markoff processes while the TDDM one does not.

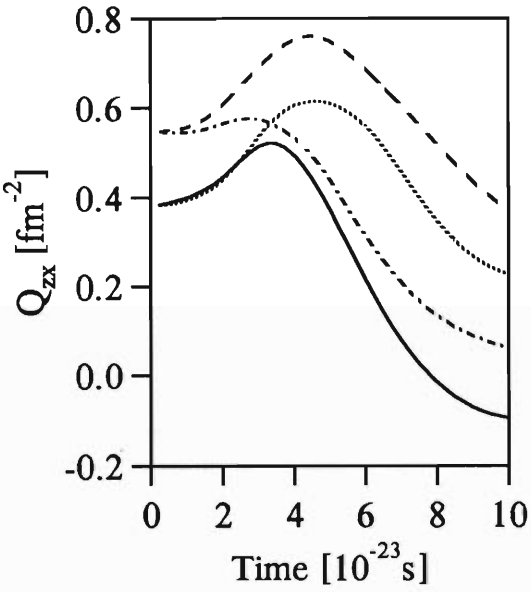

Fig. 1. Time evolution of Q_{zx} for a collision of two-dimensional slabs at Ecm/A=10MeV/nucleon. Solid, dotted, dashed and dot-dashed curves denote the results in TDDM, TDHF, Vlasov and VUU, respectively.

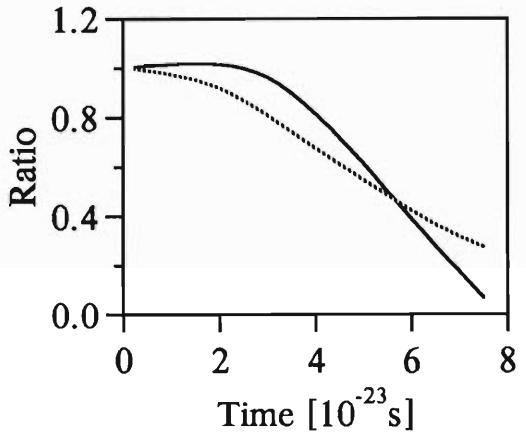

Fig. 2. Ratio of Q_{zx} with to that without NN collisions. Solid curve denotes the quantal calculation and dotted curve the semi-classical one.

References

1) M. Tohyama:*Phys.Rev.*,**C36**,187(1987).

RIKEN Accel. Prog. Rep. 26 (1992)

III-1-27. Structure of Neutron Rich Nuclei

A Typical Example of the Nucleus ^{11}Li

K. Ikeda

[Neutron halo, exotic nuclei, radioactive nuclear beams, soft giant resonances, resonance states, mean field correlations, pairing correlations.]

Recent development in the experimental technique of using radioactive nuclear beams has brought a new stage of nuclear spectroscopy of nuclei far from stability.[1] An example of the most interesting results is the fact that the p-shell nuclei near the neutron drip line, e.g., ^{11}Li, ^{14}Be and ^{17}B, have extremely large root mean square radii.

The nucleus ^{11}Li among others has been studied most extensively as a typical example of the neutron drip line nuclei. The characteristic properties of the ground state of ^{11}Li obtained by the experiment are the following: (i) The two-neutron separation energy is only 210 ± 80 keV. We note that the first open channel of ^{11}Li is the three-body channel of ^{9}Li+n+n since the two-body systems of ^{9}Li+n and n+n have no bound states. (ii) The matter root mean square radius of ^{11}Li is determind to be 3.14 ± 0.06 fm, much larger than 2.1 fm obtained from the empirical formula of the stable nuclei, $\sqrt{3/5} r_0 A^{1/3}$. (iii) The transverse momentum distribution of ^{9}Li obtained from the inclusive reaction, ^{11}Li+C$\rightarrow$^{9}Li+anything, has the narrow Gaussian component in addition to the normal wide component.[2] All these properties of ^{11}Li seem to support the so-called neutron halo in which the two valence neutrons move in a wide spatial region.

When the neutron-halo structure is realized in nuclei far from stability we expect new kinds of collective motion such that outer neutrons in the halo move against the remaing core nucleus.[3,4] The frequencies of these kinds of collective mode are expected to be low and their amplitudes to be large, compared with the corresponding collective motions in stable nuclei(or core nuclei). Therefore, we call them soft collective modes.[3] A typical example is the soft giant dipole-mode. Experimental identification of this mode has been attempted through the studies of the Coulomb excitation of the high energy projectiles of ^{11}Li and others.[5,6] If this kind of soft dipole mode will be found, the halo-structure of the ground state is considered to be supported furthermore.

The first problem which should be examined theoretically is whether or not we can reproduce the peculiar structure in which two valence nuetrons are coupled weakly with core nucleus and are correlated with each other in the interaction fields of core nucleus. Here I would like to report the theoretical studies on the structure of ^{11}Li in the framework of the microscopic hybrid model which combines two dfferent kinds of the model space, that is, the shell model space and the cluster model space. The second problem is what kinds of new excitation mode, like as the soft E1 mode, arise due to the special characteristics of the ground state structure. Based on the microscopic studies these subjects are discussed in the report of Ref.7.

References

1) I. Tanihata et al.: *Phys. Lett.*, **160B**, 380 (1985); *Phys. Rev.Lett.*, **55**, 2676 (1985); *Phys. Lett.*, **206B**, 592 (1988); I. Tanihata: *Nucl. Phys.*, **A478**, 795c (1988); *ibid.* **A488**, 113c (1988).
2) T. Kobayashi et al.: *Phys. Rev. Lett.*, **60**, 2599 (1988).
3) K. Ikeda: INS Report JHP-7(1988)[in Japanese].
4) P. G. Hansen and B. Jonson: *Europhys. Lett.*, **4**, 409 (1987).
5) T. Kobayashi et al.: *Phys. Lett.*, **B232**, 51 (1989).
6) T. Kobayashi: *Nucl. Phys.*, **A538**, 343 (1992).
7) K. Ikeda: *Nucl. Phys.*, **A538**, 355 (1992).

III-1-28. Analysis of ^{9}Li + n Resonances in ^{10}Li by the Complex Scaling Method

Interaction between ^{9}Li and Neutron

K. Ikeda and K. Kato

[Unstable nuclei, resonance, complex scaled OCM, neutron halo.]

Knowledge about the ^{9}Li-n interaction is very important to understand the exotic structure of ^{11}Li which is a typical example of neutron-rich nuclei. The experimental information about the structure of low energy resonances in the ^{10}Li system has been obtained recently by Bohlen et al..[1] The theoretical subjects are to determine quantitatively the ^{9}Li-n interaction based on those experimental results and develop understanding of the structure of ^{9}Li+2n.[2]

We have studied the resonance structure of the ^{9}Li+n system by using the complex scaled OCM within the single channel approximation and determined the reliable ^{9}Li-n interaction which consists of the central potential and ℓ·s potential. The complex scaled OCM is shown to give us the resonance energies and the resonance widths precisely. By choosing the ^{11}Be system, we have determined the ℓ·s potential by solving the neutron motion around a ^{10}Be-core so as to fit the observed data.

We have calculated resonance states of the ^{9}Li+n system by using the folding central potential and the ℓ·s potential. To fit the resonance energy (0.42 MeV) of the observed ground 1^{+} state, we found optical δ-values in the ^{9}Li-n folding central potential. The resonance states obtained by the ^{9}Li-n interaction are summarized in Fig.1. The calculated resonance widths of $(p_{1/2}, 1^{+})$ and $(p_{3/2}, 2^{+})$ have been shown to be in the same order of magnitude but larger than experimental ones. The shortcomings of the present model are that i) the calculated resonance widths are large and that ii) the second excited resonance state is calculated at a too high energy in comparison with observed data.

The shortcomings mentioned above suggest the activation in degrees of freedom of the ^{9}Li-core. We are undertaking a comprehensive study on the resonance properties of ^{10}Li in the framework of the channel coupled complex scaled OCM, in which the ^{9}Li-core excitations are taken into account. Furthermore this study should lead to a study on the ^{11}Li structure which includes the effects of the ^{9}Li-core excitations.

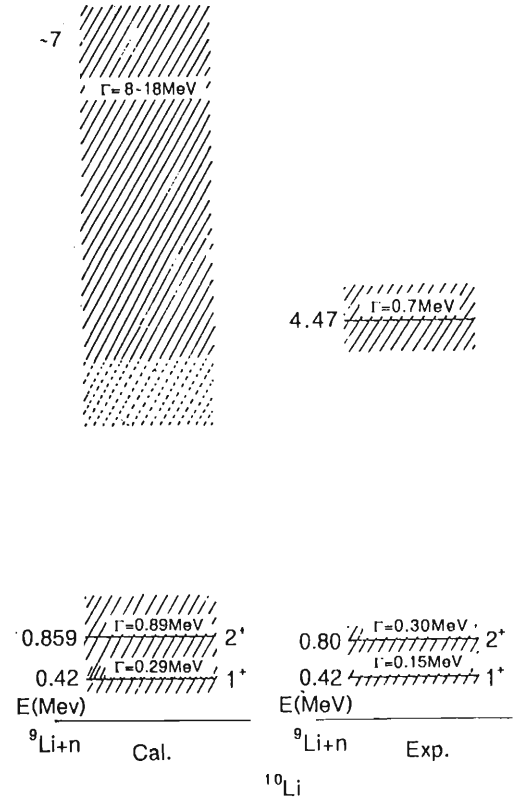

Fig.1. Calculated and obserbed resonance states of ^{10}Li. (MHN potential case)

References

1) H. G. Bohren et al.: preprint.
2) K. Ikeda: Nucl. Phys., **A538**, 355(1992).

III-1-29. Two-Neutron Removal Cross Sections of ^{11}Li

K. Soutome, S. Yamaji, and M. Sano

[Unstable nucleus, neutron halo, nuclear reaction, Glauber model.]

In the past few years there have been many studies of nuclei far from stability, especially of the extremely neutron-rich nucleus ^{11}Li. The nucleus ^{11}Li is known to have a neutron "halo", which is made of two outermost neutrons bound weakly around a ^{9}Li core. From this halo structure of ^{11}Li, it was suggested that there could exist a new type of collective excitation, soft giant dipole resonance, and this resonance will be found by experiments of Coulomb dissociation. Such experiments were performed by Kobayashi *et al.*;[1] they measured cross sections for the two-neutron removal process ^{11}Li + Target $\rightarrow$ ^{9}Li + X at E_{lab} = 0.8 GeV/nucleon. In order to discuss the Coulomb dissociation of ^{11}Li, however, one must subtract nuclear dissociation cross sections from measured cross sections. To estimate nuclear contributions, Kobayashi *et al.* adopted a naive geometrical model, the so-called "factorization model".[2]

This naive geometrical approach has been, however, criticized by several authors. For example, the "diffractive eikonal model" of Bertsch *et al.*[3] yields steeper target mass number dependence of the nuclear dissociation cross section than the factorization model. They claim that the factorized form of the cross section does not apply to the "halo" nucleus ^{11}Li.

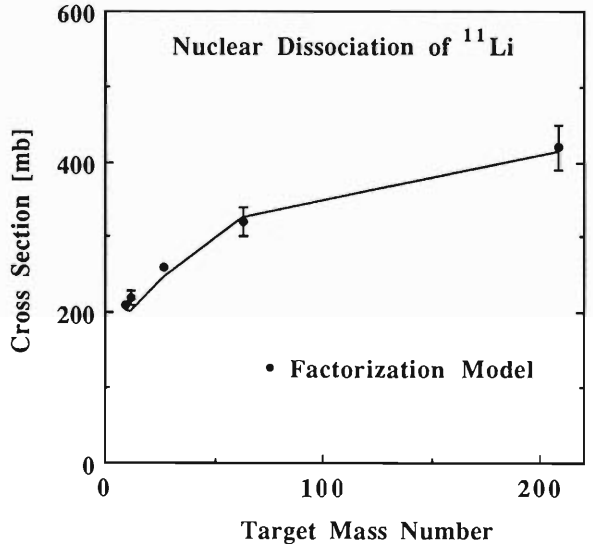

Fig. 1. Nuclear dissociation cross sections for the two-neutron removal process of ^{11}Li.

In contrast with such calculations, our recent Glauber calculation[4] indicates that the factorization model works well for the nuclear dissociation of ^{11}Li. In Fig. 1 we show calculated nuclear dissociation cross sections together with those deduced by Kobayashi *et al.* The solid curve was calculated by using the two-neutron density distribution of the following Yukawa form: $\rho(r_1, r_2) = \rho_{YK}(r_1)\,\rho_{YK}(r_2)$, $\rho_{YK}(r) = N\{1-\exp[-(r/b)^4]\} \times \exp[-ar]/r^2$, where we have chosen the values of a and b as a = 0.4 fm^{-1} and b = 2.43 fm. In order to see the "halo" structure of this model density, we show in Fig. 2 the density distribution of ^{11}Li. The shaded area represents the bounds within which interaction cross sections can be calculated consistently with experimental data.[5]

From Fig. 1 we can conclude that the factorization assumption indeed holds for the two-neutron removal process of ^{11}Li.

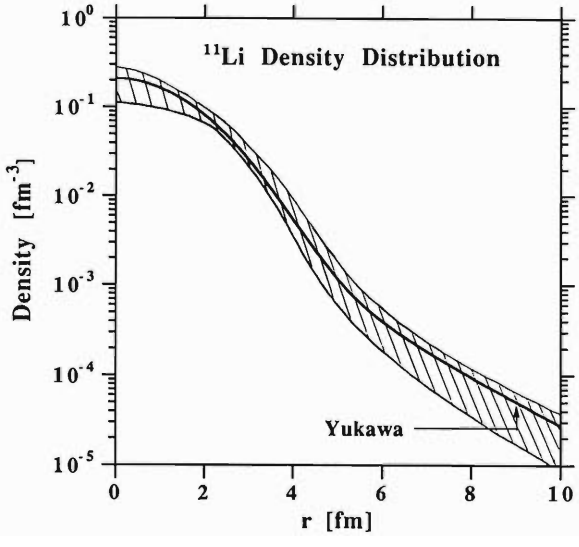

Fig. 2. Density distribution of ^{11}Li.

References
1) T. Kobayashi *et al.*: *Phys. Lett.*, **B232**, 51 (1989).
2) D. L. Olson *et al.*: *Phys. Rev.*, **C28**, 1602 (1983).
3) G. Bertsch, H. Esbensen, and A. Sustich: *Phys. Rev.* **C42**, 758 (1990).
4) K. Soutome, S. Yamaji, and M. Sano: *Nucl. Phys.*, **A538**, 383c (1992); *Prog. Theor. Phys.*, **87**, 599 (1992).
5) I. Tanihata *et al.*: RIKEN-AF-NP-119 (1992).

III-1-30. Higher Order Electromagnetic Interaction in the ^{8}B Breakup Process

N. Iwasa

[^{208}Pb (^{8}B , ^{7}Be p) ^{208}Pb; Coulomb breakup, higher order effect.]

Capture reactions at stellar temperatures can be studied by the Coulomb breakup method. If the breakup is via the one-step Coulomb excitation mechanism, direct correspondence between the cross sections of capture and breakup reactions is expected. This correspondence may be deteriorated by higher order electromagnetic interaction. G. Baur et al. developed a method to evaluate the higher order effect based on the sudden approximation.[1] They found considerable distortion in the angular distribution of the breakup fragments in their rest frame for the case of ^{11}Li + ^{208}Pb → ^{9}Li + 2n + ^{208}Pb at 30 MeV/u. In this paper the higher order effect is estimated for the E1 breakup process ^{8}B+^{208}Pb→^{7}Be+p+^{208}Pb at 47 A MeV[2] and 300 A MeV by the method of Baur et al.

Figures 1 and 2 show calculated angular distributions of the fragments in the plane perpendicular to the beam axis. The relative energy between ^{7}Be and proton is fixed to 300 keV. The impact parameter is set to be 15 fm, which corresponds to the scattering angles of 6° and 1° for the incident energies of 47 A MeV and 300 A MeV, respectively. Dotted curves represent the cross sections calculated by the first order electromagnetic interaction only, and solid curves are for the full calculation including all order. The higher order electromagnetic interaction is less important than in the ^{11}Li breakup, [1] though it is still not negligible. As shown in Fig. 2 the higher order effect diminishes at 300 A MeV. Therefore it is of interest to compare the experimental results at low and high incident energies.

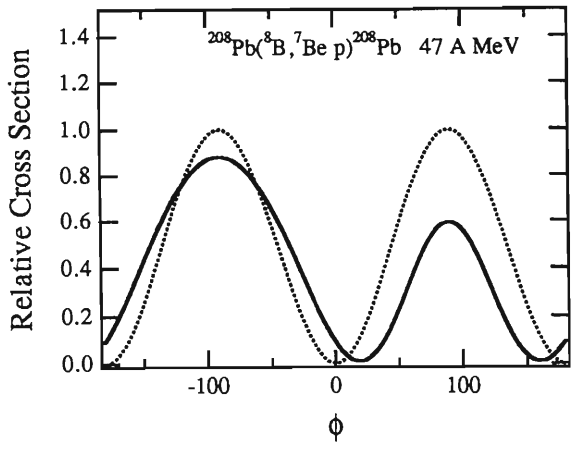

Fig. 1. Azimuthal angular distributions for the ^{208}Pb (^{8}B, ^{7}Be p) ^{208}Pb reaction at E_{in} = 47 A MeV. Dotted and solid curves represent the first and all order calculations, respectively.

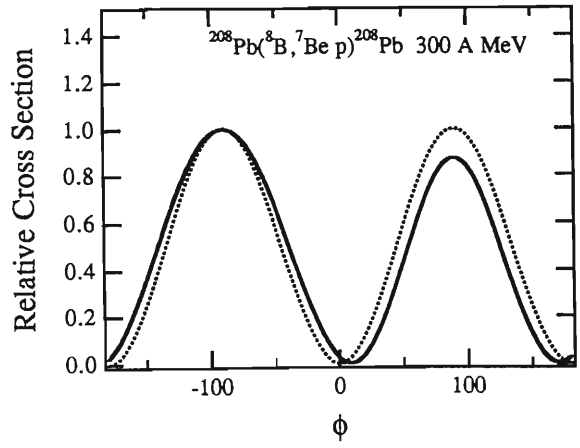

Fig. 2. The same as Fig. 1, but for the incident energy E_{in} = 300 A MeV.

References

1) G. Baur, C. A. Bertulani, and D. M. Kalassa: preprint.
2) T. Motobayashi et al.: This report, p.19.

III-1-31. Possible Existence of a Bound State in $^{7}_{\Sigma}$Li

K. Ikeda and T.Yamada*

[Σ-hypernuleus, ΣN interaction, supermultiplet.]

The possible existence of bound $^{7}_{\Sigma}$Li states[1] was investigated within the frame of the microscopic α+"2N"+Σ cluster model by employing the effective Σ-N interaction which reproduces the experimental binding energy and width of $^{4}_{\Sigma}$He.[2] We found a plausible $^{7}_{\Sigma}$Li bound state with binding energy of Σ^0 B_{Σ^0} =1.2 MeV and width $\Gamma \approx$ 5.4 MeV (See Fig. 1). The width comes only from the conversion process ΣN → ΛN because of the bound state. The bound state shows the mixed charge states with about 83% of total isospin I=1, which consists of the $[^{6}\mathrm{Li}(1^{+}_{1})\otimes\Sigma^0]$ and $[^{6}\mathrm{He}(1^{+}_{1})\otimes\Sigma^+]$ configration. This is in contrast with the fact that the $^{4}_{\Sigma}$He bound state is an almost pure isospin I=1/2 state.

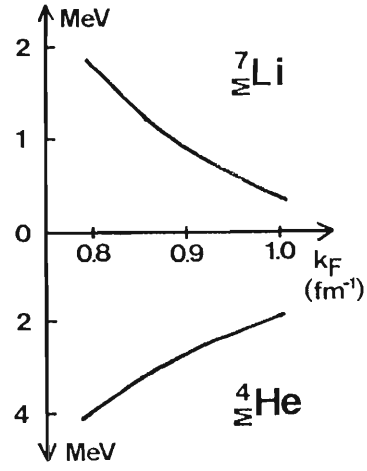

Fig. 1. Dependence of the Fermi momentum k_F on the binding enegies of $^{7}_{\Sigma}$Li and $^{4}_{\Sigma}$He.

The reason why such a bound state appears in $^{7}_{\Sigma}$Li is summarized as follows : The coupling potential between the $[^{6}\mathrm{Li}(1^{+}_{1})\otimes\Sigma^0]$ and $[^{6}\mathrm{He}(1^{+}_{1})\otimes\Sigma^+]$ states comes only from the $(\vec{t}_N\cdot\vec{t}_\Sigma)(\vec{s}_N\cdot\vec{s}_\Sigma)$term of Σ-N interaction since the $(\vec{t}_N\cdot\vec{t}_\Sigma)(\vec{s}_N\cdot\vec{s}_\Sigma)$term plays a role of coupling between the state with nulear-core spin s=1 and isospin t=0 ($^{6}\mathrm{Li}(1^{+}_{1})$) and the state with s=0 and t=1 ($^{6}\mathrm{He}(1^{+}_{1})$). The coupling strength is much larger than the energy difference (about 1 MeV) between the $[^{6}\mathrm{Li}(1^{+}_{1})\otimes\Sigma^0]$ and $[^{6}\mathrm{He}(1^{+}_{1})\otimes\Sigma^+]$ states. Therefore, the two states are coupled strongly to produce the bound state. On the other hand, the strength of the Lane potential is relatively smaller than the energy differences among $[^{6}\mathrm{Li}\otimes\Sigma^0]$, $[^{6}\mathrm{He}\otimes\Sigma^+]$ and $[^{6}\mathrm{Be}\otimes\Sigma^-]$ states with the nuclear-core isospin t=1. Therefore, the three states are not coupled strongly. $[^{6}\mathrm{He}\otimes\Sigma^+]$ configrations appear mainly due to the $(\vec{t}_N\cdot\vec{t}_\Sigma)(\vec{s}_N\cdot\vec{s}_\Sigma)$terms of Σ-N interaction. (See Fig. 2).

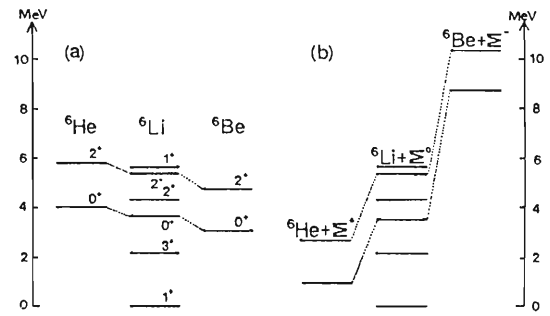

Fig. 2. (a) Isobar-diagram of the A=6 body nuclear system and (b) various Σparticle decay thresholds for $^{7}_{\Sigma}$Li.

In conclusion, we have shown the possible existence of the bound $^{7}_{\Sigma}$Li state. If this Σ-hypernucleus is observed, we can get the direct information on $(\vec{t}_N\cdot\vec{t}_\Sigma)(\vec{s}_N\cdot\vec{s}_\Sigma)$term of Σ-N interaction from the binding energy of $^{7}_{\Sigma}$Li. Therefore, it is highly desired that hypernuclear production experiments such as a $^{7}\mathrm{Li}(\mathrm{K}^-,\pi^-)^{7}_{\Sigma}\mathrm{Li}$ reaction will be performed to study the possible existense of the bound $^{7}_{\Sigma}$Li hypernucleus.

References

1) T.Yamada and K. Ikeda: *Phys. Rev.*, **C46**, 1315 (1992).
2) T. Yamada and K. Ikeda: *Prog. Theor. Phys.*, **88**, 139 (1992).

*Dept. Appl. Sci., Kochi Women's Univ.

III-1-32. $^{4}_{\Sigma}$He Hypernuclear States and Roles of the Spin-Isospin Term of Σ-N Interaction

K. Ikeda and T.Yamada*

[Hypernuclei, Σ-N interaction, isomutiplet.]

An evidence of the $^{4}_{\Sigma}$He bound state was observed in the ^{4}He(stopped K^-, π^-) experiment at KEK.[1] It is an interesting subject to investigate whether bound states and/or quasi bound states could exist in other light Σ hypernuclei with use of the effective Σ-N interaction which reproduces the experimental binding energy and width of $^{4}_{\Sigma}$He. For this purpose, we have to clarify the characteristic property of the strong spin-isospin dependent Σ-N interaction which has a role to make couple the different charge states.[2] The $[^{3}H+\Sigma^{+}]$ + $[^{3}He+\Sigma^{0}]$ model is applied to a study of the structure of $^{4}_{\Sigma}$He to make clear the roles of the spin-isospin terms of Σ-N interaction.

The eigenvalue and eigenfunction of $^{4}_{\Sigma}$He are obtained by solving the coupled channel equation. The k_F-dependence of the density dependent effective interaction obtained from the Nijmegen model D potential[3] is shown in Fig.1 (solid line) for the calculated binding energy B_{Σ^+} and width Γ. When the value of k_F is chosen to be 0.86 fm^{-1}, we found one bound state with B_{Σ^+} = 3.2 MeV and Γ = 7.8 Mev and could reproduce the experimental data. The obtained bound state shows an almost pure isospin eigenstate (I≈1/2). The reason why such an almost good isospin state appears in spite of the large energy difference (~ 2.6 MeV) between the $^{3}H+\Sigma^{+}$ and $^{3}He+\Sigma^{0}$ thresholds is given as follows : As shown in Fig. 2, the $^{3}H+\Sigma^{+}$ potentail has a repulsive part in the inner region. Therefore, there appears no bound

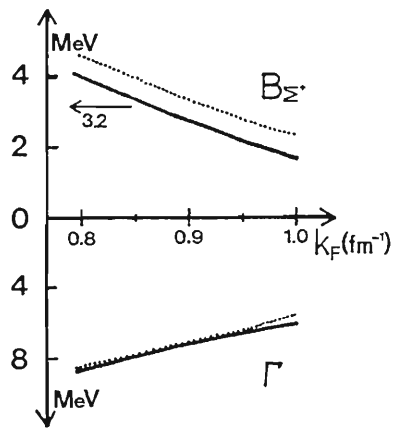

Fig. 1. k_F dependence of the calculated binding energy B_{Σ^+} and width Γ.

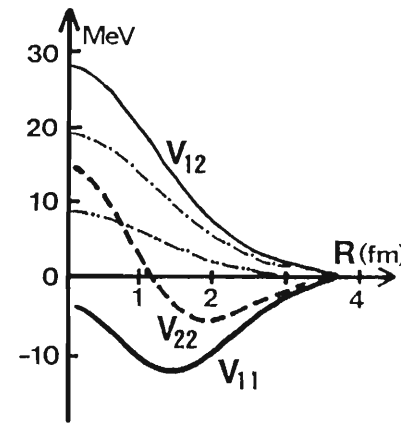

Fig. 2. Potentials for the $^{3}H+\Sigma^{+}$ (V_{11}:thick solid curve) and $^{3}He+\Sigma^{0}$ (V_{22}:thick dashed curve) channels. The fine solid curve denotes the coupling potential V_{12}.

state in the case of the $^{3}He+\Sigma^{0}$ channel. On the other hand, the coupling potential between the two channels, $V_{12}^{S=0}$, has a large magnitude. Its value amounts to about 10 MeV. It is much larger than the energy difference (~ 2.6 MeV) between the two thresholds. Therefore, the two basic charge states are coupled strongly.

As shown in Fig. 2, the origin of the large repulsive character of $V_{12}^{S=0}$ consists of the two constructive contributions ; about $\frac{1}{3}$ and $\frac{2}{3}$ of the total amount come from the $\sum_N v_{\Sigma N}^{\sigma}(\vec{s}_N \cdot \vec{s}_\Sigma)$and $\sum_N v_N^{\tau\sigma}$ $(\vec{t}_N \cdot \vec{t}_\Sigma)(\vec{s}_N \cdot \vec{s}_\Sigma)$parts of the Σ-N interactions, respectively. Thus, the $\sum_N v_N^{\tau\sigma}$ $(\vec{t}_N \cdot \vec{t}_\Sigma)(\vec{s}_N \cdot \vec{s}_\Sigma)$part of the Σ-N interaction plays an important role to form the $^{4}_{\Sigma}$He bound state.

References

1) R. S. Hayano, et al.: Phys. Lett., **B231**, 355, (1989).
2) T. Yamada and K. Ikeda: Prog. Theor. Phys., **88**, 139 (1992).
3) M. M. Nagel, T. A. Rijken, and J. J. de Swart: Phys. Rev., **D12**, 744 (1975) ; ibid.,**D15**, 2547 (1977) ; ibid., **D20**, 1633 (1979).

*Dept. Appl. Sci., Kochi Women's Univ.

III-1-33. Highly Excited States of ${}^{6}_{\Lambda}$Li by the Microscopic Cluster Model

K. Ikeda, H. Ohkura,* and T Motoba**

[Hypernuclei, hole state, cluster model, ($K^-\ \pi^-$) reaction.]

In order to explain the high-lying sharp peak observed at 18.3 MeV excitation in the ^{6}Li(K^-, π^-)${}^{6}_{\Lambda}$Li reaction,[1] which cannot be described with the α+p+Λ configuration,[2] we have applied the microscopic ^{3}He+d+Λ cluster model for the first time. This model has the broken-α degree of freedom.[3] We employ the NN interaction which describes high-lying states of ^{5}Li with the ^{3}He+d cluster model and such ΛN interaction as to reproduce the experimental Λ-binding energies of ${}^{4}_{\Lambda}$He($0^+_{g.s.}$ and 1^+ states).

In the three-body cluster calculation, as shown in Fig. 1 , it is notable first that two $J = 1^+$ eigenstates ($L = 0, S = 1$) are obtained below the ^{3}He+d+Λ threshold with their inter-cluster binding energies being 3.18 MeV and 2.10 MeV, respectively. Specifically the lowest state($1^+_1, S_N = 3/2$ dominant) is calculated to be below the ${}^{4}_{\Lambda}$He+d and ^{3}He+${}^{3}_{\Lambda}$H thresholds as a non-trivial consequence of the three-body dynamics, while the second state($1^+_2, S_N = 1/2$ dominant) is just above the ${}^{4}_{\Lambda}$He+d threshold. All the other eigenstates appear separately, more than 2 MeV above the ^{3}He+d+Λ threshold — more than 4 MeV above the 1^+_2 state.

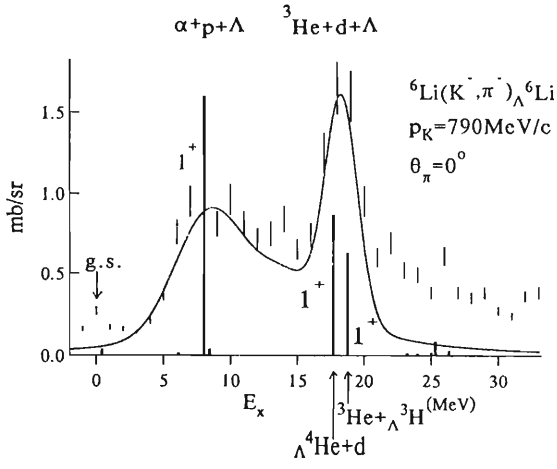

Fig. 1. Experimental[1] and theoretical excitation functions for the (K^-, π^-) reaction at p_K = 790 MeV and θ=0° with the decay channel thresholds indicated. A smooth curve shows the excitation function consisting of two Gaussian peaks(second and third peaks) and a Lorentzian bump for the experimental background.

Secondly both 1^+ states are very strongly excited in the forward (K^-, π^-) reaction on the target ^{6}Li = α+d ($\ell_N = 0, S = 1; J = 1^+$) through the recoilless $\Delta L = 0$ transition. We calculate a cross section for the (K^-, π^-) reaction by the distorted wave impulse approximation(DWIA).Thus we found that the third peak consists of these two 1^+ states. If we employ the emprical elementary cross section 4.0 mb/sr, the third peak cross section is predicted to be $\frac{d\sigma^{(3)}}{d\Omega}(0°) = 0.87(1^+_1) + 0.63(1^+_2) = 1.50$ mb/sr, which is 1.7 ~ 2.3 times as large as the shell model estimate.

Thirdly, making use of the α+p+Λ model and estimate for the second peak $\frac{d\sigma^{(2)}}{d\Omega} = 1.61$ mb/sr, the experimental ratio between the second and third peak strengths $(\frac{d\sigma^{(3)}}{d\Omega} / \frac{d\sigma^{(2)}}{d\Omega}) = 0.85 \sim 0.99$ can be reproduced satisfactorily (0.91) by the present cluster model. For such high-lying states it seems hard to explain the ratio with the shell model.

The ^{3}He+d+Λ microscopic cluster model works well for the understanding of the structure of highly excited states in view of all the consistency between the experimentally observed properties and the calculated results on the energy position, narrow width, and the reaction cross section of the third peak.

References

1) R. Bertini et al. (Heidelberg - Saclay - Strabourg Collaboration): *Nucl. Phys.*, **A368**, 365 (1981); **A360**, 315(1981).
2) T. Motoba, H. Bandō, and K. Ikeda: *Prog. Theor. Phys.*, **70**, 189(1983); **71**, 222 (1984).
3) T. Yamada, K. Ikeda, H. Bandō, and T. Motoba: *Phys. Rev.*, **C22**, 2073 (1980).

*Graduate School of Sci. and Technol., Niigata Univ.
**Lab. of Phys., Osaka Electro-Communi. Univ.

III-1-34. Light Σ Hypernuclei Σ^- Atoms

K. Ikeda and T. Yamada*

[Σ=hypernucleus, Σ^- atom, ΣN interaction, isomultiplet, supermultiplet]

This report is a review work on the structure of light Σ hypernuclei ($^4_\Sigma$He, $^7_\Sigma$Li and $^9_\Sigma$Be) and analyzed Σ atoms. We dedicate this article for the memory of prominant activities of late Prof. Jan Zofka (Nuclear Physics Institute of Czechoslovakia, Rez, Prage).[1] The summary of this article is given as follows:

(1) The structure analysis of $^4_\Sigma$He was performed within the frame of the [^{3}H+ Σ^+] + [^{3}H+Σ^0] model. [2] The bound state of $^4_\Sigma$He obtained shows an almost pure isospin eigenstate I=1/2. This is due to the fact that the coupling potential between the ^{3}H+ Σ^+ and ^{3}H+Σ^0 channels (namely, Lane potential) has large magnitude and its strengh is much larger than the sum of the mass difference and Coulomb energy difference between the two channels. It should be noted that the strong Lane potential in the case of $^4_\Sigma$He consists of two contributions from the ($t_N \cdot t_\Sigma$) and ($t_N \cdot t_\Sigma$) ($\sigma_N \cdot \sigma_\Sigma$) terms of Σ–N interaction because of the nuclear core with isospin 1/2 and spin 1/2, and the latter contribution is about twice larger than the former one.

(2) The possible existence of bound $^7_\Sigma$Li states was inverstigated within the frame of the microscopic α+ "2N" + Σ cluster model by employing the effective Σ–N interaction which reproduces the experimental binding energy and width of $^4_\Sigma$He. [3] We found the plausible $^7_\Sigma$Li bound state with B=1.2 MeV and Γ = 5.4 MeV. The width comes only from the conversion process ΣN → ΛN because of the bound state. The bound state shows the mixed charge states with abount 83% of total isospin I=1, which consists of the [^{6}Li(1$^+$) Σ^0] and [^{6}He(0$^+$) Σ^+] configurations. This is in contrast with the fact that the $^4_\Sigma$He bound state is an almost pure isospin I=1/2 state. The different binding mechanism between the $^7_\Sigma$Li and $^4_\Sigma$He hypernuclei comes from the different nuclear-core spin and isospin of the respective Σ–hypernuclei ((s,t) = (0,1) , (1,0) for ^{6}He- ^{6}Li- ^{6}Be and (s,t) = (1/2,1/2) for ^{3}H-^{3}He). If the bound $^7_\Sigma$Li hypernucleus is observed, we can get the direct information on the ($t_N \cdot t_\Sigma$) ($\sigma_N \cdot \sigma_\Sigma$) terms of Σ–N interaction from the observed binding energy of $^7_\Sigma$Li. Therefore, it is highly desired that the hypernuclear production experiment such as a ^{7}Li(K^-, π^-) $^7_\Sigma$Li reaction will be performed to study the possible existence of the bound $^7_\Sigma$Li hypernucleus.

(3) For the $^9_\Sigma$Be hypernucleus, we have applied the coupled-isomultiplet model [4] which takes into account the isospin coupling between the A=8 isotriplet (^{8}Li,^{8}Be,^{8}B) and Σ particles (Σ^+, Σ^0, Σ^-). The E_Σ=10 Mev peak observed in the ^{9}Be (K^-, π^-) $^9_\Sigma$Be reaction was interpreted as an almost pure isospin 0 state if we use the same coupling strengh of the Lane potential as that estimated by Dover et al., who analyzed the spectra of ^{12}C(K^-,π^-) $^{12}_{\Sigma}$Be, $^{12}_{\Sigma}$C reactions. The microscopic calculation for $^9_\Sigma$Be is in progress [4] with use of the effctive Σ–N interaction which repreduces the experimental binding energy and width of $^4_\Sigma$He.

(4) The combined analysis of Σ atoms and $^4_\Sigma$He was performed with use of the Nijmegen OBE potentials and was found to be useful to know the characteristic differences among them, since we can investigate the inside and outside behaviors of the Σ-nucleus potential on equal footing. [5] The model D (F and NSC (soft core)) can (cannot) reproduce both the binding energy and width of $^4_\Sigma$He. On the other hand, it is concluded that the systematic reproduction of the atomic data cannot be obtained with the existing OBE potentials in the framework of the present treatment.

References

1) T. Yamada and K. Ikeda : Czechoslovak J. Phys. (1992), to be published.
2) T. Yamada and K. Ikeda : Prog. Theor. Phys., 88, 139 (1992).
3) T. Yamada and K. Ikeda : Phys. Rev., C48 (1992), to be published.
4) K. Ikeda and T. Yamada : Int. J. Mod. Phys., A3, 2339 (1988) ; O. Richter, M. Sotona, T. Yamada, K. Ikeda, T. Motoba, and K. Itonaga : Few Body Systems, Suppl. 5, 379 (1992).
5) T. Yamada : Few Body Systems, Suppl., 5, 334 (1992).

* Dept. of Applied Sci., Kochi Woman's Univ.

III-1-35. Production of Double Λ Hypernuclei from a Formed Ξ Hypernuclear State

K. Ikeda, M. Takahashi,* and Y. Yamamoto**

[Hyper nuclei, hole state, (K^-,K^+) reaction, decay width.]

Recently a new experiment of the (K^-, K^+) reaction has been performed with use of a scintillating fiber target (KEK E-224). Because of the large momentum transfer of the elementary process $K^-N \to K^+\Xi^-$, the dominant part of K^+spectrum is of a quasi-free production of Ξ^-in the high-energy side. The production cross section of bound Ξ^-states in the terget nucleus (^{12}C) is considerd to be quite small. There is a possibility, however, to observe ΛΛ states specifically produced after $\Xi^-p \to \Lambda\Lambda$ conversion in the nucleus, even if the number of bound-Ξ^-events is not large (estimeted as about 100 events). Here we evaluate the trasition probabilities to three types of final ΛΛ states : two-Λ bound, one-Λ bound and one-Λ continuum and two-Λ continuum. Experimentally it may be possible to distinguish these three patterns of transition.

A Ξ^-particle in a nuclear bound state reacts with one of nucleons and then two Λ particles are produced. Now we define the partial conversion widths Γ_{bb},Γ_{bc} and Γ_{cc} where suffixes b, c mean bound and continumm states, respectively. Then the corresponding probabilities are given by $P_{bb} = \Gamma_{bb}/\Gamma$, $P_{bc} = \Gamma_{bc}/\Gamma$ and $P_{cc} = \Gamma_{cc}/\Gamma$ with $\Gamma = \Gamma_{bb} + \Gamma_{bc} + \Gamma_{cc}$. In the second-order perturbation we have

$$\Gamma_{bb} = \sum_{n_h\ell_h} \sum_{n_{\Lambda_1}\ell_{\Lambda_1}} \sum_{n_{\Lambda_2}\ell_{\Lambda_2}} \sum_{LST} \frac{[L][S][T]}{[\ell_\Xi][s_\Xi][t_\Xi]} \times < \alpha_\Xi \ell_\Xi n_h \ell_h | V_{\Xi N,\Lambda\Lambda} | n_{\Lambda_1}\ell_{\Lambda_1} n_{\Lambda_2}\ell_{\Lambda_2} >^2_{LST} \times \frac{\Gamma_{n_h\ell_h}}{(\epsilon_\Xi + \epsilon_{n_h\ell_h} - \epsilon_{n_{\Lambda_1}\ell_{\Lambda_1}} - \epsilon_{n_{\Lambda_2}\ell_{\Lambda_2}} + \Delta)^2 + \Gamma^2_{n_h\ell_h}/4}, \quad (1)$$

$$\Gamma_{bc} = \sum_{n_h\ell_h} \sum_{n_{\Lambda_1}\ell_{\Lambda_1}} \sum_{\ell_{\Lambda_2}} \int_0^\infty dk_{\Lambda_2} \sum_{LST} \frac{[L][S][T]}{[\ell_\Xi][s_\Xi][t_\Xi]} \times < \alpha_\Xi \ell_\Xi n_h \ell_h | V_{\Xi N,\Lambda\Lambda} | n_{\Lambda_1}\ell_{\Lambda_1} k_{\Lambda_2}\ell_{\Lambda_2} >^2_{LST} \times \frac{\Gamma_{n_h\ell_h}}{(\epsilon_\Xi + \epsilon_{n_h\ell_h} - \epsilon_{n_{\Lambda_1}\ell_{\Lambda_1}} - \hbar^2 k^2_{\Lambda_2}/2m_\Lambda + \Delta)^2 + \Gamma^2_{n_h\ell_h}/4}, \quad (2)$$

$$\Gamma_{cc} = \text{similar formula}, \quad (3)$$

where $|\alpha_\Xi \ell_\Xi >$, $|n_h\ell_h >$, $|n_\Lambda\ell_\Lambda >$ and $|k_\Lambda\ell_\Lambda >$ denote a Ξ^-nuclear state, a proton-hole state, a Λ-bound state and a Λ-continuum state, respectively, and ϵ_Ξ, $\epsilon_{n_h\ell_h}$ and $\epsilon_{n_\Lambda\ell_\Lambda}$ are corresponding single-paticle energies. A width of hole states $\Gamma_{n_h\ell_h}$, which has a large value for a ground 1s-state, is related to distribution of hole-excited states. It should be noted that Γ_{bb} gives the strength of the energy-conserving transition to two-Λ bound and hole-excited states. If $\Gamma_{n_h\ell_h} = 0$, the last parts in above expressions reduce to a delta function.

Here we calculate the partial conversion widths given in Eqs.(1)~(3) in the cases of Ξ^-absorption from nuclear orbits in ^{11}B core. The ΞN-ΛΛ coupling interaction $V_{\Xi N,\Lambda\Lambda}$ is dominated by the T=0 $^1S_0$ component and taken as three range Gaussian form. The Ξ^-in a nuclear orbit is considered to react with a deep 1s proton, whose width Γ_{1s} is taken as 10 MeV.

For convenience we represent all needed wave functions, Ξ^--nuclear,Λ-bound,Λ-continuum and proton-bound ones, on the Gaussian bases. We have calculated Ξ and Λ hypernuclear states of the $^{11}B+\Xi^-$ and $^{10}Be+\Lambda$ systems with the folding central potentials from Ξ-N and Λ-N gaussian interactions. The Λ continuum wave funciton is normalized as $\sqrt{2/\pi}\sin(kr - \pi/2 + \delta_\ell)$ asymptotically, and expanded in terms of Gaussian functions.

Table 1. Calculated partial conversion widths and corresponding probabirities. B_Ξ is the binding energy of Ξ particle.

B_Ξ(MeV)	Γ_{bb} (P_{bb})	Γ_{bc} (P_{bc})	Γ_{cc} (P_{cc})
5.1	0.199 (0.118)	1.453 (0.863)	0.032 (0.019)
9.9	0.362 (0.211)	1.323 (0.771)	0.030 (0.017)
15.7	0.978 (0.502)	0.941 (0.483)	0.028 (0.014)

In Table 1, we give preliminary calculated values of Γ_{bb}, Γ_{bc} and Γ_{cc} (P_{bb}, P_{bc} and P_{cc}). Here B_Ξ=5.1, 9.9 and 15.7(MeV) correspond to the potential strength(V_0) for -20, -30 and -40(MeV) with the range of 1.034(fm), respectively. The force strength and range for Λ are fixed to be -42.01MeV and 1.034fm. It is shown that 2Λ continuum probability is very small in comparison with others and that two Λ bound probability increases with increase of B_Ξ while one-Λ bound and one-Λ continuum one decreases with it.

References

1) M. Takahashi, Y. Yamamoto, and K. Ikeda: Physical Society's Autum Meeting, 1, 51(1992).

*Niigata Univ., **Tsuru Univ.

III-1-36. URASiMA: An Event Simulator for URHIC

S. Daté and H. Sumiyoshi

[High energy reaction, multiparticle production, event simulator.]

Activities in the field of ultrarelativistic heavy ion collisions (URHIC) are predominated by the aim of finding a new state of strongly interacting particles, the Quark-Gluon Plasma (QGP). To obtain a clear trace of the QGP formation, it is necessary to distinguish QGP signals from effects of hadronic final state interactions in nucleus-nucleus (AA) collisions. With this purpose, we have developed a new Monte Carlo event simulator URASiMA (Ultra-Relativistic AA collision Simulator based on Multiple Scattering Algorithm).

Among existing event simulators such as VENUS, MCFM, Fritiof and RQMD, URASiMA aims at being the most reliable one. URASiMA employs a conventional hadronic level multichain model[1] with known hadron-hadron (hh) and hadron-nucleus (hA) data as the input instead of introducing quark-string models as the quoted simulators do.

URASiMA code is an extension of two existing cascade codes called MCMAA and MCMHA, which have been designed to analyze cosmic ray data.[2] In contrast to the previous two codes, URASiMA deals with pp to AA collisions systematically. It regards motions and (point like) interactions of particles in the full 3+1 dimensional space-time. The code satisfies full covariance under the Lorentz transformations and the full energy-momentum conservation.

The present version of URASiMA includes elastic and inelastic NN, πN and ΔN interactions. Productions of K 's, anti nucleons and Δ resonances are considered in inelastic collisions besides with copious π productions.

We have already reported at some meetings[3] that our simulator reproduces the global data in the central rapidity region of 200 GeV ^{16}O + A reactions taken at CERN SPS. Our preliminary calculation on the transverse energy distribution in the target fragmentation region of ^{16}O + ^{184}W collisions at 200 GeV shows a good agreement with the experimental data[4] when we include internuclear interactions with the formation time τ_0 = 1.2 fm for pions.

We have made preliminary calculations to examine the role of the pion absorption. To do this, we have introduced a phenomenological parameter P_{abs} which determines the rate of the absorption among produced low energy pions. Our result shows that, in the fragmentation region, the calculation with P_{abs} = 0 (no absorption) overestimates pion yield, underestimates baryon yield and overestimates proton's p_T slope, in comparison with the experimental data.[4] These systematic deviations have been decreased significantly by introducing the pion absorption processes with non-zero P_{abs}. We have not made a full parameter search for the value of P_{abs} and we do not proceed this further in this report. We have also made a preliminary calculation on the K^+/π^+ ratio, whose observed enhancement has been regarded as a candidate of the signature of QGP. As a result, we have obtained a strong rapidity (y) dependence in the ratio; it increases rapidly when y changes to the target fragmentation region from the mid rapidity region. This dependence agrees with a measurement done by the E802 group at AGS.[5] If our understanding of the K^+/π^+ enhancement is correct, the ratio is expected to increase in proportion with nucleon density squared, since pions are mainly absorbed by two nucleon systems.

We believe that URASiMA provides an important base to study and understand mechanisms of particle production in ultra-relativistic heavy ion collisions.

References

1) A. Capella, U. Sukhatme, C. I. Tan, and J. Tranh Thanh Van: *Phys. Lett.*, **81B**, 68 (1979); K. Kinoshita, A. Minaka, and H. Sumiyoshi: *Prog. Theor. Phys.*, **61**, 165(1979); *ibid.*, **63**, 928 (1980); S. Daté, M. Gyulassy, and H. Sumiyoshi: *Phys. Rev.*, **D32**, 619(1985).
2) M. Fuki: Ph.D. thesis, printed in The Bulletin of the Okayama University of Science, **22A**,167 (1987); Y. Iga et. al.: Z. *Phys.*, **C38**, 557(1988).
3) S. Daté and H. Sumiyoshi: Proc. Int. Symp. on High Energy Nucl. Colli. and Quark Gluon Plasma, June, 1991, Kyoto, Japan (1991).
4) T. Akesson et. al.: Z. *Phys.*, **C38**, 383 (1988).
5) S. Nagamiya: talk given at the Quark Matter '91 Conf., Nov., 1991, Gatlinburg, U. S. A. (1991).

RIKEN Accel. Prog. Rep. 26 (1992)

III-1-37. Multiplicity Dependence of the Chaoticity Parameter in HBT Measurements

J. A. Casado* and S. Daté

[High energy reaction, multiparticle production, identical particle correlation.]

Chaoticity parameter in the normalized two particle correlation function for identical particles provides unique information on the quantum phase correlation between particle emission sources in high energy particle reactions. In spite of this fact, behaviors of the chaoticity parameter are not studied closely up to now.

In this work, we have tried to understand a recent measurement[1] on the multiplicity dependence of the chaoticity parameter. To do this we employ a semi-classical model of multiparticle production.[2]

In this model, pions are produced from a c-number source J(x) via Klein-Gordon equation for the second quantized pion field $\varphi(x)$. It is well known that the solution of the equation for the asymptotic final state is given by a coherent state of pions. If we assume that the pion source is composed of classically identical N sources, we can write

$$J(x) = \sum_{i=1}^{N} e^{i\phi_i} J_\pi(x-x_i) ,$$

where ϕ_i is the quantum phase and x_i is the space-time position associated with the i-th source. We assume that the positions $(x_1,\ldots,x_N)$ are distributed independent of each other according to a distribution function $\rho(x)$. Using the coherent state, we can write down the n-pion correlation function.

Given the correlation functions, the chaoticity parameter λ is expressed as

$$\lambda = \frac{\left(\int d^3k \langle P_1(k)\rangle\right)^2}{\int d^3k \langle P_1^2(k)\rangle} \frac{\int d^3k \langle P_2(k,k)\rangle}{\int d^3k_1 d^3k_2 \langle P_2(k_1,k_2)\rangle} - 1 . \quad (1)$$

Here $P_1(k)$ and $P_2(k_1,k_2)$ denote inclusive one- and two-particle densities, respectively, and <...> stands for averages over the phases, the positions and the number of sources, N.

The expressions for the correlation functions[2] provide the tandard formula of λ for the Bose-Einstein correlation when we assume randomly distributed phases. In this case, λ increases as a function of <N>, average source number, which is expected to be proportional to the charged multiplicity. This tendency apparently conflicts with the data shown in Fig. 1.

Assuming that the phases of the sources are constants, we can reproduce the data as shown in Fig.1. In this calculation, we have made further assumptions that the Fourier transform of J(x) has a flat shape in the rapidity space and that a spread of $\rho(x)$ is an order of 1 fm.

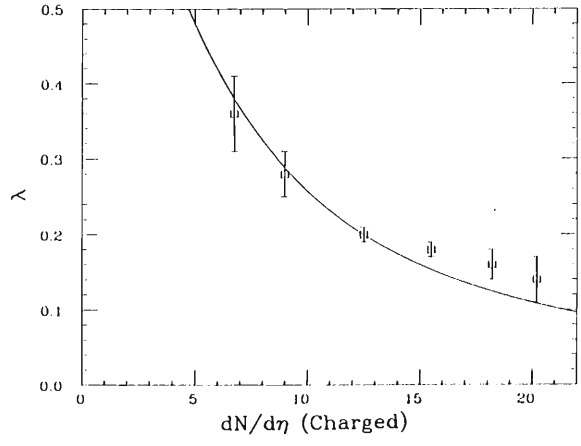

Fig. 1. The chaoticity parameter as a function of charged multiplicity. Data are taken from Ref. 1. A solid curve shows our calculation for the maximum coherent case.

Part of this work is supported by the program of Japanese Government Research Awards for Foreign Specialists promoted by the Science and Technology Agency of Japan.

References

1) C. S. Lindsey: Nucl. Phys., **A544**, 343c (1992).
2) M. Gyulassy, S. K. Kauffmann, and L. W. Wilson: Phys. Rev., **C20**, 2267 (1979).

* Departamento de Física Teorica, Universidad de Santiago de Compostela.

III-1-38. Pion Double Charge Exchange Reactions Leading to Double Pionic Atoms

J. Nieves,* E. Oset,* S. Hirenzaki, H. Toki, and M. J. Vicente-Vacas*

[Double charge exchange reactions, Double Pionic Atoms.]

Deeply bound pionic atoms in heavy nuclei are getting increasing attention from both experimentalists and theoreticians, since these states were found quasi-stable and accessible experimentally with some suitable methods.[1] Deeply bound pionic atoms have an interesting structure. The bulk part of the pion-nucleus interaction is strongly repulsive and pushes out a pion from the nucleus to protect it from being absorbed, while the Coulomb force attracts the pion to form a bound state. Hence, the pion forms a pionic halo around the nucleus. It indicates that all the observables of deeply bound atoms are very sensitive to the pion-nucleus interaction and the nuclear surface properties.

These features motivate us to think how a pionic system with many pions would look like. It would be very interesting to make an object with more than two pions in a single orbit. This will be the first case to make a microscopic system with more than two bosons in one quantum state. The double pionic atoms, in addition, would provide a unique opportunity to study the pion-pion interaction very precisely. A new field of multi-bosons with multi-fermions interacting strongly with each other will be open if we are able to create such states and study them experimentally. We may find pion condensation, which is however different from the zero energy regime discussed a lot in the past.

In this report, we would like to study theoretically a clear method to produce double pionic atoms. The idea is the use of direct reactions, in which a particle is bombarded on a target nucleus and an outgoing particle is measured. A sign for forming pionic atoms is a peak structure in the excitation function just below the two pion production threshold. As the first trial, we look into (π^-,π^+) reactions leading to double pionic atoms in ^{208}Pb.[2] This is $\pi^- + {}^{208}\mathrm{Pb} \rightarrow \pi^+ + ({}^{208}\mathrm{Pb}\ \pi_b^-\ \pi_b^-)$ with π_b^- a bound pion. We use the 4π interaction of Weinberg[3] to calculate the T matrix. We take pionic atom wave functions by solving the Klein-Gordon eq. with the optical potential of Seki and Masutani.[4] Concerning the distortion, we take the eikonal approximation. The purpose of doing this investigation is to see what is the size of the formation cross sections and what considerations are needed in order to find better methods.

We show in Fig.1 the calculated cross sections at zero degree as a function of the node quantum number n for S, P, and D states (l=0, 1, and 2). The cross sections decrease rapidly with n for each l. As for the angular momentum dependence, they increase first by going from 1s to 2p and then decrease from 2p to 3d.

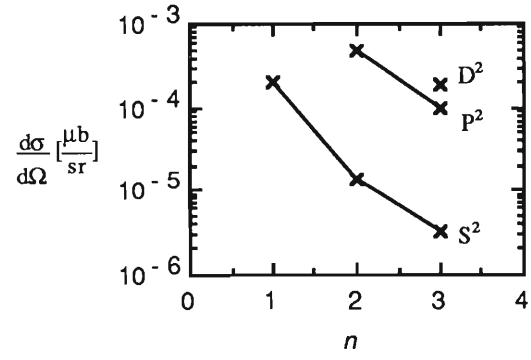

Fig. 1 The differential cross sections at zero degree leading to double pionic atom states. The energy of incident π^- is 500 MeV.

The (π^-,π^+) cross sections leading to double pionic atoms in ^{208}Pb are found quite small $d^2\sigma/dEd\Omega \sim 10^{-3} - 10^{-4}$ μb/sr/MeV. We have calculated the background double differential cross sections in the region of interest using the pion cascade model and found to be around 2 μb/sr/MeV. Hence, the (π^-,π^+) reactions seem not to be suited for double pionic atoms. The findings of the present work should be, however, of use in future exploration of alternative methods to produce these states.

References

1) H. Toki and T. Yamazaki: Phys. Lett., **B213**, 129 (1988).
2) J. Nieves, E. Oset, S. Hirenzaki, H. Toki, and M.J. Vicente-Vacas: Int. J. Mod. Phys., in press.
3) S. Weinberg: Phys. Rev. Lett., **18**, 188 (1967).
4) R. Seki and K. Masutani, Phys. Rev., **C27**, 2799 (1983).

* Department of Theoretical Physics, Univ. Valencia, Spain.

III-1-39. Formation of Deeply Bound Pionic Atoms by (d, ^{3}He) Reactions

S. Hirenzaki, H. Toki, and T. Yamazaki*

[(d,^{3}He) reactions, deeply bound pionic atoms.]

Since the suggestion of Toki and Yamazaki for the formation of deeply bound pionic atoms such as 1s and 2p states in heavy nuclei by direct reactions, there have been a number of experimental attempts to find these states. These states have a pionic halo structure due to a strong repulsive pion-nucleus interaction, which saves a pion from being absorbed by the nucleus. We pushed the use of the (d,^{3}He) reactions that use a deuteron beam.[1] This process has an advantage to be able to choose the incident deuteron energy so as to make the reaction recoilless. In this kinematics, the pion does not have to carry any momentum into the target nuclear system. Although (d,^{3}He) reactions are not coherent and hence lead to complicated nuclear configurations together with the formation of pionic states, the recoilless condition may make the process experimentally feasible. In fact, we showed that the cross sections leading to pionic atoms together with neutron hole states were comfortably large.

We have calculated double differential cross sections of (d,^{3}He) reactions on ^{208}Pb at T=600 MeV leading to deeply bound pionic atoms and also to unbound pionic states, where T is the incident deuteron kinetic energy. In a previous publication, we have developed the effective number approach for the formation of deeply bound pionic atoms in (d,^{3}He) reactions.[1] The previous publication should be referred to for all the details. Figure 1 shows the results at 0 degree leading to bound and unbound states as a function of Q value. We find that a significant amount of strength comes from bound pionic atom states coupled with a neutron hole state. On the other hand, the difference between the negative pion spectrum and the neutral pion spectrum is remarkable as can be seen by comparing the π^- and π^0 curves. The negative pion spectrum increases rapidly at the threshold, whereas the neutral pion spectrum only gradually increases from the threshold. This difference is originated by the Coulomb interaction. Adding all the contributions, we get the total cross sections as depicted by the thick solid curve. It is very interesting to note that the strength at Q =-130 ~ -140 MeV is almost exclusively due to the bound pionic states. The peak appearing at Q ~ -135MeV corresponds to the $(2p)_\pi(3p_{3/2})_n$ and $(2p)_\pi(3p_{1/2})_n$ configurations. We also have calculated the double differential cross sections at finite angles. The cross sections are smaller for larger angles. Since the momentum transfer increases with the scattering angle, the $(i_{13/2})_n$ hole contribution is dominant at larger angles.[2]

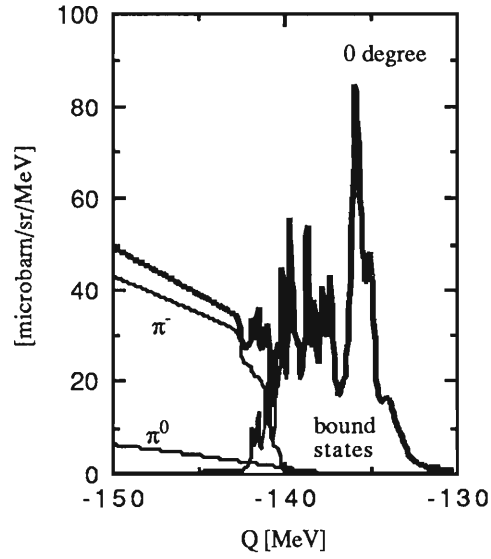

Fig. 1. ^{208}Pb(d,^{3}He) reaction cross sections calculated within the effective number approach leading to deeply bound pionic atoms and quasi-elastic pionic states at T=600MeV, 0 degree. The thick solid line means the total contribution of pionic processes. The experimental energy resolution is assumed to be 100 keV.

In conclusion, we have calculated the cross sections of ^{208}Pb(d,^{3}He) reactions in both the bound and unbound pion regions. We have found a large difference in the threshold behavior of negative and neutral quasi-free pion production cross sections due to the large Coulomb interaction. We also find that the cross section at Q =-130 ~ -140 MeV does not include the quasi-elastic pion contribution and the cross section is due to the bound pionic states.

References

1) S. Hirenzaki, H. Toki, and T. Yamazaki: Phys. Rev., **C44**, 2472 (1991).
2) S. Hirenzaki, H. Toki, and T. Yamazaki: in preparation.

* Inst. for Nuclear Study, Univ. Tokyo.

RIKEN Accel. Prog. Rep. 26 (1992)

III-1-40. Relativistic Mean Field Theory and Skyrme Hartree–Fock Theory for Unstable Nuclei

K. Sumiyoshi,* D. Hirata, H. Toki, and H. Sagawa

[Relativistic mean field theory, Skyrme Hartree-Fock theory, unstable nuclei.]

We make comparison of the relativisic mean field theory (RMF) and the Skyrme Hartree-Fock theory (SHF) for unstable nuclei. It is getting demonstrated that the RMF theory with the parameter set NL1 describes not only stable nuclei[1] but also unstable ones[2] in a wide mass region. The RMF theory with NL1 is applied also for the astrophysical use by providing the equation of state of nuclear matter at various conditions.[3] On the other hand, the SHF theory has been in use for a long time for the study of nuclear structure. It is, therefore, very interesting at this moment to see the similarity and the difference of these two frameworks in comparison with the existing nuclear data, anticipating many new data coming in the near future from the unstable nuclear beam facility.

All the details of the two models are described in the recent publication by the present authors.[4] Comparing first the nuclear matter results, we find that the incompressibility of RMF is slightly smaller than that of SHF, while the symmetry energy of RMF is larger than that of SHF. These features are reflected in the behaviors of the equations of state for nuclear matter and neutron matter around the normal density. A striking difference is, however, in the behaviour of EOS at higher density, where the EOS of RMF becomes much stiffer than that of SHF. We note also that the EOS of SHF with the most popular Skyrme paprameter set SIII is not acceptable for the astrophysical use, since the EOS of neutron matter becomes softer than that of nuclear matter.

We choose several proton magic nuclei up to the drip lines for comparison. It is very interesting to observe that the drip lines are predicted much closer to the stability line in RMF than those in SHF. The binding energies are found similar in comparison with the existing data. It seems RMF gets better in heavier nuclei. The proton radii are descibed extremely well by RMF. At the same time, the neutron radii are predicted much larger than the proton radii of the same nuclei as the nuclei deviate from the stability line. This existence of a large neutron skin is revealed in the recent unstable nuclear beam experiments for the He-isotope.[5] It would be very desirable to measure the neutron radii for nuclei far from the stability line.

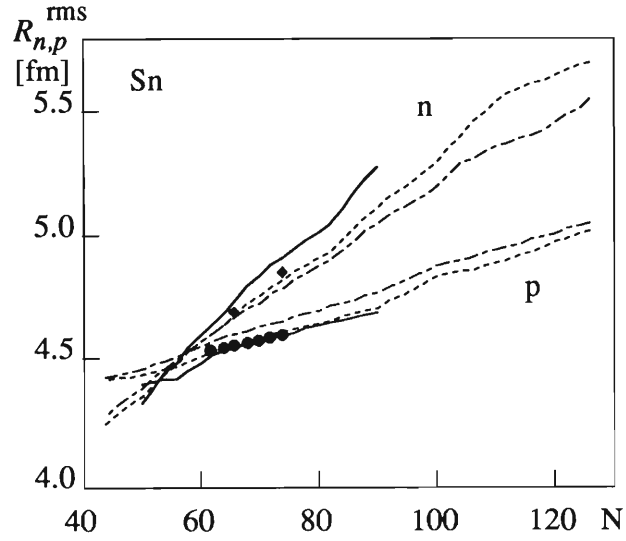

Fig. 1. The root mean square radii of Sn within RMF(NL1[solid curve]) and SHF(SIII[dash-dotted curve], Ska[dashed curve]) as a function of the neutron number in comparison with existing data which are shown by closed circles for protons and by closed squares for neutrons.

References

1) Y.K. Gambhir, P. Ring, and A. Thimet: Ann. Phys, (N.Y.), **198**, 132 (1990).
2) H. Toki, Y. Sugahara, D. Hirata, B.V. Carlson, and I. Tanihata: Nucl. Phys., **A524**, 633 (1991); D. Hirata, H. Toki, T. Watabe, I. Tanihata, and B.V. Carlson: Phys. Rev., **C44**, 1467 (1991).
3) K. Sumiyoshi, H. Toki, and R. Brockmann: Phys. Lett., **B276**, 393 (1992).
4) K. Sumiyoshi, D. Hirata, H. Toki, and H. Sagawa: Nucl. Phys., A (1992), in press.
5) I. Tanihata, D. Hirata, T. Kobayashi, S. Shimoura, K. Sugimoto, and H. Toki: Phys. Lett., **B289**, 261 (1992).

* Dept. Phys., Tokyo Metropolitan Univ.

III-1-41. Application of the Relativistic Mean Field Theory to Deformed Nuclei

D. Hirata, I. Tanihata, H. Toki, and P. Ring*

[Deformed nuclei, relativistic mean field theory]

Recently it becomes possible to study experimentally the properties of nuclei far from the stability line, in particular those with excess number of neutrons, through the use of radioactive nuclear beams. A large field of research has thus been opened. With this new technique, more data of unstable nuclei are being available.

We are interested in studying theoretically unstable nuclei using the relativistic mean theory. The application of such a theory has been demonstrated to be an excellent tool to describe the ground state properties of stable nuclei.[1] As an example, its application to unstable nuclei using a spherical symmetry gave a very good agreement with the experimental data.[2]

We have extended it to deformed nuclei. The pairing correlation was also taken into account using the constant gap approximation. A constraint was added to study the dependence of the binding energy on the amount of deformation.

When the axially symmetry was applied to Sr isotopes, it was found that the deformation changes drastically from one shape to the other at mass A=97, reproducing the observed jump in radius and the $E2^+$ energies (see Fig. 1 and 2). From the comparison with the data, it was found that this jump is due to a sudden transition of the deformation from an oblate to a prolate shape.

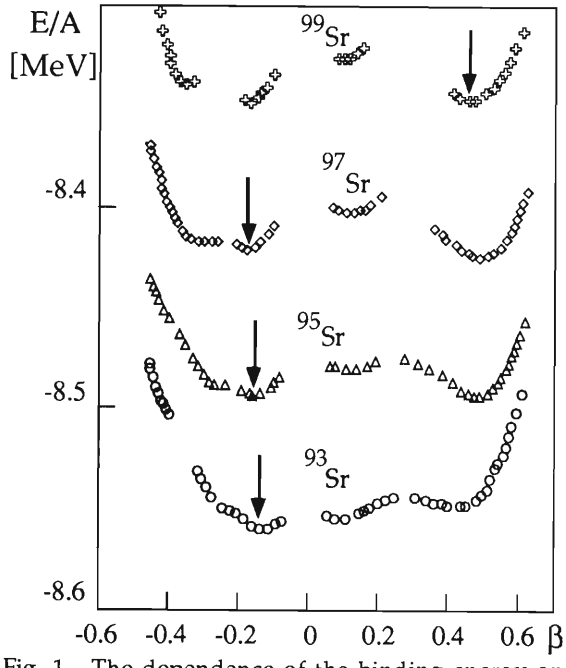

Fig. 1. The dependence of the binding energy on the amount of deformation for some odd Sr nuclei. The arrows correspond the minima choosen , showing the jump of deformation at A around 97.

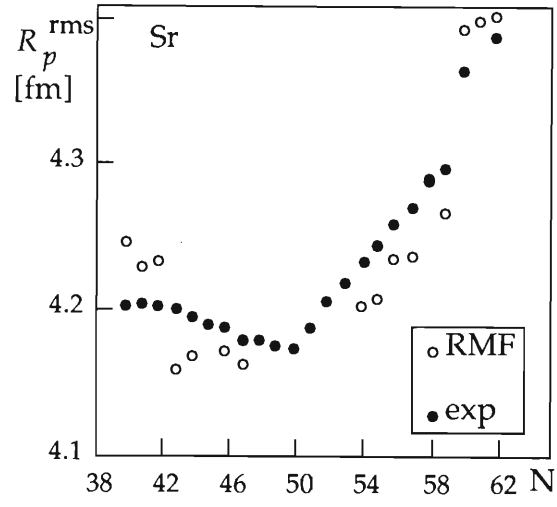

Fig.2.The rms radii of Sr isotopes as a function of the number of neutrons N.

We believe that the present work provides an important base to study and understand the structure of nuclei far from the stability line and the underlying physics of nuclei.

Part of this work is supported by the exchange program between the CNPq-Brazil and the Ministry of Education of Japan.

References

1) Y.K. Gambhir, P. Ring, and A. Thimet: Ann. Phys., **198**, 132 (1990).
2) D. Hirata et al., Phys. Rev., **C44**, 1467 (1991).

* Physikdepartment der Technischen Universität Müchen.

III-1-42. Equation of State in the $1/N$ Expansion of a Relativistic Many-Body Theory

K. Tanaka, W. Bentz,* and A. Arima*

[EOS, $1/N$ expansion, relativistic many-body theory.]

The investigation of the equation of state (EOS) for nuclear and neutron matter has been one of the most active fields in intermediate nuclear physics. The knowledge of the EOS is required for the analysis of heavy ion reactions as well as for the understanding of stellar structure and evolution. Since these applications require the EOS at densities of several times the normal nuclear matter density, the EOS's based on relativistic many-body theory are powerful candidates. The simplest and widely used version of relativistic models is the $\sigma\omega$ model.[1] However, it is known that the EOS obtained in the Hartree (mean-field) approximation to this model is unreasonably stiff.

In this paper[2] we investigate the EOS in the $\sigma\omega$ model including the higher order many-body correlations beyond the Hartree approximation. We employ the $1/N$ expansion scheme (N is the number of nucleon species), which has been recently proposed[3] as a useful method to compute the higher order corrections in the relativistic many-body theory. The Hartree approximation is obtained as the leading order term in this scheme. We include the next-to-leading order contributions, which give the RPA-type many-body correlations. The essential role of these higher order terms to reproduce the saturation property of nuclear matter has already been revealed.[3]

We find that the EOS becomes softer due to the inclusion of the higher order many-body correlations, bringing the results closer to the empirical informations. In Fig.1 we show the pressure of nuclear matter as a function of the density, comparing our result including higher order terms (the solid curve) with various other EOS's: The dot-dashed curve shows the result in the Hartree approximation, the dotted curve is the EOS based on the nonrelativistic variational calculation,[4] and the dashed curve is the phenomenological EOS modeled to give successful type-II supernovae explosions.[5] Around the normal density, the softening of our EOS is reflected by the incompressibility of 301MeV, which is close to the empirical value and should be compared with 456MeV in the Hartree approximation. For high densities our EOS is even softer than the nonrelativistic one, which becomes very stiff with increasing density due to the violation of causality.

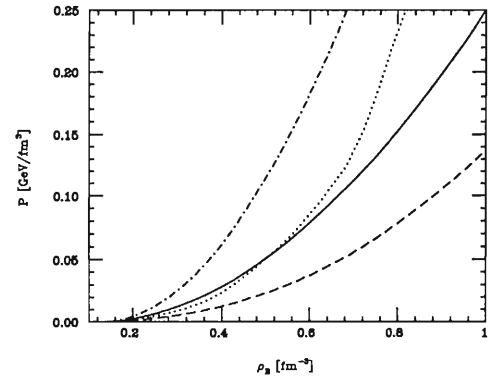

Fig. 1. Pressure vs. baryon density for nuclear matter. For the explanation of the curves, see the text.

As an application, we compute the neutron star structure based on our neutron matter EOS, integrating the Tolman-Oppenheimer-Volkoff equation.[6] We include also the ρ-meson contribution at the Hartree level into our EOS to reproduce the empirical symmetry energy of 30MeV. We find that our EOS can support the observed neutron star mass and gives the neutron star properties consistent with observations.

References

1) B. D. Serot and J. D. Walecka: "Advances in Nuclear Physics", eds., J. W. Negele and E. Vogt, Plenum, New York, **16**, 1 (1986).
2) K. Tanaka, W. Bentz, and A. Arima: preprint (1992).
3) K. Tanaka and W. Bentz: *Nucl. Phys.*, **A540**, 383 (1992).
4) B. Friedman and V. R. Pandharipande: *Nucl. Phys.*, **A361**, 502 (1981).
5) E. Baron, J. Cooperstein, and S. Kahana: *Phys. Rev. Lett.*, **55**, 126 (1985).
6) S. Weinberg: "Gravitation and Cosmology", Wiley, New York (1972).

*Dept. of Phys., Univ. of Tokyo.

III-1-43. Fermi-Liquid Properties of Nuclear Matter in the $1/N$ Expansion of a Relativistic Many-Body Theory

K. Tanaka, W. Bentz,* and A. Arima*

[Relativistic Fermi-liquid theory, $1/N$ expansion, nuclear matter.]

In recent papers[1-3] we have investigated the role of higher order many-body correlations in the relativistic $\sigma\omega$ model, based on the $1/N$ expansion method. Our results have suggested the importance of the higher order effects beyond the Hartree approximation to reproduce the bulk properties of nuclear matter, like the saturation property and the equation of state, deduced from various experimental informations. In this paper[3] we analyze these results for nuclear matter from the more fundamental aspect of the elementary excitations (quasiparticles) and their mutual interactions. We employ the general framework of the Landau theory of Fermi-liquids.[4] One essential advantage of the Landau theory is that it provides rigorous relations between the bulk properties of matter and a few universal parameters characterizing the properties of the quasiparticles. Therefore, it allows a deeper understanding of the results obtained in the preceding works.

Following the Landau theory, the quasiparticle energy and the quasiparticle interaction are obtained by taking the first and the second variational derivatives of the energy density of nuclear matter with respect to the quasiparticle distribution function. Since our energy density includes the exchange and the ring energy contributions of the next-to-leading order in the $1/N$ expansion as well as the leading Hartree contributions, our quasiparticle energy and quasiparticle interaction involve the corresponding higher order contributions; for example, those for the quasiparticle energy correspond to the RPA-type nucleon self-energies.

We find that the quasiparticle spectra as well as the quasiparticle interactions are largely modified due to the higher order effects, and these modifications bring the results for the nuclear matter properties closer to the empirical ones. In Table 1 we show the quasiparticle properties and the relevant bulk properties of nuclear matter for normal density. We see that the Fermi velocity v_F is reduced due to the higher order effects. For the quasiparticle interactions, they are reduced for the isoscalar channel (F_0, F_1) while non-zero values are generated for the isovector channel (F_0', F_1'). It is the combined effect due to the reduction of both v_F and F_0 that makes the incompressibility K considerably smaller compared to the Hartree approximation, through the rigorous relation[4] $K = 3p_F v_F(1 + F_0)$ with p_F the Fermi momentum.

As an application, we investigate the collective excitations (sound waves) of nuclear matter on the basis of the Landau kinetic equation.[4] We find that the reduction of v_F, F_0 and F_1 noted above leads to the softening of the isoscalar sound modes.

Table 1. Quasiparticle properties and bulk properties of nuclear matter at normal density. "$1/N$" refers to our full result including the higher order contributions, while "Hartree" refers to the Hartree approximation. The numbers in parenthesis show the Hartree contributions contained in the full result. Shown are the ratio of the nucleon effective mass to the free nucleon mass M^*/M, the Fermi energy ϵ_F, the Fermi velocity v_F, the dimensionless Landau parameters F_0, F_1, F_0', F_1', the incompressibility K, the first sound velocity c_1, the symmetry energy a_4, and the isoscalar and isovector orbital angular momentum g-factors $g_l^{(0)}$ and $g_l^{(1)}$. Empirically known values are $K \simeq 200 \sim 300$MeV, $a_4 \simeq 30$MeV, $g_l^{(0)} \simeq 0.52$, and $g_l^{(1)} \simeq 0.56$. ($\epsilon_F - M = -15.7$MeV is used as an input to determine the parameters of our model.)

	$1/N$		Hartree
M^*/M	0.894	(0.894)	0.730
$\epsilon_F - M$ [MeV]	−15.7	(17.7)	−15.7
v_F	0.289	(0.292)	0.350
F_0	0.356	(−0.593)	0.691
F_1	−0.113	(−0.247)	−0.621
F_0'	0.189	(0.0)	0.0
F_1'	0.096	(0.0)	0.0
K [MeV]	301	(91.5)	456
c_1	0.190	(0.103)	0.234
a_4 [MeV]	14.7	(12.5)	15.0
$g_l^{(0)}$	0.509	(0.491)	0.509
$g_l^{(1)}$	0.545	(0.535)	0.641

*Dept. of Phys., Univ. of Tokyo.

References

1) K. Tanaka and W. Bentz: *Nucl. Phys.*, **A540**, 383 (1992).
2) K. Tanaka, W. Bentz, and A. Arima: This report, p. 50.
3) K. Tanaka, W. Bentz, and A. Arima: preprint. (1992).
4) L. D. Landau: *Sov. Phys. JETP*, **3**, 920 (1956); *ibid.*, **5**, 101 (1957); *ibid.*, **8**, 70 (1959).

III-1-44. A Modified Nambu–Jona–Lasinio Model for Mesons and Baryons

M. Katô,* W. Bentz,* K. Yazaki, and K. Tanaka

[Baryons, $U_A(1)$ anomaly, NJL model.]

Hadrons are now believed to be composite particles composed of quarks and gluons, whose dynamics are governed by quantum chromodynamics (QCD). Since it is very difficult to handle QCD directly at low energies, effective theories are often used to study hadron physics. In the energy scale of hadrons, QCD has two important properties, spontaneous chiral symmetry breaking and confinement, which should be incorporated into these models as much as possible. The Nambu–Jona-Lasinio (NJL) model[1] is one of these effective theories. In this model mesons can be described as quark-antiquark bound states through the spontaneous chiral symmetry breaking. One drawback of this model is that it does not incorporate the confinement. We can expect, however, that the difference between binding and confinement has no serious consequences as long as we limit ourselves to the description of the ground state.

Recently,[2] it has been suggested that in the Hartree approximation to this model there also exists a baryon-like solution as a solitonic bound state with three valence quarks. In this paper[3] we reexamine the existence of this soliton solution toward a unified and consistent description of mesons and baryons. We use the modified flavor $SU(3)$ NJL-model,[4] which incorporates one more important property of QCD, i.e., the axial $U(1)$ ($U_A(1)$) anomaly, as well as the flavor $SU(2)$ model used in Ref. 2.

We find that in the flavor $SU(2)$ case there exists no stable solitonic solution. The solutions spread or collapse according to the value of the coupling constant of the 4-fermion interaction, and this situation does not change even if we include the vector-type interaction which is expected to stabilize the system. In the flavor $SU(3)$ case we can obtain stable solutions. The stabilization comes from the flavor mixing with the strange-quark due to the "instanton induced" 6-fermion interaction describing the $U_A(1)$ anomaly. As shown in Fig. 1, the flavor mixing leads to a position-dependent (density-dependent) effective 4-fermion coupling constant, which in turn gives a repulsive effect near the origin of the solitonic state.

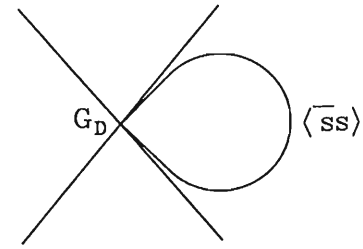

Fig. 1. The contribution of the 6-fermion interaction, which leads to a position-dependent effective coupling constant of the 4-fermion interaction $G_D\langle\bar{s}s\rangle$. G_D is the coupling constant of the 6-fermion interaction, and $\langle\bar{s}s\rangle$ is the strange-quark condensate which is position-dependent for the solitonic state.

In order that this mechanism prevents the collapse, we need an appreciably larger flavor mixing compared to the previous works.[4] We show that this large flavor mixing does not lead to inconsistencies for the physical quantities, by examining the physical observables of the nucleon and also by investigating the properties of the pseudoscalar mesons in the same framework. One of the reasons for this is the compensation by the rather small values for the quark condensates of our solution.

References

1) Y. Nambu and G. Jona-Lasinio: *Phys. Rev.*, **122**, 345 (1961); **124**, 246 (1961).
2) Th. Meissner, F. Grümmer, and K. Goeke: *Phys. Lett.*, **B227**, 296 (1989).
3) M. Katô, W. Bentz, K. Yazaki, and K. Tanaka: *Nucl. Phys.*, **A**, in press.
4) T. Hatsuda and T. Kunihiro: *Z. Phys.*, **C51**, 49 (1991).

*Department of Physics, Univ. of Tokyo.

III-1-45. Faddeev Approach to the Nucleon in the Nambu–Jona–Lasinio (NJL) Model

N. Ishii,* W. Bentz,* and K. Yazaki

[NJL-model, faddeev theory.]

The NJL model [1] has been quite successful in describing the mesons as $q\bar{q}$ bound states . [2] In recent years, it has also been used to investigate baryons, where mainly the mean field approximation [3] and the diquark-quark model [4] have been used. The Faddeev approach which takes into account the interaction between the diquark and the quark was recently used by Buck et al , [5] employing a static approximation to the quark propagator and restricting the 2-body channels to the scalar diquark one. In this work we solve the relativistic Faddeev equation [6] numerically in the scalar diquark-quark channel without any further approximation.

Our calculations are based on effective quark interaction Lagrangians $\mathcal{L}_I$ with 4-fermion coupling of the NJL-type. If we try to construct the nucleon as a bound state of a scalar diquark and a quark, the dependence of the results on the actual form of $\mathcal{L}_I$ comes in only through the ratio $r = \frac{g_{sd}}{g_\pi}$ where g_π is the strength of the interaction in the pionic (0^-) $q\bar{q}$-channel which is fixed by the pion mass, and g_{sd} is the one in the scalar (0^+) qq-channel. We will study the baryons with the ratio r as a parameter. We require that our calculation reproduces the experimental values of the pion mass and the pion decay constant. This leaves us with one free parameter, and we actually treat the constituent quark mass related to the other parameters by the gap equation as this free parameter, investigating mainly the cases $M = 350, 400$MeV. As mentioned before, we treat the ratio r as a further parameter. We solve the relativistic Faddeev equation using the quark-quark T-matrix obtained from the two-body Bethe-Salpeter equation as an input. We calculate the maximum eigenvalue $\lambda(E)$ of the Faddeev kernel as a function of the total C.M. energy E, and the baryon mass is obtained from $\lambda(m_B) = 1$. Here we confine ourselves to the nucleon.

The maximum eigenvalue $\lambda(E)$ for the case $M =$ 400MeV is shown in Fig.1 as a function of E for different ratios $r = \frac{1}{2}, \frac{2}{3}, 0.8, 1$. There exists a minimum ratio r for three quarks to be bound which in our calculation is about 0.5 in the case of $M = 400$MeV. It follows that we cannot get a bound nucleon state with the original NJL-Lagrangian for which the ratio r is $\frac{1}{6.5}$. In order to get a reasonably good nucleon mass, the ratio should be about $\frac{2}{3}$ for $M = 400$MeV.

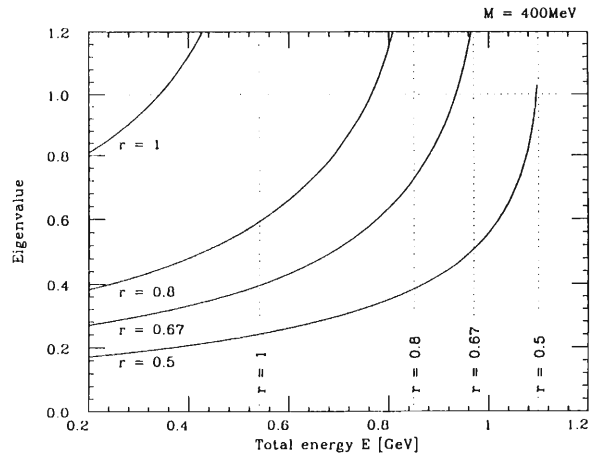

Fig.1. The maximum eigenvalue of the kernel as a function of the total energy E for several ratios r for the case of constituent quark mass $M = 400$MeV. The vertical dotted lines represent the quark-diquark thresholds for each ratio. A 3-body pole exists if the graph intersects the horizontal dotted line, and the coordinate of the intersection is the baryon mass.

This could serve as a guide for the search of an interaction Lagrangian which is able to describe both mesons and baryons. We also compared our exact solutions with the results of the static approximation of Buck et al, where the mass of the exchanged quark is virtually treated as infinitely heavy. We found that it could be used to obtain qualitative estimates, but quantitatively it gave too much attraction. Finally we mention that for more quantitative investigations we have to include at least the axial vector diquark channel in addition to the scalar one.

References

1) Y.Nambu and G.Jona-Lasinio: Phys. Rev., **122**, 345 (1960); **124**, 246 (1961).
2) T.Hatsuda and T.Kunihiro: Z. Phys., **C 51**, 49 (1991).
3) M.Kato, W.Bentz, K.Yazaki, and K.Tanaka, A Modified Nambu-Jona-Lasinio Model for Mesons and Baryons: Nucl. Phys., **A**, in press.
4) U.Vogl and W.Weise: Prog. in Part. and Nucl. Phys., **27**, 195 (1991).
5) A.Buck, R.Alkofer, and H.Reinhardt: Phys. Lett., **B 286**, 29 (1992).
6) G.Rupp and J.A.Tjon: Phys. Rev., **C 37**, 1729 (1988); **C 45**, 2133 (1992).

* Dept. Phys., Univ. Tokyo.

RIKEN Accel. Prog. Rep. 26 (1992)

III-1-46. Nuclear Transparency in $(e, e'p)$ and $(p, 2p)$ Reactions

A. Kohama,* R. Seki,** and K. Yazaki

[Nuclear transparency, Glauber approximation.]

It has been speculated[1] that the internal structure of hadrons may show up in quasi-elastic processes with nuclear targets at large momentum transfer. More specifically, the nuclear medium may become anomalously transparent for a hadron before and/or after a hard collision, since the strongly localized configuration with the smallest number of constituents in the wave function describing the internal structure of the hadron contributes dominantly to a hard process and a hadron in such a configuration is expected to interact weakly with the nuclear medium.

The nuclear transparency,[2] T, in the electron quasi-elastic process, $(e, e'p)$, is defined by the ratio between the differential cross section for nuclear target, $d\sigma_{eA}/d\Omega$, and that for e-p elastic scattering, $d\sigma_{ep}/d\Omega$, as

$$\frac{1}{Z}\frac{d\sigma_{eA}}{d\Omega} \Big/ \frac{d\sigma_{ep}}{d\Omega} = F(k)T(q)$$

where

$$\frac{d\sigma_{eA}}{d\Omega} = \int \frac{k'^2 dk'}{(2\pi)^3}\frac{d\boldsymbol{p}}{(2\pi)^3}\frac{d\sigma_{eA}}{d\boldsymbol{k}'d\boldsymbol{p}}$$

with $\boldsymbol{k}$, $\boldsymbol{k}'$ and $\boldsymbol{p}$ denoting the incident electron, the scattered electron and the knocked-out proton momenta, respectively, $F(k)$ is the kinematical factor including the Fermi averaging and q is the average momentum of the knocked-out proton. $T(q)$ approaches 1 as the nuclear medium becomes transparent for the knocked-out proton.

We have calculated $T(q)$ in the Glauber approximation without considering the internal structure of the proton which is to be compared with the experimental value for testing the above idea. With the assumptions which are better justified for heavier targets, we have obtained a simple expression for $T(q)$, i.e.

$$T(q) = \int d\boldsymbol{r}\rho(\boldsymbol{r}) \exp\left\{-A\sigma_{NN}^{r}\int_z^\infty dz'\rho(z', \boldsymbol{r}_\perp)\right\}$$

where $\rho(\boldsymbol{r})$ is the nuclear density for the target normalized to unity and σ_{NN}^{r} is the nucleon–nucleon reaction cross section. This is the same as the semi-classical estimate with the proton mean-free-path except that the total cross section is replaced by the reaction cross section. A similar expression is obtained in the case of the proton quasi-elastic process, $(p, 2p)$, where the initial state interaction for the incident proton as well as the final state interaction for the outgoing protons has to be included in the attenuation factor.[3] The results for both cases with ^{4}He, ^{12}C, ^{16}O, ^{27}Al, ^{63}Cu and ^{208}Pb as the targets are given in Table 1. The kinematical conditions correspond to those of the experiments by Carroll *et al.*[4] in the case of $(p, 2p)$ reaction and the same is taken for the case of $(e, e'p)$ reaction. σ_{NN}^{r} in this energy region is essentially constant and therefore the transparencies do not depend on the incident energy. The magnitudes of T for $(p, 2p)$ are roughly consistent with the observed ones, although the energy variation indicated in the experiment is not reproduced.

Table 1. The calculated transparencies.

target	^{4}He	^{12}C	^{16}O	^{27}Al	^{63}Cu	^{208}Pb
$T(e, e'p)$	0.81	0.68	0.59	0.51	0.42	0.28
$T(p, 2p)$	0.51	0.35	0.25	0.17	0.11	0.046

References

1) S.J. Brodsky: Proc. 13th Int. Symp. on Multiparticle Dynamics 1982, *ed.* by W. Kittel, W. Metzger and A. Stergiou, World Scientific, p.963 (1982); A.H. Mueller: Proc. 17th Recontre de Moriande (Les Ares, 1982) *ed.* by Tran Thanh Van, p.13 Ed. Frontiers, (1982).
2) A. Kohama, K. Yazaki, and R. Seki: *Nucl. Phys.* A, in press.
3) A. Kohama, K. Yazaki, and R. Seki: *Nucl. Phys.*, **A536**, 716 (1992).
4) A.S. Carroll *et al.*: *Phys. Rev. Lett.*, **61**, 1698 (1988).

*Dept. Phys., Univ. Tokyo.
**Dept. Phys., California State Univ., U.S.A.

III-1-47. Chiral Symmetry Restoration inside Flux Tubes of Hadrons

H. Suganuma

[Chiral symmetry restoration, finite-size effect, confinement.]

Hadrons can be considered as string-like tubes from the empirical evidences of the Regge trajectory and the duality of hadron reactions. We have studied the manifestation of chiral symmetry and the hadron structure based on this picture.[1] Recently, several authors have indicated that the finite-size effect may be important for the study of the $\bar{q}$-q pair creation by the Schwinger mechanism,[2-5] which is theoretically related to chiral symmetry.[1] Hence, we study the finite-size effect on the manifestation of chiral symmetry inside the flux tube of hadrons in terms of the Nambu-Jona-Lasinio (NJL) model, an effective theory of QCD.

We regard hadrons as ideal cylinders with a radius R, and impose the linear boundary condition for the quark field. When the pion field outside tubes is neglected, the effective action is simply separated into the radial and longitudinal parts, [5] so that the numerical calculation becomes possible for it. Figure 1 shows the numerical result for the dynamical quark mass in the flux tube with the cylinder radius R, when a color-electromagnetic (color-EM) field is assumed to be absent. The dynamical quark mass is found to be reduced by the finite-size effect, and the chiral-symmetry restoration takes place for the small radius $R \leq 0.45$ fm.

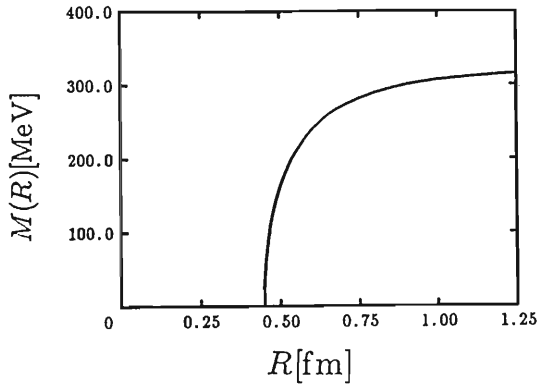

Fig.1. The dynamical quark mass as a function of the cylinder radius R, when the color-EM field is assumed to be absent. Calculation is done in the chiral limit.

We also investigate our subject in the presence of the external color-EM field. Both a color-electric field and the finite-size effect contribute the chiral-symmetry restoration additively. Hence our previous result on the chiral-symmetry restoration inside hadrons [1] is not qualitatively changed even if we include the finite-size effect of hadronic tubes, although the critical field strength $\mathcal{E}_{\rm cr}$ is reduced.

Finally we make a physical interpretation of our results. The spontaneous breakdown of chiral symmetry (χSB) is induced by the strong coupling in the low- momentum region because of the asymptotic freedom in QCD. This mechanism is effectively included in the NJL model: χSB is induced by a strong effective interaction between quarks in the low-momentum region below the ultraviolet cutoff. When the system is confined in a tube with the cylinder radius R, long wave components of quarks are forbidden in the direction vertical to the cylinder axis, so that an infrared cutoff of the order R^{-1} appears in the corresponding momentum space of the quark field. Such reduction of the strong-coupling region would weaken the nonperturbative effects on χSB, and lead to the chiral-symmetry restoration for a small R.

References

1) H. Suganuma and T. Tatsumi: *Phys. Lett.*, **B269**, 371 (1991).
2) C. Martin and D. Vautherin: *Phys. Rev.*, **D38**, 3593 (1988); *Phys. Rev.*, **D40**, 1667 (1989).
3) R. C. Wang and C. Y. Wong: *Phys. Rev.*, **D38**, 348 (1988).
4) Th. Schönfeld, A. Schäfer, B. Müller, K. Sailer, J. Reinhardt , and W. Greiner: *Phys. Lett.*, **B247**, 5 (1990).
5) H. P. Pavel and D. M. Brink: *Z. Phys.*, **C51**, 119 (1990).

RIKEN Accel. Prog. Rep. 26 (1992)

III-1-48. Chiral Solitons at Finite Temperatures

H. Suganuma

[Chiral solitons, properties of baryons at finite temperatures.]

We study properties of baryons at finite temperatures using the Skyrme soliton model.[1] The Skyrme model, an effective theory of the pion field, seems to be one of the most suitable candidates for this subject because the lightest hadrons *i.e.* pions play an important role at low temperatures. A baryon is described as a soliton of mesons in this model, so that the thermal effect for the baryons is brought by the thermal fluctuation of mesons around the soliton.

By introducing the pion fluctuation ϕ around the static soliton solution, one gets the Lagrangian of ϕ in the presence of the background field of the static soliton.[1] The partition function at finite temperatures is derived from the path integral Z by using the imaginary-time method. One obtains the thermodynamic potential in terms of soliton profile by integrating out the ϕ-field in Z. Since the original Skyrme model is an effective theory up to the four-derivative terms with respect to the derivative expansion, it would be reasonable to drop off the higher-order derivative terms by using the technic of the derivative expansion.[2]

After some complicated calculation, a finite expression of the thermodynamic potential Ω is obtained besides the temperature-independent irrelevant constant. It is noted that the symmetric four-derivative term appears in Ω at finite temperatures, however, its coefficient is rather small in comparison with that of the Skyrme term at low temperatures, e.g., $T \lesssim f_\pi$. It is also found for the expression of Ω that the pion decay constant f_π and the Skyrme parameter e seem to be effectively modified as $f_\pi^*(T) = f_\pi[1 - \frac{1}{6}\frac{T^2}{f_\pi^2} - \frac{\pi^2}{45e^2}\frac{T^4}{f_\pi^4}]^{1/2}$, $e^*(T) = e[1 + \frac{\pi^2}{90e^2}\frac{T^4}{f_\pi^4}]^{-1/2}$ at finite temperatures. The effective pion-decay constant $f_\pi^*(T)$ is reduced by the thermal effect, which may be interpreted as the chiral symmetry restoration at high temperatures.[3] On the other hand, only a little reduction is found for the effective Skyrme parameter $e^*(T)$ as long as the temperature is not so high.

One gets the hedgehog-soliton mass M_H at finite temperatures from the thermodynamic potential Ω. Since the nucleon and the delta can be regarded as adiabatically rotational solitons in this model, their masses can be obtained by the collective-coordinate method.[1] The numerical results for the baryon masses are shown in Fig.1. The delta mass M_Δ is largely reduced by the thermal effect. While, less modification is found for the masses of the hedgehog soliton and the nucleon. Then the mass difference between the nucleon and the delta becomes smaller at finite temperatures. One also finds that the size of hedgehog soliton is monotonously increased by the thermal effect. Such tendencies on the baryon properties at finite temperatures can be easily understood in terms of the behavior of $f_\pi^*(T)$ and $e^*(T)$.

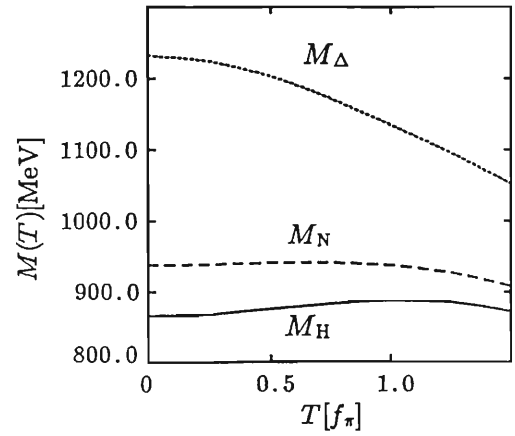

Fig.1. Temperature dependence of baryon masses for the delta, the nucleon and the hedgehog soliton.

In the solid state physics, it is known that the thermal effect reduces the soliton mass and enlarges the soliton size in the 1+1 dimensional sine-Gordon system.[4] Hence qualitatively similar features are found on the mass and size at finite temperatures between the chiral soliton and the sine-Gordon soliton.

References

1) For the recent review, *Prog. Theor. Phys. Supplement*, **109**, 1 (1992).
2) I. J. R. Aitchison and C. M. Fraser: *Phys. Rev.*, **D31**, 2605 (1985).
3) J. Gasser and H. Leutwyler: *Nucl. Phys.*, **B307**, 763 (1988).
4) K.Maki and H.Takayama: *Phys. Rev.*, **B20**, 3223 (1979).

RIKEN Accel. Prog. Rep. 26 (1992)

III-1-49. Chiral-Symmetry Restoration in a Strong Color-Electric Field and Hadron Structure

H. Suganuma and T. Tatsumi*

[Chiral symmetry restoration, hadron structure.]

Recently much effort has been devoted in order to understand hadrons and nonperturbative QCD vacuum in terms of quarks and gluons. As is well-known, the spontaneous breaking of chiral symmetry is one of the most important features in the low-energy realm of QCD. Commonly valence quarks or antiquarks are often introduced and play an important role in analyses of the hadron structure. Here we study how the color-electromagnetic field formed by valence quarks affects the properties of QCD vacuum inside hadrons in terms of the manifestation of chiral symmetry. [1,2]

We study our subject based on the Nambu-Jona-Lasinio model, an effective model of QCD. For the covariantly constant color-electromagnetic field, we can derive the compact formula of the effective potential. Its real part denotes the energy of vacuum with each value of $\langle\bar{q}q\rangle$, the order parameter of chiral symmetry breaking. We can derive the Dyson equation for the dynamical quark mass from the minimum condition for the real part of effective potential. On the other hand, its imaginary part denotes the Schwinger formula for the q-$\bar{q}$ pair creation.

We solve the Dyson equation in the presence of the external color-electric field that valence quarks would form, and obtain the dynamical quark mass as the function of $\mathcal{E} \equiv \sqrt{6\mathrm{tr}_c(gE)^2}$ as shown in Fig.1. The lower two lines denote the dynamical u,d-quark mass in Fig.1 : the solid line corresponds to the empirical case with a non-vanishing current quark mass, while the broken line corresponds to the chiral limit. The upper line denotes the dynamical s-quark mass. One finds that the chiral-symmetry restoration occurs by a strong *color-electric* field, and the rapid reduction of the dynamical (u,d-)quark mass is found around the critical field strength, $\mathcal{E}_{\mathrm{cr}} \simeq 4\mathrm{GeV/fm}$. [1,2] As for the s-quark mass, only a moderate decrease can be seen in comparison with the u,d-quark mass. [2]

Based on the color-electric flux-tube picture for hadrons, [3] one can evaluate the color-electric field strength as $\mathcal{E} = 5.3 \sim 6\mathrm{GeV/fm}(> \mathcal{E}_{\mathrm{cr}})$ inside hadrons from the empirical value of the Regge slope (see the shaded region in Fig.1). Therefore our result suggests that the chiral-symmetry restoration would take place inside the flux tube due to the strong color-electric field formed by valence quarks. [1,2] It is interesting that this result may lead to the chiral bag picture for hadrons: the chirally-symmetric phase exists inside the flux tube, while chiral symmetry remains broken outside the flux tube where color fields are absent.

In order to get deeper insight of our results, it is also desirable to refer different approach such as lattice QCD simulations. In recent years, an Austrian group has found the reduction of the quark condensate $\langle\bar{q}q\rangle$ around valence quarks or the color sources by using lattice QCD simulations, [4] which agrees with our results qualitatively.

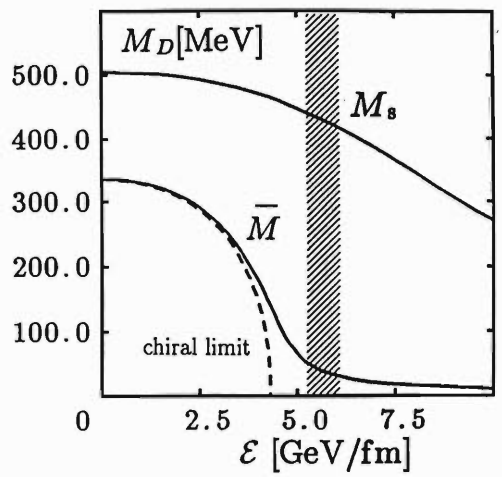

Fig.1. The dynamical quark masses as functions of $\mathcal{E}$ (magnitude of the color-electric field).

References

1) H. Suganuma and T. Tatsumi: *Phys. Lett.*, **B269**, 371 (1991).
2) H. Suganuma and T. Tatsumi: preprint KUNS, 1091, p.1 (1991).
3) A. Casher, H. Neuberger and S. Nussinov: *Phys. Rev.*, **D20**, 179 (1979).
4) W. Bürger, M. Faber, W. Feilmair, and H. Markum: *Nucl. Phys.*, **A525**, 581c (1991).

* Department of Physics, Kyoto Univ.

III-1-50. Large-scale Numerical Simulation of the Three-state Potts Model†

S. Ohta

[Potts model, quantum chromodynamics, parallel computer.]

Lattice numerical calculations of pure-gauge quantum chromodynamics (QCD) revealed that at a finite temperature the system undergoes a first-order phase transition from a low-temperature, disordered, and color-confining phase to a high-temperature, ordered, and non-confining phase. The phase transition is driven by the global Z_3 symmetry which manifests itself through the Polyakov line order parameter. The transition is weak in the sense the latent heat is small and the Polyakov line correlation length grows. The existence of a first-order phase transition and its weakness seem common among the systems with the global Z_3 symmetry such as the three-state Potts model. It is not yet understood, however, why the phase transitions are so weak. The author investigated this problem through his numerical simulation of the three-state Potts model on three dimensional simple cubic lattices.[1)]

Earlier numerical simulations of the model established a first-order phase transition separating a low-temperature ordered phase and a high-temperature disordered phase. It is considered weak because the latent heat is small. However, the small volumes caused frequent flip-flop transitions between the two phases and it was hard to tell in which the system resides at a given instant. Consequently, the natures of the individual phases could not be studied, nor the reason why the phase transition is so weak. The author overcame this difficulty by the vastly larger volume of 128^3 that became feasible by a parallel computer AP1000 of Fujitsu laboratory.[2)]

The two-point correlation function, $C_{ij}(r)$, defined as the probability to find a pair of spin i and j separated by the distance r, is numerically calculated in each of the two phases around the phase transition. In both of the phases the correlations are found to decay exponentially in Yukawa form as the distance r increases toward infinity (Fig. 1). Such behavior was known for the disordered phase but not for the ordered phase. The correlations between the like spins are always attractive and those between the unlike spins are usually repulsive with one exception. Accordingly, clustering of like spins is observed in both phases, with the sizes consistent with the correlation length of several lattice spacings.

The exception is the correlation between the two different non-favored spins in the ordered phase: it

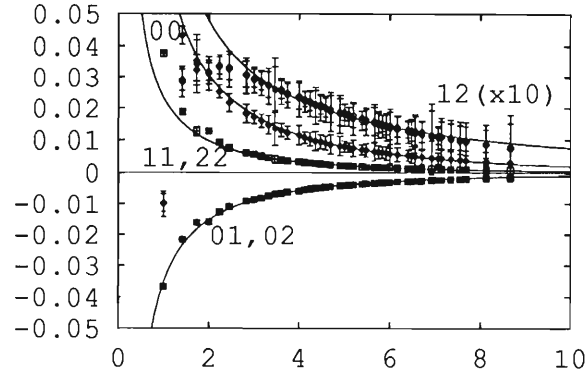

Fig. 1. Correlations in the ordered phase near the transition. The curves are the best fits to Yukawa form for ranges above 3. The favored spin is 0.

is short-range repulsive but long-range attractive. The range of attraction appears much longer, at a few ten lattice spacings, than the others. Such a long-range attraction between the two different non-favored spins is likely to cause instability of the ordered phase. In the corresponding spin distribution one finds that clusters of the two different non-favored spins appear within neighborhood of each other. It should be noted that this is an efficient way of maintaining the global Z_3 symmetry, and is probably a direct consequence of the symmetry.[3)] It is also found that such clusters do not have smooth surfaces, but have complex concave boundaries. Thus the neighborhood of such a cluster of clusters of the non-favored spins can be considered as an island of the disordered-phase left in the sea of the ordered phase. Such admixture of the disordered domains into the ordered phase gives a natural explanation of why the phase transition is so weak.

References

1) S. Ohta: in Proc. Int'l Symp. "Lattice '92," Amsterdam, the Netherlands, September 15-19, 1992, Nucl. Phys. B (Proc. Suppl.), to be published, and references cited there in.
2) S. Ohta: in Proc. Int'l Symp. "Computing in High Energy Physics '92," Annecy, France, September 21-25, 1992, to be published.
3) S. Ohta: in preparation.

†This work was supported in part by Parallel Computing Research Facility, Fujitsu Laboratory, who provided computing time on their AP1000 parallel computers.

2. Atomic and Solid-State Physics

RIKEN Accel. Prog. Rep. 26 (1992)

III-2-1. Production of Inner-Shell Vacancies in Energetic Ar Ions Penetrating Solid Targets

Y. Zou, Y. Awaya, T. Kambara, Y. Kanai, M. Oura, Y. Nakai, K. Ando, A. Hitachi, and S. Kravis

Inner-shell vacancy production in heavy-ion atom collisions is expected to be caused by the direct Coulomb ionization or electron promotion via quasi-molecular orbits. Generally the Coulomb process is dominant when the atomic numbers of the collision partners are much different or the collision velocity v_p is higher than the orbital velocity of the active electron v_e. On the other hand, the electron promotion is dominant when v_p is smaller than v_e.

We studied the K-shell vacancy production processes of Ar ions by collisions with various atoms in a velocity region between those of the direct Coulomb and the electron promotion processes ($v_p/v_e \sim 1$). We have made systematic measurements of the intensity ratio between the K_α-X rays from double K-vacancies (hypersatellites) and those from single K-vacancies of projectile Ar ions excited by penetration of solid targets. The ratio reflects the magnitude of K-shell vacancy production probability. The target atomic number Z_t ranged from 6 to 73, and the total kinetic energy of the Ar ions ranged from 43 to 300 MeV, which corresponds to $0.43 \leq v_p/v_e \leq 1.13$.

We used an Ar^{8+} beam from the RILAC in experiments at 43, 52, 65, 80.3, and 95 MeV,[1] and Ar^{5+} from the RIKEN Ring Cyclotron at 300 MeV. The beam was directed on various metallic foil targets. The K_α- X rays emitted from the beam incident side were measured by a broad-range crystal spectrometer.[2]

Figure 1 shows the intensity ratio at 43 and 300 MeV as functions of Z_t. The ratio has oscillatory behavior with two maxima at each incident energy. The positions of the maxima change with the incident energy: At lower energies, they are located at Z_t=22 - 26 and Z_t=50 - 60, and at energies higher than 80 MeV, they are located at Z_t=26 - 30 and Z_t=60 - 70.

At collision energies higher than 80 MeV, the maxima in the ratio are reproduced by the calculation with Born approximations. At lower energies the maxima shifts to small Z_t, and at

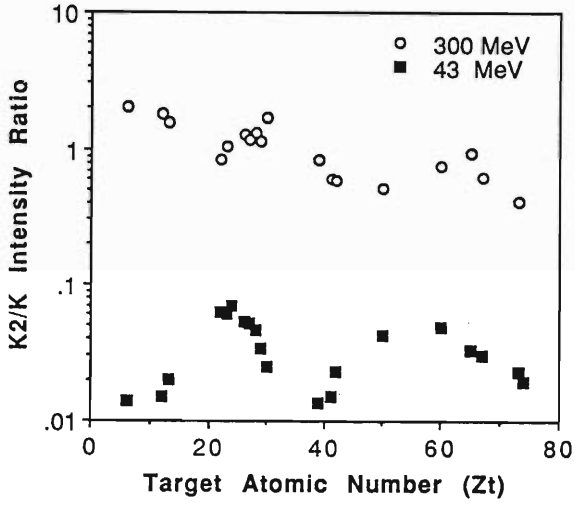

Fig. 1. K_α-X ray intensity ratio of transitions from double K-vacancies to those from single K-vacancy of Ar ions in various targets with atomic number Z_t. The energy of Ar ions are 300 MeV (upper) and 43 MeV (lower).

40 MeV they nearly correspond to the enhancement of the K-vacancy production by electron promotion process. The results show a gradual change of relative importance from the electron promotion to the Coulomb process according to the increase of the collision energy. In the intermediate energy region, the K-vacancy production cross section increases with the collision velocity, but the increase rate is much different among the targets.

A theoretical work to treat the K-shell vacancy production in this velocity region is reported elsewhere by Naitoh *et al.*[3]

References

1) Y. Zou, T. Kambara, Y. Kanai, Y. Awaya, K. Ando, M. Ohura, A. Hitachi, and S. Kravis: *RIKEN Accel. Prog. Rep.*, **25**, 69 (1991).

2) A. Hitachi, H. Kumagai, and Y. Awaya: *Nucl. Instrum. Methods* **195**, 631 (1982).

3) Y. Naitoh, Y. Zou, T. Kambara, Y. Awaya and K. Fujima: This report, p.80.

III-2-2. Measurement of RER X Rays from 0.8 MeV/nucleon Ar Ions Excited by a Foil

M.Oura, T.Kambara, Y.Kanai, S.D.Kravis, Y.Zou,
Y.Awaya, and J.Pálinkás

We have previously reported a measurement of the KL^3 RER (Radiative Electron Rearrangement) x rays from 0.8MeV/nucleon Ar ions excited by a target foil.[1] The KL^3 RER process is a correlated two-electron transition[2-4] and x rays are produced by an electron rearrangement from an initial configuration $1s^22s^22p^3$ to a final one $1s^22s^02p^4$, where superscripts are the number of electrons in each subshell. Here we report an analysis of the data. The values of the intensity ratio R3 between the KL^3 RER and the $K\alpha L^3$ satellite were estimated by a least-squares fitting procedure with Voigt functions. The extracted values are shown in table 1 for C and Al foil targets, where those are compared with the theoretical values.[4] The present intensity ratios are smaller than the typical experimental values obtained from the target atom excitation[3,4] and those are smaller than theory by a factor of 16.6 for the C target and 4.8 for the Al target.

Two 2s electrons are necessary for the RER processes. The reason for the weak KL^3 RER intensity in projectile ions can be explained by a large population of 2s vacancies in the ions with a K-vacancy since the value of intensity ratio is proportional to the square of the 2s-2p mixing coefficient in the final state.[3,4]

The projectile Ar ions in a target material quickly reach an equilibrium charge state distribution through successive outer-shell collisions. The equilibrium mean charge state of 0.8MeV/u Ar ions in the carbon foil used was about 11.5 and the mean number of the M-shell electrons is less than unity.[5] It means that the mean number of the L-electrons of Ar ions in target is about 4. If these electrons are distributed statistically among the L-subshells, the probability having two 2s electrons is about 0.2 and it results in the small intensity (by a factor of 5) of the RER transition in projectile Ar ions relative to the RER intensity via the target atom excitation. The measurement of the RER x rays gives us information about the 2s-2p electronic configuration of the initial state, therefore we can expect that it can be a tool for study of the electronic configuration of L-subshells of fast ions in a medium. Further experiments are in progress.

Table 1. Intensity ratio (KL^3 RER/$K\alpha L^3$) $R3_{exp.}$.

Projectile	Target	Origin of KL^3 RER	$R3_{exp.}$	$(R3_{theor.}/R3_{exp.})$
Ar	C	Projectile	$(7.5 \pm 2.5) \times 10^{-4}$ *	16.6#
Ar	Al		$(2.6 \pm 0.8) \times 10^{-3}$ *	4.8#
C,N	Mg	Target	$(1.34 \pm 0.33) \times 10^{-2}$ $	0.96
H~O	Al		$(8.5 \pm 2.1) \times 10^{-3}$ $	1.43
H~Cl	Si		$(1.37 \pm 0.18) \times 10^{-2}$ $	0.85

* Present data.

$ Data from Ref.3.

$(R3_{theor.})$ value was for Ar ions without M-shell electrons.

References

1) M. Ohura *et al.*: *RIKEN Accel. Prog. Rep.*, **25**, 70 (1991).
2) K.A. Jamison *et al.*: *J. Phys.*, **B8**, L458 (1975).
3) K.A. Jamison *et al.*: *Phys. Rev.*, **A14**, 937 (1976).
4) T. Åberg *et al.*: *Phys. Rev.*, **A15**, 172 (1977).
5) T. Mizogawa *et al.*: *Phys. Rev.*, **A42**, 1275 (1990).

III-2-3. Measurements of RER X Rays from 37 MeV/nucleon Ar Ions Excited by a Carbon Foil

T. Kambara, Y. Awaya, Y. Kanai, M. Oura, S. Kravis, and Y. Zou

The radiative electron rearrangement (RER) process is described as a radiative transition with a simultaneous rearrangement of two electrons.[1] We have studied the RER process in fast, few electron systems through a high-resolution X-ray measurement.

In many cases, RER is much weaker than the corresponding K_α satellite transitions, and the relative intensity of the RER to the satellite transition yields information on the configuration mixing in the excited state. However, a Li-like $1s2s^2$ state is a special case in which radiative decays are limited through the RER process. If one 1s electron is ionized from a Be-like ion in a ground state ($1s^22s^2$) by a collision and the other electron configuration is not changed, the excited state has a configuration of $1s2s^2$ which decays only through the RER to the $1s^22p$ state . Therefore we can estimate the fraction of the $1s2s^2$ state among the 1s-vacancy states by measurements of RER and K_α-X rays.

In the experiment, a beam of Ar^{14+} (Be-like) at 36.6 MeV/nucleon from the Ring Cyclotron impinged on C foil targets with thicknesses of 10, 22, 39, and 85 $\mu g/cm^2$. Since the energy of the RER X-rays in a Li-like Ar ion is about 3.04 keV which is lower than the K-X rays of the Be-like ions by only 30 eV, the X rays were measured by a broad-range crystal spectrometer. Besides the X-ray spectra, we measured the charge state distribution of the ions which passed the same targets and compared the target thickness dependence of intensity of each observed X-ray line with that of the charge state distribution. The charge state distribution of the ions was measured with a magnet and a position sensitive PPAC (Parallel Plate Avalanche Counter) behind the target.

Figure 1 shows an X-ray spectrum for the 10 $\mu g/cm^2$ target. A peak at around 3.11 keV is from $K_\alpha$satellite transitions from $1s2s^m2p^n$ to $1s^22s^m2p^{n-1}$ configurations in Ar^{15+} (Li-like; $m=1, n=1$ or $m=0, n=2$) and Ar^{16+} (He-like; $m=0, n=1$) ions, and a shoulder at about 3.08 keV is from those in Ar^{14+} (Be-like; $m+n=3, n\geq 1$) ions. Some weaker peaks around 3.3 keV are from the states with double 1s vacancies. A small peak appears at about 3.04 keV which agrees with the expected RER X-ray energy, and the intensity of the peak is smaller than a few % of that of the satellite lines of Ar^{15+}. However, it is also possible that the peak is from $K_\alpha$satellite transitions in Ar^{14+} since some transitions from the triplet or quintet states of Ar^{14+} have energies close to this region and the intensity of the peak decreases with the target thickness in a similar way to the fraction of Ar^{14+}. Therefore, from this measurement, we cannot tell whether this peak is the RER X-rays from the Li-like Ar^{15+} ions or low-energy satellite transitions of Ar^{14+}. Even if the peak is the RER-X rays, the small intensity means that Ar^{15+} ions after the target have only a small fraction of the configuration $1s2s^2$ among the 1s-vacancy states.

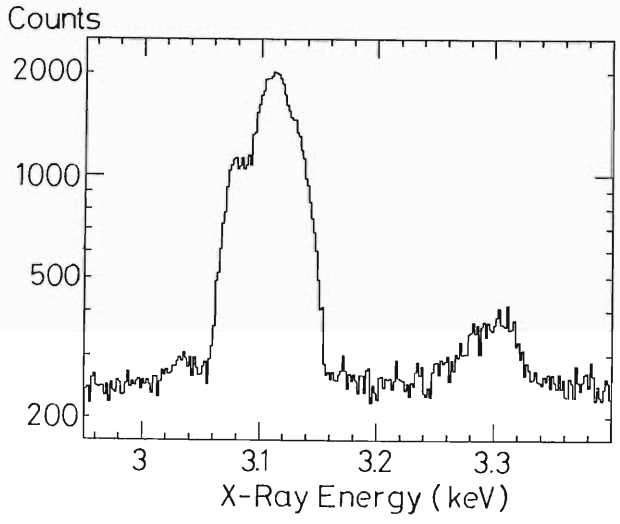

Fig. 1. Spectrum of K-X rays of Ar ions penetrating a 10 $\mu g/cm^2$ thick carbon foil.

References

1) M. Ohura, T. Kambara, Y. Kanai, S. D. Kravis, J. Pálinkás, and Y. Awaya: *RIKEN Accel. Prog. Rep.*, **25**, 70 (1991).

III-2-4. Coincident Charge States Distributions of Recoil and Scattered Ions in 26 MeV Ne–Ne Collisions

S. Lencinas, T. Kambara, S. Kravis, Y. Kanai, M. Oura,
Y. Awaya, M. Terasawa, and H. Schmidt-Böcking

Differential cross sections for the production of highly charged recoil-ions ($d\sigma(\theta, q_i^P, q_o^P, q^R)/d\theta$) have been measured for collisions of 26 MeV $Ne^{4+,7+}$ with Ne and He targets using a coincidence technique, where θ is the projectile laboratory scattering angle, q_i^P the incoming projectile charge state, q_o^P the outgoing projectile charge state, and q^R the recoil ion charge state. q_o ranges between 3 and 6 and q^R between 1 and 8. Ionisation probabilities $P(\theta)$ coincident with different recoil ion charge states were extracted for the different reaction channels like single, double and triple electron loss as well as single electron capture of the projectile.

A Ne^{4+} beam from the RILAC was collimated over a total length of 4 m to obtain an angular resolution $\Delta\theta \leq 0.1$ mrad. Having passed through a differentially pumped gas cell the projectiles were charge-state analysed and after a flight path of 7 m detected with a position sensitive PPAC (Parallel Plate Avalanche Counter). The recoil ions produced in the gas cell were extracted with an electric field, drifted in a field free region, and were detected with a channeltron detector. A standard coincidence technique was used between the signals of the PPAC and the recoil ion detector. The different recoil ion charge states were separated in the time-of-flight spectrum.

The $P(\theta)$ for different reaction channels were obtained by dividing the specific single differential cross sections by the total elastic scattering cross section. The scattering angle corresponds to an impact parameter region between $5{\cdot}10^{-2}$ and $5{\cdot}10^{-1}$ au. This covers the relevant impact parameter range for Ne K-shell ionisation accompanied by multiple ionisation of the L-shell.

Figure 1 shows the obtained $[P(\theta)]_{qR}^{qo}$ for different recoil Ne charge states and single electron loss of the projectile. The probabilities show clearly the different impact parameter contributions to the different Ne recoil ion charge states. At large impact parameters ($b > 0.5$ au) the low charged recoils dominate the charge state distribution. The principal mechanism in this range is the direct ionisation by the projectile. With decreasing impact parameter, higher charge states are produced. In this case, K-hole production is enhanced *via* Auger decay to the observed recoil-ion charge state.[1)]

Screenings of the projectile charge was investigated by changing the initial projectile charge state. For the single capture channel, Fig. 2 shows the target ionisation probabilities for $Ne^{4+,7+}$ as a projectile. At small scattering angles ($\theta \leq 0.2$ mrad) an increase of the ionisation probability by a factor of 30 is observed for Ne^{7+} projectiles and high recoil-ion charge states, while in the large scattering angle range ($\theta \geq 0.5$ mrad, $b \leq 0.1$ au.) the appreciable difference vanishes within the error bars.

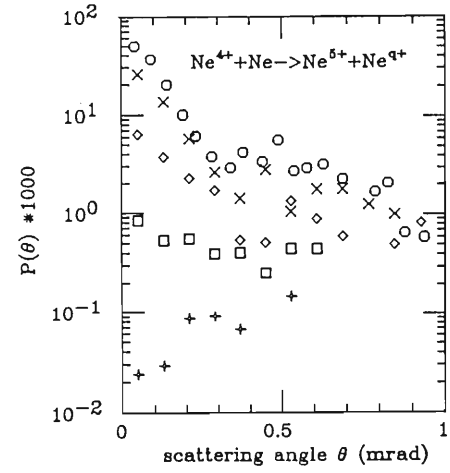

Fig. 1. Target ionisation probabilities $[P(\theta)]_{qR}^{qo}$ for different recoil Ne charge states. Symbols: ∘ Ne^{2+}, × Ne^{3+}, ◇ Ne^{4+}, □ Ne^{5+}, and + Ne^{6+}

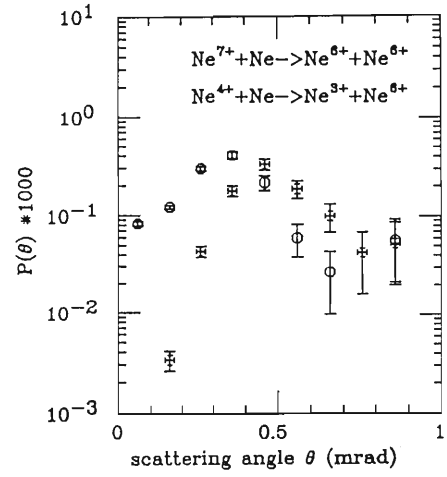

Fig. 2. Comparison between the ionisation probabilities by Ne^{4+} and Ne^{7+} as projectile for the single capture channel. Symbols: ∘ Ne^{7+} and + Ne^{4+} projectile.

References

1) H. Sharabati, K. Bethge, J. Ullrich, R. Dörner R. E. Olson, V. Dangendorf, R. Koch, and H. Schmidt-Böcking: *J. Phys. B*, **23**, 2957 (1990).

III-2-5. Multiply Charged Ions Produced from Gaseous and Condensed CO Targets under Energetic Ion Impact

H. Tawara, T. Tonuma, H. Kumagai, and T. Matsuo

Various secondary (recoil) ions have been produced under the 1.5 MeV/amu Ar^{13+} ion impact on condensed CO target using an apparatus already described.[1] A typical mass/charge spectrum of ions from a condensed CO target is shown in Fig.1(B), together with that from gaseous CO targets[2] (Fig.1(A)). In these spectra we can see the following features :

a) In gaseous targets, the parent CO^+ ion yields are larger by an order of magnitude compared with dissociation product C^+ ion yields, whereas both are comparable in condensed targets.
b) In condensed targets, C^+ ion yields are an order of magnitude larger than O^+ ion yields. Meanwhile, they are roughly equal in gaseous targets.
c) In condensed targets O^+ and O_2^+ ion yields are smaller compared with C^+ ion yields.

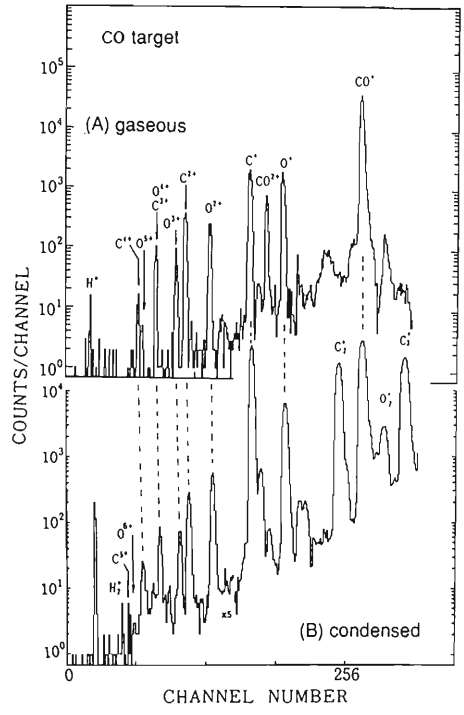

Fig.1. Mass/charge spectra of multiply charged secondary ions from (A) gaseous and (B) condensed CO targets.

d) Doubly charged parent molecular CO^{2+} ion yields are very small (10^{-3} of CO^+) in condensed targets, whereas they are about 4 % in gaseous targets.
e) Multiply charged C^{i+} ($i \geq 5$) and O^{i+} ($i \geq 6$) ion yields are observed in condensed and gaseous targets. It is noted that intensity ratios of the neighboring charge (i+1/i) for high i are roughly the same for both gaseous and condensed targets.
f) In condensed targets, cluster C_2^+ and C_3^+ ion yields are roughly comparable to those of C^+ ions (see Fig.1(B)). On the other hand, no cluster ion is observed in gaseous targets.

These features in condensed molecule targets can be understood qualitatively in comparison with those in gaseous molecular targets.[3] Namely, multiply charged atomic ions gain large initial kinetic energies which depend on the ion charge states at the time of dissociation of multiply charged molecular ions. Indeed, their kinetic energies are of the order of a few eV-a few tens of eV for ions in the present system[2]. On the other hand, the recoil energy is a few hundreds meV.[4] This difference of the initial kinetic energies results in the observed significant variations.

It is concluded that yields of multiply charged C^{i+} and O^{i+} ions including H- and He-like ions have been found to be much larger in condensed CO gas targets compared with those in condensed rare gas targets such as Ar.

References

1) H.Tawara,T.Tonuma,H.Kumagai, and T.Matsuo:J. Phys. B **25**,L423(1992).
2) T.Matsuo,T.Tonuma,M.Kase,T.Kambara, H.Kumagai, and H.Tawara:Chem.Phys. **121**,93(1988).
3) H.Tawara,T.Tonuma,K.Baba,T.Matsuo, M.Kase,T.Kambara,H.Kumagai, and I. Kohno;Nucl.Instr.Meth.B**23**,203(1987).
4) R.E.Olson,J.Ullrich, and H.Schmidt-Böcking;J.Phys. B **20**,L809(1987).

III-2-6. Measurement of Ejected Electron from Quartet State of $N^{4+**}(1s3l3l')$ Created by $N^{6+} + O_2$ Collisions

T. Negishi, N. Nakamura, S. Kitazawa, M. Nagata, S. Ohtani, T. Takayanagi, K. Wakiya, H. Suzuki, Y. Kanai, T. Kambara, and Y. Awaya

Since the last five years our group has measured ejected electrons from the doubly excited state created by highly charged ion - atom collisions.[1)]

We are now interested in ejected electrons from a multiplet state. In the last year we chose the triplet state of $O^{4+**}(1s^2 3l3l')$, $C^{4+**}(3l3l')$, by using O_2 as the target gas.[2)] And this year we carried out the measurement of electrons ejected by $N^{6+}+H_2$ and $N^{6+}+O_2$ collisions. Collisions with H_2-gas are rather simple system, because a H_2-molecule has two electrons that give a singlet state as the ground state, so that the multiplicity of any incident ion is not changed in the collision process if an incident ion captures both the electrons of a H_2-molecule. In this work, an ejected electron from the excited state $N^{4+**}(1s3l3l')$ is the doublet state in the $N^{6+}+H_2$ collisions, and it is in the $N^{6+}+O_2$ collisions the doublet or the quartet state. Therefore it is expected that we could have some informations of the quartet state of $N^{4+**}(1s3l3l')$ if we compare obtained two spectra.

We measured following prosseses,

$$N^{6+} + H_2 \longrightarrow N^{4+}(1s3l3l') + O_2^{2+}$$
$$\hookrightarrow N^{5+}(1sn''l'') + e$$

$$N^{6+} + O_2 \longrightarrow N^{4+}(1s3l3l') + O_2^{2+}$$
$$\hookrightarrow N^{5+}(1sn''l'') + e.$$

Figures 1 and 2 show examples of the obtained spectra. Incident ions are generated by the ECR Ion Source. Collision energy is 60 keV and observation angle is 0 degree with respect to the incident ion beam. Comparing these two spectra, we can find some different features in Fig.2 from that in Fig. 1. By the N^{6+}- H_2 collision, only doublet states are created. On the other hand, by the N^{6+}- O_2 collision quartet states are also possibly created in addition to doublet states. Therefore we assume that the difference between these two spectra is mainly caused by quartet state of N^{4+}. Unfortunately we could not assign these peaks. For further discussion we need more theoretical calculations.

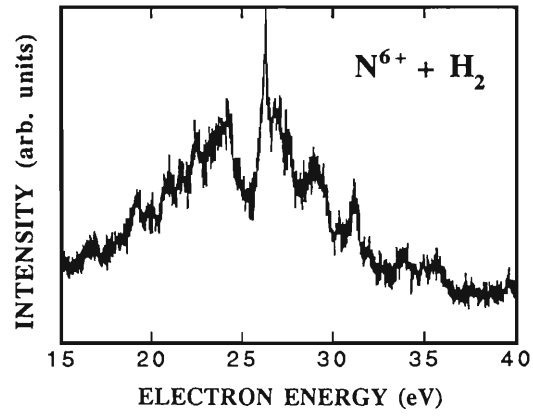

Fig. 1. High-resolution spectrum of ejected electron from the doubly excited N^{4+} (1s3l3l') ions produced in N^{6+}- H_2 collisions.

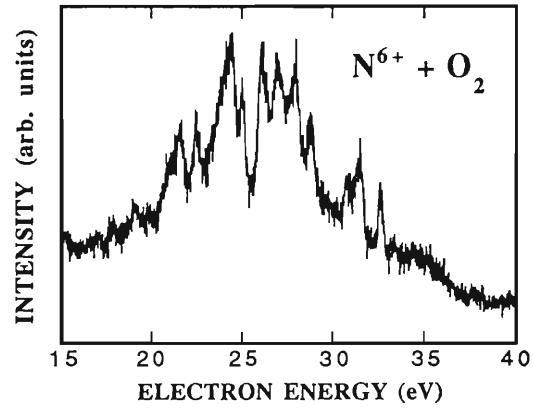

Fig. 2. High-resolution spectrum of ejected electron from the doubly excited N^{4+} (1s3l3l') ions produced in N^{6+} - O_2 collisions.

References

1) H. A. Sakaue, Y. Awaya, A. Danjo, T. Kambara, Y. Kanai, T. Nabeshima, N. Nakamura, S. Ohtani, H. Suzuki, T. Takayanagi, K. Wakiya, I. Yamada, and M. Yoshino: *J. Phys.*, **B24**, 3787 (1990).
2) T. Nabeshima, N. Nakamura, S. Ohtani, T. Takayanagi, K. Wakiya, H. Suzuki, A. Danjo, M. Yoshino, Y. Kanai, T. Kambara, and Y. Awaya: *RIKEN Accel. Prog. Rep.*, **25**, 77 (1991).

III-2-7. Binary Encounter Peaks for 0° Electrons in Collisions of 0.8 MeV/nucleon Bi^{q+} with H_2 and He

Y. Kanai, T. Kambara, M. Oura, Y. Zou, S. Kravis, and Y. Awaya

We present the charge-state dependence on the binary encounter peaks in collisions of 0.8 MeV/nucleon Bi^{q+} on H_2 and He measured at zero degree, in the region of $q_i/Z_1 < 0.4$. In this collision system, the binary encounter peak intensity increases as the charge state increases. The peak energy of the binary encounter peaks is shifted to energies lower than E_b(binary encounter peak energy for free electron targets) and this shift value increases as the charge state increases. The charge state dependence of the intensity is in good agreement with the CTMC calculations by Schultz and Olson.[1] The peak energy shift is explained qualitatively by the Bohr-Lindhard model.[2]

The experiment was performed at RILAC. The beam of $Bi^{10+,14+,32+}$ from RILAC was magnetically analyzed, collimated by two sets of four-jaw slits system and focused to the target gas cell. The target gas cell was 5 cm in length. Single collision conditions were verified experimentally.

Ejected electrons were measured at zero-degree respect to the beam direction. The spectrometer was a tandem type electron spectrometer with two 45° parallel-plate electrostatic analyzers.

In our collision system and the collision energy, the incident charge state dependence of the binary encounter electron intensity was "normal" ; the intensity increases as the incident charge state increases. According to the CTMC results, if we use high enough charge state Bi ions, we can observe the "anomalous"[3,4] charge state dependence(the intensity decreases as the incident charge state increases) and also the change from the "normal" dependence to the "anomalous" dependence.[1] But, we could not use high enough charge states (q_i > 40) to observe this.

The q_i dependence of the energy shift of the binary encounter peaks can be explained by the Bohr-Lindhard model. Details of this model were reported in ref. 2. Here, we describe it briefly. In this model, there is a characteristic distance R_r(the release distance). When the projectile ions come to this distance, target electrons are released from target atoms because of the balance between the forces from the projectile ions and the target atoms. After that, the released electrons collide with the projectile ions as free electrons. Based on this model, the energy shift ΔE_b from E_b is given by

$$\Delta E_b = 54.43 \times (q_i)^{1/2}(I_t/I_0)^{3/4}Z_2^{-1/6} \text{ (eV)}.$$

Here, q_i is the incident charge state, I_t the ionization potential of the target, I_0 the ionization potential of the hydrogen atom, and Z_2 the target atomic number.[2] Pedersen et al. used this formula to evaluate the energy shift for the fully stripped ion case.[2] But, if the R_r is larger than the radius of the clothed(partially stripped) projectile ions, it is applicable for the clothed projectile ion case.[3] Calculated shift values ΔE_b for our collision system are also shown in table 1. In our case, the R_r for H_2 targets are $\sqrt{10}$, $\sqrt{14}$, and $\sqrt{32}$ a.u. for Bi^{10+}, Bi^{14+}, and Bi^{32+}, respectively. The radius of the outer electron orbit of $Bi^{10+,14+,32+}$ ions is 1-0.5 a.u. Our assumption that R_r is larger than the radius of projectile ions is not so bad in our system.

Table 1. Binary encounter peak shift for 0.8 MeV/nucleon Bi ions on H_2 and He target.

	H_2		He	
projectile	peak shift(eV)			
	exp	Bohr-Lindhard	exp	Bohr-Lindhard
Bi^{10+}	136±20	172	216±40	239
Bi^{14+}	132±20	203	212±40	283
Bi^{32+}	220±30	308	300±40	427

References

1) D. R. Schultz and R. E. Olson: *J. Phys.* **B24**, 3409(1991).
2) J. O. P. Pedersen, P. Hvelplund, A. G. Petersen and P. D. Fainstein: *J. Phys.* **B24**, 4001(1991).
3) P. Richard, D. H. Lee, T. J. M. Zouros, J. M. Sanders, and J. L. Shinpaugh: *J. Phys.* **B23**, L213(1990).
4) P. Hvelplund, H. Tawara, K. Komaki, Y. Yamazaki, K. Kuroki, H. Watanabe, K. Kawatsura, M. Sataka, M. Imai, Y. Kanai, T. Kambara, and Y. Awaya: *J. Phys. Soc. Jpn.*, **60**, 3675(1991).

III-2-8. Search for ~MeV Electrons Produced by 95 MeV/nucleon Ar Ions Bombarding C, Ni, Au Foils

Y. Yamazaki, K. Komaki, T. Azuma, K. Kuroki, K. Kawatsura
Y. Kanai, T. Kambara, M. Ohura, and Y. Awaya

The energy and angular distributions of δ-electrons emitted in 95MeV/nucleon Ar^{17+} ions bombarding C, Ni, and Au foils have been measured with RIKEN Ring Cyclotron. As had been reported[1], electrons in the energy range of ~MeV were observed with a surprisingly high cross section (~$10^{-24}cm^2$). In the present report, we discuss a new experiment which has been done to confirm the previous observations. For this purpose, a magnetic sector analyzer was constructed with an electron detection assembly consisting of an MCP followed by a plastic scintillator. Such a combination was adopted to make sure that an electron with the right energy and the right trajectory was detected. Note that the MCP is so thin that ~MeV electrons penetrate the MCP and hit the scintillator at the same time.

Figure 1 shows a new result measured at 0° for 95MeV/nucleon Ar^{17+} bombarding a 100 $\mu g/cm^2$ carbon foil together with the previous data measured with a detector assembly consisting of four-fold surface barrier detectors (SSD), each having a depletion layer of ~500μm. We have again obtained similar results, i.e., the higher energy tail appears in the same energy range with an intensity of the same order of magnitude.

A possible explanation of such a high energy electron is an internal conversion of excited nuclei. However, we have found that the γ-ray production cross section in the same energy range is only ~$10^{-23}cm^2$. As a typical internal conversion coefficient of the present collision system is 10^{-3}~10^{-5}, the contribution of an internal conversion is of minor importance.

A non-relativistic 1st Born calculation was performed to get an order of magnitude estimate of a typical cross section of electron production. It is found that the single differential cross section for 95MeV/nucleon Ar^{18+} bombarding a 1s-electron of carbon foil is more than 7 orders of magnitude smaller than those observed.

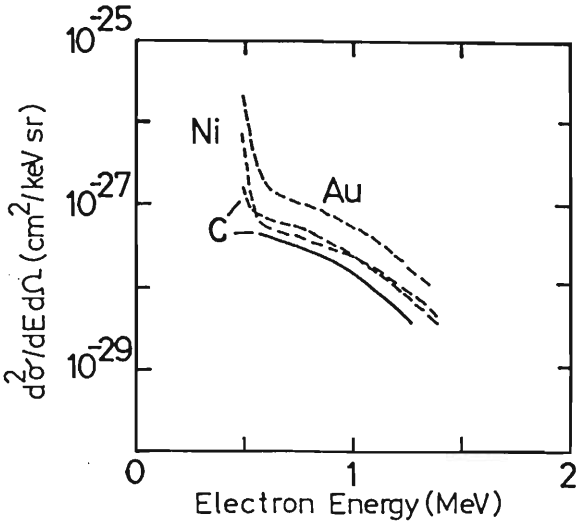

Fig. 1. Doubly differential cross sections $d^2\sigma/dEd\Omega$ of electron production as a function of electron energy measured at 0° with a magnetic sector analyzer (solid line), and at 45° with a four-fold SSD detector[1] (dashed line) for 95MeV/u Ar^{17+}.

Summarizing, we have reconfirmed a strong electron emission in an ~MeV range, which is neither attributable to a usual atomic collision process nor to an internal conversion process. Further experiments are in progress to investigate the origin of the δ-electrons.

References

1) Y.Yamazaki et al.: RIKEN Accel. Prog. Rep., 24, 54 (1990).

III-2-9. Beam–Foil Experiment of Neonlike Iron

K. Ando, Y. Zou, T. Kambara, M. Oura, Y. Nakai, Y. Awaya, and T. Tonuma

We continue the measurements of lifetimes of Ne-like isoelectronic sequence. Following Ti and Cr, we start to measure Ne-like Fe. Before the measurements of decay curves, spectra of Fe ions were taken from 250 Å to 450 Å with the spectral resolution of about 0.5 Å for the acceleration energy of 46, 58, and 73.5 MeV,

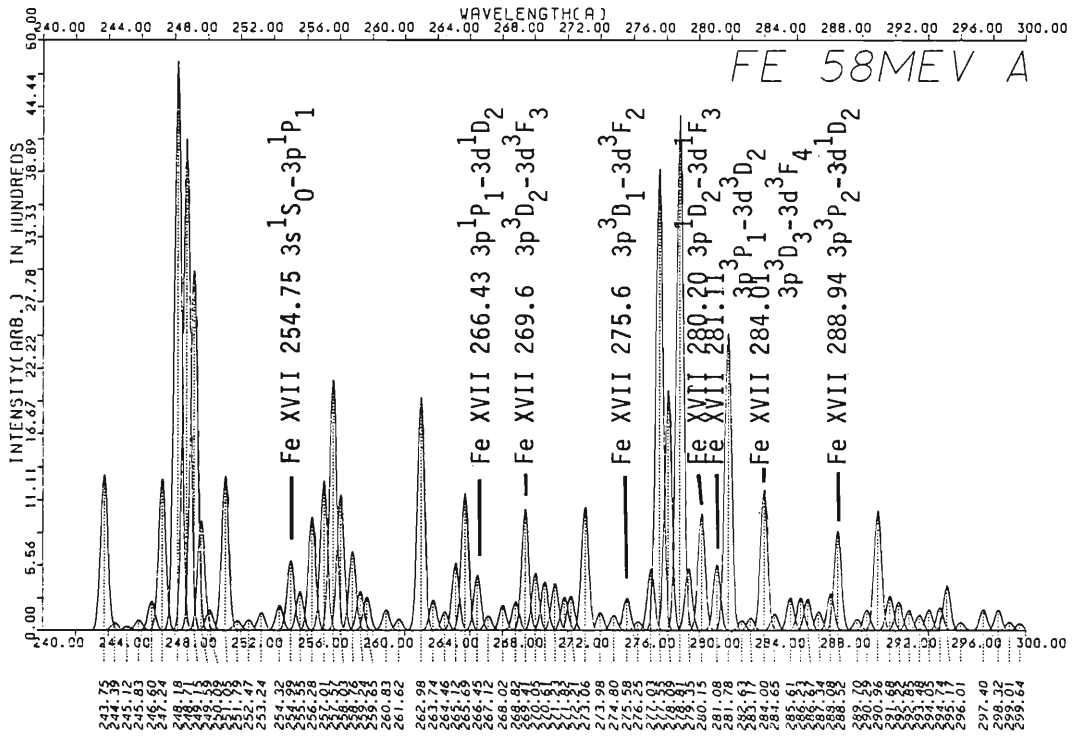

Fig. 1. Part spectrum of Iron ions with identified spectral lines of Fe XVII.

and spectral lines of Ne-like Fe (Fe XVII) were identified according to the reference 1. Intensities of lines of Fe XVII were strong at the acceleration energy of 58 MeV, as estimated from the semi-empirical formula.[2] Observed spectrum is shown in Fig. 1 with the identified spectral lines of Fe XVII.

References

1) J-P. Buchet, M-C. Buchet-Poulizac, A. Denis, J. Desesquelles, M. Druetta, S. Martin and J-F. Wyart: *J. Phys.*, **B20**, 1709 (1987).

2) K. Shima, N. Kuno, M. Yamanouchi and H. Tawara: *At. Data and Nucl. Data Tables*, **51**, 173 (1992).

III-2-10. X-ray Studies on Muon Transfer Reactions from Hydrogen to Helium

K. Ishida, S. Sakamoto,* Y. Watanabe, T. Matsuzaki, and K. Nagamine

Muon transfer reactions from muonic hydrogens to helium nuclei are of practical importance in the muon catalyzed fusion (μCF), since helium atoms are accumulated in a d-t mixture due to the tritium decay as well as the nuclear fusion. In this process, a hydrogen-helium muonic molecule is formed.[1)]

Hμ+ He -> HHeμ -> H + Heμ (H: p, d, or t)

The hydrogen-helium mesomolecule is in an excited state when formed, then is deexcited to a ground state quickly, emitting 6.8 keV X-ray.[2)]

Recently it was theoretically proposed that the excited hydrogen-helium muonic molecule has another decay mode. It may decay into a hydrogen and a muonic helium without emitting an X-ray and the transition energy is dissipated as kinetic energy.[3)] This radiationless decay rate was calculated to be comparable to that of the radiative decay and have strong dependence on the isotopes of hydrogen and helium.

We observed X-rays from $d^4He\mu$, $d^3He\mu$, and $p^4He\mu$ molecules in liquid protium or deuterium where a small admixture of helium was dissolved by charging helium gas into the target cell.[4)] The experiment was carried out at the pulsed decay muon channel of the Meson Science Laboratory of the University of Tokyo, located at KEK. X-rays were observed with a Si(Li) detector. The intensities of X-rays were found to decrease as the nuclei get lighter as in Fig. 1. In Table 1, the measured yields were compared with the calculated yields, where the helium concentrations were estimated from the Henry's law[5)] and the theoretical values of the molecular formation rate[1)] were used.

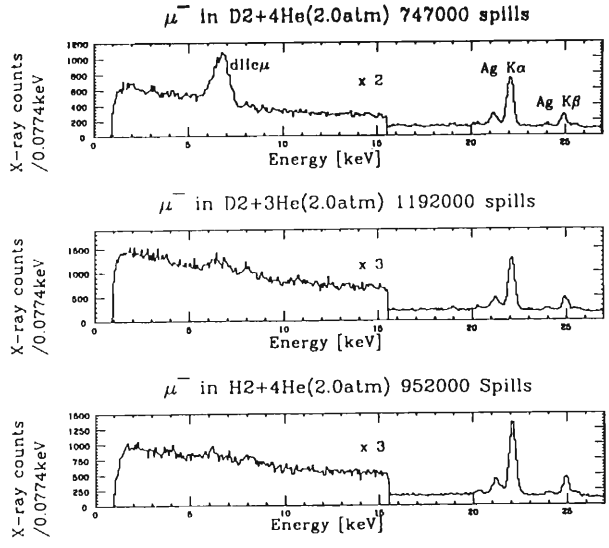

Fig. 1. Observed X-ray energy spectra for the three systems: D_2+^{4}He, D_2+^{3}He, and H_2+^{4}He.

Our measurement was consistent with the calculations which include the radiationless decay mode of hydrogen-helium muonic molecule. The result is still preliminary and we are planning to do further measurements for confirmation.

Table 1. The observed and calculated relative yields of 6.8 keV X-rays normalized to those of $d^4He\mu$.

Muonic Molecule	($d^4He\mu$)	($d^3He\mu$)	($p^4He\mu$)
Helium Atomic Concentration [ppm]	267	191	785
Observed X-ray intensity	1	0.123 ±0.019	0.002 ±0.019
Calculated X-ray intensity (without radiationless decay)	1	0.206	0.035
Calculated X-ray intensity (with radiationless decay)	1	0.096	0.007

References

1) Yu.A. Aristov *et al*: Sov. J. Nucl. Phys., **33**, 564 (1981). A.V. Kravtsov *et al.*: *J. Phys. B: At. Mol. Phys.*,**19**, 2579 (1986).
2) T. Matsuzaki, K. Ishida, K. Nagamine, Y. Hirata and R. Kadono: *Muon Catalyzed Fusion*, **2** (1988) 217.
3) Y. Kino and M. Kamimura: contribution to international workshop on muon catalyzed fusion, Uppsala, Sweden (1992).
4) S. Sakamoto *et al.*: to be appeared in UT-MSL Newsletter, ed. K. Nagamine, No. 11 (1992). K. Ishida *et al.*: contribution to international workshop on muon catalyzed fusion, Uppsala, Sweden (1992).
5) P.C. Souers: Hydrogen Properties for Fusion Energy, University of California Press, Berkeley, p.190 (1986).

* University of Tokyo.

RIKEN Accel. Prog. Rep. 26 (1992)

III-2-11. Measurement of Isotope Shift of Molybdenum by Resonance Ionization Spectroscopy

H. Katsuragawa, T. Minowa,* M. Kubota,* and H. Komatsu**

In a previous report we presented a pulsed heating method for providing atomic beams of metal elements.[1] We have studied the resonance ionization spectroscopy (RIS) of a Mo atomic beam produced by the pulsed heating method. Mo atoms were ionized resonantly by a pulsed dye laser tuned to the z^7P_3 - a^7S_3 transition of Mo.

Because the bandwidth of the pulsed laser (0.6 GHz in HWHM) is rather broad to measure the isotope shift of Mo, we separated each isotope by a mass separator and observed their resonance ionization spectra. The seven isotopes of Mo were separated by a two-stage acceleration TOF mass spectrometer. Figure 1 shows a TOF spectrum of Mo ions. The mass resolving power was about 200, which was sufficient to measure the isotope shift of each Mo isotope.

Observed widths of the RIS spectra of each Mo isotope were 0.8 GHz in HWHM. The line shape of the spectrum was fitted to a gaussian curve. The peak frequency of the spectrum was deduced by the least-squares method. Figure 2 shows the measured isotope shift, where the difference of peak frequency between ^{92}Mo and other isotopes is plotted against the mass number.

The obtained isotope shift of Mo is in good agreement with the result of Aufmuth et al.[2] Although several works on the isotope shift of Mo have been reported, our work is the first one using the resonance ionization spectroscopy. In our work only a 200 μg Mo filament was used to measure the isotope shift of Mo.

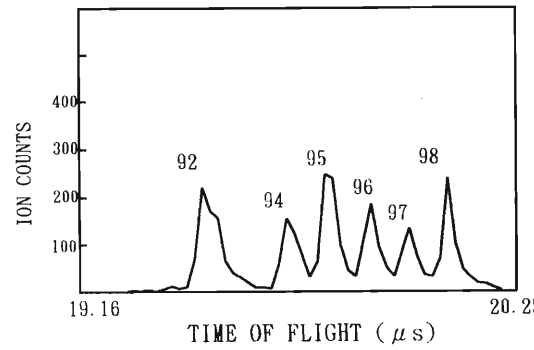

Fig. 1. Time-of-flight spectrum of Mo ion.

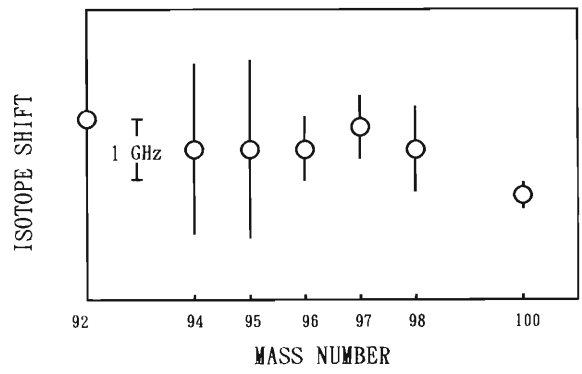

Fig. 2. Measured isotope shift.

References

1) T. Minowa, H. Komatsu, H. Katsuragawa, and T. Inamura: *RIKEN Accel. Prog. Rep.*, **24**, 58 (1990).

2) P. Aufmuth, H. P. Clieves, K. Heilig, A. Steudel, and D. Wendlant: *Z. Physik*, **A285**, 357 (1987).

* Department of Physics, Toho University.
** Tokyo Gakugei University.

III-2-12. Radiative Lifetime Measurement of Heavy Metallic Ions in an RF Trap

Hyperfine Levels in the $^3P_1$ State of Lu^+

Y. Matsuo, H. Maeda, and M. Takami

Ion trap can confine ions for a long period of time and can be combined with laser cooling that reduces the kinetic energy of gaseous atoms and ions. Laser spectroscopy in an ion trap is one of the promising techniques to determine the physical quantities of stable and unstable nuclei by measuring their isotope shifts and hyperfine structures.

We have constructed a radio-frequency (RF) ion trap that directly captures the ions produced by laser ablation[1]. The laser ablation method is useful for producing ions of heavy refractory metals and is also expected to be particularly suitable for generating multiply charged ions and revaporizing implanted atoms containing unstable nuclei.

We here report the lifetime measurement of Lu^+ with the laser ablation-ion trap method by observing laser-induced-fluorescence (LIF).

Linearly polarized light from a pulsed dye laser pumped by a XeCl excimer laser irradiates the central part of trap and the fluorescence emission from trapped ions is focused onto a photo-multiplier. The photo-electron signals are accumulated with a gated integrator or with a transient digitizer synchronized with the dye laser pulse. The former is used for frequency domain measurements and the latter for time-resolved measurements.

Lu^+ ions are excited from the ground $^1S_0$ state to the $^3P_1$ excited state. The spontaneous emission to the $^3D_{1,2}$ metastable states is observed. The laser excitation fluorescence spectra have a triplet structure caused by the hyperfine structure in the $^3P_1$ level. It is possible to record time-resolved LIF signals with a transient digitizer at each peak of those triplet transitions. Lifetimes are extracted by least-square-fitting of the decay curve to a convolution of an exponential decay and the laser pulse profile. Lifetimes of the three hyperfine levels of Lu^+ $^3P_1$ are shown in Table 1. All three levels have almost identical radiative lifetimes. Relatively longer decay times of allowed transitions suggest weaker oscillator strengths of Lu^+ ion compared with alkali-earth metal ions such as Ba^+, for which lifetime of the $^2P_{3/2}$ level, 6.4 ± 0.6 ns, is obtained with this instrument.

Table 1. Radiative lifetimes of the Lu^+ $^3P_1$ excited state

F level	lifetime(ns)
9/2	40.2 (1.3)
7/2	40.6 (1.8)
5/2	40.1 (1.4)

References

1) Y. Matsuo, H. Maeda, and M. Takami: Hyp. Int., in press.

III-2-13. ^{57}Fe Mössbauer Studies of $YBa_2(Cu_{1-x}Fe_x)_4O_8$

T. Okada and K. Asai

A high-T_c superconductor $YBa_2Cu_4O_8$ (so-called 124 compound) with T_c=80 K, has attracted much attention because its oxygen content is thermally stable up to 800°C. It has the similar structure to a 123-superconductor, $YBa_2Cu_3O_7$, but the former has doubly stacked Cu-O chains, or a ribbon, in place of single Cu-O chains of the latter. Recently, ^{57}Fe Mössbauer studies of $YBa_2(Cu_{1-x}Fe_x)_4O_8$ were performed in order to elucidate the mechanism of the superconductivity of the oxide. But there is a controversy on the site occupation of Fe ions in this compound, [1,2] and the magnetic properties of Fe ions, especially their magnetic ordering and its effect on the superconductivity of the host, have not been clarified.

In this report, a ^{57}Fe Mössbauer study of a 124-superconductor $YBa_2(Cu_{1-x}Fe_x)_4O_8$ (x=0.018) at various temperatures is made to elucidate the site occupation of Fe ions in the 124-compound.

A powder sample was synthesized by a solid-state reaction using O_2-HIP technique. The value of T_c determined by the Meissner effect is 48 K. The values of the isomer shift (*IS*) are given relative to Fe metal.

^{57}Fe Mössbauer spectra at 298 and 4.2 K are shown in Fig. 1. As shown in the Fig. 1 (a), the spectrum at 298 K can be analyzed as being composed of two quadrupole doublets denoted by (a) and (b). The values of *IS* indicate that Fe ions in (a) doublet are in trivalent state and those in (b) doublet are in tetravalent state. On lowering temperature below 40 K (not shown in the figure), the Mössbauer spectrum becomes broad and then shows a magnetic splitting. As shown in fig. 1 (b), the spectrum at 4.2 K can be analyzed with two magnetically split sextets denoted by (A) and (B) in the figure. The values of IS and population indicate that sextets (A) and (B) are associated with Fe ions in the doublets (a) and (b), respectively.

The angle between the directions of H_{hf} and the principal axis (z-axis) of the electric field gradient (EFG) in each site can be obtained from the analysis of the spectra at 4.2 K. The principal axis of EFG in Cu(2) sites is different from that in Cu(1) sites. Then we can assign the site occupation of Fe ions in the compound.

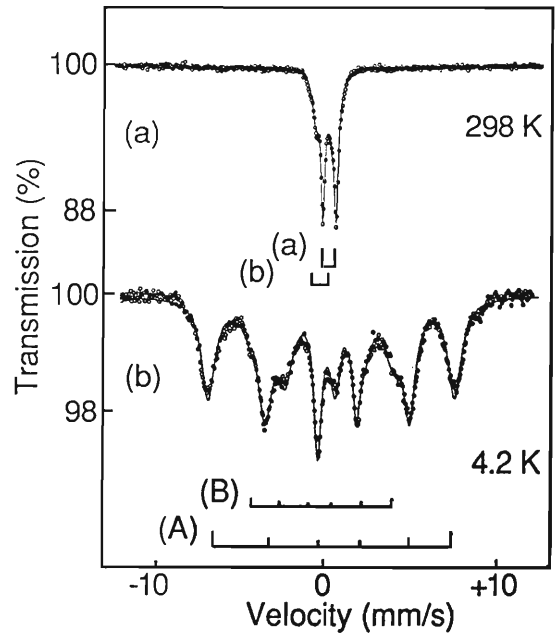

Fig. 1. ^{57}Fe Mössbauer spectra of the specimen with x =0.018 at 298 and 4.2 K.

It is concluded that the major part of Fe ions is in trivalent state and occupies the Cu(2) sites, and the minor is in tetravalent state and occupies the Cu(1) sites. They are magnetically ordered at low temperatures, meaning that the superconductivity of Cu(2) ions and the magnetic order of Fe ions coexist in the Cu(2)-O plane. It should be noted that long range exchange interactions beyond the neighboring Cu(2) ions cause the magnetic order because the content of Fe ions is as low as 0.018.

References

I) Felner et al.: Physica C **185-189** (1991) 1117.
2) P. Boolchand et al.: Phys. Rev. **B 45** (1992) 921.

III-2-14. Muon-Induced Luminescence in KBr

R. Kadono, A. Matsushita, K. Nishiyama,* and K. Nagamine

Ion implantation techniques are of basic importance to the study of condensed matter for applications in which radiative nuclei(including muons) are used as microscopic probes: they greatly facilitate the use of those probes for a wide range of materials without limitations due to surface effects, their solubility, the interaction between probes, and so on. Relatively little is known, however, about the deexcitation process of the implanted energetic probes in solids near or at the final stage when they might be affected by the existence of excitons or defects induced by the probe ions themselves. In most cases it has been commonly assumed that the probe ions are instantaneously degraded to thermal energy in solid specimens and that the associated excitations in crystalline solids are short-lived or dilute enough for such a radiolysis effect to be negligible.

We report on the luminescence induced by positive muons implanted (with 4 MeV) into KBr crystal, which evidences a long-lived (lifetime = 13.3 μs) excited state produced by muon radiolysis.[1] The temperature dependence of the luminescence yield has a strong correlation with the occurrence of "anomalous" muonium center (Mu^I)[2]: both are observed only below 50 K (see Fig. 1a). This correlation strongly suggests that, contrary to the above presumption, the muonium center is perturbed by the muon-induced excitons to cause the Mu^I state. Moreover, the luminescence energy spectrum (see Fig. 1b) and lifetime shifted considerably from those of the intrinsic π-luminescence indicate that the luminescence is associated either with i) an excited state of the self-trapped exciton (STE), e.g. $\sigma_g 2s^3\Sigma^+_u$ (or its equivalent for off-center STE), or ii) a lowest triplet state with modified ionic configuration for the hole, e.g., Br_3^{2-}, of the self-trapped exciton, which are presumably caused by the muonium formation process at its final stage.[3]

The present result also indicates that the missing amplitudes of the μSR signal in other alkali halides at lower temperatures[2] might be attributed to the formation of the Mu^I -like state which undergoes unobservably fast depolarization due to the paramagnetic interaction with these STE's produced by muon radiolysis.

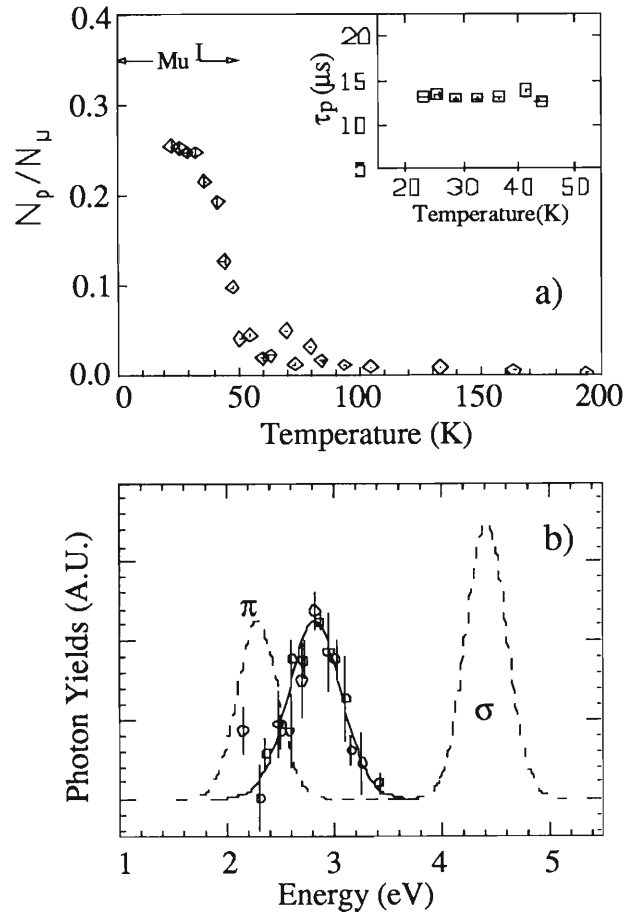

Fig.1. (a) Temperature dependence of luminescence yield and lifetime induced by positive muon implantation in KBr. (b) The energy spectrum of the luminescence at 25 K. The intrinsic luminescence spectrum is shown by a dashed curve where the peak denoted by σ or π is associated with the triplet or singlet STE state.

References

1) R. Kadono, A. Matsushita, and K. Nagamine: *Phys. Rev. Lett.*, **67**, 3689 (1991).
2) Hp. Baumeler *et al.*:*Hyp. Int.*, **32**, 659 (1986).
3) R. Kadono, A. Matsushita, K. Nishiyama, and K. Nagamine:*Phys. Rev. B*, **46**, 8586 (1992).

* Meson Science Laboratory, University of Tokyo

III-2-15. Irradiation-Enhanced Solid Krypton Formation in Kr-Implanted Aluminum

E. Yagi

It has been demonstrated that heavy inert gas atoms (Ar, Kr and Xe) implanted into metals at ambient temperature precipitate into a solid phase (solid inert gas bubbles) at high implantation doses,[1,2] and that they have an epitaxial face-centered cubic (fcc) structure in fcc matrices.

In previous studies we have investigated the nucleation and the growth of bubbles in Kr-implanted aluminum by an ion-channeling method, and observed that at the initial stage of implantation, various types of Kr-vacancy (V) complexes such as KrV_4, KrV_6 and larger ones are formed, and they act as nucleation center for the subsequent bubble formation.[3]

In the present study, in order to elucidate the mechanism of solid bubble formation, the effect of post-implantation irradiation by an analysis beam on the behavior of the Kr-implanted aluminum was investigated by the ion-channeling method and it was observed that the post-implantation irradiation enhanced the formation of solid krypton. The Kr atoms were implanted into an Al single crystal up to a dose of $1x10^{15}Kr/cm^2$ or $6x10^{15}Kr/cm^2$ at room temperature. The channeling analysis was performed for the <100>, <110> and <111> channels with a 1 MeV He beam. In the as-implanted state of the $1x10^{15}Kr/cm^2$-implanted specimen, the <100> and <111> Kr-angular profiles exhibited a shallow dip with the same half width as that of the Al-channeling dip, while the <110> Kr-profile consisted of a central peak and the shallow dip with the same half width as that of the Al-dip. After irradiation with the analysis beam up to doses higher than $4x10^{16}He/cm^2$, including the irradiation dose during the channeling analysis, a channeling dip approximately 1.5-1.8 times broader than the Al-dip became observed in <100>, <110> and <111> Kr-angular profiles. As an example the result on the <100> channel is shown in Fig. 1. This broad dip indicates the formation of solid krypton bubbles; the post-implantation-irradiation enhances the solid krypton formation. The broad dip results from the channeling effect in the solid krypton crystals. From this result, the following mechanism was proposed, In the as-implanted state the $1x10^{15}Kr/cm^2$-implanted specimen has a large number of cavities consisting of many Kr atoms (approximately

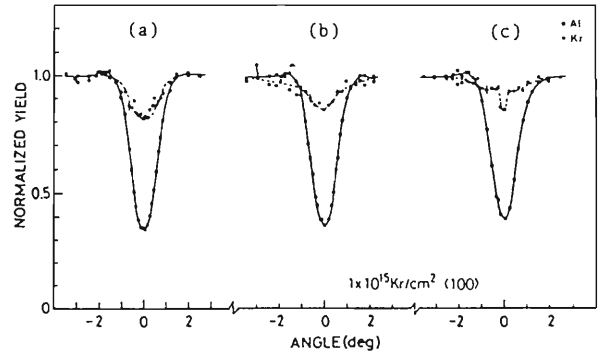

Fig. 1. <!00> channeling angular profiles for the $1x10^{15}Kr/cm^2$-implanted specimen, (a) in the as-implanted state, (b) after irradiation with $5.1x10^{16}He/cm^2$ and (c) $7.1x10^{16}He/cm^2$.

180 Kr atoms on average) and many vacancies. When a large number of cavities are present they act as effective sinks for irradiation-introduced interstitials. The vacancies in the cavities are annihilated by the absorbed interstitials, and, therefore, the ratio of the number of the Kr atoms to that of the vacancies in the cavities, i.e., the pressure of the cavities, increases. In the cavities, in which many Kr atoms are contained and the pressure reaches the threshold value required for solid krypton formation, the Kr atoms precipitate into a solid phase. This model was confirmed by the observation on the $6x10^{15}Kr/cm^2$-implanted specimen. These processes occur also during Kr implantation.

The more detailed description is given in Ref. 4.

References

1) A. vom Felde, J.Fink, Th. Müller-Heinzerling, J, Pflüger, B. Scheerer, G. Linker, and D. Kaletta: Phys. Rev. Lett., **53**, 922 (1984).
2) C. Templier, C. Janouen, J. -P. Rivière, J. Delafond, and J. Grilhé: C. R. Acad. Sci. Paris, **299**, 613 (1984).
3) E. Yagi, I. Hashimoto, and H. Yamaguchi: J. Nucl. Mater., **169**, 158 (1989).
4) E. Yagi: Phys. Rev. Lett., **67**, 3804 (1991).

III-2-16. Analysis of Damage in Both Eu- and Tb-Implanted CaF_2

K. Aono, M. Kumagai,* M. Iwaki, and Y. Aoyagi

We have carried out a study of irradiation and impurity doping effects on CaF_2 in the ion implantation for various kinds of impurities.[1] The luminescence spectra from Eu-implanted CaF_2 were blue and orange. The luminescence spectrum from Tb-implanted CaF_2 was green. The luminescence spectra from CaF_2 implanted with both Eu- and Tb- ions (double implantation) showed mainly three peaks, which were close to those of three primary colors and shifted by -430, -545 and -600 nm. In order to develop white luminescence visible to the naked eye by selecting the fluences of Eu- and Tb- ions, the most suitable condition for the fluences has been investigated. The europium and terbium are rare earth metals, and have similar atomic weights.

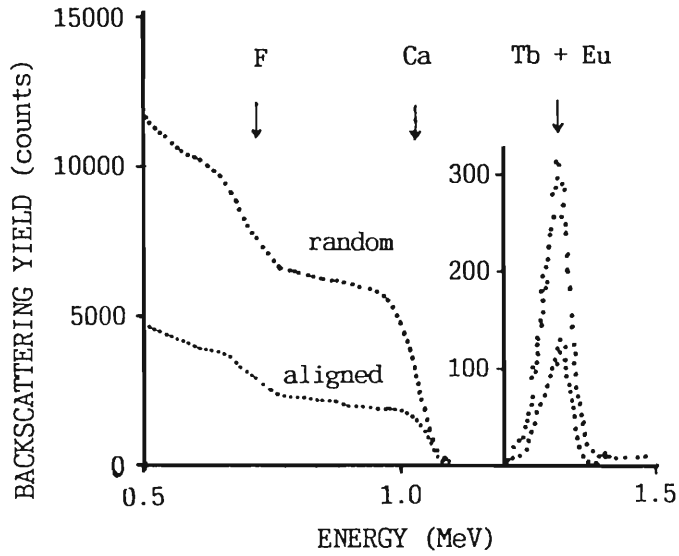

Fig. 1. Random and <111> aligned spectra obtained for CaF_2 implanted with $5x10^{14}$ Tb^+/cm^2 and $5x10^{14}$ Eu^+/cm^2.

In this study, the Eu- and Tb- implantations were performed with fluences of $5x10^{14}$ ions/cm^2 at 100 keV. The <111> single crystal CaF_2 target was in random directions and at room temperature during ion-implantation. Rutherford backscattering spectroscopy was employed for measuring depth profiles and lattice sites of Eu and Tb atoms implanted in CaF_2. Figure 1 shows random and <111> aligned spectra for the specimens implanted with $5x10^{14}$ Tb^+/cm^2 and $5x10^{14}$ Eu^+/cm^2. The random spectra obtained from as-implanted CaF_2 have the same shape as for unimplanted specimens. The depth profiles of both Eu and Tb atoms exhibit the Gaussian-type distribution. The spectra of Eu atoms have not been separated from that of Tb atoms. The angular scans were made for the host Ca- and impurity ion yields around the <111> direction. Europium and terbium have the same angler profile as Ca, suggesting that most of the implanted impurity atoms occupy substitutional lattice sites.

The implantation with $5x10^{14}$ Tb^+/cm^2 and $5x10^{14}$ Eu^+/cm^2 is not yet a suitable condition for developing white luminescence spectra. However we have the confidence that from these measurements we shall be able to find out the range of fluence introducing no serious radiation damage.

References

1) K.Aono, M.Iwaki, and S.Namba: *Nucl. Instr. Meth.*, **B46**, 220 (1990).

* Faculty of Engineering, Toyo University.

III-2-17. Single Event Burn-out in Power MOSFET by High-Energy Heavy Ion

S.Matsuda, S.Kuboyama, T.Tamura, M.Nakajima, M.Uesugi,
T.Kanno, J.Ohya, T.Ishii, T.Kohno, N.Inabe, T.Nakagawa,
K.Furutaka, Y.Futami, M.Kase, A.Goto, and Y.Yano

The power MOSFET has excellent performance as a power switching device. So it is expected to be applied to the spacecrafts. However, the power MOSFET has a possible catastrophic failure mode known as Single Event Burn-out (SEB) which is an important point to be considered in space electronic applications. The SEB is triggered upon incidence of high-energy heavy ion when the power MOSFET is biased with high voltage.

To study the SEB mechanism, a collected charge spectrum in the power MOSFET was measured by a pulse-height analyzer system with a modified charge-sensitive amplifier which has a very wide dynamic range. From the experimental data obtained last year with several kinds of ions of energy 117~200MeV, LET of 10~36MeV·cm^2/mg in Si, and range of 20~52μm in Si, it was suggested that the SEB occurred when the collected charge reached a certain value.[1] The power MOSFET used has a 43μm-thick epitaxial layer sensitive to SEB. Since uniformly created charge distribution in the whole epitaxial layer is necessary to study the detailed mechanism, high-energy Xe ions having a longer range from the RIKEN Ring Cyclotron were utilized this year. Parameter of Xe ions is shown in Table 1.

Table 1. Parameter of Xe ions.

Energy	(MeV/u)	10	26
LET in Si	(MeV·cm^2/mg)	52	36
Range in Si	(μm)	100	240

Typical collected charge spectra created by Xe ion irradiation are demonstrated in Fig.1 together with the data obtained with Ni ion irradiation. Left peak corresponds to the collected charge multiplied by the avalanche effect within the electric field of a drain junction. Right peak corresponds to the injected charge from a source junction amplified by a parasitic bipolar transistor. At a high drain bias voltage V_{DS}, both peaks move toward right, and SEB is triggered when a threshold charge Q_{TH} is reached. Since a large amount of energy is deposited by Xe ions, SEB is triggered at even lower V_{DS} compared with Ni ions.

Figure 2 shows the charge spectra obtained by Xe ion irradiation for several samples which have different drain breakdown voltages. A large collected charge is observed for a high breakdown voltage sample with a thick epitaxial layer. Each sample has different Q_{TH} and spectrum. To improve the SEB hardness of a power MOSFET, more detailed analysis will be performed for the dependence of Q_{TH} and spectrum on the device structure, impurity profile and LET of ions.

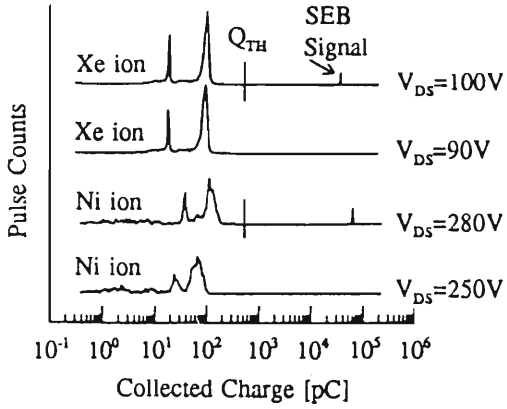

Fig.1. Collected charge spectra by 3500MeV Xe and 200MeV Ni ion irradiations as a function of drain bias voltage V_{DS}.

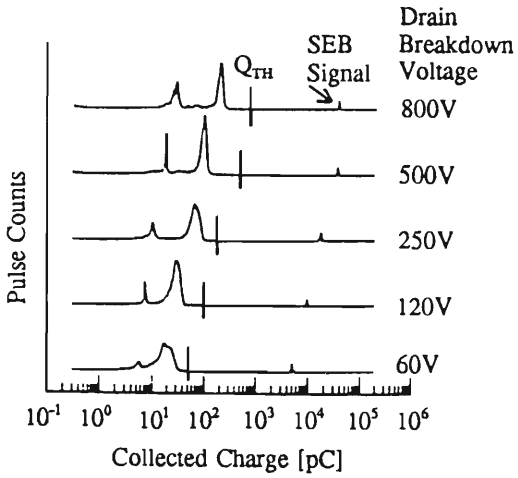

Fig.2. Collected charge spectra by 3500MeV Xe ion irradiation for various drain breakdown voltage samples.

References

1) S.Kuboyama, et al.: "Mechanism for Single-Event Burnout of power MOSFETs and Its Characterization Technique," to be published for IEEE Trans. Nucl. Sci. (1992.Dec).

III-2-18. Exact Calculation of the Second-Born Cross Sections for Particle Transfer into Excited States

N. Toshima

The Thomas-double scattering mechanism has been one of the most controversial problems in the field of atomic collisions.[1] In the original picture of Thomas, two successive binary collisions lead to electron capture by an incident ion from a target atom. In general three-body rearrangement collisions,

$$P + (Tc) \rightarrow (Pc) + T, \qquad (1)$$

three ways of Thomas mechanism are possible: (i) P hits c in the first binary collision and c makes the second collision with T; (ii) P hits c in the first collision and the recoiled P makes the second collision with T; (iii) P hits T in the first collision and the ejected T makes the second collision with c. In some cases the critical scattering angles of the above three processes coincide and they inevitably interfere. Though nonperturbative treatments of the Thomas mechanism were carried out recently and the importance of higher-order corrections was shown,[2,3] precise calculation of the second-Born amplitudes is also needed for the investigation of the interference effect of the double-scattering processes.

Exact calculations of the second-order Born amplitudes for electron capture have been reported in several papers, but all of the performed calculations are only for the capture into the $1s$ state. The contribution of capture into excited states is generally taken into account by multiplying a factor of 1.2 under the assumption that the same scaling law of $1/n^3$ (n is the principal quantum number of the final state) holds as the high-energy behavior of the first-Born approximation. It is not evident whether the second-Born, especially the differential cross sections also satisfy the same scaling law. Besides, destructive and constructive interferences, which occur only in exicited states, can be identified only if the amplitudes are calculated directly with high precision.

We have calculated the second-Born differential cross sections for exotic-atom formation into the excited states rigorously without a recourse to any further approximation.[4] The processes can be classified into three types according to the mass ratio of the three-particles. In the collision of $p + (p\mu^-)$, the Thomas mechanism takes place only via single path (i) as in the proton-hydrogen collision, while, in the collision of $e^+ + \mathrm{H}$, it can proceed via two paths that interfere destructively or constructively depending on the parity of the final bound states. In the third type, in which all the three particles have an equal mass as in positron-positronium collisions, the critical angle occurs at 180° only and the two second-order terms which are forbidden in classical mechanics are contributing significantly to the back-scattering. Although no experimental data is available for the comparison at present, the author hopes that this study may help to plan new experimental research.

References

1) R. Shakeshaft and L. Spruch: *Rev. Mod. Phys.*, **51**, 369 (1979).
2) N. Toshima and J. Eichler: *Phys. Rev. Lett.*, **66**, 1050 (1991); *Phys. Rev.*, **A46**, 2564 (1992).
3) N. Toshima: *Phys. Rev.*, **A42**, 5739 (1990); *ibid.*, **A45**, 2663 (1992)
4) A. Igarashi and N. Toshima: *Phys. Rev.*, **A46**, 1159 (1992);A. Igarashi, N. Toshima, and T. Ishihara: *Phys. Rev.*, **A46**, 5525 (1992).

III-2-19. Quantum Mechanical Calculation of Slow Ion–Atom Collisions

H. Fukuda and T. Ishihara*

The molecular orbital expansion has been a standard theoretical method for slow ion-atom collisions. The total wave function in this expansion does not satisfy the asymptotic boundary conditions because of the use of the internuclear coordinates to describe the relative motion of projectile and target. As a result, the coupled equations for the relative motion may contain spurious long-range coupling terms. The difficulty of spurious couplings does not occur if the correct relative coordinates are used instead of internuclear coordinates. Such an approach has been proposed by Kobayashi *et al.* [1]

The total wave function Ψ is expanded in terms of adiabatic basis functions defined by fixing the relative coordinates R_α of each arrangement channel α in the form

$$\Psi = \sum_{\alpha\nu} \frac{\chi_{\alpha\nu}(R_\alpha)}{R_\alpha} \psi_{\alpha\nu}(\tau_\alpha; R_\alpha). \qquad (1)$$

Radial function $\chi_{\alpha\nu}(R_\alpha)$ satisfies a set of coupled integro-differential equations,

$$-\frac{d^2\chi_{\alpha\nu}}{dR_\alpha^2} + \sum_{\nu'}[U_{\alpha\nu,\alpha\nu'} + 2P_{\alpha\nu,\alpha\nu'}\frac{d}{dR_\alpha}]\chi_{\alpha\nu'} + \sum_{\nu'}\int d\tau_\alpha V_{\alpha\nu,\beta\nu'}\chi_{\beta\nu'}(R_\beta) = 0. \qquad (2)$$

We have developed an iterative method[2] to solve Eq. (2) by expanding the radial function in the power of the ratio of the relative velocity to the electron orbital velocity,

$$\chi_{\beta\nu'}(R_\beta) = \sum_{t=0}^{\infty} \frac{(\Delta_{\beta\alpha})^t}{t!}\frac{d^t}{dR_\alpha^t}\chi_{\beta\nu'}(R_\alpha), \qquad (3)$$

where $\Delta_{\beta\alpha} = R_\beta(\tau_\alpha, R_\alpha) - R_\alpha$. Since we are interested in slow collisions, the first a few terms are retained in Eq. (3).

In Fig. 1, as a numerical example, cross sections for the charge transfer process

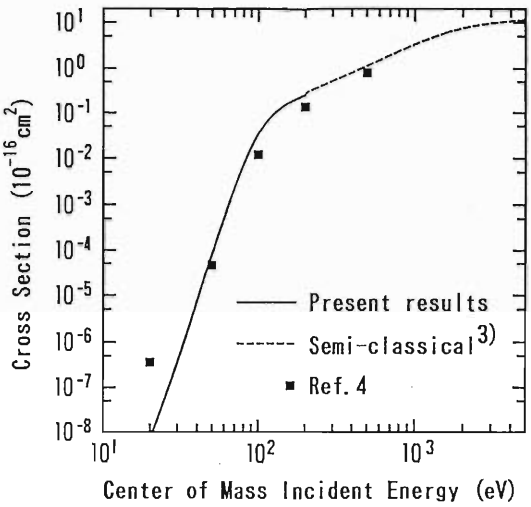

Fig. 1. Charge transfer cross sections for $H(1S)+{}^4He^{2+}$.

$$H(1S) + {}^4He^{2+} \rightarrow H^+ + {}^4He^+(n=2) \qquad (4)$$

for the incident energy E_i = 20–200 eV in the center of mass system are shown. A solid curve is the result of the present calculation and a dashed curve is the semiclassical limit of the present calculations.[3] The two curves indicate that they would merge into each other at a slightly higher energy. Solid squares in Fig. 1 are the results of the quantum mechanical calculation of Hemert *et al.* [4]

References

1) K. Kobayashi, T. Ishihara, and N. Toshima: *Muon Catalyzed Fusion.***2**, 191 (1988).

2) H. Fukuda and T. Ishihara: *Phys. Rev.*, **A46**, 5531 (1992).

3) T. G. Winter and G. J. Hatton: *Phys. Rev.*, **A21**, 793 (1980).

4) M. C. Hemert *et al.*: *Phys. Rev.*, **A31**, 2227 (1985).

* Institute of Applied Physics, University of Tsukuba.

III-2-20. Double Ionization of He by High-Energy Photon Impact

K. Hino

Double photoionization $(\gamma, 2e)$ of He is one of the simplest atomic processes for the three-body Coulomb problem. The electron-electron interaction plays a decisive role in the simultaneous ionization of two electrons. According to the results of calculations using the many-body perturbation theory (MBPT),[1] the final state correlation (FSC) has a significant contribution as does the ground state correlation (GSC) even at high photon-energy E_γ. The purpose of the present article is to evaluate the ratio, $R_\gamma = \sigma^{++}/\sigma^{+}$, of the double- to the single- photoionization cross sections of He in a high photon-energy region by use of quite accurately correlated initial and final state wave functions within the non-relativistic framework, and to compare the results with the very recent observations using synchrotron radiation by Levin *et al.*[2]

In the present calculations, attention is mainly focused on the effect of the FSC on $(\gamma, 2e)$. The ground state wave function of He is provided by the configuration interaction method and its energy is equal to -2.90276 atomic unit, differing from the exact value by 0.001 atomic unit. The final state is expressed by the analytic wave function, consisting of a product of three confluent hypergeometric functions.[3] This wave function satisfies the proper asymptotic Coulomb boundary condition of the three-body break-up channel,[4,5] and incorporates the electron-electron interaction in a non-perturbative way.

Figure 1 provides the present result of R_γ for $(\gamma, 2e)$ of He at E_γ=1.0-12.0 keV. For comparison, the result without incorporating FSC, hereafter referred to as $R_\gamma^{(0)}$, is also depicted. This essentially corresponds to the evaluation by Byron and Joachain.[6] The ratio R_γ is mostly in agreement with the experiments in the keV-region of E_γ.[2] However, R_γ is much discriminated from $R_\gamma^{(0)}$ even at very high E_γ. This result reveals the evidence of the important role of the FSC on $(\gamma, 2e)$.

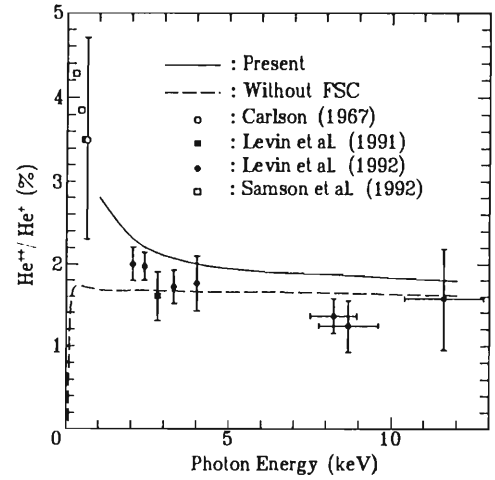

Fig.1. Ratios of the double- to the single- photoionization cross sections versus photon energy. Experimental data are taken from Refs. 2, 7 and 8.

References

1) T.Ishihara *et al.*: *Phys. Rev.*, **A44**, R6980 (1991).
2) J.C.Levin *et al.*: *Phys. Rev. Lett.*, **67**, 968 (1991) and private communications (1992).
3) C.Garibotti and J.E.Miraglia: *Phys. Rev.*, **A21**, 572 (1980).
4) P.L.Altick: *Phys. Rev.*, **A21**, 1381 (1980); *ibid.* **A25**, 128 (1982); *J. Phys.*, **B16**, 3543 (1983).
5) R.Peterkop: *J. Phys.*, **B15**, 1751 (1982).
6) F.W.Byron and C.J.Joachain: *Phys. Rev.*, **164**, 1 (1967).
7) T.A.Carlson: *Phys. Rev.*, **156**, 142 (1967).
8) J.A.Samson *et al.*: *Phys. Rev.*, 7277 (1992).

III-2-21. Double Excitation of H^- by Fast Proton and Anti-Proton Impact

K. Hino, M. Nagase,* H. Okamoto,* M. Matsuzawa, and M. Kimura**

Recent advance of experimental technique has made it possible to reveal evidences of electron correlation effects in the course of ion-atom collisions.[1-3] In this article, we evaluate cross sections of double excitation of H^- induced by p and $\bar{p}$ impact in the MeV/u-energy region. Wave functions of H^- are generated using the hyperspherical coordinate method.

To calculate the excitation cross sections of H^-, a set of 67 states is employed as basis functions to analyze the collision dynamics. The set consists of the discrete states $1s^2\ ^1S^e$, $2s^2\ ^1S^e$ and $2p^2\ ^1D^e$, the shape-resonance state $2s2p\ ^1P^o$, and the low-lying singly ionized state $1skp\ ^1P^o$. The $2s2p\ ^1P^o$ and $1skp\ ^1P^o$ states are made discrete into 10 energy-meshes for the present calculation. Tabel 1 indicates our calculated results based on the close-coupling method (CC), the first-order plane-wave Born approximation (PWB1), and the first- and the second-order distorted-wave Born approximation (DWB1 and DWB2) at the energies of 0.1 and 1.5 MeV/u, respectively.

Table 1. Calculated cross sections (in the unit of $10^{-20}cm^2$) for double excitation process of H^- at impact energy of (a) 1.5 MeV/u and (b) 0.1 MeV/u, respectively.

(a) 1.5 MeV/u

	$2s^2\ ^1S^e$		$2p^2\ ^1D^e$	
	proton	anti-proton	proton	anti-proton
PWB1	9.43	9.43	0.458	0.458
DWB1	9.35	9.41	0.456	0.458
DWB2	9.40	9.31	1.29	1.57
CC	9.62	9.49	1.26	1.43

(b) 0.1 MeV/u

	$2s^2\ ^1S^e$		$2p^2\ ^1D^e$	
	proton	anti-proton	proton	anti-proton
PWB1	141	141	6.85	6.85
CC	118	124	24.4	79.5

References

1) P.W.Arcuni and D.Schneider: *Phys. Rev.*, **A36**, 3059 (1987).
2) J.O.P.Pedersen and P.Hvelplund: *Phys. Rev. Lett.*, **62**, 2373 (1989).
3) J.P.Giese *et al.*: *Phys. Rev.*, **A42**, 1231 (1990).

*Department of Applied Physics and Chemistry, University of Electro-Communications.
**Argonne National Laboratory and Department of Physics, Rice University.

III-2-22. Inner-Shell Vacancy Production of Fast Ar Ions in Collision with Various Target Elements

Y. Naitoh,* Y. Zou, T. Kambara, Y. Awaya, and K. Fujima

Experimental observations have shown that the intensity of K_α-hypersatellites of projectile Ar ions oscillates against the target atomic number Z_t, when the projectile Ar ions are ionized at collision energy between 30 and 100 MeV.[1] Since direct excitation cross sections by a fast charged particles show monotonous dependence on Z_t, the shell structure of the target and projectile makes this observed oscillation, in other word, the binding energy matching rather than momentum plays an important role.

Figure 1 shows 1s to 2p excitation cross sections of Ar ions in collisions with various targets calculated by a simple Born approximation. Note that the Born cross section depends only on the effective charge of the target and the velocity of the ions. As is expected, there is no sign of oscillation which is clearly seen in the experiments.

Now we turn to the Fano-Lichten excitation model in which energy crossing of the target and projectile ions stimulates the inner shell vacancy production. The theoretical estimation based on this idea needs a rather complicated procedure. First we have to calculate the correlation diagrams of the system. Figure 2 shows the correlation diagrams of Ni-Ar and Cr-Ar systems using the DV-Xα method. In the Cr-Ar system, the Ar 1s state matches with the Ar 2p state at the united atom limit. However, Ni 2p correlates to

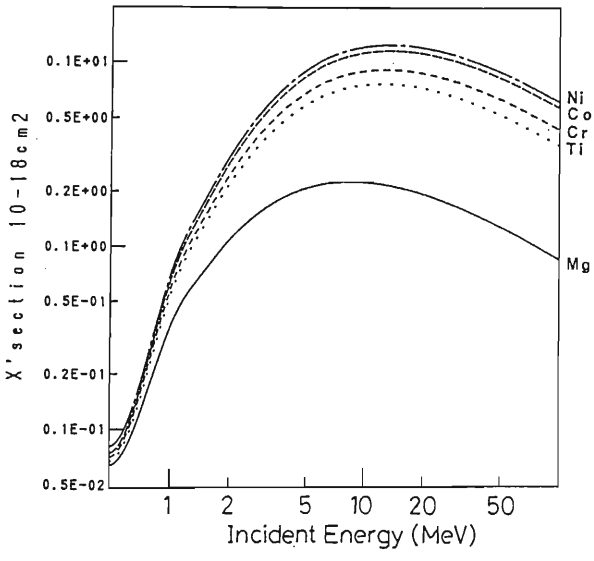

Fig. 1. Cross section of 1s to 2p excitation of Ar calculated by a Born approximation.

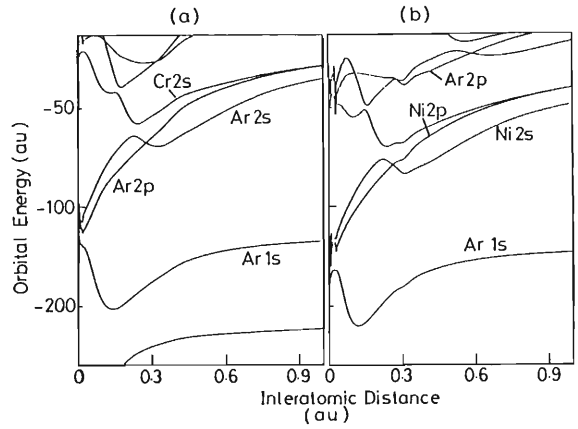

Fig. 2. Calculated molecular-orbital potential energy for (a) Ar+Cr and (b) Ar+Ni.

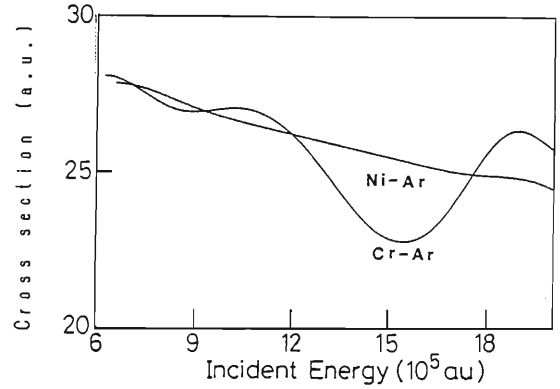

Fig. 3. Total cross section of Ar 1sσ to Ar 2pπ excitation as a function of the collision energy.

Ar 1s in the Ni-Ar system. The inner-shell excitation cross sections shown in Fig. 3 are calculated by integrating so called a close coupling equation with five states. The cross section for Ni-Ar is smooth against collision energy. On the contrary, the Cr-Ar system shows oscillation and exhibits a valley at collision energy of about 0.15×10^7 a.u. (Center of mass). This is thought to be a reason for K_α hypersatellite intensity oscillation observed experimentally.

References

1) Y. Zou, T. Kambara, Y. Kanai, Y. Awaya, K. Ando, M. Ohura, A. Hitachi, and S. Kravis: *Riken Accel. Prog. Rep.*, **25**, 69 (1991).

*Fac. Eng., Yamanashi Univ.

III-2-23. Resonant States of Two Electron Atomic Systems

H. Sato and S. Hara

In this research, the projection operator formalism is applied to obtain the energies for the resonant (autoionising) states of two electron atomic systems.

The Hamiltonian H of the system is given by

$$H = \Sigma(-\Delta_i/2 - z/r_i) + 1/r_{12}$$

where z is the nuclear charge, r_i the distance of i-th electron from the nucleus and r_{12} that between two electrons. The total wave function $\Psi(r_1,r_2)$ and the energy E_0 of the autoionising state are given, in the first approximation, by the solution of the eigen value equation

$$(QHQ - E_0)\,\Psi(r_1,r_2) = 0,$$

where Q is the projection operator introduced by Feshbach,[1]

$$Q = (1-p_1)(1-p_2),$$

where

$$p_1 = \phi_0(1)><\phi_0(1),$$

and $\phi_0(1)$ is the ground state wave function for the one electron system. The total wave function $\Psi(r_1,r_2)$ is expanded as

$$\Psi(r_1,r_2) = \Sigma\, a_i\, \Phi_i(r_1,r_2).$$

In the above expression, the configuration function Φ_i is given by

$$\Phi_i(r_1,r_2) = [f_{i1}(r_1)f_{i2}(r_2) + f_{i1}(r_2)f_{i2}(r_1)],$$

where f(r) is the Sturmian functions. The coefficients a_i are determined by a variational procedure.

We have constructed a general computer code to calculate the resonant energies and the wave functions for the two electron atomic systems. The results for He atom are given in Table 1 as an example.

Table 1. Resonant energies for He autoionising states in atomic units.

	present	Ref. 2)	Ref. 3)
$^1S(2s^2)$	-0.77872705	-0.7787	-0.7781585
$^3p(2p^2)$	-0.76145106	-0.760497	
$^3P(2s2p)$	-0.71041379		
$^1D(2p^2)$	-0.70248016		
$^1P(2s2p)$	-0.69251193	-0.69313	-0.6917983
$^1S(2p^2)$	-0.62164874	-0.621927	-0.6205051

References

1) H. Feshbach: *Ann. Phys.*, N. Y., **19**, 287 (1962).
2) Y. K. Ho: *Phys. Rep.*, **99**, 1 (1983).
3) B. H. Bransden and C. Joachain: "Physics of Atoms and Molecules", Longman, London and New York (1983).

3. Radiochemistry and Nuclear Chemistry

III-3-1. Preparation of Radioactive Multitracer Solutions from a High-Energy Heavy-Ion Irradiated Au Target by Means of a Supported Liquid Membrane (I)†

S. Ambe, Y. Ohkubo, Y. Kobayashi, M. Iwamoto, M. Yanokura, and F. Ambe

A large number of radioactive nuclides useful as tracers are produced in targets by high-energy heavy-ion irradiations by the RIKEN Ring Cyclotron.[1,2] With the aim of developing automated methods of preparing multitracer solutions, we are investigating separation of radioactive nuclides by means of supported liquid membranes. Separation by supported liquid membranes is considered to be especially suitable for preparation of multitracer solutions because of (i) simplicity of operation leading to facile automation, (ii) feasibility of concentrating tracers into a small volume of a solution, and (iii) necessity of a far smaller amount of extractants than conventional solvent extraction. This paper describes successful removal of the target material Au from multitracers by means of a TBP-decalin membrane.

The irradiated Au disk was dissolved in 10 cm^3 of aqua regia. A portion of the solution was evaporated to dryness. The residue was dissolved in 1 mol dm^{-3} HNO_3. The solution containing about 170 mg of Au^{3+} ions was used as a feed solution. A supported liquid membrane was prepared by impregnating a microporous polytetrafluoroethylene sheet with a 0.8 mol dm^{-3} TBP-decalin solution. Distilled water was used as strip solutions.

The supported liquid membrane was fixed at the bottom of a Teflon vessel with a Teflon ring. The feed solution in the outer vessel was stirred at 1000 rpm with a magnetic stirrer. The strip solution was circulated at the rate of 3 cm^3 min^{-1}, a given portion of the circulating solution being trapped in a Teflon vessel put on a pure-Ge detector for measurement of γ-rays. Measurement of 1200 s duration for the strip solution was automatically repeated and the γ-ray spectra obtained were recorded on a disk. The strip solution was replaced by fresh distilled water after 300 and 1300 min in each experimental run.

Figure 1 shows the transport of Au^{3+} ions, monitored by the γ-rays of radioactive Au nuclides, from the 1 mol dm^{-3} HNO_3 feed solution. Transport of Au^{3+} ions started immediately after the contact of the feed and strip solutions with the membrane from each side. The amount of transported Au^{3+} ions increased almost linearly up to 55 %, where the increase tended to saturate. By replacing the strip solution with fresh distilled water, the transport of Au^{3+} ions was recovered. After permeation overnight the strip solution was replaced with fresh water again and conc HNO_3 (2 volume % of feed solution) was added to the feed solution in order to compensate the loss of HNO_3 into the strip solutions. The transport of Au^{3+} ions completed in less than 2000 min from the beginning. Radioactive nuclides of the elements, Sc, Fe, Co, Rb, Sr, Y, Zr, Nb, Rh, Ag, Te, Ba, Ce, Eu, Gd, Yb, Lu, Hf, Ir, and Pt were found remaining in the feed solution after the permeation of those of Au. In the strip solutions, 20 % of total Ag^+ ions were observed and the transport of the other elements was less than 5 %.

It is concluded from the observations described above that the supported liquid membrane of TBP-decalin is effective for separating multitracers from an Au target irradiated with high-energy heavy ions. Essentially all the radioactive nuclides remain in the 1 mol dm^{-3} HNO_3 feed solution, though removal of Au takes somewhat long time. The time required for eliminating Au is expected to be considerably shortened by supplying fresh distilled water continuously as the strip solution and also keeping the HNO_3 concentration of the feed solution close to 1 mol dm^{-3} by automatically controlled addition of HNO_3.

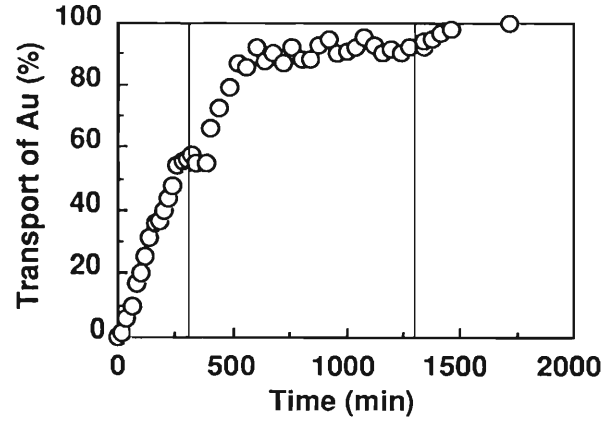

Fig. 1. Transport of Au^{3+} ions from a 1 mol dm^{-3} HNO_3 feed solution. The two vertical lines in the frame indicate the time of replacement of the strip solution with fresh distilled water.

References

1) S. Ambe, S. Y. Chen, Y. Ohkubo, Y. Kobayashi, M. Iwamoto, M. Yanokura, and F. Ambe: *Chem. Lett.*, **1991**, 149.

2) S. Ambe, S. Y. Chen, Y. Ohkubo, Y. Kobayashi, M. Iwamoto, M. Yanokura, and F. Ambe: *Anal. Sci.*, **7**, Suppl. 317 (1992).

† Condensed from the article in *Appl. Radiat. Isot.* **43**, 1533 (1992).

III-3-2. Preparation of Radioactive Multitracer Solutions from a High-Energy Heavy-Ion Irradiated Au Target by Means of a Supported Liquid Membrane (II)†

S. Ambe, Y. Ohkubo, Y. Kobayashi, M. Iwamoto, M. Yanokura, and F. Ambe

This paper describes successful removal of the target material Au from multitracers in 8 mol dm^{-3} HCl by means of a TBP-decalin membrane supported on a microporous polytetrafluoroethylene sheet. TBP was adopted since Au^{3+} has the largest distribution coefficient of all the elements reported in extraction from 1-12 mol dm^{-3} HCl.

The irradiated Au disk was dissolved in 10 cm^3 of aqua regia. A portion of the solution was evaporated to dryness. The residue was dissolved in 8 mol dm^{-3} HCl. The solutions containing about 170 mg of Au^{3+} ions were used as a feed solution in each separation. The other experimental conditions are similar to the previous report.[1)]

The result on the 8 mol dm^{-3} HCl feed solution is shown in Fig. 1. Transport of Au^{3+} ions proceeded much faster than in the case of the 1 mol dm^{-3} HNO_3 solution, attaining 93 % in 300 min by the first strip solution. In the second and third, 6 % and 1 % of total Au ions were found, respectively. No γ-rays due to Au nuclides were found in the feed solution, indicating complete transport of Au^{3+} into the three strip solutions.

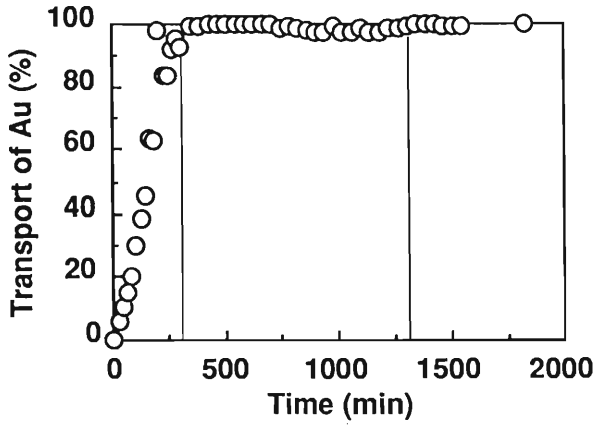

Fig. 1. Transport of Au^{3+} ions from an 8 mol dm^{-3} HCl feed solution. The two vertical lines in the frame indicate the time of replacement of the strip solution with fresh distilled water.

In the case of 8 mol dm^{-3} HCl feed solution, however, elements other than Au were observed to be transported more or less to the strip solutions as shown in Fig. 2. In the feed solution remained more than 60 % of the radioactive nuclides of Co, Rb, Sr, Y, Rh, Ag, Ba, Ce, Eu, Gd, Yb, and Lu, and about half of those of Hf, Ir, and Pt. On the other hand, more than 80 % of Sc and Zr, and essentially all of Fe, Nb, and Te nuclides were transported into the strip solutions together with Au. The stripping behavior of the elements is well correlated with their distribution coefficients in TBP-HCl solvent extraction.

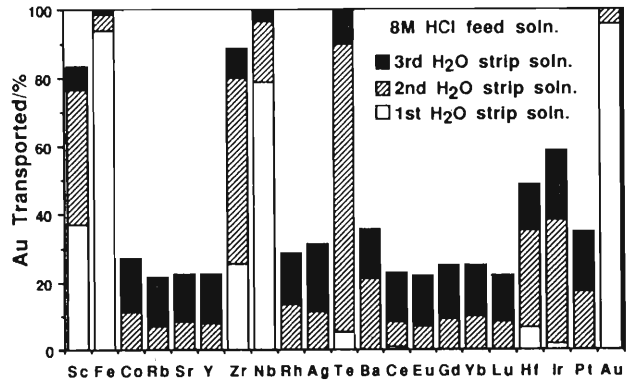

Fig. 2. Transport of various elements from an 8 mol dm^{-3} HCl feed solution.

It is concluded from the observations described above that the supported liquid membrane of TBP-decalin is effective for separating multitracers from an Au target irradiated with high-energy heavy ions. The 8 mol dm^{-3} HCl feed solution is recommended for certain elements because of the quicker separation of Au. Choice of a feed solution also depends on the experiment in which the multitracer solution is used.

A series of experiments are now under way to establish efficient procedures for preparing multitracer solutions from different kinds of targets irradiated by high-energy heavy ions. A search will be made for liquid membranes, leaving a target element in the feed solution and letting all tracers permeate the strip solution. Combination of two or more liquid membranes is expected to yield groups of tracers useful for different specific purposes.

References

1) S. Ambe, Y. Ohkubo, Y. Kobayashi, M. Iwamoto, M. Yanokura, and F. Ambe: This report, p. 83.

† Condensed from the article in *Appl. Radiat. Isot.* **43**, 1533 (1992).

III-3-3. Separation of Multitracer from Heavy-Ion Irradiated Targets by Heating under Reduced Pressure

M. Iwamoto, S. Ambe, Y. Ohkubo, Y. Kobayashi, M. Yanokura,
H. Maeda, and F. Ambe

We continued in this period a series of experiments on the separation of multitracers from targets irradiated with heavy ions from the RIKEN Ring Cyclotron by heating under reduced pressure.[1,2]

The apparatus was improved in several points resulting in high yields of tracers. The cold finger used in previous experiments[2] was no more used, because the radioactive nuclides evaporating from the molten target were found to be efficiently collected on a part of the inner wall of the quartz tube. They formed a band having a width of a few cm just at the exit of the furnace.

Since the cold finger was abandoned, the sizes of both the quartz tube and the electric furnace were made smaller. The volume of washing solution was consequently made much smaller than before.

After heating a target under reduced pressure of a few Pa, the quartz tube was drawn out of the furnace and the target was removed. Then 5 cm^3 of 6 mol/dm^3 HCl was poured into the quartz tube. The tube was set on an apparatus being inclined enough so that the inside wall of the tube got wet with the acid solution (Fig.1). The quartz tube was rotated slowly by means of a motor for more than 1 hour. Thus, a 6 mol/dm^3 HCl solution of multitracers was obtained. The percentage of recovery on average was 70~80% of the radioactive nuclides deposited on the inner wall of the quartz tube. Detailed yields for each nuclide will be reported elsewhere.

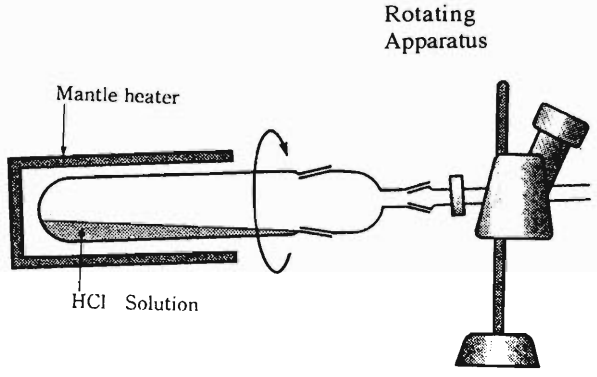

Fig. 1.The apparatus for dissolving radioactive nuclides.

References

1) M. Iwamoto et al.: RIKEN Accel. Prog. Rep.,**25**, 96 (1991).
2) M. Iwamoto et al.: Anal. Sci., **7**, Suppl. 313 (1991).

III-3-4. Application of the Radioactive Multitracer Technique to a Study of Adsorption of Metal Ions on α-Fe_2O_3†

S. Ambe, S. Y. Chen,* Y. Ohkubo, Y. Kobayashi, M. Iwamoto, and F. Ambe

We established convenient and reliable radiochemical procedures by which radioactive multitracer solutions free from carriers are prepared from Au, Ag, and Cu targets irradiated with a high-energy heavy-ion beam accelerated by the RIKEN Ring Cyclotron.[1,2] Use of the multitracer solutions enables us to determine the characteristic behavior of different elements under strictly identical experimental conditions and to make a precise comparison among them.

Here, the multitracer technique was applied to the study of the adsorption of elements on a model compound, α-Fe_2O_3, from aqueous solutions. The pH dependence of the adsorption of the elements, Sc, Ga, As(V), Se(IV), Rb, Sr, Y, Zr, Nb, and Mo(VI), was simultaneously determined using a multitracer solution separated from an Ag target irradiated by a 135 MeV/nucleon ^{12}C beam.

α-Fe_2O_3 was added to the multitracer solution at pH 2. The pH of the resulting suspension was adjusted to different values with a dilute NaOH solution. The suspension was shaken at room temperature for 1 h. After centrifugation of the suspension, the supernatant solution was withdrawn for measurement of γ-ray spectra.

Figure 1 shows the pH dependence of adsorption of 10 elements obtained simultaneously in an experimental run. The patterns of adsorption can be classified into the following five groups: A) Sc, Y, and Zr, whose percentage of adsorption increases with increase of pH, attaining complete adsorption in the alkaline region, B) Se(IV) and Mo(VI), which are adsorbed almost completely in the acid pH range, but whose adsorption decreases with increase in pH, C) Ga, which is adsorbed completely in the neutral region, but whose adsorption decreases in both acid and alkaline pH ranges, D) Rb and Sr, which show little or low adsorption within the entire pH range studied, and E) As(V) and Nb, which give high adsorption yield within the entire pH range.

The results described above demonstrate the usefulness of the multitracer technique in studying the behavior of a number of elements under identical experimental conditions. The adsorption characteristics of the elements revealed in the present work provide a basis for understanding their behavior in natural environments.

Detailed discussion on the mechanisms of the adsorption in terms of the surface charge of α-Fe_2O_3 and chemical species of the elements in the multitracer solution will be described elsewhere, along with experimental data on other elements and those on kinetic aspects of adsorption. Similar work on different adsorbates is also in progress.

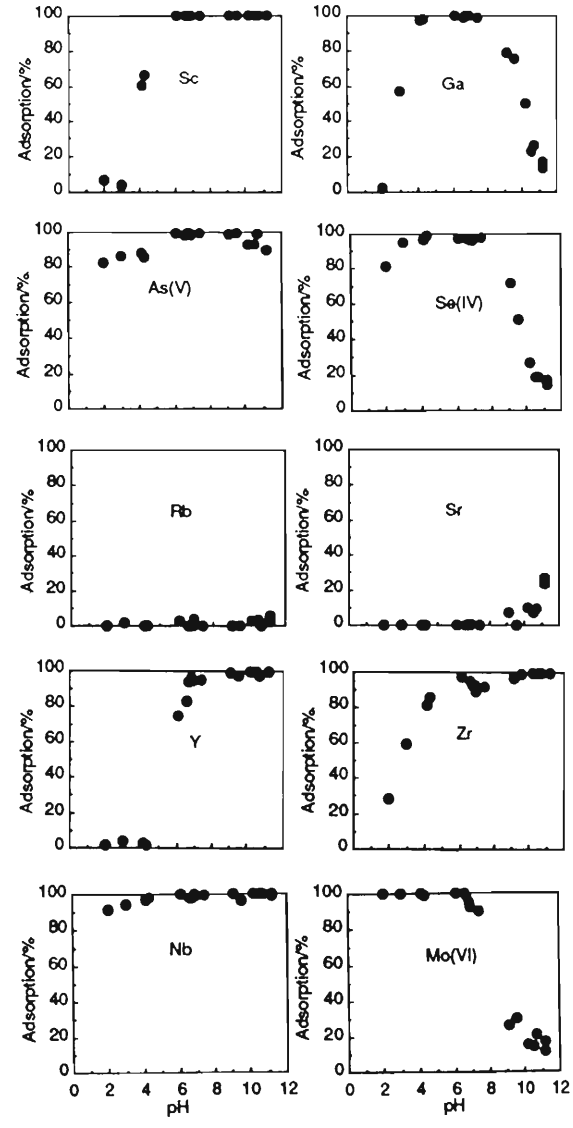

Fig. 1. The pH dependence of adsorption of the elements, Sc, Ga, As, Se, Rb, Sr, Y, Zr, Zb, and Mo.

References

1) S. Ambe, S. Y. Chen, Y. Ohkubo, Y. Kobayashi, M. Iwamoto, M. Yanokura, and F. Ambe: *Chem. Lett.*, **1991**, 149.
2) S. Ambe, S. Y. Chen, Y. Ohkubo, Y. Kobayashi, M. Iwamoto, M. Yanokura, and F. Ambe: *Anal. Sci.*, **7**, Suppl. 317 (1992).

† Condensed from the article in *Chem. Lett.*. **6**,1059(1992).

* South China Sea Institute of Oceanology.

III-3-5. Radiochemical Study of Adsorption Behavior of Various Elements in Hydrochloric Acid Solutions on Activated Carbon Fiber and Non-ionic Macro-reticular Copolymer Using Multitracer

S. Shibata, K. Watari,* Y. Noda,* S. Ambe, Y. Ohkubo, M. Iwamoto, Y. Kobayashi, M. Yanokura, H. Maeda, and F. Ambe

Activated carbon and non-ionic macro-reticular (MR) copolymers have been reported to be effective adsorbents for a number of organic materials in aqueous solutions, but not enough attention has been paid on the adsorption of inorganic substances. Those materials have particulary high distribution ratios (Kd) for tetrachloro complex anions of Fe(III), Ga(III) and Au(III) in above 6 mol·dm^{-3} HCl solutions without any other organic ligands.[1,2] Such peculiar adsorption behavior has been observed with cation exchange resins.[3] In the present work, the adsorption behavior of inorganic elements in 0.01 - 10 mol·dm^{-3} HCl solutions of multitracer prepared from Ag foils irradiated with 135 MeV/nucleon ^{12}C [4] on a novoloid-based activated carbon fiber, Kynol ACF-1605-15, and a non-ionic MR copolymer, Amberlite XAD-7, was studied.

The retention of the elements was studied under static conditions (batch method). The multitracer solutions were shaken with the adsorbents for 2 h. Aliquots of a half volume of the supernatant were separated at the end of sorption time. The radioactivity of the phases was measured with a high-resolution γ-ray spectrometer, and was analyzed with the BOB code [5] on a SUN workstation.

The distribution of the elements was determined by counting the radioactivity of both the aqueous aliquot and the remaining sorbent fraction. The distribution ratio was calculated from

$$Kd = (A_r - A_s) / 2A_s \cdot V/m,$$

where A_s and A_r are the peak areas of the aqueous aliquot and the remaining portion, respecively, and V/m denotes the volume to weight rario in cm$^3 \cdot$g^{-1}.

Figure 1 shows the adsorption profiles of 18 elements in log-log plottings of Kd against the concentration of HCl. An important feature of these profiles compared to those in the HNO_3 solution system is that increasing concentration of HCl above 5 mol·dm^{-3} tends to increase Kd in several elements.

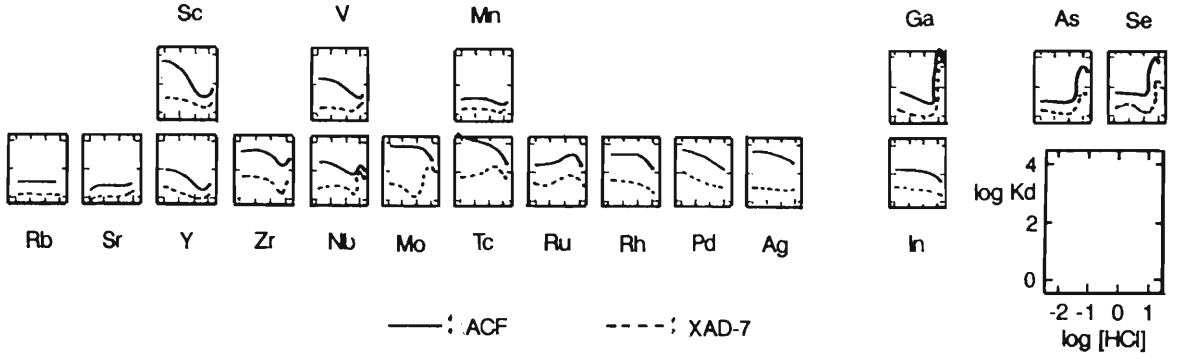

Fig. 1. Adsorption of the inorganic multitracer prepared from Ag foils on ACF-1605-15 and XAD-7 from aqueous solutions as a function of the concentration of HCl.

References

1) K. Watari, K. Imai, S. Shibata, and M. Miura: *J. At. Energy Soc., Japan*, **26**, 384 (1984).
2) S. Shibata, K. Watari, and K. Kaneko: *Radioisotopes*, **39**, 226 (1990).
3) F. Nelson, T. Murase, and K. A. Kraus: *J. Chromatog.*, **13**, 503 (1964).
4) S. Ambe, S. Y. Chen, Y. Ohkubo, Y. Kobayashi, M. Iwamoto, M. Yanokura, and F. Ambe: *Anal. Sci.*, **7**, Suppl., 317 (1991).
5) H. Baba, H. Okashita, S. Baba, T. Suzuki, H. Umezawa, and H. Natsume: *J. Nucl. Sci. Technol.*, **8**, 1227 (1972).

* National Institute of Radiological Sciences.

III-3-6. Utilization of Multitracer Solutions for Studies on the Ion Exchange Behavior of a Strongly Acidic Resin NAFION

T. Bamba, H. Harakawa, Y. Saito, K. Kimura, T. Yaita, S. Shibata, S. Ambe, Y. Ohkubo, M. Iwamoto, Y. Kobayashi, M. Yanokura, H. Maeda, and F. Ambe

Radioactive multitracer solutions, in a carrier- and salt-free condition, prepared from silver[1,2] and gold[2-4] foils irradiated with 135 MeV/nucleon ^{12}C ions were used for the titled studies in a NAFION-$HClO_4$ system after converting to a perchloric acid solution. The NAFION-501 resin, manufactured by DuPont, is a perfluorinated polymer containing ~5 mmol g^{-1} sulfonic acid group as shown below. Because of the strong acidity of the resin, a comparison of its exchange behavior with that of a common cation exchange resin attracts much attention.

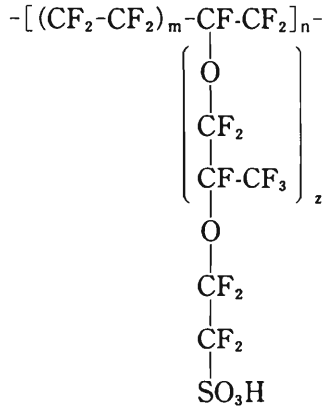

The resin, commercially available as a cylindrical shape of ca. 1mmϕ ×1~3 mm, was crushed with a stamp mill at liquid nitrogen temperature, passed through a 50-mesh screen, and used. Into a small polyethylene bottle, 0.1ml of the multitracer solution and 2.4g of the resin were introduced, and the acidity of the system was adjusted to 0.10, 1.1, and 5.6mol dm^{-3} with perchloric acid by making the volume of the solution to 10ml. The contents of the bottle were shaken vigorously at 25°C with an 8-shape mode shaker. Time of the shaking was 16 hours for the silver-multitracer and 75 hours for the gold-multitracer. After filtration, γ-ray spectrometry was carried out for both phases. The γ-ray spectra were analyzed on a FACOM M780 computer.

The distribution ratios (D) of Na, Sc, V, Co, Ga, Rb, Sr, Y, Zr, Nb, Ru, Rh, and Pd were obtained from the silver-multitracer runs and those of Sc, Rb, Y, Zr, Ag, Ba, Eu, Gd, Tb, Tm, Yb, Lu, and Pt from the gold-multitracer runs. The D's for Sc, Rb, Y, and Zr obtained from the silver and the gold runs showed that more than 80% of the equilibrium was attained by the 16 hours shaking. As shown in Fig. 1, the slopes for alkali and alkaline earth metal ions in the log-log plottings were approximately -1 and -2, respectively, that is characteristic of the ion exchange. D's for noble metals remained rather constant with increasing acidities and 5~10 times higher than those in a NAFION-hydrochloric acid system.[5]

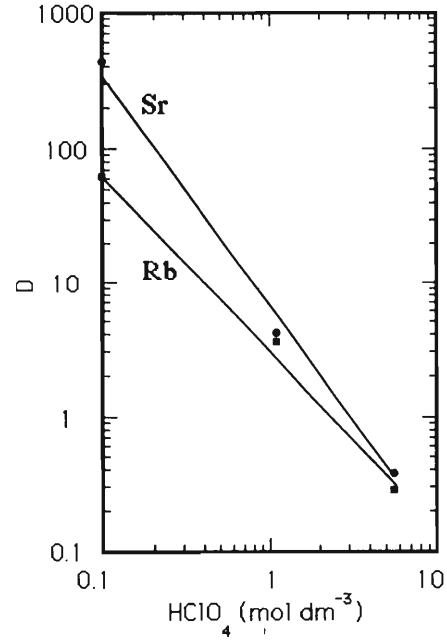

Fig. 1. Relationship between the D and the acidity.

References

1) S. Ambe, S.Y. Chen, Y. Ohkubo, Y. Kobayashi, M. Iwamoto, M. Yanokura, and F. Ambe: RIKEN Accel. Prog. Rep., **25**, 95(1991).
2) S. Ambe, S.Y. Chen, Y. Ohkubo, Y. Kobayashi, M. Iwamoto, M. Yanokura, and F. Ambe: *Anal. Sci.*, **7**, Suppl.,317(1991).
3) S. Ambe, S.Y. Chen, Y. Ohkubo, Y. Kobayashi, M. Iwamoto, and F. Ambe: RIKEN Accel. Prog. Rep., **24**, 73(1990).
4) S. Ambe, S.Y. Chen, Y. Ohkubo, Y. Kobayashi, M. Iwamoto, M. Yanokura, and F. Ambe: *Chem. Lett.*, **1991**, 149.
5) J. Kawarada, T. Yaita, Y. Saito, K. Kimura, S. Ambe, S.Y. Chen, Y. Ohkubo, M. Iwamoto, Y. Kobayashi, and F. Ambe: RIKEN Accel. Prog. Rep., **25**, 98(1991).

III-3-7. Multitracer Study on Complex Formation of Humic Acid

Y. Minai, Y. Takahashi, M. K. Kubo, S. Toyoda,* M. Ishibashi,*
S. Ambe, Y. Kobayashi, Y. Ohkubo, M. Iwamoto, M. Yanokura, H. Maeda,
S. Shibata, N. Takematsu, F. Ambe, and T. Tominaga

Humic acid is a naturally-occurring organic polyacids which can combine with various metal cations in natural and artificially-modified environments. Estimated stabilities of the metal-humic acid complexes were strong enough to influence the behavior of several elements in the environments. For instance, large values of complex formation constants of actinide(III)-humates have been reported in recent studies, indicating considerable amounts of actinide(III)-humates can be formed in aqueous environments.[1] However, reliable stability constants were not obtained for most of the elements which are important in environmental chemistry and geochemistry.

In this study the multitracer technique was employed to evaluate stabilities of humate complexes of various metal cations including several geochemically important elements (e.g., lanthanides). Besides, it was intended to elucidate the dependence of the stabilities on ionic radius and charge which have been believed to affect the stability of the complexes.

Multitracer solutions (3M HCl) were obtained from the targets (silver and gold foils) irradiated with a ^{12}C beam accelerated in RIKEN Ring Cyclotron. The procedures for separation of the multitracer from the targets were given elsewhere.[2,3] After evaporation of the multitracer solutions containing hydrochloric acid, 0.001M perchloric acid was added to yield the multitracer solutions for further experiments.

In order to evaluate the stabilities of the metal-humate complexes we employed ion exchange, solvent extraction, ultrafiltration, and paper chromatography. Free cations are partially removed from the solutions with ion exchange and solvent extraction. Since the fraction of the cations removed is a function of the concentrations of the humic acids which can be combined to the cations, we can estimate the stability of the metal-humate complexes. Determination of stability constants with ultrafiltration is based on the property of humic acid as a polyacid; the cations bound to humic acid molecules cannot pass an ultrafiltration membrane. Relative radioactivity of the filtrate depends on the concentrations of humic acid in the solution for ultrafiltration. Paper chromatography was used for qualitative evaluation of binding affinity of the cations with humic acid. Multitracers spotted on a piece of humic acid-impregnated paper was developed by an 80% ethanol aqueous solution of manganese acetate.

Preliminary results on the complexation affinity from a paper chromatogram indicated that, at least, technetium and several lanthanides preferred to make complexes with humic acid. Solvent extraction and ion exchange studies on the complexation also indicated that these elements can make stable complexes with humic acid. Further analysis on ion exchange and extraction properties of the resin and the extracts employed should give the quantitative information regarding the affinity of the complex formation between the cations and humic acid.

References

1) Y. Minai, Y. Meguro, and T. Tominaga: Proc. 3rd. Int. Symp. Adv. Nucl. Energ. Res., p.229 (1991) and the references cited therein.
2) S. Ambe, S. Y. Chen, Y. Ohkubo, Y. Kobayashi, M. Iwamoto, M. Yanokura, and F. Ambe: Chem. Lett., **1991**, 149.
3) S. Ambe, S. Y. Chen, Y. Ohkubo, Y. Kobayashi, M. Iwamoto, M. Yanokura, and F. Ambe: Anal. Sci., Suppl., **7**, 317 (1991).

* Dept. of Chem., Fac. of Sci., Univ. of Tokyo

III-3-8. Investigation of 7 MeV/nucleon ^{58}Ni Induced Reaction on Cu and Rh Targets

M. Kiriu, T. Saito, A. Yokoyama, E. Taniguchi,
H. Baba, and Y. Ohkubo

Linear and angular momentum transfers involved in heavy-ion collisions are fascinating phenomena[1] and the succeeding decay mechanism is so complex that extended studies are still required.

An experiment was performed at the E3b beam course of RIKEN Ring Cyclotron. A 7 MeV/nucleon ^{58}Ni beam was used to bombard Cu and Rh targets (and Al target as a monitor) in order to compare the mass distribution of the reaction products from an essentially symmetric composite system to that from an asymmetric one.

The thicknesses of a Cu target foil (foil 1) and two Al downstream catcher foils (foil 2 and 3) were 1.84 mg/cm^2, 2.74 mg/cm^2 and 6.07 mg/cm^2, respectively. Not to degrade the beam energy, all these catcher foils were placed in the downstream.

A Rh target stack consisted of a 2.75 mg/cm^2 Al upstream catcher foil, a Rh target foil, and a 6.03 mg/cm^2 Al downstream catcher foil. The Rh target was an about 2.5 mg/cm^2 foil with an about 18 mg/cm^2 polyester support in the downstream.

The beam intensities on Cu and Rh foils were about 0.15 and 0.7 particle nA, respectively. After the irradiation, γ-rays from each foil were repeatedly measured with Ge detectors for about two months. About a hundred product nuclides were identified based on the photopeak energy and half-life data.

The formation cross sections were obtained for each nuclide by decay analysis. Assuming the charge dispersions to be Gaussian, we could determine the most probable charge, Z_P, only for the Cu target stack because there were no isobaric triplets for the Rh target stack.

Figure 1 shows mass yields of each Cu target stack foil, where the contribution of reaction products with Al catchers was subtracted. Figure 2 shows formation cross sections vs. atomic mass, where the contribution of reaction products with upstream Al and polyester could not be subtracted.

As Fig. 1 shows, there appear a broad peak around mass 107 for foil 3 and broad peaks around mass 60 for all the three foils, where the former is due to evaporation residues and the latters are to fission fragments. In Fig. 2 a large peak is observed around mass 67 which is mainly due to the reaction products with polyester. But any other clear information could not be obtained.

We should, therefore, study further on the reaction mechanism.

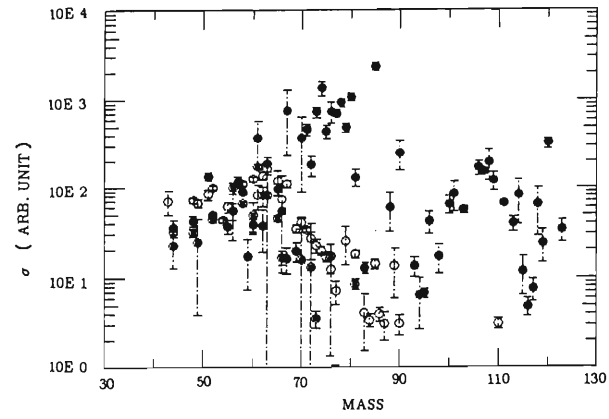

Fig. 1. Mass distribution of 7 MeV/nucleon ^{58}Ni + Cu system (See text). [foil 1 : ◉ , foil 2 : ○ , foil 3 : ●]

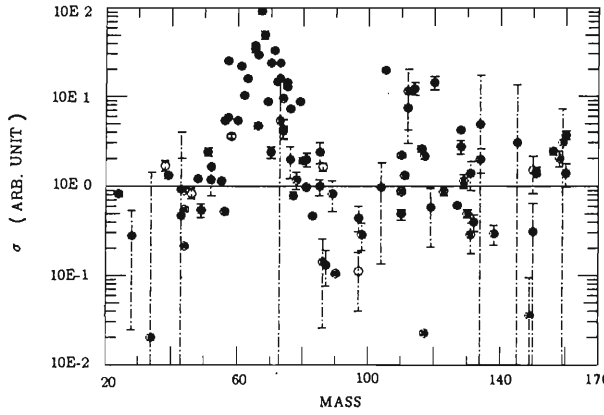

Fig. 2. Mass distribution of 7 MeV/nucleon ^{58}Ni + Rh system (See text).

References

1) R. Bass : "Nuclear Reactions with Heavy Ions", Springer-Verlag, Berlin (1980).

III-3-9. Target Fragmentation of ^{141}Pr and ^{165}Ho Induced by Heavy Projectiles

K. Takesako, T. Saito, H. Kusawake*, A. Yokoyama, H. Baba, Y. Ohkubo, A. Shinohara, and M. Furukawa

In an earlier study[1] for target fragmentation by highly energetic light projectiles such as proton and ^{4}He, the following relationship was shown to hold between the mass yield $Y(A)$ and the fragment mass number A:

$$Y(A) \propto \exp(pA). \quad (1)$$

This parameter p is known to depend only on the incident energy for various combinations of target and light projectile. It was further found that the parameter value decreases as the incident energy increases and levels off above 1 GeV. We performed experiments in order to test this limiting behavior in the case of heavy-ion projectiles.

The monoisotopic ^{141}Pr and ^{165}Ho target foils sandwiched among aluminum or Mylar foils were irradiated with ^{14}N, ^{15}N, or ^{40}Ar projectiles at the E3b beam course of RIKEN Ring Cyclotron. We performed γ-ray measurements with Ge detectors to obtain the cross sections of reaction products and the cumulative mass yields.

Figure 1 shows the values of p derived for each incident energy. For the systems with ^{14}N (1.89 GeV) and ^{40}Ar (2.36 and 3.80 GeV) the data seem to be in good agreement with the limiting value reported in Ref. 2.

Target fragmentation is usually treated as a two-step process, excitation by the projectile and sequential deexcitation. We tentatively attributed the limiting value of p to the appearance of the upper limit in the nuclear temperature that the initially formed nuclei can possess. We considered p to be related to the mean evaporation energy per nucleon $\langle E_{ev} \rangle$, the nuclear temperature T, and the level density parameter a as

$$p = \frac{\langle E_{ev} \rangle}{aT^2}. \quad (2)$$

Following the method described in Ref. 3, we found that the limiting nuclear temperature from our data is around 5.4 MeV as listed in Table 1. This value is consistent with various theoretical predictions.[4]

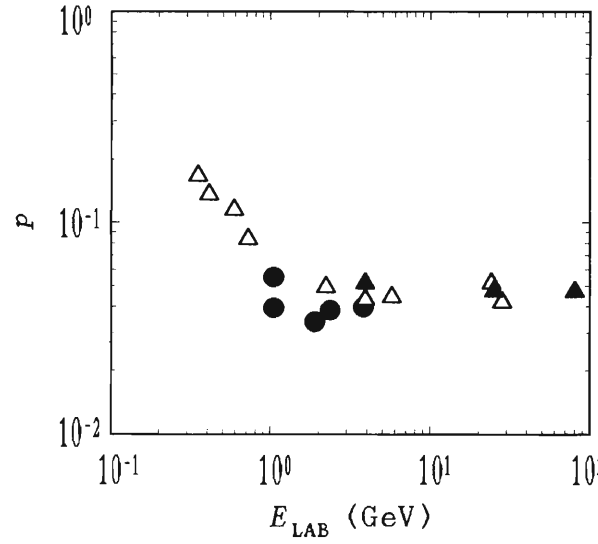

Fig. 1. Dependence of the parameter p on incident energy E_{LAB}. Circles represent the data in this work, and triangles the data by Cumming et al.[2] Closed marks mean the systems with heavy-ion projectile, and open marks light-ion projectile.

Table 1. Parameter p and deduced nuclear temperature T.

	E_{LAB} (GeV)	p (10^{-2})	T (MeV)
^{15}N + ^{141}Pr	1.05	3.93±1.78	5.40±2.35
^{15}N + ^{165}Ho	1.05	5.52±2.12	4.08±1.40
^{14}N + ^{165}Ho	1.89	3.39±0.15	5.49±0.14
^{40}Ar + ^{141}Pr	2.36	3.85±0.11	5.47±0.09
^{40}Ar + ^{141}Pr	3.80	3.97±0.11	5.37±0.09

* Tsukuba Space Center, NASDA

References

1) G. Rudstam: *Z. Naturforsch.*, **21a**, 1027 (1966).
2) J.B. Cumming et al.: *Phys. Rev.*, **C17**, 1632 (1978).
3) S. Shlomo and J.B. Natowitz: *Phys. Rev.*, **C44**, 2878 (1991).
4) See, e.g., H.W. Barz et al.: *Phys. Lett.*, **B184**, 125 (1987).

III-3-10. Symmetric Mass Division in the Ir-Composite System

S. Watanabe, K. Takesako, T. Saito, H. Baba, Y. Ohkubo,
A. Shinohara, E.Taniguchi, and M. Furukawa

A nuclear chemistry experiment with a light target and a heavy projectile was carried out to investigate the heavy-ion reaction mechanism under the inverse kinematical conditions contrary to usual experiments. A vanadium foil with a thickness of 8.47 mg/cm^2 was bombarded with a ^{136}Xe beam (8.5 MeV/nucleon) at the E3b beam course of RIKEN Ring Cyclotron. Two Al catcher foils (5.67 mg/cm^2 thick) were placed downstream of the target. Irradiation time of the stack was about 90 min. After the bombardment, the irradiated foils were separately subjected to γ-ray spectrometry with Ge spectrometers. Product yields of 143 nuclides were obtained.

The charge dispersion was considered to be a Gaussian. The most probable charge (Z_p) seems to have linear dependence on mass number A, $Z_p = 0.39A+4.3$. The product charge dispersion for the mass region from 50 to 176 was found to have a width parameter of σ=1.05. The total chain yields for each foil (target and two Al catcher foils) were deduced from the obtained width parameter, Z_p, and product yields. Figure 1 shows the product-mass distributions for the target and the two catcher foils. The target-like deep inelastic transfer (DIT) products can be observed mainly in the target, whereas the projectile-like DIT products in the second catcher foil. The peak around mass 170 is attributed to fusion-evaporation residues which were predominantly transferred to the most downstream catcher.

Although fusion-fission products are reported[1] to make a broad peak in the symmetric mass region in the system of ^{132}Xe+^{NAT}Fe, this component may be buried in the tails of the target- and the projectile-like DIT components in this experiment. Further experiments at other incident energies are needed to obtain clearer insights into the reaction mechanism.

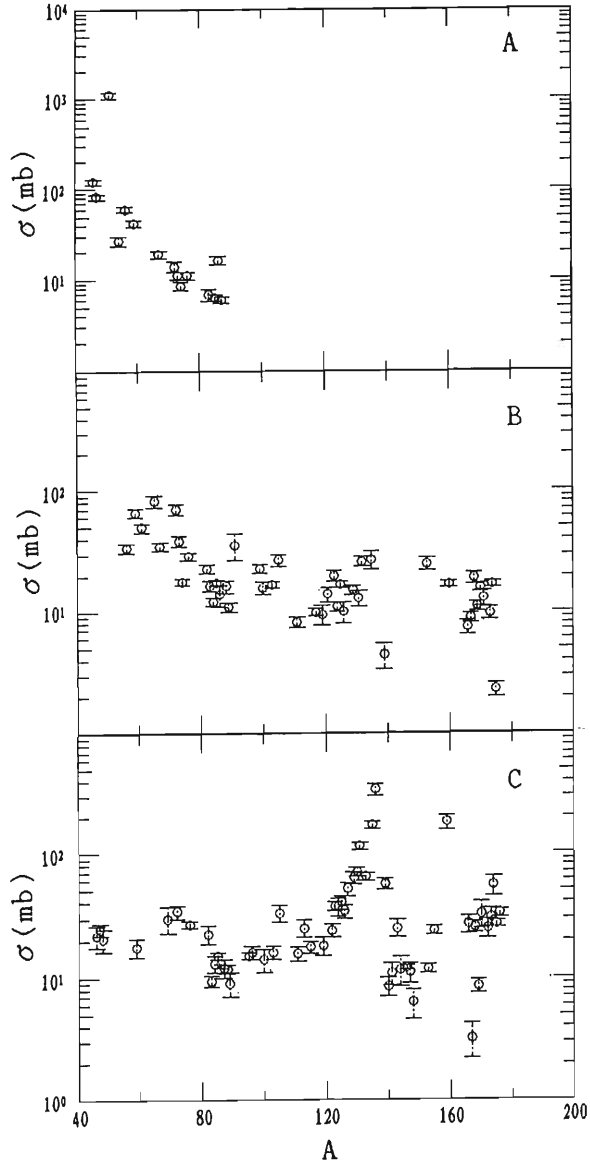

Fig.1 The mass distributions for the target (A), the first catcher (B), and the second catcher(C).

References

1) R. A. Esterlund, W. Westmeier, U. Reus, A. M. Habbestad Wätzig, and P. Patzelt: *Nucl. Phys.*, **A435**, 597 (1985).

III-3-11. Nuclear Reactions with Intermediate Energy Heavy Ions on V, Cu, Nb, and I

E. Taniguchi, J. Kurachi, A. Shinohara, M. Furukawa, S. Kojima, K. Takesako, T. Saito, Y. Ohkubo, S. Shibata, and F. Ambe

Nuclear reactions induced by intermediate energy heavy ions have been extensively studied. Further studies are, however, still required to elucidate the reaction mechanism in detail. We have measured cross sections and recoil properties in the reactions of V, Cu, Nb, and I with ^{40}Ar (38, 59, 95MeV/nucleon), ^{14}N (135MeV/nucleon), and ^{15}N (70MeV/nucleon) ions. The target stack was irradiated at the falling-ball irradiation facility[1] installed at the E3b course of the RIKEN Ring Cyclotron. Targets were metal foils (10~30μm thick) and KI discs covered with polyester films or aluminum foils to catch the recoil products. Non-destructive γ-ray spectrometry was performed with Ge detectors for three months after bombardment. Mass yield distributions were obtained from the measured cross sections on the basis of the charge distributions. Mean longitudinal momentum transfer was deduced from the measured mean recoil ranges.

As an example, the mass yield curve of ^{93}Nb + ^{40}Ar reaction is shown in Fig. 1. In the target fragmentation region (A=40~80), the slope of the mass yield curve for 38MeV/nucleon is higher than that for 59MeV/nucleon. However, much difference cannot be seen between 59MeV/nucleon and 95MeV/nucleon. From our experimental data, the higher projectile energy results in the lower slope of the mass yield curve until the projectile energy reaches 2~3GeV. Above the energy, the slope of the mass yield curve approaches a constant value. Mass dependence of the mean longitudinal momentum transfer for the same reaction system is shown in Fig. 2. The results show that the mean longitudinal momentum transfer decreases with increasing projectile energy.

The changes of the slope of the mass yield curve with various targets at the same bombarding energy are insignificant. The mean longitudinal momentum transfer decreases with the increase of the target mass. The reaction mechanism will be examined from detailed analysis of the experimental data.

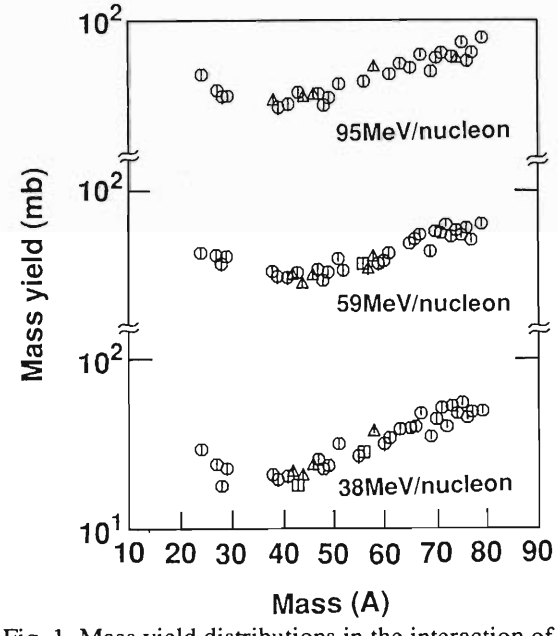

Fig. 1. Mass yield distributions in the interaction of ^{93}Nb with ^{40}Ar ions (○:observed nuclides<30% △: observed nulcides≥30% □:observed nuclides≥60%)

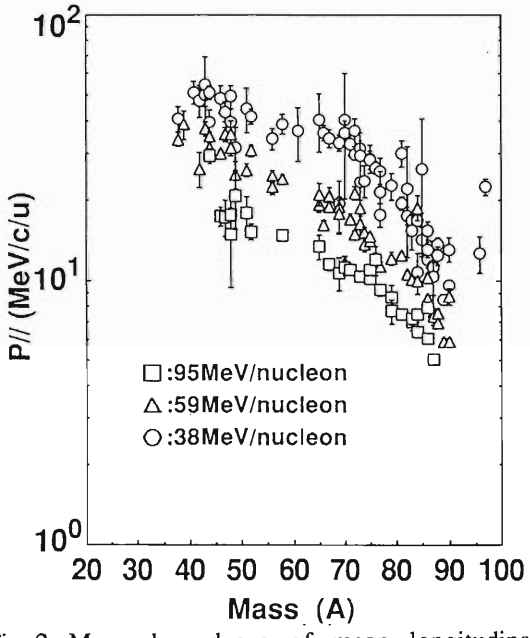

Fig. 2. Mass dependence of mean longitudinal momentum transfer for ^{93}Nb + ^{40}Ar reaction.

References

1) S. Ambe *et al.*: *Chem. Lett.*, **1991**, 149.

III-3-12. Nuclear Reaction Products in the Interaction of ^{197}Au and Intermediate Energy Heavy Ions ^{14}N, ^{15}N, and ^{40}Ar

J. Kurachi, E. Taniguchi, A. Shinohara, M. Furukawa, S. Kojima, K. Takesako, T. Saito, Y. Ohkubo, F. Ambe, and S. Shibata

Au targets were irradiated with heavy-ion beams ^{15}N (70MeV/nucleon), ^{14}N (135MeV /nucleon) and ^{40}Ar(38, 59MeV/nucleon) to study the projectile dependence of the nuclear reactions including fission induced by intermediate energy heavy ions.

Irradiations were performed at the falling ball irradiation facility[1] installed at the E3b course of the RIKEN Ring Cyclotron. Target stacks consisted of Au foils (37~43mg/cm^2 thick) surrounded by Mylar and aluminium catchers. After irradiations, γ -rays from the targets and the catcher foils were measured with Ge detectors. Mass yield distributions were deduced from measured formation cross sections (Fig. 1). Linear momentum transfer per nucleon ($v_{//}$) and isotropic momentum components (V) were deduced from measured recoil ranges by means of the two step vector model[2] (Fig. 2). The products were classified into fission (A=55~110), spallation (A=130 ~180) and nucleon transfer (A>180) reaction products from the mass and momentum distribution. The fission yields were obtained by subtracting spallation components from mass yields in the region, A=59~111. The spallation component yields were extrapolated from the mass yields in the region of A=135~ 175. The fission yields were fitted to Gaussian to obtain the fission cross section. The results of analysis for fission are presented in Table 1. The fission cross section decreases with increasing projectile energy per nucleon. The mass of fissioning nucleus was estimated to be 160~180 from the center of the mass distribution. The $v_{//}$ values of fission products are similar to those of products in the vicinity of the target. These suggest that these products originate from the fission of target-like nuclei.

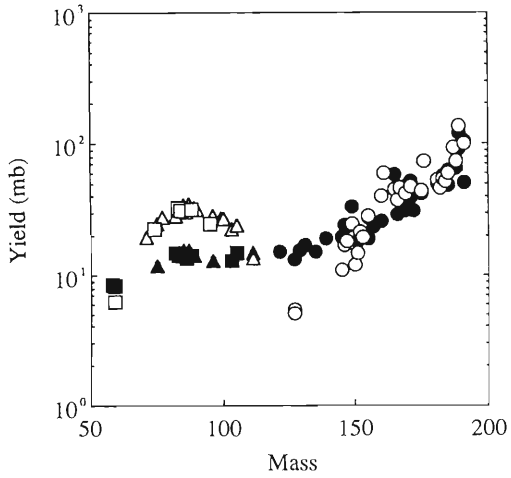

Fig. 1. Mass yield distributions in the interaction of Au with ^{14}N 135MeV/nucleon (solid) and ^{15}N 70 MeV/nucleon (open). Symbol ○ denotes that it is cumulative yield. The other symbols indicate the fraction of each yield that was measured: △: <40%; □: >40%.

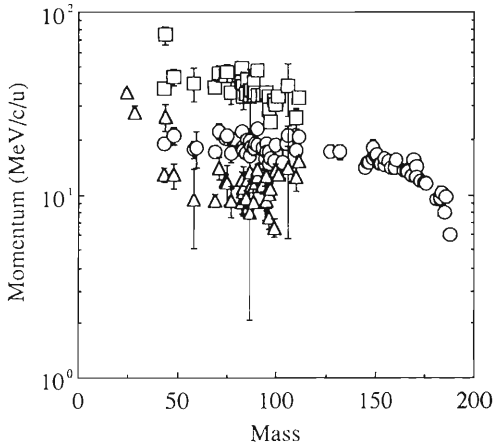

Fig. 2. Momentum distribution of products in the interaction of Au with ^{15}N 70MeV/nucleon. Symbols denote: ○, $v_{//}$ from the average forward range; △, $v_{//}$ from the two step model, □: V from the two step model.

Table 1. Parameters of fission mass distribution.

Projectile (MeV/nucleon)	Center (A)	FWHM (A)	Fission Cross Section (A)
^{14}N (135)	81.4±1.5	52±4	0.24±.06
^{15}N (70)	87.3±.3	36.8±.7	0.62±.05
^{40}Ar (59)	89 ±7	49 ±3	0.61±.17
^{40}Ar (38)	92.9±.2	48.9±.2	1.18±.16

References

1) S. Ambe *et al.*: *Chem. Lett.*, **1991**, 149.
2) L. Winsberg: *Nucl. Instrum. Methods:* **150**, 465 (1978).

III-3-13. Time-Differential Perturbed-Angular-Correlation (TDPAC) of γ-Rays and Emission Mössbauer Spectroscopy of ^{99}Ru in $YBa_2Cu_3O_{7-x}$ Using ^{99}Rh as a Source Nuclide

Y. Ohkubo, Y. Kobayashi, K. Harasawa, S. Ambe, T. Okada, K. Asai, S. Shibata, S. Takeno,* and F. Ambe

The perovskite-like oxide, $YBa_2Cu_3O_{7-x}$, is superconducting for $0 \leq x \leq 0.7$ (Region I), and is semiconducting for $0.7 \leq x \leq 1$ (Region II). Both phases have two distinctive copper sites. The first site (Cu-1) forms one-dimensional Cu-O chains only in Region I. The second site (Cu-2) constitutes a corrugated two-dimensional plane in both Regions I and II. The variation of oxygen content involves only the population and depopulation of one oxygen site, along the Cu-1-oxygen chains. Thus, the copper ions at the Cu-2 site exist as Cu^{2+} in both Regions I and II. On the other hand, the copper ions at the Cu-1 in Region I exist as Cu^{2+} and Cu^{3+}, and those in Region II Cu^{1+} and Cu^{2+}. It is generally accepted that a copper ion in perovskite-like oxides is easily replaced by a metal ion with its ionic radius close to that of the copper ion. We first prepared a $YBa_2Cu_3O_{7-x}$ with $x \lesssim 0.2$ (YBCO7) containing a 1ppb order of radioactive $^{99}Rh^{3+}$, which decays to ^{99}Ru with $t_{1/2}$ = 15 d.[1,2] All heating processes were done in flowing oxygen. We then prepared a sample with $x \approx 1$ (YBCO6) by heating the YBCO7(^{99}Rh) sample under reduced pressure at 760°C for 1 h. The ionic radius of $^{99}Rh^{3+}$ is close to that of Cu^{2+}, and hence rhodium ions are expected to occupy the Cu-1 and Cu-2 sites. We measured TDPAC spectra of the ^{99}Ru 3/2+ level ($t_{1/2}$ = 20.5 ns) in the two samples to determine the Ru or Rh site occupancy. The emission Mössbauer spectra of the two samples were measured at 5 K.

Figures 1(a) and (b) show the frequency spectra derived from the TDPAC spectra of ^{99}Ru in YBCO7 and in YBCO6, respectively. Figure 1(a) shows two electric field gradients (EFG's) corresponding to two peaks. These two EFG's might be ascribed to two Ru sites corresponding to the Cu-1 and Cu-2 sites. But, as shown in Fig. 1(b), there is only one Ru site in YBCO6 corresponding to either Cu site. We must consider the possibility that during the heating process under reduced pressure at 760°C mentioned above, Rh ions at one Cu site moved to the Cu site of the other type. In order to examine this possibility, we heated the YBCO6(^{99}Rh) sample in flowing oxygen at 280°C for 0.5 h and measured a TDPAC spectrum for this sample. We obtained an essentially identical spectrum to that of YBCO7(^{99}Ru). At this low temperature, it is unlikely for heavy Rh ions to move to another site. We thus conclude that Ru ions occupy one type of Cu site and that the two EFG's seen in Fig. 1(a) correspond to two oxygen configurations at Ru ions and one EFG in Fig. 1(b) to one configuration.

We note that the frequency distribution for YBCO6 at 10 K in Fig. 1(b) is widespread. Compared to the Mössbauer spectrum for YBCO7, the spectrum for YBCO6 has a second component with a larger width. From these observations, we consider that there is a hyperfine magnetic field at ^{99}Ru in YBCO6 in addition to the EFG at low temperatures. At least above 80 K this magnetic field is insignificant. The magnitude of the hyperfine magnetic field at the Cu-2 site at 80 K was found to be comparable to that at 10 K, using ^{57}Fe as a probe.[3] On the other hand, the magnetic field at the Cu-1 site at 80 K is a few times less than that at 10 K.[3] We therefore conclude that Ru ions occupy the Cu-1 site in both YBCO7 and YBCO6 exclusively.

We suppose that metal ions like Rh ions which favor high oxidation states are hardly substituted for Cu ions in low oxidation states. Since we first prepared YBCO7 in flowing oxygen and the average valence of the Cu ions at the Cu-1 site is larger than that of the Cu-2 site, Rh ions are considered to have occupied the Cu-1 site.

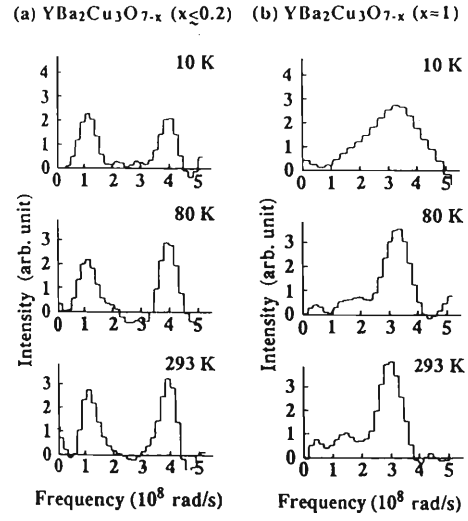

Fig. 1. Frequency spectra of ^{99}Ru in (a) $YBa_2Cu_3O_{7-x}$($x \lesssim 0.2$) and in (b) $YBa_2Cu_3O_{7-x}$($x \approx 1$) at 10, 80, and 293 K derived from their TDPAC spectra.

References

1) Y. Ohkubo, Y. Kobayashi, K. Harasawa, S. Ambe, T. Okada, F. Ambe, S. Shibata, and K. Asai: RIKEN Accel. Prog. Rep., **25**, 89 (1991).
2) Y. Ohkubo, Y. Kobayashi, S. Ambe, K. Harasawa, M. Takeda, S. Shibata, K. Asai, T. Okada, and F. Ambe: Chem. Lett., **1992**, 2069.
3) T. Shinjo, S. Nasu, T. Kohara, T. Takabatake, and M. Ishikawa: J. Physique, **49**, C8-2207 (1988).

* Toshiba Corp., R&D Cent.

III-3-14. Magnetic Moment of Ru Atoms in $Fe_{3-x}Ru_xSi$

Y. Kobayashi, K. Asai, T. Okada, and F. Ambe

^{57}Fe and ^{99}Ru Mössbauer spectra were measured on the ternary alloys $Fe_{3-x}Ru_xSi$ with the Ru concentrations of $0.1 \leq x \leq 1.0$. From ^{57}Fe Mössbauer spectra obtained at 77 K, the distribution of the hyperfine magnetic fields (H_{hf}) at ^{57}Fe nuclei were derived as shown in Fig. 1. It is seen that the distribution of H_{hf} for $0.1 \leq x \leq 1.0$ has two obvious peaks at about 220 and 300 kOe as in the case of Fe_3Si. The starting material of Fe_3Si has two obvious the distribution peaks of H_{hf} at 220 and 300 kOe, on the basis of the magnetic moments (m[A, C] = 1.35 μ_B and m[B] = 2.20 μ_B). The intensity ratio of these two components is roughly 2:1, being consistent with the relative population of Fe atoms on both sites. The distribution of H_{hf} at ^{57}Fe for $Ru_{0.1}Fe_{2.9}Si$ is understood well in line with this. It is found that the peak position of H_{hf} for Fe[B] gradually decreases and the relative intensity increases with an increase of x, while the peak position of Fe[A, C] increases slightly in the Ru concentration range studied. The intensity ratio between the two components decreases from the value of 2 for Fe_3Si and is reversed at $0.9 < x$. It is found that the mean value of H_{hf} for all ^{57}Fe shifts slightly to be larger with the Ru substitution. On the other hand, from ^{99}Ru Mössbauer spectra it is found that H_{hf} of Ru atoms are distributed in a broadened component. The values of H_{hf} are calculated to be 340 kOe and 270 kOe for x=0.5 and 1.0 respectively.

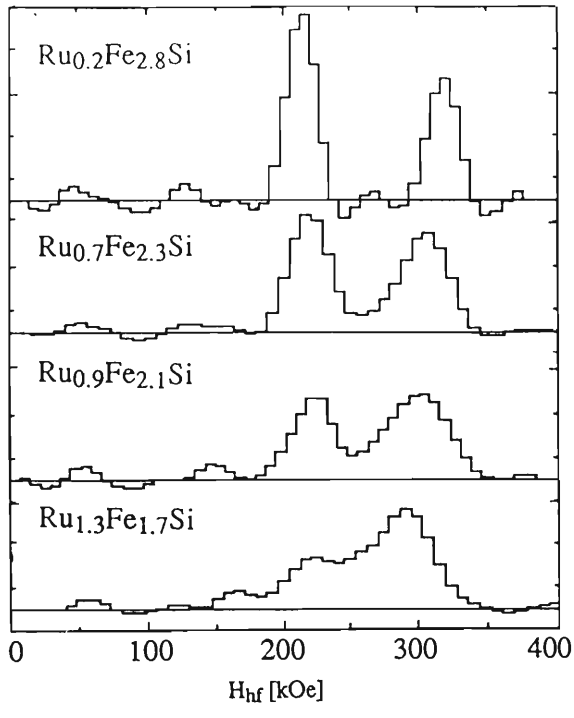

Fig. 1. Hyperfine magnetic field distribution at ^{57}Fe nuclei of the ternary alloys $Fe_{3-x}Ru_xSi$.

In general, all the alloys which contain ruthenium as the main substance are nonmagnetic. In the region of $0.1 \leq x \leq 1.0$, the phenomenon that H_{hf} of Fe[B] diminishes with Ru substitution can be understood qualitatively by a decrease of Fe atoms on the [A, C] sites in number. From the result of NMR measurement,[1] Ru atoms are expected to substitute selectively Fe atoms on the [A, C] sites with the quite dilute concentration of ruthenium (x=0.04) in this system. H_{hf} transferred from Fe[A, C] is reduced with the increase of the substituted Ru atoms. It is considered, however, that the previous result does not refer to our present study because the range of substituted Ru concentration is different. In order to interpret the fact that the magnetization per chemical formula in this system show little appreciable change in spite of decreasing H_{hf} of Fe[B], two possibilities can be considered; Ru atoms on [A,C] sites possess a magnetic moment, or nonmagnetic Ru atoms enhance the magnetic moment of adjacent Fe[A, C] and/or [B]. The composition dependence of H_{hf} at ^{57}Fe in the present study indicates that the magnetic moments of some Fe[A, C] may be enhanced by substituting Ru atoms for Fe atoms in [A, C] and/or [B] sites.

More quantitative discussion will be given elsewhere together with experimental results on the series of this system.

References

1) V. A. Niculescu, T. J. Burch, and J. I. Budnick: *J. Mag. Mag. Mater.*, **39**, 223 (1983).

III-3-15. The Influence of Light Element Mixture on the Lifetime of Carbon Stripper Foils

I. Sugai, M. Oyaizu, M. Aratani, and M. Yanokura

We have been investigating the best methods to make not only long lifetime, but also mechanically strong carbon stripper foils with high reproducibility.[1,2] Through a series of recent experiments, we developed a quite new type method,[3] which was based on the ion beam sputtering(IBS). In that work the lifetime of foils was strongly affected by the amount of hydrogen, nitrogen and oxygen light elements in the foils.

In order to confirm the effect of the amount of light elements used as the reactive ion beam to sputter carbon on lifetime, we made foils by using single gases H_2, N_2 or O_2, or binary mixing gases such as diluted (H_2 + Ne), (N_2 + Ne) or (O_2 + Ne), and compared the lifetime with those of foils made by the thermal evaporation methods. All foils have surface densities of 15 to 25 μg/cm^2 and their size is 15 x 15 mm^2.

The lifetime measurements of foil were carried out by 3.2 MeV Ne^+ beams of intensity of 3 - 4 μA from the Van de Graaff Accelerator at the Tokyo Institute of Technology. The lifetime was defined as an integrated current incident upon the foil till rupture.

The contaminants of light elements such as H, N and O in the foils were examined by ERDA (Elastic Recoil Detection Analysis) and RFS (Rutherford Forward Scattering) methods using 50 MeV Ar^{4+} beams from the RILAC.

Figure 1 shows the result of lifetime meaurement of the foil made by the single and binary mixing gas methods, together with that of a commercially available carbon(CM) foil. As shown in the figure, an extraordinarily long lifetime was achieved in the case of ion beam sputtering of reactive single nitrogen(IBSRN), and the foil made by binary mixing gas of (N_2 + Ne) also shows rather long lifetime. On the other hand, we can clearly see that foils made by the single or binary mixing of hydrogen or oxygen gases had very short lifetimes. The lifetime of a foil made by the thermal evaporation method is nearly the same as that of a CM foil. As a reference the lifetime of the foils made by the IBS of Ne gas is shown in Fig.1.

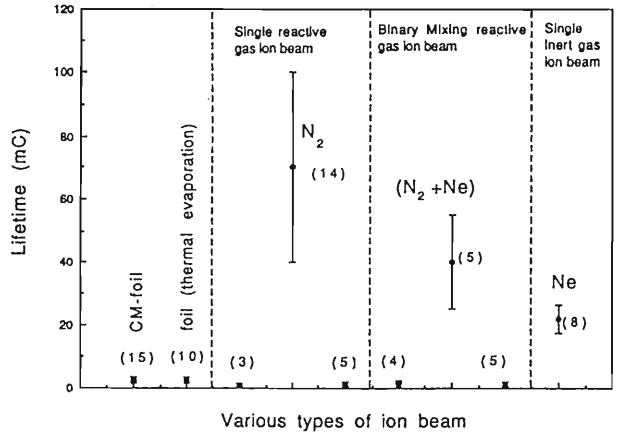

Fig.1. Comparison of relative lifetimes of foils made by different types of gas ion sputtering. The lifetimes were measured by using 3.2 MeV Ne^+ beams of 3-4 μA intensity. The foil thickness was about 15 μg/cm^2. The average total incident current in mC(milli-Coulomb) until rapture is plotted with the number of samples investigated in parentheses beside the point.

It is worth while to notice that the foils made by the binary mixing gas of (N_2+Ne) have the longest lifetime among the binary mixing gases, but the life is shorter than the IBSRN, and the foils sputtered by the single or mixing of hydrogen or oxygen gases show a shorter lifetime than a CM foil.

The admixture of oxygen or hydrogen in carbon foils always reduces the lifetime. The bondings between carbon and nitrogen atoms in the foil are probably stronger and more stable than those of hydrogen or oxygen atoms for the beam bombardment.

The most important point in prodution of extraordinary long-lived foils is to reduce the amounts of hydrogen and oxygen contaminants as much as possible.

References

1) I. Sugai et al.: *Nucl. Instrum. & Methods. Phys. Res.*, **A236,** 576 (1985).
2) I. Sugai et al.: *Nucl. Instrum. & Methods. Phys. Res.*, **A282,** 164 (1989).
3) I. Sugai et al.: *Nucl. Instrum. & Methods. Phys. Res.*, **A303,** 59 (1991).

III-3-16. Positron Annihilation Study on Nanometer Cavities in Porous Silicon

Y. Itoh, H. Murakami, A. Kinoshita,* and R. Iwata**

A porous silicon obtained by anodization of a silicon crystal in hydrofluoric acid contains a network of nearly parallel pores. The physical and chemical properties of porous silicon have attracted strong attention. The photoluminescence was found out recently from a porous silicon.[1] The mechanism of the photoluminescence is actively studied while the utilization is discussed as an optical device and a gas and humidity sensor. The surface of pores is covered by an Si-H layer. The study of an Si-H layer is interesting from a view point of positronium chemistry and surface science.

Silicon substrates used were boron-doped wafers of 1~2 ohm-cm with (100) surface. The substrates were anodized in hydrofluoric acids of 20 wt.% - 55 wt.% at a constant current density from 10.2 mA/cm^2 to 100.0 mA/cm^2. The thickness of a porous layer ranges from 30.0 nm to 100.0 nm. The porosity, which is defined as the ratio of the reduced mass from the anodized layer to its mass before the anodization, varies from 0.526 to 0.686.

Measurements of positron lifetime and Doppler broadening were carried out on the anodized samples sandwiching a positron source of ^{22}NaCl. Some of the samples were mounted on a heating stage in a vacuum chamber with a positron source of ^{48}V and evacuated to 3 x 10^{-6} Torr at 350 °C for 4 hr. The spectra of lifetime and Doppler broadening were obtained before and after the evacuation as keeping the sample on the stage in the chamber. The positron lifetime was measured with a fast-fast coincidence system whose time resolution is 210 ps. The Doppler spectrum was obtained with the aid of a pure Ge detector. The energy resolution of the system is 1.07 keV. The lifetime spectra were analyzed with a computer program POSITRONFIT (Kirkgaard).[2] A very long lifetime is clearly observed on porous silicons of #1, #2, and #3 as shown in Fig. 1. The pick-off annihilation of ortho-positronium corresponds to the long lifetime. A value of the lifetime is about a few tens of nanoseconds which is anomalously long as a positronium lifetime in a solid except for a few kinds of zeolites (Ito et al.).[3] Fig. 2 shows Doppler spectra for the porous silicon of #2 (a) and the bulk silicon (b).

A narrow component seems to be overlapped on a broad gaussian component. This suggests the para-positronium formation in a porous silicon. A positron/positronium spectroscopy is very useful in the study of physical and chemical properties of porous silicon. The effect of hydrogen on the surface in the pore is under investigation.

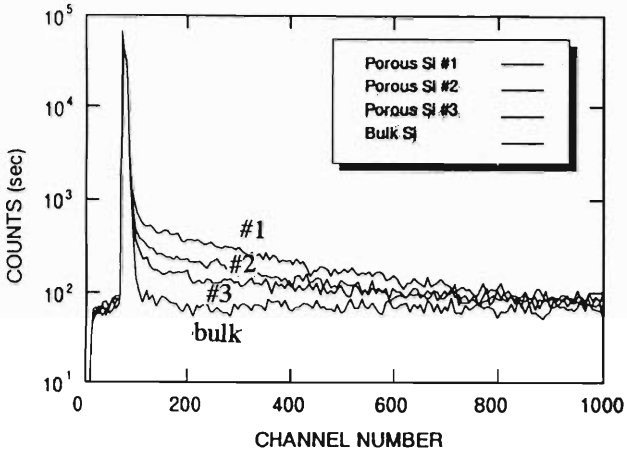

Fig. 1. The lifetime spectra of porous silicons (#1, #2, #3) compared with bulk silicon.

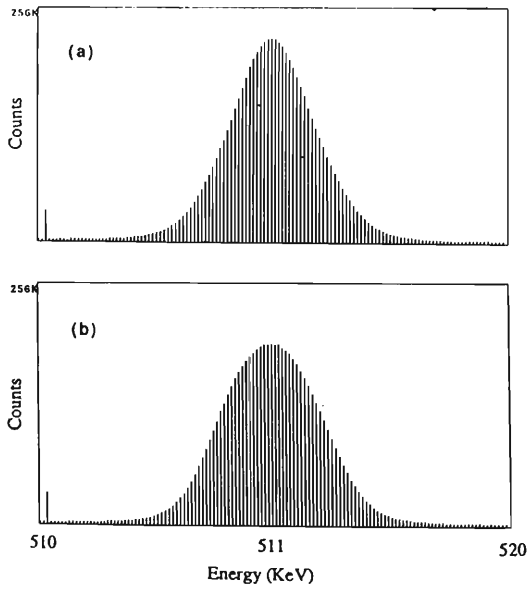

Fig. 2. S-parameter of porous silicon (a) compared with bulk silicon (b).

References

1) L. T. Canham: Appl. Phys. Lett., **57**, 1046(1990)
2) P. Kirkgaard, M. Eldrup, O. E. Mogensen, and N. J. Pedersen: Computer Physics Commun., **23**, 307 (1981).
3) Y. Ito, T. Takano, and M. Hasegawa: Appl. Phys., **A45**, 193 (1988).

* Fac.of Sci.and Eng. Tokyo Denki Univ.
** Cyc. RI center, Tohoku Univ.

III-3-17. Recovery and Clustering of Defects in GaAs Studied by Means of Positron Annihilation

Y. Itoh, H. Murakami, and R. Iwata*

The identification of induced defects and the recovery stage of electron-irradiated GaAs have been studied by positron lifetime and Doppler broadening measurements. Samples used are liquid encapsulated Czochralski(LEC) GaAs whose carrier density is 2.03 x 10^{17} cm^{-3}. Some of the LEC-GaAs were doped with Si atoms of 1.3 x 10^{18} cm^{-3}. They were irradiated by 3 MeV electrons to a dose of 5 x 10^{17} cm^{-2}. The irradiation temperature was held below 50 ℃. The irradiated samples were isochronally annealed for 30 min at various temperatures from 373 K to 973 K and measured at 300 K after each annealing. Some of the irradiated samples were cooled down to a temperature below 300 K to 10 K and measured at the temperature. ^{22}Na was used as a positron source. The lifetime was measured with a fast-fast coincidence system whose time resolution is 210 ps. The Doppler broadening was obtained with the aid of a pure Ge detector whose energy resolution is 1.07 keV.

Figure 1 shows temperature dependence of lifetime(a) and S-parameter(b) of electron-irradiated undoped and Si-doped GaAs. The lifetime decreases as the temperature decreases. The lifetime of 260 ps at 300 K is classified as a gallium vacancy,V_{Ga}.[1-3] The charge state of V_{Ga} is considered to change from a negative state to a neutral state as the temperature decreases since V_{Ga} is an acceptor type defect.[1] Then the lifetime is expected to increase as the temperature decreases but the observed lifetime shows an opposite tendency. One possible explanation is deduced from the coexistence of antisite

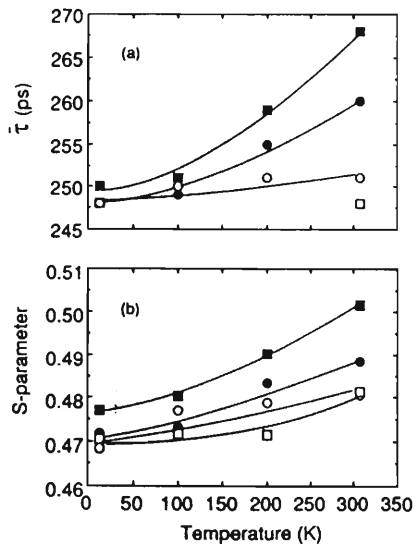

Fig. 1. Temperature dependence of positron lifetimes(a) and S-parameter(b) in undoped(■) and Si-doped (●) GaAs irradiated with electrons. The results obtained before irradiation on undoped (□) and Si-doped (○) samples are also included.

Ga, Ga_{As}, induced upon the irradiation, together with V_{Ga}. Ga_{As} is considered to act as a weak trap of positron at low temperatures. The lifetime of positrons trapped by this shallow trap is shorter than that in V_{Ga}. The decrease of S-parameter as the temperature decreases supports strongly the coexistence of Ga_{As} and this conclusion agrees with the proposal by Corbel et al.[3]

The lifetime and S-parameter of electron-irradiated undoped and Si-doped GaAs change during the isochronal annealing as shown in Fig. 2(a) (b). Two annealing stages were observed in the both samples. This suggests that V_{Ga}'s gather and form clusters in the lower temperature stage, and the clusters are annealed out in the higher temperature stage. The effect of Si dopants shifts the annealing stage to the higher temperature. The detailed discussion was presented in UN3PC92 conference.

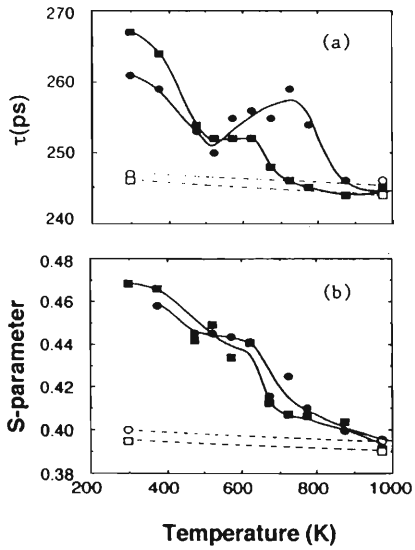

Fig. 2. Isochronal annealing of the positron lifetime and S-parameter in electron-irradiated GaAs; (■) undoped and (●)Si-doped samples. The results obtained before irradiation on undoped □) and Si-doped (○) samples are also included.

References

1) G. Dlubek, A. Dlubek, P. Bremmer, K. Frieddland and R. Rentszch: Phys sat.. sol. (a), **106**, 419(1988); G. Dlubek, A. Dlubek, R. Krause, and O. Brummer: Phys. stat. sol. (a), **107**, 111 (1988).
2) S, Dannefaer, B. Hogg and D. Kerr; Phys. Rev.. **B30**, 335 (1984).
3) C. Corbel, M. Stucky, P. Hautojarvi, K. Saarinen, and P. Moser: Phys. Rev., **B38**, 8192.(1988); C. Corbel, F. Pierre, P. Hautojarvi, K. Saarinen, and P. Moser: Phys. Rev., **B41**, 10632 (1990).

* Cyc. RI center, Tohoku Univ.

4. Radiation Chemistry and Radiation Biology

III-4-1. LET Dependent Competition between Radiative and Nonradiative Annihilations of Core Holes Produced by Ion Irradiation of BaF_2 Single Crystal

K. Kimura, R. Nemoto, S. Nakamura, K. Morita, and H. Kumagai

VUV-photon or electron excited BaF_2 single crystal is known to exhibit a 2200 A luminescence band. This luminescence is named the Auger-free luminescence in the sense that the valence electron of F2p transits to the core hole of Ba5p radiatively instead of emission of Auger electrons. One of characteristics of this luminescence is that its decay time is as short as 800 ps, which cannot be explained by self-trapped excitons. We have measured luminescence decay with various ion irradiations, using SISP[1] which is an equipment for measurement of fast luminescence decay. Results were different from those of the photo-irradiation. The decay could be decomposed into two exponentials. A fast component decreases in its decay time with increasing LET(linear energy transfer of ions), while the decay time of a slow one shows no systematic variation to LET although the value for He ions is too large (Table 1). These results can be explained by the following model[2]. In case of the ion irradiation, there exist free electrons ejected at a high density and they can recombine with the core hole competitively with the Auger-free luminescence process (See Fig. 1). From competition kinetics, the instantaneous luminescence I(t) can be expressed as,

$$I(t) = k_1[Ba^{3+}]_0 \exp\{-k_1 + k_2[e_{free}]t\}$$

Table 1. LET-dependent decay times.

Excit.	VUV-light	He	N	Ar	Kr	Xe
fast/ps	800	440	300	240	220	220
slow/ps	——	1500	814	800	790	840

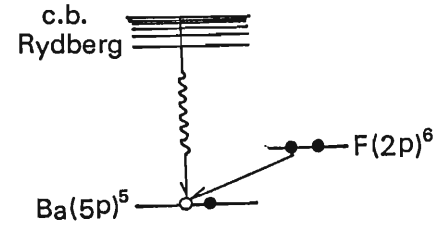

Fig.1. A competition between nonradiative transition and Auger-free luminescence.

where k_1 denotes the rate constant of the Auger-free luminescence and $k_2[e_{free}]$, that of above nonradiative recombination. LET dependence of the latter can be plotted as Fig. 2. The value attains to a constant value at LET of 15 MeV/cm^2/mg due to that for Kr-ions. A reciprocal of the value ceiled means a life time of the Ba5p core exciton.

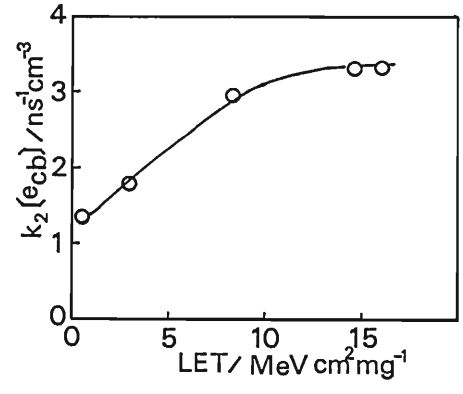

Fig.2. $k_2[e_{free}]$ as a function of LET.

References
1)K.Kimura, T.Matsuyama, and H. Kumagai: Radiat.Phys.Chem. 34,575(1989);K. Kimura and H. Kumagai: to be published in Radiat. Ef. Defect. Sol.126, Dec.(1992)
2)K. Kimura and J. Wada: submitted to Phys. Rev. Let.

III-4-2. Depth Resolved Dynamics of Ion-tracks

Correlation between VUV- and VIS-Excimer Luminescence from Ion-Irradiated Dense Helium

K. Kimura, R. Nemoto, S. Nakamura, and K. Morita

A track scope, composed of an imaging quartz fiber and a position-sensitive photon counter, was developed. Luminescence spectra, their specific intensities dL/dx, and efficiencies dL/dE, were measured as functions of the helium density and of depth along the N- and He-ion tracks in dense gas and liquid helium. Observed visible luminescences were limited to those due to Rydberg states of excimers, ^3d, ^3D, ^3H, and ^3J, according to Herzberg's notation. It can be concluded that they are produced only by the bimolecular reaction of the lowest triplet excimer, ^3a, and that excess energy of this reaction must be removed by the third body. With increasing penetration depth, dL/dx was enhanced and exhibited a peak maximum whose position depends on the helium density. This behavior of dL/dx could be expressed by the excitation density (Fig.1). In an extreme case near the track termination, dL/dx was turned to be suppressed. A new-type quenching process that the three-body reaction cannot find the third body except for the excimer ^3a could explain the result.[1)]

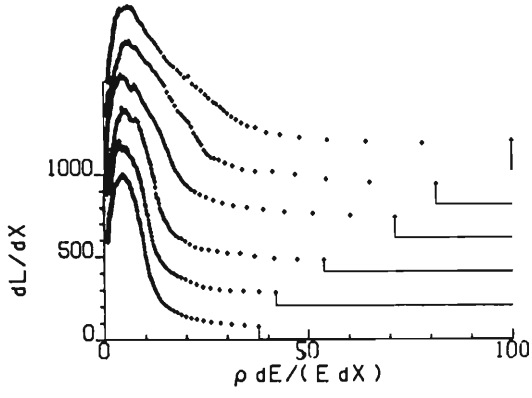

Fig.1. VIS-dL/dx vs excitation density induced by 4MeV/amu N ion with various helium densities from 0.02 at top to 0.0638 g/cm^3 at bottom.

Also, depth-resolved VUV(vacuum ultraviolet)-luminescence due to the transition ^1A-^1X has been measured on a dense helium target with variation of helium density. With increasing excitation density, the formation of ^1A is enhanced by $^3a+^3a$ reaction and suppressed by $^3a+^3a+^3a$ reaction, as was the case of VIS-luminescence. However, the dL/dx peak shifted to smaller excitation density. An additional peak in luminescence efficiency dL/dE , appeared near 4.8×10^2 cm/sec of ion velocity, was much more intense than that for VIS-dL/dE(Fig.2). The peak was explained by charge exchange and direct excitation processes.[2)]

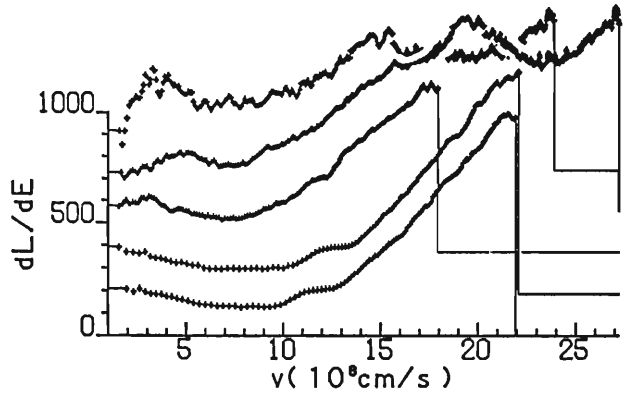

Fig.2. VUV-dL/dx vs N-ion velocity in helium at the densities from 0.02 at top to 0.062 g/cm^3 at bottom.

References

1)K.Kimura, Phys. Rev. A to be published in Vol47 Jan.(1993); Nucl.Instrum.Meth. B53, 301(1991)

2)K.Kimura, Nucl.Instrum.Methods B, in press.

III-4-3. Radiation Effects of Ion-particles on Various DNA Structures

S. Kitayama, K. Nakano, T. Takahashi, M. Suzuki, M. Kikuchi, and H. Watanabe*

Ionizing radiation including accelerated particles induces various damages in DNA of living cells. Although most of them are repairable in the cell, unrepairable damages are thought to be the cause of cell inactivation. However, little is known about what kinds of DNA damage are unrepairable in the living cells. It is also unknown whether unrepairable DNA damages are qualitatively and/or quantitatively different in eukaryotic or in prokaryotic cells. In eukaryotic cells double - helical DNA coils around histone hexamers (=beads). These beads make a helical string of them with H1 histone and other non-histone proteins. The native DNA is wrapped further into a structure of higher order by tying up these strings in a bundle. Therefore, it can be expected that the type and /or number of radiation damages in a naked DNA might be different from those induced in the folded structure such as chromosome. In prokaryotic cells double-strand DNA is also folded with many DNA binding proteins and binds to the cell membrane. From these reasons it is quite important to avoid the artificial damage during the extraction and analysis of irradiated DNA. Recent technical progress in the analysis of a large DNA, such as the pulse field gel electrophoresis, makes it possible to measure the strand breakages in a large DNA. Whole chromosome of bacteria such as *E. coli* is the order of ~10^6 base pairs (bp). Therefore, it can be cleaved at defined positions with a restriction endonuclease into several fragments which have hundreds kilo bp. Using this technique it is possible to compare radiation damage in each DNA fragment in contrast to analyze the damages in an unidentified gross DNA fragment mixture.

In order to compare the radiation effects of N-ions (~135 MeV/μ) on naked, folded or packaged DNA in a cell, cells of *Deinococcus radiodurans* were solidified with agarose. Before the irradiation the cells were lysed in the presence of RNases and treated with or without proteinase. The "naked", "folded" or "packaged" DNAs were irradiated with various doses of the ions. Following the lysis of cells and treatment with proteinase, DNAs were digested with a restriction endonuclease. Not I, and analysed by the pulse field gel electrophoresis. This enzyme digested the unirradiated chromosomal DNA into 11 pieces whose sizes are as follows; 216, 230, 253, 277, 303, 307, 320, 365, 388, 418 and 498 kbp.[1)]

A preliminary experiment was carried out to determine the dose of irradiation adequate to find out the change of DNA fragments listed above. It was observed that bigger DNA fragments of a "folded" DNA disappeared substantially in contrast to those of other two samples. The figure will be presented after confirmation by more detailed experiments since the result was observed once at a dose of irradiation.

References

1) J.K. Grimsley, C.I.Masters, E.P. Clark, and K.W. Minton: *Int. J. Radiat. Biol.*, **60**, 613 (1991).

* Japan Atomic Energy Research Institute

III-4-4. Further Studies on Sensitivity of XP Cells to Heavy Ions

F. Yatagai, K. Nakano, K. Eguchi, T. Kanai, T. Takahashi, and F. Hanaoka

Xeroderama pigmentosum (XP) is an autosomal recessive human disease, clinically characterized by high incidence of skin cancers on sun exposed areas. XP cells are hypersensitive to killing by ultraviolet light (UV) due to their defect in nucleotide-excision repair of UV-induced DNA damages[1]. Genetic complementation analysis by cell fusion has identified 7 genetic complementation groups, designated groups A to E, G, and variant.

In this study, we planed to get some insights into the possibility that DNA damages, reparable by the same nucleotide-excision pathway as that for UV lesions, are also produced by heavy-ion irradiation. As well as normal human fibroblast cells (NB-1), XP cells of complementation groups, C and D, were exposed to carbon ions (135MeV/n) accelerated by the cyclotron. Linear energy transfer of the carbon ion corresponded to 22.5 keV/μm. The survival curves in Fig.1 demonstrated that the radio-sensitivity for XP-C cells was a little higher than those for NB-1 and XP-D cells.

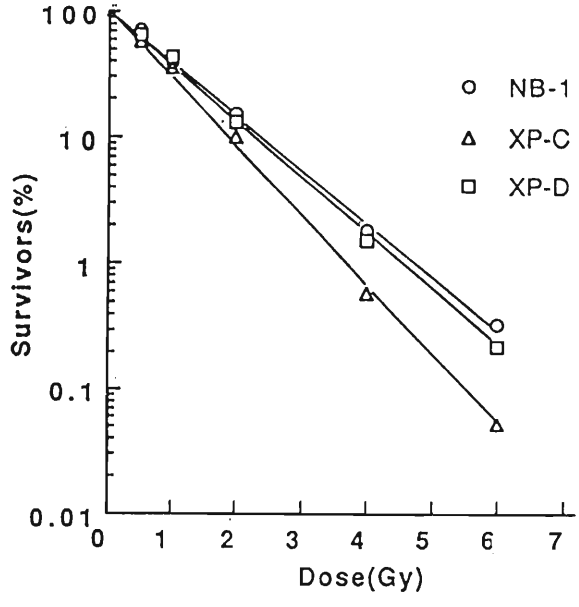

Fig.1. The survival curves of XP and NB-1 cells for carbon ion (LET=22.5keV/μm)

An analysis by the natural elution technique was made to explain this small difference in the sensitivity by the DNA double-strand breakage (dsb) remaining after ~15hours post-irradiation incubation. Unfortunately, comparison between XP-C and XP-D revealed almost no difference in the relative number of remaining dsb (Fig.2). For better understanding, the relative number of dsb following Co-60 gamma rays irradiation was also shown in Fig. 2 and those data do not contradict with the small decrease in the killing effect compared to that by carbon ion (22.5 keV/μm).

In this elution analysis, there is a possibility that we could detect not the damages related to the excision repair but only the dsb induced by direct hit of c-ions and its high-energy secondary electrons.

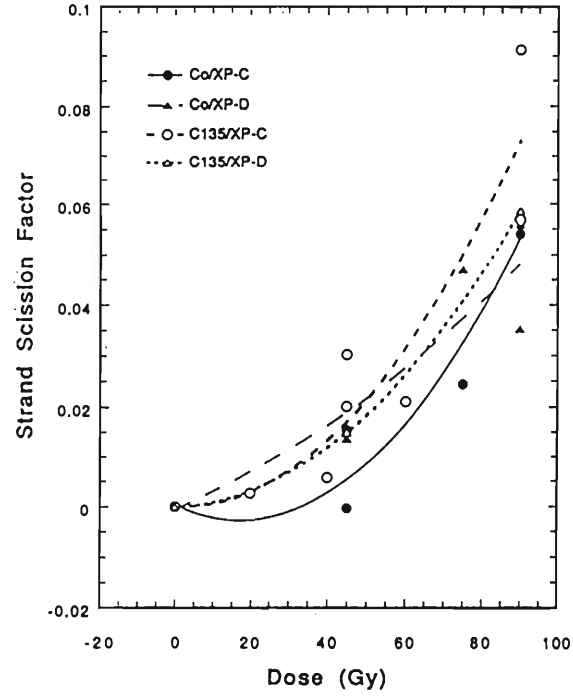

Fig.2. The neutral elution analysis for dsb remaining after ~15 hours post-irradiation incubation. Strand scission factor was calculated from the relative radioactivity remainig on the filter to the total, reflecting the relative number of dsb.

References

1) K. Tanaka: *Cell Technology.*, **9**, 972 (1990).

III-4-5. Effect of Carbon Beam Irradiation on Human Monolayer Cells

H. Ito, S. Yamashita, I. Nishiguchi,* W. Ka,* F. Yatagai, and T. Kanai

This study was performed to determine the biological effect of carbon beams on human monolayer cells (HeLa, RMUG), comparing with that of 200kVp X-rays. Carbon beams were generated by the Riken Ring Cyclotron. The cells were maintained in an F10 medium with 10% fetal bovine serum in a 5% CO2 incubator. The cells in a proliferative phase were irradiated at room temperature. The irradiated cells were trypsinized and survival curves were determined by the colony assay.

"Figure 1 (left)" showed the relationship between the linear energy transfer (LET) and relative biological effect (RBE) at a 0.1 survival. The increase of the RBE was observed in both cell lines according to the increment of the LET of carbon beam between 20 and 80keV/μm. The RBE depended on the dose of irradiation at higher LET region (80keV/μm) and the increase of the dose from 0.8Gy to 3.2Gy decreased the RBE from 2.9 to 2.7 (Figure 1 right). The recovery between split doses was expected, since the survival curves of both cell lines irradiated with 20keV/μm carbon beams showed the initial shoulder (n=1.4). Figure 2 showed the recovery between two split doses (4 hours interval). When RMUG was irradiated of 4Gy of 200kVp X-ray (in split dose experiment, 2Gy x 2), the recovery rate between two split doses was 1.7. (Recovery rate was calculated by dividing the surviving fraction with split irradiation by that with single irradiation.) RMUG irradiated with 20keV/μm carbon beams (2Gy x 2) showed the recovery rate of 1.4. The recovery between split dose irradiation was observed in both X-ray and carbon beam irradiation. However, thr recovery rate was smaller in carbon beams. The cells irradiated with higher LET than 40keV/μm did not show recovery between split doses. HeLa showed the almost similar results to RUMG.

These results suggested that the fractionated radiotherapy might give some benefits to the normal tissues if the normal tissues in the irradiated volume were given with the low LET beams.

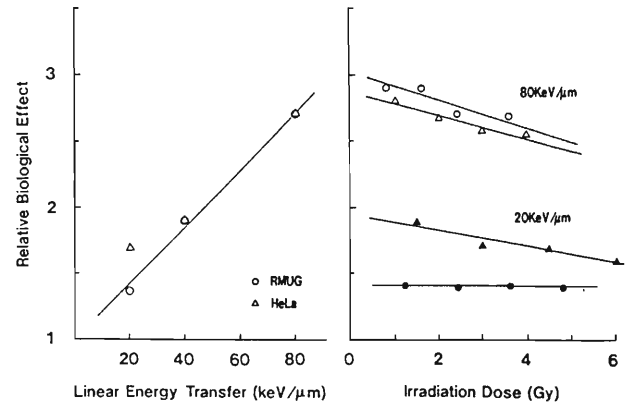

Fig. 1. RBE plotted against LET (left) and dose (right).

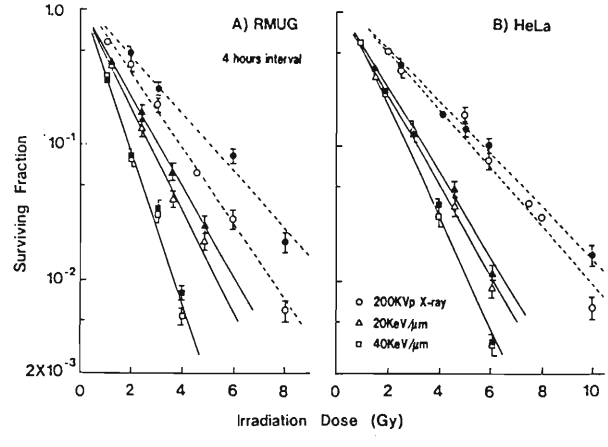

Fig. 2. Survival curves which were irradiated with either single doses (open symbols) or two split doses (closed symbols).

* Keio Univ.

III-4-6. LET Dependence of PCC Breaks in Human Embryo Cells Irradiated with Carbon Ions

M. Watanabe, M. Suzuki,* K. Suzuki,** K. Nakano, F. Yatagai, and T. Kanai

The technique of premature chromosome condensation (PCC) is very useful in detecting both radiation- and chemical-induced damages since the cell cycle delay after irradiation needs not to be considered. It may be a powerful method to compare effects of high and low linear energy transfer (LET) radiations which may produce difference in the cell cycle progression after irradiation (1). X-ray-induced damages have been investigated using the PCC technique by several investigators and their data suggested that the PCC technique is a very sensitive method for detecting chromatin damages (PCC) in interphase cells. Limited reports, however, have been published concerning chromatin damages induced by high LET radiations. Bedford an Goodhead (2) reported the dose-response relationship of the chromatin break formation induced by alpha particles. They showed that the chromatin breaks increased linearly with absorbed dose in the case of both alpha particles and X-rays . However, the relative biological effectiveness (RBE) for alpha particles was 2.3 times larger than that for X-rays. Goodwin at al. (3) studied biological effects of Ne ions (LET= 182keV/um) and X-rays, and found that the amount of chromatin breaks by Ne ions was 1.5 times more than that by X-rays. In addition, although 90 % of the chromatin breaks induced by X-rays were rejoined within 8 hours after irradiation, only 50% of the chromatin breaks induced by Ne ions were rejoined. These data suggest that high LET radiations are more biologically effective in producing chromatin damages than low LET radiations. We previously reported that ^{14}N and ^{4}He ions were more effective in cell killing, mutation, PCC breaks and neoplastic cell transformation than gamma ray in SHE cells (1,4,5).

In this study, we detected chromosome aberrations as chromatin breaks in G_1/G_o interphase human embryo (HE) cells using the PCC technique. We assessed the RBE of the induction of chromatin breaks induced by carbon ion and examined the repair kinetics to qualitatively determine the difference in PCC damages induced by carbon ions with several LETs(22, 39,68,75,110 124, 148, and 230 keV/um). HE cells were irradiated with carbon ions (135MeV/um) generated by the cyclotron at the Institute of Physical and Chemical Research in Japan. Irradiated HE cells were fused with mitotic XP cells by the polyethylene glycol mediated cell fusion to induce PCC.

The incidence of chromatin breaks in cells irradiated with carbon ions was higher than that in cells irradiated with ^{137}Cs gamma-rays. The RBEs, compared to ^{137}Cs gamma ray, were between 1.8-2.3 for carbon ions when they were compared at the same absorbed dose level and the highest value was 2.3 for 110 -124 keV/um carbon ions. This LET dependence is coincident with those for induction of mutants at HGPRT locus and for the degree of lethal effects . Although over 90 % of PCC breaks induced by gamma ray were rejoined within 8 hours of the post-irradiation incubation, only 50-75% of the initial breaks were rejoined. In the case of 110-124 keV/um carbon ions, degree of unrepaired breaks at 12 h after irradiation was 50% of initial breaks and it was the highest value. If protein synthesis in irradiated cells was inhibited, there were no difference in the incidence of PCC breaks. This suggests that newly synthesized protein(s) may play an important role to make LET-dependent-differences in biological effects by high LET radiations.

These results suggest that there is a qualitative difference in the chromatin damage caused by high LET radiations and low LET radiations.

References

1) M.Watanabe, M. Suzuki, K. Suzuki, and K. Watanabe : *In Vitro Toxicology*, **4**, 93 (1991).
2) J.S Bedford, and D.T.Goodhead: *Int. J. Radait. Biol.*, **55**, 211 (1989).
3) E. Goodwin, E. Blakely, G. Ivery, and C. Tobias : ; *Adv. Space Res.*, **9**, 83 (1989).
4) M.Suzuki, M.Watanabe, K. Suzuki, K. Nakano, I. Kaneko:*Radiat. Res.*, **120**, 468 (1989).
5) M. Suzuki, M. Watanabe, K. Nakao, K. Suzuki, and K. Matsui: *Int. J. Radiat. Biol.*, **62**, 581 (1992).

* Division of Radiation Biology, Dept. of Health Sci., Nagasaki Univ.
** Division of RAdiation Biology, School of Medicine, Yokohana City Univ.

III-4-7. Tumor Control Probabilities and Tumor Growth Delay after Accelerated Carbon Ions

K. Ando, S. Koike, M. Kimoto, M. Iizuka, T. Kiuchi,* T. Aruga,* W. Shimizu,*

T. Sugita,* C. K. Cho,* T. Kanai, H. Kato,* and F. Yatagai

Biological effects of carbon-12 (135MeV/n) accelerated by RIKEN Ring Cyclotron were investigated for transplantable NFSa fibrosarcomas growing hind legs in syngeneic C3H male mice. Under pentobarbital anesthesia, right hind legs with tumors (7mm diameter) were placed in a doughnut-shaped radiation field with a 2.5cm rim. A Bragg peak of carbon beams was spread out by a range modulator to a 3-cm width. The leg tumors received single doses of carbon-12 with Spread-Out-Bragg-Peak (SOBP) and unmodulated plateau. As references, Cs-137 γ-rays and cyclotron-produced fast neutrons (13MeV) were also used here. For initial experiments, a 1st generation range modulator was used to generate SOBP. Tumor control probabilities were determined 120 days after irradiation. TCD50/120 (radiation doses for halves of mice to achieve tumor cure 120 days after irradiation) after unmodulated plateau, entrance to SOBP, proximal SOBP, and mid SOBP were 56.4Gy, 58.3 Gy, 36.5Gy, 35.8Gy, respectively (Fig.1). Comparison of these values to reference ones indicated that RBEs (γ/C) were 1.5 for unmodulated plateau, 1.4 for entrance, and 2.3 for both proximal and mid SOBPs. Fast neutrons gave a TCD50 of 28.2Gy and a resultant RBE (γ/n) of 3.0. For second experiments where the tumor growth delay was measured, a 2nd generation range modulator was employed. The tumor growth was measured by calipers every day after irradiation, and the tumor growth delay relative to untreated controls was obtained (Fig.2) Data of combined four experiments indicated that RBEs of mid SOBP and distal SOBP at 1Gy were as large as 7.0, and that RBEs decreased when dose increased (Fig.3). At a high dose region, fast neutrons again gave larger RBEs than carbons. These results suggested that both oxygen enhancement ratio (OER) and oxic cell kill effects would be larger for carbon ions than for fast neutrons.

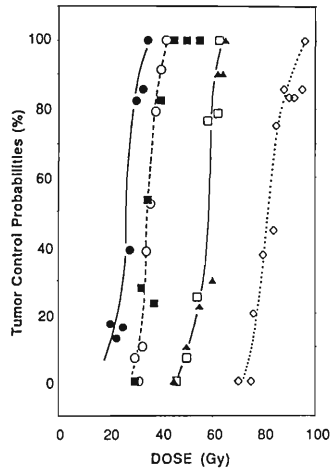

Fig.1 Tumor control probabilities after fast neutrons(●), γ rays (◇), carbon unmodulated plateau (□), entrance (▲), proximal (■) and middle (○) of SOBP.

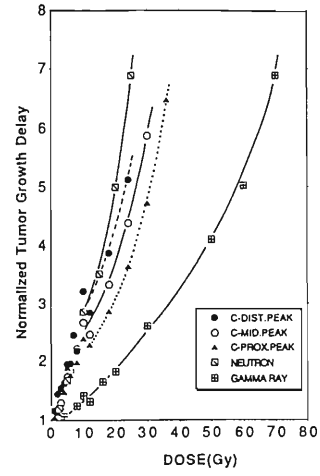

Fig.2 Dose-tumor growth delay relationship.

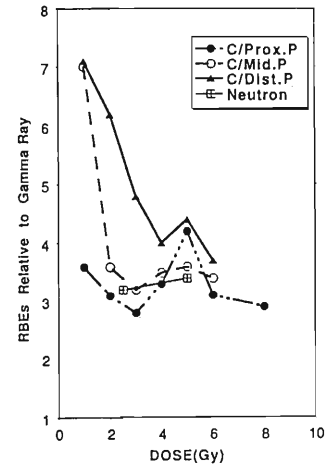

Fig.3 RBEs of carbon-12 and fast neutrons relative to Cs-137 γ rays for tumor growth delay.

*Natl. Inst. Radiol. Sci.

RIKEN Accel. Prog. Rep. 26 (1992)

III-4-8. Early Skin Damage in Mice after Single Doses of Accelerated Carbons

K. Ando, S. Koike, M. Kimoto, M. Iizuka, T. Kiuchi*, T. Aruga,* W. Shimizu,*

T. Sugita,* C. K. Cho,* T. Kanai, S. Furukawa,* H. Kato,* and F. Yatagai

Biological effects of carbon-12 (135MeV/n) accelerated by RIKEN Ring Cyclotron were investigated for a leg skin of C3H female mice. Two spots were tattooed with Indian ink into the skin of outer side of right hind legs prior to irradiation. The distance between the spots was measured one month after irradiation, and compared with the preirradiated value to obtain percent skin shrinkage. Skin reaction was also scored by a scoring method which is convenient but semiquantitative. Mice were anesthetized by an injection of pentobarbital, and their right hind legs were placed in a doughnut-shaped radiation field with 2.5cm rim. Single doses were used. Unmodulated carbon beams entered through the outer skin of legs. Skin shrinkage at Day 30 indicated that the biological effectiveness of carbon -12 relative to γ rays (RBE) was ranging from 1.5 to 4.0, depending on the linear energy transfer (LET) and on the severity of damage (Fig.1).

Skin shrinkage increases with a dose-dependent fashion till certain doses over which saturation of skin shrinkage was observed for all four different LETs of carbon beam (Fig.2). Higher LETs showed a lower saturation level than lower LETs. As the highest LET used here (100keV/μm) penetrated only 0.6mm deep while the lowest LET (22keV/μm) could completely (38mm deep) pass through entire legs (5 mm thick), the saturation level would be due to either LET or dose-distribution or both. The damage saturation was also observed for the skin reaction determined by a scoring method. When a counter dose with 100keV/μm of Carbon-12 was delivered to the inner skin in addition to the outer skin, the skin reaction in the outer skin was enhanced even though the counter dose did not reach the outer skin (Fig.3). These results indicated that particle beams would be useful for studying the volume effect of normal tissue damage.

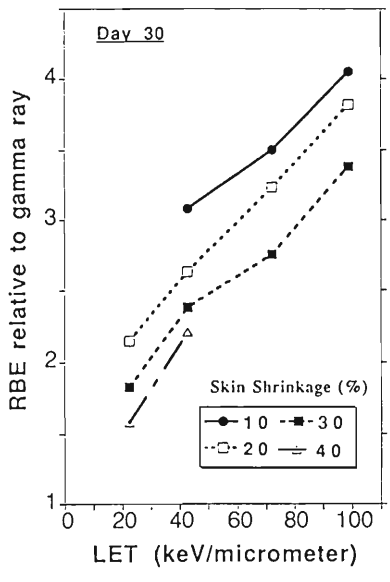

Fig.1 Dependence of RBE for Skin Shrinkag on Linear Energy Transfer.

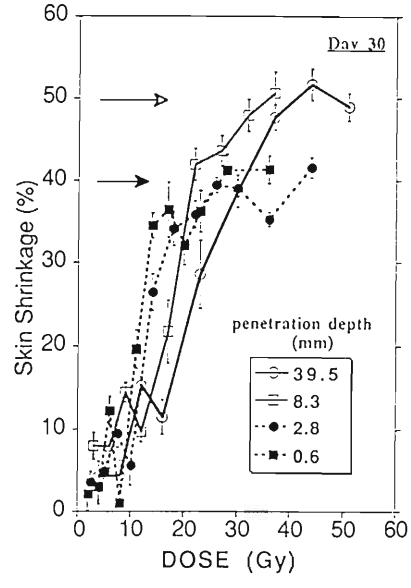

Fig.2 Volume Effect on Skin Shrinkage after 135 MeV Carbon-12. Saturation of skin shrinkage is indicated by arrows.

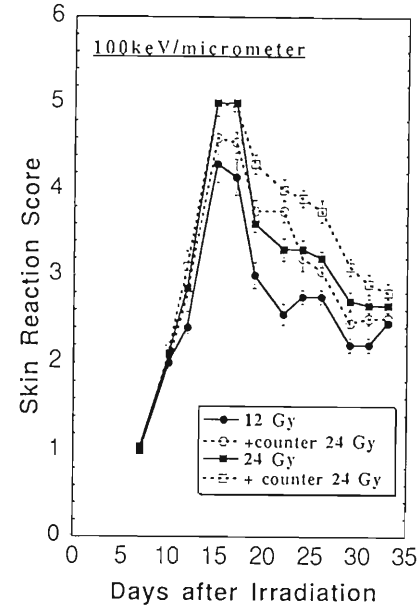

Fig.3 Enhacement of Skin Reaction by Counter Dose of Carbon-12.

*Natl. Inst. Radiol. Sci.

III-4-9. Studies on Induced Mutations by Ion Beam in Plants

Induced Mutants of Rice Resistant to Bacterial Leaf Blight

H. Nakai, H. Watanabe,* Y. Kobayashi,* S. Kitayama, T. Takahashi, and T. Asai**

Bacterial leaf blight(BLB) of rice caused by *Xanthomonas campestris* pv. *oryzae* is one of the most important diseases seriously affecting the production of rice in rice growing areas all over the world.[1,2] M_2 Plants (the second generation after mutagen treatment) of rice derived from the seeds irradiated by ion beams($^{14}N^+$), thermal neutrons and gamma-rays[3] were inoculated by clipping the leaf tip using scissors previously dipped in a suspension of 10^9~10^{10} BLB cells/ml of isolate T7133. The inoculated plants were scored for disease severity by measuring the length of the lesions three weeks after the inoculation. The resistant plants whose lesions were significantly shorter than the control were selected.

Table 1. Frequency of bacterial leaf blight resistant mutants of rice in the mutagens of ion beams, thermal neutrons and gamma-rays.

Mutagen	Dose (krad)	Seed fertility in M_1(%)	No. of M_2 seedlings*	No. of Plants selected	Frequency of resistant mutant
Ion beam	10	52	30,000	25	8.3×10^{-4}
Thermal neutron	1.0~1.5	53	30,000	15	5.0×10^{-4}
Gamma-ray	30	49	15,000	12	8.0×10^{-4}

* No. of seeds sown

The results are presented in Table 1. In the table, frequency of the resistant mutants was calculated as the number of resistant plants selected per the number of total M_2 seedlings analyzed. It was noted that the frequency of BLB resistant mutants by ion beam bombardment was similar to that by gamma-ray irradiation, and was higher than that by thermal neutron treatment. Further screening tests for BLB resistance in the later generations are needed in order to obtain more precise data on the mutagenic effect on the induction of BLB resistant mutants. It can be concluded from the present experiment, however, that ion beams could be one of the most effective mutagens for induction of useful mutants for the plant breeding.

References

1) H. Nakai et al.: *J. Agric. Sci. Camb.*, **111**, 309 (1988).
2) H. Nakai et al.:*ibid.*, **114**, 219 (1990).
3) H. Nakai et al.:*RIKEN Accel. Prog. Rep.*, **25**, 110 (1991).

* Atomic Energy Res. Inst.
** Sizuoka Univ.

III-4-10. Somatic Mutation Frequencies Induced by Ion Irradiations in Soybean Strain L65 Heterozygous at the Leaf Color Locus Y_{11}

O. Yatou and T. Takahashi

Somatic mutation frequencies induced by ion irradiations in soybean strain L65 were observed. The soybean strain has been extensively used to detect the genetic effect of various mutagens.[1] Plants of the strain are heterozygotes of a mutant gene in a leaf color locus y_{11}. Three types of somatic mutation sectors, green sector, yellow sector and yellow-green double sector, are observed after mutagenic treatment.

Air dried soybean seeds were irradiated with Ar (88 MeV/n, 0.06-8 Gy), N (136 MeV/n, 0.06-8 Gy) or gamma ray (0.1-1.6 Gy) of ^{60}Co. The ions were accelerated in RIKEN Ring Cyclotron and the gamma-ray irradiation was conducted in the Institute of Radiation Breeding. In each irradiation, mutant sectors of 5 to 20 plants, i.e. 10 to 40 leaves, were observed.

Mutation frequencies induced by the three radiations were shown in Figure 1, in which numbers of the three types of sectors were pooled. Unexpectedly gamma ray induced the mutations at higher frequencies than the higher LET radiations, Ar and N ion beams. In the Ar irradiation, variation in number of sectors among irradiated plants was extremely large, e.g. from 1 to 28 in a leaf (coefficient of variation = 0.92) at 2 Gy. This indicates the possible effect of shielding of the seeds, 7 mm diameter at maximum, against the ion beam, because the seeds were set in 2 to 3 layers. Then in the following irradiation of N, the seeds were placed in a single layer with their embryos at the beam direction. This improved uniformity of the irradiation effect, cv.= 0.59 at 2 Gy.

The numbers of yellow sectors were compared with those of the other two types of sectors (Table 1). Yellow sectors are considered to be derived from, at higher

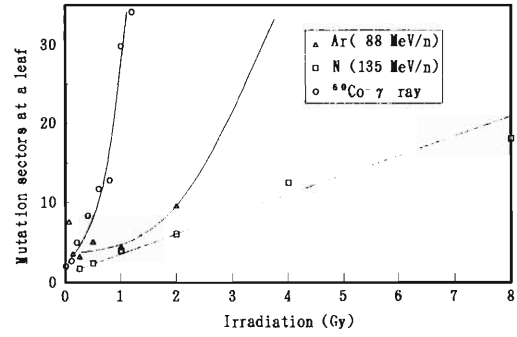

Fig. 1. Somatic mutation frequencies in y_{11} locus of soybean strain L65. The number of all three types of mutant sectors was pooled in each irradiations. The sectors induced by 4 Gy irradiation of Ar were not counted because the number was too many.

Table 1. Relative frequency of yellow sectors in all sectors observed.

	Yellow sectors A	Others B	A/B
N	573	75	7.64
^{60}Co-γ	1118	319	3.50

possibility, deletion or inactivation of the gene.[1] The relative frequency of yellow sector was higher in the N ion irradiation than in the gamma ray irradiation, which suggests that a single hit of the ion beam has a lareger impact to the soybean chromosome. A similar result was reported in the thermal neutron irradiation in this soybean strain.[2]

References

1) B.K.Vig:*Mutation Res.*, **31**, 49(1975).
2) T.Itoh, and S. Kondo:*Jpn. J. of Genetics*, **66**, 461(1991).

III-4-11. Effects of Heavy Ions on Fish Development

K. Ijiri, T. Takahash, M. Suzuki, S. Minohara, and T. Kanai

The effect of heavy ions on the development of the fish, *Oryzias latipes* was studied. Fertilized eggs were collected after natural spawning between the 1-year-old adult fish, and were incubated at 25°C for further development. Matui's normal table of this species was employed for the identification of the stages of their development.

Embryos were irradiated with the beams accelerated by RIKEN Ring Cyclotron. C ions (135 MeV/nucleon), N ions (135 MeV/nucleon) and Ar ions (95 MeV/ nucleon) were employed. The beam dosimetry was carried out using an ionizing chamber. Then, the flux of the beam was calculated using the ratio of the count of a parallel-plate avalanche counter(PPAC) to that of the ionizing chamber. Twenty to forty embryos were irradiated for each data point. They were then placed in glass vessels with stored tap water to develop at 25° C.

Embryos were irradiated at different developmental stages ranging from 0 to 3 days. For N and C ion beams, various LET values were realized, placing the Al absorbers along the beam axis. Hatching percentage of irradiated embryos was obtained as a function of the dose at each LET value.[1,2]

When these data were compared with the

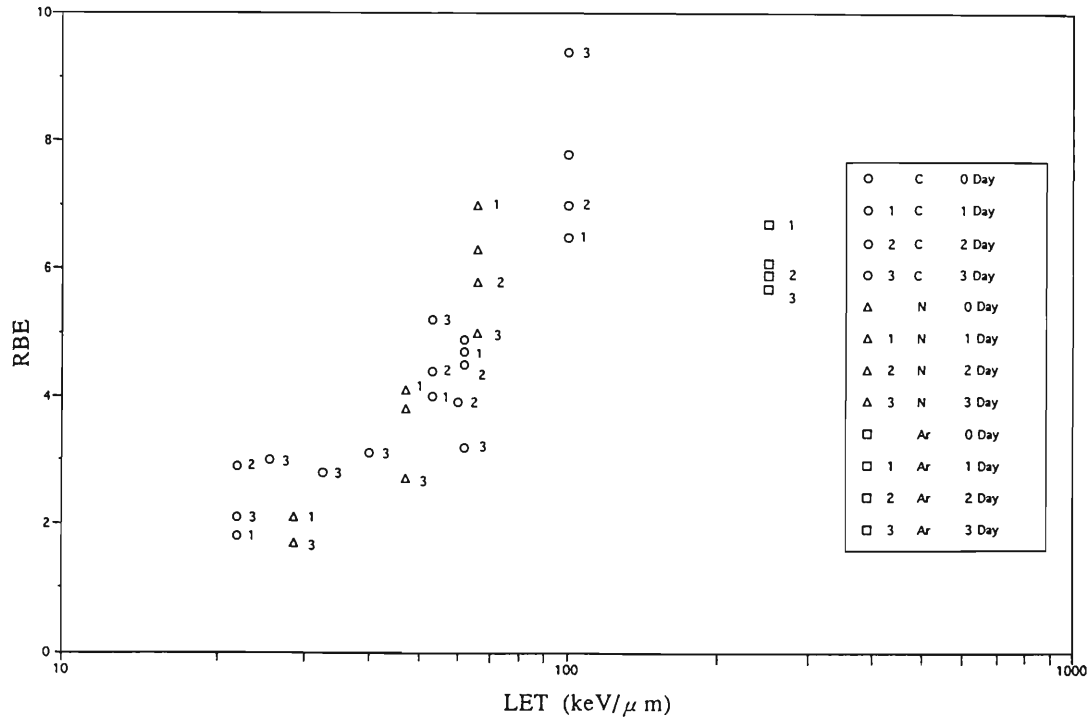

Fig.1. The relationship between LET and RBE for hatching of medaka (*Oryzias latipes*) embryos (Preliminary data). Developmental stages of embryos irradiated are expressed as 0 (stage 11), 1 (stage 19), 2 (stage 24), and 3 (stage 26).

hatching percentage after the γ-rays irradiation, ^{137}Cs was used as a source of γ-rays to obtain the relative biological effectiveness (RBE). Figure 1 summarises the relationship between LET and RBE so far obtained for four different developmental stages of embryos. With an increase in LET, RBE also becomes larger. The lack of data points for LET larger than 100 keV/μm, is soon to be filled when irradiations with Ne ions are carried out.

References

1) K. Ijiri, K Tao, K Nakano, M. Suzuki, and T. Takahashi: *RIKEN Accl. Prog. Rep.*, **25**, 112 (1991).
2) K. Ijiri and T. Takahashi:*Biol. Sci. Space*, **5**, 244 (1991).

5. Instrumentation

III-5-1. Development of New Data Acquisition System at RIKEN Ring Cyclotron Facility

N.Aoi, Y.Doki, Y.Watanabe, T.Ichihara, and A.Yoshida

We are now developing a data acquisition system for CAMAC using a new SCSI[a] crate controller 3929 developed by Kinetic System Corporation. We will show results of the test and its usefulness in this report.

The present data acquisition system at RIKEN Ring Cyclotron[1] consists of a microVAXII (0.9MIPS) and Kinetic 3922/2922 crate controllers connected by a Q22 bus. Recently, the performance of computers increased dramatically, and a fast and cheep computer, "workstation", appeared. On the other hand, nuclear experiments become more complicated nowadays and much faster computers are needed.

But a workstation was not used for nuclear experiments since it did not have a suitable interface to CAMAC. The new crate controller allows us to connect a CAMAC system to a workstation through a SCSI because a SCSI is very general and almost every workstation has it. The bus length limitation of a SCSI (6m) can be resolved by using a bus extender.

We measured the time requirement of CAMAC functions using the new system under the following condition as shown in the Fig. 1.

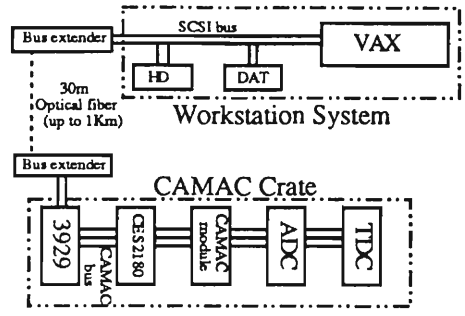

Fig. 1. The setup of a test bench.

1. Crate Controller : Kinetic 3929
2. Computer : VAXstation[b]
3. CAMAC module : CES2180[c]
4. Bus extender : APPLIED CONCEPTS Laser link with a 30m optical fiber.

The results are shown inTable 1. The transfer rates are somewhat slower than those of the present system but fast enough for most applications at the RIKEN Ring Cyclotron.

We also measured the time requirement of asynchronous interrupt for VAXstation3100. It takes 26ms which is about one order of magnitude slower than the present system. We will study further whether it results from the hardware or the software. On the VAXstation4000, interrupt does not work due to a known bug and will be fixed soon.

We used this system in an actual experiment of about 1block transfer per secound. Then it was confirmed that this system works well if the event rate is not so high. In case of high-rate experiments, we cannot tell whether this system works or not at the present time.

Though this system still contains some problems as we mentioned above, we succeeded in introducing a powerful tool, "workstation", to the experimental scene at the RIKEN Ring Cyclotron.

Table 1. The transfer rate of CAMAC function.

		VAXstation4000-60		VAXstation3100-76	
		Direct*	Optical link**	Direct	Optical link
single*** transfer	read [words/sec]	472	469	370	338
	write[words/sec]	448	448	370	338
block**** transfer	read [kwords/sec]	369	144	281	125
	[blocks/sec]	46	18	34	16

* Directly connected by a SCSI cable.
** Connected through a 30m optical fiber.
*** Data transfer using a single CAMAC function.
**** Data transfer by the block transfer (1block=16kbytes)
We could not measure the Block transfer write because of its unstableness.

References

1) T.Ichihara et al.:*IEEE TRANS. ON NUCL. SCI.***36-5**, 1628(1989).

a) SCSI or Small Computer System Interface: Interface standard widely used for a peripheral device such as a disk drive or a magnetic tape.

b) VAXstation3100-76(7.6MIPS) and VAXstation4000-60(13MIPS)

c) CES2180:CAMAC Auxiliary Crate Controller. It is generally used in RRC experiments as a front end buffer.

III-5-2. Computing Environment around the Accelerator Facility

T. Ichihara, A. Yoshida, and Y. Watanabe

A general description of the data acquisition system at the RIKEN accelerator research facility can be found elsewhere.[1] In this report, we will describe the recent improvement of the system.

(1) On-line data acquisition system

Currently, seven Micro VAX's are used for the on-line experiments at the RIKEN accelerator research facility. The node names and locations are as follows:

RIKMV1:: Micro VAX II (1F)
RIKMV2:: Micro VAX II (B2F E3)
RIKMV3:: Micro VAX II (Linac)
RIKMV4:: Micro VAX II (B2F RIPS)
SMART:: VAX Station 3520 (B2F SMART)
SMARTF:: VAX Server 3300 (B2F SMART)
RIKLV2:: VAX Station 3100 M76 (1F)

Independent measurements and counter tests can be performed without interference. The current version of the data-taking program supports the CAMAC multi-crate parallel-readout using multi-J11's (starbursts). The throughput of the data acquisition is increased by using these parallel readout features. Recently several digital audio tape (DAT) units of 2 GB capacity have been installed for on-line data recording. Now a DAT is the most standard recording media for the on-line experiment.

(2) Off-line data processing system -1

The following VAX's are available for the off-line data analysis and for general purposes.

RIKEN:: (virtual node name of the cluster)
RIKVAX:: VAX-6610 (Central)
RIKVS0:: VAX Station 4000-60
RIKVS2:: VAX Station 4000-60
RIKVS3:: VAX Station 4000-60
RIK835:: VAX Station 4000-60
RIKLV1:: VAX Station 3100 M76
RIKSNA:: DECnet/SNA Gateway

Theses computers are connected by LAVC (Local Area VAX Clusters) via the ethernet. They are also connected to the HEPnet(DECnet) and TISN Internet (DECnet/IP) and reachable from all over the world.

Since the load of the VAX-6510 was too heavy, we have upgraded the VAX-6510 to VAX-6610 in May 1992. By this upgrade, the performance of RIKVAX:: has been increased about a factor of 3 (from 12 VUPS to 32 VUPS).

(3) Off-line data processing system -2

Following FACOM main-frame computers are available at the accelerator facility.

FACOM M-380 (Ring cyclotron)
FACOM M-1800/20 (Computer center)

These two computers are connected by the Netwrok Job Entry (NJE) and DSLINK via the ethernet. These two computers are also connected to the DECnet/SNA Gateway.

Operation of the FACOM M-380 will be terminated in the end of March 1993, because a recent RISC-based computer is much more efficient and faster than the old-style main-frame computer.

(4) Wide area network

The RIKEN accelerator research facility is connected to the world-wide network of HEPnet (High Energy Physics NETwork) / SPAN (Space Physics Analysis Network) as Area 40, which is a part of the DECnet Internet, and the TISN internet (Todai International Science Network) which is a part of "The Internet" (NSFnet, ESnet, NSI, DDN etc.).

In order to support these wide area network connections, we are now supporting following 6 leased lines at the accelerator research facility.

512 kbps to University of Tokyo
64 kbps to RIKEN Tsukuba Center
19.2 kbps to RIKEN Komagome
9.6 kbps to KEK, Tsukuba
9.6 kbps to Tokyo Institute of Technology
9.6 kbps to NTT X.25 (DDX-80)

The link to University of Tokyo was upgraded from 64 kbps to 512 kbps in June 1992 using the optical fiber. The leased line between RIKEN-Wako and RIKEN-Tsukuba was also upgraded from 9.6 kbps to 64 kbps in February 1992.

(5)Address of the electric-mail

The address of the electric-mail for general user of the RIKEN accelerator research facility is described as follows, where the *userid* should be replaced by a proper name.

(HEPnet/DECnet)
RIKEN::*USERID* (or 41910::*USERID*)

(Internet/Bitnet)
USERID@RIKVAX.RIKEN.GO.JP

References

1) T. Ichihara et al.: IEEE Transaction on Nuclear Science, 36-5 p. 1628 (1989).

III-5-3. High-Resolution Dispersive-Mode Beam Transport to the Spectrograph SMART

T. Ichihara, Y. Fuchi, K. Hatanaka, H. Kawashima, S. Kubono,
S. Miyamoto, T. Niizeki, S. Takaku, M.H. Tanaka, T. Yamamoto, and H. Ohnuma

High-resolution dispersive-mode beam transport to the spectrograph SMART has been developed. Since the momentum spread of the accelerated beams from the RIKEN Ring Cyclotron is estimated to be about 0.05%, the high resolution dispersive-mode beam transport is required for high-resolution experiments using the spectrograph SMART.

(1) High-Resolution Beam Transport

This transport has a horizontal focus point with large dispersion (13m), where the beam can be cut by the slit in the wall (A11). The transport matrix of the beam at this focal point is written as follows,

-1.199	0.000	0.000	0.000	0.000	13.179
-3.783	-0.833	0.000	0.000	0.000	31.961
0.000	0.000	-0.239	-0.276	0.000	0.000
0.000	0.000	1.975	-1.894	0.000	0.000
-1.151	-1.098	0.000	0.000	1.000	11.430
0.000	0.000	0.000	0.000	0.000	1.000

where the notation of the beam matrix follows the program TRANSPORT.

The momentum resolution at this focal point is estimated as P/ΔP=11,000, assuming that the beam is cut by a horizontal slit of 1mm width.

(2) Disparsive-Mode Beam Transport

The dispersion of the beam spot on a target of the spectrograph SMART can be adjusted by changing some quadrupole magnets in the beam transport system to archive the dispersion matching of the beam transport and the spectrograph. This is necessary for light-ion beams because the slit cannot be used for the intermediate energy light-ion beams. For example, in a typical measurement of the 0 degree change-exchange reaction, the beam matrix on the target is set to be as follows.

-0.540	0.018	0.000	0.000	0.000	14.247
0.000	-1.851	0.000	0.000	0.000	-26.242
0.000	0.000	-0.760	0.000	0.000	0.000
0.000	0.000	-2.247	-1.315	0.000	0.000
-1.416	-2.589	0.000	0.000	1.000	23.049
0.000	0.000	0.000	0.000	0.000	1.000

In this case, the beam matrix on a counter of the second focal plane of the spectrograph becomes as follows.

-0.288	0.009	0.000	0.000	0.000	-0.000
-10.023	-3.119	0.000	0.000	0.000	176.531
0.000	0.000	-0.838	0.064	0.000	0.000
0.000	0.000	-15.175	-0.032	0.000	0.000
5.095	-0.175	0.000	0.000	1.000	90.116
0.000	0.000	0.000	0.000	0.000	1.000

The matrix element of M16 (dispersion) at the counter is 0, thus the dispersion matching being achieved.

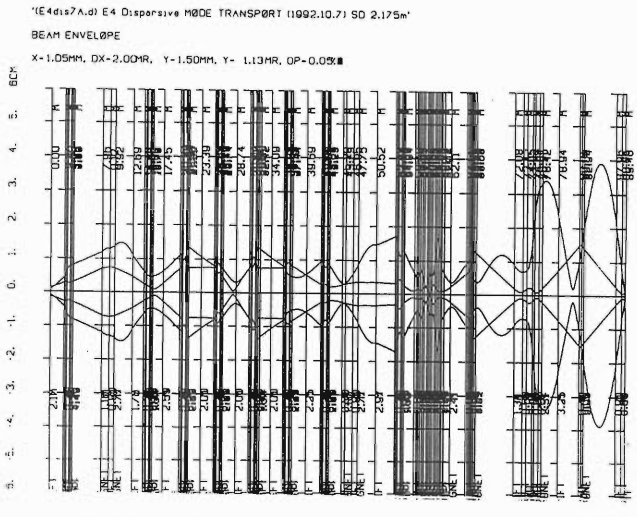

Fig.1. Typical beam envelope of this transport.

Figure 1 shows the typical beam envelope of this beam transport.

So far, we have achieved the momentum resolution of P/ΔP=5,000 using the spectrograph SMART. A typical example of the spectra of the $^{12}C(^{12}C,^{12}N)^{12}B$ reaction at E/A=135 MeV obtained by the spectrograph SMART can be found elsewhere in this volume.[1] In this case, the overall energy resolution was 700 keV(FWHM) using a 1.62 GeV ^{12}C beam. We are expecting to obtain a twice better resolution in the near future by improving the beam transport and the method of tuning the disperssion matching.

References

1) T. Ichihara et al.: This reports, p. 17.

RIKEN Accel. Prog. Rep. 26 (1992)

III-5-4. A Proportional Scintillation Imaging Chamber for Heavy Ion Detection

M. Suzuki , T. Takahashi, and K.Kuwahara

In understanding the overall effect of heavy ion irradiation on biological systems, it is essential to determine the spatial distribution of the deposited energy along ionization tracks. In this respect a proportional scintillation imaging chamber (PSIC) represents an ideal instrument, since it can visualize the spatial distribution of the secondary electrons in the ionization tracks produced by heavy ions in the chamber gas.[1] In this report we describe a prototype PSIC constructed, and report the observed optical images of the ionization tracks of N ions (135MeV/nucleon) and of Ar ions (95MeV/nucleon) both accelerated by the RIKEN Ring Cyclotron.

As shown in Fig.1, the prototype consists of a drift chamber and a parallel plate avalanche chamber (PPAC), each section being separated by stainless steel meshes. The chamber gas used is a gaseous mixture of argon (88%) + methane (10%) + triethelamine (2%). Entering the drift chamber through an entrance window made of a stainless steel with a thickness of 200μm, heavy ions generate the secondary electrons along their paths. These electrons will drift towards the PPAC under the influence of an applied electric field. Passing through the first mesh, the electrons initiate electron avalanches due to the high electric field in the PPAC. The luminescence associated with the electron avalanches is observed with an image intensifier coupled with a CCD camera, focused on the second mesh in the PPAC. Since the luminescence induced is highly localized at the site of the electron avalanches, the luminous pattern observed will be the projection image of the secondary electrons generated by the incident heavy ion. The optical images detected are monitored on a TV screen, and are recorded on a video tape. The video signals are digitized and processed with a computer for further analysis and storage.

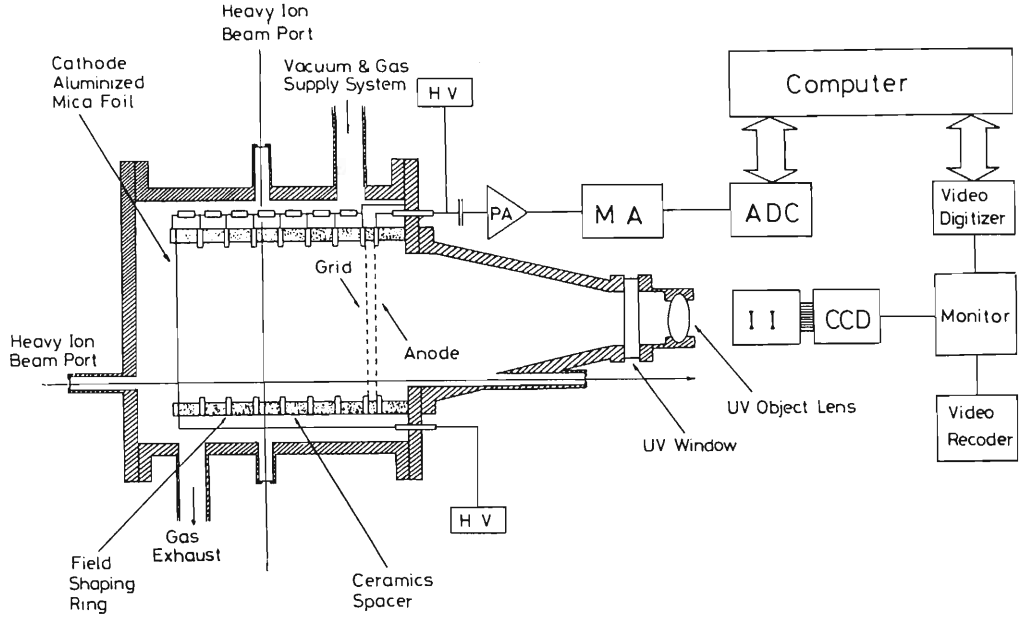

Fig. 1. Cross sectional view of the proportional scintillation imaging chamber and its associated optical readout system.

The observed ionization track images produced by a N ion of 135MeV/nucleon and by an Ar ion of 95MeV/nucleon are shown in Fig.2 and 3, respectively, together with the variations of the relative brightness perpendicular to the tracks. The real size of each picture is 71 mm × 95 mm. The brightness curve indicating the electron density has a peak at the center of the ionization track, and decreases on both sides symmetrically. It can be also seen that the peak appearing in the Ar ion track is sharper than that in the N ion track, and that the Ar ion track is not tailing as long as the N ion does. The values of dE/dx for the Ar ion and for the N ion can be estimated to be 2.5 (MeV•cm^2/mg in water) and 0.29 (MeV•cm^2/mg in water), and the maximum range of the δ-rays to be 23 (cm) and 45 (cm) in the present chamber gas, respectively.[2] It is, therefore, expected that the secondary electrons in the ionization track are more localized near the central part in the Ar track than in the N track, being consistent with the present results.

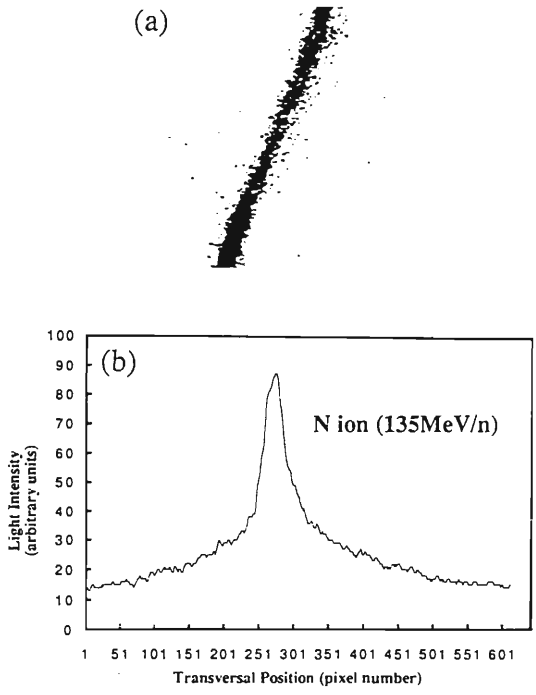

Fig. 2. (a) Photograph of the ionization track produced by a N ion (135MeV/nucleon) and (b) the transversal brightness variation of the track image.

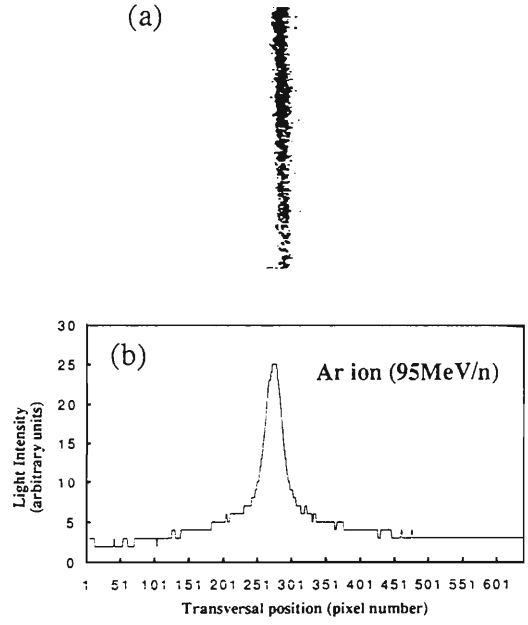

Fig. 3. (a) Photograph of the ionization track produced by an Ar ion (95MeV/nucleon) and (b) the transversal brightness variation of the track image.

References

1) M.Suzuki and T.Takahashi: in *Proceedings of International Conference on Evolution in Beam Application*, p.397, November 5-8,1991, Takasaki, Japan.
2) M.P.R.Waligorski, R.N.Hamm, and R.Katz: *Nucl. Tracks Radiat. Meas.*, 11, 309(1986).

III-5-5. Heavy-Ion Radiation Damage on Position-Sensitive Silicon Detector

M. Kurokawa, T. Motobayashi, T. Nomura, K. Morita, and A. Yoshida

An ion-implanted position-sensitive detector was designed and fabricated[1] for the experiment of superheavy element search.[2] During the experiment it is exposed in the radiation environment of heavy charged particles (A>200). We studied the effect of radiation damage induced by ^{110}Xe ions at 53 MeV. The radiation damage for heavy charged particles has not been well studied so far as compared with that for light particles like proton and neutron.

The ^{110}Xe ion was produced by the fusion reaction ^{58}Ni(^{58}Ni,α2n)^{110}Xe and transported by the gas-filled recoil separator (GARIS) at RIKEN. The resultant damage factors for ^{110}Xe are listed in Table 1 together with those for protons and ^{28}Si[3]. The first row corresponds to the damage factor α(A/cm), which is often used for expressing the degree of damage. It is used to,

$$\alpha = \frac{dJ}{d\Phi} \qquad (1)$$

where J(A/cm^3) and Φ(cm^{-2}) are the leakage current density and the irradiated fluence, respectively. The significant difference of the order of about 4 is seen between the damage factors α for protons and heavy ions. This might be partly due to the difference in the total energy deposit to the detector. To take this into account, the fluence Φ is replaced by the doze D(J/Kg), and a new damage factor k is defined as,

$$k = \frac{dJ}{dD} \qquad (2)$$

As seen in the table, the k values for protons are almost constant despite of the huge difference in the incident energy. This suggests that the damage is determined by the amount of the irradiated dose. However, those for heavy charged particles are still larger than for protons. The damage reflets the number of the defects made by the nuclear collision or the non-ionizing energy loss of incident particles with silicon, whereas the most part of energy deposit is due to the ionization process. The constant k value means that the ratio of energy loss by nuclear collision to that by ionization is almost constant. The larger k values for heavy ions may be explained by the increase of the nuclear collision contribution at very low velocity region, where the ionization process is suppressed by the decrease of the effective charge of ions. Note that the velocities are very low for the ^{28}Si and ^{110}Xe listed in Table 1, whereas those of the protons are higher enough to be free from the effective charge effect.

Table 1. Damage factors for various incident ions.

particle	energy	α (nA/cm)	k	ref.
proton	21 MeV	2.7×10^{-7}	8.7×10^{-8}	[4]
proton	25 MeV	2.2×10^{-7}	8.1×10^{-8}	[5]
proton	65 MeV	1.1×10^{-7}	8.6×10^{-8}	[6]
proton	12 GeV	3.0×10^{-8}	1.0×10^{-7}	[7]
proton	800 GeV	2.9×10^{-8}	7.6×10^{-8}	[8]
^{28}Si	80 MeV	3.2×10^{-4}	1.6×10^{-7}	[3]
^{110}Xe	53 MeV	5.6×10^{-3}	1.9×10^{-6}	present

References

1) M. Kurokawa *et al.*: *RIKEN Accel Prog. Rep.*, **25**, 120 (1991).
2) T. Nomura *et al.*: *RIKEN Accel Prog. Rep.*, **24**, 25 (1990).
3) N. Kato: *Nucl. Inst. and Meth.*, **B51**, 425(1990).
4) G. Lindstrom *et al.*: *Silicon Detector for Calorimetry - Developments for H1 at HERA - V International Conference on Instrumentation for Colliding Beam Physics*, Novosibrisk, March 1990.
5) G. Lindstrom *et al.*: DESY Report 89(August, 1989).
6) M.Kubota *et al.*: *Conference Record of the 1991 IEEE Nuclear Science Symposioum and Medical Imaging Conference* November 2-9, 1991 Santa Fe, New Mexico USA, **vol. 1**, 1246.
7) T. Ohsugi *et al.*: *Nucl. Inst. and Meth.*, **A265**, 105 (1988).
8) N. Nakagawa *et al.*: *Nucl. Inst. and Meth.*, **A270**, 421 (1988).

III-5-6. Straggling of High Energy Heavy Ions in Silicon Detectors

K. Nagata, T. Doke, K. Itsumi, T. Shino, T. Kashiwagi, J. Kikuchi, N. Hasebe, H. Moriya, A. Nakamoto, T. Yanagimachi, H. Murakami, S. Sugino*, and T. Kohno

The energy loss straggling in silicon detectors for high energy heavy ions are compared with the theoretical gaussian distribution.[1,2] The enegy loss distributions are measured in silicon detectors of 0.515 - 3.130 mm in thickness for 135 MeV/u ^{12}C, 135 MeV/u ^{14}N, 100 MeV/u ^{18}O, and 95 MeV/u ^{40}Ar nuclei.

An experimental energy loss distribution for 95 MeV/u ^{40}Ar in 1.848 mm thick silicon detector is shown in Fig.1. A solid curve shows the experimental distribution, and a chain curve shows the theoretical gaussian distibution. The experimental deposited energy loss 908.6 MeV is 3.6% lower than the calculated value of 939.3 MeV, and the distribution width (FWHM) is greater than the theoretical width.

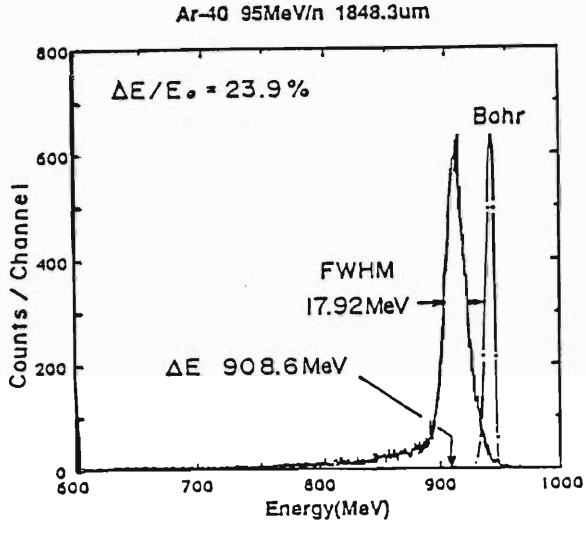

Fig. 1. Experimantal energy loss distribution for 95 MeV/u ^{40}Ar in a 1.848 mm silicon detector. A chain curve shows the theoretical gaussian distribution.

The ratio of the width obtained experimentally to the width from Bohr's theory is plotted in Fig.2 as a function of the ratio of fractional energy loss to the incident particle kinetic energy. A solid curve shows the ratios of the Payne's theoretical widths[3] for very large energy losses to the Bohr's theoretical widths . The result shows that the measured distribution widths are in agreement with the theoretical widths when the ratio of the fractional energy loss to the particle kinetic energy is less than about 20%. And the experimental widths become to be too wide for the energy losses over 20% in comparison with the theoretical Payne's widths.

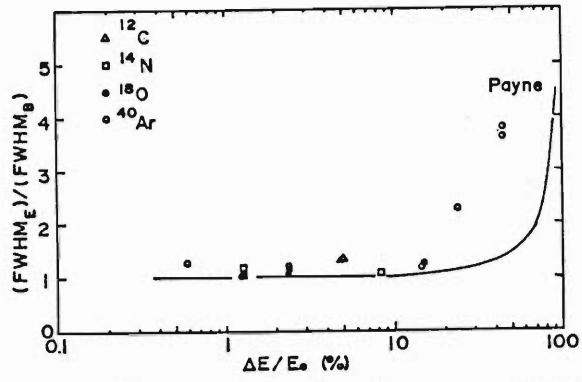

Fig.2. The ratio of the experimental distribution width (FWHM) to the theoretical gaussian width (FWHM) as a function of the ratio of the fractional energy loss to the particle kinetic energy. Solid curve is the ratio of the Payne's distribution widths to the gaussian distribution widths.

References

1) K. Nagata *et al.*: *RIKEN Accel. Prog. Rep.*, **24**, 115 (1990).
2) K. Nagata *et al.*: *ibid.*, **25**, 132(1991).
3) M. G. Payne: *Phys. Rev.*, **185**, 611(1969).

* Rikkyo Univ.

III-5-7. Calibration Experiments for the Identification of Isotopes by Telescopes HEP-MIs aboard the Geotail Satellite

N. Hasebe, H. Moriya, K. Fujiki, T. Kashiwagi, J. Kikuchi, T. Doke, T. Hayashi, K. Itsumi, T. Shino, T. Ito, K. Nagata, A. Nakamoto, H. Murakami, T. Yanagimachi, S. Sugino,*and T. Kohno

The science satellite Geotail was launched for the research in the tail of the earth magnetosphere in July, 1992. Medium energy Isotope telescopes, HEP-MIs, were installed on the Geotail for the purpose of observing the elemental and isotopic composition of cosmic rays.[1] The telescopes include several silicon detectors to measure heavy particles of $2 \leq Z \leq 28$ in the energy range 2.2 to 110 MeV/n using a well-known $\Delta E \times E$ method. A cross sectional view of the MI2 is shown in the inset of Fig.1. The telescopes consist of 6 silicon detectors which are 2 two-dimensional position sensitive detectors[2] (PSD1 and PSD2) and 4 ΔE-detectors (D1-D4).

The calibration experiment for the MI2s was carried out at the RIKEN Ring Cyclotron accelerator facility. Good Si detectors were selected in advance for the experiment. O and Ar beams with energies of 100 MeV/n and 95 MeV/n, respectively, were used to measure the fundamental characteristics of the telescopes. The fragmented beam produced by the nuclear reaction of the oxygen beam with a target of an acrylic plate was irradiated at the incident angle of 0° to the MI2 telescopes. Figure 1 shows a scatter plot of energy loss ΔE versus total energy E for the fragmented particles stopped in the D3 detector, where ΔE and E represent the sum of the energy losses D1(0.2mm) and D2(0.4mm), and the sum from D1 to D3(2.0mm), respectively. As seen from the figure, isotopes from Li to N are clearly resolved.

Figure 2 shows mass histograms of Be, B, C and N. Excellent mass resolutions, better than 0.37amu expressed in fwhm for isotopes from Li to N, have been achieved for the HEP-MI telescopes.

It is found from the beam experiments using O and Ar ions that isotopes heavier than carbon are clearly resolved by the MI telescopes.

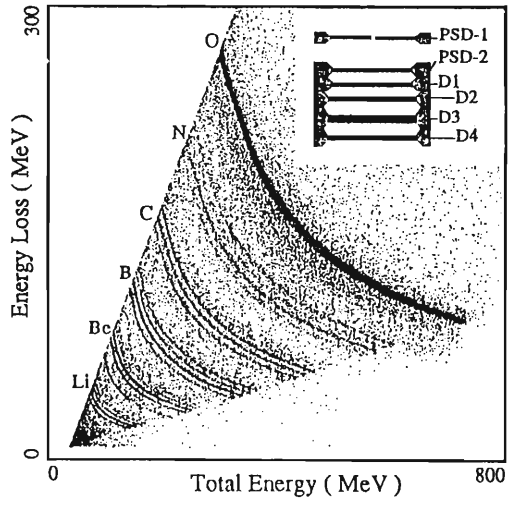

Fig. 1. Total energy E vs. energy loss ΔE scatter plot obtained from the fragmented beam produced by 100 MeV/n oxygen.

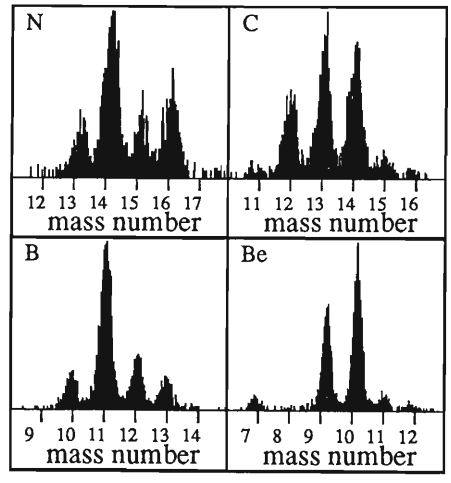

Fig. 2. Mass histgrams of Be, B, C and N isotopes.

References

1) T. Doke *et al.* : ISAS, SP, No. 10 (1989).
2) N. Hasebe *et al.* : JJAP., **31**, 1191, (1992).

* Faculty of Science, Rikkyo Univ.

III-5-8. Detection of Scintillation Photons in Liquid Xe from Heavy Ions and Their Attenuation Length

T. Doke, S. Ben, A. Hitachi, N. Ishida, K. Ito, M. Kase, K. Masuda,
Y. Qu, M.Suzuki, and T. Takahashi

Liquid xenon (LXe) is a good scintillator for radiation detection and will be possibly used in nuclear and particle physics in near future. The critical factors for detection of LXe scintillation photons are the reflection of the scintillation light (170 nm) on walls and the attenuation length of the light in the liquid.

Last year we measured the dependence of the light intensity on the distance between the incident position of heavy ions and the photodiode as a photon detector. An effective attenuation length of about 10 cm was obtained for the scintillation in LXe by using several kinds of reflector walls for VUV photons.[1] This value of the effective attenuation length includes the geometric factor (solid angle), the reflectivity of the mirrors and the light attenuation length of the LXe itself. In the present experiment, black walls with no reflection are used to clarify which factor is dominant in this effective attenuation length.

The apparatus is the double vacuum chamber which is the same as that used previously.[1] The effective length of the chamber is 65 cm. The chamber has seven beam windows which are separated by 10 cm from the neighbors along its length. A photon detector is a silicon photodiode or a vacuum triode. The liquid volume is surrounded by black walls which are made of almite.

The incident ions entered and stopped in LXe after passing through a Mylar window of the beam line, about 10 cm air, and then the chamber windows (40 μm Havar and 200 mm SUS). A thin (100 μm) plastic scintillator was sometimes used to obtain a beam trigger. The ions used were 135 MeV/n N, 100 MeV/n O and 95 MeV/n Ar from the RIKEN Ring Cyclotron.

Xe gas was purified by passing through an Oxisorb purifier and molecular sieves (4A) with a flow rate of 5 l/min and then liquefied in the chamber. The LXe temperature was kept at -75°C with dry ice.

Charge signals from the photodiode or the triode were processed with a preamplifier, a shaping amplifier (peaking time of 1μs) and an ADC.

The obtained effective attenuation length is about 9 cm for all cases of incident ions and photon detectors. This value is very close to that obtained with reflection mirrors inside the chamber. Namely this fact means that the reflection mirrors do not work well for VUV photons of the wavelength of 175 nm as considered previously.

In order to confirm the intrinsic attenuation length of the VUV photons in LXe itself, we measured photon yields due to alpha particles in LXe as a function of the distance between the source and the photomultiplier in a small test chamber.[2] An intrinsic attenuation length of about 3 meters is obtained. This has confirmed the above results for heavy ions.

For good uniformity of scintillation response as a high energy calorimeter, development of good mirrors in LXe is necessary.

References

1) T. Doke et al.: *RIKEN Accel. Prog. Rep.*, **25**, 140 (1991).
2) N.Ishida et al.: Proc. Int. Conf. on Liquid Radiation Detectors, p.353, April (1992), Tokyo, Japan; N. Ishida et al.: *Nucl. Instr. and Meth.* to be published.

III-5-9. Isotope Separation of a Cosmic Ray Telescope

C. Kato, T. Kohno, T. Imai, H. Kato, and K. Munakata

We have developed a cosmic ray Heavy Ion Telescope (HIT) with a very large geometric factor of 30 $cm^2 \cdot sr$. The HIT is going to be launched into a geosynchronous orbit in 1994. The brief description of the telescope is given elsewhere.[1] In addition to the numerical simulation,[2] the ground calibrations of the telescope using heavy ion beams of an accelerator are a very important and indispensable procedure for confirmation of the instrument ability and the reliability of the obtained data in space.

We used a beam of ^{16}O with an energy of 135 MeV/nucleon for a ground calibration experiment of a flight model of the telescope. The beam will stop in the telescope. The obtained mass resolution for the incident ^{16}O is reported in a previous report.[3] Since we have no magnetic analyzer at our beam port, we did not use any target for fragmentation production. Therefore we considered that the mass resolution measurement for only ^{16}O was possible with this experimental set up. But we found a different situation in the obtained data. We used a collimator to determine the characteristics of Position Sensitive Detectors (PSD).

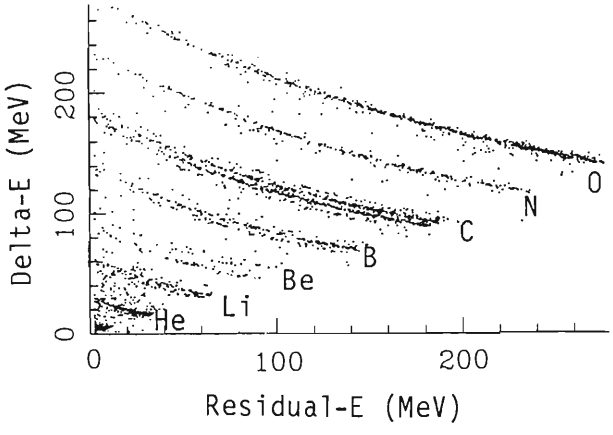

Fig. 1. Scatter plots for two detectors named PIN2 and PIN3 for events stopped in PIN3.

This collimator made of a 6 mm thick brass plate had 1 mm φ holes on the 13 x 13 lattice points at 5 mm intervals. In order to get a wide beam profile to cover the large area of the PSDs (62 mm x 62 mm), we strongly defocused the beam using Q-magnets. As a result it is conceivable that the beam lines were bent from a pure parallel beam line. Therefore some parts of this bent beam could passed through the hole by grazing the edge of the narrow hole of 1 mm φ x 6 mm length. By this effect, a part of the collimator could be a target and some secondary fragments were produced in the beam. Fig.1. shows a continuous energy loss of ^{16}O itself and the existence of lighter nuclides produced by nuclear fragmentation.

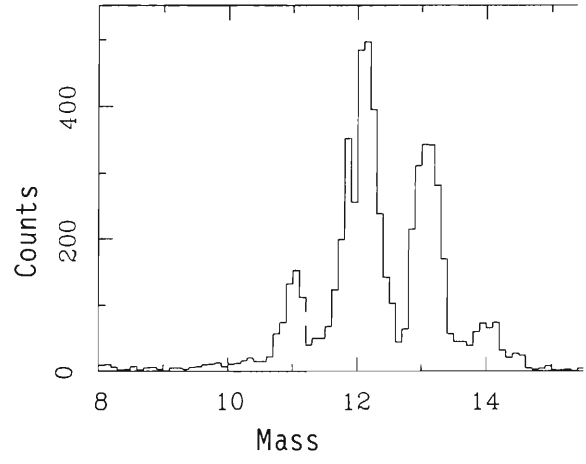

Fig. 2 . Mass histogram for an element of carbon.

A histogram example of isotopic separation for carbon is shown in Fig.2. The obtained mass resolution is about 0.4 amu in FWHM. This value is much better than 0.6 amu which was obtained for ^{16}O.[3] This comes from the low noise characteristics of the PIN-type detector used for this analysis in contrast with the relatively large noise existence for the Si(Li) type detector in which ^{16}O stops because of their large thickness.

References

1) T.Kohno: *Space Sci. Rev.*, **51**, 185 (1989).
2) K.Munakata et al.: *Nucl. Instrm. Methods*, **A276**, 306 (1989).
3) T.Kohno et al.: *RIKEN Accel. Prog. Rep.*, **25**, 134 (1991).

III-5-10. Collinear Laser Spectroscopy with Ion-Guide Beam

M. Wakasugi, T. Horiguchi, T.T. Inamura, T. Ishizuka, W.G. Jin, H. Katsuragawa, M. Koizumi, S. Matsuki, K. Morita, T. Murayama, I. Nakamura, K. Shimomura, T. Shinozuka, I. Sugai, Y. Tagishi, M. Takami, and A. Yoshida

Collinear laser spectroscopy has been successfully made for many radioactive isotopes but not for refractory elements.[1] Nuclear spins, electromagnetic moments and mean square nuclear charge radii can be investigated systematically over a long isotopic chain with this technique. We are going to make the collinear laser spectroscopy experiment for refractory elements with a ion-guide beams from RIKEN-IGISOL. Here we report the test experiment off-line. The possibility of the experiment has been shown in our previous work.[2]

To make preparatory collinear laser spectroscopy off-line, we constructed a laser-ablation ion source for IGISOL using a Nd:YAG laser. With this ion source, we extracted ions of stable Hf and Ba isotopes, and tested our collinear laser spectroscopy system with Ba ion beam. From this experiments the extraction efficiency and the extraction time of IGISOL were measured, and the efficiency of the photon detection system was obtained.

The Nd:YAG laser beam was focused on a metallic target which was placed inside the IGISOL gas cell filled with a helium gas. The ion current produced by the laser ablation amounted to 1μA in the gas cell and 1-2 % of the current was extracted from an exit hole of the gas cell. The yield of ions produced in the gas cell and the extraction efficiency strongly depend on the helium gas pressure. Although it may depends on the geometry of the gas cell, the most efficient gas pressure has been found to be 40 mb in this experiment. Because the Nd:YAG laser is a high power pulse laser with the pulse width of 10 ns and the repetition rate of 10 Hz, we could measure the time profile of the extracted ion-guide beam. In the case of the helium gas pressure of 40 mb, the measured time profile of the pulsed ion beam has an averaged deley time of 13 ms, the time width of 11 ms and decay time of 9 ms. These values gradually increase as the helium gas pressure increases.

The extracted ion beams were accelerated up to 60 keV and mass-separated with an analysing magnet. The highest mass resolving power of 470 and 370 was also obtained at the gas pressure of 40 mb for Ba and Hf, respectively.

The separated ion beam was crossed with a laser beam collinearly and detected by a resonance fluorescence method. We measured isotope shifts of the 614 nm transition for seven Ba isotopes. This is the first time measurement of optical isotope shift with the ion-gude beam. In the fluorescence spectrum, the line width was 350 MHz, and it corresponds to an energy spread of ion beam of 90 eV. This value is enough for the isotope shift measurement but not for the hyperfine structure measurement. We can expect the line width to be reduced by using a focusing devise such as a SQUEEZER.[2]

The fluorescence spectrum for ^{132}Ba, which has the smallest abundance of 0.101 %, was also clearly observed with the ion beam current of 0.2 pA. From this measurement, the estimated photon detection efficiency was 10^{-5}. This value is not sufficient to make this kind of experiment with radioactive isotopes. We are now improving the detection system.

References

1) E.W. Otten: Treaties on Heavy-Ion Science, Vol. 8, ed. by D.A. Bromley, Plenum Pub. Co., New York, (1989).
2) M. Koizumi et al.: Nucl. Instr. and Meth., **A313**, 1 (1992).

III-5-11. Atomic Beam Magnetic Resonance Apparatus for Systematic Measurement of Hyperfine Structure Anomalies (Bohr–Weisskopf effect)

H. T. Duong,[*1] C. Ekström,[*2] M. Gustafsson,[*3] T. T. Inamura, P. Juncar,[*4] P. Lievens,[*5] I. Lindgren,[*3] S. Matsuki, T. Murayama, R. Neugart,[*6] T. Nilsson,[*3] T. Nomura, M.Pellarin,[*7] S. Penselin,[*8] J. Persson,[*3] J. Pinard,[*1] I. Ragnarsson,[*9] O. Redi,[*10] H. H. Stroke,[*10] J. L. Vialle,[*7] and the ISOLDE Collaboration

The Bohr-Weisskopf effect, or hfs anomaly, which results from the effect of the distribution of nuclear magnetization on the atomic electron-nuclear interaction, will be studied systematically, first for a long chain of radioactive cesium isotopes, analogously to isotope shifts, at the CERN PS Booster ISOLDE. Results are expected to provide an independent test for nuclear wave functions. Precision measurements of the hfs splitting and nuclear magnetic moments are required, with sensitivity adequate for the radioactive isotopes produced.

We have constructed at Orsay in France a triple resonance atomic beam magnetic resonance apparatus with optical pumping state selection. Detection of the beam is by laser induced fluorescence or mass spectrometry. The performance of the apparatus was tested with stable K and Rb beams. Results obtained for g-values and hfs anomalies are in excellent agreement with published data, and show the technique to be suitable for the on-line experiments at ISOLDE. A precision better than 10^{-4} for g-value has been obtained in the tests, leading to hfs anomaly measurements better than 10 percent. Details of the system will be described elsewhere.[1)]

The apparatus has been installed at the ISOLDE facility and is presently being tuned up for the on-line measurements of a sequence of radioactive cesium isotopes.

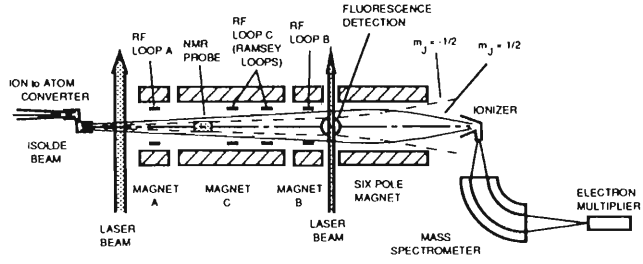

Fig. 1. Schematic of the experimental setup of ABMR at ISOLDE.

Part of this collaboration is supported by the Yamada Science Foundation, the Ministry of Education, Science and Culture in Japan, the U.S. National Science Foundation, the Swedish Natural Science Research Council and the C.N.R.S. in France.

References

1) H. T. Duong et al.: *Nucl. Instr. Methods* A, in press.

*1 Laboratoire Aimé Cotton, CNRS II
*2 The Svedberg Laboratory, Uppsala Univ.
*3 Dept. Physi. Chalmers Univ.
*4 Inst. Natl. Métrologie du CNAM
*5 CERN
*6 Inst. Physik, Univ. Mianz
*7 Laboratoire de Spectrométrie Ionique et Moléculaire, Univ. Lyon I
*8 Inst. Angewandte Physik, Univ. Bonn
*9 Dept. Mathemat. Phys. , Lund Inst. Technology
*10 Dept. Phys., New York Univ.

III-5-12. High Resolution PIXE Using Imaging Plate

J. Kawai and K. Maeda

An imaging plate (IP) is composed of a flexible plastic plate coated with photostimulable phosphor crystal powder ($BaFBr:Eu^{2+}$).[1] PIXE (particle induced x-ray emission) is one of the trace and micro-analysis methods of elements without troublesome sample preparations. For the purpose of elemental analysis, an energy dispersive spectrometer (EDS) is used. On the other hand, if a high resolution x-ray spectrometer such as a wavelength dispersive spectrometer (WDS) is used, then chemical specifications of elements in the compounds are also possible as was first demonstrated by Kamada *et al.*[2] We have tried to use an IP for an x-ray detector of the Bragg type PIXE spectrometer to compensate the weak analyte signal due to the trace or micro-analysis, or due to the short measuring time.

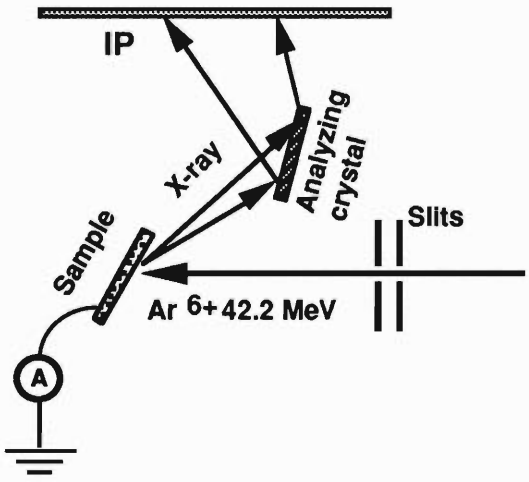

Fig. 1. Schematic drawing of the experimental setup. The slits were 0.3 mm wide. Practically, the IP was wrapped by an aluminium foil. The analyzing crystal was LiF(220).

X-ray emission measurements were performed at the RIKEN Linear Accelerator (RILAC). The setup of the experiment is shown in Fig.1. The x-rays were induced by 42.2 MeV Ar^{6+} ions projected on a steel AISI 430 (Fe 81.4 % and Cr 17.1 %). The reason we chose this steel was that the Ba L_3 absorption edge (5.2 keV) is just below the Cr K-L energy (5.4 keV). Therefore the detection efficiency was higher for transition metals than for other elements. The IP used was Fuji Film Type BAS-III IP. Six-fold spectral measurement was made by changing the irradiation time (1 sec ~ 6 hours) as well as the Ar^{6+} current (0.1 ~ 100 nA). Consequently, the total sample currents were 0.01, 0.1, 1, 100, 500, 1800 μC for six measurements in a limited beam time of the linear accelerator. After the exposure of x rays, the x-ray intensity was read by a Bioimaging Analyzer FUJI FILM BAS 2000 as shown in Fig.2.

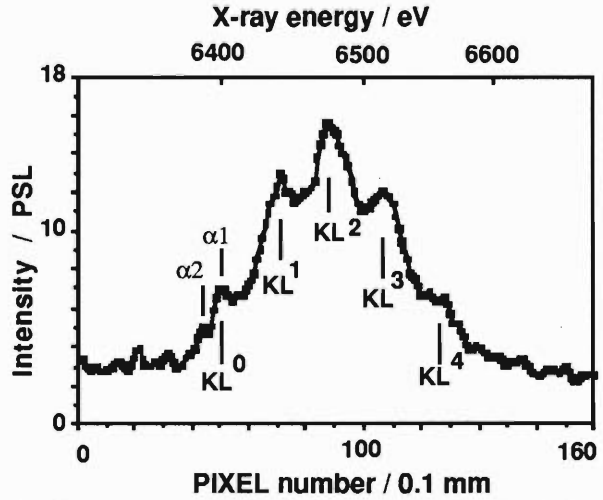

Fig. 2. Plot of Fe KL^n-L^{n+1} spectrum digitized from the IP image of a width of 1.5 mm. The total beam current was 1800 μC.

The multivacancy satellite intensity distribution is expressed by a binomial law $I(KL^n) = {}_8C_n\, P_L{}^n\, (1 - P_L)^{8-n}$, where P_L is the ionization probability from L shell, and n the number of the L shell vacancy.[3] We analyzed the spectrum in Fig.2, and obtained P_L=0.27. Folkmann[4] reported that P_L=0.33 and 0.22 for Cr when excited by 1.4 MeV/u Cl^{8+} and O^{4+}, respectively. Our value (0.27 of Fe excited by 1.1 MeV/u Ar^{6+}) is quite reasonable compared with those of Folkmann.

To get a sufficient spectral intensity in the present experimental condition, the total beam

current was enough for 500 μC, which was achieved by irradiation of less than 1.5 hours when the beam current was 100 nA. This means a rapid measurement is possible when the IP is used.

In conclusion, we have first demonstrated that an IP is a better x-ray detector of a high resolution PIXE spectrometer compared with x-ray films or position sensitive proportional counters. It requires a short measuring time (1.5 hours) and a small amount of specimen (1.5×0.3 mm^2); it achieves a high energy resolution; and a wide energy range is detectable simultaneously.

References

1) K. Takahashi, J. Miyahara, and Y. Shibahara: *J. Electrochem. Soc.*, **132**, 1492 (1985).
2) H. Kamada, R. Inoue, M. Terasawa, Y. Gohshi, H. Kamei, and I. Fujii: *Anal. Chim. Acta*, **46**, 107 (1969).
3) K. W. Hill, B. L. Doyle, S. M. Shafroth, D. H. Madison, and R. D. Deslattes: *Phys. Rev.*, **A13**, 1334 (1976).
4) F. Folkmann: *Proc. 6th Intern. Conf. on PIXE, Tokyo Japan, Nucl. Instrum. Methods*, **B** (in press).

III-5-13. Total Reflection X-Ray Photoelectron Spectroscopy

J. Kawai, S. Hayakawa, S. Suzuki, Y. Kitajima,* T. Urai, K. Maeda, and Y. Gohshi

Total reflection x-ray photoelectron spectroscopy (TRXPS), which has been proposed by some of the present authors and coworkers,[1] is a surface characterization method. The excitation x-rays impinge on a specular surface and go through total reflection. Then the x-rays do not penetrate deeper than the evanescent length from the surface. The incident and reflected x-rays form a standing wave on the surface. The intensity of the standing wave is four times as strong as that of the incident x-ray beam. Therefore the TRXPS will be a powerful tool for surface characterization when the next generation synchrotron radiation source is realized.[2] Another advantage of the TRXPS is that the background in the ordinary x-ray photoelectron spectroscopy (XPS) due to the inelastic scattering of electrons which are photoionized below the surface is reduced to less than one half when the TRXPS technique is used as was numerically simulated using optical constants for x-rays.[1]

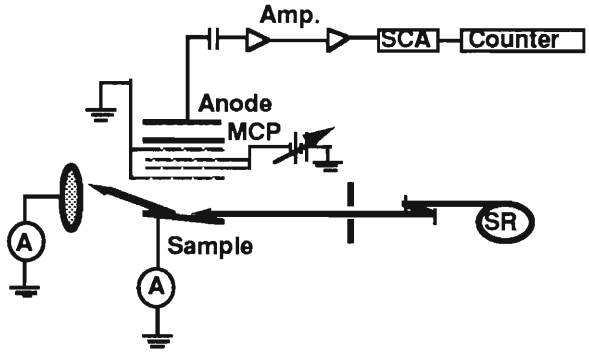

Fig. 1. Schematic illustration of the experimental setup.

We have designed a prototype TRXPS spectrometer to check the numerical simulation results, and measured the photoelectron spectra using a synchrotron radiation source at the Photon Factory, KEK, as shown in Fig. 1. The sample was GaAs single crystal wafer, and the beam size was 5×0.2 mm^2. The x-ray energy was 2 keV monochromatized by an InSb double crystal monochromator. We measured the sample current during the TRXPS measurement excited by the synchrotron radiation as a function of the glancing angle of the x-rays to the sample surface. Usually, when one measures the XPS spectra, one does not measure the sample current, because it is believed to be negligibly small, and, no matter how strong it is, one believes that it has no physical meaning. However, based on the traditional manner in which experiments are done at the RIKEN linear accelerator (RILAC), where the target (sample) current is always measured to monitor the ion beam stability as well as to know the total current of the ion beam, we have added a circuit to measure the sample current in the prototype TRXPS spectrometer as shown in Fig. 1.

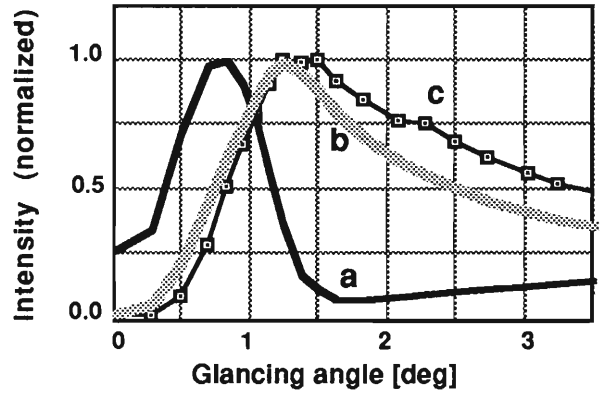

Fig. 2. Glancing-angle dependence of reflected x-ray intensity (a), sample current (b), and photoemission current (c) for 2 keV x-ray beam impinging on GaAs wafer.

The sample current had a maximum at the critical angle of the total reflection as shown in Fig. 2. This is the first observation of the existence of the sample current maximum at the critical angle. The behavior of the photoelectron current and the sample current was similar each other. The sample current was of the order of $10^{-11} \sim 10^{-10}$ A.

In conclusion, though we have not yet obtained high resolution TRXPS spectra, it has been found that the sample current has a maximum at the critical angle of total reflection. This effect will become a useful technique to characterize surfaces (e.g., to determine oxide layer thickness, adsorbates, and amount of defects on the surface) or to determine the critical angle.

References

1) J. Kawai, M. Takami, M. Fujinami, Y. Hashiguchi, S. Hayakawa, and Y. Gohshi: *Spectrochim. Acta*, **47B**, 983 (1992).
2) Y. Hashiguchi: *SPring-8 PROJECT, Part II, Scientific Program, Draft*, The JAERI-RIKEN SPring-8 Project Team, p.114 (1992).

* Photon Factory, KEK

6. Material Analysis

III-6-1. Molecular Orbital Calculation of Sulfur $K\beta$ X-Ray Spectra

J. Kawai, E. Uda, and M. Uda

High resolution $K\beta_{1,3}$ (K-$M_{3,2}$) x-ray fluorescence spectra of the elements of atomic number between 12 and 17 have complicated line shapes reflecting the valence electronic structure of the compound. However the fine structures of the x-ray spectra are not well understood still now. Therefore we have tried to reproduce the x-ray fluorescence spectra quantum chemically using a molecular orbital method. We have chosen sulfur because it has various oxidation states (the formal oxidation numbers are 6+, 4+, 2+, 0, and 2-), and also because the sulfur spectra of various compounds were measured with very high resolution.

We have assumed that the $K\beta$ line shape equals to the local (sulfur atom site) and partial ($3p$) electron density of states (DOS).[2,3] The S $3p$ DOS was calculated by the net $3p$ atomic orbital population in the LCAO approximation using the DV-Xα LCAO-MO method.[4] We have calculated the $K\beta_{1,3}$ line profiles of various sulfur compounds: covalent and ionic compounds; solids and molecules; and compounds of various oxidation numbers. For infinite size solids or large molecules, we have used the molecular cluster approximation.

Figure 1 shows a representative result of the present study using $C_6H_5SO_3Na$. Though $C_6H_5SO_3Na$ is an ionic solid, the local structure of it is represented by molecular clusters, SO_3^{2-} or $C_6H_5SO_3^-$. Therefore we have calculated the x-ray spectra of both SO_3^{2-} (Fig.1b) and $C_6H_5SO_3^-$ (Fig.1c). The experimental spectrum of solid $C_6H_5SO_3Na$ by Takahashi *et al.*[1] is also shown in Fig.1a for comparison.

Table 1. Orbital component of the x-ray peak of SO_3^{2-} (%).

Orbital	2452 eV	2462 eV	2466 eV	2470 eV
S 3*s*	0	34	0	3
S 3*p*	14	22	25	6
O 2*s*	82	32	15	0
O 2*p*	3	12	60	92

The experimental spectrum (Fig.1a) has four spectral components (2452, 2462, 2466, and 2470 eV), which are well reproduced by the calculation of SO_3^{2-}. However, the larger cluster calculation yields additional 2458 eV peak (Fig.1c), which is found as a small shoulder in the experimental spectrum. The molecular orbital assignment is easier when the cluster has a simpler structure. The molecular orbital assignment is shown in Table 1.

In conclusion, we have calculated the $K\beta$ x-ray fluorescence spectra of various sulfur compounds, and the agreement between theory and experiment is satisfactory even for small size clusters for all the sulfur compounds we tried.

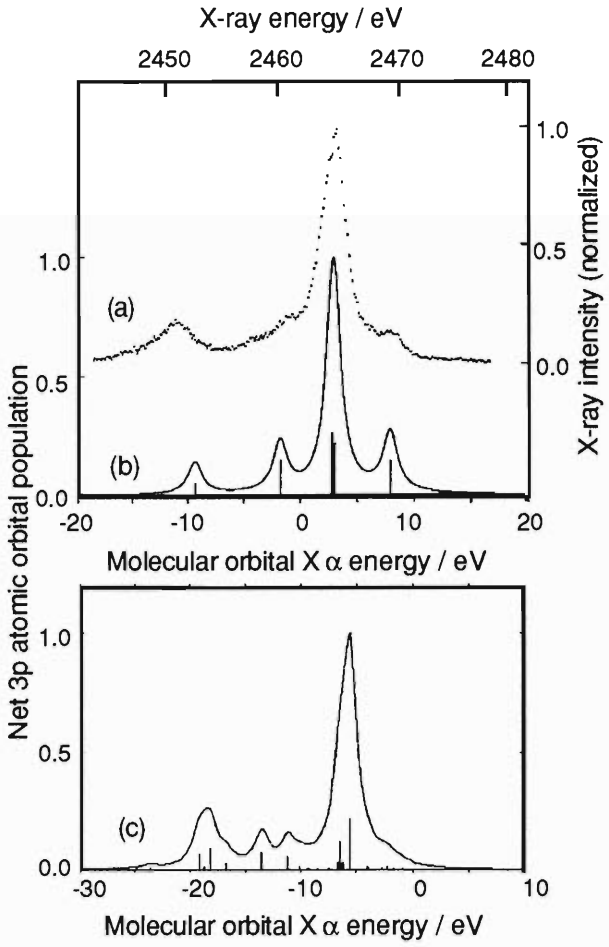

Fig. 1. Sulfur $K\beta$ spectra of SO_3^{2-}. (a) Observed spectrum of $C_6H_5SO_3Na$ by Takahashi *et al.*[1] (b) Calculated spectrum of SO_3^{2-} cluster. (c) Calculated spectrum of $C_6H_5SO_3^-$ cluster. Vertical line: $3p$ orbital population. Solid line: S $3p$ DOS (vertical line spectra are convoluted by a 1.5-eV-FWHM Lorentzian function).

References

1) T. Takahashi, W. Qi, M. Enomoto, S. Nojima, J. Kawai, and Y. Gohshi: *Adv. X-ray Chem. Anal. Japan (X-sen Bunseki no Shinpo)*, **17**, 37 (1986).
2) D. S. Urch: *J. Phys. C: Solid St. Phys.*, **3**, 1275 (1970).
3) R. Manne: *J. Chem. Phys.*, **52**, 5733 (1970).
4) A. Rosén, D. E. Ellis, H. Adachi, and F. W. Averill: *J. Chem. Phys.*, **65**, 3629 (1976).

III-6-2. Low-Energy Satellite Structure of Ca~Fe Kα

K. Maeda and J. Kawai

X-ray diagram lines (e.g. Kα and Kβ) are accompanied with various types of satellites. In the highly-sensitive multielement analysis by energy-dispersive X-ray spectrometry, satellites emitted from matrix elements often obstruct the detection of trace elements, even if the satellites were very weak compared with their parent diagram lines. However, there is little information available as to weak satellites. We report here the broad satellite structure which was detected on the low-energy side of the Kα lines of elements of atomic number Z=20~26. As an excitation source we chose He ions instead of X rays which are generally used for X-ray chemical analysis. When X rays are used for excitation, the incident (i.e. primary) X rays are scattered by the target sample and superimposed on a spectrum of secondary X-rays emitted from the sample. Ion-induced X-ray spectra are free from such scattered X rays.

High purity metal sheets of V (>99.99%), Cr (>99.99%), Mn (>99.9%) and Fe (>99.998%), and a disk of CaF_2 powders (Merck Spurapur, K<5ppm, Cd<0.5ppm) were used as target samples. The samples were irradiated with 8 MeV He ions accelerated by RILAC. Emitted X rays were analyzed by a Si(Li) semiconductor detector with a resolution of 170 eV at 6 keV. X-ray spectra were measured directly at first using the arrangement shown in Fig.1a, and after monochromatizing the X rays using the arrangement as shown in Fig.1b. The latter measurement was carried out to determine the response function of the Si(Li) detector, which is composed of an escape peak, a low-energy exponential tail and a low-energy flat continuum.

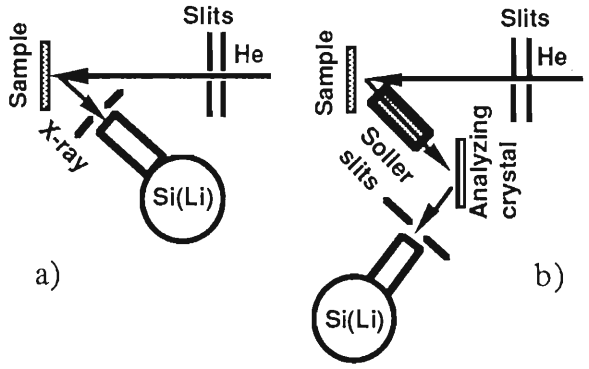

Fig. 1. Schematic drawing of experimental arrangements: a) without a monochromator and b) with a monochromator (Soller slits, an analyzing crystal and a detector were arranged so as to satisfy the Bragg condition for the Kα line of the target element).

Figure 2 shows the X-ray spectrum in an energy region lower than the Mn Kα. The spectrum was obtained by subtracting the response function for the Mn Kα from the directly measured spectrum so that the background due to the detector could be removed.

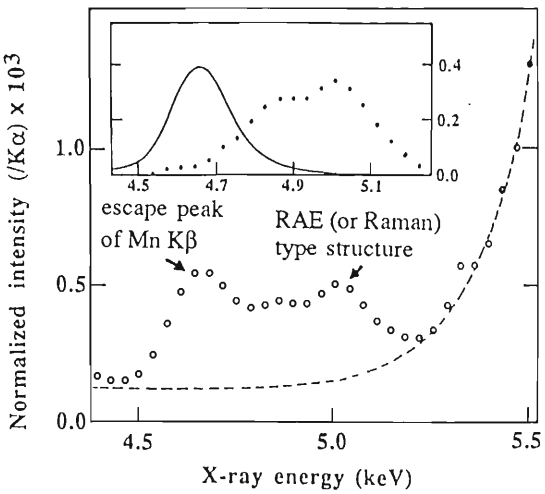

Fig.2. X-ray spectrum in the low-energy region of Kα obtained from a Mn metal.

A broad satellite structure was clearly observed in the energy region (around 5 keV) corresponding to K-LL Auger transitions. A similar structure was found in all spectra obtained from other samples. From the peak energies and spectral shapes, the structure may be ascribed to the K-LL radiative Auger effect (RAE) type transition[1] or Kα-L Raman type scattering.[2] The peak energies and intensities of the structure are summarized in Table 1. The integrated intensity was obtained after subtracting the background and the escape peak of Kβ, shown in Fig.2, and then correcting the detection sensitivity and self-absorption factors.

Table 1. Energies and intensities of low energy structure.

Element	Peak energy (keV)	Integrated peak intensity (/Kα,%)
Ca	3.16	0.17
V	4.24	0.20
Cr	4.66	0.12
Mn	5.03	0.08
Fe	5.49	0.07

The intensity of the low-energy satellite structure relative to Kα was determined to be 0.1~0.2 % for Z=20~26. This implies that the low-energy satellites are not so weak as to be neglected in analysis of trace and minor elements. The contribution from these satellites should be taken into consideration when the quantitative trace analysis is made by X-ray spectrometry.

References

1) E. Magareter, W. Wegscheider, and K. Muller: *X-Ray Spectrometry*, **13**, 78 (1984).
2) Y. D. Koo and K. Das. Gupta: *Phys. Rev.*, **A42**, 5441 (1990).

III-6-3. Chemical Specification by High Resolution PIXE

T. Isomura, K. Maeda, J. Kawai, M. Takami, and M. Uda

Particle induced X-ray emission (PIXE) spectroscopy has the following three advantages among many X-ray spectroscopies for the purpose of chemical specification:
(1) The sensitivity of PIXE is one order of magnitude higher than that of X-ray fluorescence spectrometry.
(2) External beam techniques make it possible to analyze a sample in atmospheric pressure.
(3) Focused ion beam techniques give information on the local area of materials.

In particular X-ray emission spectra of valence-core electron transitions, e.g. $K\beta$ spectra of Al, Si, P, S and Cl, reflect the valence electronic structures. Therefore chemical specification is possible if the X-ray spectra are measured by a high energy resolution crystal spectrometer.

To show the potential of PIXE for chemical specification, sulfur $K\beta$ X-ray spectra of S_8 and $MgSO_4$ were measured with a Bragg type spectrometer (Fig. 1). The sample was set in air and was irradiated by a 1 MeV H^+ beam produced by the Tandetron. The beam diameter was 4.5 mm and the beam current was ca. 100 nA. The spectrometer was positioned at 90° with respect to the incident beam (45° with respect to the sample). The pressure in the spectrometer chamber was 1 Torr. A 7.5 μm thick Kapton film was used as an X-ray entrance window which separated the vacuum from atmospheric pressure. The emitted X-rays were collimated by Soller slits (0.17°) and analyzed by a Ge(111) ($2d$ = 6.532 Å) flat crystal.

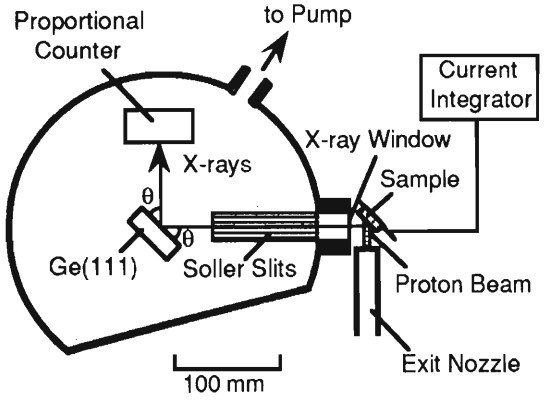

Fig. 1. Experimental setup for high resolution PIXE.

The X-rays were detected by a proportional counter. The spectrometer was step-scanned at an interval of a constant Bragg angle and the beam current was integrated to 10 μC for each step. The dwelling time of one step was shorter than 100 seconds.

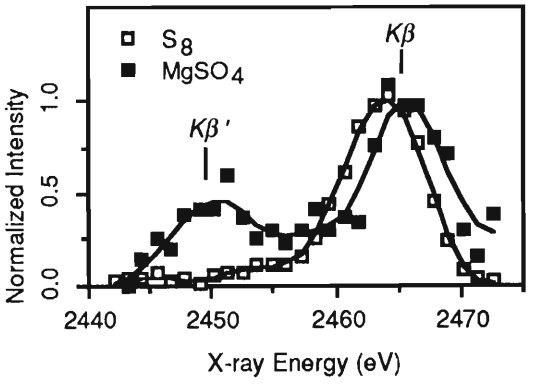

Fig. 2. Sulfur $K\beta$ spectra of S_8 and $MgSO_4$. Square dots show the raw data and solid lines show the smoothed data.

The measured spectra are shown in Fig. 2. The data were processed by a smoothing method.[1] The $K\beta'$ peak, which was characteristic of an S-O bond, was observed at 2450 eV for $MgSO_4$. It is also found that the $K\beta$ main peak of $MgSO_4$ is 1 eV higher than that of S_8. The oxidation number of sulfur was determined by these differences in the spectra. Hurley and White[2] proposed that the measurement of only four channels was required to determine the chemical form of sulfur. Therefore the oxidation number of sulfur can be determined by a measurement shorter than 7 minutes (= dwelling time of four channels) if the beam current is as strong as 100 nA.

In conclusion we have demonstrated that the high resolution PIXE distinguishes between sulfur (S^0) and sulfate (SO_4^{2-}) in air with a spatial resolution of ~1 mm^2.

References

1) A. Proctor and P. M. A. Sherwood: *Anal. Chem.*, **52**, 2315 (1980).
2) R. G. Hurley and E. W. White: *Anal. Chem.*, **46**, 2234 (1974).

III-6-4. Singularity of Clay Minerals and Iridium Concentration at a Cretaceous-Tertiary (K-T) Boundary

K. Tazaki, M. Aratani, M. Yanokura,
K. Kaiho,* and S. Noda**

The K-T boundary sediments have relatively high Ir concentrations suggesting that an asteroid struck the Earth and caused mass extinctions at the end of the Cretaceous.[1] Spherical clays heated probably by shock were found in the Cretaceous-Tertiary (K-T) boundary sediments in the eastern district of Hokkaido, northern Japan.[2] Mineralogical and chemical investigations of the claystone have been carried out by the use of X-ray powder diffraction, high resolution electron microscope, energy dispersive X-ray and heavy ion Rutherford scattering (HIRS analysis).

Heavy ion probes of $^{40}Ar^{4+}$or $^{40}Ar^{6+}$(50MeV), $^{84}Kr^{9+}$(131.1MeV) and $^{129}Xe^{13+}$(164.7MeV) were used. HIRS analysis of the clay powder ($<2\mu$m) from the K-T boundary layer using $^{84}Kr^{9+}$(131.1 MeV) at glancing detector angles of 60° and 30° revealed the existence of Ga, Zr, Mo, In and a trace of Ir (Fig. 1).

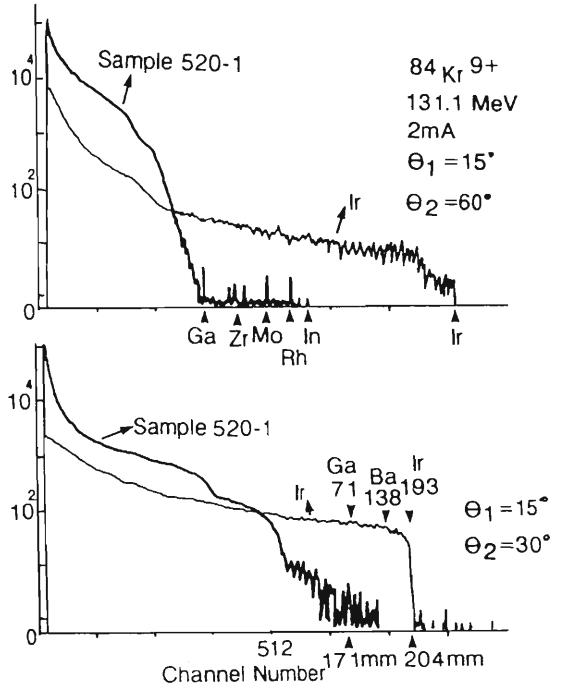

Fig. 1. HIRS energy spectra of the black-grey clay at the K-T boundary show that heavy metals are contained in sample 520-1.

In the sedimentary layers just above and below the K-T boundary, the content of Ir was under the detection limit. Sample 520-1 from the K-T boundary layer indicated the existence of Ir at glancing detector angles of 40° and 50° (Fig. 2).

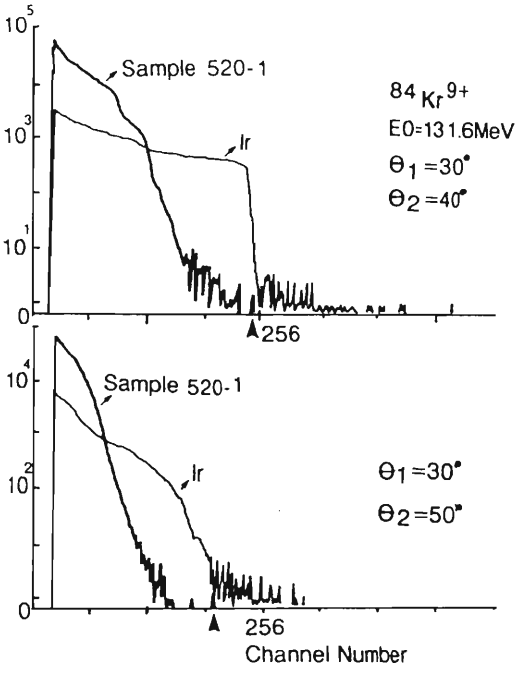

Fig. 2. HIRS energy spectra of the black-grey clay show that Ir is contained in the sediment (sample 520-1) at the K-T boundary.

Mineralogical examinations of a continuous stratigraphic section spanning the K-T boundary revealed that the spherical interstratified clays in the K-T boundary layer are largely decomposed. The spherical clays showed characteristic stacking disorder of 14 Å, 10 Å and 7 Å phases. These results suggest that there were heating events in the K-T boundary.

References

1) W. Alvarez, E.G. Kauffman, F. Surlyk, L.W. Alvarez, F. Asaro and H.V. Michel: *Geol. Soc. Amer.*, Special Paper, **190**, 423 (1982).
2) K. Kaiho and T. Saito: *Proc. Japan Academy*, **62**, 145 (1986).

* Tohoku Univ.
** Inst. Ind. Sci. Technol.

III-6-5. Structural Water in Volcanic Glass

K. Tazaki, T. Tiba,* M. Aratani, and M. Miyachi**

Hydrogen and deuterium distribution in the volcanic glass from Mt. Daisen in Tottori Prefecture, SW Japan was examined by heavy-ion Rutherford scattering using the RIKEN heavy-ion linear accelerater (RILAC)[1].

A 50MeV Ar^{4+} or Cu^{2+} beam of 50nA was used as incident particles. The beam size was about 1.5mm×3mm on a target angled at 45°.

Quantitative energy dispersive X-ray analysis of the glass grains gave 77-78% SiO_2, 12-13% Al_2O_3, 1.1-1.9% FeO, 1.0-1.3% CaO, 3.3-3.9% Na_2O and 3.0-3.3% K_2O suggesting fresh dacitic glass. The DTA curve, free from any visible endo- or exothermic peaks, is indicative of neither clay minerals nor crystalline materials (Fig.1).

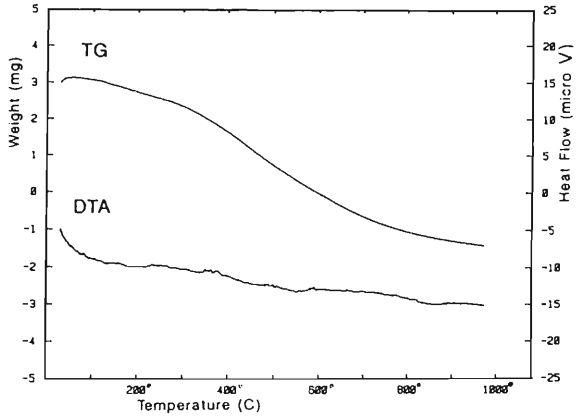

Fig. 1 Differential thermal analysis (DTA) and thermogravimetry (TGA) of glass grains.

Heavy-ion Rutherford scattering (HIRS) depth profiles indicated high contents of H, O, Si, Ca and Fe in the volcanic glass (Fig. 2).

The profile showed no significant difference between the outside and the inside of the structure. The hemispherical hydrogen slope showed that hydrogen atoms are distributed uniformly in the glass with no evidence of surface absorption. The data indicated that the structural water is in uniform structural distribution with O, Si, Ca and Fe. High resolution HIRS showed not only hydrogen but also a deuterium ion spectrum (Fig. 3).

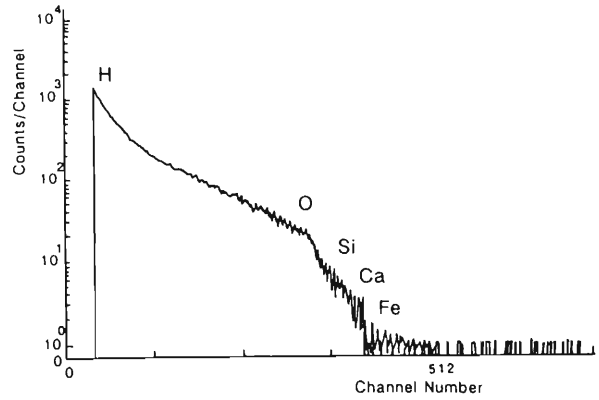

Fig. 2 Energy spectrum of the volcanic glass using HIRS showing uniform distribution of structural water.

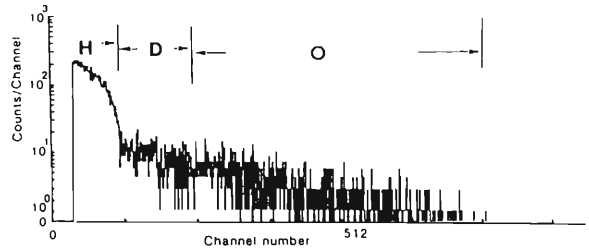

Fig. 3 Energy spectrum of recoiled hydrogen, deuterium and oxygen ions (35° to the incident argon ion beam).

Another volcanic glass of a similar age, collected from Mt. Aira in southern Kyushu, Japan was also analysed by HIRS for comparison. Spectra of the Aira glass also showed the presence of structural hydrogen, even though the amount of water was five times less than that in the volcanic glass from Mt. Daisen.

References

1) M. Aratani: *Radioisotopes*, **37**, 43 (1988).

* Natl. Sci. Museum
** General Education, Kyushu Univ.

IV. NUCLEAR DATA

IV-1. Status Report of the Nuclear Data Group

Y. Tendow, A. Yoshida, Y. Ohkubo, A. Hashizume, and K. Kitao

The Nuclear Data Group has been continuing the following data activities since previous years.

(1) Nuclear reaction cross-section data (EXFOR)

Compilation of nuclear reaction cross sections induced by charged particles into the EXFOR format has been continued. We have been restricted our scope of compilation to the production cross section for only 20 radioisotopes commonly used in the biomedical application field; ^{11}C, ^{13}N, ^{15}O, ^{18}F, ^{28}Mg, ^{52}Fe, ^{67}Ga, ^{68}Ge, ^{74}As, ^{77}Br, ^{82}Br, ^{77}Kr, ^{81}Rb, ^{82m}Rb, ^{111}In, ^{123}Xe, ^{127}Xe, ^{123}I, ^{124}I and ^{125}I.

New measurements for these isotopes rarely appear in recent references. However, a considerable number of old data are still missing in the EXFOR master file. For the completeness of the EXFOR master, we started to pick up missing works. About 60 papers have already been found so far. The compilation of these data into EXFOR format is now in progress. There are many useful medical radioisotopes other than our 20 nuclides. We are considering to expand our scope of choice to a wider range of isotopes.

A transmission tape R007 containing the corrected and revised EXFOR files that previously transmitted by us as a tape R006 has been sent to the IAEA Nuclear Data Section (NDS) this year.

Cross section data for the production of radiobromine isotopes especially ^{75}Br were surveyed extensively. [2] Radiobromine is one of the useful members of the widely used radiohalogen isotopes in medical diagnosis and biochemical studies.

(2) Evaluated nuclear structure data file (ENSDF)

We have been participating in the ENSDF compilation network coordinated by the Brookhaven National Nuclear Data Center (NNDC). The evaluation and compilation for A = 129 mass chain nuclides are in progress and reaching the final stage of completion.

(3) Nuclear structure reference file (NSR)

We are engaged in collection and compilation of secondary references (annual reports, conference proceedings etc.) published in Japan since previous year into the Nuclear Structure Reference (NSR) file and sending it to NNDC. The NSR file is offered for the on-line retrieval service by NNDC and also published periodically as the RECENT REFERENCES.

Compilation of the 1990 references has been completed and sent to the NNDC. Secondary sources surveyed are following annual reports (in code name in NSR); RIKEN (*RIKEN Accel. Prog. Rep.*), JAERI-TLV (*JAERI Tandem, Lin. & V.D.G.*), INS (*INS Univ. Tokyo*), UTTAC (*Univ. Tsukuba Tandem Accel. Center*), RCNP (*Res. Center Nucl. Phys. Osaka Univ.*) and CYRIC (*Cyclo. Radioisot. Center, Tohoku Univ.*).

Compilation of the new 1991 references along with some missing reports of 1988 through 1990 is in progress.

(4) Others

The IAEA Consultants' Meeting on Technical Aspects of the Co-operation of Nuclear Reaction Data Centers was held on 1 - 3 September 1992 at the NDS in Vienna. Participants from nine data centers in the world mainly discussed matters of technical aspects of EXFOR and CINDA as well as NDS's changeover from the mainframe computer to a VAX system.

References

1) Y. Tendow, A. Yoshida, Y. Ohkubo, A. Hashizume, and K. Kitao: *RIKEN Accel. Prog. Rep.*, 25, 154 (1991).
2) Y. Tendow, A. Hashizume, and K.Kitao: This report, p.136.

IV-2. Radiobromine Nuclides and ^{75}Br Production Cross Section

Y. Tendow, A. Hashizume, and K. Kitao

Radioactive halogen isotopes are widely used for labelling organic compounds of biomedical use as substitutes for hydrogen atoms. ^{18}F and ^{123}I have been commonly used for *in vivo* functional imaging in diagnosis and biomedical studies. Radiobromine is also found to be useful in the same application. An advantage of using radiobromine is in that several isotopes from ^{75}Br through ^{82}Br are available according to their physical properties such as half-life or decay mode. Of all the radiobromines, ^{77}Br has been most extensively used in a gamma camera because of its moderate half-life (57 h) and EC decay with a very weak positron emission rate (0.74 %). [1]

^{76}Br (16 h) is also used in the positron emission computed tomography (PECT) but it has a disadvantage in positron decay properties; a high positron energy (3.98 MeV) and a low emission rate (57 %).

^{82}Br is a β^- decay isotope and produced by an (n, γ) reaction in low specific activity. It is not suitable for the *in vivo* imaging application. ^{82}Br appears as an impurity activity in the ^{nat}Se (p, xn)^{75,76,77}Br reaction for easy production of a neutron deficient radiobromine mixture.

^{75}Br would be the most convenient isotope for PECT having a moderate half-life (1.6 h) and a proper positron energy (1.74 MeV) with a high emission rate (75.5 %). ^{75}Br is produced through various reactions; ^{76}Se (p, 2n), ^{76}Se (d, 3n), ^{76}Se (^{3}He, 3np), ^{75}As (^{3}He, 3n), ^{75}As (α, 4n) and an indirect reaction ^{nat}Br (d, xn)^{75}Kr - ^{75}Br. ^{76}Br is the main impurity mixed through these reactions with 1 ~ 3 % content typically. The excitation functions for various reactions are shown in Fig.1 and the cross section data are summarized in Table 1.

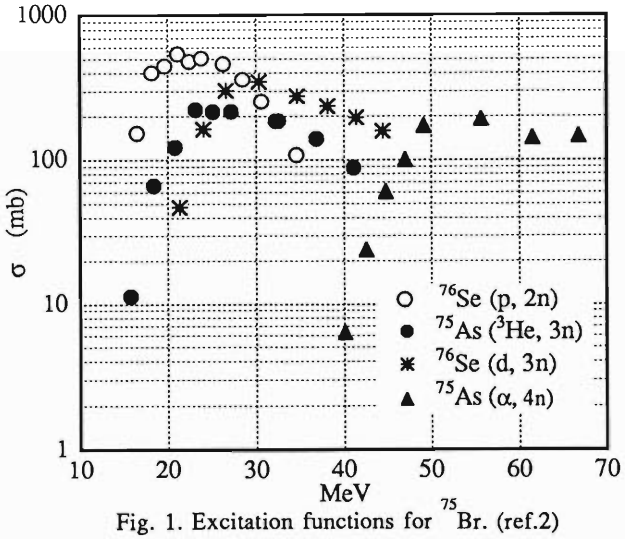

Fig. 1. Excitation functions for ^{75}Br. (ref.2)

Table 1. Cross section data for ^{75}Br production.

Reaction	Energy (MeV)	σ max (mb)	Ref.
^{76}Se(p, 2n)	16.5 - 34.5	520	2)
	15.8 - 40	410	3)
^{76}Se(d, 3n)	21.8 - 44.3	370	2)
^{76}Se(^{3}He,3np)	26.5 - 35	>53	4)
^{75}As(^{3}He,3n)	15.8 - 41.4	203	2)
	15.2 - 62.2	352	5)
^{75}As(α, 4n)	40.3 - 71.7	186	2)
	42.6 - 106	268	5)
^{nat}Br(d,xn)^{75}Kr - ^{75}Br	60 - 80	4	6)

Of all these reactions, ^{76}Se (p, 2n) and ^{75}As (^{3}He, 3n) are most suitable for the ^{75}Br production. To improve the resistivity to the high beam current, Cu-Se or Cu-As alloys are employed as target materials. ^{75}Br is recovered by the high temperature dry distillation of targets after the bombardment. The ^{76}Se (p, 2n) reaction gives the highest yield and purity. Disadvantage of this reaction is that an enriched target material has to be employed. The ^{75}As (^{3}He, 3n) reaction is also a convenient method. Advantage is in that natural arsenic can be used, but the yield is lower than that of ^{76}Se (p, 2n) reaction.

References

1) K. Kitao, A. Hashizume, Y. Tendow, Y. Ohkubo, and K. Sueki: *RIKEN Accel. Prog. Rep.*, **21**, 192 (1987).
2) A. M. J. Paans, J. Welleweerd, W. Vaalburg, S. Reiffers, and M. G. Woldring: *Int. J. Appl. Radiat. Isot.*, **31**, 267 (1980).
3) Z. Kovács, G. Blessing, S. M. Qaim, and G. Stöcklin: *Int. J. Appl. Radiat. Isot.*, **36**, 635 (1985).
4) He Youfeng, S. M. Qaim, G. Stöcklin: *Int. J. Appl. Radiat. Isot.*, **33**, 13 (1982).
5) Z. B. Alfassi, R. Weinreich: *Radiochim. Acta*, **30**, 67 (1982).
6) S. M. Qaim, and R. Weinreich: *Int. J. Appl. Radiat. Isot.*, **32**, 823 (1981).

V. DEVELOPMENT OF ACCELERATOR FACILITIES

1. Ion Accelerator Development

V-1-1. Recent Development of RIKEN 10 GHz Electron Cyclotron Resonance Ion Source

T. Nakagawa, T.Kageyama, M. Kase, A. Goto, and Y. Yano

In order to increase the beam intensity of highly charged ions from an electron cyclotron resonance ion source(ECRIS), it is surely necessary to increase the electron density of plasma or to prolong the exposure time of ions in the electron cloud, because only the efficient way to obtain highly charged ions is the successive ionization. Several methods for increasing the electron density have been successfully used in many laboratories[1-3]. One of the methods for increasing the electron density is to insert electrons into the plasma. In order to make such a condition, we changed the structure of the first stage of RIKEN 10 GHz ECRIS, which is so-called the plasma cathode method.

Figure 1 shows the schematic drawing of the first stage for the plasma cathode method. The design and performance before the change of structure of the first stage is described in Ref.4. The first stage is isolated from the second stage electrically. An acceleration plate which has a central hole is placed in front of the first stage and connected with the second stage electrically. A negative bias voltage is supplied between the first stage and the acceleration plate to extract electrons from the first stage to the second stage.

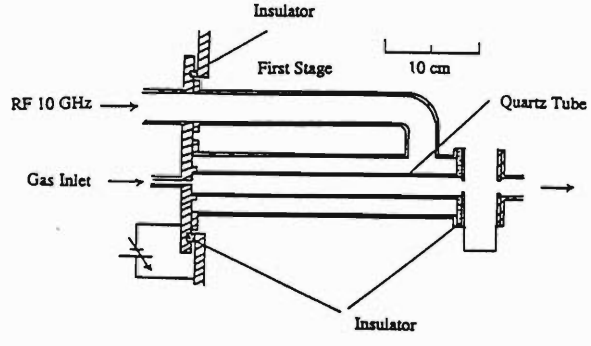

Fig.1. Schematic drawing of the first stage of RIKEN 10GHZ ECRIS for the Plasma cathode method.

Figure 2 shows the beam intensity for highly charged nitrogen, neon, argon and krypton ions as a function of the charge stage. The RF powers of the first and second stages are 0 and 800W, respectively. The extraction voltage is 10 kV. The gas pressures of the first, second, and extraction stage are 5-7x10^{-6}, 4-6x10^{-7},and 6-8x10^{-8} Torrs, respectively. These values are eight or nine times as low as the values obtained without using the plasma cathode method. The beam intensity of Ar^{11+} increases from 30 to 80 eμA, and that of Kr^{20+} increases from 0.6 eμA to 8 eμA. It is clear that the beam intensity of the highly charged ions are remarkably increased by using this method.

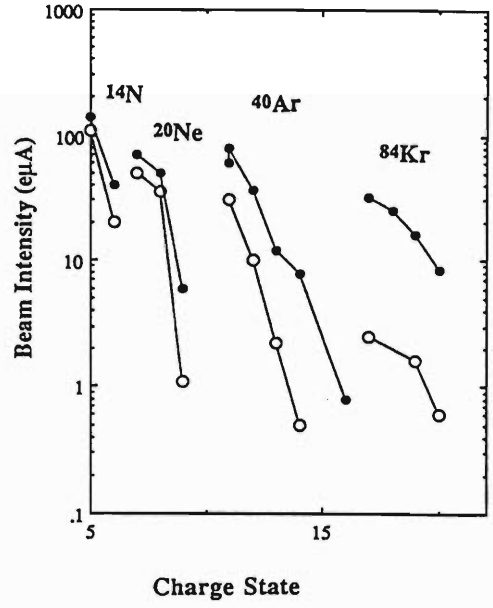

Fig.2. Beam intensities of nitrogen, neon, argon, and krypton ions as a function of charge states. Open and closed circles are the results obtained without and with using the plasma cathode method, respectively.

References

1)R. Geller: Annul. Rev. Nucl. Part. Sci.,**40**, 15(1990) and references therein
2)Z. Q. Xie, C. M. Lyneis, R. S. Lum and A. Lundgern : Rev. Sci, Instrum.,**62**, 775(1991).
3)T. Nakagawa, T. Kageyama: Jpn. J. Appl. Phys., **30**, L1588(1991).
4)K. Hatanaka and H. Nonaka: Proc. Int. Conf. Physics of Multiply Charged Ions and Int. workshop of ECR Ion Source, Grenoble, 1988, J. Phys.,C1, 821(1989) .

V-1-2. RIKEN High Intensity Polarized Ion Source and Deuteron Polarimeters

N.Sakamoto, H.Okamura, H.Sakai, T.Uesaka, T.Kubo, N.Inabe, K.Ikegami, J.Fujita, M.Kase, A.Goto, Y.Yano, and K.Hatanaka

The assembling of a high-intensity polarized-ion source (PIS) for the injector AVF cyclotron was finished in this May. We are presently trying to upgrade the performance of the PIS.

In July we succeeded in getting a 14MeV polarized deuteron beam from the cyclotron for the first time. The typical intensity obtained at the exit of PIS was 20μA; the polarizations of the extracted beam were as shown in Table 1.

Table 1. The polarizations obtained

polarization modes		p_z	p_{zz}
pure vector	up	0.40	-
	down	0.42	-
pure spin states	m=+1	0.46	0.38
	m= 0	- 0.07	- 0.36
	m= -1	- 0.44	0.28

The PIS still has drawbacks mainly in two places: the first one is concerned with the dissociator. The "white stuff" comes from the inner wall surface of a dissociation Pyrex tube which is sputtered by rf-discharge plasma and builds up in the cold nozzle(35K) for cooling the atomic beam. Another is concerned with the beam extraction system of the ECR ionizer. It has not yet been well optimized and therefore the extraction efficiency is very low. We are modifying the extraction electrodes to achieve higher efficiency.

The PIS can provide all modes of polarizations of pure vector, pure tensor and pure spin states by the combinations of two strong and two weak field rf transitions. The spin direction can be controlled by using a Wien filter which is installed at the exit of the PIS. Two different polarimeter systems monitor the vector and tensor polarizations(p_z and p_{zz}) and their polarization axis of the accelerated deuteron beam. One of them is placed between the AVF and Ring cyclotrons. The polarimetry will be made by utilizing the $^{12}C(d,p)^{13}C(g.s.)$ reaction at 14MeV. For this purpose we have measured the complete set of the analyzing powers (A_y , A_{yy} , A_{zz} and A_{xz}) of this reaction at the Kyushu University tandem accelerator laboratory (Fig.1).

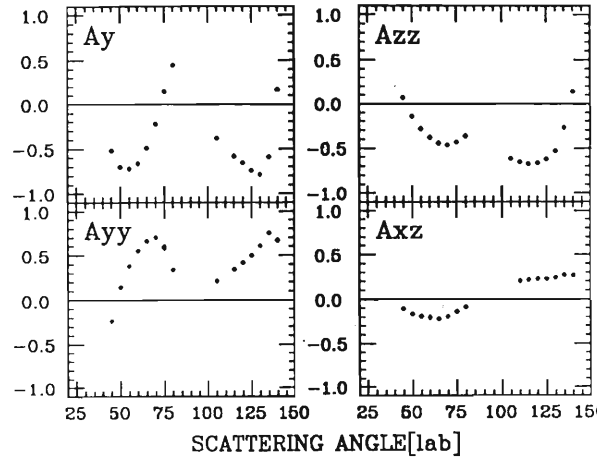

Fig. 1. Analyzing powers of $^{12}C(d,p)^{13}C$ [Ed=14MeV]

Another polarimeter for a 270MeV deuteron beam is installed on the beam transport line of the Ring cyclotron. In this November we, for the first time, accelerated a polarized deuteron beam up to 270MeV by the Ring cyclotron. We measured the vector and tensor analyzing powers (Ay and Ayy) of the H(d,d)H reaction at the scattering chamber ASCHRA. These data will be used as fundamental data of the polarimetry. Detailed analysis is now in progress.

Since the complete sets of analyzing powers (Ay,Ayy,Axx and Axz) are needed to determine the polarization axis of a deuteron beam, an experiment to measure Axx and Axz of the H(d,d)H reaction at 270MeV is scheduled for the next February.

V-1-3. Development of the LNA Laser for Polarized ^{3}He Ion Source of the Injector AVF Cyclotron (III)

A. Minoh, K. Ogiwara, and T. Fujisawa

It was shown by Leduc et al[1] that the laser frequency has to be tuned on one of the hyperfine components of the ^{3}He 2S-->2P transition to make the nuclear polarization of ^{3}He by the optical pumping. In our previous experiment, the 0.1mm air gap etalon reduced the spectral width of the LNA laser from 300GHz to 30GHz and it was believed that another etalon must be set in the cavity to reduce the width to the Doppler width of the 2GHz(in 2S-->2P transition of ^{3}He).[2] Thus the free spectral range(FSR) of the second etalon should be more than 30GHz. We estimate the spacing of the etalon is 2--3mm because the second etalon must tune the laser frequency on one hyperfine level in the width of 30GHz.

We made experimentally sure the cavity parameters by using the LNA laser of the Institute for Molecular Science, because the output power of our Ar^+ laser exciting the LNA laser is too weak to insert two etalons in the cavity.

Optogalvanic effect induced by the laser beam was observed to study the tuning on the hyperfine transition.[3] The optogalvanic cell was of 15mm inner diameter and 25cm long. The cell was filled with 0.4Torr ^{3}He gas and the DC discharge current was 10mA.

The output power of the LNA laser was 15mW. A part of the laser beam was split by a non-coated glass plate, and was introduced into the optogalvanic cell.

The LNA laser frequency was scanned from 9228.59cm^{-1} to 9230.28cm^{-1} by the 2mm air gap etalon controlled by a piezo-electric transducer. The optogalvanic signals corresponding to the all hyperfine components of 2S-->2P transition were observed. The observed intensity of the optogalvanic signal was as strong as 60mV p-p and a saturation dip was observed at the center of the Doppler broaden line. We plan to use this saturation dip to lock the laser frequency on hyperfine level during the long time optical pumping.

The threshold pumping power of the Ar^+ laser was 1.3W for the LNA laser inserted two etalons. The maximum power of our Ar^+ laser is 1.6W. Then the output power of our LNA laser will be too weak to obtain the sufficient nuclear polarization.

We plan to measure the polarization of the ^{3}He nucleus by measuring the circular

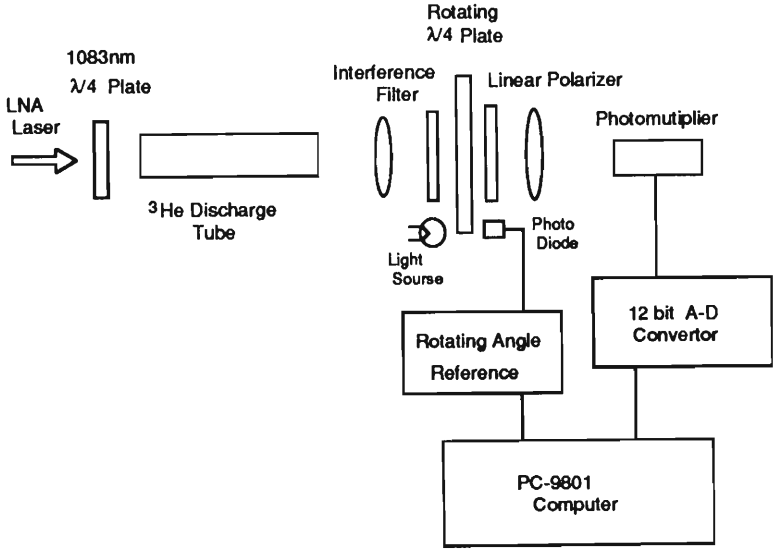

Fig. 1. Detection system of the nuclear polarization of ^{3}He.

polarization of the 667.8nm light of the 3D-->2P transition.[2] The detection system is shown in Fig.1. The 1083nm light from the laser is circularly polarized by a λ/4 plate and fed into a ^{3}He discharge tube. An interference filter cuts off all the light except the 667.8nm light. The 667.8nm light is focused by a lens, passes through a λ/4 plate rotating constantly and a linear polarizer, and measured by a photomultiplier. The output signals from the photomultiplier are sampled at each rotation angle of 90° of the λ/4 plate and stored in a PC-9801 personal computer through a 12 bit A-D converter. After several tenth rotation of the λ/4 plate, the polarization of the 667.8nm light is calculated by comparing the difference between the data of the two groups corresponding the diagonal angle of the rotating λ/4 plate. This system detects one percent of the circular polarization of the light. This analyzing power corresponds to a few percent nuclear polarization.

We thank Dr. Morita and Dr. Kumakura for providing us an opportunity to use the LNA laser system of the Institute for Molecular Science.

References

1) M. Leduc, S.B. Crampton, P. J. Nacher, and F. Laloe: Nuclear Science Application, **1**, 1 (1983).
2) A. Minoh, and T. Fujisawa: *RIKEN Accel. Prog. Rep.*, **25**, 103 (1991).
3) L. D. Shearer, and Pedetha Tin : J. Opt. Soc. Am. B, **6**, 1771 (1989).

V-1-4. A Beam Chopper for RILAC Using High Speed MOS-FET Modules

M.Hemmi, H.Kumagai, and Y.Miyazawa

In order to get a short beam pulse from RILAC, a new beam chopper was installed in the beam injection line. The chopper was composed of a deflector and a simple pulser, as shown in Fig.1.

The deflector has two parallel plate electrodes (8 cm in length along the beam line and 8 cm wide) with a gap of 2.6 cm. When a pulsed high voltage (3kV) is applied to the deflector, the beam from a 500 kV injector is deflected and stopped by a beam slit located just in front of the RILAC first cavity.

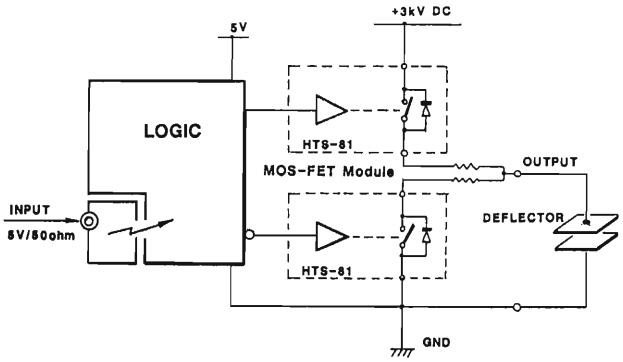

Fig. 1. Conceptional diagram of the beam chopper.

The pulser for the beam chopper is made by using a commercially available MOS-FET module.* This module is capable of switching 8kV, 30A with a turn-on rise time of 5 ns and conveniently providing 10 kV isolation between the power output and the TTL input port. To reduce the rise and fall time of the pulse two of the modules were connected in series and operated in the push-pull mode. The input signal is isolated with a high speed photo-coupler to eliminate common noise.

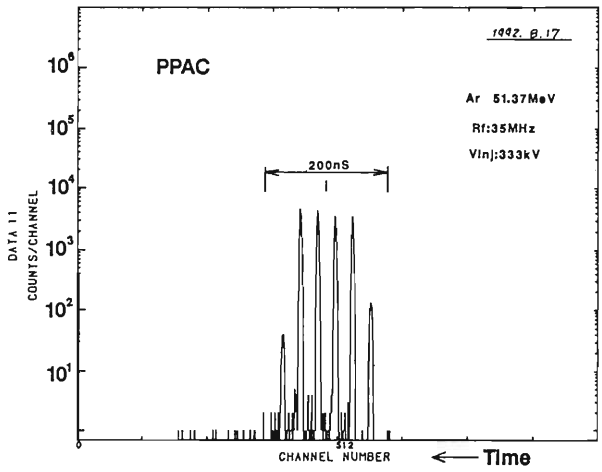

Fig. 2. A time spectrum of 51.37 MeV argon beam on the 35 MHz rf phase. It was detected by a Parallel Plate Avalanche counter.[1] The time resolution of the counter is 0.67 ns.

The pulser can drive the deflector electrodes having a capacitance of 16 pF at 3 kV with rise and fall times of about 20 ns. The pulse width of chopper can be changed from 200 ns to DC operation. Maximum repetition rate is 40000 pps.

Figure 2 shows a time spectrum of a pulsed beam accelerated by RILAC with a phase modulation of 200 ns which was synchronized to the master oscillator of RILAC. Six beam pulses in a single bunch were observed on the chopper modulation pulse.

References

1) H. Kumagai et al.: *RIKEN Accel. Prog. Rep.*, **19**, 148 (1985).

* BEHLKE HTS-81

V-1-5. Construction of the Second-Harmonic Buncher for RILAC

S. Kohara, M. Kase, Y. Miyazawa, M. Hemmi,
T. Chiba, Y.Chiba, and A. Goto

The design of a second-harmonic buncher reported previously[1] was modified by taking into account the following problems:

1) Moderating an increase of rf loss in the low frequency region.
2) Keeping a good impedance matching to the power feed line (50 ohm) without making any adjustment of elements and any external compensation through the frequency range (34-90 MHz).
3) Reducing as much as possible the parts placed in vacuum for easy fabrication.

A cross sectional view of the new buncher is shown in Fig. 1. The resonator of the buncher is of a coaxial quater-wave-length type, which has two open ends oscillating in phase and at nearly equal voltage; one end consists of a drift tube and the other a capacitive voltage divider, through which rf power is fed. The ratio of the drift tube voltage to the feed terminal voltage is kept nearly constant, 30, in the frequency range. The resonant frequency is varied by using both a movable short and a variable capacitor instead of using the latter only in the previous design; this alteration moderates the frequency dependence of rf loss. Thus low voltage standing wave ratios (VSWR) on the power feed line is obtained through the frequency range. Driving range of the movable short is 63 cm. Capacitance range of the variable vacuum capacitor is from 12 to 60 pF. The drift tube and its opposite electrodes, only components in vacuum, are sealed off with a vacuum feed-through of ceramics insulator.

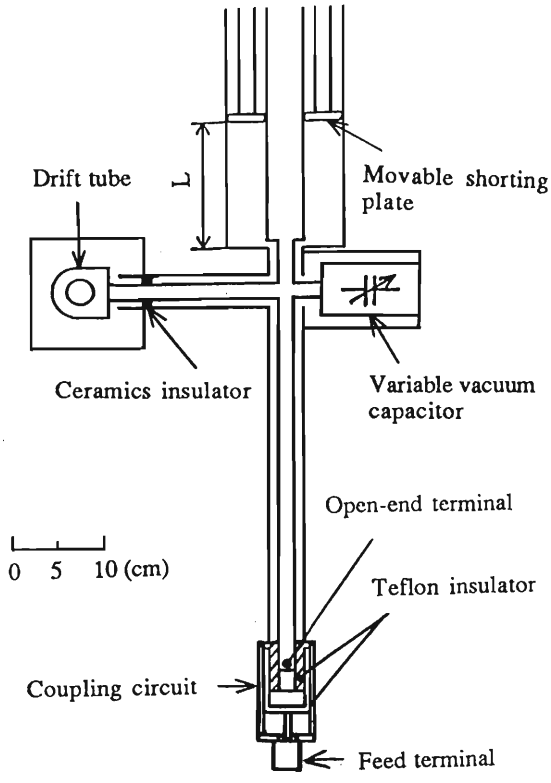

Fig. 1. Cross sectional view of the second-harmonic buncher.

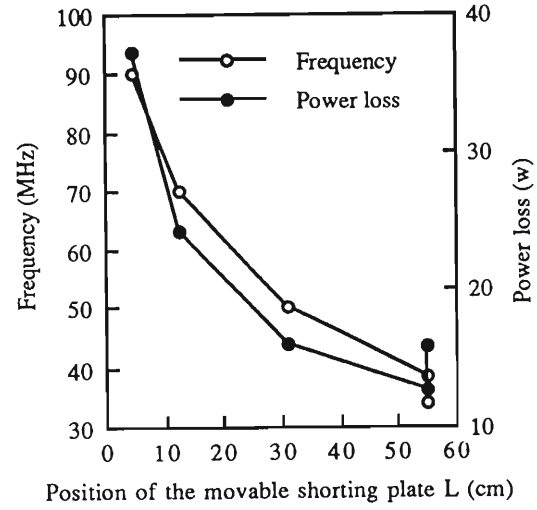

Fig. 2. Positions L of the movable shorting plate (see Fig. 1), power losses , and capacitances of the variable capacitor calculated as a function of the frequency. Power losses are calculated for the peak gap voltage of 1.5 kV.

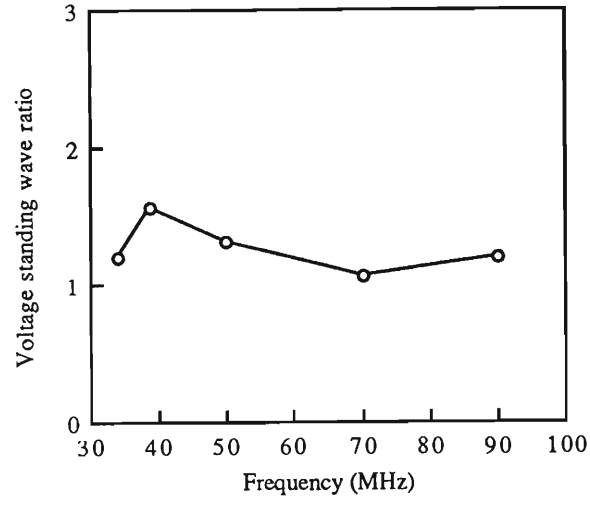

Fig.3. Voltage standing wave ratio at the feed terminal calculated as a function of frequency.

Resonant frequencies and power losses calculated with the transmission-line approximation are shown in Fig. 2. The resonant frequencies calculated are varied from 39 MHz at 55 cm of position of the movable short to 90 MHz at 4.45 cm when the variable capacitor is set at 15 pF. The resonant frequency of 34 MHz is obtained when the capacitance is 50 pF and at the position 55 cm. The maximum power loss is 37 W to get the peak gap voltage of 1.5 kV. The maximum current of the variable capacitor is reduced to 20 A from previous 120 A, so that a small size capacitor is enough for the purpose. VSWR calculated at the feed terminal is shown in Fig. 3. It is less than 1.55.

The buncher will be completed at the end of next March.

References

1) S. Kohara, M. Kase, and A. Goto : RIKEN Accel. Progr. Rep., **25**, 167 (1991).

V-1-6. Profile Monitor for Light-Ion Beams with High Energy

M. Kase, T. Kawama,* and I. Yokoyama

A three-wire type beam scanner has been used for the beam profile measurement at every beam line in the RIKEN Ring Cyclotron.

As its sensor material, a gold-plated tungsten wire with a diameter of 100 μm has been used. It has enough sensitivities for a beam of ions heavier than carbon with any energy available here (0.001 ~ 135 MeV/nucleon). On the other hand, for light ions, such as proton and deuteron with energies greater than 100 MeV/nucleon, the sensitivity is very low and sometimes one cannot measure a beam profile of their low-intensity beams. It is troublesome especially in case of beam tuning, when a beam intensity must be low enough to lighten useless radioactivation on chamber walls and so on.

To solve this problem, a new type of sensor material was introduced, namely a copper plate with a thickness of 300 μm and a width of 3 mm. The plate had been made by the chemical etching to eliminate any mechanical distortion. Three plates are held on the probe head with a Macor insulator in stead of three wires in the old type probe.[1] Figure 1 shows a view of probe head of the new profile monitor.

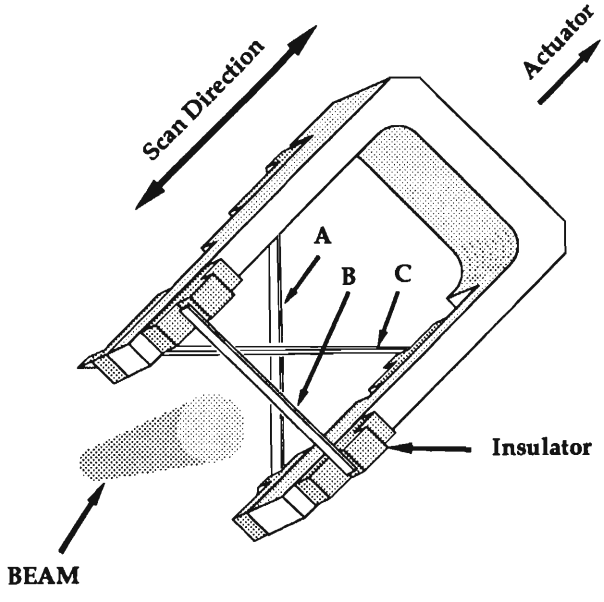

Fig. 1. A view of new type of profile monitor. A is the sensor plate for a horizontal measurement, B for a vertical one and C for a 45 deg. line one.

Figure 2 shows the comparison of the beam profile data obtained with the old and new monitors under the same conditions. The new probe has much higher sensitivity than the old one, although the two give almost the same profile shapes. The enhancement of sensitivity amounts to be a factor of 100, which corresponds to the ratio of intersection volumes for the two sensor materials. Similar data were obtained for a 135MeV proton beam.

The new monitor cannot stand for a heat damage by a 135 MeV/nucleon heavy-ion beam with an intensity over 100 pnA. Therefore the two types of probes must be installed together in one beam diagnostic station of beam lines from the RIKEN Ring Cyclotron in order to cover the all variation of beams available here.

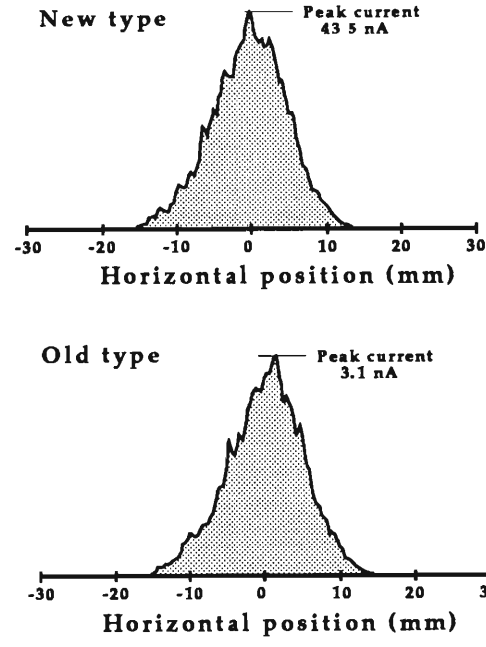

Fig.2. The horizontal beam profile data obtained by two types of probes for 270 MeV deuteron beam with an intensity of 60 nA. Vertical axes show electric currents from the sensor irradiated by the beam. The both data are normalized to their respective peak currents.

References

1) M. Kase, I. Yokoyama, I. Takeshita, Y. Oikawa, M. Saito, and Y. Yano : Proc. 11th Int. Conf. on Cyclotrons and Their Applications, Tokyo, p.443 (1987).

* Sumijyu Accelerator Service, Ltd.

2. Synchrotron Radiation Source Development

V-2-1. Study on the Low α Operation of SPring-8 Storage Ring

H. Tanaka and N. Kumagai

On the normal operation of the storage ring of SPring-8, the bunch length is expected to be a few tens psec. Although this value is quite small compared with the 2nd generation light sources based on the FODO lattice, it is required by some special users to make the bunch length as short as possible. We study the possibility of the operation for an extremely short bunch in this paper.

The bunch length in the light source is determined by the balance between radiation excitation and damping. It is expressed as follows without the current-dependent turbulence.

$$\sigma_L = \sqrt{\frac{\alpha T E}{eV'}} \cdot \frac{\sigma_\varepsilon}{E}, \qquad (1)$$

where, E, T, V', α, and σ_ε are beam energy, revolution time, slope of a RF field, a momentum compaction factor, and energy spread of circulating beams, respectively. In these parameters, T and E are not free and σ_ε is determined by E and geometrical factors. And also V' cannot be easily increased because it is limited by the RF power supply. We therefore try to shorten the bunch length by reducing α as a preliminary study. This idea was first proposed by D. A. G. Deacon[1] and confirmed by the experimental study in UVSOR.[2] Momentum compaction factor, α, is written as the following form,

$$\alpha = \frac{1}{C}\oint \frac{\eta}{\rho} ds, \qquad (2)$$

where C, η, and ρ denote the circumference of a ring, a horizontal dispersion function, and a radius of curvature, respectively. Theoretically, α can be reduced by vanishing the loop integral until the second order term of η is not negligible. Since η is positive along the ring, negative η is introduced to reduce the integral value at the straight sections for insertion devices.

We perform the parameter search under the following constrain[3]; the strength of quadrupoles and sextupoles is less than 0.675 m^{-2} and 15.75 m^{-2}, respectively.

Table 1 shows the results obtained for the case that the operation point is fixed at ν_x =51.22

Table 1. Lattice data for the case that the operation point is fixed.

	HLC2B	LALFA-B1	LALFA-B2	LALFA-B3	LALFA-B4
Emittance (nm•rad)	6.96	28.3	31.4	30.6	34.9
Tune-X	51.22	45.388	44.498	44.22	44.22
Tune-Y	16.16	16	16.332	17.16	11.16
Chrom-X	-119.21	-82.39	-81.833	-83.43	-81.174
Chrom-Y	-40.769	-41.11	-39.603	-38.1	-38.243
α_c	1.46E-04	7.96E-05	4.64E-05	4.41E-05	1.02E-05
Disp-X at HST (m)	0	-0.25	-0.25	-0.26	-0.29
Disp-X at LST (m)	0	-0.05	-0.05	-0.05	-0.05
Max BX (m)	30.4	39.4	39.6	44.66	43.7
Max BY (m)	26.8	33	32	28.56	38
Max Disp-X (m)	0.4	0.54	0.52	0.51	0.51
Quad.(1/m2)					
Q1 (0.35m)	-0.2804218	-0.31477036	-0.32143032	-0.3336449	-0.4371839
Q2 (0.97m)	0.3982004	0.3715247	0.3674327	0.3751093	0.4025077
Q3 (0.51m)	-0.4384298	-0.3856111	-0.38669375	-0.4040179	-0.4054399
Q4 (0.41m)	-0.6005168	-0.59130037	-0.58711399	-0.57624131	-0.4720318
Q5 (0.51m)	0.6349426	0.6540738	0.6588736	0.674034	0.6599572
Q6 (0.51m)	0.6349426	0.6295413	0.633524	0.6137483	0.5969747
Q7 (0.41m)	-0.6005168	-0.57310385	-0.5677595	-0.557599	-0.5013098
Q8 (0.51m)	-0.5639839	-0.58376106	-0.59185676	-0.610212	-0.5391905
Q9 (0.97m)	0.6131862	0.5916253	0.5914277	0.5883734	0.5626772
Q10 (0.35m)	-0.4772537	-0.55852177	-0.56483411	-0.5470004	-0.4760235
1/2*Sext. (1/m2)					
S1 (0.3m)	3.90425				
S2 (0.3m)	-4.3				
S3 (0.3m)	-3.95936	-3.2459	-4.0385	-4.029	-4.4551
S4 (0.5m)	7.12567	6.1845	7.96025	7.8091	8.79915
S5 (0.3m)	-3.95936	-3.2459	-4.0385	-4.029	-4.4551
S6 (0.3m)	-2.38462				
S7 (0.3m)	4.28489				

Table 2. Lattice data for the case that the operation point is not fixed.

	HLC2B	LALFA-A1	LALFA-A2	LALFA-A3	LALFA-A4
Emittance (nm•rad)	6.96	12.1	19.3	28.7	40.5
Tune-X	51.22	51.22	51.22	51.22	51.22
Tune-Y	16.16	16.16	16.16	16.16	16.16
Chrom-X	-119.21	-114.97	-115.25	-115.98	-117.12
Chrom-Y	-40.769	-41.224	-40.441	-40.802	-40.91
α_c	1.46E-04	1.98E-04	2.47E-04	3.07E-04	3.82E-04
Disp-X at HST (m)	0	-0.1	-0.2	-0.3	-0.4
Disp-X at LST (m)	0	-0.03	-0.06	-0.09	-0.13
Max BX (m)	30.4	30.3	30.4	30.5	30.7
Max BY (m)	26.8	28.3	27.5	28.4	29.8
Max Disp-X (m)	0.4	0.5	0.6	0.72	0.84
Quad.(1/m2)					
Q1 (0.35m)	-0.2804218	-0.2819887	-0.2849845	-0.28992387	-0.26994134
Q2 (0.97m)	0.3982004	0.3991698	0.4041829	0.4072485	0.4044493
Q3 (0.51m)	-0.4384298	-0.4270565	-0.43584623	-0.4302093	-0.43009175
Q4 (0.41m)	-0.6005168	-0.6069119	-0.59887883	-0.60283015	-0.60823549
Q5 (0.51m)	0.6349426	0.6305796	0.6231438	0.6193608	0.6163892
Q6 (0.51m)	0.6349426	0.3525007	0.1082802	0.0054031	0.1718881
Q7 (0.41m)	-0.6005168	-0.5395966	-0.17169347	-0.66188263	-0.0845667
Q8 (0.51m)	-0.5639839	-0.5609783	-0.56130915	-0.5554901	-0.53834575
Q9 (0.97m)	0.6131862	0.6145512	0.6185984	0.6211569	0.6250086
Q10 (0.35m)	-0.4772537	-0.4730372	-0.48495141	-0.49278872	-0.5258064
1/2* Sext. (1/m2)					
S1 (0.3m)	3.90425				
S2 (0.3m)	-4.3				
S3 (0.3m)	-3.95936	-2.7372	-2.2091	-1.7712	-1.4491
S4 (0.5m)	7.12567	4.879489	3.89505	3.0964	2.5173
S5 (0.3m)	-3.95936	-2.7372	-2.2091	-1.7712	-1.4491
S6 (0.3m)	-2.38462				
S7 (0.3m)	4.28489				

and ν_y=16.16. In the tables, HLC2B represents the parameters of the typical operation mode and the values for the sextupoles represent one half of the sextupole strength. We cannot find the proper operation mode with smaller α than the typical one in this condition. This may be because the lattice with dispersion free straight sections is optimized at this operation point. It is difficult to completely delete the dependence of fitting results on the initial condition, even with a good fitting routine.

Table 2 shows the results obtained for the case that the operation point is not fixed. The momentum compaction factor α can be reduced from one half to one fifth of the typical value. According to Eq. (1), the bunch length can be reduced down to one fourth of the typical value, several psec. On the other hand, the natural emittance becomes 4~5 times larger than the typical one and the strength of sextupole magnets becomes strong. Especially in LALFA-B4, the strength is much beyond the constrain. Although

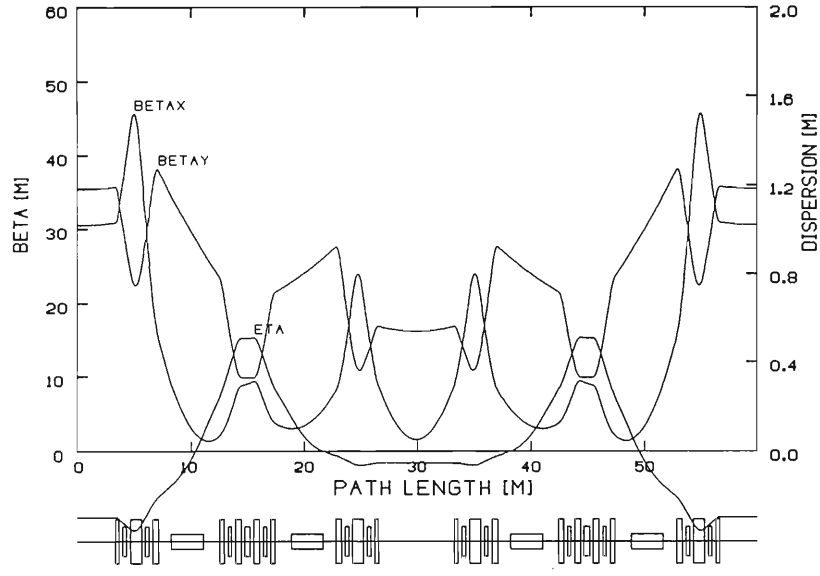

Fig. 1. Lattice functions of one normal cell for LALFA-B4.

there is a possibility to reduce the strength of the sextupoles by the sophisticated optimization with the other sextupoles for the harmonic correction, it seems not to be easy to obtain a large dynamic aperture. We show the lattice functions for the operation mode, LALFA-B4 listed in the table, in Fig. 1.

References

1) D. A. G. Deacon: Phys. Rep. **76**, 349 (1981).
2) H. Hama, S. Takano, and G. Isoyama: Proc. Workshop on 4th Generation Light Sources, Stanford, USA, Feb. 24-27, 208(1992).
3) H. Tanaka and N. Kumagai: RIKEN Accel. Prog. Rep. 25, 175(1991).

V-2-2. Estimation of Increase in Vertical Emittance Due to the Vertical Dispersion Induced by Magnetic Errors

H. Tanaka and A. Ando

In an X-ray region, brilliance of synchrotron radiations is not limited by their diffraction but limited by the emittance of an electron beam. Especially, it is important to the keep vertical emittance small for achieving high brilliance.

The vertical emittance is excited by two mechanisms; the radiation-excitation and the coupling between horizontal and vertical betatron oscillations. Since the scheme for its reduction depends on its excitation-mechanism, the contributions on the vertical emittance from the both should be estimated to design the reduction scheme. We have already investigated the effect of coupling between the transverse betatron oscillations on the vertical emittance[1] and here investigate how much the vertical emittance is excited by the radiation-excitation under practical magnetic errors in the storage ring of SPring-8.

The vertical emittance, ε_y, due to the radiation-excitation is represented as follows,[2] assuming that the partition number of a vertical damping rate is equal to unity and neglecting the angular divergence of photons emitted by an electron.

$$\varepsilon_y = C_q \cdot \left(\frac{E}{mc^2}\right)^2 \cdot \frac{\oint \frac{H_y}{|\rho^3|} ds}{\oint \frac{1}{|\rho^2|} ds} , \qquad (1)$$

$$H_y = \gamma_y \eta_y^2 + 2\alpha_y \eta_y \eta_y' + \beta \eta_y'^2 ,$$

$$C_q = \frac{55}{32\sqrt{3}} \cdot \frac{h}{2\pi mc} = 3.84 \times 10^{-13} ,$$

where, E, h, β_y, α_y, γ_y, ρ, η_y, and η_y' are the beam energy, the Planck constant, a betatron, an alfa, and a gamma functions, a radius of curvature, a dispersion function and its derivative, respectively. The subscript y denotes a vertical axis. For an ideal ring without magnetic errors, the vertical emittance defined by Eq. (1) is completely equal to zero, because η_y and η_y' vanish along the ring. We calculate the vertical emittance using the residual closed orbit distortion (COD) as a parameter. The calculation is performed by the simulation code, which is made of a linear calculation part of RACETRACK[3] and original calculation routines for statistics and correction. Magnetic errors included here are listed in Table 1.

Table 1. Random magnetic errors used in the simulation.

Dipole Magnet		
Tilt Error	1×10^{-4}	[rad]
Field Error	5×10^{-4}	
Quadrupole Magnet		
Tilt Error	2×10^{-4}	[rad]
Field Error	5×10^{-4}	
Misalignment	0.2	[mm]
Sextupole		
Tilt Error	2×10^{-4}	[rad]
Field Error	1×10^{-3}	
Misalignment	0.2	[mm]

Calculation results for three different sets of random magnetic errors, are shown in Fig. 1. The vertical emittance decreases as the r.m.s. of

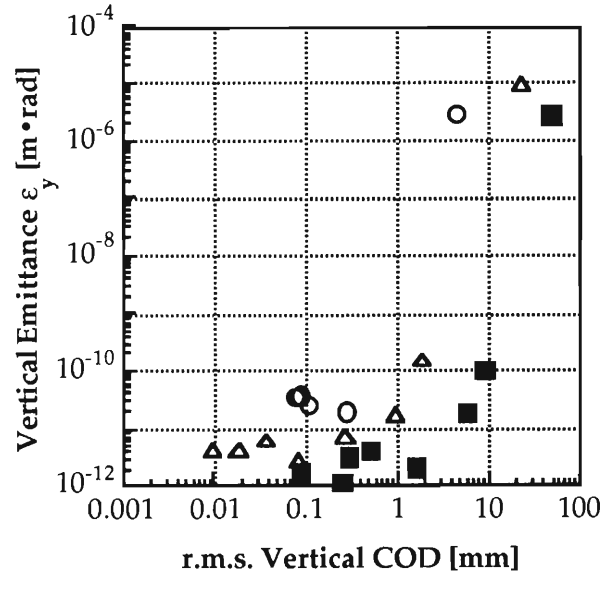

Fig. 1. Vertical emittance versus r.m.s. vertical COD.

vertical COD decreases. It reaches a few tens pm•rad when the COD is corrected below 0.2 mm by the present COD correction system.[4,5] These results show that the correction of vertical dispersion is not necessary for achieving 1 % of emittance-coupling defined as the ratio of vertical emittance to horizontal one. The horizontal emittance in the storage ring is expected to be several nm•rad.

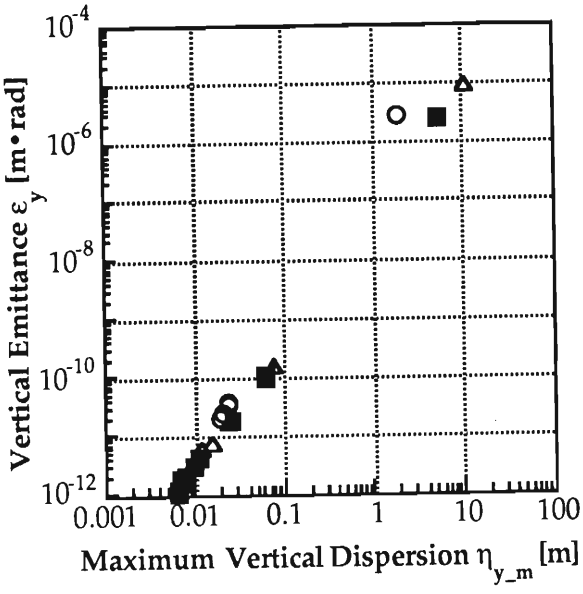

Fig. 2. Vertical emittance versus maximum vertical dispersion.

In Fig. 2, the vertical emittance is shown against the maximum vertical dispersion induced by the random errors. This value can be also adjusted by using the COD correction system. A good positive correlation between the two parameters is obtained. To keep the vertical emittance less than 10 pm•rad, the maximum vertical dispersion in the ring should be suppressed below 1 cm.

References

1) H. Tanaka and M. Hara: RIKEN Accel. Prog. Rep., **24**, 143 (1990).
2) M. Sands: SLAC-121 (1979).
3) A. Wrulich: DESY Rep., 84-026 (1984).
4) H. Tanaka, R. Nagaoka, K. Tsumaki, K. Yoshida, and M. Hara: RIKEN Accel. Prog. Rep., **22**, 231 (1988).
5) H. Tanaka, R. Nagaoka, K. Tsumaki, K. Yoshida, and M. Hara: ibid., p.235.

V-2-3. Effects of Multipole Errors on the Dynamic Aperture of SPring-8 Storage Ring (III)

H. Tanaka, Y. Ishii,* and N. Kumagai

At the initial phase of commissioning, beams are injected into a storage ring with all sextupole magnets turned off to obtain the beam stability in a short period. In this case, we should avoid the situation that multipole errors limit the beam stability within a vacuum chamber. From this point of view, the previous works[1,2] were performed. On the other hand, sextupole magnets are turned on at the steady operation to increase the beam current by suppression of the head-tail instability. Multipole errors also should not seriously affect the dynamic aperture determined by the nonlinearity of sextupole magnets in this operation phase. We here investigate the effects of multipole errors on the dynamic aperture with sextupole magnets turned on.

Figure 1 shows the dynamic aperture using the strength of octapoles and decapoles as a parameter. The multipole errors used in this calculation are listed in Table 1. Under the condition represented by the empty circles, the dynamic aperture was larger than the chamber aperture with the sextupole magnets turned off,[2] but it becomes about 25 % smaller than the chamber's with the sextupole magnets turned on. We see in the figure that the empty symbols represent smaller dynamic aperture than the filled ones and that there is not a marked difference between the empty circles and squares. This means that the reduction of the dynamic aperture is due to the octapole components under the calculation condition. By one fifth reduction of the strength of the octapole components, the horizontal dynamic aperture recovers from 28 mm up to 31 mm in the low coupling.

Table 1. Multipole errors used for the calculation of dynamic aperture. The values for each multipole component in the table represent the ratios to the measured data[3] corresponding to the same component. The symbols 'R' and 'S' denote the random and the systematic errors, respectively.

	6 pole		8 pole		10 pole		12 pole	
Symbol	R	S	R	S	R	S	R	S
O	0.5	5	5	50	0.5	5	0.1	1
□	0.5	5	5	50	0.1	1	0.1	1
◆	0.5	5	1	10	0.5	5	0.1	1
▲	0.5	5	1	10	0.1	1	0.1	1

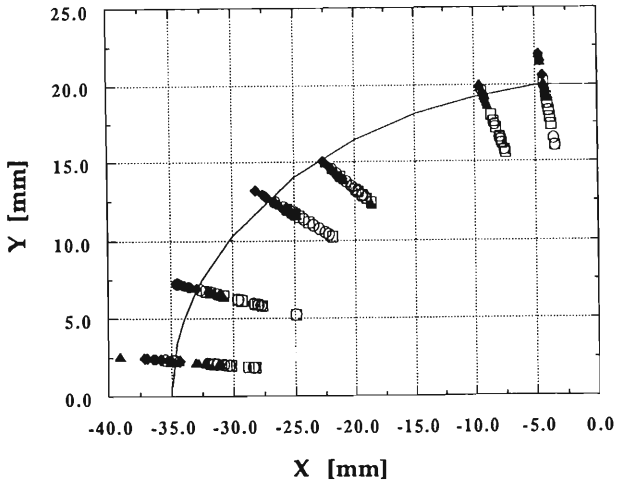

Fig. 1. Reduction of the dynamic aperture du to the multipole errors with the sextupole magnets turned on. The solid line represents the vacuum chamber aperture. In this calculation, the multipole errors listed in Table 1 were used.

Figure 2 shows the effect of end-shims on the enlargement of the dynamic aperture. The

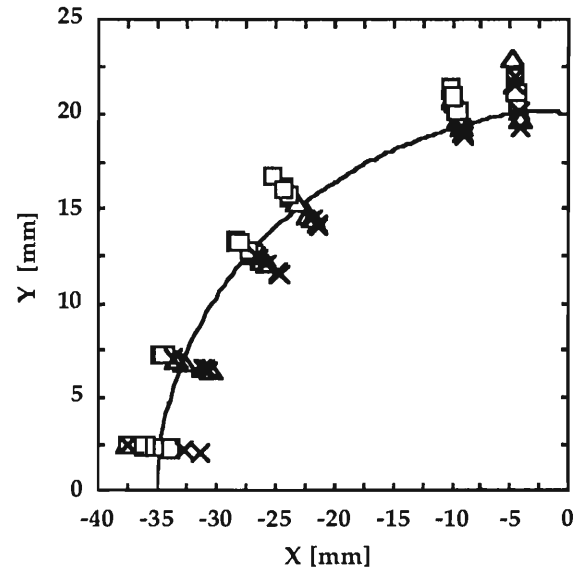

Fig. 2. Enlargement of the dynamic aperture due to the end-shims with sextupole magnets turned on. In this calculation, the multipole errors listed in Table 2 were used.

* Takasaki Rad. Chem. Establish., Japan Atomic Energy Res. Inst.

Table 2. Condition of the multipole errors used in Fig. 2. The symbols 'R', S', and each value in the table denote the same as in Table 1.

Symbol	6 pole R	6 pole S	8 pole R	8 pole S	10 pole R	10 pole S	12 pole R	12 pole S
×	0.5	5	1	10	0.5	5	0.1	1
Δ	0.5	5	1	1	0.5	5	0.1	0.1
❑	0.5	0.5	1	1	0.5	0.5	0.1	0.1

multipole errors used in this calculation are listed in Table 2. The crosses represent the case without end-shims. The empty triangles and squares represent the cases with end-shims to correct the multipole errors of the quadrupole magnets and to correct those of the both quadrupole and sextupole magnets, respectively. In this calculation, it is assumed that only systematic multipole errors are reduced to one tenth by using the end-shim correction. We see in Fig. 2 that; (1) the enlargement of ~10 % is obtained by the end-shim correction in the low coupling ratio, (2) the end-shim correction is not effective for the enlargement in the high coupling ratio, and (3) there is not a marked difference between the cases where the end-shim correction is applied to the quadrupole magnets only and to both of the quadrupole and bending magnets.

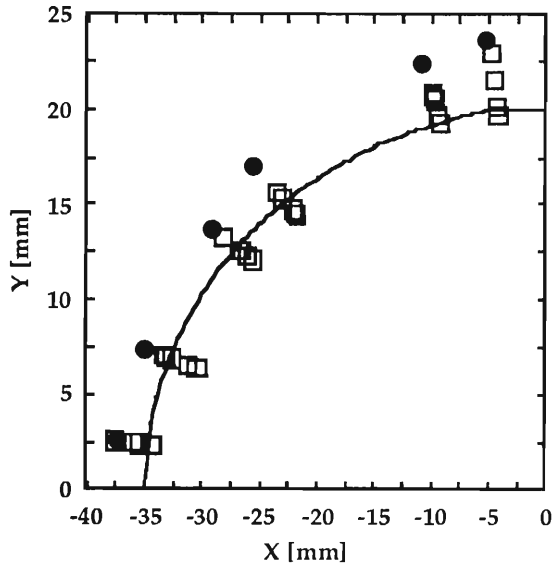

Fig. 3. Comparison between the dynamic apertures with and without the multipole errors under the condition that the sextupole magnets are turned on. The empty squares and the filled circles denote the dynamic aperture with and without the multipole errors, respectively.

Figure 3 shows the comparison between the dynamic apertures with and without the multipole errors. As the multipole errors, those represented by the empty triangle in Table 2 are used. The multipole errors do not much reduce the dynamic aperture in this condition.

Figure 4 shows the comparison between the dynamic apertures with the sextupole magnets turned on and off. The same multipole errors as in Fig. 3 are used. In this multipole error condition, the dynamic aperture is about twice larger than the chamber's with the sextupole magnets turned off.

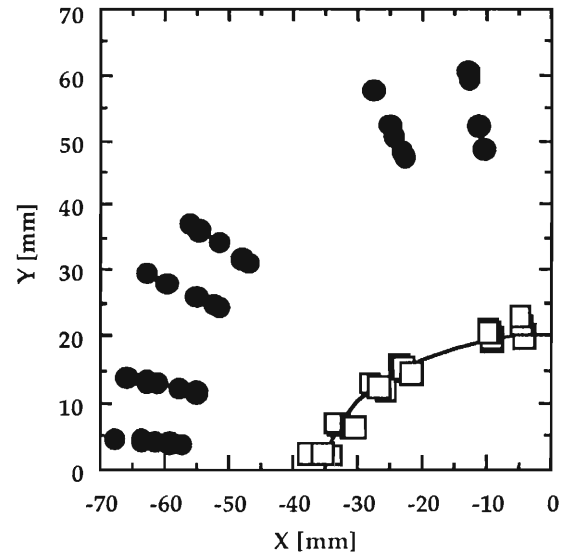

Fig. 4. Comparison between the dynamic apertures with the sextupole magnets turned off and on in the presence of the multipole errors. The filled circles and the empty squares denote the dynamic aperture with sextupole magnets turned off and on, respectively.

References

1) Y. Ishii, H. Tanaka, and N. Kumagai: RIKEN Accel. Prog. Rep., 25, 180(1991).
2) Y. Ishii, H. Tanaka, and N. Kumagai: ibid, 25, 182(1991).
3) J. Ohnishi, H. Takebe, K. Kumagai, and S. Motonaga: IEEE Trans. Mag., 28, No.1, 546(1992).

V-2-4. Effects of Ground Tremor on the Orbit Distortion of SPring-8 Storage Ring

H. Tanaka and A. Ando

To obtain highly brilliant photons emitted by circulating beams, it is important to reduce practical emittance. This emittance can be calculated with the photon density on a sample averaged through an experimental period. When time-dependent orbit modulation occurs and its frequency is large enough, the practical emittance increases and it is approximately expressed as a convolutional form:

$$\frac{\varepsilon_{\text{total } z}-\varepsilon_z}{\varepsilon_z}=\frac{\Delta\varepsilon_z}{\varepsilon_z}=2\cdot\sqrt{\frac{\varepsilon_{\text{vib } z}}{\varepsilon_z}}+\frac{\varepsilon_{\text{vib } z}}{\varepsilon_z},\ z=x,y, \tag{1}$$

where ε_{vib} represents emittance of the orbit modulation and subscripts x and y represent a horizontal and a vertical plane, respectively. In order to estimate the emittance growth due to ground tremor, we investigate its effects on the orbit distortion.

Plane ground wave model[1] is used here. In this model, we assume the following; (1) the ground tremor is decomposed into plane waves, (2) the waves propagate straight and with a constant velocity, (3) the waves are uniformly distributed on the surface and cover the ring completely, (4) a ring is regarded as a circle, and (5) magnets along the ring oscillate synchronizing with the waves. Schematic figure for the model is shown in Fig. 1.

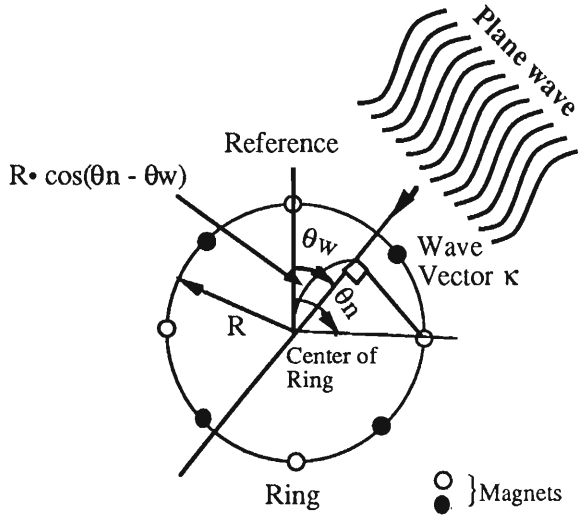

Fig. 1. Schematic geometry described by the model.

In the figure, θw, θn, and R denote a direction of wave-propagation, an arbitrary azimuthal position, and a mean radius of a ring, respectively. We introduce a parameter Δφ to represent the phase-difference from the center of the ring. At the position θn, Δφ(θn, θw) is written as

$$\Delta\phi(\theta n,\theta w)=\kappa\cdot\bar{r}=|\kappa|\cdot R\cdot\cos(\theta n-\theta w),$$
$$=\frac{\omega\cdot R}{v_t}\cdot\cos(\theta n-\theta w), \tag{2}$$

where ω and v_t are an angular frequency and a propagation velocity of the wave, respectively. Therefore, the transverse displacement due to the wave at θn is expressed with Δφ(θn, θw) as

$$\Delta x_n=A\cdot\cos(\theta n-\theta w)\cdot\mathrm{Re}[\exp i\{\omega t+\Delta\phi(\theta n,\theta w)+\phi_0\}], \tag{3}$$
$$\Delta y_n=A\cdot\mathrm{Re}[\exp i\{\omega t+\Delta\phi(\theta n,\theta w)+\phi_0\}]. \tag{4}$$

In the above, Δx_n, Δy_n, A, and ϕ_0 are a horizontal and a vertical displacement at θn, an amplitude of the wave, and an initial phase of the oscillation, respectively. Equations (3) and (4) are substituted into well known formulae[2] for a closed orbit distortion and then they are averaged on the initial phase ϕ_0 and the amplitude A. We obtain normalized amplification factors F_z as

$$F_z^2=\frac{\langle\varepsilon^2_{\text{vib } z}\rangle}{\langle A^2\rangle}=\frac{1}{16\sin\pi\nu_z}\sum_i\sum_j\sqrt{\beta_{zi}}\cdot\sqrt{\beta_{zj}}\cdot\frac{(B'L)_i}{B\rho}\cdot\frac{(B'L)_j}{B\rho}\cdot\cos(\mu_{zi}-\mu_{zj})\cdot\Lambda\cdot\{\cos(\Delta\phi(\theta i,\theta w))\cdot\cos(\Delta\phi(\theta j,\theta w))+\sin(\Delta\phi(\theta i,\theta w))\cdot\sin(\Delta\phi(\theta j,\theta w))\},$$

$$\Lambda=\begin{cases}\cos(\theta i-\theta w)\cdot\cos(\theta j-\theta w) & \text{at } z=x\\ 1 & \text{at } z=y\end{cases}, \tag{5}$$

where ν_z, μ_z, B'L, and Bρ denote a tune and phase advance of a betatron oscillation, integrated strength of a quadrupole magnet, and magnet rigidity, respectively. The angle bracket represents the ensemble mean of a parameter within it. For a Chasman Green lattice which is complicated compared with an FODO lattice, eq. (5) cannot be written with a series of Bessel functions used in Ref. 1.

In the following calculation, a propagation velocity is assumed to be 1000 m/sec on the basis of the data measured at Harima Science Garden City.[3] The amplification factors are also calculated at the center of the high β straight section. In Fig. 2, we show the dependence of the normalized amplification factors on the frequency of the wave. From these results, we see

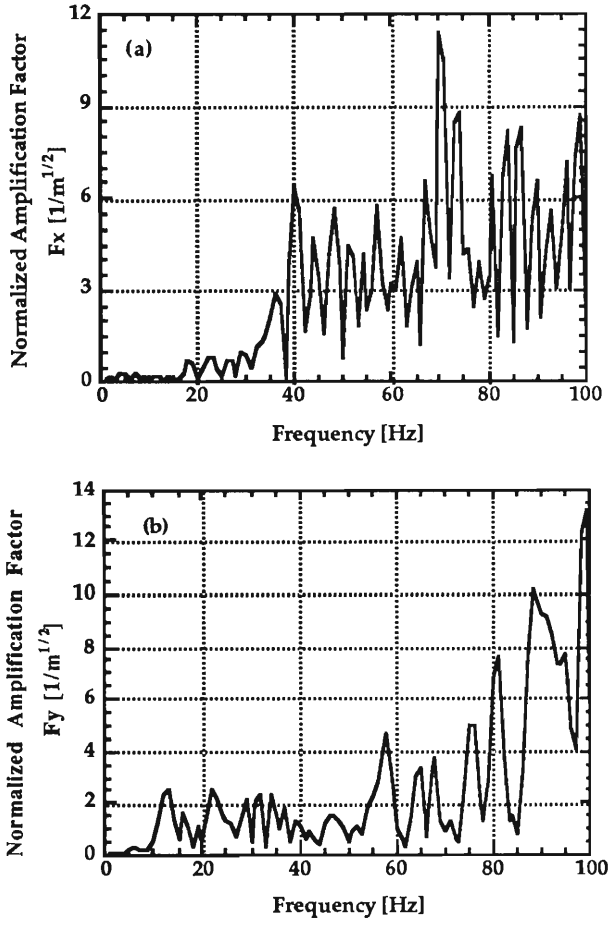

Fig. 2. Normalized amplification factors versus the frequency of the wave. The incident angle is set to be 0.0 degree. (a) and (b) show the horizontal and the vertical dependences, respectively.

the following: (1) The normalized amplification factors are at most ~10 in the regime that the frequency is less than 100 Hz. (2) The orbit distortion is not induced in both planes in the regime that the frequency is less than ~10 Hz. In this regime, the wave-length is so large that the oscillations of all magnets within a few straight sections have almost the same oscillation phases. This cancels out the contributions to COD from each magnet.

In Fig. 3, we show the dependence of the normalized amplification factors on the angle of incidence of the wave. Since a resonant peak is observed at 10~13 Hz in the power spectrum of the measured data,[3] the frequency of the wave is fixed at 13 Hz. We see that the horizontal

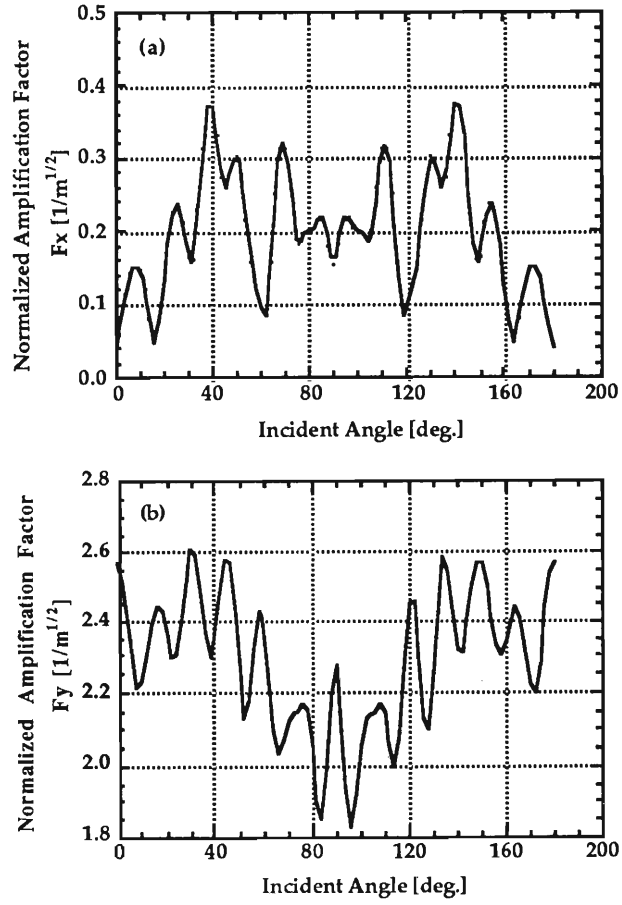

Fig. 3. Normalized amplification factors versus the incident angle. The frequency is 13 Hz. (a) and (b) show the horizontal and the vertical dependence, respectively.

amplification factor strongly depends on the incident angle in this frequency regime, but it is not beyond 0.4 .

According to the measured data, the peak amplitude at 10~13 Hz is about 10^{-3} μm. By using this value and the calculation results, $\varepsilon_{vib\ z}$ is estimated to be less than ~1×10^{-17} and $\Delta\varepsilon_x$ and $\Delta\varepsilon_y$ are 0.01 % and 0.1 %, respectively. We find that the emittance growth due to the ground tremor is small in the storage ring of SPring-8.

References

1) J. Rossbach: Particle Accelerators, **23** , 121 (1988).
2) E. D. Courant and H. S. Snyder: Annals of Physics, **3**,1 (1958).
3) Conceptual Design Report, SPring-8 Project Part I Facility Design 1991 [REVISED], JAERI-RIKEN SPring-8 Project Team.

V-2-5. Geodesy for the Storage Ring of SPring-8

S.Matsui and I.Takeshita

The SPring-8 surrounds Mihara-Kurriyama Hill which is 50 m higher than the storage ring level. Ten geodetic points (SR1~SR10) are positioned outside the ring as shown in Fig.1. The style, which is a Japanese standard fiducial point, is shown in Fig.2.

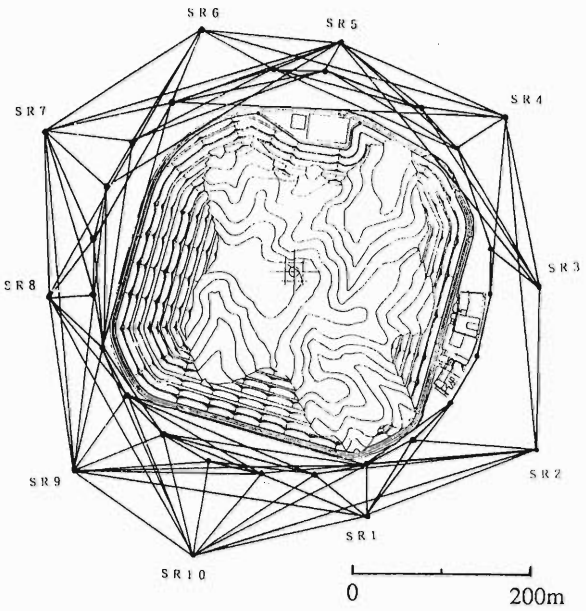

Fig. 1. Surface network.

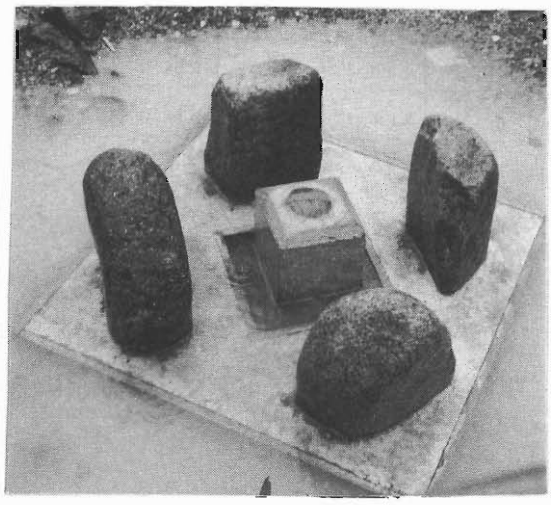

Fig.2. Geodetic point outside the ring.

A weak point is that it is hard to connect these points with triangles because of the Hill.

Figure 3 shows one of the 23 monuments for the magnet alignment on the ring and the cross section of the tunnel. This concrete block is fixed by anchor bolts to prevent it from shifting.

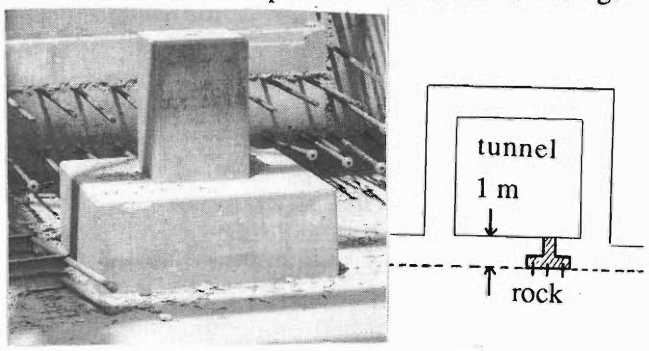

Fig.3. A monument for magnet alignment.

These monuments can be used not only for the magnet alignment but also as a mark for the construction of the accurate wall of the tunnel.

It is possible to align the magnet even if the number of monuments is reduced. However the accuracy becomes better as the number of monuments is increased, and a 60 m interval between two monuments is adequate for measuring the distance with ease between the monument and the wall. If the interval is 120 m, it is hard to measure the distance from the monument to the wall when the tunnel is constructed.

A stand for survey instruments is mounted on the monument as shown in Fig.4. The measurement becomes easy and accurate by using these stands.

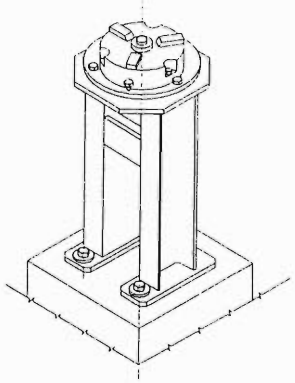

Fig.4. A stand for survey instruments.

The distance is measured by a Kern Mekometer ME5000 (measuring accuracy 0.2mm+0.2ppm) and the angle by a Wild Theodolite T3000 (accuracy 0.5″).

V-2-6. Status of SPring-8 Magnet System

J. Ohnishi, N. Kumagai, S. Motonaga, S. Matsui, H. Takebe, and K. Kumagai

Prior to the mass production of about nine hundreds magnets of the SPring-8 storage ring, a dipole, two quadrupole, and a sextupole have been fabricated and delivered to our laboratory. There was no great problem for their fabrication except only one quadrupole that did not satisfy the required dimensional accuracy. It had large asymmetrical yokes and was not strong structurally. The same type of quadrupoles will be changed a little in the design of yoke supports.

We measured their magnetic characteristics such as excitation curves, magnetic lengths, and multipole field components. The dipole magnet was measured with a hall probe, the quadrupoles with twin search coils and harmonic coils, and the sextupole with the harmonic coils with a rotary encoder.[1,2]

Table 1 lists the measured coefficients of multipole fields. Those of the dipole and the sextupole magnet were smaller than the tolerance limits required by the beam dynamics. However, the strength of the dodecapole field of the quadrupole magnet was larger than the requirement, though that had been predicted. This component will be corrected by attaching shims to the end plates of the magnets. Moreover, since other components of the quadrupole magnet were slightly large due to the fabrication inaccuracy, it is necessary to check the influence on the beam by the tracking simulations.

Presently, mass production of the storage ring magnets has begun and a few ten magnets are completed. By next spring, thirteen dipoles, about a hundred quadrupoles, and a hundred sextupoles will be delivered to the construction site of the storage ring. We will start to make a series of measurements of all the delivered magnets in order to confirm their magnetic characteristics.

Table 1. Multipole field strengths of the fabricated magnets.

multipole		dipole	quadrupole	sextupole	octupole	decapole	dodecapole	14-pole	16-pole	18-pole	30-pole
n		0	1	2	3	4	5	6	7	8	14
BM	b_n	7.1×10^{-2}	1.1×10^{-4}	-2.8×10^{-2}	-4.1×10^{-2}	1.5×10^{1}	3.1×10^{1}	2.0×10^{4}	-3.8×10^{4}	-1.2×10^{7}	
QM	$\lvert a_n+ib_n\rvert$		2.3×10^{-1}	1.7×10^{-3}	7.5×10^{-2}	1.6	4.7×10^{2}				
SM	b_n			2.4	5.0×10^{-2}	5.0×10^{-2}	8.1	4.5×10^{1}	3.8×10^{3}	1.2×10^{6}	2.8×10^{15}
	a_n				2.2×10^{-2}	2.5×10^{-1}	3.2	5.6×10^{1}	3.2×10^{3}	1.1×10^{5}	7.7×10^{12}

notation:

$$\frac{BL}{B\rho}=\sum_n (b_n+ia_n)(x+iy)^n$$

condition of measurements:

BM:Bo=0.679 [T], L=2.804 [m], QM:B'=17.4 [T/m], L=0.354 [m], SM:B"=420 [T/m^2], L=0.30 [m]

References

1) J. Ohnishi, H. Takebe, K. Kumagai, and S. Motonaga: IEEE Magnetics, 28, 1, 546 (1992),

2) J. Ohnishi and N. Kumagai: This report, p.155.

RIKEN Accel. Prog. Rep. 26 (1992)

V-2-7. Magnetic Field Measurements with Improved Harmonic Coils

J. Ohnishi and N. Kumagai

All the magnets of the SPring-8 storage ring will be inspected by field measurements before the installation in the ring. In the field measurements we measure excitation curves, magnetic field lengths, multipole fields, and positions of the magnetic center. We will use a field measurement device called harmonic coils in order to make precise measurements in short time.

Figure 1 shows a schematic view of the harmonic coils. When they are rotated in quadrupole or sextupole magnets, harmonic voltages are generated proportional to multipole fields. In the first system, the induced voltages were directly analyzed with FFT. However, since induced voltages are influenced by the angular velocity of the coils, it is difficult to measure the field strengths and the multipole field coefficients precisely.

Then, we attached a rotary encoder to the harmonic coil, and integrated voltages at regular intervals of rotating angle. Because the integrated voltages are independent of the angular velocity of the coils, we can measure the field strengths with the accuracy of about 1×10^{-4} and the multipoles stably. Moreover the measurements of the rotating angles enabled us to

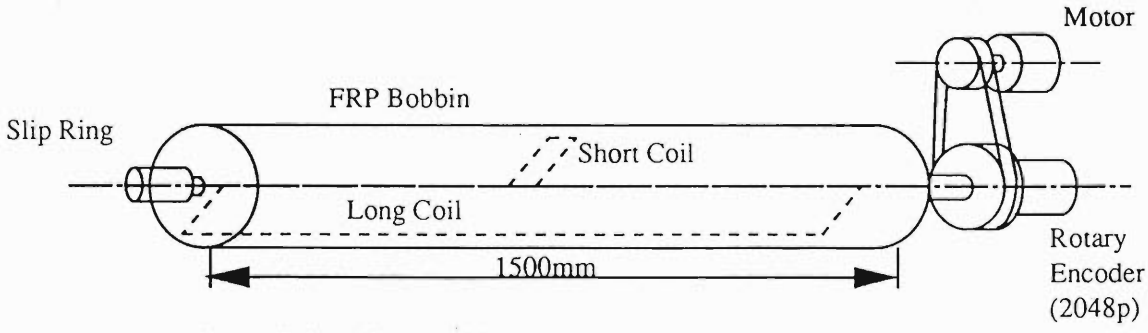

Long Coil: w40 x L1500, 1turn
Short Coil: w35.5 x L20, 50turns

Fig. 1. Schematic view of the harmonic coil.

decompose each multipole field into a normal and a skew component.

Figure 2 shows multipole field strengths of the first fabricated magnet of 336 sextupoles as an example. Black and white bars indicate a normal and a skew components for each multipole field respectively. The strengths of multipole fields are represented at a point on the circle with a radius of 35 mm by a unit of gauss. It is found from the figure that a normal component is dominant for the 18-pole (n=9) and the 30-pole (n=15) components because of the geometric symmetry of the magnet. The quadrupole and the 28-pole components are induced from the sextupole and the 30-pole respectively by the displacement between the magnetic center and the rotating center of the harmonic coil.

Series measurements of the storage ring magnets with the harmonic coils described above will start in spring next year.

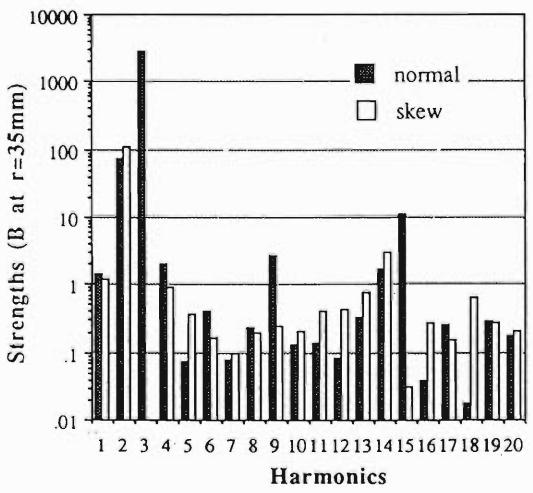

Fig. 2. Multipole field strengths of the first fabricated sextupole magnet measured with the harmonic coils.

V-2-8. Design of Injection Section for the SPring-8 Storage Ring

K. Kumagai and S. Matsui

Detailed design of the injection section for the SPring-8 storage ring is in progress. The beam from the synchrotron is injected into the storage ring at one of the straight sections through three DC septum magnets (SEP5,SEP6, and SEP7) and a pulsed septum magnet (SEP8). These magnets are required to provide about 8.4 degree deflection to the injection beam, while not disturbing the stored beam. Figure 1. shows the arrangement of the septum magnets.

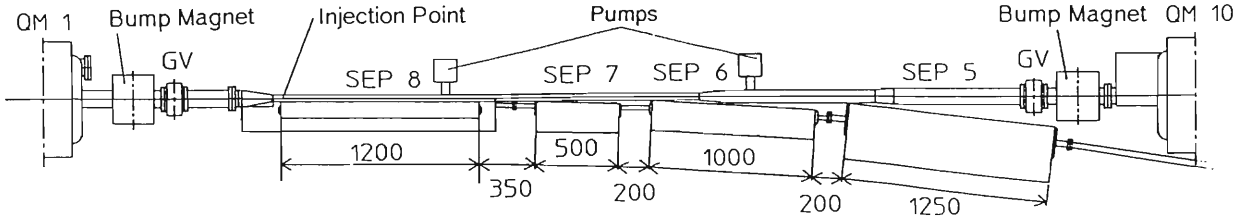

Fig.1. Arrangement of the injection section.

The main parameters of DC septum magnets are listed in Table 1. SEP5, SEP6, and SEP7 are excited in series by the DC power supply, and operated in air with a stainless steel vacuum chamber passing through the magnet gap. These magnets have straight axes, and the cores of SEP6 and SEP7 have the same cross section to save the construction cost.

Table 1. Parameters of the DC septum magnets.

	SEP5	SEP6	SEP7
Core Length(m)	1.25	1.0	0.5
Bending Angle (mrad)	65.9	42.2	14.1
Peak Field (T)	1.406	1.125	0.75
Number of Turns	10	6	4
Peak Current (A)	2240	2240	2240
Stability (%)	0.01	0.01	0.01

SEP8 is a pulsed septum magnet. The cross section is shown in Fig.2 and the parameters are given in Table.2. The magnetic field in the gap is generated by a single turn conductor wound around the return yoke, and it is excited by a half sine wave pulse of current.

The septum wall has a thickness of 9.5 mm, reducing to 1.5 mm at the injection point. This wall is made of a copper plate combined outside with a magnetic stainless. The copper plate is effective as an eddy current screen while the magnetic stainless is effective for shielding the magnetic field and is also a part of the storage ring vacuum chamber. The magnet core of SEP8 is laminated plates of 0.1 mm thick silicon steel.

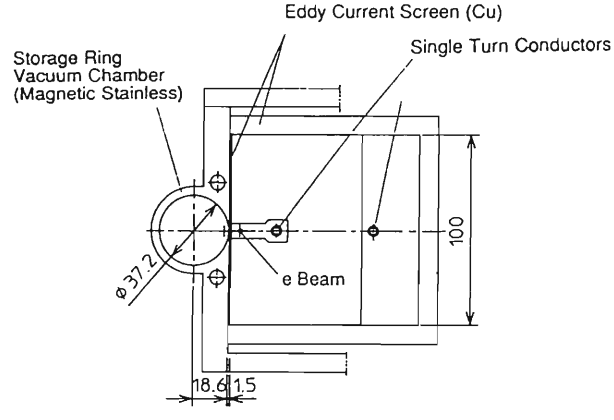

Fig.2. Cross sectional view of the pulsed septum magnet, SEP8.

Table 2. Parameters of the pulsed septum magnet.

	SEP8
Core Length (m)	1.2
Bending Angle (mrad)	24.7
Peak Field (T)	0.55
Number of Turns	1
Peak Current (A)	3510
Pulse Width (μsec)	30
Stability (%)	0.1

V-2-9. Power Supply System for SPring-8 Magnet

H. Takebe, N.Kumagai, J.Ohnishi, K.Kumagai, S.Matsui, and S.Motonaga

A detailed design of the power supply (PS) system for the SPring-8 Storage Ring was completed this Summer. Based on the excitation measurement using the R&D magnets(B, Q, and Sx), their maximum currents were decided. All the big PSs are located in PS-room A, and steering and auxiliary (QA-) PSs[1] are located in PS-rooms A, B, C, and D. Connecting cables between the PS and magnets are designed to have a current density under 1.2 A/mm^2. The maximum voltages are also fixed.

The maximum current, voltage, power and cubicle number for the B-PS are 1270A, 1157V, 1515kW, and 1, respectively. Those for Q magnets are 392A ~ 570A, 480 ~ 1281V, 192 ~ 728kW and 10. And those for Sx magnets are 300A, 669 ~ 781V, 201 ~ 234 kW and 7. Total inductances of the B,Q, Sx magnets over 48 cells are 0.76 H, 0.45 ~ 1.25 H, and 0.62~0.72 H, respectively.

Each steering magnet(St) is connected to one PS of 5 A and 51 V. Total number of the St-PS is 192. Thirty-six sets of St-PS are mounted in 1 cubicle and are supplied a DC bus together.

The Bending-magnet-PS has an input transformer for 6.6kV, 24th phase thyrister diodes and a passive filter system.

Figure 1 shows a block diagram of the Q-PS system. Input voltage for the Q-PS is 400 V. It has 12th phase thyrister diodes and a reactor transformer active filter system. Input transformer phases of the Q-PSs are shifted for half sets in order to reduce the harmonic current distortion. QP-2,5,6,9 have bypass (2%) circuits to compensate a small difference of the excitation factors caused by the magnet yoke shape difference. Q magnets in the long straight sections can be compensated by an auxiliary power supply system(QA-PS). They (40 sets, initially) are 11~17 A and 19~33 V floating PSs.

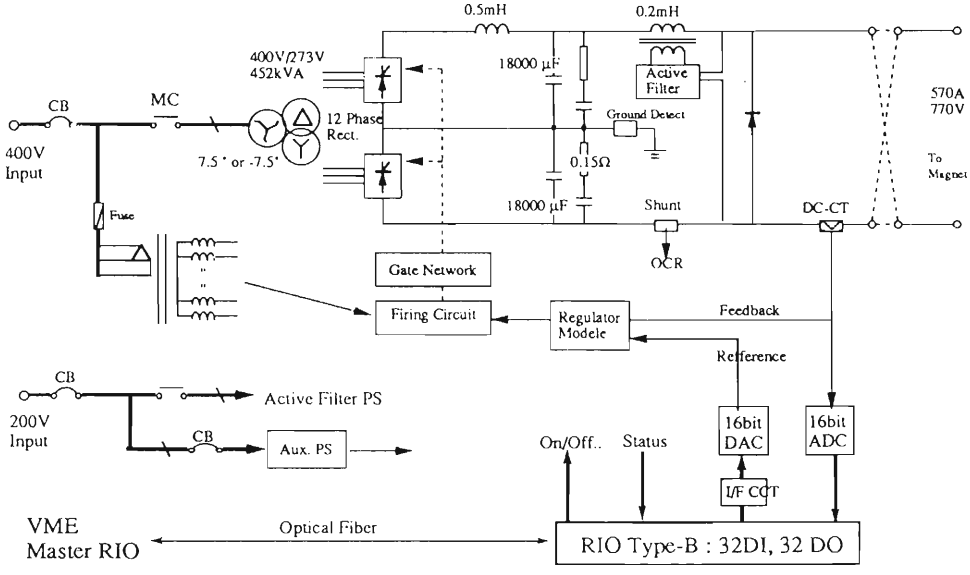

Fig. 1. Block diagram of the Q PS.

Input voltage of the Sx-PS is 400 V. A six phase thyrister diode system is stacked with a 30 kHz switching regulator system. Input voltage of the St-PS is 200 V and a 100 kHz switching regulator system is used. Thirty-six sets of St-PSs are mounted in one cubicle. An RIO star branch is connected to 36 RIO cards of type-A.[2] One RIO-A card controls the DC bus in the cubicle.

B-, Q-, and Sx-PSs are controlled by the RIO type-B. The current control data are given by a 16 bits parallel I/O[3]. QA and St-PSs are controlled by the RIO type-A and the current control signal is given by an analog voltage of the RIO-A. The shunt voltage of the St and QA PS is directly connected to the RIO's ADC inputs buffer amplifier.

References

1) SPring-8 Project, I, 2-68 (1991).
2) H.Takebe et al.: This Report, p. 176.
3) H.Takebe et al. : *RIKEN Accel. Prog. Rep.* **25**, 209, (1991).

V-2-10. High Power Test Results of a Prototype Single-cell Cavity for the SPring-8 Storage Ring

K.Inoue, H.Ego, Y.Ohashi, Y.Kawashima, H.Suzuki,* H.Yonehara,*
I.Takeshita, and M.Hara

Two single-cell prototype cavities for the SPring-8 storage ring were fabricated with different methods, which were a diffusion bonding (type A) and an electron beam welding (type B) [1]. Both cavities were made of oxygen free high conductivity copper(OFHC) class 1. These two cavities have been tested independently.

In the first step, vacuum pressure test was done. Only a turbo molecular pump of which pumping speed is 200 l/sec was operated during baking at 150 °C for 24 hours. After then, a sputter ion pump with the pumping speed of 140 l/sec was operated. Obtained minimum vacuum pressure was $7.5¥10^{-8}$ Pa through such a procedure. As to vacuum pressure of both single-cell cavities, their values were almost the same. No difference depending upon the fabrication methods was observed, but the pressure was only dependent on the outgases from the surface of materials.

In the second step, RF high power loading test of these two prototype cavities has been done at 1-MW klystron test stand [2]. After the RF equipments, an input coupler, an adjustable tuner, two fixed tuners, a pick-up probe and a turbo molecular pump of which pumping speed is 300 l/sec, were fully assembled, a CW RF power within a few kirowatts has been fed to the cavity for several hours in order to condition the inner surface of the cavity. As an RF input coupler, a cylindrical ceramic RF window which was developed for KEK TRISTAN MR, used for the same frequency 508.58 MHz as SPring-8 storage ring RF system, was adopted [3]. At the beginning of the conditioning procedure, the vacuum pressure of the cavity often got higher. The operation was stopped until the vacuum pressure was recovered below the threshold level which was set at an interlock system. The recovering time of the vacuum pressure got shorter and shorter as conditioning proceeded. After enough conditioning, RF input power has gradually been increased to 100 kW in about 24 hours. In order to cool down the cavity in a high power test, pure water of which flow rate is 150 l/min was supplied to the cooling water channels of the cavity. Two single-cell cavities showed different temperature rises. The conditions were as follows; RF input power was fixed at 50 kW and input water temperature was 33 °C. The temperatures of these two cavities were measured by thermocouples at the same places and obtained 45 °C for the type B and 41 °C for the type A. Water channels of type A are located nearer the inner surface of the cavity than those of the type B. The place of the highest temperature was at the port of pick-up probe because no water channels were there.

A different input coupler whose ceramic window was of a disk type has been developed [4]. The coupler was designed to have a power limit of 100 kW for the single-cell cavity. But, in a high power test, temperature rise at the ceramic window was steeper than expected. The input coupler with disk type windows is under the development.

References

1) K.Inoue, T.Nakamura, Y.Kawashima and M.Hara, IEEE Par. Acc. Conf.,San Francisco, (1991) 667.
2) K.Inoue, Y.Kawashima, T.Nakamura, and M.Hara: RIKEN Accel. Prog. Rep. 24 166 (1990).
3) M.Akemoto and Y.Yamazaki, Proc. of the 7th Symp. Accel. Scien. and Tech., Osaka Japan (1989) 106.
4) K.Inoue, T.Kusaka, H.Suzuki, T.Kojo, H.Ego, Y.Ohashi, Y.Kawashima, and M.Hara: RIKEN Accel. Prog. Rep. 25 212 (1991).

*JAERI SPring-8 design team.

V-2-11. Higher Order Modes of Single Cell Cavities for the SPring-8

H. Ego, M. Hara, K. Inoue, Y. Kawashima, Y. Ohashi,
H. Suzuki,* I. Takeshita, and H. Yonehara*

For a storage ring of the SPring-8, it is most important to accumulate an intensive electron beam having a low emittance in order to obtain a high brilliance photon beam. The beam quality is strongly dependent on beam instabilities. As frequencies of a parasitic higher order mode (HOM) of RF cavities are multiples of a revolution frequency, the coupled-bunch instabilities grow up and induce beam blow-up[1]. A bell-shaped single cell cavity is favorable for a storage ring since transverse and longitudinal HOM impedances of the cavity are smaller than those of a normal re-entrant cavity[2]. Then HOMs must be studied in detail to obtain the stable and low emittance beam. On account of limited space, this report describes the TM110 mode which has a large transverse impedance.

The bead perturbation measurements[3] have been executed to specify HOMs in the cavity. Various types of beads were used. Then directions and distribution of the electric and magnetic fields of HOMs were determined.

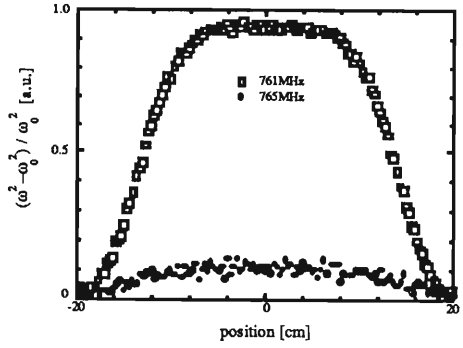

Fig.1. Frequency shifts by perturbation of a metallic plane directed vertically.

The TM110 mode frequency was calculated with computer codes [2]. In a real cavity, however, the degenerating TM110 mode splits into two modes . Figure 1 shows frequency shifts by perturbation of a metallic rectangular planes directed vertically and on a beam axis. This indicates that the direction of the magnetic field of the 761MHz mode across the axis is horizontal and that of the 765MHz mode is vertical.

To suppress instabilites[4], it is effective to move the HOM's frequencies without changing the accelerating mode (TM010) frequency. Figure 2 shows frequency shifts of the TM110 mode as a function of tuner position. The frequency of the 765MHz mode becomes larger as a horizontal tuner is put into the cavity, but that of the 761MHz modes does smaller. On the other hand, the vertical change of the tuner position causes a large shift for the 761MHz mode and a small shift for the 761MHz mode .

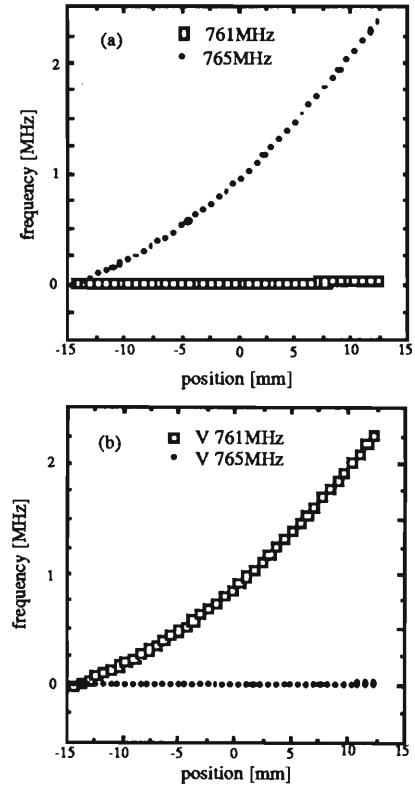

Fig.2. A frequency shift by (a) a horizontal tuner and (b) a vertical tuner

An about 1MHz shift in TM110 mode could be made by small modification of the cavity size. In this case, however, the frequency of the accelerating mode of these cavities is adjusted to 508.88MHz by tuners.

With frequency tuners and a small change of the cavity size, HOM's frequencies, at least TM110 mode frequencies, can be adjusted not to meet conditions of the coupled-bunch instabilities.

References

1) H.Kobayakawa, Y.Yamazaki, Y.Kamiya and M.Kihara, Jap. Jour. App. Phys. **25** 864 (1986)
2) K.Inoue, T.Nakamura, Y.Kawashima and M.Hara, IEEE Par. Accel. Conf., San Francisco 667 (1991)
3) L.C.Maier,Jr. and J.C.Slater, Jour. App. Phys. **23**, 68 (1952)
4) H.Kobayakawa, M.Izawa, S.Sakanaka and S.Tokumoto, Rev.Sci.Instrum. **60** (7), (1989).

* Japan Atomic Energy Research Institute.

V-2-12. Impedance Estimation of the SPring-8 Storage Ring

T. Nakamura

The broad band longitudinal impedance of the vacuum chamber of the SPring-8 storage ring was estimated assuming cylindrical symmetry. Analytical equations and results of the simulation with MAFIA T2 are used, some of the analytical equations are derived to approximate the results of simulations[1-3] (pair of shallow transitions) and the others are derived theoretically[4,5](cavity, gap, slot, resistive wall, synchrotron radiation). In the simulation with MAFIA T2[6], several model shapes of wake functions[2,3](inductive, resistive, cavitylike) are assumed to fit the results. The result is shown in Table 1.

Table 1 - Impedances of the components of the vacuum chamber of the SPring-8 storage ring.

	single $\frac{Z_{//}}{n}$ [Ω]		Number	total $\frac{Z_{//}}{n}$ [Ω]	
	Equations	MAFIA T2		Equations	MAFIA T2
RF cavities	$4.8\times10^{3}\,\frac{1+i}{n\sqrt{n}}$	$4.0\times10^{3}\,\frac{1+i}{n\sqrt{n}}$	32	$1.5\times10^{5}\,\frac{1+i}{n\sqrt{n}}$	$1.3\times10^{5}\,\frac{1+i}{n\sqrt{n}}$
weldments	-2.6×10^{-6} i	-3.1×10^{-6} i	2000	-0.005 i	-0.006 i
flanges	-	-7.8×10^{-6} i	700	-0.005 i	-0.005 i
offsets	-4.9×10^{-6} i	-7.2×10^{-6} i	2700	-0.013 i	-0.019 i
BPMs	-	$\frac{1.2}{n}$	300	-	$\frac{360}{n}$
ID sections	-4.6×10^{-4} i	-3×10^{-4} i	40	-0.018 i	-0.012 i
pumping slots	$-\frac{0.012}{n}$ i	-	6000	$-\frac{72}{n}$ i	-
transitions at RF	-0.0013 i	-0.0016 i	4	-0.005 i	-0.006 i
absorbers at RF	-6×10^{-4} i	-7×10^{-4} i	12	-0.007 i	-0.008 i
bellows	-	-1×10^{-4} i	400	-	-0.040 i
valves	$-(2.7\times10^{-5}+0.002/n)\,i+\frac{0.2}{n}$	-	100	$-(0.003+0.2/n)\,i+\frac{20}{n}$	-
steps in ante-chambers	$-\frac{0.3}{n}$ i	-	600	$-\frac{180}{n}$ i	-
resistive wall	-	-	-	$1.9\,\frac{(1-i)}{\sqrt{n}}$	-
synchrotron radiation	-	-	-	0.026	-

The total impedance is expressed as

$$\frac{Z_{//}}{n} = 1.9\,\frac{(1-i)}{\sqrt{n}} + 1.5\times10^{5}\,\frac{(1+i)}{n\sqrt{n}} + \frac{(3.8-2.5i)}{n}\times10^{2} + 0.03 - 0.11\,i \quad .$$

Here n is ω/ω_{rev}, ω_{rev} is the revolution frequency, and i is $\sqrt{-1}$. The frequency ω where the instabilities will occur is expected to be higher than c/σ, where σ is the r.m.s. bunch length and c is the speed of light. Hence n is greater than 23000. The absolute value of total impedance $|Z_{//}/n|$ is ~0.13Ω.

References

1) K. L. F. Bane, SLAC-PUB-5177 (1990).
2) M. Takao, T. Higo and K. L. F. Bane, Proc. of the 1991 IEEE Particle Accelerator Conference, San Francisco, 1991, p. 506.
3) S. Heifets, SLAC/AP-93 (1992).
4) R. L. Gluckstern, Phys. Rev. D 39, p. 2773(1989).
5) S . Heifets, SLAC-PUB-5792 (1992).
6) R. Klatt and T. Weiland, Proc. of Linear Acc elerator Confference, SLAC, 1986, p. 282.

V-2-13. Design of Aluminum Alloy Conflat Flange for SPring-8 Storage Ring

Y.Yanagi, K.Shibuya, M.Tsuchiya, S.Yokouchi,
H.A.Sakaue, K.Watanabe and S.H.Be

Conflat type flanges are used as vacuum chamber joints of the Spring-8 storage ring. The flange materials are shown in Table 1. The aluminum alloy A2219-T852 is suitable for the flanges because of the high hardness and the good welding compatibility with the chamber material A6063-T5.

In view of the flange-flange interface, the SPring-8 conflat flanges are classified into the following groups: Al/Al(aluminum to aluminium conflat flange) ,Al/SUS and SUS/SUS.

An Al(Al050H24) gasket is mounted in Al/Al flanges. A Cu(OFHC) gasket is mounted in SUS/SUS flanges. As for the gasket in Al/SUS flanges, an Al gasket is chosen because of easy deformation with the assembling torque. The surfaces of bolts, nuts and washers are coated with alumite, solid film lubricant and hard alumite respectively to reduce the bolt/nut friction.

Table 1 . Flange materials.

	Al flange	SUS flange
material	A2219-T852	SUS 304L
sarface finish	Rmax 1.6	manufacturer's standard
hardness	>120HV * >400HV * *	manufacturer's standard

* Hardness without TiC coating
* * Hardness with TiC (> 1 μm) coating

gascket, bolt and washer

	Al/Al	Al/SUS	SUS/SUS
gasket	A1050H24	A1050H24	Cu(OFHC)
bolt	A2024-T4	A2024-T4	SUS304
nut	A6061-T6	A6061-T6	SUS304
washer	A2017-T4	A2017-T4	SUS304

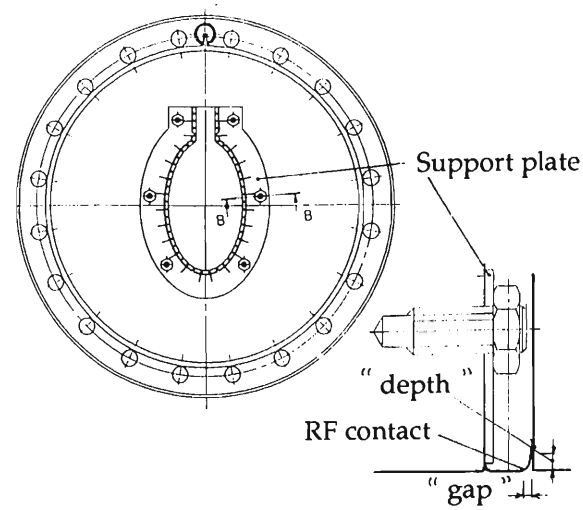

Fig.1. RF contacts assembling method.

Table 2 . RF contacts specification.

material	Be-Cu (JISC1720 P-1/4HT)
design target	° contact fouce >50 g ° surface stress <85kg/mm2

To minimize the RF impedance caused by abrupt changes in the cross section of the vacuum chamber, we use RF contact fingers to bridge the 3.5 mm gap of the gasket groove.

The cross section view of the flanges with RF contacts is shown in Fig.1 and the requirement to the RF contacts is summarized in Table 2.

In the design of RF contacts the following attention has been payed:The gap and depth of RF contacts are to be kept as small as possible, while to ensure mechanical performance the following criteria must be satisfied:

(1) The surface stress of RF contacts should be lower than the spring limit stress(85kg/mm^2)

(2) The minimum contact force is more than 50 g to reduce the electrical resistance on the contact surfaces.

A test for comfirming these requirements by the measurement of the contact force and the surface resistance is planned to be made in Nov,'92

RIKEN Accel. Prog. Rep. 26 (1992)

V-2-14. Sealing Performance of AL/SUS Conflat Flanges

K. Shibuya,* H.A. Sakaue, K. Watanabe, S. Yokouchi, and S.H. Be

We experimentally investigated the reliability of leak tightness for multiple extreme operations in baking combination flanges of different metals such as AL-alloy and SUS (stainless steel). The leakage is usually caused by the relaxation of tightening force during baking. Table 1 shows the specification of materials used in this investigation.

Table 1. Main specification.

Cover frange	A 2219 - T 852
Chamber frange	SUS 304
Gasket	A 1050 - H 24
Bolt Nut Washer	A 2024 A 6061 A 2017

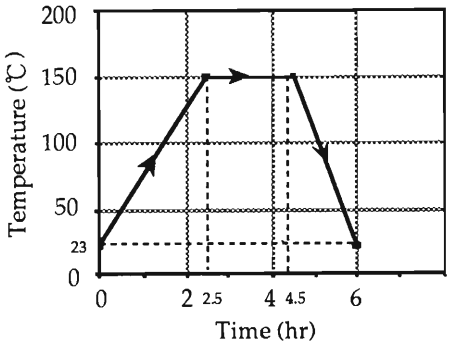

Fig.1. Baking temperature.

Table 2. Various type of flanges used for leak test.

Flange size	Baking cycles	Sets
ICF 253	20	3
ICF 203	10	2
ICF 114	6	1

Tightening of flanges with bolts are as following : Firstly, a flange is alternately tightened at intervals of 180° with bolts by torque of 50kgf-cm and then by that of 90kgf-cm. Finally,the flange is retightened in turn by the same torque of 90 kgf-cm. A repeated baking cycle of the flange is shown in Fig. 1. Here the tightening force is defined as the load per sealing length [kgf/mm].

A leak test was done before and after baking. Table 2 shows the size of flanges, their numbers used in the test, and baking cycles. In all cases no leakage was detected even with the maximum sensitivity of a leak detector. The relaxation of tightening force for the bolts during the baking is shown in Fig. 2. This figure shows that the tightening force is reduced about 30 to 40 % in the initial 10 baking cycles, but after then, the tightening force is kept to be constant. This result is for the flange size of ICF 253, but we think this tendency is also applied to other flange sizes (ICF 203,114,etc). This means that the leakage is not caused by the relaxation of tightening force. At present time, the reason for the leakage is not clear. This problem is to be pursued furthermore.

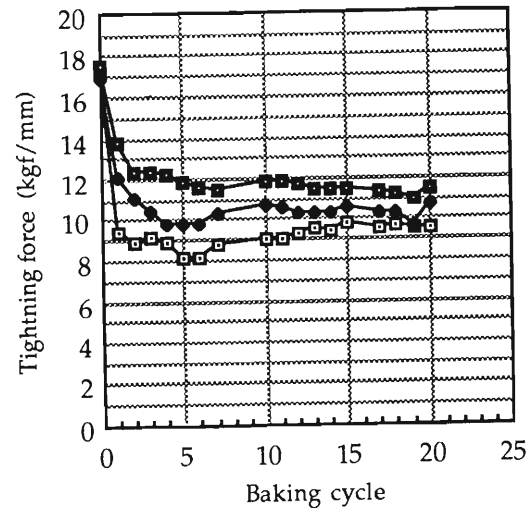

Fig.2. Relations of tightening force vs baking cycle for an ICF 253.

* SMC Ltd.

V-2-15. Photodesorption for OFHC-class1 by High Energy Photon

K. Watanabe, T. Hanasaka, Y. Hirano,* H.A. Sakaue,
K. Yano, S. Yokouchi, and S.H. Be

One of main problems to be considered in the design and manufacturing of the vacuum system for the SPring-8 storage ring is interactions of synchrotron radiation (SR) with absorbers. To investigate the interactions we measured the photodesorption yield of OFHC-class1 (oxygen free copper), the material of the absorbers, using the high energy the photon beam (the critical energy 26 keV) from the Accumulation Ring (AR) of TRISTAN at KEK.

Experimental scheme is shown in Fig.1. SR was adjusted with a collimator slit of 5mm×5mm, and perpendicularly directed onto the inner wall of test chamber. The test chamber was a cylindrical tube of 300mm×φ60mm made of OFHC-class1. The production of the test chamber is roughly as follows; machining (oil-free) → brazing → chemical cleaning (acetone, ethanol) → baking (10 hours at 450 °C). The chamber was evacuated and baked out about for 13 hours at 150 °C in advance of the SR irradiation, and thereby the final pressure, namely the background pressure for experiments was 6.8×10^{-10} Torr. The chamber was cooled with water to reduce thermal desorption during experiments. The outgassing rate due to photodesorption was obtained by through-put-method.

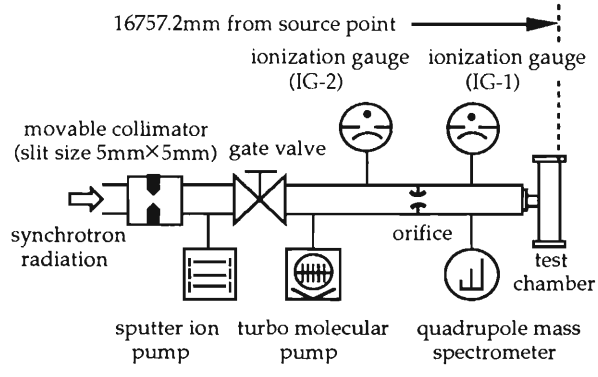

Fig. 1. Schematic drawing of the photon beam line (NE9).

Figure 2 shows the relation between the photodesorption yield (η) and photon dose (Dp). η is reduced to 1.3×10^{-4} molecules/photon (equivalent nitrogen pressure) at Dp of 1×10^{21} photons/slit. This value is higher by about one order compared to the experimental results made with the critical photon energy of 4 keV from the 2.5 GeV storage ring of Photon Factory at KEK[1]. The reason is not clear yet, and this is the problem to be discussed further. η is as following:

1) $Dp\leq10^{20}$ photons/slit
   $\eta=4\times10^{-4}$ (molecules/photon),
2) $Dp>0^{20}$ photons/slit
   $\eta=1.23\times10^{10}\cdot Dp^{-2/3}$ (molecules/photon).

As the critical photon energy at AR is approximately equal to that (=29 keV) at SPring-8, we obtain η of OFHC-class1 at SPring-8 assuming that η at SPring-8 is equal to η at AR:

$\eta=1.1\times10^{-4}\cdot Di^{-2/3}$ (molecules/photon),

where Di (A•hours) is the electron beam dose. As a result, the outgassing rate per 1 mrad is obtained as

$Q=3.4\times10^{-7}\cdot Di^{-2/3}$ (Torr•l/sec).

For example, if Di=100 A•hours, we obtain $Q=1.6\times10^{-8}$ Torr•l/sec/mrad. Further we are planning experiments of elucidation of the photodesorption mechanism.

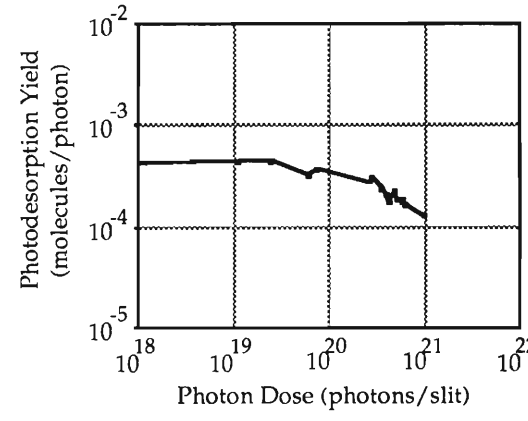

Fig.2. Photodesorption yield of OFHC-class1 (equivalent nitrogen pressure).

References

1) S.Ueda et al.: Vacuum, 41, No.7-9, 1928 (1990).

* ANELVA Co.

V-2-16. Electrical Parameters for the Operation of a Titanium Sublimation Pump

S.Yokouchi, H.A.Sakaue, K.Watanabe, and S.H.Be

We investigated electrical parameters for the operation of a titanium sublimation pump (TSP), which is considered as a vacuum pump of the SPring-8 storage ring, during the performance experiment of a TSP.[1] A sublimator of the TSP consists of three filaments, each of which is 85%Ti-15%Mo alloy wire, 2 mm in diameter, and 200 mm in length. The filament is heated by applying electric current directly to it from a power supply. The experiment was continued untill the filament cut.

Figure 1 shows the measuring system for the electrical parameters of the TSP. The power supply has a dropping characteristics so as to supply a stable power independent of the change of filament resistance (R_{fil}). The V_{fil}'s and I_{lin}'s were measured with respect to various primary voltages (V_{pri}'s) during the experiment. From the V_{fil} and I_{lin}, we also got the R_{fil} of the filament and the power (P_{fil}) to sublimate titanium.

Figure 2 shows variations of the R_{fil} and P_{fil} during the experiment. The R_{fil} increases with the running time since the filament becomes thinner owing to sublimation of titanium. Although the R_{fil} must depend on the V_{pri} because of the dependence of the filament temperature on the P_{fil}, we cannot find the tendency in this figure.Initial P_{fil} at V_{pri} = 200 V is a little smaller than 270 W, which is recommended as the power for normal operation by the manufacturer. The P_{fil} gradually decreases with the running time, and finally becomes to 80% of the initial value. This suggests that we should use such a power supply as can supply a power more stably than the present one in the real ring. From the result, one filament can be opreated for about 90 hours, but we have not investigated how long the filament, whose diameter gradually becomes thinner, can give a sufficient pumping speed. This is a problem to be investigated from now.

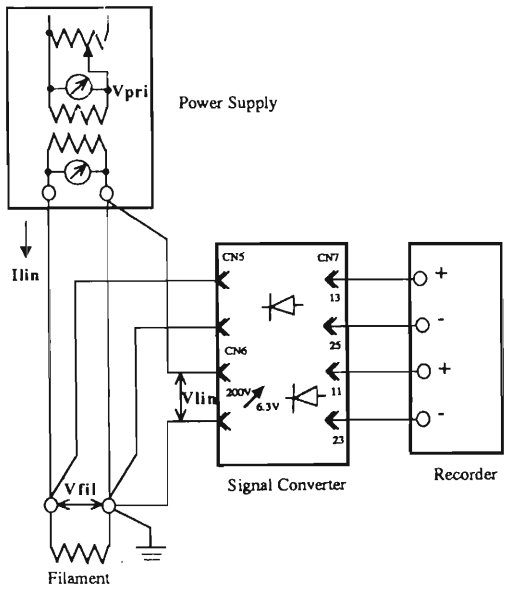

Fig. 1. Schematic diagram of the measuring system for the electrical parameters of the TSP. V_{fil} is the voltage applied to the filament, V_{lin} the voltage drop in the current feed line, and I_{lin} the electric current flowing through the filament. The I_{lin} can be got from the V_{lin} by using the relation between I_{lin} and V_{lin} measured previously. The V_{fil} and V_{lin} are converted to DC voltage with the signal converter.

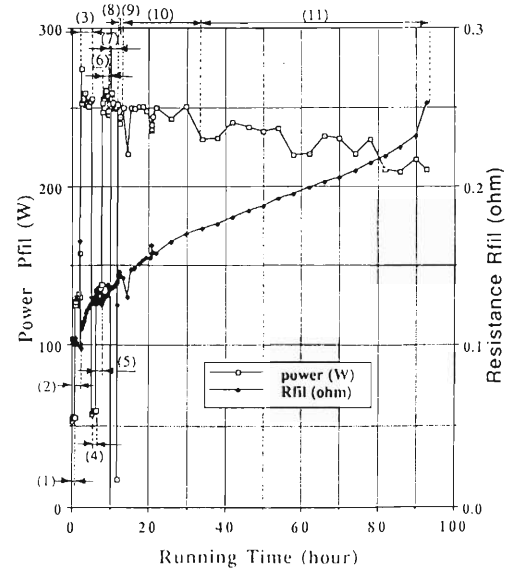

Fig. 2. R_{fil} and P_{fil} vs running time of the TSP during the experiment. Operating conditions in each stage (1)-(11) are as follows. (1),(4) : V_{pri} = 100 V,continuously. (2),(5) : V_{pri} = 150 V,continuously. (3),(6),(7),(10),(11) : V_{pri} = 200 V,continuously. (8),(9) : V_{pri} = 200 V for 30 sec, 0 V for 60 sec,alternatively.

References

1) H.A.Sakaue et al.: This report, p.165.

V-2-17. The Outgassing Characteristics of Titanium Sublimation Pump

H. A. Sakaue, S. Yokouchi, K. Watanabe, and S. H. Be

In the experimental beam line absorber system of the SPring-8 storage ring, titanium sublimation pumps (TSP) will be installed. A TSP has a problem of outgassing at the sublimation of titanium. In case of using a TSP at the ultla high vacuum, it is important to degass by the initial passage of an electric current. Therefore we measured the outgassing rates and observed the behavior of various molecules which were released from a titanium filament when the filament was heated.

Figure 1 shows the experimental setup for measuring the outgassing characteristics of a TSP. The titanium filament is installed in chamber 1. A BA gauge (BAG1) and a quadrupole mass spectrometer in chamber 2, a BA gauge (BAG2) and a turbo-molecular pump (TMP) in chamber 3 are installed. The outgassing rate Q of a TSP was obtained from $Q=C(P_1-P_2)$, where P_1 is the pressure of the chamber 2, P_2 that of the chamber 3, and C the conductance (2.3 l/s for N_2) of the orifice whose diameter is 5mm.

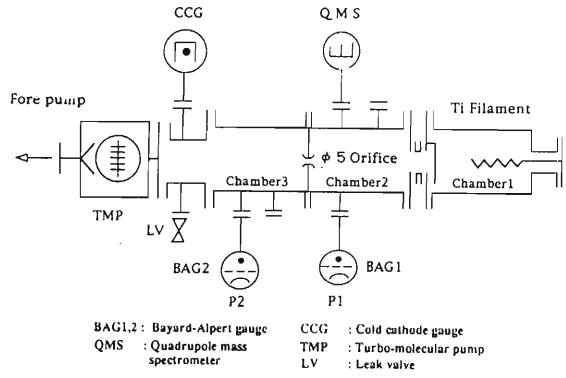

Fig. 1. Experimental setup for measuring the performance characteristics of TSP.

The outgassing rates and mass spectrum were measured with respect to various primary voltages of a TSP power supply (V_{pri}=100V, 150V, and 200V). This experimental methods are explained in detail elsewhere.[1] Measured outgassing rates of a TSP are shown in Fig.2. The Q increased from 1×10^{-4} to 4×10^{-4} Torr·l/s at the first heating (V_{pri}=100V). However, after several heatings, the outgassing rate scarcely increased at the same voltage, because of degassing of filament by several passages of an electric current.

Figures 3 and 4 show the behavior of various molecules (M/e=2,16,18,28,44) from the filament at each flashing. The quantities of H_2O (M/e=18), CO (M/e=28) and CO_2 (M/e=44) were suddenly increased at the initial heating and, after repeated heating, these quantities almost became constant due to the heating of filament. This phenomenon was caused by degassing of filament due to several passages of an electric current. On the other hand, the quantities of H_2 (M/e=2) and CH_4 (M/e=16) were always increased at each heating of filament, because hydrogen was released from both surface and

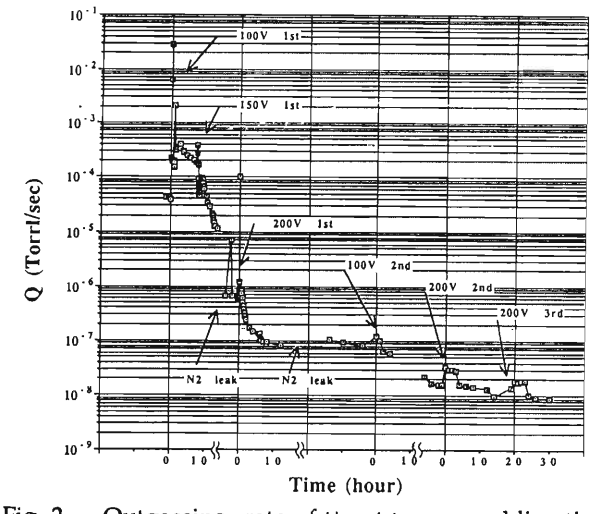

Fig. 2. Outgassing rate of the titanium sublimation pump.

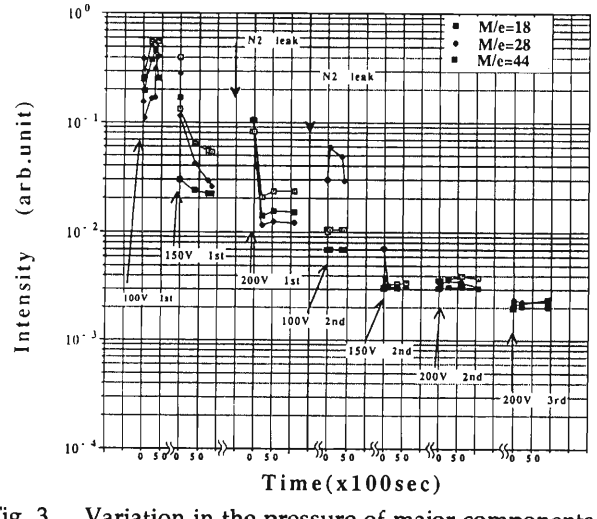

Fig. 3. Variation in the pressure of major components (M/e=18,28,and 44.) of the outgassing flux as a function of heating time of titanium filament.

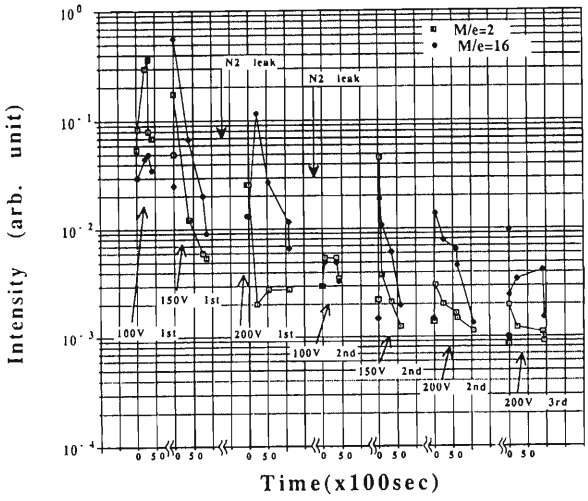

Fig. 4 Variation in the pressure of major components (M/e=2 and 16)of the outgassing flux as a function of heating time of titanium filament.

inside of titanium filament by heating. The quantity of CH_4 especially depended on the V_{pri}. The quantity of CH_4 at V_{pri} =100V increased little in comparison with other voltages. This phenomenon is caused by a small quantity of sublimation of titanium, because methane is produced with hydrogen and carbon released from the titanium filament during flushing of the titanium.[2] However it is necessary to ascertain the above phenomenon by the measurement of the filament heating temperature and pumping speed.

The outgassing of H_2 and CH_4 from titanium filament cannot be negligible at each titanium sublimation. However the other outgassing may be sufficiently decreased by a good condition of initial degassing of filament.

References

1) S.Yokouchi et al.:This Report,p.164.
2) A.Roth:"Vacuum technology",North-holland publishing company,Amsterdam p.268(1982).

V-2-18. Reproducibility of Outgassing Rate at UHV Chamber

T. Hanasaka, K. Watanabe, S. Yokouchi, and S. H. Be

We measured the reproducibility of outgassing rate at a UHV(Ultra High Vacuum) chamber by means of a so-called throughput method.

The apparatus is to measure outgassing rate of UHV materials in a sample chamber. But only the reproducibility of outgassing rate at an empty chamber (the background) was described in this paper. When we measure the outgassing rate of some sample pieces, we must subtract the background from the values measured with samples. The measurement of background level and its reproducibility are, therefore, very important for the accurate measurement of outgassing rate.

Figure 1 shows the schematic diagram of the apparatus. The system is mainly made of SUS304 stainless steel. The surface area of the sample chamber is 0.196 m^2. The conductance of orifice between the sample chamber and pump side chamber is 2.15×10^{-3} m^3/s (for N_2, at 22 °C). The pumping speed of the main pump is 360l/s for N_2. The ultimate pressure at pump side chamber is of the order of 10^{-8} Pa.

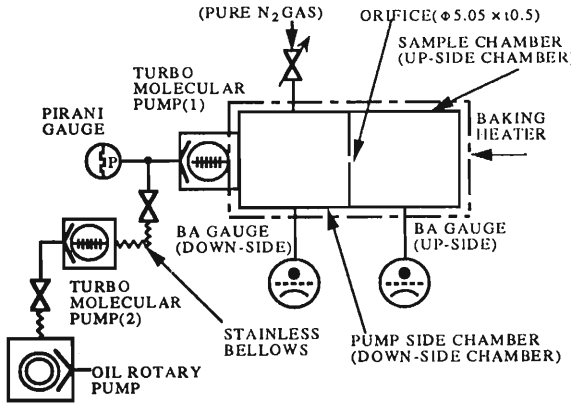

Fig. 1. Schematic diagram of experimental apparatus.

The main procedures of the measurement were as follows.

(1) The apparatus was vented by N_2 gas.
(2) The sample inlet flange was opened for 10 min or 37 min (but no sample was installed).
(3) The apparatus was evacuated at room temperature for obtaining background data.
(4) The baking was carried out and background data after baking were taken.
(5) The pressures of the sample and pump side chamber (P_1 and P_2) and the evacuation time were measured, then the outgassing rate from the sample chamber at each time was calculated by

$$Q=C(P_1-P_2)/S.$$

Where, Q: outgassing rate,
C: conductance between sample and pump side chamber,
P_1:pressure of sample chamber,
P_2:pressure of pump side chamber,
S: surface area of sample chamber.

The pressure measurement was carried out by using calibrated BA gauges.

Figure 2 shows the influence of venting gas on the outgassing rate. As shown, the difference between wet air and 99.9998 % N_2 in the reproducibility is small in our case.

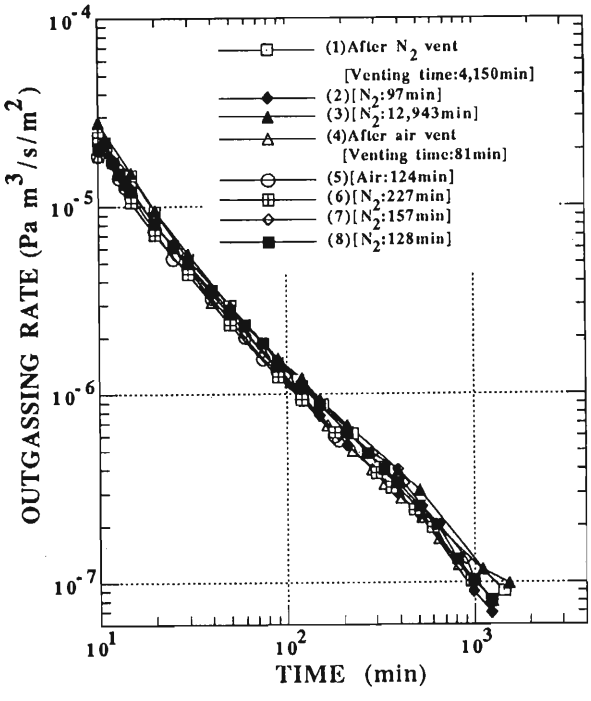

Fig. 2. Influence of venting gas and venting time on the outgassing rate.

Figure 2 also shows the influence of venting time (time from the start of vent to the start of next evacuation) on the outgassing rate.

Figure 3 shows the effect of exposure time (time from the opening of sample inlet flange to its closing) on the outgassing rate.

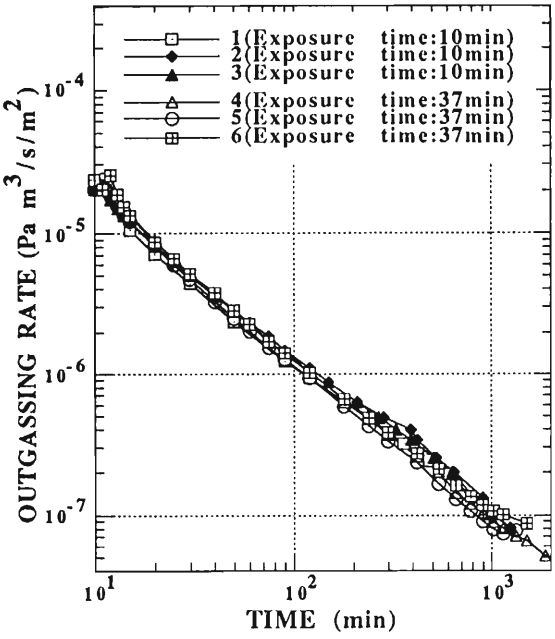

Fig. 3. Influence of exposure time.

As shown in Fig. 4, we obtained overall reproducibility of about ±35 %(± 25% by the exception of N18) in the background level, at the evacuation time of around 1,000 min, during seven months. The symbols N8, N9 etc. in Fig. 4 show the order of experiment after nitrogen venting.

Similar curves taken after baking (not shown in this paper) also show reproducibility of about ±25%. From above, we can obtain following conclusions.

(1) Venting by 99.9998 % N_2 gas is sufficient to obtain the reproducibility. Wet air might be used in some limited cases.

(2) Venting time is not so critical in case of pure N_2 gas venting.

(3) Exposure time is also not so critical .

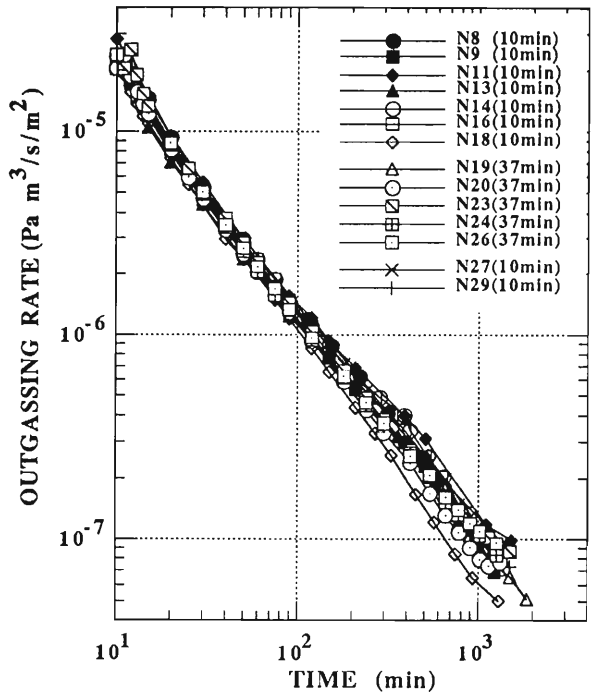

Fig. 4. Reproducibility in background level at room temperature during seven months.

(4) Our standard evacuation procedure, including some fluctuation because of the manual operation, is sufficient to obtain the reproducibility.

(5) We did no degas operation for BA gauges. Because outgassing from BA gauges is to be cancelled out by the subtraction of the background at the actual outgassing measurement (in case of the sample piece method). This simple procedure seems to be adequate for obtaining the reproducibility.

Temperature of the sample chamber is also a very important factor for the reproducibility of background. In our experience, outgassing rate changes around 5per-cent by the change in the chamber temperature of 1 °C.

Individual control of the chamber temperature is not possible now but, if it is possible, control of the chamber temperature within ±1 °C is desirable for the better reproducibility of background.

V-2-19. Outgassing Rate Measurement of Alumina Sample

T. Hanasaka, K. Watanabe, S. Yokouchi, Y. Niioka, and S. H. Be

We measured the outgassing rate of an alumina(Al_2O_3) sample by means of a so-called throughput method.

The measurement apparatus is shown schematically in Fig. 1. The details will be described elsewhere.[1] The surface area of a sample chamber is 0.196 m^2. The conductance of the orifice between the sample chamber and pump side chamber was 2.15×10^{-3} m^3/s (for N_2, at 22 °C). The background level and the reproducibility of the outgassing rate will be described in Ref. 1).

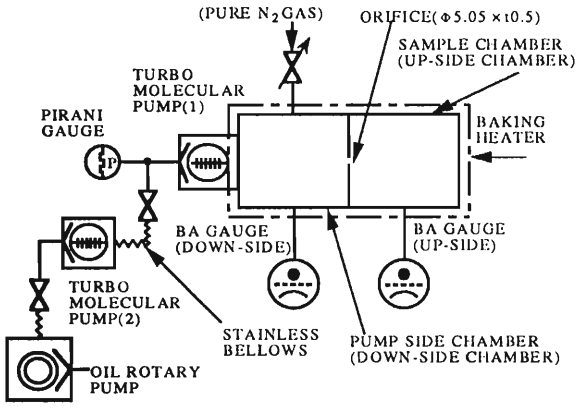

Fig. 1. Measurement apparatus.

The sample is made of 99 % alumina (type A-479, KYOCERA INDUSTRIAL CERAMICS CORPORATION). Figure 2 shows the sample block, and its surface area is 0.588 m^2. 68 pieces of stainless steel M2 nut were used as the spacers to separate each alumina plate. The surface area of nuts is less than 1 % of that of the alumina plates. Several characteristics of the sample are shown in Table 1.

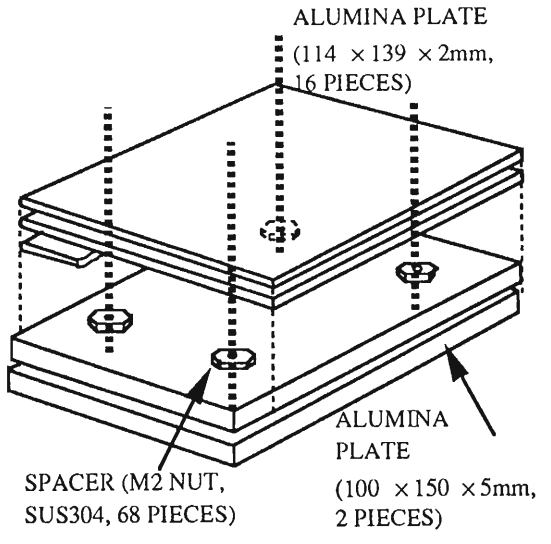

Fig. 2. Laminated alumina sample.

Table 1. Several characteristics of the alumina sample.

Material	Alumina (dense type, A-479, KYOCERA)
Plate size and number of plate	1)114×139×2 (mm) 16 pieces 2)100×150×5 2 pieces
Surface area	5,883 (cm^2)
Surface treatment of material at KYOCERA	Ultrasonic cleaning and drying (after sintering)
Density	3.8 (g/cm^3)
Alumina contents	99 %

The cleaning procedures of the sample at RIKEN were as follows.

[1] Alumina plates.
(1) Supersonic cleaning in pure hot water. (10 sec, at 60~70 °C.)
(2) Drying in a dry furnace. (several hours, at 80 °C.)

[2] M2 nuts.
(1) Degrease in 1.1.1 trichloroethane vapor. (10 min, at 78 °C.)
(2) Rinse in 10 % hydrochloric acid. (2~3 sec, at room temperature.)
(3) Rinse in running water. (4 times, in 4 stage flow bath.)
(4) Rinse in pure water. (10~20 sec, at room temperature.)
(5) Rinse in pure hot water. (10~20 sec, at 60~70 °C.)
(6) Drying in a dry furnace. (several hours at 80 °C.)

Note: Conductivity of pure water used was below 0.2 μS/cm.

The cleaned alumina plates and nuts were installed in a clean glass beaker with a glass lid and kept in a desiccator till the measurement started.

The main procedures of the measurement were as follows.

(1) The apparatus was vented by N_2 gas.

(2) The flange for sample change was opened for 37 min (without sample installation).

(3) The apparatus was evacuated without the sample at room temperature for obtaining background data.

(4) The baking was carried out without the sample, and background data after baking were taken.

(5) The total outgassing rate from the sample chamber at each time was calculated by the following formula.

$$Q=C(P_1-P_2),$$

Q: outgassing rate,

C: conductance between sample and pump side chamber,

P_1: pressure of sample chamber,

P_2: pressure of pump side chamber.

(6) The same procedures as in (1) and (2), but the sample was installed at step (2).

(7) The same procedures as in (3), (4) and (5) with the sample.

(8) The same procedures as in (1)~(5), but the sample was taken out at step (2).

(9) Average value of two background measurements was subtracted from the measured value with the sample.

(10) The outgassing rate per unit area of the sample was calculated.

After one cycle, the sample was back to the desiccator , and, after a few days, the next cycle has started again with the same sample.

The outgassing rate vs. pumping time curves for two cycles are shown in Fig. 3. The origins of pumping time are (1) the starting point of evacuation for the "room temperature evacuation" and (2) the starting point of cool down for the "after baking". Obtained values are of the same order as the outgassing rates for clean stainless steel or clean aluminum alloy.

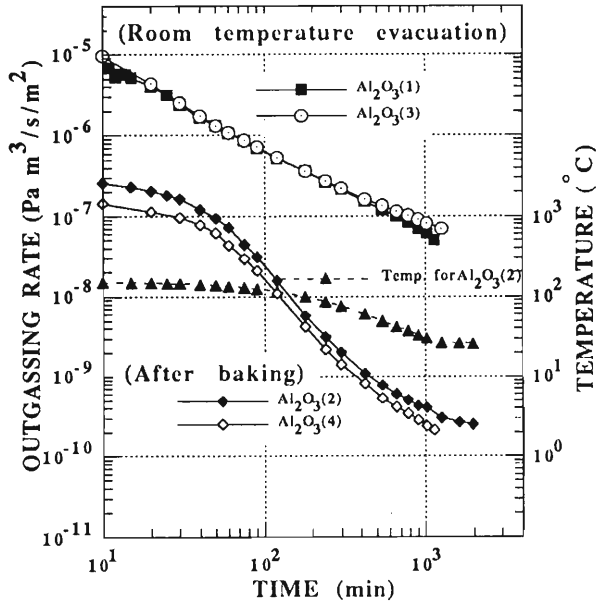

Fig. 3. Outgassing rate of alumina sample.

References

1) T. Hanasaka *et al.*: This Report, p.167.

V-2-20. Outgassing Rate Measurement of BeCu Sample

T. Hanasaka, K. Watanabe, S. Yokouchi, Y. Niioka, and S. H. Be

Outgassing rate of a BeCu sample is measured by means of a so-called throughput method.

The measurement apparatus is shown schematically in Fig. 1. The details will be described elsewhere.[1] The surface area of a sample chamber is 0.196 m^2. The conductance of the orifice between the sample chamber and pump side chamber was 2.15×10^{-3} m^3/s (for N_2, at 22°C). The background level and the reproducibility of the outgassing rate is described in Ref. 1).

The sample plate is a JIS C1720P-1/4H (BeCu25-1/4H) copper-beryllium alloy (made by NGK INSULATORS LTD). Figure 2 shows the shape of the sample, and its surface area is 2.02 m^2. Several characteristics of the sample are shown in Table 1.

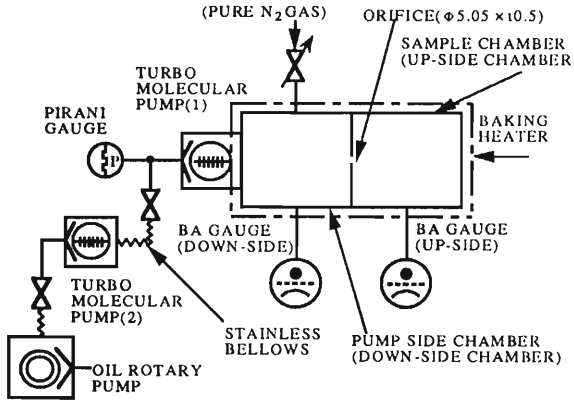

Fig. 1. Measurement apparatus.

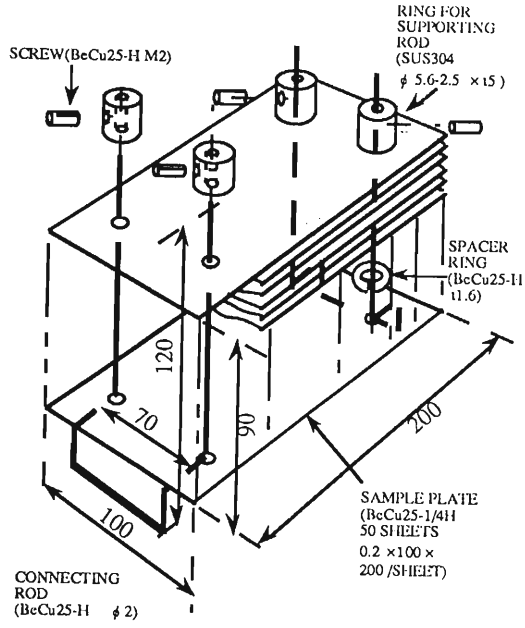

Fig. 2. BeCu sample.

Table 1. Several characteristics of the sample.

Material	(1)BeCu25-1/4H plate (JIS C1720P-1/4H) (2)BeCu25-H rod (JIS C1720B-H)
Plate size	0.2×200×100(mm)
Number of plate	50 sheets
Surface area	(1)Plate: 20,043cm^2 (2)Rod : 187cm^2 Total : 20,230cm^2
Surface treatment of material at NGK	(1) Plate: Degreasein1.1.1.trichloro-ethane and benzotriazole treatment for rust preventing (2) Rod: Benzotriazole treatment for rust preventing (after centerless grinding)
Chemical component of sample plate	Be : 1.85(%) Co+Ni : 0.27 Co+Ni+Fe : 0.30 Cu+Be+Co+Ni+Fe : 99.95

The cleaning procedures of the sample at RIKEN were as follows:

(1) Degrease in 1.1.1 trichloroethane vapor. (10 min, at 78 °C.)
(2) Rinse in 10 % hydrochloric acid. (2~3 sec, at room temperature.)
(3) Rinse in running water. (4 times, in 4 stage flow bath.)
(4) Neutralization in 5 % sodium cyanide. (2~3 sec, at room temperature.)
(5) Rinse in running water. (4 times, in 4 stage flow bath.)
(6) Rinse in pure water. (10~20 sec, at room temperature.)
(7) Rinse in pure hot water. (10~20 sec, at 60~70 °C.)
(8) Rinse in acetone [special grade]. (1 min, at room temperature.)

(9) Drying in a dry furnace. (several hours, at 80 °C.)

Note: Conductivity of pure water used was below 0.2 μS/cm.

The cleaned sample was installed in a clean glass beaker with a glass lid and kept in a desiccator till the measurement started.

The main procedures of the measurement were as follows:

(1) The apparatus was vented by N_2 gas.

(2) The flange for sample change was opened for 10 min (without sample installation).

(3) The apparatus was evacuated without sample at room temperature for obtaining background data.

(4) The baking was carried out without sample, and background data after baking were taken.

(5) The total outgassing rate from the sample chamber at each time was caluculated by the following formula.

$$Q=C(P_1-P_2),$$

Q: outgassing rate,

C: conductance between sample and pump side chamber,

P_1: pressure of sample chamber,

P_2: pressure of pump side chamber

(6) The same procedures as in (1) and (2), but the sample was installed at step (2).

(7) The same procedures as in (3), (4) and (5) with the sample.

(8) The same procedures as in (1)~(5),but the sample was taken out at step (2).

(9) Average value of two background measurements was subtracted from the measured value with the sample.

(10) The outgassing rate per unit area of the sample was calculated.

After one cycle, the sample was back to the desiccator , and, after a few days, the next cycle again started with the same sample.

The outgassing rate vs. pumping time for several cycles are shown in Fig. 3. The origins of pumping time are (1) the starting point of evacuation for the "room temperature evacuation" and (2) the starting point of cool down for the "after baking".

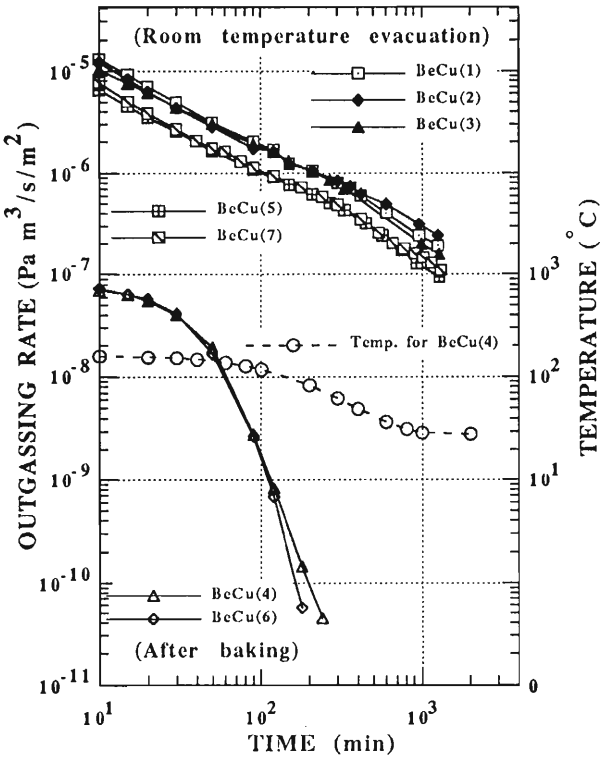

Fig. 3 Outgassing rate of BeCu sample.

Obtained values are of the same order as the outgassing rates for a clean stainless steel or a clean aluminum alloy for the "room temperature evacuation", and those for the "after baking" are extremely low. The reason for the extremely low value may be due to the high diffusion constant of a copper-rich alloy.

References

1) T. Hanasaka *et al.*: This Report, p.167.

V-2-21. Support for a Normal Cell Vacuum System

C.Y. Xu, K. Watanabe, H.A. Sakaue, M. Tsuchiya, and S.H. Be

The vacuum channel of a normal cell 30 m in length consists of two bending magnet chambers (BMC), three straight section ones (SSC) with an absorber, an insertion device dummy one (ID-C) and two crotches. Each chamber is mounted on a rigid holder and a sliding support and connected with the bellows which allow the chamber to move during installation and baking. The chamber thermal expansion caused by baking at 150°C is shown in the following table.

Table 1. Thermal expansion caused by baking at 150°C

	Length (mm)	Thermal expansion (mm) Beam direction	Horizontal
SSC1	4621	14.60	
SSC2	5460.6	17.25	
SSC3	4356	13.76	
BMC1	3191.5	10.08	0.078
BMC2	3073	9.70	0.070
ID-C	4589	14.50	
Crotch	775	2.45	
Crotch	575	1.82	

The mounts for the SSC1 of three different SSC's and BMC1 of two BMC's are described. The SSC1 is installed on the magnet girder using two mounts near the station of the beam position monitor (BPM) as shown in Fig.1 after adjusting precisely a chamber position by a pair of special adjustors. The rigid mount does not allow chamber motion at the rigid point in any direction. The other mount is composed of a leaf spring and the support with a clamping screw as shown in Fig.2. The former is to allow a slight chamber thermal expansion along the electron beam direction during the chamber baking cycle, and the latter is for supporting the chamber weight. These mounts can suppress the chamber displacement at the station of BPM's within the accuracy of 0.03 mm after each baking cycle. The deflection of the leaf spring due to thermal expansion makes the chamber downward, which interferes with the function of clamping screw. To solve this problem, we bolt the leaf spring at the rib which is welded on the chamber, so that the vertical thermal expansion of the rib compensates this downward deflection.

The BMC1 is inserted in the gap of the bending magnet. The chamber weight is supported by three stainless steel plates on the bending magnet and the chamber is set up accurately with three adjustors located at the middle and near both ends of the BMC1, respectively, as shown in Fig.3. The middle adjustor is usually locked, but other ones can allow a slight chamber thermal expansion in the beam and the horizontal directions during the chamber baking.

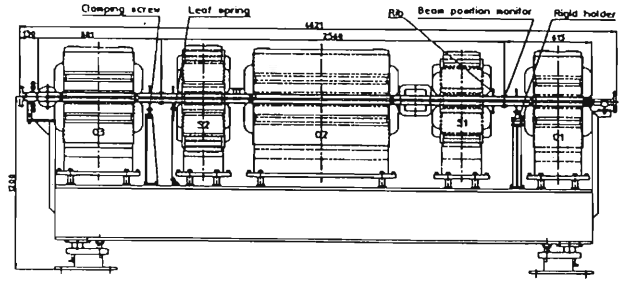

Fig.1. Schematic arrangement of the SSC1.

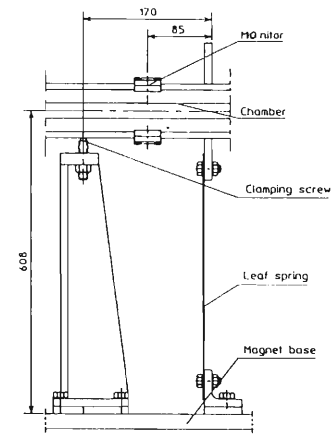

Fig.2. Assembly of the sliding support.

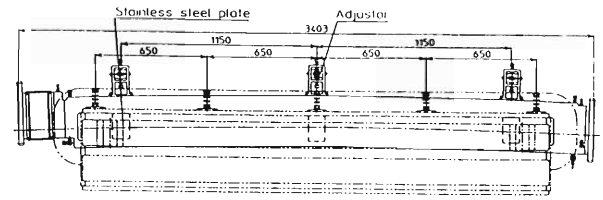

Fig.3. Schematic arrangement of the BM1.

RIKEN Accel. Prog. Rep. 26 (1992)

V-2-22. Development of the LynxOS Device Drivers

T.Masuda, T.Nakamura, H.Takebe, and T.Wada

The control sub-system of the SPring-8 storage ring is designed to have a hierarchical structure which consists of three layers such as presentation, processing and equipment ones. Recently such a structure is going to become a standard model of accelerator and large experimental physics control systems in the world as shown in Fig.1. In a processing layer, the SPring-8 project team has decided to adopt a VME (Versa Module European)bus system with microprocessors as FEPs (Front End Processors). These VMEbus systems which have a real time OS (Operating System) are linked by a computer network and distributed around the storage ring. For an R&D study, we have introduced Motorola Delta systems which contain a MVME147S 32-bit single board computer based on MC68030 and LynxOS as a real time OS on a MVME147S. The LynxOS is comparatively new and is one of the so-called "real time UNIX" operating systems. The LynxOS complies with POSIX 1003.1 (Application program Interface) and POSIX 1003.4 (Real Time Extension). POSIX (Portable Operating System Interface for Computer Environment) is a standard OS proposed by the IEEE committee.

We intend to control a klystron test stand by using this Delta system. Hence we need to operate some I/O boards on a VMEbus. There are two solutions to access and to control I/O boards. One is the way with "shared memory" and the other is with a "device driver". We have achieved an operation of I/O boards with shared memory in the first step, because the implementation is easier. But the way with a device driver is more advantageous because it can treat hardware interruption and 1 msec timer interruption, and it makes application program hardware independent. Hence as the second step, we have developed the LynxOS device drivers for VME boards used for a klystron test stand such as DI (PENTLAND, MPV910), DO (Digital, DVME DOUT2) and AI (PENTLAND, MPV906) .

Device drivers are embeded in an OS kernel and is glued between a kernel and I/O devices. For keeping hardware independency of the kernel, UNIX device driver consists of a collection of function routines called the "entry point" which is called by the kernel in the same way as functions called by a main program written in C language. We can access to the I/O devices only from these entry points through the kernel. LynxOS device driver has the same structure as that of UNIX and has eight entry points per one device driver. The name of entry points and their purposes are shown in Table.1. Since the device driver is embeded in the kernel, we usually need to modify a configuration table file and reboot system to remake the kernel if we want to add a new device driver. This process is called static loading of the driver. But static loading is very troublesome especially at the development time

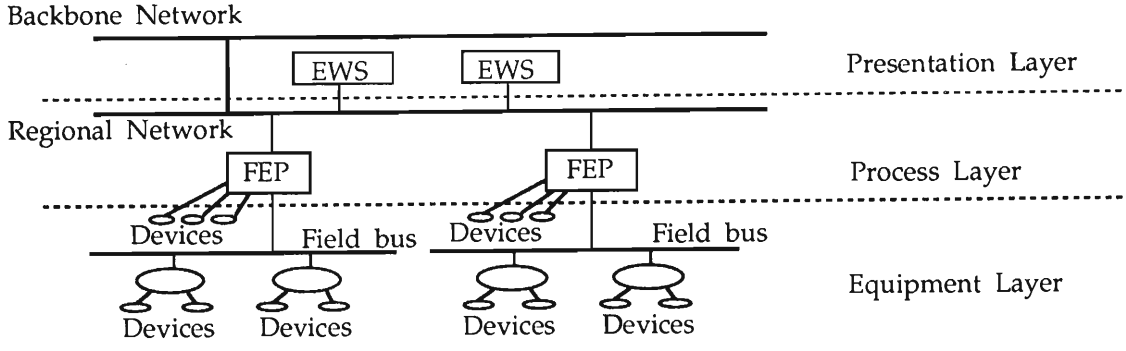

Fig.1. The standard model for accelerator and large experimental physics control systems.

Table 1. LynxOS device driver entry points and its purpose.

Entry Point	Purpose
open	called when device is opened
close	called when device is closed
read	called to read data
write	called to write data
select	support select system call
ioctl	device control
install	called to install major device
uninstall	called to remove major device

of the device driver. LynxOS offers powerful and useful functions for development of device drivers which are called dynamic loading. We can link/unlink the device drivers to the kernel with some shell commands. All things we need to do are merely to declare the entry points in a form of the specific structure at the end of the device driver. We need not to modify a configuration file and to reboot the system. There are no performance penalty by using dynamically loaded device drivers. If we finish the development and test of LynxOS device driver with dynamic loading, then we can load it statically according to the LynxOS static loading procedure.

Since device drivers are embeded in the kernel, we cannot use system calls or standard C library functions, but some special functions with a C interface are provided only for device drivers. These functions naturally depend on the OS which are called "driver service calls" on LynxOS. The LynxOS supports many driver service calls such as dynamic memory allocation, timer interruption (10 msec and 1 msec), hardware interruption dispatch, software interruption, thread, semaphore, signal, DMA chain and so on. Hence we can describe the LynxOS device driver almost in C language with these device service calls.

We have implemented hardware interruption from the I/O boards on VMEbus with LynxOS device driver. All things we have to do in the device driver are to describe an interrupt software handler and to establish a relation between the header address of interrupt software handler and interrupt vector number which is sent to CPU from the I/O device which demands for an interruption. The latter is implemented with a specific driver service call which has interrupt vector number and address of an interrupt software handler as arguments in installing entry point. It is very easy to implement hardware interruption with this service call.

We have composed the LynxOS device driver for a MPV906 AI board. Generally speaking, an AI board has more powerful and complicated functions than a DI/DO board, hence it is more difficult to make a device driver for an AI board. The MPV906 is a 12-bit analog-to-digital converter board with 64 single ended/32 differential input channels, and the board operation can be selected from two operating modes (continuous/transient), two data acquisition modes (polling/interrupt mode), four trigger sources (internal/software/event/external trigger), 64/32 data acquisition channels, three gain settings (×1/×10/×100), conversion period (for internal trigger), seven interrupt levels and interrupt status/ID (interrupt vector number) by the software program. It has 64 words memory for converted data. Since we can set the board operation from an application program through a device driver, the device driver must be written to support these available functions. It is not necessary to implement all functions to drive the klystron test bench. Hence we have fixed the data taking way as taking 64 samples per one read cycle for a specific input channel with a transient operation mode. It takes about 16.5 msec per one read cycle by polling mode with an internal trigger (30 μsec per one conversion) , and about 17 msec by interrupt mode with an internal trigger (30 μsec). One read cycle time includes one to open the device, set the device, read data and close the device.

We intend to establish the ways of exclusive and synchronous control of processes with device access and communication between these processes. We must implement these ways at both device driver level and upper application program level. After these ways are established, we intend to control VMEbus systems from a presentation layer which consists of EWS (Engineering Work Station) through network.

References

1) T. Wada: *RIKEN Accel. Prog. Rep.*, **24**, 202 (1990).
2) T. Masuda, T. Nakamura, T. Wada,and Z. Wang: *RIKEN Accel. Prog. Rep.*, **25**, 240 (1991).
3) R. Rausch, Ch. Serre: "Common Control System for the CERN accelerators", International Conference on Accelerator and Large Experimental Physics Control Systems, Tsukuba, Japan (1991).

V-2-23. Test of VME Remote I/O System Slave Card Type-A

H. Takebe, M. Hasegawa,* and K. Matsuo*

Power supplies for the SPring-8 Storage Ring magnets[1] are controlled by a VME[2] remote I/O card (RIO) system[3]. RIO cards of type-A and -B were made and tested in this year. This RIO system was initially developed for the HIMAC HEBT system at the NIRS (National Institute of Radiation Science) with a Multi-Bus system, and modified for the VME bus system at this time, by Mitsubishi Electric Corporation.

Figure 1 shows a block diagram of the RIO slave card type-A. The RIO card type-A has a 16 bits ADC (AD7701), a 16 bits DAC(AD669), 8 bits

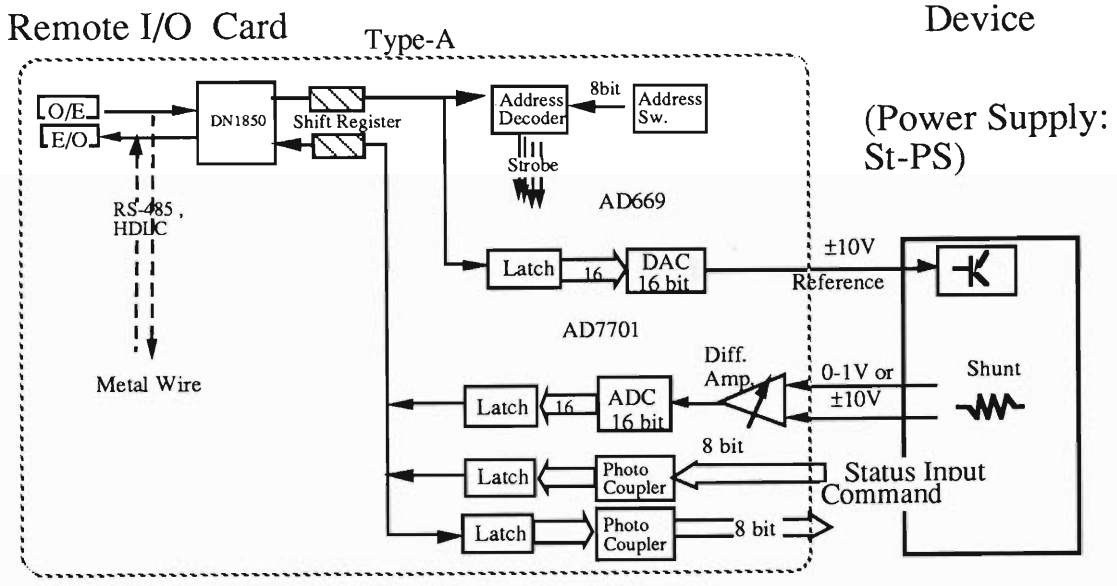

Fig.1. Block diagram of the RIO slave card type-A.

digital outputs and 8 bits digital inputs. This card is a single height of a Euro-card size as shown in Fig.2. Type-B has a 32 bits digital output and input with a double height of Euro-card size. The digital I/O's are all photo isolated, and can be connected to relay circuits, photo-coupler, and TTL level circuits.

The test bench system consists of a VME chassis and RIO cards. They are linked by an optical fiber cable. This VME system consists of a VME CPU module (MVME147), an Ethernet module, an RIO master module (Fig. 3), and an active star coupler. An operation test and a DAC accuracy check were done by using VME Lynx-OS[4] and C language test program. The following tests of the ADC and DAC of the RIO type-A were achieved:

1) Accuracy and linearity of the DAC,
2) DAC out drift check during 500 hours,
3) Accuracy and linearity of the ADC,
4) ADC out drift check for 500 hours.

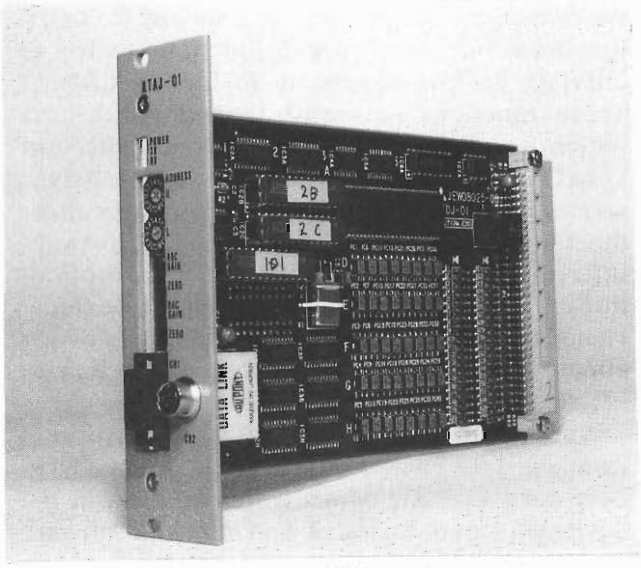

Fig. 2. Prototype RIO-A slave card.

* Mitsubishi Electronic Co.

These tests were done by using a DVM (HP : 3458A) at room temperature (25 ~ 28 ℃). The DAC output is connected to the ADC and DVM.

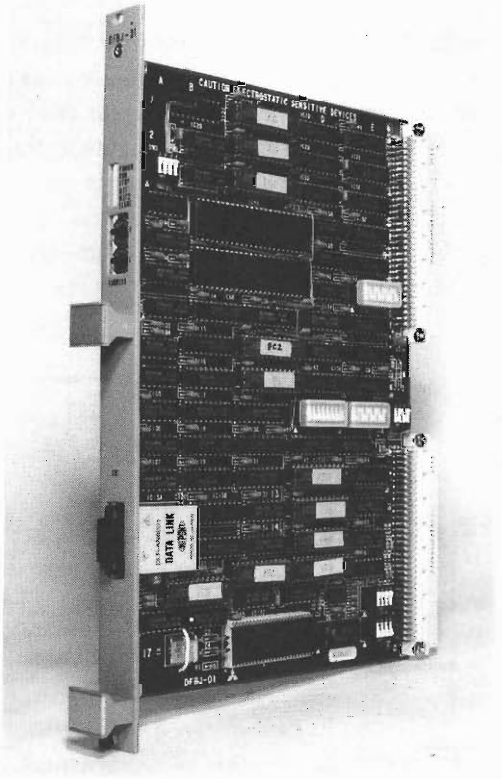

Fig.3. Prototype RIO master card.

Figure 4 shows a difference in percent between the measured DAC output data obtained by the DVM and the ideal DAC voltage along the DAC set value. The DAC was set in 1024 step from 0 to 65535(FFFF). It was changed in upper 4 bits only. This measurement was also done by changing all the bits of DAC set value which were turned on alternatively. The errors were within 0.012% and -0.025%. These can be reduced by adjusting the VR of the card, and the linearity error will become within $\pm 3 \times 10^{-5}$.

Figure 5 shows a long time drift of the DAC output when the data is FFFF and 10.03 V over 500 hours. The maximum drift is less than ±0.0003 V ($\pm 3 \times 10^{-5}$ against the full scale).

Differences between the DVM readings and the values calculated from the ADC data are less than ±1.2 mV ($\pm 1.2 \times 10^{-4}$ to the full scale value). These can be also reducedto $\pm 5 \times 10^{-5}$ by adjusting the scaling VR. Reproducibility of the reading of the ADC is better than $\pm 8 \times 10^{-5}$ in 2 days.

A cyclic time of the RIO serial data transfer was measured to be 0.19 ms for a 1 slave card. An RIO control program development in the VME Lynx-OS and design of RIO network is now in progress. A test of connection between the RIO type-B and a main power supply is scheduled in 1993.

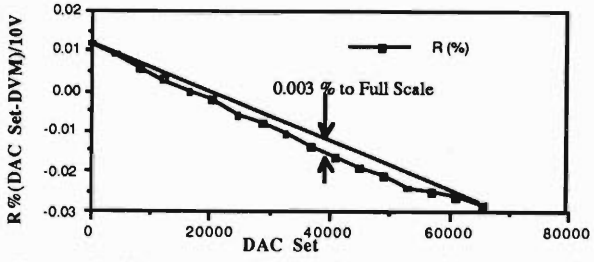

Fig. 4. Difference in percent between the measured DAC output voltage (DVM) and an ideal DAC voltage along the DAC set value. The linearity error will be reduced to within $\pm 3 \times 10^{-5}$ when the scaling VR is adjusted.

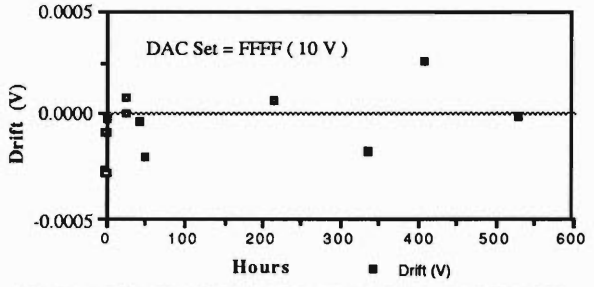

Fig. 5. Drift of the DAC output data , checked by the DVM when the DAC set value is FFFF in hexadecimal for 500 hours.

References

1) H.Takebe, N.Kumagai, J.Ohnishi, S.Matsui, K. Kumagai, and S.Motonaga : This report, p . 157.
2) Versa Module for European.
3) H.Takebe et. al. : *RIKEN Accel. Prog. ,Rep.* **25**, 209, (1991).
4) Real -Time Systems. Inc.

V-2-24. Design of RF Low Power System for the SPring-8 Storage Ring

Y. Ohashi, H. Ego, M. Hara, K. Inoue, Y. Kawashima, H. Suzuki,* I. Takeshita, and H. Yonehara*

A low power control system design of the SPring-8 storage ring has basically completed. The system described in this report includes 508.58 MHz reference signal transmission, klystron out phase and amplitude, and cavity tuning controls.

An ultra-stable reference signal generator, which will be installed in the RF "A" station (or central control room), will supply the main RF frequency of 508.58MHz. The signal is distributed in succession to the nearby stations and the synchrotron as shown in Fig.1. A special single-mode fiber-optic cable,[1] which compensates temperature drifts, is used for the signal transmission. Phase accuracy for transmitting signal over a 500m fiber-optic cable is about ±1° without a phase-lock loop(PLL) under the ambient temperature range between 20 and 30°C (about ±5° between 20 and 40°C).[2] Individual two fiber-optic cables are to be used to compensate phase drifts within 1° by the PLL and

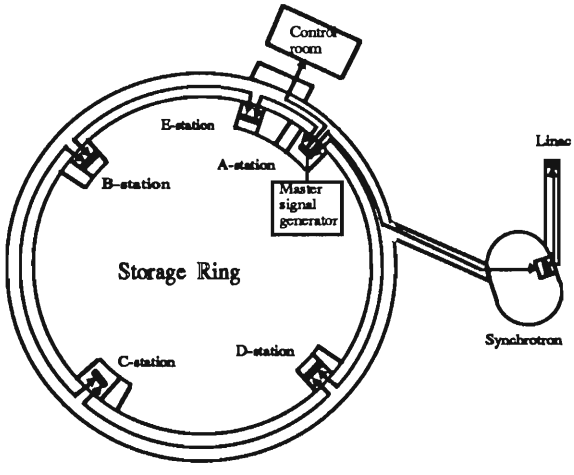

Fig.1. Fiber-optic link for the 508.58MHz reference signal trnsmission.

to watch actual drifts or any troubles in the reference line by monitoring phase control voltages as well.[3] A single fiber-optic cable might be used with optical directional couplers if a difference in the characteristics in both cables is a problem. A first timing signal transmission will be done with the same fiber-optic system.

As in Fig.2 RF signals picked-up from 8 cavities are sent to a vector sum over phase stable coaxial cables. The vector-summed signal is split into two. One is linearly detected and used for the amplitude control of the klystron. Since the cavity voltage is used for the klystron output power control, a beam loading effect is spontaneously compensated. The other sum-signal is fed into a phase detector to lock the klystron out RF signal phase.

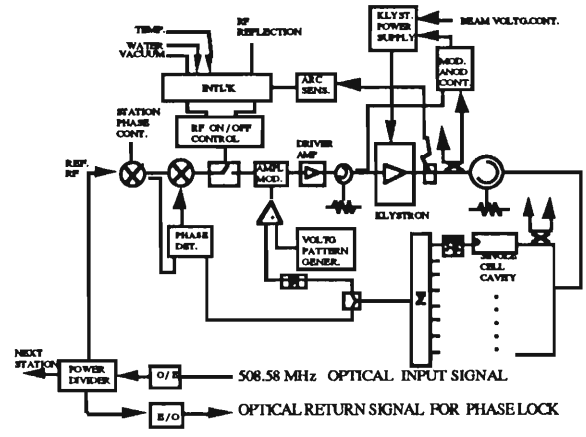

Fig.2. Schematic diagram of RF control system.

A picked up signal phase from each cavity is compared with the input phase. A phase drift, which is caused by the thermal detuning or reactive beam loading effect appeared in each cavity, is compensated by driving a stepping motor of the tuner.

A part of the system has been examined during a high power test. RF components needed to test and improve the overall system are being purchased, and a study of the whole system will be extensively carried out in a half year. The low power system described here is to be basically adopted in the booster synchrotron.

* Japan Atomic Energy Research Institute,

References

1) J. Urakawa: Particle Accelerators, **29**, 251 (1990).
2) Y. Kawashima, H. Ego, M. Hara, K. Inoue, Y. Ohashi, H.Suzuki, I.Takeshita,and H.Yonehara: "On the temperature dependence of an optical fiber and related modules for the timing system of the SPring-8" in this report, p.179.
3) E.Ezura, K.Akai, H.Hayano, M.Ono, M.Suetake, and T. Takashima: "The low level RF system for TRISTAN main ring" in Proc. 1987 Particle Accelerator Conf. (Washington, D.C., USA, 1987)

V-2-25. On the Temperature Dependence of an Optical Fiber and Related Modules for the Timing System of the SPring-8

Y.Kawashima, H.Ego, M.Hara, K.Inoue, Y.Ohashi, H.Suzuki,*
I.Takeshita, and H.Yonehara*

We have developed a transport system of the timing signal for the SPring-8. The method and relevant instruments are briefly described.

The fundamental radio frequency (RF) of 508.58 MHz is transmitted to the four RF power stations distributed in a storage ring with a circumference of 1436 m and an injector system. An RF, for example, is transmitted from a station to the other one. Received RF is divided into two, then one of them is returned to the original station, where the two RF signals, transmitted and received, are compared, and a phase difference between them is obtained. The phase difference of the RF between power stations must be kept within 1°, which corresponds to about 5 psec. The longest distance from a station to the neighboring one is about 400 m and the phase between them must be stable. Its stability must be kept in all seasons.

To realize our purpose, we adopted optical fibers to transmit RF signal. We also use them as a timing signal transmitter for the beam kicker. An optical fiber is much more useful compared with a co-axial wire cable in point of some problems such as attenuation in a long distance transmission and an electro-magnetic noise. In these days, we easily get an optical fiber whose phase stabilization is guaranteed in a room temperature around 20°C. The only issue to treat the optical fiber was modules such as an electrical to optical (E/O) and an optical to electrical (O/E) fiberoptic transmitter and a receiver with good response up to several tens GHz-high radio frequency, but they have also been developed and we can get them as commercialized products.

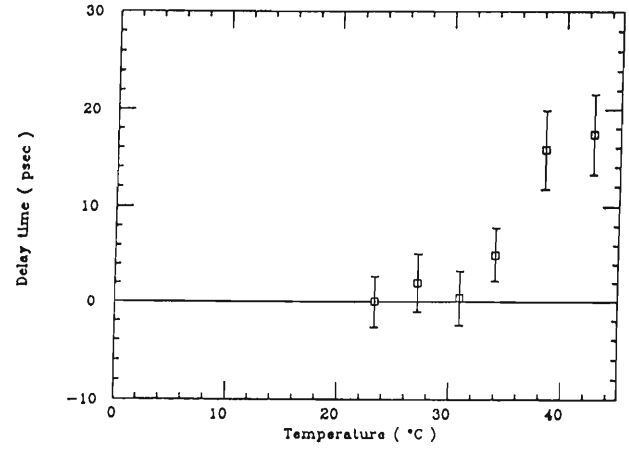

Fig.1. Temperature dependences of E/O and O/E obtained by a digital oscilloscope.

We have measured the temperature dependence concerning a time jitter of an E/O, an O/E and an optical fiber. First of all, the E/O and O/E connected with a 1-m long optical fiber was placed in a constant temperature box. We measured their specifications in a temperature range from 23.3°C to 42.6°C. The obtained results are shown in Fig.1, where the fluctuation of the delay time in a wide range of temperature is as small as the phase tolerance of the RF. The room temperature of a storage ring is to be kept at 27±1°C, so that we may expect the stabilities of the E/O and O/E. As to a 500-m long optical fiber, we have done the same experiment and obtained the same result as shown in Fig.2.

Consequently, we can expect the stability of a timing system comprising RF signal transmitter, receiver and optical fiber with enough reliability, as long as the room

*Japan Atomic Energy Research Institute

temperature in the storage ring and the booster synchrotron would be kept around 27°C within a few degrees as a temperature drift.

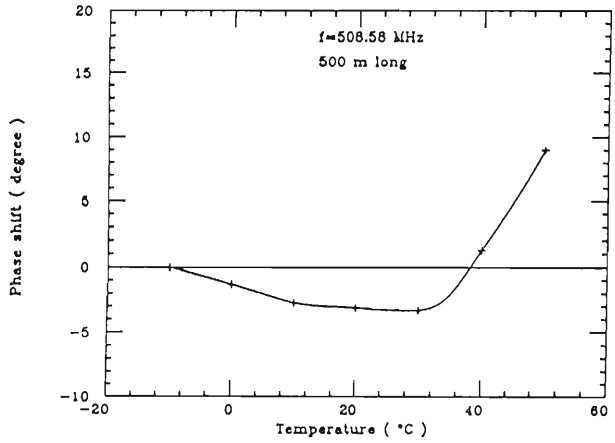

Fig.2. Temperature dependence of a phase stabilized optical fiber detected by a vector voltmeter.

In an actual system, in order to cancel a phase difference between stations, a phase lock system which consists of hardware is to be equipped, and the phase stability would be completed perfectly.

We are going to use the same E/O, O/E and optical fiber to kick a beam from a linac to a booster synchrotron and also from the synchrotron to the storage ring. In this system, a pulse signal is transmitted. We have to, therefore, use a pulse shaper circuit (PS) after the O/E module because of attenuation. Taking into account the small change of a pulse height due to a little temperature dependence of a transmission system, a constant-fraction-discriminator (CFD) module was inserted after the O/E. In case of a constant pulse height, total time jitter including E/O, O/E connected with a 500-m long optical fiber and a CFD was obtained to be 13 psec as a sigma value. Even if the pulse height is varied from -100 mV to -200 mV, the transit time of the CFD is changed by only 20 psec.

In the SPring-8, new devices such as an optical fiber and the related modules are employed, and the reliability of RF transmission and timing system must be remarkably improved.

VI. RADIATION MONITORING

RIKEN Accel. Prog. Rep. 26 (1992)

VI-1. Radiation Monitoring of RILAC, TANDETRON, and Hot Laboratory

I. Sakamoto, M. Yanokura, T. Kobayashi, M. Iwamoto,
I. Kohno, and T. Inamura

Radiation monitoring was carried out for RILAC, TANDETRON, and the hot laboratory in the cyclotron building from October 1991 to September 1992.

(1) Radiation monitoring of RILAC

The leakage radiation was measured at various points outside the RILAC building in July. When RILAC was used for the RRC injector with $^{40}Ar^{5+}$ beam of 18.7-MeV, no leakage of γ rays and neutrons from the RILAC building was detected. No contamination due to residual activities was found on the floors of the controlled area in the RILAC building in this period.

(2) Radiation monitoring of TANDETRON

X-ray monitoring was carried out for TANDETRON, when a copper target was bombarded with 1.6-MeV H^+ ions of 500 nA. The maximum dose (1 cm dose-equivalent) rate measured around TANDETRON was 1 μSv/h. No leakage of X-rays was detected not only outside the TANDETRON room but also around the target chamber.

(3) Air and surface contamination in the hot laboratory

Radioactive substances were handled in the hot laboratory. The radioactivity in air at the exit of draft chambers was measured every month, and the radioactivity was found small (the order of 10^{-8} Bq/cm^3). The surface contamination on the floors was below 10^{-2} Bq/cm^2.

(4) Contamination of drainage

Each time the drainage from the hot laboratory was drained outside the cyclotron building, the radioactivities in the drain water were measured. The radioactivities were found to be of the order of 10^{-4} Bq/cm^3. The total activity in aqueous effluents was 12 kBq.

VI-2. Exposure Dose Monitoring for Radiation Workers at RIKEN Accelerator Research Facilities

M. Miyagawa, I. Sakamoto, T. Katou, Y. Matsuzawa,
S. Kagaya, H. Katou, and T. Inamura

The external exposure dose of radiation workers at RIKEN Accelerator Research Facilities was mearsured by using γ-ray and neutron film badges. Four hundred and twenty-eight radiation workers were registered in fiscal 1991 (April 1991-March 1992), and their external doses recorded are given in Table 1. One nuclear chemist was exposed to γ-rays at an external dose of 0.1 mSv. (This is about one-tenth of the natural external dose/year in Japan.) The external doses owing to thermal and fast neutron exposures were below the detection limit.

Table 1. External exposure doses (effective dose-equivalent in mSv) recorded for radiation workers at RIKEN Accelerator Research Facilities in fiscal 1991(April 1991-March 1992).

Field	Number of personel				Collective dose (mSv)
	Dose undetectable	0.1-1 (mSv)	>1 (mSv)	Total	
Accelerator physicists and Operators#	83	0	0	83	0
Nuclear physicists	198	0	0	198	0
Researchers in other fields	118	1	0	119	0.1
TANDETRON workers	20	0	0	20	0
Health physicists	8	0	0	8	0
Total	427	1	0	428	0.1

#: Operators of the RIKEN Ring Cyclotron, RIKEN AVF Cyclotron and RILAC.
The average dose per person was 0.0002mSv; the maximum individual dose was 0.1mSv.

VI-3. Measurement of Neutron Flux with the Activation Method

S. Nakajima, N. Nakanishi, S. Fujita, H. Matsumoto,
K. Tanaka, and T. Shikata*

A series of experiments to measure the secondary neutrons produced by a reaction of the 135MeV/nucleon ^{14}N ions with a thick iron target has been made to obtain information for shielding caluculations. The neutron energy spectra and their angular dependence were measured last year using the activation analysis technique[1]. It is difficult to get accurate spectrum by this method, but its approximate shape was obtained . We found that the method is simple and inexpensive but is useful to determine the approximate shape of the spectrum. Systematical dependence on the target elements, the incident particles and enegies may be easily obtained with this technique.

This report is concerned with a similiar measurement for 135MeV/nucleon deuterons incident on a thick iron target (about 7cm long) in which the primary beam was completely stopped. The same elements as in the previous case(a carbon block and the seven metal foils of Al, Fe, Co, Ni, Ag, In, Au) were used for the activation samples, and placed at the angles of 0, 30, 60, 90, and 120 degree with respect to the incident beam. The carbon block was irradiated for approximately 2 hours and the seven metal foils were irradiated for about 16 hours by the secondary neutrons.

The measurements of γ-rays from the activated elements were performed after the irradiation . As an example, a γ-ray spectrum from the activated ^{59}Co foil is shown in Fig. 1 together with that taken in the case of 135 MeV/nucleon ^{14}N + iron reaction. The γ-rays whose energies correspond to those from the reaction products of (n,2n), (n,3n), (n,4n), (n,5n) were observed in both the spectra. The reaction Q-value is about 30MeV for the (n,4n) reaction and about 40MeV for the (n,5n) reaction. Significant presence of neutrons with energies of larger than 40 MeV is indicated.

The relative intensities among the peaks (n,2n), (n,4n), and (n,5n) were some-what different in two cases. A prominent peak was the (n,4n) for the ^{14}N's case and the (n,2n) for the deuteron's case. This is probably because much heigher energy neutrons were produced in the ^{14}N induced reaction. Any other remarkable difference was not readily seen in the two spectra. Detailed analysis is in progress.

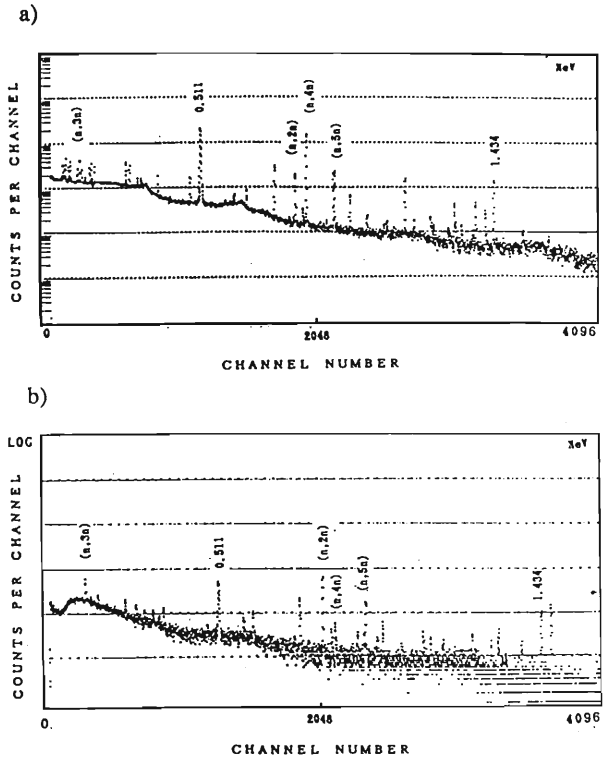

Fig. 1. γ-ray spectra from activated ^{59}Co foils taken in the cases of a) ^{14}N + iron reaction , b) deuteron + iron reaction.

References

1) T. Shikata et al.:RIKEN Accel. Prog. Rep., 25,171 (1991)

* Diseased

VI-4. Leakage Radiation Measurements in the Ring Cyclotron Facility

S. Fujita, S. Nakajima, N. Nakanishi, S. Okamoto,* H. Matsumoto, T. Takagi,**
K. Ikegami, and T. Inamura

The radiation safety control system has worked steadily this year, performing radiation monitoring continuously and automatically. We, however, encountered the following problem.

When experiments in an experimental vault E6 are carried out in the course of RIPS, a primary beam is separated from secondary beams with a magnet D1 in a distribution corridor (See Fig.1 (a)), and stopped in it. In some cases of experiments in the E6 vault, a gas activity detector NaI (2" x 2" NaI) was activated in spite of a very low radiation level in the vault. The gas activity detector is on the 2nd basement floor at a distance of 6.6 m from the magnet D1, and 1.8 m thick concrete exists between them.

To solve this problem, we measured leakage radiations around the gas activity detector using a primary beam of 135 MeV/u $^{12}C^{6+}$ particles. At that time, leakage neutrons from the AVF cyclotron, Ring cyclotron, E6 experimental vault, and the distribution corridor were monitored using a neutron dose meter at various points in the facility(See Figs.1 a,b). Results are summarized in Table 1.

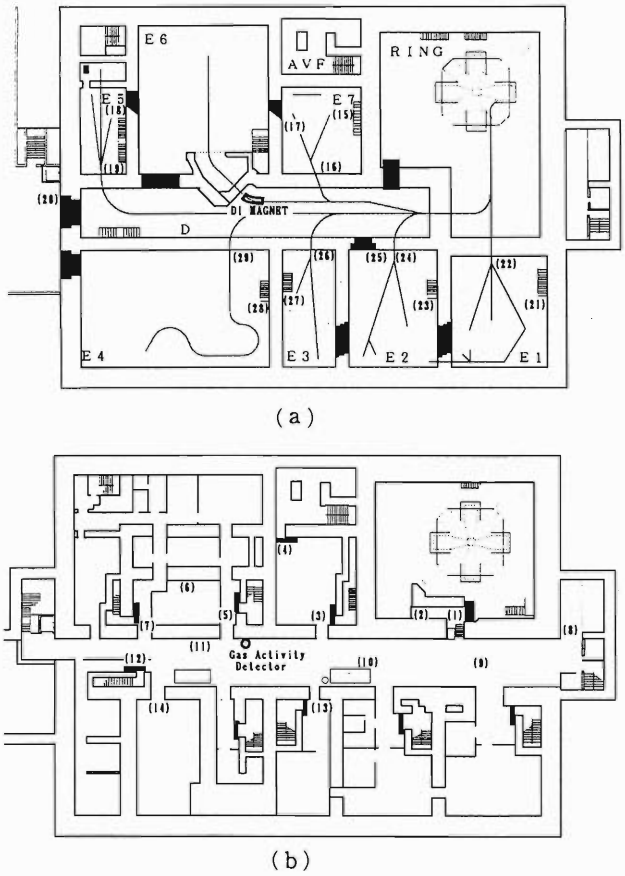

Fig. 1. Layout of RIKEN Ring Cyclotron facility as of 1992. a) Plan view of the 1st basement floor; b) Plan view of the 2nd basement floor. Points, where leakage radiations were measured, are denoted by the numbers in the parentheses.

Table 1. Dose rates of neutron leakage radiation from the magnet D1 in the beam distribution corridor. (See Figs.1-a,b).

Measured Point	Dose Rate (μSv/h)/(pμA)
(1)	25.1
(2)	505.2
(3)	0.610
(4)	0.0414
(5)	1.09
(6)	0.391
(7)	0.0617
(8)	0.02
(9)	3.35
(10)	2.12
(11)	7.43
(12)	1.76
(13)	0.325
(14)	0.306
(15)	1.77
(16)	12.5
(17)	5.42
(18)	0.04
(19)	0.130
(20)	0.163
(21)	9.04
(22)	292.1
(23)	0.0622
(24)	0.113
(25)	1.94
(26)	1.89
(27)	2.18
(28)	15.5
(29)	52.2

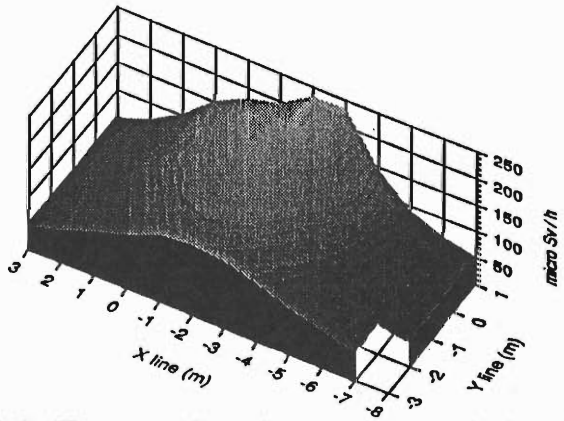

Fig.2. The contour lines of neutron dose rates /pμA on the 2nd basement floor. The position of activity detector is (-3,1) in the X-Y coodinates.

* Institute of Physics, University of Tukuba.
** Fukudagiken.

Leakage neutrons from the RIPS primary target point in the distribution corridor were also measured with neutron dose meters at 60 points in steps of 1 m on the 2nd basement floor. The contour lines of radiation levels are shown in Fig.2, where X and Y lines stand for parallel and perpendicular ones with the beam line in the distribution corridor. The origin of the coordinate is taken at the position on the 2nd basement floor just right under the magnet D1. The highest dose rate was detected at the position of the gas activity detector, that is, the X line (-3 m) and the Y line (1 m). It seems that the gas activity detector was activated by high energy neutrons from the magnet D1.

We also measured γ rays with a Ge detector around the gas activity detector. We shielded the Ge detector with lead of 5 cm thick because the gas activity detector is enclosed with lead of 5 cm thick. Figure 3 shows the energy spectrum; high energy components up to about 10 MeV are observed, which may be coming from high-energy neutron-induced secondary γ rays.

From those results it is concluded that we have to change the position of the gas activity detector and to shield locally the target chamber. It is very much desirable to develop monitors which are suitable for high energy γ rays and neutrons.

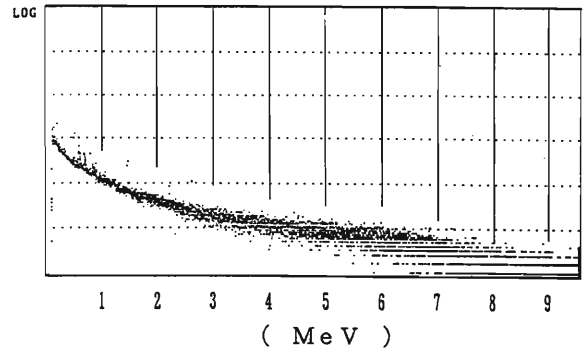

Fig. 3. An energy spectrum of γ rays by a Ge detector at the activity detector.

VI-5. Residual Activities in the Ring Cyclotron Facility

S. Fujita, S. Okamoto, *H. Matsumoto, K. Tanaka, N. Nakanishi, and T. Inamura

Residual activities were measured at various points in the Ring Cyclotron Facility after almost every beam time and during the overhaul throughout the year. In the following we describe significant residual activities

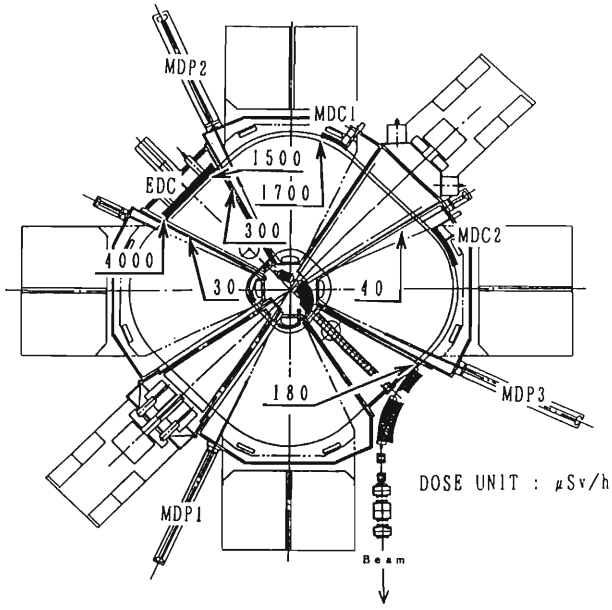

Fig. 1. Detection points around the RIKEN Ring Cyclotron: an electrostatic deflection channel, EDC; a magnetic deflection channel 1, MDC1; a magnetic deflection channel 2, MDC2; a main differential probe 1, MDP1; a main differential probe 2, MDP2; a main differential probe 3, MDP3. Indicated numerals are dose rates in units of μSv/h.

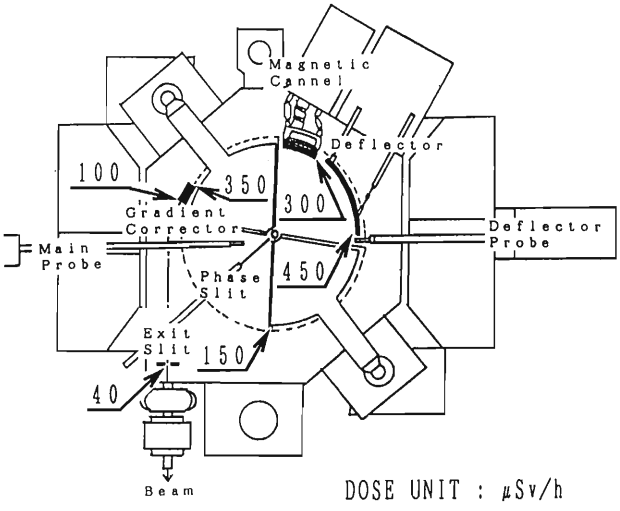

Fig. 2. Dose rates detected inside the injector AVF cyclotron. They are given in units of μSv/h.

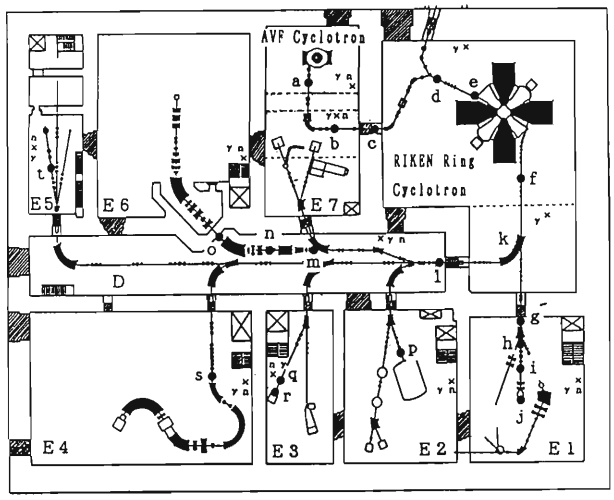

Fig. 3. Layout of the RIKEN Ring Cycrotron facility as of 1992. Monitoring positions are denoted by X . Detection points of residual activities on the beam lines are denoted by alphabets.

Table 1. Summary of the residual activities measured along the beam lines with an ionization chamber survey meter. Alphabets indicate the detection points in Fig. 3.

Detection point	Detected dose rate (μSv/h)	Date
a	50	Nov. 5,1991
b	30	Mar.10,1992
c	45	Mar.10,1992
d	20	Mar.10,1992
e	28	Mar.10,1992
f	80	Mar.10,1992
g	1150	Oct.12,1992
h	730	Oct.12,1992
i	160	Oct.12,1992
j	170	Oct.12,1992
k	40	Feb. 5,1992
l	40	Aug. 6,1992
m	50	Aug. 6,1992
n	5000	Feb. 5,1992
o	60	Aug. 6,1992
p	46	Oct. 9,1992
q	100	May.28,1992
r	300	Oct. 7,1992
s	28	Jul. 3,1992
t	27	May. 1,1992

* Institute of Physics, Uiversity of Tukuba.

observed.

From July 29 to August 1, the last experiment in the spring term was carried out with an $^{40}Ar^{16+}$ beam of 90 MeV/u in the experimental vault E6.

A routine overhaul was made in August, and the dose rates due to residual activities of the Ring Cyclotron and the injector AVF cyclotron were measured on Aug. 4 and 24, respectively. Those results are shown in Figs. 1 and 2 together with detection points. The residual activities at the deflectors of the Ring Cyclotron and injector AVF cyclotron were slightly increased than those of a previous report.[1)]

In the period from Oct. 16, 1991 to Oct. 15, 1992, residual activites were measured along the beam lines with a portable ionization chamber. The detection points above 20 μSv/h are shown in Fig.3. Table 1 summarizes the detected dose rates with measured dates. The maximum dose rate was 5000 μSv/h at the point n (the production target chamber of RIPS) in the beam distribution corridor.

References

1) S. Fujita, S. Okamoto, N. Nakanishi, I. Sakamoto, and T. Inamura: ***RIKEN*** *Accel. Prog. Rep.*,**22**,246 (1991).

VII. LIST OF PUBLICATIONS

VII. LIST OF PUBLICATIONS

1. Accelerator development and accelerator physics

1) J. Ohnishi, H. Takebe, K. Kumagai, and S. Motonaga: "Field Measurements of Prototype Magnets for the SPring-8 Storage Ring", *IEEE Magnetics*, **28**, 546 (1992).
2) C. Kato, A. Yoneda, T. Imai, K. Munakata, and T. Kohno: "Test of Two-Dimensional Position Sensitive Silicon Detector for Cosmic Ray Telescope by a Light Pulser", *Jpn. J. Appl. Phys.*, **30**, 3549(1991).
3) T. Nakagawa, T. Kageyama, M. Kase, A. Goto, and Y. Yano: "Mechanism of the Increase of Highly Charged Ion Intensity by Use of an Electrode in the First-Stage Chamber of the RIKEN 10 GHz Electron Cyclotron Resonance Ion Source", *ibid.*, **31L**, 1129 (1992).
4) Ch. Ellert, D. Habs, E. Jaeschke, T. Kambara, M. Music, D. Schwalm, P. Sigray, and A. Wolf: "An Induction Accelerator for the Heidelberg Test Storage Ring TSR", *Nucl. Instrum. Methods Phys. Res.*, **A314**, 399 (1992).
5) K. Watanabe, Y. Oikawa, H.A. Sakaue, S. Takahashi, C.Y. Xu, T. Hanasaka, Y. Hirano, S.H. Be, S. Yokouchi, T. Nishidono, and R.S. In: "Vacuum System for SPring-8 Storage Ring", Proc. 8th Meet. on Ultra High Vacuum Techniques for Accelerators and Storage Rings KEK (Natl. Lab. for High Energy Phys.), p.21 (1992).
6) H.A. Sakaue, Y. Oikawa, S. Takahashi, C.Y. Xu, T. Hanasaka, Y. Hirano, S.H. Be, S. Yokouchi, and K. Watanabe: "Pumping System for SPring-8 Storage Ring", *ibid.*, p.88.
7) S. Yokouchi, Y. Hirano, K. Watanabe, S.R. In, and S.H. Be: "Pumping Speed of a Distributed NEG Strip", *ibid.*, p.129.
8) S. Hirenzaki, H. Toki, and T. Yamazaki: "(d, ^{3}He) Reactions for the Formation of Deeply Bound Pionic Atoms", *Phys. Rev. C*, **44**, 2472 (1991).
9) M. Katō, W. Bentz, and K. Tanaka: "Neutral Pion Condensation in Quark Matter including Vacuum Fluctuation Effects", *ibid.*, **45**, 2445 (1992).
10) S. Kubono, N. Ikeda, Y. Funatsu, M. H. Tanaka, T. Nomura, H. Orihara, S. Kato, M. Ohura, T. Kubo, N. Inabe, A. Yoshida, T. Ichihara, M. Ishihara, I. Tanihata, H. Okuno, T. Nakamura, S. Shimoura, H. Toyokawa, C.C. Yun, H. Ohnuma, K. Asahi, A. Chakrabarti, T. Mukhopadhyay, and T. Kajino: "Decay Property of ^{20}Na for the Onset Mechanism of the Rapid-Proton Process", *ibid.*, **46**, 361 (1992).
11) K. Yoshida, J. Kasagi, H. Hama, M. Sakurai, M. Kodama, K. Furutaka, K. Ieki, W. Galster, T. Kubo, M. Ishihara, and A. Galonsky: "Neutron Emission for the Fusion of ^{40}Ar+Ni, ^{92}Mo, ^{122}Sn Reactions at E/A=26MeV", *ibid.*, p.961.
12) H. Kusakari, M.Oshima, A. Uchikura, M. Sugawara, A. Tomotani, S. Ichikawa, H. Iimura, T. Morikawa, T. Inamura, and M. Matsuzaki: "Electromagnetic Transition Probabilities in the Natural-Parity Rotational Bands of ^{155,157}Gd", *ibid.*, p.1257.
13) S. Kim and S. Ohta: "QCD Thermodynamics with Eight Staggered Quark Flavors on a $16^3\times6$ Lattice", *Phys. Rev. D*, **46**, 3607 (1992).

2. Nuclear physics and nuclear instrumentation

1) S. Kubono, N. Ikeda, M.H. Tanaka, T. Nomura, I. Katayama, Y. Fuchi, H. Kawashima, C.C. Yun, Y. Tajima, M. Yosoi, H. Ohnuma, M. Ohura, T. Kubo, I. Tanihata, H. Toyokawa, H. Orihara, H. Miyatake, T. Shimoda, R. N. Boyd, and T. Kajino: "Study of the Key Reaction ^{8}Li(α,n)^{11}B for the Primordial Nucleosynthesis", Proc. Int. Workshop on Unstable Nuclei in Astrophysics, eds. S. Kubono and T. Kajino, World Scientific, Singapore, p.131 (1991).
2) K. Yuasa-Nakagawa, Y.H. Pu, S.C. Jeong, H. Fuziwara, T. Mizota, S.M. Lee, T. Nakagawa, B. Heusch, K. Ieki, T. Sugimitu, and T. Matsuse: "Complex Fragment Mass Distributions in ^{84}Kr+^{27}Al at E_{lab}=10.6MeV/u", Towards a Unified Picture of Nuclear Dynamics AIP Conf. Proc., No. 250, p.100 (1992).

3) T. Matsuse, S.M. Lee, Y.H. Pu, K. Yuasa-Nakagawa, C. Beck, T. Nakagawa: "Statistical Emission of Complex Fragments from Highly Excited Compound Nucleus", *ibid.*, p.112.
4) K. Yazaki: "Quark-Meson Hybrid Model for Nuclear Force and Nuclear Currents", *Few-Body Systems*, Suppl., **5**, 441 (1992).
5) M. Koizumi, M. Azuma, T. Horiguchi, T. Inamura, T. Ishizuka, A. Iivonen, H. Katsuragawa, S. Matsuki, K. Morita, T. Murayama, I. Nakamura, M. Nakaoka, K. Shimomura, T. Shinozuka, I. Sugai, Y. Tagishi, M. Takami, K. Valli, M. Wakasugi, and A. Yoshida: "Collinear Fast Atomic-Beam Laser Spectroscopy at RIKEN GARIS/IGISOL", *Hyperfine Interact.*, **74**, 181 (1992).
6) S. Matsuki, K. Shimomura, I. Ogawa, K. Suzuki, M. Koizumi, T. Nakamura, M. Okuno, N. Inabe, S. Hamada, Y. Fukashiro, H. Sunaoshi, M. Wada, T. Kohmoto, T. Kubo, T. Shinozuka, K. Asahi, T. Inamura, M. Ishihara, and M. Fujioka: "Radiation-Detected Optical Pumping in Solids", *ibid.*, p.223.
7) T. Doke, J. Kikuchi, N. Hasebe, H. Murakami, A. Nakamoto, T. Yanagimachi, T. Kohno, K. Nagata, B. Wilken, K. Maezawa, Y. Muraki, T. Terasawa, S. Yanagita, K. Munakata, and A. Nishida: "High Energy Particle Experiment (HEP)", Geotail Prelaunch Report, ISAS SES-TD-92-007SY, Sagamihara, p.71 (1992).
8) M. Kodama, T. Kohno, and H. Kanzawa: "Stratospheric Sudden Cooling after Solar Proton Event over Syowa Station Antarctica", *J. Geomag. Geoelectr.*, **44**, 361 (1992).
9) M.A. Miah, K. Nagata, T. Kohno, H. Murakami, A. Nakamoto, N. Hasebe, J. Kikuchi, and T. Doke: "Spatial and Temporal Features of 0.64-35 MeV Protons in the Space Station Environment: EXOS-C Observations", *ibid.*, p.591.
10) K. Ieki, N. Iwasa, Y. Ando, K. Hata, T. Motobayashi, H. Murakami, M. Ogiwara, Jian-zhi Ruan (Gen), S. Shibuya, S. Shirato, H. Fujiwara, S. C. Jeong, S.M. Lee, T. Mizota, Y. Nagashima, M. Ogihara, S. Okumura, Y.H. Pu, and M. Ishihara: "Dynamics of the Projectile-like Fragment Emission in the $^{40}Ar+^{209}Bi$ Reaction at 26 MeV/u", *J. Phys. G: Nucl. Particle Phys.*, **18**, 401 (1992).
11) K. Suzuki and H. Toki: "Flavor SU(4) Baryon and Meson Masses in Diquark-quark Model Using the Pauli-Gursey Symmetry", *Mod. Phys. Lett.*, **A7**, 2867 (1992).
12) A. Kohama, K. Yazaki, and R. Seki: "Nuclear Transparency in the Glauber Approximation", *Nucl. Phys.*, **A536**, 716 (1992).
13) J. Peter, J.P. Sullivan, G. Bizard, W. Q. Shen, R. Brou, D. Cussol, M. Louvel, J.P. Patry, R. Regimbard, J. C. Stecmeyer, B. Tamain, E. Crema, H. Doubre, K. Hagel, G.M. Jin, A. Perhaire, F. Saint-Laurent, Y. Cassagnou, R. Legrain, C. Lebrun, E. Rosato, R. MacGrath, S.C. Jeong, S. M. Lee, Y. Nagashima, T. Nakagawa, M. Ogihara, J. Kasagi, and T. Motobayashi: "Inversion of the Collective Matter Flow in Nucleus-Nucleus Collisions, Measured with a 4π Charged Particle Array", *ibid.*, **A538**, 75c (1992).
14) T. Suzuki: "Pion Production in Intermediate Energy Nucleus-Nucleus Collisions", *ibid.*, p.113c.
15) T. Kobayashi: "Projectile Fragmentation of Exotic Nuclear Beams", *ibid.*, p.343c.
16) K. Soutome, S. Yamaji, and M. Sano: "Target-Charge Dependence of the Coulomb Dissociation Cross Section of ^{11}Li", *ibid.*, p.383c.
17) R.N. Boyd, D. Hirata, N. Inabe, T. Kubo, T. Nakagawa, T. Suzuki, I. Tanihata, M. Yanokura, X.X. Bai, K. Kimura, S. Kubono, S. Shimoura, and H.S. Xu: "The $^{8}Li(^{4}He,n)^{11}B$ Reaction Cross Section at Low Energies", *ibid.*, p.523c.
18) J. Kasagi, K. Furutaka, T. Murakami, A. Yajima, M. Ohshima, S. Niiya, H. Tominaga, K. Yoshida, H. Hama, K. Ieki, W. Galster, K. Kubo, M. Ishihara, and A. Galonsky: "Excitation Energy and Spin Dependence of the Giant Dipole Resonance at Finite Temperature", *ibid.*, p.585c.
19) K. Tanaka and W. Bentz: "$1/N$ Expansion and the Correlation Energy of Nuclear Matter in the Relativistic $\sigma\omega$

Model", *ibid.*, **A540**, 383 (1992).
20) R.N. Boyd, S. Kubono, N. Ikeda, M. Y. Tanaka, T. Nomura, Y. Fuchi, H. Kawashima, M. Ohura, H. Orihara, S. Yun, H. Toyokawa, M. Yosoi, and H. Ohnuma: "^{9}Be(α,p)^{12}B Reaction and Primordial Nucleosynthesis", *ibid.*, **A542**, 97 (1992).
21) M. Arima, K. Shimizu, K. Yazaki: "A Study of π-Nucleon S-Wave Resonances and the η-Nucleon Interaction", *ibid.*, **A543**, 613 (1992).
22) T. Sakai, A. Buchmann, K. Yazaki, and K. Shimizu: "The Nucleon-H-Particle Interaction in the Quark Model", *ibid.*, p.661.
23) M. Oshima, Y. Gono, T. Murakami, H. Kusakari, M. Sugawara, S. Ichikawa, Y. Hatsukawa, T. Morikawa, and B.J. Min: "Observation of Coulomb Excitation of Unstable Nuclei: Utilization of a Secondary Beam", *Nucl. Instrum. Methods Phys. Res.*, **A312**, 425 (1992).
24) M. Koizumi, Y. Yoshida, K. Morita, M. Takami, T. Inamura, M. Azuma, H. Katsuragawa, M. Nakaoka, I. Nakamura, T. Ishizuka, T. Murayama, A. Iivonen, K. Valli, K. Shimomura, S. Matsuki, and I. Sugai: "Velocity Distribution of Ion Beams from the RIKEN IGISOL", *ibid.*, **A313**, 1 (1992).
25) H. Ichinose, T. Doke, A. Hitachi, J. Kikuchi, K. Masuda, and E. Shibamura: "Energy Resolutions for Gamma-Rays and Electrons from ^{207}Bi in Liquid Xe Doped with TEA", *ibid.*, **A322**, 216 (1992).
26) T. Matsuzaki, R. Kadono, K. Ishida, A. Matsushita, and K. Nagamine: "Low Energy Unstable Nuclear Beam Channel 'SLOW' at the RIKEN Ring Cyclotron", *ibid.*, **B70**, 101 (1992).
27) A. Iivonen, J. Kuhalainen, R. Saintola, K. Valli, T. Inamura, M. Koizumi, K. Morita, and A. Yoshida: "The Squeezer Ion Guide", *ibid.*, p.213.
28) T. Inamura, M. Koizumi, K. Morita, A. Yoshida, M. Takami, T. Ishizuka, I. Nakamura, M. Nakaoka, T. Murayama, I. Sugai, M. Azuma, H. Katsuragawa, K. Shimomura, S. Matsuki, A. Iivonen, and K. Valli: "Velocity Distribution of RIKEN IGISOL Ion Beams", *ibid.*, p.226.
29) K. Matsuta, A. Ozawa, Y. Nojiri, T. Minamisono, M. Fukuda, A. Kitagawa, S. Momota, T. Ohtsubo, Y. Matsuo, H. Takechi, S. Fukuda, I. Minami, K. Sugimoto, I. Tanihata, K. Omata, S. Shimoura, J.R. Alonso, G. F. Krebs, and T.J.M. Symons: "A Fragment Separator at LBL for the Beta-NMR Experiment", *ibid.*, p.304.
30) T. Kubo, M.Ishihara, N. Inabe, H. Kumagai, I. Tanihata, K. Yoshida, T. Nakamura, H. Okuno, S. Shimoura, and K. Asahi: "The RIKEN Radioactive Beam Facility", *ibid.*, p.309.
31) K. Ishida, T. Matsuzaki, and K. Nagamine: "A Large Solid-angle Secondary-beam Collector Using Axially Symmetric Superconducting Magnetic Field", *ibid.*, p.366.
32) K. Shimomura, I. Ogawa, K. Suzuki, S. Hamada, T. Nakamura, H. Okuno, M. Koizumi, N. Inabe, Y. Fukashiro, H. Sunaoshi, M. Wada, S. Hatori, T. Murayama, T. Kohmoto, Y. Fukuda, T. Kubo, T. Shinozuka, K. Asahi, S. Morinobu, T. Inamura, M. Ishihara, M. Fujioka, M. Kondo, and S. Matsuki: "OPERA: An On-line System of Optical Pumping in Solids for Unstable Nuclei", *ibid.*, p.513.
33) S. Kubono, Y. Funatsu, N. Ikeda, M. H. Tanaka, T. Nomura, H. Orihara, S. Kato, M. Ohura, T. Kubo, N. Inabe, T. Ichihara, M. Ishihara, I. Tanihata, H. Okuno, T. Nakamura, S. Shimoura, H. Toyokawa, C.C. Yun, H. Ohnuma, K. Asahi, A. Chakrabarti, T. Mukhopadhyay, and T. Kajino: "Proton Decay Measurement with RIPS for Astrophysical Interest", *ibid.*, p.583.
34) G. Bizard, D. Durand, A. Genoux-Lubain, M. Louvel, R. Bougault, R. Brou, H. Doubre, Y. El-Masri, H. Fugiwara, K. Hagel, A. Hajfani, F. Hanappe, S. Jeong, G.M. Jin, S. Kato, J.L. Laville, C. Le Brun, J.F. Lecolley, S. Lee, T. Matsuse, T. Motobayashi, J.P. Patry, A. Peghaire, J. Peter, N. Prot, R. Regimbart, F. Saint-Laurent, J.C. Steckmeyer, and B. Tamain: "Three Fragment Sequential Decay of Heavy Nuclei around 3 MeV/u Excitation Energy", *Phys. Lett. B*, **276**, 413 (1992).
35) K. Matsuta, A. Ozawa, Y. Nojiri, T.

Minamisono, S. Fukuda, A. Kitagawa, S. Momota, T. Ohtsubo, Y. Matsuo, H. Takechi, S. Fukuda, I. Minami, K. Sugimoto, I. Tanihata, K. Omata, J.R. Alonso, G.F. Krebs, and T.J.M. Symons: "Observation of Spin Polarization of Projectile Fragments from 106 A MeV ^{40}Ca+Au Collisions", *ibid.*, **281**, 214 (1992).
36) K. Yuasa-Nakagawa, Y.H. Pu, S.C. Jeong, Y. Futami, T. Mizota, S.M. Lee, T. Nakagawa, B. Heusch, K. Ieki, and T. Matsuse: "Complex Fragment Distributions in ^{84}Kr+^{27}Al at E_{lab}=10.6 MeV/u", *ibid.*, **283**, 185 (1992).
37) H. Hofmann, S. Yamaji, and A.S. Jensen: "Distribution of Strength for Isoscalar Modes at Finite Temperature", *ibid.*, **286**, 1 (1992).
38) H. Kawakami, S. Kato, T. Ohshima, C. Rosenfeld, H. Sakamoto, T. Sato, S. Shibata, J. Shirai, Y. Sugaya, T. Suzuki, K. Takahashi, T. Tsukamoto, K. Ueno, K. Ukai, S. Wilson, and Y. Yonezawa: "High Sensitivity Search for a 17 keV Neutrino. Negative Indication with an Upper Limit of 0.095%", *ibid.*, **287**, 45 (1992).
39) I. Tanihata, T. Kobayashi, T. Suzuki, K. Yoshida, S. Shimoura, K. Sugimoto, K. Matsuta, T. Minamisono, W. Christie, D. Olson, and H. Wieman: "Determination of the Density Distribution and the Correlation of Halo Neutrons in ^{11}Li", *ibid.*, p.307.
40) I. Tanihata, D. Hirata, T. Kobayashi, S. Shimoura, K. Sugimoto, and H. Toki: "Revealing of Thick Neutron Skins in Nuclei", *ibid.*, **289**, 261 (1992).
41) R.N. Boyd, I. Tanihata, N. Inabe, T. Kubo, T. Nakagawa, T. Suzuki, M. Yanokura, X.X. Bai, K. Kimura, S. Kubono, S. Shimoura, H.S. Xu, and D. Hirata: "Measurement of the ^{8}Li (α, n)^{11}B Reaction Cross Section at Energies of Astrophysical Interest", *Phys. Rev. Lett.*, **68**, 1283 (1992).
42) F.V. De Blasio, W. Cassing, M. Tohyama, P.F. Bortignon, and R.A. Broglia: "Non-perturbative Study of the Damping of Giant Resonances in Hot Nuclei", *ibid.*, p.1663.
43) R. Brockmann and H. Toki: "Relativistic Density Dependent Hartree Approach for Finite Nuclei", *ibid.*, p.3408.
44) R.N. Boyd and I. Tanihata:"Physics with Radioactive Nuclear Beams", *Physics Today*, June, p.44 (1992).
45) K. Soutome, S. Yamaji, and M. Sano: "Coulomb Dissociation of the Weakly-Bound Nucleus ^{11}Li", *Prog. Theor. Phys.*, **87**, 599 (1992).
46) T. Watabe and H. Toki: "The Chiral Quark-soliton Model for the Nucleon", *ibid.*, p.651.
47) H. Toki and K. Suzuki: "Scale Invariant Nambu and Jona-Lasinio Model with Confinement for Hadrons", *ibid.*, p.1435.
48) K. Soutome, S. Yamaji, and M. Sano: "Role of Minimum Momentum Transfer in Coulomb Dissociation of ^{11}Li Projectiles", *ibid.*, **88**, 703 (1992).
49) A. Hosaka and H. Toki: "Chiral Bag Model", *ibid.*, Suppl., **109**, 137 (1992).
50) K. Nagata and HEP Group: "Calibration Experiment of GEOTAIL High Energy Particle Observation", *Solar Terr. Environ. Res. Jpn.*, **15**, 40 (1992).
51) S. Kubono, Y. Funatsu, N. Ikeda, M. H. Tanaka, T. Nomura, H. Orihara, S. Kato, M. Ohura, T. Kubo, N. Inabe, T. Ichihara, M. Ishihara, I. Tanihata, H. Okuno, T. Nakamura, S. Shimoura, H. Toyokawa, C.C. Yun, H. Ohnuma, K. Asahi, A. Chakrabarti, T. Mukhopadhyay, and T. Kajino: "Study of the Decay Property of ^{20}Na for the Onset Mechanism of the Rapidproton Process", Radioactive Nuclear Beams 1991, IOP Publishing, p.317 (1992).
52) S. Kubono, N. Ikeda, M.H. Tanaka, T. Nomura, I. Katayama, Y. Fuchi, H. Kawashima, C.C. Yun, Y. Tajima, M. Yosoi, H. Ohnuma, M. Ohura, T. Kubo, I. Tanihata, H. Toyokawa, H. Orihara, H. Miyatake, T. Shimoda, R. N. Boyd, and T. Kajino:"Experimantal Study of the Key Reaction ^{8}Li(α,n)^{11}B for the Primordial Nucleosynthesis", *ibid.*, p.323.
53) T. Wada, N. Carjan, and Y. Abe: "Multi-Dimensional Langevin Approach to the Dissipative Dynamics of Nuclear Fission", Proc. Tours Symp. on Nucl. Phys., World Scientific, Singapore, p.136 (1992).
54) I.Tanihata: "Studies with Radioactive Beams-Preperties of Neutron Halo-",

ibid., p.150.
55) K. Soutome, S. Yamaji, and M. Sano: "Target-Charge Dependence of the Coulomb Dissociation Cross Section of the Weakly-Bound Nucleus ^{11}Li", Proc. of Int. Symp. on Structure and Reactions of Unstable Nuclei, Niigata, Japan, 1991, World Scientific, Singapore, p.167 (1992).
56) T. Kobayashi: "Spectroscopy of the Exotic Nucleus ^{11}Li via Pion Double Charge Exchange Reaction ^{11}B(π^-, π^+)^{11}Li", *ibid.*, p.187.
57) I. Tanihata: "On the Momentum Distributions of Fragments of ^{11}Li and ^{11}Be-Possible Indication of di-Neutron Formation-", *ibid.*, p.233.
58) H. Sato: "Nucleus as a Canonical Ensemble", Proc. Int. Workshop on Gross Properties of Nuclei and Nuclear Excitations XX, GSI, Darmstadt, p.89 (1992).
59) T. Kobayashi: "Spectroscopy of the Exotic Nucleus ^{11}Li via Pion Double Charge Exchange Reaction ^{11}B(π^-, π^+) ^{11}Li", Proc. Int. Workshop on Pions in Nuclei, Peniscola, Spain, 1991, Edited by T.Osset, World Scientific, Singapore, p.58 (1992).
60) S. Hirenzaki, H. Toki, and T. Yamazaki: "Formation of Deeply Bound Pionic Atoms", *ibid.*, p.345.
61) H. Sato: "Nucleus as a Canonical Ensemble: Level Density", Proc. Specialists' Meet. on High Energy Nuclear Data JAERI-M92-039 (JEARI, 1992), p.162 (1992).
62) H. Sato: "Nucleus as a Canonical Ensemble: Deformed Nucleus", Proc. of the Symp. on Group Theory and Special Symmetries in Nuclear Physics, World Scientific, Singapore, p.359 (1992).

3. Atomic and solid-state physics

1) I. Shimamura: "R-Matrix Method and Doubly Excited Rydberg States", Adv. in Atomic and Molecular Physics, ed. M.S.Z. Chaghtai, Today & Tomorrow's Printers and Publishers, New Delhi, p.17 (1992).
2) A. Matsushita, R. Kadono, K. Nishiyama, Y. Miyake, A. Nakao, J. Takahashi, M. Iwaki, and K. Nagamine: "Muonium Formation on Powdered Platinum Surface", *Chem. Phys. Lett.*, **197**, 297 (1992).
3) M. Sakurai, T. Sekioka, M. Kimura, T. Niizeki, T. Hirayama, M. Terasawa, H. Yamaoka, Y. Awaya, J. Yoda, A. Ogata, and S. Ohtani: "Storage and Lifetime Measurements of Multiply Charged Ions Produced by Synchrotron Radiation", *Jpn. J. Appl. Phys.*, **30**, 1899 (1991).
4) S.C. Mukherjee, D.P. Sural, J.F. McCann, and I. Shimamura: "Theory of Electron Capture in Ion-Atom Collisions at High Energies", *Comments At. Mol. Phys.*, **28**, 25 (1992).
5) P. Hvelplund, H. Tawara, K. Komaki, Y. Yamazaki, K. Kuroki, H. Watanabe, K. Kawatsura, M. Sataka, M. Imai, Y. Kanai, T. Kambara, and Y.Awaya: "Binary Encounter Peaks for 0° Electrons in Collisions between 2 MeV/amu Si^{q+} and He", *J. Phys. Soc. Jpn.*, **60**, 3675 (1991).
6) K. Tanaka, E. Yagi, K. Kawakami, and A. Ono: "Channeling Analysis of Ge Epitaxial Layer on Si Substrate and Doped Ga Atoms by Using RBS and PIXE Methods", *Int. J. PIXE*, **2**, 137 (1992).
7) E. Yagi: "Behaviour of Kr Atoms in Kr-Implanted Aluminium", *Ionics*, (in Japanese), **18**, No. 2, p.3 (1992).
8) H. Tawara, T. Tonuma, H. Kumagai, and T. Matsuo: "Multiply-Charged Ions Produced from Condensed Gas Targets under Heavy Ion Impact: Comparison between Atom and Molecule Targets", *J. Phys. B: At. Mol. Opt. Phys.*, **25**, L423 (1992).
9) T. Mizogawa, Y. Awaya, Y. Isozumi, R. Katano, S. Ito, and N. Maeda: "New Readout Technique for Two-Dimensional Position-Sensitive Detectors", *Nucl. Instrum. Methods Phys. Res.*, **A312**, 547 (1992).
10) M. Imai, M. Sataka, H. Naramoto, Y. Yamazaki, K. Komaki, K. Kawatsura, and Y. Kanai: "Dynamical Behaviour of Angular Momentum Distributions of Autoionizing $1s^22pnl$ States of S^{12+} Ions Excited through Carbon Foils", *ibid.*, **B67**, 142 (1992).
11) T. Tonuma, H. Kumagai, T. Matsuo, H. Shibata, and H. Tawara: "Molecular and Cluster Ions Produced from Frozen C_2H_2 Molecules under Energetic, Heavy Ion Impact", *ibid.*, p. 544.
12) T. Okada, M.D. Lan, J.Z. Liu, R.N.

Shelton, and K. Asai: "Mössbauer Studies of Single Crystal $YBa_2Cu_{3-x}Fe_xO_{7-y}$", *Physica C*, **185-189**, 783 (1991).
13) T. Okada, Y. Kobayashi, K. Asai, N. Yamada, and T. Yamadaya: "^{57}Fe Mössbauer Studies of $BiPbSr_2FeO_6$", *ibid.*, p.1125.
14) M. Sataka, K. Kawatsura, H. Naramoto, Y. Nakai, Y. Yamazaki, K. Komaki, K. Kuroki, Y. Kanai, T. Kambara, Y. Awaya, J.E. Hansen, I. Kádár, and N. Stolterfoht: "High-resolution L-shell Auger Spectroscopy of Mg-like Scandium Produced in 89MeV Sc^{8+}+He Collisions", *Phys. Rev. A*, **44**, 7290 (1991).
15) M. R. Harston, I. Shimamura, and M. Kamimura: "Energy Shift in the [(dtμ)-d]ee Molecule Due to the Finite Size of the Muonic Molecular Ion $(dt\mu)^+$", *ibid.*, **45**,94 (1992).
16) A. Igarashi and N. Toshima: "Destructive and Constructive Interferences of the Second Born Amplitudes for Positronium Formation", *ibid.*, **46**, 1159 (1992).
17) I. Shimamura: "Scaling of the Cross Sections for Vibrational Transitions", *ibid.*, p.1394.
18) N. Toshima and J. Eichler: "Nonperturbative Treatment of the Thomas Mechanism in Electron Capture", *ibid.*, p.2564.
19) I. Shimamura: "Moleculelike Metastable States of Antiprotonic and Mesic Helium", *ibid.*, p.3776.
20) H. Fukuda and T. Ishihara: "Distorted Atomic-Orbital Expansion for Slow Ion-Atom Collisions", *ibid.*, p.5531.
21) R. Kadono, A. Matsushita, K. Nishiyama, and K. Nagamine: "Muon-Induced Luminescence in KBr", *Phys. Rev. B*, **46**, 8586 (1992).
22) K. Ando, U.I. Safronova, and I.Y. Tolstikhina: "Energy Levels $1s^2 21nl'$ (n=2, 3, 4) of Na VIII-S XIII Ions. Comparison of Two Calculation Methods: MCDF and MZ", *Phys. Scr.*, **46**, 107 (1992).
23) E. Yagi: "Channelling Experiments on the Lattice Location of Hydrogen in Metals by Using a Nuclear Reaction ^{1}H (^{11}B, α)$\alpha\alpha$", *Rad. Eff. Def. Sol.*, **124**, 21 (1992).
24) M. Sakurai, M. Kimura, T. Sekioka, M. Terasawa, H. Yamaoka, T. Niizeki, Y. Awaya, T. Hirayama, J. Yoda, A. Ogata, and S. Ohtani: "Trapping and Probing of Multiply Charged Xe Ions Produced by Synchrotron Radiation", *Rev. Sci. Instrum.*, **63**, 1186 (1992).
25) S. Kravis: "SPring-8 Workshop on Atomic Physics", *Synchrotron Radiat. News*, **5**, 3 (1992).
26) H. Tawara, T. Tonuma, H. Kumagai, T. Matsuo, and H. Shibata: "Multiply-Charged Ions and Cluster Ions Produced from Frozen CO_2 and H_2O Targets in Energetic, Heavy Ion Impact", *Z. Phys. D, At. Mol. and Clusters*, **21**, S257 (1991).
27) T. Kambara, R. Schuch, Y. Awaya, T. Mizogawa, H. Kumagai, Y. Kanai, H. Shibata, and K. Shima: "Solid-gas Effect in K-Vacancy Production in Near Symmetric Slow Heavy-Ion-Atom Collisions", *ibid.*, **22**, 451 (1992).
28) M.R. Harston, I. Shimamura, and M. Kamimura: "Energy Shift in (dtμ)e Due to the Finite Size of the Muonic Molecular Ion $(dt\mu)^+$", *ibid.*, p.635.

4. Radiochemistry, radiation chemistry, and radiation biology

1) M. Iwamoto, Y. Kobayashi, S.Y. Chen, Y. Ohkubo, S. Ambe, M. Yanokura, A.N. Garg, and F. Ambe: "Separation of Multitracers from Heavy-Ion-Irradiated Targets by Melting under Reduced Pressure", *Anal. Sci.*, **7**, Suppl., 313 (1991).
2) S. Ambe, S.Y. Chen, Y. Ohkubo, Y. Kobayashi, M. Iwamoto, M. Yanokura, and F. Ambe: "Preparation of Radioactive Multitracer Solutions from Au, Ag, and Cu Foils Irradiated with High-Energy Heavy Ions", *ibid.*, p.317.
3) S.Y. Chen, S. Ambe, Y. Ohkubo, M. Iwamoto, Y. Kobayashi, N. Takematsu, and F. Ambe: "Study of Removal Mechanisms of Metal Elements from Seawater Using Radioactive Multitracers", *ibid.*, p.1105.
4) T. Takahashi, F. Yatagai, and K. Izumo: "Microdosimetric Considerations of Effect of Heavy Ions on *E. coli* K-12 Mutants", *Adv. Space Res.*, **131**, No. 2, p.65 (1992).
5) S. Ambe, Y. Ohkubo, Y. Kobayashi, M. Iwamoto, M. Yanokura, and F. Ambe: "Preparation of Radioactive Multitracer Solutions from a High-

Energy Heavy-Ion Irradiated Au Target by Means of a Supported Liquid Membrane", *Appl. Radiat. Isot.*, **43**, 1533 (1992).
6) M. Nakada, Y. Watanabe, K. Endo, H. Nakahara, H. Sano, K. Mishima, M.K. Kubo, Y. Sakai, T. Tominaga, K. Asai, I. Kohno, and F. Ambe: "Mössbauer Emission Spectroscopy of ^{57}Fe Arising from ^{57}Mn in Metal and Oxides of Chromium", *Bull. Chem. Soc. Jpn.*, **65**, 1 (1992).
7) S. Ambe, S.Y. Chen, Y. Ohkubo, Y. Kobayashi, M. Iwamoto, and F. Ambe: "Application of the Radioactive Multitracer Technique to a Study of Adsorption of Metal Ions on α-Fe_2O_3", *Chem. Lett.*, **1992**, 1059.
8) Y. Ohkubo, Y. Kobayashi, S. Ambe, K. Harasawa, M. Takeda, S. Shibata, K. Asai, T. Okada, and F. Ambe: "^{99}Ru($\leftarrow^{99}$Rh) as a TDPAC Probe in the Study of a High-T_c Superconductor", *ibid.*, p.2069.
9) Y. Kobayashi, M. Watanabe, M. Katada, H. Sano, T. Okada, and F. Ambe: "^{99}Ru Mössbauer Spectroscopic Studies on Salts of Ruthenocene with Halogens", *Hyperfine Interact.*, **68**, 189 (1991).
10) J.S. Zheng, Y. Kobayashi, J. Nakamura, K. Asai, G. L. Zhang, and F. Ambe: "Europium-151 Mössbauer Effect Study of Europium Orthovanadite", *ibid.*, p.307.
11) J. Nakamura, Y. Kobayashi, F. Ambe, K. Asai, and N. Yamada: "^{121}Sb Mössbauer Spectroscopy of $Mn_{1+x}Sb$", *ibid.*, p.311.
12) G.L. Zhang, S.Y. Chen, S. Ambe, K. Maeda, K. Suzuki, Y. Sasa, E. Yagi, H. Yabuki, Z.W. Huang, and F. Ambe: "Characterization of Iron Oxides and Hydroxides in the Sand of Flaming Mountain", *ibid.*, **70**, 973 (1992).
13) T. Nagamune, J. Honda, Y. Kobayashi, H. Sasabe, I. Endo, F. Ambe, Y. Teratani, and A. Hirata: "Mössbauer, Electron Paramagnetic Susceptibility Studies of Photosensitive Nitrile Hydratase from *Rhodococcus* sp. N-771", *ibid.*, **71**, 1271 (1992).
14) Y. Kobayashi, T. Okada, K. Asai, M. Katada, H. Sano, and F. Ambe: "Mössbauer Spectroscopy and Magnetization Studies of α- and β-$RuCl_3$", *Inorg. Chem.*, **31**, 4570 (1992).
15) M. Suzuki, M. Watanabe, K. Nakano, K. Suzuki, and K. Matsui: "Heavy-ion-Induced Chromosome Breakage Studied by Premature Chromosome Condensation (PCC) in Syrian Golden Hamster Embryo Cells", *Int. J. Radiat. Biol.*, **62**, 581 (1992).
16) M. Watanabe, M. Suzuki, K. Suzuki, K. Nakano, and K. Watanabe: "Effect of Multiple Irradiation with Low Doses of Gamma-Rays on Morphological Transformation and Growth Ability of Human Embryo Cells *in vitro*", *ibid.*, p.711.
17) F. Yatagai, M.J. Horsfall, and B.W. Glickman: "Specificity of SOS Mutagenesis in Native M13 *lacI* Phage", *J. Bacteriol.*, **173**, 7996 (1991).
18) O. Yatou and T. Takahashi: "Evaluation of Mutation Induction Effect of Ion Irradiation in Soybean Strain L65 with the Heterozygous Leaf Color Locus y11.", *Jpn. J. Breeding*, **42**, Suppl., 2, p.472 (1991).
19) M. Watanabe, M. Suzuki, K. Suzuki, K. Nakano, and F. Yatagai: "Radiation-Induced Chromosome Damage in G_1-Phase Cells as Breaks in Premature Chromosome Condensation (PCC) and Analysis of Its Biological Meaning", *J. Radiat. Res.*, **33**, 87 (1992).
20) F. Yatagai, S. Hachiya, Y. Hama, A. J.E. Gordon, and F. Hanaoka: "Resolution and Characterization of Polymorphic DNA by SSCP and Chemical Cleavage Methodologies", *ibid.*, p.95.
21) F. Yatagai, J.A. Halliday, and B.W. Glickman: "Specificity of *recA* 441-Mediated (*tif-1*) Mutational Events", *Mol. Gen. Genet.*, **230**, 75 (1991).
22) K. Kimura: "Track-depth Resolved Dynamics of Helium Excimers along 4 in Near-liquid and Liquid Helium", Proc. Int. Conf. on Liquid Radiation Detectors: Their Fundamental Properties and Applications, p.38 (1992).
23) Y. Itoh, H. Murakami, and T. Suzuki: "Defects in Electron or Proton Irradiated Undoped and Si-doped GaAs by Positron Annihilation", Positron Annihilation Proc. 9th Int. Conf. Positron Annihilation, Materials Science Forum, Trans Tech Publications, Switzerland, **105-110**, 1085 (1992).

5. Material analysis

1) K. Tazaki, T. Tiba, M. Aratani, and M. Miyachi: "Structural Water in Volcanic Glass", *Clays and Clay Minerals*, **40**, 122 (1991).

2) K. Maeda, Y. Sasa, and M. Uda: "High Resolution Soft X-Ray Spectrometer for Chemical State Analysis by PIXE", *Int. J. PIXE*, **2**, 19 (1992).

3) M. Suzuki and T. Takahashi: "Proportional Scintillation Imaging Chamber and Its Application", *Ioniz. Radiat.*, (in Japanese), **19**, 54 (1992).

4) K. Tazaki, M. Aratani, M. Yanokura, K. Kaiho, and S. Noda: "Singularity of Clay Minerals and Iridium Concentration at Cretaceous-Tertiary (K-T) Boundary", *J. Clay Sci. Soc. Jpn.*, **32**, 86 (1992).

5) I. Sugai, M. Oyaizu, M. Aratani, M. Yanokura, and K. Yamazaki: "Development of Heavy Ion Beam Sputtering Method for Long-Lived Carbon Stipper Foils", *Nucl. Instrum. Methods Phys. Res.*, **A320**, 15 (1992).

6) K. Maeda and J. Kawai: "Report on 6th Int. Conf. on PIXE and 1st Int. Symp. on Bio-PIXE", *Oyo Butsuri* (in Japanese), **61**, 1180 (1992).

7) J. Kawai, M. Takami, M. Fujinami, Y. Hashiguchi, S. Hayakawa, and Y. Gohshi: "A Numerical Simulation of Total Reflection X-Ray Photoelectron Spectroscopy (TRXPS)", *Spectrochim. Acta*, **47B**, 983 (1992).

VIII. LIST OF PREPRINTS

VIII. LIST OF PREPRINTS

1992

RIKEN-AF-NP

119 I. Tanihata, T. Kobayashi, T. Suzuki, K. Yoshida, S. Shimoura, K. Sugimoto, K. Matsuta, T. Minamisono, W. Christie, D. Olson, and H. Wieman: "Determination of the Density Distribution and the Correlation of Halo Neutrons in ^{11}Li"

120 T. Harada: "Production and Structure of Light Σ-Hypernuclei"

121 H. Toki and K. Suzuki: "Scale Invariant Nambu and Jona-Lasinio Model with Confinement for Hadrons"

122 V.V. Lyukov and N.I. Starkov: "Properties and Some Production Possibilities of the Charmed Nuclei"

123 I. Tanihata, D. Hirata, T. Kobayashi, S. Shimoura, K. Sugimoto, and H. Toki: "Revealing of Thick Neutron Skins in Nuclei"

124 T. Yamada and K. Ikeda: "$^{4}_{\Lambda}$He Hypernuclear States and Roles of the Spin-Isospin Terms of Σ-N Interaction"

125 T. Yamada and K. Ikeda: "Possible Existence of a Bound State in $^{7}_{\Lambda}$Li"

126 C. -B. Moon, M. Fujimaki, S. Hirenzaki, N. Inabe, K. Katori, J.C. Kim, Y.K. Kim, T. Kobayashi, Y. Kubo, H. Kumagai, S. Shimoura, T. Suzuki, and I. Tanihata: "Measurements of ^{11}Li+p and ^{9}Li+p Elastic Scatterings at 60 MeV"

127 S. Hirenzaki, H. Toki, and I. Tanihata: "Proton Elastic Scattering with ^{9}Li and ^{11}Li and its Halo Structure"

128 K. Yoshida, J. Kasagi, H. Hama, M. Sakurai, M. Kodama, K. Furutaka, K. Ieki, W. Galster, T. Kubo, M. Ishihara, and A. Galonsky: "Neutron Emission for the Fusion of ^{40}Ar+Ni, ^{92}Mo, ^{122}Sn Reactions at E/A=26 MeV"

129 H.T. Duong, C. Ekstrom, M. Gustafsson, T.T. Inamura, and P. Juncar: "Atomic Beam Magnetic Resonance Apparatus for Systematic Measurement of Hyperfine Structure Anomalies (Bohr-Wesskope Effect)"

130 Y. Yamamoto, M. Wakai, T. Fukuda, and M. Sano: "Formation of Double-Lamda Hypernucleus from Quasi-Free Ξ Absorption"

131 K. Sugimoto and I. Tanihata: "Nuclear Structures Studied with Exotic Nuclear Beams"

132 A. Ozawa: "Projectile-Fragmentation Process Studied by Detecting the Spin Polarization of Heavy Fragments of 100 MeV/nucleon (thesis)"

133 C. -B. Moon, M. Fujimaki, N. Inabe, K. Katori, J.C. Kim, T. Kobayashi, T. Kubo, H. Kumagai, S. Shimoura, T. Suzuki, and I. Tanihata: "Measurement of Angular Distribution for the ^{11}Li+p and ^{9}Li Elastic Scatterings"

I. Tanihata, D. Hirata, T. Kobayashi, S. Shimoura, K. Sugimoto, and H. Toki: "Revelation of Thick Neutron Skin in Nuclei"

T. Kobayashi: "Nuclear Structure Experiments on ^{11}Li"

I. Tanihata: "Radioactive Beam Facilities and Their Physics Program"

134 S. Shimoura, T. Nakamura, H. Okamura, H. Okuno, H. Sakai, and M. Ishihara: "Density Distribution of Neutron Halo in ^{11}Li"

135 H. Okuno, K. Asahi, H. Ueno, H. Sato, M. Adachi, T. Kubo, T. Nakamura, N. Inabe, A. Yoshida, Y. Ohkubo, T. Ichihara, M. Ishihara, T. Shimoda, H. Miyatake, and N. Takahashi: "Polarization in Projectile Fragmentation and g-Factor Measurements for Neutron-Rich Nuclei"

136 K. Kato and K. Ikeda: "Analyses of ^{9}Li+n Resonances in ^{10}Li by the Complex Scaling Method=Interaction between ^{9}Li and Neutron"

137 B.V. Danilin, A.A. Korsheninnikov, and M.V. Zhukov: "Possible Existence of ^{10}He as Narrow Three-Body Resonance"

138 Y. Futami, T. Mizota, Y.H. Pu, Y. Honjo, K. Yuasa-Nakagawa, H. Toyokawa, S.M. Lee, K. Furutaka, T. Murakami, J. Kasagi, K. Yoshida, and T. Nakagawa: "Performance of a Phoswich Detector Composed of a Thin Plastic and a Thick BaF_2 Scintillators"

139 M. Sano, K. Soutome, and S. Yamaji: "Projectile Fragmentation in Heavy-Ion Collisions"

140 S. Yamaji, A.S. Jensen, and H. Hofmann: "Isoscalar Vibrational States in Hot Nuclei"

IX. PAPERS PRESENTED AT MEETINGS

IX. PAPERS PRESENTED AT MEETINGS

1. Accelerator development and accelerator physics

1) A. Goto:"Acceleration of Proton Beams with RIKEN Ring Cyclotron", The Specialists' Meet. on High Energy Nuclear Data, Tokai, Oct. (1991).
2) S. Yokouchi, Y. Hirano, K. Watanabe, S.R. In, and S.H. Be: "Pumping Speed of a Distributed NEG Strip", 8th Meet. on Ultra High Vacuum Techniques for Accelerators and Storage Rings, Tsukuba, Mar. (1992).
3) K. Watanabe, Y. Oikawa, H.A. Sakaue, S. Takahashi, C.Y. Xu, T. Hanasaka, Y. Hirano, S.H. Be, S. Yokouchi, T. Nishidono, and R.S. In: "Vacuum System for SPring-8 Storage Ring", *ibid*.
4) H.A. Sakaue, Y. Oikawa, S. Takahashi, C.Y. Xu, T. Hanasaka Y. Hira no, S.H. Be, S. Yokouchi, and K. Watanabe: "Pumping System for SPring-8 Storage Ring", *ibid*.
5) Y. Hasegawa, H. Yuta, F. Suekane, T. Kondo, Y. Unno, H. Iwasaki, Y. Sakai, Y. Watanabe, T. Tanimori, K. Kaneyuki, L. Soso, T. Doke, A. Hitachi, T. Ito, E. Shibamura, K. Masuda, and T. Takahashi: "Photoionization of Dopants in Liquid Argon-Xenon Mixture", Int. Conf. on Liquid Radiation Detectors, Tokyo, Apr. (1992).
6) N. Ishida, T. Doke, J. Kikuchi, K. Kuwahara, T. Kashiwagi, M. Ichige, K. Hasuike, K. Ito, S. Ben, A. Hitachi, Y.H. Qu, K. Masuda, M. Suzuki, M. Kase, and T. Takahashi: "Fundamental Test of Liquid Xe and Ar/Xe Scintillation Detector Using Silicon Photodiode", *ibid*.
7) K. Watanabe, S. Takahashi, T. Hanasaka, Y. Hirano, H.A. Sakaue, C.Y. Xu, K. Yano, S. Yokouchi, S. H. Be, N. Ota, Y. Suetsugu, K. Kanazawa, Y. Morimoto, T. Shirakura, and K. Konishi: "Synchrotron Radiation Interactions in the Crotch and Absorbers, and Their Design", XVth Int. Conf. on High Energy Accelerators, Hamburg, Germany, July (1992).
8) Y. Yano: "Recent Achievements at the RIKEN Ring Cyclotron", 13th Int. Conf. on Cyclotrons and their Applications, Vancouver, Canada, July (1992).
9) Y. Yano: "Status Report on RIKEN Accelerator Research Facility", RIKEN Int. Symp. on Unstable Nuclei and Particles as Probes in Physics and Chemistry, Wako, Aug. (1992).
10) Y. Yano: "RIKEN Accelerator Research Facility (RARF)", Joint Italian - Japanese Meet. within the INFN-RIKEN Agreement 'Perspectives in Heavy Ion Physics', Catania, Italy, Sept. (1992).
11) J. Ohnishi: "Magnetic Field Measurements with Harmonic Coils", Autumn Meet. Phys. Soc. Jpn., Niigata, Oct. (1992).
12) H.S. Sakaue, Y. Hirano, S.R. In, S. Yokouchi, K. Watanabe, and S.H. Be: "Lumped NEG Pump for Crotch and Pumping System of SPring-8 Storage Ring", 12th Int. Vacuum Congr., Hague, the Netherlands, Oct. (1992).
13) Y. Yano: "RARF and Other New Ion Accelerator Facilities in Japan", Joint Symp. on Synchrotron Radiation Sources, Pohang, Korea, Nov. (1992).

2. Nuclear physics and nuclear instrumentation

1) M. Hosaka, H. Orihara, M. Ohura, G. C. Jon, K. Ishii, K. Furutaka, and J. Kasagi: "Development of BaF_2 γ-Ray Detector", 46th Ann. Meet. Phys. Soc. Jpn., Sapporo, Sept. (1991).
2) K. Hosomi, T. Tohei, T. Nakagawa, J. Takamatsu, A. Terakawa, A. Narita, T. Inomata, H. Orihara, K. Ishii, M. Ohura, M. Hosaka, G.C. Jon, T. Suehiro, K. Miura, K. Abe, and H. Ohnuma: "The ^{4}He, ^{16}O(^{3}He,n)^{6}Be, ^{18}Ne Reaction at E=45MeV", *ibid*.
3) A. Narita, T Tohei, T. Nakagawa, A. Sato, J. Takamatsu, M. Mori, A. Terakawa, K. Hosomi, H. Orihara, T. Niizeki, M. Ohura, S. Hirasaki, M. Hosaka, G.C. Jon, K. Miura, and H. Ohnuma: "The ^{42}Ca(d,n) Reaction and the Hole Strenghths of the sd-shells", *ibid*.
4) A. Terakawa, T. Tohei, T. Nakagawa, J. Takamatsu, A. Narita, K. Hosomi, H. Orihara, K. Ishii, T. Niizeki, M. Ohura, M. Hosaka, G.C. Jon, K.Miura, and H. Ohnuma: "Inves-

tigation of the Single-Proton States in ^{19}F through the (d,n) Reaction", *ibid*.
5) H. Toyokawa, Y. Honjo, K. Ohkushi, N. Tomita, H. Ohnuma, T. Niizeki, H.Y. Yoshida, Y. Tajima, C.C. Yoon, M. Yosoi, H. Orihara, M. Ohura, M. Hosaka, S. Kubono, M.H. Tanaka, and N. Ikeda: "^{13}C(p,$d_{s=0}$)^{12}C Reaction with 35 MeV Proton", *ibid*.
6) A. Terakawa, T. Tohei, T. Nakagawa, A. Narita, K. Hosomi, T. Inomata, H. Orihara, K. Ishii, M. Ohura, M. Hosaka, S. Miyamoto, G.C. Jon, K. Miura, and H. Ohnuma: "Deuteron Adiabatic Analysis of the ^{208}Pb(d,n) ^{209}Bi Reaction at Ed=25 MeV", *ibid*.
7) S. Hirenzaki, C.-B. Moon, T. Suzuki, T. Kobayashi, and I. Tanihata: "An Optical Model Study of the Li+p Elastic Scattering", RIKEN Symp. on Nucl. Phys. by Unstable Nucl. Beam, Wako, Jan. (1992).
8) K. Soutome, S. Yamaji, and M. Sano: "Nuclear Dissociation of ^{11}Li", *ibid*.
9) M. Koizumi, T. Inamura, T. Ishizuka, H. Katsuragawa, K. Shimomura, T. Shinozuka, I. Sugai, M. Takami, Y. Tagishi, M. Nakaoka, I. Nakamura, T. Horiguchi, S. Matsuki, T. Murayama, K. Morita, A. Yoshida, and M. Wakasugi : "Laser Spectroscopy with IGISOL", Symp. on Radiation-detected Hyperfine Interaction, Osaka, Jan. (1992).
10) H. Sato: "The Production Cross Section of Nuclides-The Mass Distribution of Fission Products-", RIKEN Symp. on the Study of Nuclear Structures and Reactions with the Unstable Nucleus, Wako, Jan. (1992).
11) C.-B. Moon: "Angular Distributions for the ^{9,11}Li+p Elastic Scattering", *ibid*.
12) T. Wada: "Nuclear Dissipative Dynamics", RIKEN Symp. on Nuclear Fusion and Fission Reactions, Wako, Jan. (1992).
13) S. Daté and H. Sumiyoshi: "Event Simulator URASiMA for Ultrarelativistic Heavy Ion Collisions", RIKEN Symp. on Physics of High Energy Heavy Ion Collisions, Wako, Jan. (1992).
14) H. Sato: "Nucleus as a Canonical Ensemble", Int. Workshop XX on Gross Properties of Nuclei and Nuclear Excitations held at Hirsheg, Kleiwalsertal, Austria, Jan. (1992).
15) S. Daté and H. Sumiyoshi: "Event Simulator: URASiMA", Int. Mini-Symp. on High-Energy Heavy-Ion Reactions, Hiroshima, Feb. (1992).
16) S. Daté and H. Sumiyoshi: "Event Simulation of High Energy Heavy Ion Collisions based on a Multiple Scattering Model", 47th Ann. Meet. Phys. Soc. Jpn., Yokohama, Mar. (1992).
17) N. Ishida, T. Doke, J. Kikuchi, T. Kashiwagi, M. Ichige, A. Hitachi, K. Ito, K. Masuda, E. Aprile, M. Suzuki, and T. Takahashi: "Measurement of the Attenuation Length of Scintillation Light in Liquid Xenon", *ibid*.
18) K. Soutome, S. Yamaji, and M. Sano: "Dissociation Cross Sections of ^{11}Li", *ibid*.
19) T. Murayama, H.T. Duong, J. Pinard, T.T. Inamura, and S. Matsuki: "Systematic Measurement of Hyperfine Structure Anomaly", *ibid*.
20) F.V. De Blasio, W. Cassing, M. Tohyama, P.F. Bortignon, and R.A. Broglia: "Temperature Dependence of the Widths of the Giant Resonances", *ibid*.
21) K. Ishida, T. Matsuzaki, R. Kadono, A. Matsushita, and K. Nagamine: "Production of Surface Muons by ^{14}N at 135 MeV/A and ^{40}Ar at 95 MeV/A", *ibid*.
22) S. Hirenzaki, C.-B. Moon, T. Suzuki, T. Kobayashi, and I. Tanihata: "Proton-Li Elastic Scattering", *ibid*.
23) S. Ohta: "Lattice QCD Numerical Calculations on Parallel Computer AP 1000", *ibid*.
24) T. Wada, N. Carjan, and Y. Abe: "Light-Particle Emissions in Induced Nuclear Fission", *ibid*.
25) K. Shimomura, I. Ogawa, K. Suzuki, S. Hamada, T. Nakamura, H. Okuno, M. Koizumi, N. Inabe, Y. Fukashiro, H. Sunaoshi, M. Wada, T. Murayama, T. Kohmoto, T.Kubo, T. Shinozuka, K. Asahi, T. Inamura, H. Ishihara, M. Fujioka, and S. Matsuki: "Nuclear Structure Studies of Neutron-Rich Nuclei with Radiation-Detected Optical Pumping in Solids", *ibid*.
26) T. Inamura, M. Nakaoka, A. Iivonen, R. Saintola, K. Valli, J.-H. Gu, and H.-J. Song: "Measurements of the Energy Spread of Ion-Guide Beams", *ibid*.
27) H. Toyokawa, Y. Honjo, K.Ohkushi,

N. Tomita, H. Ohnuma, T. Niizeki, H.Y. Yoshida, Y. Tajima, C.C. Yoon, M. Yosoi, H. Orihara, M. Ohura, M. Hosaka, S. Kubono, M.H. Tanaka, and N. Ikeda: "$^{13}C(p,d_{s=0})^{12}C$ Reaction by 35MeV Proton", *ibid*.

28) A. Terakawa, T. Tohei, T. Nakagawa, A. Narita, K. Hosomi, T. Inomata, H. Orihara, K. Ishii, M. Ohura, M. Hosaka, S. Miyamoto, G. C. Jon, K. Miura, and H. Ohnuma: "Deuteron Adiabatic Analysis of the $^{208}Pb(d,n)^{209}Bi$ Reaction at Ed=25 MeV", *ibid*.
29) K. Tanaka and W. Bentz: "Nuclear Matter Properties including Higher Order Quantum Corrections II", *ibid*.
30) M. Kato, W. Bentz, K. Tanaka, and K. Yazaki: "A Modified Nambu-Jona-Lasinio Model for Mesons and Baryons", *ibid*.
31) N. Sakamoto: "Analyzing Powers of $^{12}C(d,p)^{13}C$(g.s.) and ^{12}C(d.do) [Ed=14MeV]", *ibid*.
32) H. Sato: "Nucleus as a Canonical Ensemble: Deformed Nucleus", *ibid*.
33) T. Inamura: "Atomic Beam Magnetic Resonance Experiment —for Bohr-Weisskopf Effect Measurement with ISOLDE at CERN—", Workshop on Electromagnetic Isotope Separators and their Application, Kumatori, Mar. (1992).
34) H. Toki: "Scale Invaliant Nambu and Jona-Lasinio Model", Int. Symp. on Extended Objects and Bound Systems, Karuizawa, Mar. (1992).
35) K. Ishida: "Large Solid-angle Superconducting Muon Channel", Workshop on Research and Developments for JHP and Related Scientific Topics, Tanashi, Mar. (1992).
36) T. Kobayashi: "Experiments with Light Neutron-Rich Projectiles", Symp. on Production and Utilization of Radioactive Beams, Am. Chem. Soc. Meet., San Francisco, U.S.A., Apr. (1992).
37) A. Iivonen, R. Saintola, K. Valli, T. Inamura, K. Morita, and A. Yoshida: "Ion-Guide Quadrupole Mass Spectrometer for On-Line Studies of Short-Lived Nuclei", Finnish Phys. Soc. Meet., Lahti, Finland, Apr. (1992).
38) T. Motobayashi: "Nuclear Astrophysics Studied by Unstable Nuclear Beams", Ann. Meet. Phys. Soc. Jpn., Tokyo, Apr. (1992)
39) H. Toki: "Pauli-Gursey Symmetry in Mesons and Baryons", German-Eastasia Symp. on Symmetries and Dynamics in Nuclear and Low-Energy Particle Physics, Blaubeuren, Germany, May (1992).
40) K. Yazaki: "Nuclear Transparency in High Energy Collisions", 1st Japanese-Israeli Binational Symp. on Theoretical Physics, Rehovot, Israel, May (1992).
41) H. Suganuma and T. Tatsumi: "Chiral Symmetry Restoration in a Strong Color-Electromagnetic Field and Hadron Structure", RCNP Workshop on Dynamics of Quarks and Hadrons in Nuclei, Ibaraki, June (1992).
42) K. Tanaka and W. Bentz: "Nuclear Matter Properties including Higher Order Quantum Corrections in the Relativistic σ-ω Model", *ibid*.
43) S. Ohta: "Why are Finite-Temperature QCD Phase Transitions So Weak?", RCNP Workshop, Osaka, June (1992).
44) E.A.G. Armour, D.M. Lewis, and S. Hara: "Calculation of the Auger Deexcitation Rate of the dtμ 'Nucleus' of the Muonic Quasi-Molecule [(dtμ) dee]", Int. Workshop on Muon Catalyzed Fusion (μCF-92), Uppsala, Sweden, June (1992).
45) T. Motobayashi: "The $^{13}N(p,\gamma)^{14}O$ Reaction from Coulomb Dissociation", 180th Meet. of Am. Astron. Soc., Columbus, U.S.A., June (1992).
46) H.T. Duong, C. Ekström, M. Gustafsson, T.T. Inamura, P.Juncar, P. Leivens, I. Lindgren, S. Matsuki, T. Murayama, R. Neugart, T. Nilsson, T. Nomura, M. Pellarin, S. Penselin, J. Persson, J. Pinard, I. Ragnarsson, O. Redi, H.H. Stroke, and J.L. Vialle: "Atomic Beam Magnetic Resonance Apparatus for Systematic Study of Bohr - Weisskopf effect at Booster - Isolde", 6th Int. Conf. on Nuclei far from Stability, Bernkastel-Kues, Germany, July (1992).
47) C.-B. Moon, M. Fujimaki, N. Inabe, K. Katori, J.C. Kim, T. Kobayashi, T. Kubo, H. Kumagai, S. Shimoura, T. Suzuki, and I. Tanihata: "Measurements of Angular Distributions for the $^{11}Li+p$ and $^{9}Li+p$ Elastic Scatterings", *ibid*.
48) I. Tanihata, D. Hirata, T. Kobayashi,

and H. Toki: "Disclosure of Thick Neutron Skins", *ibid*.

49) I. Tanihata, D. Hirata, T. Kobayashi, S. Shimoura, K. Sugimoto and H. Toki: "Revealing of Thick Neutron Skins in Nuclei", *ibid*.

50) S. Shimoura, T. Nakamura, M. Ishihara, N. Inabe, T. Kobayashi, T. Kubo, R.H. Siemssen, I. Tanihata, and Y. Watanabe: "El Strength Distribution of ^{11}Li by Invariant Mass Spectroscopy", 6th Int. Conf. on Nuclei far from Stability and 9th Int. Conf. on Atomic Masses and Fundamental Constants, Berenkastel-Kues, Germany, July (1992).

51) J. Chiba, D. Aschery, H. Ito, K. Kimura, Yu T. Kiselev, S. Koda, K. Miyano, T. Murakami, T. Nagae, Y. Nakai, M. Nomachi, S. Sawada, M. Sekimoto, T. Suzuki, K.H. Tanaka, M.K. Vlasov, and Y. Yoshimura: "Enhancement of Subthreshold Antiproton Production in Deuteron Induced Reactions", Int. Nuclear Physics Conf., Wiesbaden, Germany, July (1992).

52) I. Tanihata: "Radioactive Beam Facilities and Their Physics Program", *ibid*.

53) T. Kobayashi: "Nuclear Structure Experiments with ^{11}Li", *ibid*.

54) S. Date: "Ultrarelativistic AA Collision Simulator Based on Multichain Algorithm", XXII Int. Symp. on Multiparticle Dynamics, Santiago de Compostela, Spain, July (1992).

55) M. Fujii *et al*.: "Performance of Medium Energy Isotope Telescope for Geotail High Energy Particle Experiment", Chu-Shikoku Section Meeting Phys. Soc. Jpn., Ehime, July (1992).

56) W.G. Jin, M. Wakasugi, T. Inamura, T. Murayama, T. Wakui, T. Kashiwabara, H. Katsuragawa, T. Ariga, T. Ishizuka, M. Koizumi, and I. Sugai: "Isotope Shift and Hyperfine Structure of Refractory Elements by Laser Spectroscopy with Sputtered Atomic Beams", RIKEN Int. Symp. on Unstable Nuclei and Particles as Probes in Physics and Chemistry, Wako, Aug. (1992).

57) I. Tanihata: "Neutron Halo in Nuclei", *ibid*.

58) I. Tanihata: "Unstable Nuclear Beams for Study of Nuclei far from Stability", 5th Asia Pacific Physics Conf., Kuala Lumpur, Malaysia, Aug. (1992).

59) H. Okuno: "Polarization in Projectile Fragmentation and g-Factor Measurements for Neutron-Rich Nuclei", IXth Int. Conf. on Hyperfine Interactions, Osaka, Aug. (1992).

60) K. Nagata, T. Kashiwagi, J. Kikuchi, T. Doke, K. Itsumi, T. Shino, N. Hasebe, H. Moriya, A. Nakamoto, T. Yanagimachi, H. Murakami, S. Sugino, and T. Kohno: "Energy Loss and its Straggling of High Energy Heavy Ions in Silicon Detector", 1992 Fall Meet. Phys. Soc. Jpn., Tokyo, Sept. (1992).

61) C. Kato, T. Imai, A. Yoneda, K. Munakata and T. Kohno: "On a Probability of Nuclear Fragmentation in Cosmic Ray Silicon Detector Telescope", *ibid*., Niigata, Sept. (1992).

62) Y. Gono, S. Mitarai, A. Odahara, E. Ideguchi, T. Shizuma, N. Kidera, T. Morikawa, Y.H. Zhang, A. Ferragut, K. Morita, A. Yoshida, K. Murakami, M. Ogawa, M. Nakajima, M. Oshima, H. Kusakari, M. Sugawara, B.J. Min, J.C. Kim, and S.J. Chae: "High-Spin Isomer of ^{145}Sm", *ibid*., Oct. (1992).

63) K. Tanaka and W. Bentz: "Equation of State for Nuclear Matter including Higher Orders in a Relativistic Many-Body Theory", *ibid*.

64) N. Ishida, T. Doke, K. Kuwahara, M. Ichige, S. Ben, M. Suzuki, A. Hitachi, K. Masuda: "Efficiency of Light Collection in Liquid Xenon", *ibid*.

65) T. Wakui, T. Ariga, T. Ishizuka, T. Inamura, T. Kashiwabara, H. Katsuragawa, W.G. Jin, M. Koizumi, T. Shinozuka, K. Shimomura, I. Sugai, M. Takami, Y. Tagishi, I. Nakamura, T. Horiguchi, S. Matsuki, T. Murayama, K. Morita, Y. Yano, A. Yoshida, and M. Wakasugi: "Collinear Laser Spectroscopy with Laser - Ablation IGISOL", *ibid*.

66) K. Sumiyoshi, D. Hirata, H. Toki, H. Sagawa: "Comparison of the Relativistic Mean Field Approach with the Skyrme Interaction for Infinite Matter and Nuclei", *ibid*.

67) D. Hirata, I. Tanihata, H. Toki, P. Ring: "Relativistic Mean Field Theory for Deformed Nuclei", *ibid*.

68) S. Yamaji, A.S. Jensen, and H. Hofmann: "Isoscalar Vibrational States in

Kubo, T. Nakagawa, Y. Watanabe, S. Shimoura, and T. Tanihata: "Search for a Pineut", *ibid*.

69) K. Soutome, S. Yamaji, and M. Sano: "Nuclear Dissociation Cross Sections of ^{11}Li", *ibid*.

70) S. Hirenzaki and H. Toki: "Formation of Deeply Bound Pionic Atoms by (d, ^{3}He) Reactions", *ibid*.

71) N. Sakamoto: "The Construction of RIKEN Polarized Ion Source", *ibid*.

72) M. Tohyama: "Comparison between TDDM and VUU", *ibid*.

73) H. Suganuma: "Chiral Solitons without Nonlinear Constraint and Chiral Bag Picture", *ibid*.

74) H. Ueno: "Measurement of ^{21}F Nuclear Moment Using Spin-Polarization in Fragmentation Reaction", *ibid*.

75) S. Yamaji, A.S. Jensen, and H. Hofmann: "Isoscalar Vibrational States in Hot Nuclei", 1st INFN-RIKEN Joint Meet. on Perspective in Heavy Ion Physics, Catania, Italy, Sept. (1992).

76) Y. Gono, T. Morikawa, T. Murakami, A. Ferragut, Y.H. Zhang, K. Morita, A. Yoshida, M. Oshima, H. Kusakari, M. Sugawara, M. Ogawa, M. Nakajima, J.C. Kim, S.J. Chae, B.J. Min, S. Mitarai, A. Odahara, E. Ideguchi, T. Shizuma, and N. Kidera: "Physics on/with Extremely High-Spin Isomers", *ibid*.

77) T. Nakagawa, K. Yuasa-Nakagawa, S.C. Jeong, H. Fujiwara, Y.H. Pu, Y. Futami, B. Heusch, K. Ieki, T. Sugimitsu, T. Matsuse, and S.M. Lee: "Complex Fragment Emission from the Hot Compound Nucleus", *ibid*.

78) S. Shimoura:"Invariant Mass Spectroscopy on Excitation Modes of Neutron Drip Line Nuclei", *ibid*.

79) S. Ohta: "Lattice QCD Numerical Calculations on AP1000", Int. Conf. on Computing in High Energy Physics '92, Annecy, France, Sept. (1992).

80) S. Ohta: "Large Scale Numerical Simulation of the Three-State Potts Model", Int. Conf. on "Lattice '92," Amsterdam, the Netherlands, Sept. (1992).

81) T. Doke, J. Kikuchi, T. Hayashi, T. Kashiwagi, K. Itsumi, T. Shino, T. Ito, N. Hasebe, H. Moriya, K. Fujiki, A. Nakamoto, H. Murakami, T. Yanagimachi, S. Sugino, K. Nagata, and T. Kohno: "Identification of Isotopes by Telescope HEP-MI aboard the Geotail Satellite Using RIKEN Ring Cyclotron Accelerator", *ibid*.

82) Y. Gono, T. Morikawa, T. Murakami, A. Ferragut, Y.H. Zhang, K. Morita, A. Yoshida, M. Oshima, H. Kusakari, M. Sugawara, M. Ogawa, M. Nakajima, J.C. Kim, S.J. Chae, B.J. Min, S. Mitarai, A. Odahara, E. Ideguchi, T. Shizuma, and N. Kidera: "High-Spin Isomers and High-Spin Isomer Beams", 21st INS Int. Symp. on Rapidly Rotating Nuclei 92, Tokyo, Oct. (1992).

83) M. Oshima, H. Kusakari, M. Sugawara, Y. Gono, A. Ferragut, Y.H. Zhang, S. Ichikawa, and T. Inamura: "Double-γ Vibrational State in ^{168}Er", *ibid*.

84) S. Yamaji, H. Hofmann, and A.S. Jensen: "Distribution of Strength for Isoscalar Modes at Finite Temperature", *ibid*.

85) Y. Gono, T. Morikawa, T. Murakami, A. Ferragut, Y.H. Zhang, K. Morita, A. Yoshida, M. Oshima, H. Kusakari, M. Sugawara, M. Ogawa, M. Nakajima, J.C. Kim, S.J. Chae, B.J. Min, S. Mitarai, A. Odahara, E. Ideguchi, T. Shizuma, and N. Kidera: "High-Spin Isomers and High-Spin Isomer Beams", 6th Franco-Japanese Colloquim on Nuclear Structure and Interdisciplinary Topics, Saint-Malo, France, Oct. (1992).

86) T. Motobayashi: "Coulomb Excitation of Unstable Nuclei: Application to Nuclear Astrophysics and Nuclear Spectroscopy", *ibid*.

87) K. Yazaki: "Quark Degress of Freedom in Nuclei", *ibid*.

88) T. Motobayashi: "Coulomb Breakup Measurements for Determination of Astrophysical (p, γ) Reaction Rates", Ann. Fall Meet. Div. Nucl. Phys., Am. Phys. Soc., Santa Fe, U.S.A., Oct. (1992).

89) H. Toki and Y. Sugahara: "Relativistic Equation of State with Strangeness for Neutron Stars", Int. Symp. on Origin and Evolution of the Elements, INS, Tokyo, Oct. (1992).

90) T. Kobayashi: "Momentum Distribution of Projectile Fragments from Neutron-Rich Nuclei", INFN-RIKEN Symp. on Intermediate-Energy Nuclear Physics,

Catania, Italy, Oct. (1992).

91) Y. Gono, T. Morikawa, T. Murakami, A. Ferragut, Y.H. Zhang, K. Morita, A. Yoshida, M. Oshima, H. Kusakari, M. Sugawara, M. Ogawa, M. Nakajima, J.C. Kim, S.J. Chae, B.J. Min, S. Mitarai, A. Odahara, E. Ideguchi, T. Shizuma, and N. Kidera: "High-Spin Isomer Beams", RIKEN Symp. on Nuclear Spectroscopy with Unstable Nuclear Beams, Wako, Nov. (1992).

92) Y. Gono: "High Spin Isomer Beams", *ibid*.

93) I. Tanihata: "Study of Neutron-Drigline Nuclei Using Radioactive Nuclear Beams", 12th Int. Conf. on the Application of Accelerators in Research & Industry, Denton, U.S.A., Nov. (1992).

94) T. Ichihara: "^{12}C (^{12}C, ^{12}N)^{12}B Charge -Exchange Reaction at E/A=135MeV", Japan-China Joint Symp., Tokyo, Nov. (1992).

3. Atomic and solid-state physics

1) K. Kuroki, Y. Yamazaki, K. Komaki, T. Azuma, N. Kakutani, K. Kawatsura, Y. Kanai, T. Kambara, and Y. Awaya: "Observation of Relativistic Electrons in Relativistic Heavy-Ion-Atom Collisions", Int. Conf. Atomic Collisions in Solids, Salford, U.K., July (1991).

2) K. Aono, M. Iwaki, Y. Aoyagi, and S. Namba: "Tb-ion Implantation into CaF_2 III", 52nd Autumn Meet. Jpn. Soc. Appl. Phys., Okayama, Oct. (1991).

3) K. Ando: "The Present State of X-Ray Laser", RIKEN Symp. on Studies of Solid State Physics and Materials, Atomic Processes, Nuclear Chemistry, and Biology and Medical Science by Using RIKEN Ring Cyclotron, Wako, Jan. (1992).

4) R. Kadono: "Anomalous Muonium Centers and Relaxed Excitonic States", *ibid*.

5) I. Shimamura: "Positron-Atom and Positron-Molecule Collisions", ISSP Symp. on Solid State Physics by Monochromatic Slow Positron-Beam, Tokyo, Jan. (1992).

6) T. Kambara: "Atomic Collision Experiments at Heidelberg TSR", Meet. Atomic Physics with Cooler Ring, Tanashi, Feb. (1992).

7) Y. Matsuo, H. Maeda, and M. Takami: "Spectroscopy and Dynamics of Heavy Metallic Ions in an RF Trap", RIKEN Symp. on 14th Laser Science, Wako, Feb. (1992).

8) H. Fukuda and I. Shimamura: "AO-MO Matching for μ-Transfer Reactions", 47th Ann. Meet. Phys. Soc. Jpn., Yokohama, Mar. (1992).

9) I. Shimamura: "Moleculelike Description of Metastable, Highly Excited Antiprotonic Helium", *ibid*.

10) T. Kambara: "Atomic Physics Experiments at RIKEN", *ibid*.

11) T. Nabeshima, N. Nakamura, Y. Kanai, S. Ohtani, S. Kitazawa, M. Nagata, T. Takayanagi, K. Wakiya, H. Suzuki, T. Kambara, and Y. Awaya: "Ejected Electron Spectra from Triplet States of $O^{4+}(1s^2nln'l')$ Produced by $O^{6+} + O_2$ Collision", *ibid*.

12) Y. Zou, Y. Awaya, T. Kambara, Y. Kanai, M. Ohura, K. Ando, A. Hitachi, and S.D. Kravis: "Foil Target Element and Incident Energy Dependence of Multiple Inner-shell Vacancy Production of Projectile Ar Ions", *ibid*.

13) Y. Yamazaki, K. Komaki, T. Azuma, K. Kuroki, K. Kawatsura, Y. Kanai, T. Kambara, M. Ohura, and Y. Awaya: "High Energy Electron Production in Relativistic Heavy Ion Atom Collision II", *ibid*.

14) K. Ando, Y. Zou, Y. Awaya, T. Kambara, M. Ohura, T. Tonuma, and S. Tsurubuchi: "Lifetimes of Ne-Like Cr Ion Measured by Beamfoil Spectroscopy", *ibid*.

15) J. Mitani, I. Hashimoto, H. Yamaguchi, E. Yagi, and M. Iwaki: "Annealing Effect on Kr Bubbles in Kr-Implanted Aluminium", *ibid*.

16) E. Yagi: "Kr Bubbles in Aluminium", *ibid*.

17) S. Sakamoto, K. Ishida, T. Matsuzaki, K. Nagamine, P. Strasser, and Y. Watanabe: "Muon Transfer Reactions in Liquid Deuterium with Helium Impurity III", *ibid*.

18) Y. Matsuo, H. Maeda, and M. Takami: "RF Trap of Heavy Metallic Ions from Laser-Produced-Plasma II", *ibid*.

19) K. Ando, Y. Zou, Y. Awaya, T. Kambara, M. Oura, T. Tonuma, and S. Tsurubuchi: "Lifetimes of Ne-like Cr Ion Measured by Beam-Foil Spectros-

copy", *ibid*.
20) R. Kadono, A. Matsushita, K. Nishiyama, and K. Nagamine: "Muonium Fluorescence: Anomalous Muonium Centers and Relaxed Excited States in KBr", *ibid*.
21) Y. Awaya and M. Kimura: "Research and Development for Experiments at SPring-8", SPring-8 Workshop on Atom. Phys. at High Brilliance Synchrotron Radiation Facilities (11th RIKEN Symp.), Himeji, Mar. (1992).
22) S.D. Kravis: "Atomic Physics Experiments with an EBIS and Synchrotron Radiation", *ibid*.
23) K. Aono, M. Kumagai, M. Iwaki, and Y. Aoyagi: "Tb-ion Implantation into CaF_2 IV", 39th Spring Meet., Jpn. Soc. Appl. Phys. Related Soc., Narashino, Mar. (1992).
24) E. Yagi: "Behaviour of Kr Atoms Implanted into Aluminium", RIKEN Symp. on Relation between Ion Beams and Surface Layer and Interface, Wako, Mar. (1992).
25) T. Kambara, Y. Awaya, Y. Kanai, and A. Hitachi: "Multiple Inner-Shell Ionization of Target Atoms by High-Energy Heavy-Ion Impact", 2nd Int. Symp. on Swift Heavy Ions in Matter, Bensheim, Germany, May (1992).
26) Y. Zou, Y. Awaya, T. Kambara, Y. Kanai, M. Oura, K. Ando, A. Hitachi, and S. Kravis: "Foil Target Element and Incident Energy Dependence of Multiple Inner-Shell Vacancy Production of Projectile Ar Ions", *ibid*.
27) Y. Yamazaki, K. Kuroki, H. Knudsen, K. Komaki, T. Azuma, K. Kawatsura, Y. Kanai, T. Kambara, M. Oura, and Y. Awaya: "Relativistic Electron Emission in Ion-Atom Collisions", *ibid*.
28) R. Kadono: "Muon Diffusion in Dissipative Systems", Int. Symp. on Metal-Hydrogen Systems, Fundamentals and Applications, Uppsala, Sweden, June (1992).
29) M.R. Harston, I. Shimamura, and M. Kamimura: "Energy Shift in the dtμdee Molecular Hybrid due to the Finite Size of the Muonic Molecular Ion dtμ", Int. Workshop on Muon Catalyzed Fusion (μCF-92), Uppsala, Sweden, June (1992).
30) K. Ishida, T. Matsuzaki, Y. Watanabe, S. Sakamoto, K. Nagamine, and P. Strasser: "X-ray Studies of Muon Transfer Reactions from Hydrogen to Helium", *ibid*.
31) P. Strasser, K. Ishida, S. Sakamoto, M. Iwasaki, E. Torikai, K. Nagamine, and G.M. Marshall: "Towards Slow μ^- Production via Muon Catalyzed Fusion", *ibid*.
32) K. Nagamine: "X-Ray Studies of Muon-alpha Sticking and Muon Transfer in Muon Catalyzed Fusion", *ibid*.
33) K. Nagamine: "Slow and Monoenergetic ($^3He\mu^-$) Beam Production and Novel Applications", *ibid*.
34) K. Nagamine: "Future μCF Program with Pulsed Muons at RIKEN-RAL and at UTMSL-KEK", *ibid*.
35) M. Oura, T. Kambara, Y. Kanai, S. Kravis, Y. Zou, J. Pálinkás, and Y. Awaya: "Study of Radiative Electron Rearrangement (RER) Processes", 17th Meet. Soc. for Atomic Colli. Res., Wako, Aug. (1992).
36) Y. Zou, Y. Awaya, T. Kambara, Y. Kanai, M. Oura, K. Ando, Y. Nakai, A. Hitachi, and S. Kravis: "Study of Inner-Shell Vacancy Production of Ar Projectile in Collision with Foil Target", *ibid*.
37) S. Kravis, K. Okuno, H. Saitoh, K. Soejima, Y. Kaneko, M. Oura, and Y. Awaya: "New Results for Single and Double Charge Transfer Cross Sections in $Ar^{q+} + H_2$ Collisions at Low Energies for $6 \leq q \leq 8$", *ibid*.
38) A. Matsushita, R. Kadono, K. Nishiyama, Y. Miyake, A. Nakao, J. Takahashi, M. Iwaki, and K. Nagamine: "Muonium Emission and Reaction on the Platinum and Gold Powder Surfaces Revealed by MuSR", 9th Int. Conf. Hyperfine Interactions, Toyonaka, Aug. (1992).
39) R. Kadono, A. Matsushita, K. Nishiyama, and K. Nagamine: "Relaxed Excited States and Anomalous Hyperfine Structure of Muonium Centers in KBr", *ibid*.
40) T. Okada, K. Asai, N. Yamada, Y. Yamada, T. Matsumoto, and Y. Kodama: "^{57}Fe Mössbauer Studies of $YBa_2(Cu_{1-x}Fe_x)_4O_8$", 3rd Int. Symp. on the Industrial Applications of the Mössbauer Effect, Otsu, Aug. (1992).
41) E. Yagi: "Channelling Study on the

Lattice Location of Hydrogen in Metals by a Nuclear Reaction-Channelling Method", RIKEN Int. Symp. on Unstable Nuclei and Particles as Probes in Phys. and Chem., Wako, Aug. (1992).

42) T. Okada, K. Asai, N. Yamada, T. Matsumoto, Y. Yamada, and Y. Kodama: "^{57}Fe Mössbauer Fraction of $YBa_2(Cu_{1-x}Fe_x)_4O_8$", *ibid*., Sept. (1992).

43) Y. Kanai: "Doubly-Excited States of He-Like and Be-Like Ions in Highly Charged Ions", 6th Int. Conf. on the Physics of Highly Charged Ions, Manhattan, U.S.A., Sept. (1992).

44) Y. Kanai, T. Kambara, M. Oura, Y. Zou, S. Kravis, and Y. Awaya: "Binary Encounter Peaks for 0° Electrons in Collisions of 0.8MeV/amu Bi^{q+} with H_2 and He", *ibid*.

45) M. Oura, T. Kambara, Y. Kanai, S. Kravis, Y. Zou, J. Pálinkás, and Y. Awaya: "Measurement of RER X Rays from 0.8MeV/u Ar Ions Passing through Target Foil", *ibid*.

46) S. Kravis, K. Okuno, H. Saitoh, K. Soejima, Y. Kaneko, M. Oura, and Y. Awaya: "Single and Double Charge Exchange Cross Sections for $Ar^{q+} + H_2$ (q=6, 7, and 8) from 8eV to 8keV", *ibid*.

47) S. Kravis, K. Okuno, T. Kojima, M. Kimura, S. Ohtani, T. Kambara, Y. Kanai, and Y. Awaya: "An EBIS for Use with Synchrotron Radiation (Photoionization of Highly Charged Ions)", *ibid*.

48) N. Nakamura, T. Negishi, Y. Kanai, S. Ohtani, S. Kitazawa, M. Nagata, T. Takayanagi, K. Wakiya, H. Suzuki, T. Kambara, and Y. Awaya: "Ejected Electron Spectra from Quartet States of $N^{4+**}(1s3l3l')$ Produced by $N^{6+} + O_2$ Collisions", 1992 Fall Meet. Phys. Soc. Jpn., Tokyo, Sept. (1992).

49) T. Yoshida and I. Shimamura: "Highly Excited States of Antiprotonic Neon", *ibid*.

50) I. Shimamura: "Scaling of the Cross Sections for Molecular Vibrational Transitions by Electron Impact", *ibid*.

51) Y. Matsuo, H. Maeda, and M. Takami: "Heavy Metallic Ions in an RF Trap: Reaction with Molecules and Spectroscopy", *ibid*.

52) T. Okada, K. Asai, N. Yamada, T. Matsumoto, Y. Yamada, and Y. Kodama: "Mössbauer Fraction of $YBa_2(Cu_{1-x}Fe_x)_4O_8$", *ibid*.

53) E. Yagi and S. Koike: "Lattice Location of Hydrogen in Nb-Mo Alloys", *ibid*.

54) M. Takami and Y. Matsuo: "Spectroscopy and Chemical Reactions of Heavy Metallic Ions in an RF Trap", 1992 Symp. on Molecular Science, Kyoto, Sept. (1992).

55) K. Aono, M. Kumagai, M. Iwaki, Y. Aoyagi, and S. Namba: "Radiation Damage in Tb-implanted CaF_2 Observed by the Channeling Method and Luminescence IBMM '92", Heidelberg, Germany, Sept. (1992).

56) E. Yagi: "Solid Krypton Precipitates in Kr-Implanted Aluminium", Int. Conf. on Diffusion in Mater., Kyoto, Sept. (1992).

57) R. Kadono: "Muon Diffusion in Solids", *ibid*.

58) I. Shimamura: "The Theory of Extraordinarily Long-lived Antiprotonic Helium", Symp. on the Dynamic Processes Involving Exotic Atoms, Wako, Sept. (1992).

59) Y. Yamazaki, K. Komaki, M. Sataka, M. Imai, Y. Kanai, K. Kawatsura, H. Tawara, and D.R. Schultz: "Electron Emission in Energetic Heavy Ion-Atom Collisions", 4th China-Japan Seminar and 1st East Asian Int. Seminar on Atomic and Molecular Physics, Tokyo, Oct. (1992).

60) Y. Awaya, T. Kambara, and Y. Kanai: "Multiple Inner-Shell Ionization in Heavy Ion-Atom Collisions", *ibid*.

61) I. Shimamura: "Moleculelike Metastable States of Antiprotonic Helium", *ibid*.

62) H. Shibata, T. Tonuma, T. Matsuo, H. Kumagai, and H. Tawara: "Multiply Charged Ions from Gaseous and Frozen SF_6 and CF_4 Produced by Energetic Heavy Ion Impact", 6th Int. Conf. on the Physics of Highly Charged Ions, Kansas, U.S.A., Oct. (1992).

63) H. Tawara, T. Tonuma, H. Kumagai, and T. Matsuo: "Multiple Ionization: Comparison between Gas and Condensed Matter", Joint Int. Seminar on Atomic and Molecular Physics, Tokyo, Oct. (1992).

4. Radiochemistry, radiation chemistry, and radiation biology

1) J. Kurachi, E. Taniguchi, A. Shinohara, M. Furukawa, S. Kojima, Y. Ohkubo, F. Ambe, K. Takesako, T. Saito, and S. Shibata: "Nuclear Reaction Products in the Interaction of ^{197}Au with Intermediate Energy Heavy Ions", 63rd Natl. Meet. Chem. Soc. Jpn. (Spring), Osaka, Mar. (1992).
2) K. Takesako, T. Saito, H. Kusawake, S. Watanabe, K. Goto, A. Yokoyama, H. Baba, Y. Ohkubo, A. Shinohara, and M. Furukawa: "Target Fragmentation of ^{141}Pr and ^{165}Ho Induced by ^{14}N, ^{15}N, and ^{40}Ar Projectiles", *ibid*.
3) J. Kurachi, E. Taniguchi, A. Shinohara, M. Furukawa, S. Kojima, Y. Ohkubo, F. Ambe, K. Takesako, T. Saito, and S. Shibata: "Nuclear Reaction Products in the Interactions of ^{197}Au with Intermediate Energy Heavy Ions", *ibid*.
4) N. Ohmori, A. Kimura, A. Ejiri, K. Kimura, and K. Nakagawa: "Electron-ion Recombination in Photoionization of Anthracene Doped in Non-polar Solvents", Spring Meet. Phys. Soc. Jpn., Hiyoshi, Mar. (1992).
5) K. Nakagawa, A. Ejiri, K. Kimura, K. Tanaka, A. Kimura, N. Ohmori, and D. Nurdiawati: "Origin of Structure of Photocurrent Spectrum of Anthracene Doped in Non-Polar Solvents", *ibid*.
6) K. Ando, S. Koike, C.K. Cho, and T. Kanai: "Mouse Skin Damage after Carbon Irradiation", 31st Ann. Meet. Radiation Biology Division of Jpn. Radiol. Soc., Yokohama, Apr. (1992).
7) S. Koike, K. Ando, T. Kanai, and M. Kimoto: "Therapeutic Effectiveness of Carbon Spread-Out-Bragg-Peak", *ibid*.
8) K. Kimura: "Track-depth Resolved Dynamics of Helium Excimers in 4 MeV/amu N-ion Tracks in Near-Liquid and Liquid Helium", Int. Conf. Liquid Radiat. Detector, Tokyo, Apr. (1992).
9) K. Kimura: "Lifetime Shortening and Quenching of the Excitons of a BaF_2 Single Crystal Created by Heavy-Ion Induced High Density Excitation", 2nd Int. Symp. on Swift Heavy Ions in Matt., Bensheim, Germany, May (1992).
10) K. Kimura: "Excited State Dynamics Resolved along the Depth of Ion Tracks in Dense Rare Gases", *ibid*.
11) S. Ambe, Y. Ohkubo, M. Iwamoto, Y. Kobayashi, and F. Ambe: "Preparation of Radioactive Multitracer Solutions from a High-Energy Heavy-Ion Irradiated Au Target by Means of a Supported Liquid Membrane", 53rd Symp. on Anal. Chem., Akita, May (1992).
12) F. Yatagai, S. Hachiya, Y. Hama, A. J.E. Gordon, M. Izumi, H. Miyazawa, S. Harakawa, and F. Hanaoka: "Resolution and Characterization of Polymorphic DNA by SSCP and Chemical Cleavage Methodologies", Gordon Res. Conf. (Mutagenesis), Plymouth, U.S.A., June (1992).
13) K. Ando and H. Tatsuzaki: "Volume Effect: from a Radio-biological Point of View", 22nd Symp. on Cancer Control, Sapporo, June (1992).
14) K. Kimura: "Lifetime Shortening and Quenching of the Excitons of a BaF_2 Single Crystal Created by Heavy-Ion Induced High Density Excitation", Gordon Conf., Newport, U.S.A., July (1992).
15) K. Kimura: "Excited State Dynamics Resolved along the Depth of Ion Tracks in Dense Rare Gases", *ibid*.
16) T. Takahashi, M. Suzuki, F. Yatagai, and K. Izumo: "Calculation and a Preliminary Experiment on the Energy Deposition around the Path of an Ion", 29th Ann. Meet. Radioisotopes in the Physical Sciences and Industries, Tokyo, July (1992).
17) S. Ambe, Y. Ohkubo, M. Iwamoto, Y. Kobayashi, M. Yanokura, and F. Ambe: "Preparation of Multitracers and Their Application to a Study on Plant", *ibid*.
18) K. Nakagawa, A. Ejiri, K. Kimura, K. Tanaka, D. Nurdiawati, N. Ohmori, and A. Kimura: "Density Dependence of Structures in Photocurrent and Optical Absorption Spectra of Anthracene Doped in Supercritical Xenon Fluids", 10th Int. Conf. VUV Radiat. Phys., Paris, France, July (1992).
19) Y. Itoh, H. Murakami, and A. Kinoshita: "Positron Annihilation Study on Nanometer Cavities in Porous Silicon", RIKEN Int. Symp. on Unstable Nuclei and Particles as Probes in Physics and

Chemistry, Wako, Aug. (1992).

20) Y. Itoh and H. Murakami: "Recovery and Clustering of Defects in GaAs Studied by Means of Positron Annihilation", *ibid*.

21) Y. Ohkubo, Y. Kobayashi, K. Harasawa, S. Ambe, T. Okada, K. Asai, S. Shibata, M.Takeda, and F. Ambe: "Time-Differential γ-Ray Perturbed-Angular-Correlation (TDPAC) and Emission Mössbauer Spectroscopy of ^{99}Ru in $YBa_2Cu_3O_{7-x}$ Using ^{99}Rh as a Source Nuclide", *ibid*.

22) H. Ueno, H. Okuno, K. Asahi, H. Sato, M. Adachi, T. Kubo, T. Nakamura, N. Inabe, A. Yoshida, Y. Ohkubo, T. Ichihara, M. Ishihara, T. Shimoda, H. Miyatake, N. Takahashi, and W.-D. Schmidt-Ott: "Spin-Polarized Radioactive Beams and β-NMR Experiments", *ibid*.

23) Y. Kobayashi, K. Asai, T. Okada, and F. Ambe: "Mössbauer and Magnetization Studies on Ferromagnet $Fe_{3-x}Ru_xSi$", *ibid*.

24) K. Ando, K. Koike, K. Fukutsu, M. Kimoto, M. Iizuka, T. Kiuchi, T. Aruga, W. Shimizu, T. Sugita, C.K. Cho, T. Kanai, S. Furukawa, H. Kato, S. Matsushita, Y. Furusawa, and F. Yatagai: "Effects of Accelerated Carbon Ions on Normal Tissues and Tumors in Experimental Animals", 2nd Workshop of Heavy Ion Research, Chiba, Aug. (1992).

25) Y. Ohkubo, Y. Kobayashi, K. Asai, T. Okada, and F. Ambe: "TDPAC and Emission Mössbauer Studies of Fe_3O_4 (^{99}Ru)", 9th Int. Conf. on Hyperfine Interact., Toyonaka, Aug. (1992).

26) K. Ogura, M. Matusima, Y. Yamada, T. Takahashi, F. Yatagai, H. Ohnishi, T. Kasuya, T. Doke, K. Kuwahara, and S. Nagaoka: "Determination of High LET Cosmic Particles, Trajectories for Space Radiobiological Studies", 16th Int. Conf. on Nuclear Tracks in Solids, Beijin, China, Sept. (1992).

27) K. Ogura, T. Naito, K. Nakano, and T. Takahashi: "Application of the Pre-Soaking Effects to the Production of CR-39 Microfilters", *ibid*.

28) K. Kimura, K. Morita, R. Nemoto, and S. Nakamura: "Depth-resolved Dynamics of VUV Luminescence in Ion Tracks in Dense Helium Gase", 1992 Fall Meet. Phys. Soc. Jpn., Tokyo, Sept. (1992)

29) K. Kimura, K. Morita, R. Nemoto, S. Nakamura, and H. Kumagai: "Mechanism of Lifetime Shortening of Auger-free Luminescence from Ion-Irradiated BaF_2", *ibid*.

30) Y. Ohkubo, Y. Kobayashi, K. Asai, T. Okada, and F. Ambe: "TDPAC and Emission Mössbauer Studies of Fe_3O_4 (^{99}Ru)", *ibid*.

31) Y. Itoh, H. Murakami, and A. Kinoshita: "Positron Annihilation Study on Nanometer Cabities in Porous Silicon", 53th Fall Meet. Jpn. Soc. Appl. Phys., Osaka, Sept. (1992).

32) Y. Ohkubo, Y. Kobayashi, S. Ambe, T. Okada, F. Ambe, K. Harasawa, M. Takeda, K. Asai, and S. Shibata: "TDPAC and Emission Mössbauer Studies on ^{99}Ru Arising from ^{99}Rh in $YBa_2Cu_3O_{7-x}$", 36th Symp. on Radiochemistry, Hachioji, Oct. (1992).

33) M. Iwamoto, S. Ambe, Y. Ohkubo, Y. Kobayashi, M. Yanokura, H. Maeda, and F. Ambe: "Separation of Multitracer by Heating under Reduced Pressure", *ibid*.

34) S. Ambe, Y. Ohkubo, M. Iwamoto, Y. Kobayashi, M. Yanokura, H. Maeda, F. Ambe, S. Shibata, T. Yaita, F. Bamba, H. Harakawa, H. Saito, and K. Kimura: "Study on the Ion Exchange Adsorption of Various Elements on Superacid Resin NAFION Using a Multitracer", *ibid*.

35) Y. Minai, Y. Takahashi, M.K. Kubo, S. Toyoda, M. Ishibashi, S. Ambe, Y. Kobayashi, Y. Ohkubo, M. Iwamoto, M. Yanokura, H. Maeda, S. Shibata, N. Takematsu, F. Ambe, and T. Tominaga: "Multitracer Study on Complex Formation of Humic Acid", *ibid*.

36) S. Ambe, S. Tanaka, Y. Kobayashi, Y. Ohkubo, M. Iwamoto, H. Maeda, M. Yanokura, and F. Ambe: "Study of Selective Transport of Metal-Ions by Means of a Supported Liquid Membrane Using a Multitracer (I)", *ibid*.

37) S. Tanaka, S. Ambe, Y. Kobayashi, Y. Ohkubo, M. Iwamoto, H. Maeda, M. Yanokura, and F. Ambe: "Study of Selective Transport of Metal-Ions by Means of a Supported Liquid Membrane Using a Multitracer (II)", *ibid*.

38) S. Shibata, K. Watari, Y. Noda, S. Ambe, Y. Ohkubo, M. Iwamoto, Y. Kobayashi, M. Yanokura, H. Maeda, and F. Ambe: "Study on the Adsorption Behavior of Various Elements in Chloride Solutions on a MR Type Resin and an Activated Carbon Fiber Using a Multitracer", *ibid*.
39) S. Watanabe, K. Takesako, T. Saito, H. Baba, Y. Ohkubo, A. Shinohara, E. Taniguchi, and M. Furukawa: "Symmetric Mass Division in the Ir-Composite System", *ibid*.
40) M. Kiriu, T. Saito, A. Yokoyama, H. Baba, E. Taniguchi, and Y. Ohkubo: "Investigation of the 7MeV/nucleon ^{58}Ni-Induced Reaction on Cu and Rh Targets", *ibid*.
41) J. Kurachi, E. Taniguchi, A. Shinohara, M. Furukawa, S. Kojima, Y. Ohkubo, F. Ambe, K. Takesako, T. Saito, and S. Shibata: "Nuclear Reaction Products in the Interactions of ^{197}Au and Intermediate Energy Heavy Ions ^{14}N, ^{15}N, and ^{40}Ar", *ibid*.
42) E. Taniguchi, J. Kurachi, A. Shinohara, M. Furukawa, S. Kojima, Y. Ohkubo, F. Ambe, K. Takesako, T. Saito, and S. Shibata: "Nuclear Reactions with Intermediate Energy Heavy Ions on V, Cu, Nb, and I-The Dependence on Projectiles and Targets-", *ibid*.
43) K. Takesako, T. Saito, H. Kusawake, A. Yokoyama, H. Bamba, Y. Ohkubo, A. Shinohara, and M. Furukawa: "Target Fragmentation of ^{145}Pr and ^{165}Ho Induced by Heavy Projectiles", *ibid*.
44) Y. Kobayashi, T. Okada, F. Ambe, and K. Asai: "Magnetization and Mössbauer Effect Studies of $Fe_{3-x}Ru_xSi$", *ibid*.
45) K. Ida, Y. Itoh, A. Kinosita, and H. Murakami: "The Study on Porous Silicon by Means of Positron Annihilation", *ibid*.
46) K. Fukutsu, T. Kanai, S. Koike, C.K. Cho, T. Aruga, Y. Furusawa, and K. Ando: "Response of Crypt Cell Surivals of Mouse Intestine after Single Doses of Accelerated Carbon-Ion with Spread-Out Bragg Peak", 35th Ann. Meet. Jpn. Radiat. Res. Soc., Ohtsu, Oct. (1992).
47) T. Takatsuji, H. Okumura, T. Takahashi, F. Yatagai, and T. Kanai: "Effect of Spatial Distribution of Absorbed Energy to the Chromosome Aberration", *ibid*.
48) K. Ijiri, T. Takahashi, and T. Kanai: "Effects of Carbon, Nitrogen, and Argon Ions on the Development of Fish Embrios", *ibid*.
49) F. Yatagai, K. Nakano, H. Ikehata, K. Eguchi, T. Kanai, and F. Hanaoka; "Understanding of Heavy-Ion Induced Biological Damages: Approach from Radiation Sensitivities of Mammalian Cells", *ibid*.
50) M. Suzuki, M. Watanabe, K. Nakano, K. Suzuki, T. Kanai, and F. Yatagai: "Biological Effects in Normal Human Cells Induced by Accelerated Carbon Ions", *ibid*.
51) K. Kimura, K. Morita, R. Nemoto, S. Nakamura, and H. Kumagai: "Effect of High-Density Excitation to Augerfree Luminescence of Ion-Irradiated BaF_2", 35th Conf. Radiat. Chem., Takasaki, Oct. (1992).
52) K. Kimura: "Study on Depth-Resolved Track Structure: Correlation between UV-and VUV-Luminescences from Ion-Irradiated near Liquid Helium", *ibid*.
53) K. Ushida, A. Kira, K. Kimura, H. Shibata, S. Tagawa, and Y. Yoshida: "γ- Radiolysis of Ceramics as a Radiation Monitor", *ibid*.
54) K. Nakagawa, A. Ejiri, K. Kimura, K. Tanaka, A. Kimura, N. Ohmori, and D. Nurdiawati: "Origin of Structure of Photocurrent Spectrum of Anthracene Doped in Non-Polar Solvents", *ibid*.
55) H. Murakami, Y. Itoh, and A. Kinoshita: "Positron Annihilation on Porous Silicon", 47th Ann. Meet. Phys. Soc. Jpn., Tokyo, Oct. (1992).
56) Y. Ohnishi, A. Moriguchi, T. Takahashi, and F. Yatagai: "Effects of HZE Particles on *B. subtilis* Spores", 6th Ann. Meet. Jpn. Soc. Biol. Sci. Space, Sendai, Oct. (1992).
57) K. Ando, T. Kanai, S. Koike, Y. Furusawa, K. Kasai, H. Itsukaichi, H. Ohara, S. Furukawa, C.K. Cho, M. Kimoto, M. Iizuka, T. Kiuchi, W. Shimizu, T. Sugita, T. Aruga, N. Hori, and F. Yatagai: "Biological Effectiveness of Particle Beams on Cells and Tissues", 3rd Symp. on Beams Engineering of Advanced Material

Syntheses (BEAMS 1992), Tokyo, Nov. (1992).

58) S. Ambe, S. Tanaka, Y. Kobayashi, Y. Ohkubo, M. Iwamoto, H. Maeda, M. Yanokura, and F. Ambe: "Study of Selective Transport of Metal-Ions by Means of a Supported Liquid Membrane Using a Multitracer", Symp. on Membrane, Kyoto, Nov. (1992).

59) S. Shibata, K. Watari, Y. Noda, S. Ambe, Y. Ohkubo, M. Iwamoto, Y. Kobayashi, N. Takematsu, M. Yanokura, H. Maeda, and F. Ambe: "Application of Radioactive Multitracers to Studies on Adsorption Behavior of Inorganic Elements on Solids from Solution", 6th General Meet. Jpn. Soc. Adsorption, Utsunomiya, Nov. (1992).

5. Material analysis

1) M. Suzuki and T. Takahashi: "Proportional Scintillation Imaging Chamber and Its Application", 39th Spring Meet. Jpn. Soc. Appl. Phys., Funabashi, Mar. (1992).

2) E. Uda, J. Kawai, and M. Uda: "Calculation of $K\beta$ X-Ray Spectra of Sulfur Compounds by DV-$X\alpha$ Molecular Orbital Method", 63th Natl. Meet. Chem. Soc. Jpn. (Spring), Osaka, Mar. (1992).

3) S. Kubota, M. Hishida, M. Suzuki, and J. Ruan(Gen): "Light Output and Collected Charge in Xenon-doped Liquid Argon", Int. Conf. on Liquid Radiation Detectors, Tokyo, Apr. (1992).

4) S. Kubota, M. Hishida, M. Suzuki, and J. Ruan(Gen): "The Suppression of the Slow Component in Xenon-doped Liquid Argon Scintillation", *ibid*.

5) K. Maeda, Y. Sasa, M. Takami, and M. Uda: "Determination of the Surface Angle of a Non-flat Target from the L/K X-Ray Yield Ratio for Quantitative PIXE Analysis", 3rd Int. Conf. on Nuclear Microprobe Technology and Applications, Uppsala, Sweden, June (1992).

6) J. Kawai, K. Maeda, and T. Yamane: "High Resolution PIXE Using Imaging Plate as a Position Sensitive Detector", 6th Int. Conf on Particle Induced X-Ray Emission and its Analytical Applications, Tokyo, July (1992).

7) E. Uda, J. Kawai, and M. Uda: "Calculation of Sulfur $K\beta$ Spectra", *ibid*.

8) T. Hanada, M. Mogi, J. Kawai, K. Maeda, Y. Sasa, and M. Uda: "Intensity Analysis of Nickel $L\alpha$ Spectra Measured by a High-Resolution Spectrometer for PIXE", *ibid*.

9) K. Ishii, K. Maeda, M. Takami, Y. Sasa, M. Uda and S. Morita: "Continuous Background in Heavy Ion PIXE", *ibid*.

10) Y. Nishide, E. Hayashi, K. Maeda, Y. Sasa, and M. Uda: "PIXE Analysis of Calcified Tissues by Use of a Combined X-Ray Absorber", *ibid*.

11) K.I. Yoshida, H. Kusuyama, K. Maeda, Y. Sasa, and M. Uda: "PIXE Analysis of Human Spermatozoa: Comparative Studies of Composition of Spermatozoa from Different Degrees of Fertilizing Potential", *ibid*.

12) K. Suzuki, K. Maeda, Y. Sasa, A. Okada, K. Sakamoto, and T. Ozawa: "Application of PIXE Analysis to Source Indentification of KOSA Aerozol", *ibid*.

13) T. Isomura, K. Maeda, J. Kawai, M. Kobayashi, M. Takami, and M. Uda: "Materials Characterization by High Resolution PIXE", *ibid*.

14) K. Maeda, Y. Sasa, and M. Uda: "Effective Use of In-Air PIXE Analysis", *ibid*.

15) T. Tsunokami, Y. Sasa, R. Murai, K. Maeda, I. Harigai, Y. Nakayama, S. Yoshimura, T. Kikuchi, K. Sakurai, and M. Uda: "Quantitative Analysis of Ancient Egyptian Pigments by External PIXE", *ibid*.

16) S. Adachi, K. Takemoto, Y. Sasa, and K. Maeda: "Fate of Inhaled Airborne Particles -PIXE for Hilar Gland and AAS for Lung Tissue", Int. Symp. on Bio-PIXE, Sendai, July (1992).

17) K. Kakihara, S. Gohhara, T. Nishijima, S. Itoh, K. Maeda, and Y. Sasa: "Metal Analysis of Liver Tissue by PIXE in Patients with Liver Diseases", *ibid*.

18) M. Suzuki and T. Takahashi: "Track Structure of Ionizing Radiation Observed by Proportional Scintillation Imaging Chamber", 1992 Fall Meet. Phys. Soc. Jpn., Tokyo, Sept. (1992).

19) J. Kawai, E. Uda, and M. Uda: "DV-$X\alpha$ Calculation of X-Ray Fluorescence Spectra of the Third Period Elements", 2nd Int. Conf. on Computer Applica-

tions to Materials and Molecular Science and Engineering, Yokohama, Sept. (1992).
20) M. Aratani, M. Yanokura, K. Tazaki, and K. Kaiho: "Profiling of Heavy Elements in Clay Mineral Samples", 36th Symp. on Radiochemistry, Hachioji, Oct. (1992).
21) I. Sugai, M. Oyaizu, M. Aratani, and M. Yanokura: "Total Characterization of Self-Supporting Foils", *ibid*.
22) M. Yanokura, M. Aratani, and A. Okada: "Nondestructive Analysis for Hydrogen/Deuterium Ratio Using ERD and NR Methods", *ibid*.
23) K. Kanazawa, M. Yanokura, and M. Aratani: "Quantitative Measurement of Light Elements on the Surface of Vacuum Chamber Materials for Electron Storage Rings", *ibid*.
24) T. Hanasaka, K. Watanabe, S. Yokouchi, Y. Niioka, and S.H. Be: "Outgassing Rate Measurement of BeCu and Alumina Sample", 32th Vacuum Symp. Jpn. (Sponsored by the Vacuum Society of Japan), Osaka, Oct. (1992).
25) K. Maeda and J. Kawai: "Interfering Line in Energy-Dispersive X-Ray Spectrometry: Radiative Auger Peak", 28th Meet. for X-Ray Chem. Anal. Jpn., Tokyo, Nov. (1992).
26) J. Kawai, K. Maeda, and T. Yamane: "Imaging Plate X-Ray Emission Spectrometer", *ibid*.

X. LIST OF SYMPOSIA

X. LIST OF SYMPOSIA

(Jan. — Dec. 1992)

1) Studies of Condensed Matter Physics, Atomic Physics, Nuclear Chemistry, and Bio-Medical Science with the RIKEN Ring Cyclotron.
14 Jan. , Wako RIKEN, Metal Physics Lab.

2) Physics of High-Energy Heavy-Ion Collisions
23 Jan., Wako RIKEN, Cyclotron Lab.

3) Nuclear Physics at Intermediate Energy
24 Jan., Wako RIKEN, Linac Lab.

4) Nuclear Structure Studies using Radioactive Nuclear Beams
27 Jan., Wako RIKEN, Linac Lab.

5) Fusion Reaction and Fissions
28 Jan., Wako RIKEN, Cyclotron Lab.

6) Nuclear Physics with Radioactive Beam
29 Jan., Wako RIKEN, Radiation Lab.

7) Dinosaur Research in RIKEN
11 May, Wako RIKEN, Nuclear Chemistry Lab., Association of Vertebrate Paleontologists in Japan

8) Unstable Nuclei and Particles as Probes in Physics and Chemistry (UN3PC 92)
31 Aug. – 2 Sept., Wako RIKEN, Nuclear Chemistry Lab., The Chemical Society of Japan, The Japan Society for Analytical Chemistry, The Japan Society of Applied Physics, The Physical Society of Japan

9) Perspectives in Heavy Ion Physics (First Joint Italian-Japanese Meeting)
28 Sept. – 2 Oct., Catania, Italy, Accelerator Research Facility, Institute National Fisica Nuclear (INFN)

10) Nuclear Spectroscopy with Radioactive Beam
2, 3 Nov., Wako RIKEN, Radiation Lab.

11) Muon Science 1992
9 Dec., Wako RIKEN, Metal Physics Lab.

XI. LIST OF SEMINARS

XI. LIST OF SEMINARS

(Jan.-Dec. 1992)

Radiation Lab., Cyclotron Lab., and Linear Accelerator Lab.

1) H. Toki, Tokyo Metropolitan Univ. (Tokyo), 20 Jan.
"Scale Invariant Nambu and Jona-Lasinio Model for Hadrons"

2) N. Starkov, Lebedev Physical Institute, Moscow (Russia), 5 Feb.
"The Properties and the Formation Probabilities of Charmed Nuclei"

3) K. Sumiyoshi, Tokyo Metropolitan Univ. (Tokyo), 26 Feb.
"Neutron Star, Hot Neutron Star and Supernova with Equation of State in Relativistic Field Theory"

4) A. Kudryavtsev, ITEP, Moscow (Russia), 11 Mar.
"Krell-Zel'dovich Phenomena in Particle and Nuclear Physics"

5) P. Kienle, GSI, Darmstadt (Germany), 16 Mar.
"Latest News about the GSI Positron Lines"

6) M. Gai, Yale Univ., New Haven (USA), 25 Mar.
"Probing the Cosmos with Secondary (Radioactive) Beams"

7) P. Kienle, GSI, Darmstadt (Germany), 26 Mar.
"New Results from the GSI SIS/ESR"

8) Y. Ogawa, Niigata Univ. (Niigata), 16 Apr.
"On Momentum Spectra of ^{9}Li in Two Neutron Removal Reactions of ^{11}Li"

9) V.G. Soloviev, JINR, Dubna (Russia), 22 Apr.
"Microscopic Description of Vibrational States in Deformed Nuclei"

10) D. Ashery, Tel Aviv Univ., Tel Aviv (Israel), 28 Apr.
"Pion Absorption and Short Range Correlations"

11) H. Sato, RIKEN, 8 June
"Systematics of Isotope Production Rates: Fission Products and Their Barrier Penetration"

12) J.K.P. Lee, McGill Univ., Montreal (Canada), 10 June
"COMPLIS—A New Laser Spectroscopic Facility at ISOLDE, CERN"

13) A. Nakamura, Waseda Univ. (Tokyo), 17 June
"Behavior of Hadrons at Finite Temperature"

14) Y. Koike, Maryland Univ., Maryland (USA), 25 June
"Finite Temperature QCD Sum Rules Reexamined: Rho/Omega/and A-1 Mesons"

15) K. Takayanagi, Tokyo Denki Univ. (Saitama), 26 June
"Isospin-dependent Effective Interaction in Nucleon-nucleus Scattering"

16) T. Otsuka, Univ. of Tokyo (Tokyo), 6 July
"Some Speculations on the Physics of Unstable Neutron-Rich Nuclei"

17) H. Ikegami, RCNP (Osaka), 7 July
"Cyclotron Maser Cooling of Electron and Ion Beams"

18) Zhang Qi-Ren, Peking Univ., Peking (China), 22 July
"On Quantum Bag Dynamics"

19) K. Kato, Hokkaido Univ. (Hokkaido), 5 Aug.
"Unstable Nuclei and Complex Scaling Method"

20) G. Bollen, Mainz Univ. (Germany), 26 Aug.
"Mass Measurements with Exotic Beams"

21) H. Yabu, South Carolina Univ. (USA), 2 Sep.
"Nucleon Spin Structure in a Relativistic Constituent Quark Model"

22) M. Asakawa, Texas A&M Univ. (USA), 7 Sep.
"The M_T Scaling in Dilepton Spectrum as a Signature for the Quark-Gluon Plasma"

23) Jose A. Casado, Univ. de Santiago de Compostela (Spain), 16 Sep.
"Measurement of the Radii of Time Dependent Chaotic Pion Sources"

24) L.G. Liu, Zhongshan Univ. (China), 25 Sep.
"Studies of ρ^0-ω Mixing"

25) I. Nomura, RIKEN, 7 Oct.
"Pion Absorption in GeV Region: Beyond the Meson Factories"

26) M. Uehara, Saga Univ. (Saga), 19-20 Oct.
"The Chiral Soliton Model of a Nucleon"

27) M. Thoennessen, NSCL, Michigan State Univ. (USA), 23 Oct.
"Dissipation and the Population and Decay of Compound Nuclei"

28) H. Conzett, LBL (USA), 27 Oct.
"A Sensitive New Test of Time-Reversal Invariance"

29) I. Katayama, INS (Tokyo), 29 Oct.
"A New Focusing and Cooling Device for Ion from Ion Guide"

30) T. Nakatsukasa, Kyoto Univ. (Kyoto), 2 Nov.
"Octupole Correlations in Superdeformed Nuclei"

31) Y.K. Gambhir, IIT, Bombay (India), 5 Nov.
"Relativistic Mean Field Description of Nuclear Properties"

32) M.N. Harakeh, Vrije Univ., Amsterdam (the Netherlands), 6 Nov.
"Dipole Excitations in Inelastic Alpha Scattering"

33) V. Tsarev, Lebedev Physical Institute, Moscow (Russia), 11 Nov.
"Cold Fusion Researches in Russia"

34) I. Hamamoto, Univ. of Lund (Sweden), 18 Nov.
"Octupole Deformation in Large Fermion System"

35) J. Chiba, KEK (Ibaraki), 25 Nov.
"Behavior of Delta in Nuclei"

36) T. Kunihiro, Ryukoku Univ. (Shiga), 30 Nov.
"Chiral Phase Transition at Finite Temperature in QCD"

37) Y. Sakuragi, Osaka City Univ. (Osaka), 3 Dec.
"Is Coulomb Dissociation Method Applicable to Astrophysics?"

38) G.D. Alton, Oak Ridge National Lab. (USA), 3 Dec.
"The Radioactive Ion Beam Project at The Oak Ridge National Lab."

39) Zhou Yizhong, Inst. of Atomic Energy (China), 7 Dec.
"The Study of Relativistic Heavy-Ion Collisions with RBUU Theory"

40) Liu Jianye, Inst. of Modern Physics (China), 7 Dec.
"Heavy-Ion Collision Theory with the Medium Effects and Momentum Dependent Interaction"

41) Y. Yoshizawa, College of Industrial Technology (Hyogo), 7 Dec.
"Coulomb Excitation of Deformed Nuclei and Future of Nuclear Spectroscopy"

42) Zhang Xizen, Inst. of Atomic Energy (China), 9 Dec.
"Collective Spectrum of Octupole Deformed System"

43) T. Udagawa, Univ. of Texas, Austin (USA), 24 Dec.
"Delta and Its Decay in Nuclei"

Atomic Physics Lab.

1) K-I Kowari, Univ. British Columbia (Canada), 13 Jan.
"Moderation and Thermalization of Subexcitation Electrons in Methane"

2) M. Inokuti, ANL (USA), 13 Jan.
"Fano Factor of Argon for Electrons,

Photons, and Alpha Particles"

3) C. Bhalla, Kansas State Univ. (USA), 18 Jan.
"Dielectronic Recombination and Resonance Transfer Excitation"

4) B.D. DePaola, Kansas State Univ. (USA), 30 Jan.
"Charge Capture from a Laser Excited Target"

5) A.D. Bandrauk, Univ. Sherbrook (Canada), 28 Feb.
"Molecules in Intense Laser Field"

6) H. Schmidt-Böcking, Univ. Frankfurt (Germany), 2 Mar.
"Electron Emission in Heavy Ion-Atom Collisions"

7) S. Lencinas, Univ. Frankfurt (Germany), 15 Apr.
"Recoil Ion Momentum Spectroscopy"

8) D. Berényi, Hungarian Academy Science (Hungary), 5 June
"Recent Results on the Cusp in the Spectrum of Electrons Emitted in Ion-Atom Collisions"

9) W. Meyerhof, Stanford Univ. (USA), 13 July
"Atomic Clocks for Nuclear and Fission Times"

10) P.H. Mokler, GSI (Germany), 14 July
"Atomic Collisions with Heavy Ions (Recent Development at GSI)"

11) S. Hara, Tsukuba Coll. Tech., 10 Sep.
"Theoretical Studies of Atomic Doubly-Excited States"

XII. LIST OF PERSONNEL

XII. LIST OF PERSONNEL

RIKEN Accelerator Research Facility Personnel

ISHIHARA Masayasu 石原正泰 (Facility Director)
AWAYA Yohko 粟屋容子 (Vice Facility Director)
YANO Yasushige 矢野安重 (Vice Facility Director)

Linac Division

CHIBA Toshiya 千葉利哉
CHIBA Yoshiaki 千葉好明
HEMMI Masatake 逸見政武
IKEZAWA Eiji 池沢英二
KASE Masayuki 加瀬昌之
KOHARA Shigeo 小原重夫
MIYAZAWA Yoshitoshi 宮沢佳敏*

Ring Cyclotron Division

FUJITA Jiro 藤田二郎
GOTO Akira 後藤 彰*
IKEGAMI Kumio 池上九三男
INABE Naohito 稲辺尚人
KAGEYAMA Tadashi 影山 正
KAMIGAITO Osamu 上垣外修一
KASE Masayuki 加瀬昌之
KOHARA Shigeo 小原重夫
KUBO Toshiyuki 久保敏幸
NAGASE Makoto 長瀬 誠
NAKAGAWA Takahide 中川孝秀
OGIWARA Kiyoshi 荻原 清
YOKOYAMA Ichiro 横山一郎

Experimental Support Division

ICHIHARA Takashi 市原 卓
KAMBARA Tadashi 神原 正
KANAI Yasuyuki 金井保之
KOBAYASHI Toshio 小林俊雄*
KUMAGAI Hidekazu 熊谷秀和
MATSUZAKI Teiichiro 松﨑禎市郎
MORITA Kosuke 森田浩介
OHKUBO Yoshitaka 大久保嘉高
WATANABE Yasushi 渡邊 康
YANOKURA Minoru 矢野倉 実
YATAGAI Fumio 谷田貝文夫

Radioisotope Facilities Division

AMBE Fumitoshi 安部文敏*
IWAMOTO Masako 岩本正子
KOBAYASHI Yoshio 小林義男

Administration Staff

NAKAMURA Toshiko 中村とし子
YOSHIDA Tohru 吉田 徹**

Steering Committee

AMBE Fumitoshi 安部文敏
AWAYA Yohko 粟屋容子
CHIBA Yoshiaki 千葉好明
GOTO Akira 後藤 彰
HANAOKA Fumio 花岡文雄
INAMURA Takashi 稲村 卓
ISHIHARA Masayasu 石原正泰
KAMITSUBO Hiromichi 上坪宏道
KATSUMATA Koichi 勝又紘一
KIRA Akira 吉良 爽
KOBAYASHI Toshio 小林俊雄
KUMAGAI Noritaka 熊谷教孝
MATSUOKA Masaru 松岡 勝
MIYAZAWA Yoshitoshi 宮沢佳敏
NAGAMINE Kanetada 永嶺謙忠
TAKAHASHI Tan 高橋 旦

*Group Leader **Administrative Manager

TAKAMI Michio 高見道生
YAGI Eiichi 八木栄一
TANIHATA Isao 谷畑勇夫*
YANO Yasushige 矢野安重

Scientific and Engineering Personnel

Cosmic Radiation Laboratory

IMAI Takashi 今井 喬
KOHNO Tsuyoshi 河野 毅

(Visitors)
HASEBE Nobuyuki 長谷部信行 (Fac. Gen. Educ., Ehime Univ.)
KASHIWAGI Toshisuke 柏木利介 (Sci. Eng. Res. Lab., Waseda Univ.)
KATO Chihiro 加藤千尋
MUNAKATA Kazuoki 宗像一起 (Fac. Sci., Shinshu Univ.)
MURAKAMI Hiroyuki 村上浩之 (Fac. Sci., Rikkyo Univ.)
NAGATA Katsuaki 永田勝明 (Fac. Eng., Tamagawa Univ.)
NAKAMOTO Atsushi 中本 淳 (Fac. Sci., Rikkyo Univ.)
YANAGIMACHI Tomoki 柳町朋樹 (Fac. Sci., Rikkyo Univ.)

(Students)
FUJIKI Kenichi 藤木謙一 (Fac. Sci., Ehime Univ.)
ITO Tomoyuki 伊藤朋行 (Fac. Sci. Eng., Waseda Univ.)
ITSUMI Norifumi 逸見憲史 (Fac. Sci. Eng., Waseda Univ.)
MORIYA Hitoshi 守屋 整 (Fac. Sci., Ehime Univ.)
SHINO Tomoaki 篠 智彰 (Fac. Sci. Eng., Waseda Univ.)

Cyclotron Laboratory

DATE Schin 伊達 伸
FUJITA Shin 藤田 新
HARADA Toru 原田 融
INABE Naohito 稲辺尚人
JIN Wei-Guo 金 衛国
KAMIGAITO Osamu 上垣外修一
KUBO Toshiyuki 久保敏幸
NAGASE Makoto 長瀬 誠
NAKAJIMA Shunji 中島諄二
OGIWARA Kiyoshi 荻原 清
SAITO Motozo 斎藤始三
SOUTOME Kouichi 早乙女光一
WAKASUGI Masanori 若杉昌徳
YANO Yasushige 矢野安重
FUJITA Jiro 藤田二郎
GOTO Akira 後藤 彰
IKEGAMI Kumio 池上九三男
INAMURA Takashi 稲村 卓
KAGEYAMA Tadashi 影山 正
KOHARA Shigeo 小原重夫
MORITA Kosuke 森田浩介
NAKAGAWA Takahide 中川孝秀
NAKANISHI Noriyoshi 中西紀喜
OHTA Shigemi 太田滋生
SHIKATA Takashi 四方隆史
SUGANUMA Hideo 菅沼秀夫
YAMAJI Shuhei 山路修平
YOKOYAMA Ichiro 横山一郎

(Visitors)
ABE Yasuhisa 阿部恭久 (Res. Inst. Funda. Phys., Kyoto Univ.)
ARAI Eiichi 新井栄一 (Res. Lab. Nucl. Reactors, Tokyo Inst. Tech.)
EJIRI Hiroyasu 江尻宏泰 (Dep. Phys., Osaka Univ.)
FUJIOKA Manabu 藤岡 学 (Cyclotron Radioisot. Cent., Tohoku Univ.)
FUJISAWA Takashi 藤沢高志 (Denki Kogyo Co. Ltd.)
FUJITA Yoshitaka 藤田佳孝 (Dep. Phys., Osaka Univ.)
FUKUMOTO Sadayoshi 福本貞義 (KEK)
FURUNO Kohei 古野興平 (Inst. Phys. Tandem Accel. Cent., Univ. Tsukuba)

*Chairperson

HASHIMOTO Osamu 橋本　治 (Inst. Nucl. Study, Tokyo Univ.)
HATANAKA Kichiji 畑中吉治 (RCNP, Osaka Univ.)
HATSUKAWA Yuichi 初川雄一 (JAERI, Tokai)
HAYANO Ryugo 早野龍五 (Dep. Phys., Tokyo Univ.)
HEIGUCHI Kazuhiko 平口和彦 (Graduate Sch. of Sci. & Tech., Niigata Univ.)
HIRAO Yasuo 平尾泰男 (Nat. Inst. Radiol. Sci.)
HORIGUCHI Takayoshi 堀口隆良 (Dep. Phys., Hiroshima Univ.)
HORIUCHI Hisashi 堀内ひさし (Dep. Phys., Kyoto Univ.)
IKEDA Kiyomi 池田清美 (Dep. Phys., Niigata Univ.)
IKEDA Nobuo 池田伸夫 (Inst. Nucl. Study, Tokyo Univ.)
IKEGAMI Hidetsugu 池上栄胤 (RCNP, Osaka Univ.)
INOUE Makoto 井上　信 (RCNP, Osaka Univ.)
ISHIZUKA Takeo 石塚武男 (Dep. Phys., Saitama Univ.)
IWAMOTO Akira 岩本　昭 (Japan Atomic Energy Res. Inst.)
IWASHITA Yoshihisa 岩下芳久 (Inst. Chem. Res., Kyoto Univ.)
KAMEYAMA Hirobumi 亀山浩文 (Dep. Phys., Chiba Keizai Jr. Coll.)
KAMIMURA Masayasu 上村正康 (Dep. Phys., Kyushu Univ.)
KANMURI Tetsuo 冠　哲夫 (Dep. Phys., Osaka Univ.)
KATAYAMA Ichiro 片山一郎 (RCNP, Osaka Univ.)
KATORI Kenji 鹿取謙二 (Dep. Phys., Osaka Univ.)
KATO Kiyoshi 加藤幾芳 (Dep. Phys., Hokkaido Univ.)
KATSURAGAWA Hidetsugu 桂川秀嗣 (Dep. Phys., Toho Univ.)
KAWAI Mitsuji 川合光路 (Dep. Phys., Kyushu Univ.)
KIKUCHI Fumio 菊池文男 (Coll. Arts Sci., Univ. Tokyo)
KOBAYASHI Shinsaku 小林晨作 (Dep. Phys., Kyoto Univ.)
KOHMOTO Susumu 河本　進 (Univ. Electro-Commun.)
KOHMOTO Toshiro 河本敏郎 (Dep. Phys., Kyoto Univ.)
KOIZUMI Mitsuo 小泉光生 (Dep. Phys., Hiroshima Univ.)
KONDOU Michiya 近藤道也 (RCNP, Osaka Univ.)
KOSAKO Toshiso 小佐古敏荘 (Atomic Energy Res. Cent., Univ. Tokyo)
KUDO Hisaaki 工藤久昭 (Dep. Chem., Niigata Univ.)
KUROYANAGI Tokihiro 黒柳登喜大 (Dep. Phys., Kyushu Univ.)
LEE Sanmu 李　相茂 (Dep. Phys., Univ. Tsukuba)
LI Zhuxia (Atomic Energy Sci. & Tech.)
MARUMORI Toshio 丸森寿夫 (Dep. Phys., Univ. Tsukuba)
MATSUKI Seishi 松木征史 (RCNP, Osaka Univ.)
MATSUSE Takehiro 松瀬丈浩 (Dep. Phys., Shinshu Univ.)
MATSUYANAGI Kenichi 松柳研一 (Dep. Phys., Kyoto Univ.)
MINAMISONO Tadanori 南園忠則 (Dep. Phys., Osaka Univ.)
MIURA Iwao 三浦　岩 (RCNP, Osaka Univ.)
MIYAMURA Osamu 宮村　修 (Fac. Sci., Osaka Univ.)
MIYATAKE Hiroari 宮武宇也 (Fac. Sci., Osaka Univ.)
MORI Yoshiharu 森　義治 (KEK)
MURAKAMI Tetsuya 村上哲也 (Dep. Phys., Kyoto Univ.)
MURAOKA Mitsuo 村岡光男 (Dep. Educat., Chiba Univ.)
MURAYAMA Toshiyuki 村山利幸 (Tokyo Univ. Mercantil Marine)
MUROTANI Shin 室谷　心 (Sch. Sci & Engi., Waseda Univ.)
NAGAI Yasuki 永井泰樹 (Dep. Appl. Phys., Tokyo Inst. Technol.)
NAKAHARA Hiromichi 中原弘道 (Dep. Chem., Tokyo Metrop. Univ.)
NAKAI Koji 中井浩二 (KEK)
NAKAMURA Ichiro 中村市郎 (Dep. Phys., Saitama Univ.)
NAKAMURA Takashi 中村尚司 (Cyclotron Radioisot. Cent., Tohoku Univ.)
NIITA Koji 仁井田浩二 (Dep. Phys., Univ. of Giessen, Giessen)
NOMURA Toru 野村　亨 (Inst. Nucl. Study, Univ. Tokyo)
OGATA Hiroshi 小方　寛 (RCNP, Osaka Univ.)
ONISHI Naoki 大西直毅 (Dep. Phys., Coll. Gen. Educ., Univ. Tokyo)

OSUGA Toshiaki 大須賀敏明 (Col. Art & Sci., Chiba Univ.)
PU YUE HU 蒲 越虎 (Dep. Phys., Univ. Tsukuba)
SAKAI Hideyuki 酒井英行 (Dep. Phys., Univ. Tokyo)
SASAGAWA Tatsuya 笹川辰弥 (Dep. Phys., Tohoku Univ.)
SATOU Kenichi 佐藤憲一 (Dep. Phys., Tohoku Coll. Pharm.)
SEKINE Toshiaki 関根俊明 (JAERI, Tokai)
SHIKAZONO Naoki 鹿園直基 (JAERI, Tokai)
SHIMOMURA Koichiro 下村浩一郎 (RCNP, Osaka Univ.)
SHINOZUKA Tsutomu 篠塚 勉 (Cyclotron Radioisot. Cent., Tohoku Univ.)
SUEKI Keisuke 末木啓介 (Inst. Nucl. Study, Univ. Tokyo)
SUGAI Isao 菅井 勲 (Inst. Nucl. Study, Univ. Tokyo)
SUMIYOSHI Hiroyuki 住吉広行 (Matsusho-Gakuen Junior Col.)
TAGISHI Yoshihiro 田岸義宏 (Tandem Accl. Cent., Univ. Tsukuba)
TAKADA Kenjiro 高田健次郎 (Dep. Phys., Kyushu Univ.)
TAKEMASA Tadashi 武政尹士 (Dep. Phys., Saga Univ.)
TAKIGAWA Noboru 滝川 昇 (Dep. Phys., Tohoku Univ.)
TAMAGAKI Ryozo 玉垣良三 (Dep. Phys., Kyoto Univ.)
TANAKA Jinichi 田中仁市 (Inst. Nucl. Study, Univ. Tokyo)
TOHYAMA Mitsuru 遠山 満 (Dep. Phys., Kyorin Univ.)
TOMIMASU Takio 富増多喜夫 (Electro Tech. Lab.)
TORIYAMA Tamotsu 鳥山 保 (Dep. Appl. Phys., Tokyo Inst. Technol.)
TSUNEMOTO Hiroshi 恒元 博 (Natl. Inst. Radio. Sci.)
WADA Michiharu 和田道治 (Dep. Phys., Tohoku Univ.)
WAKAI Masamichi 若井正道 (Dep. Phys., Osaka Univ.)
WANG Zhen 王 真 (Inst. Modern Phys., Academia Sinica)
YAMANOUCHI Mikio 山内幹雄 (Tandem Accel. Cent., Univ. Tsukuba)
YAMAZAKI Takashi 山崎 魏 (RCNP, Osaka Univ.)
YOSHIDA Nobuaki 吉田宣章 (Dep. Phys., Univ. Tokyo)
YOSHIDA Shiro 吉田思郎 (Dep. Phys., Tohoku Univ.)
YOSHINAGA Naotaka 吉永尚孝 (Comput. Cent., Univ. Tokyo)

(Students)
ARIGA Takehiro 有賀健博 (Dep. Phys., Saitama Univ.)
FUKASHIRO Yasuyuki 深代康之 (Dep. Phys., Tohoku Univ.)
FURUYA Shinji 古谷信司 (Dep. Appl. Phys., Tokyo Inst. Technol.)
HAMADA Shingo 濱田真悟 (Dep. Nucl. Eng., Kyoto Univ.)
HIRASAWA Junichiro 平澤淳一郎 (Dep. Appl. Phys., Tokyo Inst. Technol.)
KASHIWABARA Taketo 柏原健人 (Dep. Phys., Toho Univ.)
KATOU Haruhiko 加藤治彦 (Dep. Phys., Chuo Univ.)
KOBAYASHI Takayuki 小林貴之 (Dep. Chem., Tokyo Metrop. Univ.)
KUMAGAI Kenji 熊谷健二 (Dep. Phys., Hiroshima Univ.)
KURAMOTO Takeshi 蔵本武志 (Dep. Phys., Tokyo Univ.)
MARUYAMA Toshiki 丸山敏毅 (Dep. Phys., Kyoto Univ.)
NAKAOKA Masaya 中岡正哉 (Dep. Phys., Saitama Univ.)
NISHINAKA Ichiro 西中一朗 (Dep. Phys., Tokyo Metrop. Univ.)
OGAWA Izumi 小川 泉 (Dep. Phys., Kyoto Univ.)
OONISHI Akira 大西 明 (Dep. Phys., Kyoto Univ.)
OOSAKI Toshiro 大崎敏郎 (Dep. Appl. Phys., Tokyo Inst. Technol.)
SEINO Satoshi 清野 聡 (Dep. Appl. Phys., Tokyo Inst. Technol.)
SENOO Kenichi 妹尾賢一 (Dep. Appl. Phys., Tokyo Inst. Technol.)
SUNAOSHI Hitoshi 砂押 仁 (Dep. Phys., Tohoku Univ.)
SUZUKI Katsuhiro 鈴木勝博 (Dep. Phys., Kyoto Univ.)
TAKAYANAGI Masao 高柳昌夫 (Dep. Phys., Toho Univ.)
TAKEDA Kenji 竹田賢志 (Dep. Appl. Phys., Tokyo Inst. Technol.)
TANIKAWA Masashi 谷川勝至 (Dep. Phys., Tokyo Metrop. Univ.)
WAKUI Takashi 湧井崇志 (Dep. Phys., Toho Univ.)

WATANABE Koutarou 渡辺康太郎 (Dep. Appl. Phys., Tokyo Inst. Technol.)

Linear Accelerator Laboratory

CHIBA Toshiya 千葉利哉
CHIBA Yoshiaki 千葉好明
FUJIMAKI Masaki 藤巻正樹
HEMMI Masatake 逸見政武
HIRENZAKI Satoru 比連崎 悟
IKEZAWA Eiji 池沢英二
KASE Masayuki 加瀬昌之
KOBAYASHI Toshio 小林俊雄
KUMAGAI Hidekazu 熊谷秀和
MIYAZAWA Yoshitoshi 宮沢佳敏
OZAWA Akira 小沢 顕
SUZUKI Takeshi 鈴木 健
TANIHATA Isao 谷畑勇夫
TONUMA Tadao 戸沼正雄
YANOKURA Minoru 矢野倉 実
YOSHIDA Koichi 吉田光一

(Visitors)
ALOKSANDROV D. V. (Kurochatov Inst.)
FUJIWARA Mamoru 藤原 守 (RCNP, Osaka Univ.)
HIRATA Daisy (CTA, Inst. Estudos Avancados, Brasil)
HURUTANI Keiichi 古谷圭一 (Fac. Sci., Sci. Univ. Tokyo)
ITO Noriaki 伊藤憲昭 (Dep. Cryst. Mater., Nagoya Univ.)
KANAZAWA Kenichi 金澤健一 (KEK)
KATORI Kenji 鹿取謙二 (Fac. Sci., Osaka Univ.)
KIKUCHI Jun 菊池 順 (Sci. Eng. Res. Lab., Waseda Univ.)
KIMURA Kikuo 木村喜久雄 (Fac. Eng., Nagasaki Inst. Appl. Sci.)
KORCHENINNIKOV A. A. (Kurochatov Inst.)
MATUOKA Nobuyuki 松岡伸行 (Res. Centr. Nucl. Phys., Osaka Univ.)
MOON Chang-Bun (Seoul Univ.)
MURAOKA Mituo 村岡光男 (Coll. Arts Sci., Chiba Univ.)
NIKOLSKI E. Y. (Kurochatov Inst.)
OBUTI Marcia M. (Sao Paulo Univ.; Saitama Univ.)
OGAWA Kengo 小川建吾 (Coll. Arts Sci., Chiba Univ.)
OGLOBLIN Alexei (Kurochatov Inst.)
OMATA Kazuo 小俣和夫 (Inst. Nucl. Study, Univ. Tokyo)
SAGAWA Hiroyuki 佐川弘幸 (Fac. Sci., Univ.Tokyo)
SAKAI Hideyuki 酒井英行 (Fac. Sci., Univ. Tokyo)
SUDA Toshimi 須田利美 (Fac. Sci., Tohoku Univ.)
SUGAWARA Masahiko 菅原昌彦 (Fundam. Sci., Chiba Inst. Technol.)
SUZUKI Yasuyuki 鈴木宣之 (Fac. Sci., Niigata Univ.)
YAMAGUCHI Hiromi 山口裕美 (Sci. Eng. Res. Lab., Waseda Univ.)

Radiation Laboratory

FERRAGUT Alain
ICHIHARA Takashi 市原 卓
ISHIHARA Masayasu 石原正泰
IZUMO Koichi 出雲光一
KONNO Satoshi 金野 智
NOMURA Izumi 野村和泉
SUZUKI Masayo 鈴木昌世
TAKAHASHI Tan 高橋 旦
TANAKA Kazuhiro 田中和宏
TENDOW Yoshihiko 天道芳彦
WATANABE Yasushi 渡邉 康
YOSHIDA Atsushi 吉田 敦

(Visitors)
ABE Yasuhisa 阿部恭久 (Res. Inst. Fundam. Phys., Kyoto Univ.)
ADACHI Minoru 足立 實 (Dep. Appl. Phys., Tokyo Inst. Technol.)
ANDO Yoshiaki 安藤嘉章 (Dep. Phys., Rikkyo Univ.)
APRILE Elena (Columbia Univ., U.S.A)
ASAHI Koichiro 旭 耕一郎 (Fac. Sci., Tokyo Inst. Technol.)
BECK F.A. (Groupe RSN, Strasbourg, France)

BROGLIA R. (Milano Univ., Italy)
DELBAR Thierry, JM (Univ. Catholique de Louvain, Belgium)
DOKE Tadayoshi 道家忠義 (Sci. Eng. Res. Lab., Waseda Univ.)
FLOCARD Hubert (Inst. Phys. Nucl., Orsay, France)
FUCHI Yoshihide 渕 好秀 (Inst. Nucl. Study, Univ. Tokyo)
FUJIOKA Manabu 藤岡 学 (Dep. Phys., Tohoku Univ.)
FUKUDA Mitsunori 福田光順 (Fac. Sci., Osaka Univ.)
FUKUDA Tomokazu 福田共和 (Inst. Nucl. Study, Univ. Tokyo)
GAI Moche (Yale Univ., U.S.A.)
GONO Yasuyuki 郷農靖之 (Dep. Phys., Kyushu Univ.)
GUY Y. Bizard (CAEN Univ., France)
HAMAMOTO Ikuko 浜本育子 (Lund Univ. Sweden)
HASEGAWA Takeo 長谷川武夫 (Fac. Eng., Miyazaki Univ.)
HASHIZUME Akira 橋爪 朗 (Japan Atomic Energy Relations Organization)
HITACHI Akira 月出 章 (Sci. Eng. Res. Lab., Waseda Univ.)
ICHIMURA Munetake 市村宗武 (Coll. Arts Sci., Univ. Tokyo)
IEKI Kazuo 家城和夫 (Fac. Sci., Rikkyo Univ.)
IJIRI Kenichi 井尻憲一 (Radioisot., Cent., Univ. Tokyo)
ISHIDA Nobumichi 石田伸道 (Seikei Univ.)
ISHIKAWA Masanobu 石川雅紀 (Tokyo Univ. Fisheries)
IWASAKI Hiroyuki 岩崎博行 (KEK)
KANEYUKI Kenji 金行健治 (Fac. Sci., Tokyo Inst. Technol.)
KASAGI Jirohta 笠木治郎太 (Lab. Nucl. Sci., Tohoku Univ.)
KASAI Kiyomi 笠井清美 (Natl. Inst. Radiol. Sci.)
KATAYAMA Ichiro 片山一郎 (Inst. Nucl. Study, Univ. Tokyo)
KATO Seigo 加藤静吾 (Fac. Educ., Yamagata Univ.)
KATORI Kenji 鹿取謙二 (Fac. Sci., Osaka Univ.)
KAWAKAMI Hirokane 川上宏金 (Inst. Nucl. Study, Univ. Tokyo)
KAWASHIMA Hideo 川島英雄 (Inst. Nucl. Study, Univ. Tokyo)
KIKUCHI Jun 菊池 順 (Sci. Eng. Res. Lab., Waseda Univ.)
KIM Hee J. (Oak Ridge Natl. Lab., U.S.A.)
KIM Jong-Chan 金 鐘賛 (Seoul Natl. Univ., Korea)
KISHIDA Takashi 岸田 隆 (Fac. Sci., Univ. Tokyo)
KITAHARA Yoshitaka 北原義孝 (Hoya Corp.)
KITAO Kensuke 喜多尾憲助 (Natl. Inst. Radiol. Sci.)
KOMAGATA Kazuyuki 駒形和行 (Asahi Glass Co., Ltd.)
KONDO Takahiko 近藤敬比古 (KEK)
KUBONO Shigeru 久保野 茂 (Inst. Nucl. Study, Univ. Tokyo)
KUBOTA Shinzou 窪田信三 (Fac. Sci., Rikkyo Univ.)
KUSAKARI Hideshige 草刈英榮 (Fac. Educ., Chiba Univ.)
LEE Sang Mu 李 相茂 (Inst. Phys., Univ. Tsukuba)
LIU Jian Ye (Inst. Mod. Phys., Acad. Sinica, China)
LIU Lyan Gan 劉 良鋼 (Zhong Shan Univ., China)
MAEDA Kazushige 前田和茂 (Coll. Gen. Educ., Tohoku Univ.)
MASUDA Kimiaki 増田公明 (Saitama Coll. Health)
MATSUDA Takeshi 松田 武 (KEK)
MATSUYANAGI Kenichi 松柳研一 (Dep. Phys., Kyoto Univ.)
MIN Byung-Joo 閔 丙珠 (Korea Atomic Energy Res. Inst., Korea)
MITARAI Shiro 御手洗志郎 (Dep. Phys., Kyushu Univ.)
MIYACHI Takashi 宮地 孝 (Inst. Nucl. Study, Univ. Tokyo)
MIYATAKE Hiroari 宮武宇也 (Coll. Gen. Educ., Osaka Univ.)
MORIKAWA Tsuneyasu 森川恒安
MORINOBU Shunpei 森信俊平 (Dep. Phys., Kyushu Univ.)
MOTOBAYASHI Tohru 本林 透 (Fac. Sci., Rikkyo Univ.)
MOTTELSON Ben R. (NORDITA, Copenhagen, Denmark)
MUKERJEE Reshmi (Columbia Univ., U.S.A.)

MURAKAMI Takeshi 村上 健 (Natl. Inst. Radiol. Sci.)
NAGAI Yasuki 永井泰樹 (Fac. Sci., Tokyo Inst. Technol.)
NAGASHIMA Yasuo 長島泰夫 (Dep. Phys., Univ. Tsukuba)
NAKAJIMA Mitsuo 中島充夫 (Graduate Sch. Nagatsuda, Tokyo Inst. Technol.)
NAKAMURA Syougo 中村正吾 (Fac. Educ., Yokohama Nat. Univ.)
NAKAYAMA Shintaro 中山信太郎 (Coll. Gen. Educ., Tokushima Univ.)
NEUGART Rainer (Mainz Univ. German)
NIIZEKI Takashi 新関 隆 (Fac. Sci., Tokyo Inst. Technol.)
NORO Tetsuo 野呂哲夫 (RCNP, Osaka Univ.)
OGAWA Masao 小川雅生 (Graduate Sch. Nagatsuda, Tokyo Inst. Technol.)
OGURA Koichi 小倉紘一 (Coll. Indus. Technol., Nihon Univ.)
OHNUMA Hajime 大沼 甫 (Fac. Sci., Tokyo Inst. Technol.)
OHTSUKA Takaharu 大塚孝治 (Fac. Sci., Univ. Tokyo)
OKAMURA Hiroyuki 岡村弘之 (Fac. Sci., Univ. Tokyo)
ORIHARA Hikonojo 織原彦之丞 (Cyclotron and Radioisot. Cent., Tohoku Univ.)
OSHIMA Masumi 大島眞澄 (Japan Atomic Energy Res. Inst.)
OSHIRO Takashi 尾城 隆 (Tokyo Univ. Fisheries)
OYAIZU Michihiro 小柳津充広 (Inst. Nucl. Study, Univ. Tokyo)
QU Yun-he 屈 云河 (Inst. High Energy Phys., Chinese Acad. Sci., China)
RUAN (GEN) Jian-zhi 阮 建治 (Dep. Phys., Rikkyo Univ.)
SAKAGUCHI Harutaka 坂口治隆 (Dep. Phys., Kyoto Univ.)
SAKAI Mitsuo 坂井光夫 (Inst. Nucl. Study, Univ. Tokyo)
SAKAI Yoshihide 堺井義秀 (KEK)
SATO Hiroshi 佐藤 竑 (Seikei Univ.)
SHIBAMURA Eido 柴村英道 (Saitama Coll. Health)
SHIMIZU Hajime 清水 肇 (Fac. Educ., Yamagata Univ.)
SHIMIZU Yoshifumi 清水良文 (Dep. Phys., Kyushu Univ.)
SHIMODA Tadashi 下田 正 (Coll. Gen. Educ., Osaka Univ.)
SHIMOURA Susumu 下浦 享 (Dep. Phys., Rikkyo Univ.)
SHIRATO Shoji 白土鈔二 (Dep. Phys., Rikkyo Univ.)
SHIROYAMA Masaki 城山正樹 (Asahi Glass Co., Ltd.)
SUEKANE Fumihiko 末包文彦 (Fac. Sci., Tohoku Univ.)
SUGAWARA Masahiko 菅原昌彦 (Chiba Inst. Technol.)
SUZUKI Yasuyuki 鈴木宜之 (Dep. Phys., Niigata Univ.)
TAKADA Eiichi 高田栄一 (Natl. Inst. Radiol. Sci.)
TAKAHASHI Noriaki 高橋憲明 (Coll. Gen. Educ., Osaka Univ.)
TAKAKU Shinsaku 高久清作 (Inst. Nucl. Study, Univ. Tokyo)
TAKIGAWA Noboru 滝川 昇 (Dep. Phys., Tohoku Univ.)
TANAKA Masahiko 田中雅彦 (Inst. Nucl. Study, Univ. Tokyo)
TANIMORI Tohru 谷森 達 (Fac. Sci., Tokyo Inst. Technol.)
TAO Kazuyuki 垰 和之 (Radioisot. Cent., Univ. Tokyo)
TOKI Hiroshi 土岐 博 (Dep. Phys., Tokyo Metrop. Univ.)
TOYOKAWA Hidenori 豊川秀訓 (Inst. Phys., Univ. Tsukuba)
TSAREV V. (Lebedev Phys. Inst., Moscow)
UNO Masahiro 宇野正宏 (The Ministry of Education)
UNNO Yoshinobu 海野義信 (KEK)
WATANABE Yasushi 渡辺靖志 (Fac. Sci., Tokyo Inst. Technol.)
YAMAYA Takashi 山屋 堯 (Dep. Phys., Tohoku Univ.)
YATO Osamu 矢頭 治 (Kagoshima Agr. Exp. Stn.)
YOSHIDA Kazuo 吉田和夫 (Hoya Corp.)
YOSHINAGA Naotaka 吉永尚孝 (Saitama Univ.)
YOSOI Masaru 與曽井 優 (Dep. Phys., Kyoto Univ.)
YUTA Haruo 湯田春雄 (Fac. Sci., Tohoku Univ.)
ZHANG Yu-hu 張 玉虎 (Inst. Mod. Phys., Acad. Sin., China)
ZHU Yongtai 諸 永泰 (Inst. Mod. Phys., Acad. Sin., China)

(Students)
AKEBOSHI Yoshihiro 明星慶洋 (Fac. Sci., Tokyo Inst. Technol.)
AOI Nori 青井 考 (Fac. Sci., Univ. Tokyo)
BEN Sei 下 正 (Sch. Sci. Eng., Waseda Univ.)
CHAE Soo-Joh (Seoul Univ., Korea)
DOI Masashi 土井雅史 (Fac. Sci., Tokyo Inst. Technol.)
DOKI Yasuhiro 土記康博 (Fac. Sci., Univ. Tokyo)
FRANCE Jr. Ralph Hayward (Yale Univ., U.S.A.)
FURUTAKA Kazuyoshi 古高和禎 (Fac. Sci., Tokyo Inst. Technol.)
FUTAMI Yasuyuki 二見康之 (Inst. Phys., Univ. Tsukuba)
GUIMARAES Valdir (Inst. Nucl. Study, Univ. Tokyo)
HAHN Kevin I (Yale Univ., U.S.A.)
HARADA Masaki 原田昌樹 (Fac. Sci., Tokyo Inst. Technol.)
HASEGAWA Yoji 長谷川庸司 (Fac. Sci., Tohoku Univ.)
HASUIKE Katsuhito 蓮池勝人 (Sch. Sci. Eng., Waseda Univ.)
HONJO Yoshio 本城義夫 (Inst. Phys., Univ. Tsukuba)
HORI Yoichi 堀 陽一 (Fac. Sci., Tokyo Inst. Technol.)
HOSAKA Masahito 保坂将人 (Cyclotron and Radioisot. Cent., Tohoku Univ.)
ICHIGE Masayuki 市毛正之 (Sch. Sci. Eng., Waseda Univ.)
IDEGUCHI Eiji 井手口栄治 (Dep. Phys., Kyushu Univ.)
IKEDA Yasufumi 池田泰文 (Dep. Phys., Rikkyo Univ.)
ISHIDA Satoru 石田 悟 (Fac. Sci., Univ. Tokyo)
ITO Ken 伊藤 研 (Sch. Sci. Eng., Waseda Univ.)
ITO Tomoyuki 伊藤朋行 (Sci. Eng. Res. Lab., Waseda Univ.)
IWASA Naohito 岩佐直仁 (Dep. Phys., Rikkyo Univ.)
IZUMI Hideaki 出水秀明 (Fac. Sci., Tokyo Inst. Technol.)
KOBAYASI Misaki 小林美咲 (Sch. Sci. Eng., Waseda Univ.)
KOGANEMARU Kenichi 小金丸健一 (Graduate Sch. Nagatsuda, Tokyo Inst. Technol.)
KOMIYAMA Tatsuto 込山立人 (Sch. Sci. Eng., Waseda Univ.)
KURA Jumpei 蔵 純平 (Fac. Sci., Tokyo Inst. Technol.)
KUROKAWA Meiko 黒川明子 (Dep. Phys., Rikkyo Univ.)
KUWAHARA Kōta 桑原宏太 (Sch. Sci. Eng., Waseda Univ.)
LU Jun 呂 駿 (Inst. Phys., Univ. Tsukuba)
MATSUDA Kiyohide 松田清秀 (Fac. Sci., Tokyo Inst. Technol.)
MIYAMOTO Shouichi 宮本昭一 (Cyclotron and Radioisot. Cent., Tohoku Univ.)
MIZOI Yutaka 溝井 浩 (Coll. Gen. Educ., Osaka Univ.)
MIZOTA Takeshi 溝田武志 (Inst. Phys., Univ. Tsukuba)
MORIGUCHI Ako 森口亜子 (Japan Women's Univ.)
NAGANUMA Masayuki 永沼正行 (Graduate Sch. Nagatsuda, Tokyo Inst. Technol.)
NAGATA Kazuhiko 長田和彦 (Fac. Sci., Tokyo Inst. Technol.)
NAKAI Yoichi 中井陽一 (Dep. Phys., Kyoto Univ.)
NAKAMURA Takashi 中村隆司 (Fac. Sci., Univ. Tokyo)
NISHIO Teiji 西尾禎治 (Dep. Phys., Rikkyo Univ.)
NUNOYA Yoshihiko 布谷嘉彦 (Dep. Phys., Rikkyo Univ.)
ODAHARA Atsuko 小田原厚子 (Dep. Phys., Kyushu Univ.)
OHNISHI Hiroko 大西裕子 (Coll. Agric. Vet. Med., Nihon Univ.)
OHNO Mariko 大野真理子 (Radioisot. Cent., Univ. Tokyo)
OHSAKI Yoshinori 大嵜美紀 (Graduate Sch. Nagatsuda, Tokyo Inst. Technol.)
OHTSU Hideaki 大津秀暁 (Fac. Sci., Univ. Tokyo)
OKADA Hiroyuki 岡田宏之 (Sch. Sci. Eng., Waseda Univ.)
OKUNO Hiroki 奥野広樹 (Fac. Sci., Univ. Tokyo)
PU Y.H. 蒲 越虎 (Inst. Phys., Univ. Tsukuba)
SAKAMOTO Naruhiko 坂本成彦 (Fac. Sci., Univ. Tokyo)
SATO Hiromi 佐藤広海 (Fac. Sci., Tokyo Inst. Technol.)
SAWADA Shinya 澤田真也 (Dep. Phys., Kyoto Univ.)
SEKI Hiroyuki 関 宏之 (Graduate Sch. Nagatsuda, Tokyo Inst. Technol.)

SEKINE Takashi 関根　隆 (Fac. Sci., Tokyo Inst. Technol.)
SHIMADA Kenji 島田健児 (Fac. Sci., Tokyo Inst. Technol.)
SHIZUMA Toshiyuki 静間俊行 (Dep. Phys., Kyushu Univ.)
SOSO Lucio (Fac. Sci., Tokyo Inst. Technol.)
SUEMATSU Shigeyuki 末松繁行 (Dep. Phys., Kyushu Univ.)
TAJIMA Yasuhisa 田島靖久 (Fac. Sci., Tokyo Inst. Technol.)
TAKEDA Kenji 竹田賢志 (Fac. Sci., Tokyo Inst. Technol.)
TERANISHI Takashi 寺西　高 (Fac. Sci., Univ. Tokyo)
TOMITA Shigeo 冨田成夫 (Inst. Phys., Univ. Tsukuba)
TOMURA Hiromi 外村浩美 (Dep. Phys., Kyushu Univ.)
UEDA Tomomi 上田知美 (Japan Women's Univ.)
UENO Hideki 上野秀樹 (Fac. Sci., Tokyo Inst. Technol.)
UESAKA Tomohiro 上坂友洋 (Fac. Sci., Univ. Tokyo)
WAKASA Tomotsugu 若狭智嗣 (Fac. Sci., Univ. Tokyo)
YAJIMA Akira 矢嶋　亨 (Fac. Sci., Tokyo Inst. Technol.)
YAMAMOTO Takuhisa 山本琢久 (Fac. Sci., Tokyo Inst. Technol.)
YAMAZAKI Hiroshi 山崎弘詞 (Fac. Sci., Tokyo Inst. Technol.)
YASHIRO Yoshinori 矢代義徳 (Fac. Sci., Tokyo Inst. Technol.)
YOON Chong Cheol 尹　鐘哲 (Fac. Sci., Tokyo Inst. Technol.)
YOSHIDA Hiroshi 吉田浩司 (Fac. Sci., Tokyo Inst. Technol.)
YOSHIDA Kenichiro 吉田健一郎 (Dept. Phys., Kyoto Univ.)
YUASA-NAKAGAWA Keiko 中川恵子 (Inst. Phys., Univ. Tsukuba)
ZHAO Zhiping (Yale Univ., U.S.A.)

Atomic Physics Laboratory

ANDO Kozo 安藤剛三
KAMBARA Tadashi 神原　正
KRAVIS Scott (STA-fellow)
NISHIDA Masami 西田雅美
SHIMAMURA Isao 島村　勲
AWAYA Yohko 粟屋容子
KANAI Yasuyuki 金井保之
NAKAI Yoichi 中井陽一
OURA Masaki 大浦正樹
YOSHIDA Takashi 吉田高志

(Visitor)
AZUMA Toshiyuki 東　俊行 (Coll. Arts Sci., Univ. Tokyo)
BERENYI Dénes (ATOMKI, Hungary)
BHALLA Chander P. (Kansas State Univ., U.S.A.)
DANJO Atsunori 壇上篤徳 (Dep. Phys., Niigata Univ.)
DePAOLA Brett D. (Kansas State Univ., U.S.A.)
FUJIMA Kazumi 藤間一美 (Fac. Eng., Yamanashi Univ.)
FUKUDA Hiroshi 福田　宏 (Sch. Administration and Informatics, Univ. Shizuoka)
HARA Shunsuke 原　俊介 (Dep. Gen. Educ., Tsukuba Coll. Technol.)
HARSTON Michael R. (Oxford Univ., England)
HINO Kenichi 日野健一 (Dep. Eng. Phys., Univ. Electro-Commun.)
HITACHI Akira 月出　章 (Sci. & Eng. Res. Lab. Waseda Univ.)
ISHII Keishi 石井慶之 (Dep. Eng. Sci., Kyoto Univ.)
ISOZUMI Yasuhito 五十棲泰人 (Inst. Chem. Res., Kyoto Univ.)
ITO Shin 伊藤　真 (Radioisot. Res. Cent., Kyoto Univ.)
ITOH Akio 伊藤秋男 (Fac. Eng., Kyoto Univ.)
ITOH Yoh 伊藤　陽 (Fac. Sci., Josai Univ.)
KARASHIMA Shosuke 唐島照介 (Dep. Electron. Eng., Tokyo Univ. Sci.)
KAWATSURA Kiyoshi 川面　澄 (Kyoto Inst. Technol.)
KOBAYASHI Nobuo 小林信夫 (Dep. Phys., Tokyo Metrop. Univ.)
KOHARA Takao 小原孝夫 (Fac. Sci., Himeji Inst. Technol.)
KOIKE Fumihiro 小池文博 (Sch. Med., Kitasato Univ.)
KOIZUMI Tetsuo 小泉哲夫 (Dep. Phys., Rikkyo Univ.)

KOMAKI Kenichiro 小牧研一郎 (Coll. Arts Sci., Univ. Tokyo)
KUROKI Kenro 黒木健郎 (Natl. Res. Inst. Police Sci.; Coll. Arts Sci., Univ. Tokyo)
LENCINAS Sergio (Univ. Frankfurt, Germany)
MATSUO Takashi 松尾 崇 (Dep. Pathol., Tokyo Med. Dent. Univ.)
MATSUZAWA Michio 松澤通生 (Dep. Eng. Phys., Univ. Electro-Commun.)
MITAMURA Tohru 三田村 徹 (Fac. Eng., Himeji Inst. Technol.)
MIZOGAWA Tatsumi 溝川辰巳 (Nagaoka Coll. Technol.)
MUKOYAMA Takeshi 向山 毅 (Inst. Chem. Res., Kyoto Univ.)
OHTANI Shunsuke 大谷俊介 (Inst. Laser Sci., Univ. Electro-Commun.)
OKUNO Kazuhiko 奥野和彦 (Dep. Phys., Tokyo Metrop. Univ.)
SATO Hiroshi 佐藤浩史 (Dep. Phys. Ochanomizu Univ.)
SCHMIDT-BÖCKING Horst (Univ. Frankfurt, Germany)
SEKIOKA Tsuguhisa 関岡嗣久 (Fac. Eng., Himeji Inst. Technol.)
SHIBATA Hiromi 柴田裕美 (Res. Cent. Nucl. Sci., Univ. Tokyo)
SHIMA Kunihiro 島 邦博 (Tandem Accel. Cent., Univ. Tsukuba)
SHIMAKURA Noriyuki 島倉紀之 (Gen, Educ. Dep., Niigata Univ.)
SUZUKI Hirosi 鈴木 洋 (Inst. Laser Sci., Univ. Electro-Commun.)
TAWARA Hiroyuki 俵 博之 (Natl. Inst. Fusion Sci.)
TERASAWA Mititaka 寺澤倫孝 (Fac. Eng., Himeji Inst. Technol.)
TOSHIMA Nobuyuki 戸嶋信幸 (Inst. Appl. Phys., Univ. Tsukuba)
TSURUBUCHI Seiji 鶴淵誠二 (Fac. Technol., Tokyo Univ. Agric. Technol.)
WAKIYA Kazuyoshi 脇谷一義 (Dep. Phys., Sophia Univ.)
WATANABE Shinichi 渡辺信一 (Dep. Eng. Phys., Univ. Electro-Commun.)
YAMAZAKI Yasunori 山崎泰規 (Coll. Arts Sci., Univ. Tokyo)
YOSHINO Masuhiro 吉野益弘 (Lab. Phys., Shibaura Inst. Technol.)
ZOU Yaming 邹 亚明 (Jiao Tong Univ., China)

(Students)
KAKUTANI Nobukazu 角谷暢一 (Coll. Arts Sci., Univ. Tokyo)
KASUGA Masahito 春日真人 (Coll. Arts Sci., Univ. Tokyo)
KYOH Suigen 姜 師現 (Fac. Eng., Kyoto Univ.)
NAGATA Michi 永田美知 (Dep. Phys., Meisei Univ.)
NAKAMURA Nobuyuki 中村信行 (Inst. Laser Sci., Univ. Electro-Commun.)
NEGISHI Tomoo 根岸智夫 (Dep. Phys., Sophia Univ.)
SANO Mutsumi 佐野 睦 (Dep. Phys., Rikkyo Univ.)
YAMAGATA Masahiro 山形昌広 (Coll. Arts Sci., Univ. Tokyo)
YAMASHITA Tetsurou 山下徹郎 (Dep. Phys., Rikkyo Univ.)

Metal Physics Laboratory

ISHIDA Katsuhiko 石田勝彦
KOYAMA Akio 小山昭雄
MATSUSHITA Akira 松下 明
NAGAMINE Kanetada 永嶺謙忠
YAGI Eiichi 八木栄一
KADONO Ryosuke 門野良典
MATSUNO Shun-ichi 松野俊一
MATSUZAKI Teiichiro 松﨑禎市郎
WATANABE Isao 渡邊功雄

(Visitors)
AKAISHI Yoshinori 赤石義紀 (Fac. Sci., Hokkaido Univ.)
FUJIOKA Manabu 藤岡 学 (Cyclotron Radioisot. Cent., Tohoku Univ.)
JONES E. Steven (Dep. Phys. and Astronomy, Brigham Young Univ., U.S.A.)
KAMIMURA Masayasu 上村正康 (Fac. Sci., Kyushu Univ.)
KUMAGAI Kenichi 熊谷健一 (Fac. Sci., Hokkaido Univ.)
MINAMISONO Tadanori 南園忠則 (Fac. Sci., Osaka Univ.)
MIYAKE Yasuhiro 三宅康博 (Meson Sci. Lab., Univ. Tokyo)
MORITA Masato 森田正人 (Fac. Sci., Jyosai Univ.)

TORIKAI Eiko 鳥養映子 (Fac. Eng., Yamanashi Univ.)
WATANABE Tsutomu 渡部 力 (ICU)

(Student)
STRASSER Partrick (Fac. Eng., Univ. Tokyo)

Magnetic Materials Laboratory

OKADA Takuya 岡田卓也

Plasma Physics Laboratory

OYAMA Hitoshi 大山 等
YANO Katsuki 矢野勝喜

(Visitor)
SAKAMOTO Yuichi 坂本雄一 (Electr. Eng. Dep., Toyo Univ.)

Microwave Physics Laboratory

MINOH Arimichi 箕曲在道

Earth Science Laboratory

TAKEMATSU Noburu 竹松 伸

Semiconductor Laboratory

AOYAGI Yoshinobu 青柳克信

(Visitor)
AONO Keiko 青野桂子 (Coll. Lib. Arts, Kitasato Univ.)

Inorganic Chemical Physics Laboratory

AMBE Shizuko 安部静子
KAWAI Jun 河合 潤
MAEDA Kuniko 前田邦子
MATSUO Yukari 松尾由賀利
TAKAMI Michio 高見道生

(Visitors)
ISHII Keizo 石井慶造 (Cyclotron Radioisot. Cent., Tohoku Univ.)
SASA Yoshihiko 佐々嘉彦 (Lab. Mater. Sci. Technol., Waseda Univ.)
UDA Masayuki 宇田応之 (Dep. Mater. Sci. Eng., Waseda Univ.)

(Students)
ISOMURA Tomoyuki 磯村知之 (Dept. Mat. Sci. Eng., Waseda Univ.)
SUZUKI Setsuo 鈴木説男 (Dept. Ind. Chem., Univ. Tokyo)
UDA Eiichirou 宇田英一郎 (Dept. Mat. Sci. Eng., Waseda Univ.)

Nuclear Chemistry Laboratory

AMBE Fumitoshi 安部文敏
ARATANI Michi 荒谷美智
ITOH Yoshiko 伊東芳子
IWAMOTO Masako 岩本正子
KOBAYASHI Yoshio 小林義男
OHKUBO Yoshitaka 大久保嘉高

MAEDA Haruka 前田はるか

(Visitors)
ASAI Kichizo 浅井吉蔵 (Univ. Electro-Commun.)
BABA Hiroshi 馬場 宏 (Fac. Sci., Osaka Univ.)
CHEN Shaoyong 陳 紹勇 (South China Sea Inst. Oceanol., China)
FURUKAWA Michiaki 古川路明 (Fac. Sci., Nagoya Univ.)
IMAI Masato 今井正人 (Komatsu Electronic Metals Co., Ltd.)
HARAKAWA Hiroaki 原川裕章 (Coll. Sci. and Eng., Aoyamagakuin Univ.)
KIMURA Kan 木村 幹 (Coll. Sci. and Eng., Aoyamagakuin Univ.)
KOJIMA Sadao 小島貞男 (Nucl. Med. Cent., Aichi Medical Univ.)
KUBO Michael Kenya 久保謙也 (Fac. Sci., Univ. Tokyo)
MINAI Yoshitaka 薬袋佳孝 (Fac. Sci., Univ. Tokyo)
MURAKAMI Hideoki 村上英興 (Tokyo Gakugei Univ.)
NOZAKI Tadashi 野崎 正 (Sch. of Hygienic Sci., Kitasato Univ.)
OKADA Shigenobu 岡田繁信 (R/D Eng., Shimazu Corp.)
OOHIRA Shigeo 大平重男 (Nikkei Technol. Res. Co., Ltd.)
SAITO Kazuo 斉藤和男 (Toshiba Corp., R&D Cent.)
SAITO Tadashi 斎藤 直 (Fac. Sci., Osaka Univ.)
SHIBATA Sadao 柴田貞夫 (Natl. Inst. Radiol. Sci.)
SHIBATA Seiichi 柴田誠一 (Inst. Nucl. Study, Univ. Tokyo)
SHINOHARA Atsushi 篠原 厚 (Fac. Sci., Nagoya Univ.)
SUGAI Isao 菅井 勲 (Inst. Nucl. Study, Univ. Tokyo)
TAZAKI Kazue 田崎和江 (Fac. Sci., Shimane Univ.)
TOMINAGA Takeshi 富永 健 (Fac. Sci., Univ. Tokyo)
YAITA Tsuyoshi 矢板 毅 (Japan Atomic Energy Res. Inst.)
YOKOTA Yuko 横田裕子 (Coll. Sci. and Eng., Aoyamagakuin Univ.)
YOKOYAMA Akihiko 横山明彦 (Fac. Sci., Osaka Univ.)
YUKAWA Masae 湯川雅枝 (Natl. Inst. Radiol. Sci.)

(Students)
AKIYAMA Hiroshi 秋山 浩 (Dep. Metal Eng., Shibaura Inst. Technol.)
BAMBA Takehiro 番場丈博 (Coll. Sci. and Eng., Aoyamagakuin Univ.)
IDA Katsuyuki 井田勝之 (Fac. Sci. & Eng., Tokyo Denki Univ.)
KAWARADA Jun 河原田 淳 (Coll. Sci. and Eng., Aoyamagakuin Univ.)
KIRIU Masaru 桐生 大 (Fac. Sci., Osaka Univ.)
KURACHI Junji 倉知淳史 (Fac. Sci., Nagoya Univ.)
MUROYAMA Toshiharu 室山俊浩 (Fac. Sci., Nagoya Univ.)
NAKAMURA Jin 中村 仁 (Univ. Electro-Commun.)
OHTSUKA Hiroshi 大塚博史 (Fac. Sci., Univ. Tokyo)
SHINTAI Junichirou 新帯淳一郎 (Fac. Sci., Nagoya Univ.)
TAKAHASHI Yoshio 高橋嘉夫 (Fac. Sci., Univ. Tokyo)
TAKESAKO Kazuhiro 竹迫和浩 (Fac. Sci., Osaka Univ.)
TANAKA Shigeo 田中茂男 (Fac. Sci., Toho Univ.)
TANIGUCHI Eugene 谷口勇仁 (Fac. Sci., Nagoya Univ.)
UMEMURA Yasushi 梅村泰史 (Fac. Sci., Univ. Tokyo)
WATANABE Seiya 渡辺誠也 (Fac. Sci., Osaka Univ.)
YANO Daisaku 矢野大作 (Fac. Sci., Osaka Univ.)
YOSHINAGA Hiroshi 吉永 宏 (Dep. Metal Eng., Shibaura Inst. Technol.)

Chemical Dynamics Laboratory

KIMURA Kazuie 木村一宇

(Visitor)

ITO Yasuo 伊藤泰男 (Res. Cent. Nucl. Sci. Technol., Univ. Tokyo)

(Students)
MORITA Kazuo 森田和雄 (Dept. Phys., Chuo Univ.)
NAKAMURA Seiji 中村清志 (Dept. Phys., Chuo Univ.)
NEMOTO Ryuji 根本隆治 (Dept. Phys., Chuo Univ.)

Cellular Physiology Laboratory

HANAOKA Fumio 花岡文雄
KITAYAMA Shigeru 北山 滋
YATAGAI Fumio 谷田貝文夫

(Visitors)
ANDO Koichi 安藤興一 (Natl. Inst. Radiol. Sci.)
BAVERSTOCK Keith F. (Radiobiol. Unit, Med. Res. Counc., U.K.)
FUKUMURA Akifumi 福村明史 (Natl. Inst. Radiol. Sci.)
FURUSAWA Yoshiya 古沢佳也 (Natl. Inst. Radiol. Sci.)
HASHIMOTO Shozo 橋本省三 (Fac. Med., Keio Univ.)
HOSHINO Kazuo 星野一雄 (Natl. Inst. Radiol. Sci.)
IIZUKA Masayuki 飯塚正之 (Natl. Inst. Radiol. Sci.)
ITOH Hiroko 伊藤浩子 (Natl. Inst. Radiol. Sci)
ITO Hisao 伊東久夫 (Fac. Med., Keio Univ.)
KANAI Tatsuaki 金井達明 (Natl. Inst. Radiol. Sci.)
KAWACHI Kiyomitsu 河内清光 (Natl. Inst. Radiol. Sci.)
KAWASHIMA Katsuhiro 川島勝弘 (Natl. Inst. Radiol. Sci.)
KIKUCHI Masahiro 菊地正博 (Japan Atomic Res. Inst., Takasaki)
KIMOTO Masafumi 木元正史 (Natl. Inst. Radiol. Sci.)
KOBAYASHI Yasuhiko 小林泰彦 (Japan Atomic Energy Res. Inst.)
KOHNO Toshiyuki 河野俊之 (Natl. Inst. Radiol. Sci.)
KOIKE Sachiko 小池幸子 (Natl. Inst. Radiol. Sci.)
KOJIMA Eiichi 小島栄一 (Natl. Inst. Radiol. Sci.)
KOSAKA Toshifumi 小坂俊文 (Dep. Vet. Radiol., Nihon Univ.)
KUBOTA Nobuo 窪田宜夫 (Fac. Med., Yokohama City Univ.)
McINTYRE Cindy L. (Radiobiol. Unit, Med. Res. Counc., U.K.)
MINOHARA Shinichi 簑原伸一 (Natl. Inst. Radiol. Sci.)
NAKAI Hirokazu 中井弘和 (Dep. Agric., Shizuoka Univ.)
OHARA Hiroshi 大原 弘 (Dep. Gen. Cul., Okayama Univ.)
SOGA Fuminori 曽我文宣 (Inst. Nucl. Study, Univ. Tokyo)
SUDO Michio 須藤美智雄 (Natl. Inst. Radiol. Sci.)
TAKATUJI Toshihiro 高辻俊宏 (RI Cent., Nagasaki Univ.)
TANAKA Kaoru 田中 薫 (Natl. Inst. Radiol. Sci.)
TSUBOI Atsushi 坪井 篤 (Natl. Inst. Radiol. Sci.)
WATANABE Hiroshi 渡辺 宏 (Japan Atomic Energy Res. Inst.)
WATANABE Masami 渡辺正己 (RI Cent., Fac. Med., Yokohama City Univ.)
YAMASHITA Shoji 山下昌次 (Natl. Saitama Hospital)

(Student)
SUZUKI Masao 鈴木雅雄 (RI Cent., Fac. Med., Yokohama City Univ.)

Safety Center

INAMURA Takashi 稲村 卓
INOUE Yoshio 井上義夫
KAGAYA Satoru 加賀屋 悟
KATOU Hiroko 加藤博子
KATOU Takeo 加藤武雄
MATSUZAWA Yasuhide 松沢安秀
MIYAGAWA Makoto 宮川真言
SAKAMOTO Ichiro 坂本一郎

SHINOHARA Shigemi 篠原茂己　　USUBA Isao 薄葉　勲

Surface Characterization Center

IWAKI Masaya 岩木正哉　　KOBAYASHI Takane 小林　峰
SAKAIRI Hideo 坂入英雄

Radioisotope Technology Division

NAKANO Kazushiro 中野和城　　YATAGAI Fumio 谷田貝文夫

Synchrotron Radiation Facility Design Group

ANDO Ainosuke 安東愛之輔　　BE Suck Hee 裵　碩喜
EGO Hiroyasu 恵郷博文　　FUJIWARA Shigeki 藤原茂樹
HARA Masahiro 原　雅弘　　KAMITSUBO Hiromichi 上坪宏道
KAWASHIMA Yoshitaka 川島祥孝　　KUMAGAI Keiko 熊谷桂子
KUMAGAI Noritaka 熊谷教孝　　MASUDA Takemasa 増田剛正
MATSUI Sakuo 松井佐久夫　　MOTONAGA Shoshichi 元永昭七
NAKAMURA Takeshi 中村　剛　　OHASHI Yuji 大橋裕二
OHNISHI Jun-ichi 大西純一　　OIKAWA Yoshifumi 老川嘉郁
OUCHI Tetsuya 大内徹也　　SAKAUE Hiroyuki 坂上裕之
SASAKI Shigeki 佐々木茂樹　　SOUTOME Kouichi 早乙女光一
TAKANO Shirou 高野史郎　　TAKEBE Hideki 武部英樹
TAKESHITA Isao 竹下勇夫　　TANAKA Hitoshi 田中　均
WADA Takahiro 和田隆宏　　WADA Takeshi 和田　雄
WANG Yong 王　勇　　WATANABE Kowashi 渡邊　剛
XU Choyin 徐　朝銀

(Visitors)
GOHSHI Yohichi 合志陽一 (Dept. Indust. Chem., Univ. Tokyo)
HANASAKA Takao 花坂孝雄 (Shimazu Co.)
HAYAKAWA Shinjiro 早川慎二郎 (Dept. Indust. Chem., Univ. Tokyo)
HIRANO Yoshiki 平野芳樹 (Anelva Co.)
INOUE Kouji 井上浩司 (Kobe Steel, Ltd.)
SHIBUYA Keiichi 渋谷敬一 (SMC Ltd.)
TAKAHASHI Sunao 高橋　直 (Kobe Steel, Ltd.)
TSUCHIYA Masao 土屋将夫 (IHI Co.)
YANAGI Yoshihiko 柳　義彦 (Hitachi, Ltd.)
YOKOUCHI Shigeru 横内　茂 (Osaka Vacuum Ltd.)

(Students)
IGARI Sin-ichi 猪狩真一 (Coll. Hum. Sci., Nihon Univ)
KATO Haruhiko 加藤治彦 (Fac. Eng. Sci., Chuo Univ)
SUGANUMA Kenji 菅沼健治 (Coll. Hum. Sci., Nihon Univ)

AUTHOR INDEX

RIKEN Accelerator Progress Report

理化学研究所加速器年次報告　第26巻（1992）

印　刷　平成5年（1993）3月23日
発　行　平成5年（1993）3月31日

発行者　理化学研究所
代表者　小　田　稔
〒351-01　埼玉県和光市広沢2番1号
電話（048）462—1111

編集者　理化学研究所加速器研究施設
運営委員会

印刷所　勝美印刷株式会社
〒112　東京都文京区小石川1丁目3番7号

定価 5,000円
（消費税別）

理化学研究所

埼玉県　和光市　広沢